1

AGARDograph 109

AD657092

AGARDograph 109

AGARD

ADVISORY GROUP FOR AEROSPACE RESEARCH & DEVELOPMENT

64 RUE DE VARENNE PARIS-7E FRANCE

Subsonic Wind Tunnel Wall Corrections

by H. C. Garner, E. W. E. Rogers
W. E. A. Acum and E. C. Maskell

★

AUG [illegible] 1967

OCTOBER 1966

NORTH ATLANTIC TREATY ORGANIZATION

464

AGARDograph 109

NORTH ATLANTIC TREATY ORGANIZATION

ADVISORY GROUP FOR AEROSPACE RESEARCH AND DEVELOPMENT

(ORGANISATION DU TRAITE DE L'ATLANTIQUE NORD)

SUBSONIC WIND TUNNEL WALL CORRECTIONS

by

H.C.Garner, E.W.E.Rogers,
W.E.A.Acum and E.C.Maskell

Editor
H.C.Garner
Aerodynamics Division, National Physical Laboratory,
Teddington, Middlesex, England.

October 1966

This AGARDograph is one of a series of publications sponsored by the
NATO-AGARD Fluid Dynamics Panel under the editorship of
Professor Wilbur C.Nelson

SUMMARY

The subject of wall interference spans nearly half a century and remains a field of active research. The classical theories of lift and blockage interference in two-dimensional and three-dimensional tunnels are now highly developed for steady subsonic flows without separation in fully closed or open tunnels. Oscillatory experiments, cases of separated flow, and tunnels with slotted or perforated walls can be treated by more recent analysis, but results are relatively limited.

The theoretical background is reviewed and modern developments in the formulation, calculation and application of interference corrections are discussed in seven chapters. Chapter I gives a general review and lists areas in which further research is needed. Each of the more specialized chapters contains selected graphs of numerical data and a summary or table of principal formulae.

RESUME

L'étude de la question de l'interférence due à la paroi remonte à presque un demi-siècle et continue à faire l'objet de recherches actives. Les théories classiques concernant l'interférence due à la portance ou au blocage dans les souffleries bi- et tridimensionnelles ont maintenant été élaborées à un haut degré pour les écoulements subsoniques stationnaires sans séparation dans des souffleries à circuit entièrement fermé ou ouvert. Les expériments oscillatoires, les écoulements séparés et les souffleries à parois à fentes ou perforées peuvent être traités par des méthodes d'analyse plus récentes, mais les résultats ainsi fournis ne sont que relativement limités.

Les sept chapitres constituant la présente Agardographie passent en revue l'historique des théories à ce sujet et examinent des développements modernes dans la formulation, calcul et application des corrections de parois. Le premier chapitre donne un aperçu general et indique les domaines dans lesquels de nouvelles recherches sont nécessaires. Chacun des chapitres plus spécialisés comporte des graphiques choisis de données numériques, ainsi qu'un résumé ou tableau récapitulatif des principales formules utilisées.

533.6.071.4

CONTENTS

Page

SUMMARY iii

RESUME iii

CHAPTER I STATUS OF INTERFERENCE EFFECTS by H.C. Garner 1

1.1 Introduction 5
1.2 General References 6
1.3 Present Knowledge 8
1.4 Outstanding Problems for Research 14
1.5 Acknowledgements 16

CHAPTER II LIFT INTERFERENCE ON TWO-DIMENSIONAL WINGS by H.C. Garner 21

2.1 Introduction 29
2.2 Wings of Zero Thickness in Closed Tunnels 31
2.3 Wings of Finite Thickness in Closed Tunnels 37
2.4 Aerofoils with Hinged Flaps 44
2.5 Open-Jet Tunnels 46
2.6 Experimental Considerations 53

CHAPTER III LIFT INTERFERENCE ON THREE-DIMENSIONAL WINGS by H.C. Garner 75

3.1 Introduction 87
3.2 Small Wings in Closed and Open Tunnels 90
3.3 General Theory of Lift Interference 103
3.4 Evaluation of Interference Parameters 117
3.5 Numerical Interference Corrections 141
3.6 Special Configurations 153
3.7 Experimental Considerations 167
3.8 Index of Formulae and Data 173

CHAPTER IV INTERFERENCE EFFECTS IN UNSTEADY EXPERIMENTS by W.E.A. Acum 219

4.1 Introduction 223
4.2 Two-Dimensional Wings in Incompressible Flow 232
4.3 Two-Dimensional Wings in Compressible Flow 236
4.4 General Theory for Three-Dimensional Wings 239
4.5 Application to Three-Dimensional Wings in Closed Tunnels 247
4.6 Perforated and Slotted Walls 256
4.7 Steadily Rotating Models 258
4.8 Applications to Common Experimental Situations 264

Page

CHAPTER V BLOCKAGE EFFECTS IN CLOSED OR OPEN TUNNELS by E. W. E. Rogers 279

5.1 Introduction 287
5.2 Solid Blockage Factors in Closed Rectangular Tunnels 289
5.3 Solid Blockage Factors in Closed Non-Rectangular Tunnels 299
5.4 Wake Blockage Factors in Closed Tunnels 304
5.5 Blockage Factors in Open-Jet Tunnels 308
5.6 Estimation of Blockage from Wall Measurements 311
5.7 Blockage Corrections at Very High Subsonic Speeds in Closed Tunnels 315
5.8 Use of Blockage Factors in Correcting Measured Quantities 317
5.9 Summary of Principal Blockage Formulae 321

CHAPTER VI WALL INTERFERENCE IN TUNNELS WITH VENTILATED WALLS by E. W. E. Rogers 341

6.1 Introduction 351
6.2 Boundary Conditions for Walls with Longitudinal Slots 353
6.3 Two-Dimensional Blockage in Tunnels with Longitudinal Slots 357
6.4 Three-Dimensional Blockage in Tunnels with Longitudinal Slots 362
6.5 Lift Interference in Tunnels with Longitudinal Slots 369
6.6 Some General Remarks on Interference Effects in Tunnels with Longitudinal Slots 379
6.7 The Perforated Wall 380
6.8 Two-Dimensional Blockage in Tunnels with Perforated Walls 383
6.9 Three-Dimensional Blockage in Tunnels with Perforated Walls 385
6.10 Lift Interference in Tunnels with Perforated Walls 386
6.11 Application of Correction Factors 389

CHAPTER VII BLUFF BODIES AND HIGH-LIFT SYSTEMS by E. C. Maskell 431

7.1 Introduction 437
7.2 Blockage Effects on Bluff Bodies 438
7.3 Lifting Wings with Separated Flow 441
7.4 V/STOL Configurations 444

DISTRIBUTION

CHAPTER I

STATUS OF INTERFERENCE EFFECTS

by

H.C.Garner

Aerodynamics Division, National Physical Laboratory,
Teddington, Middlesex, England

CONTENTS

Page

1.1 INTRODUCTION 5

1.2 GENERAL REFERENCES 6

1.3 PRESENT KNOWLEDGE 8
- 1.3.1 Lift Interference 8
- 1.3.2 Blockage Interference 10
- 1.3.3 Ventilated Tunnels 11
- 1.3.4 Unsteady Interference 13
- 1.3.5 High-Lift Systems 14

1.4 OUTSTANDING PROBLEMS FOR RESEARCH 14

1.5 ACKNOWLEDGEMENTS 16

REFERENCES 16

STATUS OF INTERFERENCE EFFECTS

H.C.Garner

1.1 INTRODUCTION

By its very nature the most perfect subsonic wind tunnel cannot reproduce an unconstrained flow past a model. The problem of wall interference has been of lasting concern to experimenters and theoreticians while tunnel design, model shapes and experimental techniques have been developing through the years. The decision to prepare a monograph on subsonic wind-tunnel wall corrections was made during the planning of an AGARD meeting on interference effects in aerodynamic test facilities, held in Brussels in March 1959. Goethert's[1.1] monograph on transonic wind-tunnel testing, then in course of preparation, concentrates more especially on flows at high subsonic and low supersonic Mach numbers. As regards wall interference, this and the present AGARDograph are largely complementary. The slight overlap on the subject of ventilated tunnels is not inappropriate as there have been recent developments in this important field. A review of progress and current problems was presented by Rogers[1.2] in the introductory paper to the AGARD meeting. Further advances and new problems have since emerged, and such facts confirm the continuing importance of a study that has already occupied nearly half a century.

The foundation of research on tunnel-wall interference is attributed to Prandtl (Ref.1.3; 1919), because his lifting-line theory led to many experimental investigations with the object of verifying the theory. Moreover, the basic principles of the lifting-line theory are essential to an understanding of the simplest calculations of wall interference on finite lifting wings. The method of analysis for closed and open tunnels is established in Reference 1.3, where Prandtl develops the concept of trailing vortices so that the problem of wall interference at a lifting line involves two dimensions only. Theoretical and empirical studies then followed in quick succession, and after some ten years of research the elements of wall interference had been built into a practical framework so as to influence model testing and the design of wind tunnels. A comprehensive account of these early developments is given in Glauert's classic monograph (Ref.1.4; 1933).

Interference effects in subsonic wind tunnels may arise from the influence of tunnel-wall boundary layers, disturbances from measuring gear and model supports within the airstream, and irregularities of the airstream itself due to non-uniformity, unsteadiness or small-scale turbulence. In different ways these can all be important, but they are mainly outside the scope of the present monograph. The nature of tunnel-wall constraint can be deduced from physical principles of streamline flow. It is also associated directly with the theoretical consideration that, although the differential equations of the flow are the same in the tunnel as in free air, the outer boundary conditions are different. A logical and precise evaluation of the interference flow near the model by linearized theory would involve firstly a solution for the velocity potential in the presence of the tunnel boundaries, and secondly a solution for the velocity field near the model when all the boundaries, including that of the model, are removed and the velocity potential at the surface of the model from the first solution is preserved. The resulting perturbations of velocity-potential gradient normal to the surface of the model represent the interference-flow field which may be regarded as a correction to the free stream. In practice this correction has significant vertical and streamwise components. If the model is small enough, these can be interpreted as respective corrections to the direction and speed of the stream: if the model has appreciable span, average values may suffice: if the model has appreciable length, the respective components involve a streamline curvature and a longitudinal pressure gradient with consequent corrections to pitching moment and drag. The correction to stream direction and the streamline curvature are known as lift interference, since they are usually associated with circulation or vorticity round the model; in most applications they are considered to be independent of the changes in longitudinal velocity, known as blockage interference and usually arising from the volume occupied by the model and its wake. Although the basic problem is to determine the interference-flow field, this needs to be interpreted in the form of corrections to nearly all the measured aerodynamic quantities.

From Reference 1.4 it is clear that many of the early developments were associated with lift interference, and that the concept of streamline curvature. though implicit in tailplane interference, first arose as the essence of two-dimensional interference. Glauert's monograph is of more than historical importance; it continues to provide a comparative back-ground for most of the subsequent developments. Above all it gives a full and lucid account of the many principles underlying lift and blockage interference. Some more recent works of reference are briefly reviewed in Section 1.2 from the standpoint of tunnel-wall interference in subsonic flow. Section 1.3 discusses the contents of Chapters II to VII of the AGARDograph, and conclusions regarding important fields for further research are presented in Section 1.4.

1.2 GENERAL REFERENCES

References 1.1 and 1.5 to 1.12 comprise a representative collection of treatises concerning, among other important topics, the theory and application of subsonic wind-tunnel wall corrections. These are considered below in chronological order.

The contribution in Reference 1.5 by von Kármán and Burgers followed shortly after Glauert's[1.4] monograph. They consider only lift interference and give the analysis for two-dimensional flows with closed boundaries and for a lifting line in closed and open rectangular and circular tunnels. By far the most important contribution is the general solution, due to Burgers, for the three-dimensional flow field of a lifting element in a closed or open circular tunnel. Under the editorship of Durand also, there is the chapter in Reference 1.6 by Toussaint. This includes a discussion of blockage interference fuller than that of Reference 1.4 without improving its practical content. The treatment of two-dimensional lift interference in Reference 1.6 is unreliable, but the uniformly loaded lifting line in rectangular tunnels is considered in more detail than in Reference 1.5. In particular, the correct expression is given for the case of solid side-walls and open floor and roof, for which Glauert quoted an erroneous result*.

In an AVA monograph Riegels[1.7] gives a most comprehensive collection of graphs to illustrate many aspects of lift interference in incompressible flow. These include off-centre models, streamline curvature along the tunnel axis, and types of mixed boundary to achieve zero interference. With brief discussion of some sixty references of later date than References 1.4 to 1.6, the monograph represents a major advance, especially with regard to circular and elliptical tunnels with closed, open or mixed boundaries. Solid and wake blockage are also considered in some detail. Of the same period there is a short informative article by Katzoff[1.8] that deserves to be read by all wind-tunnel users. These two references highlight the impact of research on wall interference in the dozen years following the preparation of References 1.4 to 1.6.

Two valuable works on wind-tunnel practice by Pankhurst and Holder[1.9] and Pope[1.10] appeared early in the following decade, both of which give full accounts of wall interference corrections. Three-dimensional lift interference is regarded primarily as a function of tunnel shape and wing span, apart from the treatment of tailplane interference. Blockage interference effects, including the buoyancy correction to drag due to longitudinal pressure gradient, are well discussed. In many configurations of the present day, however, the influence of streamline curvature on lifting wings is usually much more important than the buoyancy correction, and in this respect References 1.9 and 1.10 have both been overtaken by developments. By way of contrast, Pankhurst and Holder[1.9] give more information on octagonal tunnels and alternative methods of applying the two-dimensional lift interference corrections, with particular attention to the neighbourhood of the stall. Pope[1.10], however, gives a fuller account of corrections to downwash in the wake of a lifting wing and includes some numerical data on streamline curvature; moreover, he gives more discussion of reflection-plane models and the case of asymmetrical spanwise loading. Pope gives considerably more graphical data, but perhaps concentrates too much on lift interference for uniform spanwise loading in conjunction with the equivalent span of the rolled-up trailing vortex; however, elliptic spanwise loading is by no means neglected. Pankhurst and Holder include some particularly useful tables and reinforce their more limited graphical data with tabulated values; by contrast, Pope includes no tables but does give illustrative worked examples of calculated interference corrections. Both works serve the wide needs of the wind-tunnel operator most admirably and cannot be judged from the standpoint of wall interference alone.

It is unfortunate that ventilated tunnels were subject to security classification when References 1.9 and 1.10 were prepared; their most serious limitation arises from the intensive development and wide use of ventilated tunnels for transonic testing. Goethert's[1.1] monograph deals comprehensively with this subject for the first time. Subsonic wall interference is reviewed in some detail. There is a good physical discussion of solid blockage in open and closed tunnels preparatory to a chapter on tunnels with longitudinal slots. The replacement of the singular boundary conditions of discrete slots by a homogeneous one is discussed, and there follows the general conclusion that with inviscid flow the open area ratio of slotted tunnels for zero interference decreases exponentially as the number of slots increases. The homogeneous boundary condition is generalized to account for slot depth and viscous effects such as friction or local separation inside the slots. Goethert argues that the slots are treated as in slender-wing theory, so that the boundary condition is essentially independent of Mach number, although the viscous effects may be altered by compressibility. The more detailed theoretical treatment of lift and blockage interference is confined to two-dimensional and circular slotted tunnels. There is a physical discussion of the flow near perforated walls and of the existence of an image system when the model and the tunnel are two-dimensional; again the theoretical results are limited to two-dimensional and circular tunnels. Finally Goethert points out a basic difference between perforated tunnels and ideal slotted tunnels without viscous effects. The boundary condition for a perforated tunnel (and indeed for a slotted tunnel with viscous effects) behaves like that for a closed tunnel in the distant wake of a lifting wing. Hence the Trefftz condition that the downwash at large distances behind the wing is twice as large as the downwash at the plane of the wing does not hold true. The importance of ventilated tunnels is emphasised in the account of subsonic wall interference by Allen and Spiegel[1.11]. Closed and open boundaries are regarded virtually as special cases of slotted or perforated walls. The theoretical lift and blockage interference in tunnels of circular section are used to illustrate the fundamental characteristics of the two types of ventilated tunnel and the manner in which they are intermediate between closed and open tunnels and can achieve zero interference.

---

* This, the only error the author has detected in Reference 1.4, is discussed in Chapter III (Section 3.2.2).

The previous references give very little attention to wind-tunnel interference in unsteady experiments. Molyneux[1.12] has recently written a useful review of the problems. For dynamic investigations there is a more extensive range of interference effects which include resonances associated with transverse acoustic waves, the tunnel-drive system and induced flows external to an open jet. There is also the possibility of random disturbances in a ventilated working section from turbulent mixing at the downstream end of slotted or perforated walls. Reference 1.12 gives a brief discussion of other aspects of wall constraint on oscillating models and provides a practical introduction to the subject.

1.3 PRESENT KNOWLEDGE

From many aspects of wall interference there have been considerable advances since the preparation of the important works of reference discussed in Section 1.2. Chapters II to VII of this AGARDograph incorporate such advances and also include original contributions and unpublished numerical data. Some of these recent developments are outlined below in relation to earlier achievements.

1.3.1 Lift Interference

For two-dimensional tests in closed tunnels the most well-known corrections apply to small, thin wings and neglect terms in aerofoil thickness to chord ratio t/c and in $(c/h)^4$ where h is the tunnel height. But Goldstein's[1.13] analysis includes interactions of thickness and incidence in wall interference, such as the effect of thickness on lift interference and that of incidence on solid blockage. In Chapter II his theory is presented in a simplified form for symmetrical aerofoils, so that the corrections include terms in $(c/h)^2$ and $(c/h)^4$ with coefficients linearly dependent on t/c. The formulae are easily generalized to incorporate first-order effects of compressibility and some allowance for viscous effects. The complete corrections are applied to the systematic experiments of Knechtel[1.14] on the NACA 4412 profile with encouraging success.

There is a tendency in theoretical work to express wall interference in terms of correction factors to the measured forces. In practice the interference on a lifting aerofoil is interpreted more appropriately as incremental corrections to the measured quantities, including the incidence. This is particularly true of aerofoils with hinged flaps. The theory of Preston and Manwell[1.13] is developed to give the necessary corrections to incidence, lift, pitching moment and hinge moment. A later theory by de Jager and van de Vooren[1.16], also discussed in Chapter II, considers the non-linear characteristics of flaps at large angles of deflection for which the interference corrections are shown to change sign.

It seems profitless to treat two-dimensional testing in open tunnels in great detail. Either the flow is far from two-dimensional, or else with the model between solid side-walls the interference corrections are large, of order c/h, and of dubious accuracy so as to place a very restricted limit on model size. However, there is considerable theoretical interest in the configuration of an aerofoil spanning a rectangular tunnel with solid side-walls, when the working section has open floor and roof between a closed entrance nozzle and a collector downstream. The usual boundary condition imposes the same constant pressure at the two free boundaries. Katzoff[1.17] introduces differential pressures to prevent spillage at the collector, and under such conditions the wall interference of order c/h and the streamline curvature can both be nearly eliminated.

Chapter III draws more heavily than other chapters from classical theory as compiled by Glauert[1.4]. By 1935 the basic theory for simple lifting-line wings with a tail arm was available for most tunnel shapes. Improved methods have been developed subsequently for calculating the interference upwash in rectangular and circular tunnels, but the basic theory survives. New tunnel configurations have necessitated the theoretical development for closed octagonal tunnels by Batchelor[1.18], and Katzoff et al.[1.17] have analysed the problem of open circular tunnels of finite jet length. The testing of half-models mounted on a reflection plane has in effect introduced other shapes of tunnel; the bipolar shapes corresponding to circular tunnels have been treated with closed boundaries by Sivells and Salmi[1.19] and with open boundaries by Davison and Rosenhead[1.20]. Other developments for the lifting-line model of a wing with tail include off-centre models considered by Silverstein and White[1.21] and interference corrections on ground effect by Brown[1.22] when the floor of the tunnel is used to simulate the ground. The ultimate refinement of the lifting-line treatment is that of Sanders and Pounder[1.23] for closed rectangular tunnels.

The main developments of three-dimensional lift interference in the past twenty years have concerned the sweptback, and later slender, wings designed for high-speed flight. The lifting-line model no longer applies, so that a different representation of the lifting wing by distributed vortices is needed, together with more elaborate methods of interpreting the interference upwash. Difficulties of presentation in Chapter III arise from the wide variety of vortex models, notations and procedures for obtaining the interference corrections. The models vary from distributions of lifting elements along the locus of sectional streamwise centres of pressure used by Acum[1.24] to the point concentrations of lift used by Katzoff and Hannah[1.25]. The formulation varies from the admirable approximate expressions in Reference 1.19 to that of Reference 1.26 which requires the use of one of the lifting-surface theories that have come to replace the inadequate lifting-line theory. Allowance for Mach number M is included, wherever possible, by using the Prandtl-Glauert analogy and inserting the appropriate power of $\beta = \sqrt{(1 - M^2)}$ as a factor in the geometric and aerodynamic parameters of an equivalent incompressible flow. In this way the results can usually be presented for a general subsonic Mach number and in a unified notation. The special case of slender wings involves a distribution of lifting elements along the axis of the tunnel, and in this sense can be regarded as an extension of the theory for small wings. Berndt[1.27] has given an exact theory for slender wings, to which a useful simplifying approximation can be made.

There are some aspects of lift-interference correction that are much less satisfactory. These arise primarily through deficiencies or complexities in the theoretical treatment of the corresponding problem in unconstrained flow. Three particular instances, when the corrections are quite large, are control-surface hinge moments, vortex-induced yawing moment and wing-body combinations. The hinge moments involve uncertainties of large viscous effects, and the corrections of Bryant and Garner[1.28] allow for these on a crude two-dimensional basis. More serious are thought to be the shortcomings of the interference corrections to yawing moment. Apparently all existing formulae for these are derived from lifting-line theory. Likewise the theory of wall interference on lifting wing-body combinations is inadequate, and the author concludes that the literature on this aspect of lift interference is misleading.

It is observed experimentally by Knight and Harris[1.29] on wings of moderately high aspect ratio, that the interference parameter for the drag coefficient C_D is closer to the lifting-line correction than is the interference parameter for correcting the incidence α; that is to say, the streamline curvature associated with the streamwise extent of the model has a larger effect on $\Delta\alpha$ than on ΔC_D. However, circumstances are different for slender wings with leading-edge separation. With the loss of leading-edge suction the effects of streamline curvature on $\Delta\alpha$ and ΔC_D become equally important, but the evaluation poses an unsolved non-linear problem.

The diversity of methods and notations is coupled with scarcity of published numerical examples. An attempt is made in Chapter III to digest numerical data in the most general form, with particular emphasis on formulae that are applicable to general subsonic Mach number, general planform and a range of tunnel shape. Simplified methods of evaluating the interference corrections are developed where possible. Specific comparisons between the results of different methods are quite encouraging and show which of them are useful approximations and which give primarily a rapid estimate of the order of magnitude of the corrections.

1.3.2 Blockage Interference

Chapter V is based on assumptions that the lift is not large and that solid and wake blockage effects are independent. It further assumes that only longitudinal flow is subject to blockage interference, which is only true if the model is mounted in the centre of the tunnel. For closed boundaries the condition of zero normal velocity is reliable. The corresponding assumption for an open-jet boundary is one of constant pressure; mixing effects are ignored and a linearized condition is applied at the undisturbed boundary. Moreover, it is frequently assumed that the jet is of infinite length, but in practice the nozzle and collector are relatively near the model and may strongly influence the constraint corrections[1.17]. It follows that the open-jet corrections, though usually smaller in magnitude, are less soundly based than those for a closed tunnel; furthermore, there are few experimental data from which to assess the validity of the estimated corrections for open tunnels.

With these limitations the range of available corrections is fairly complete. Two-dimensional solid and wake blockage are discussed by Thom in Reference 1.30, and Goldstein[1.13] gives a more general treatment including terms in $(c/h)^4$. With particular reference to the work of Herriot[1.31], the solid and wake blockage corrections to the usual aerodynamic coefficients may be calculated with some confidence for three-dimensional models in tunnels having a wide range of rectangular cross-sections. The circular tunnel also presents no great problems, but for elliptical and octagonal cross-sections certain simplifying assumptions need to be made to relate these to corresponding simpler shapes. Allen and Vincenti[1.32] give a sound basis on which the effect of compressibility at subcritical Mach numbers can be incorporated simply by linear-perturbation techniques; even the presence of local regions of supersonic flow about the model, with attendant shock waves, may be allowed for in an empirical manner.

Thus the topic of blockage interference on small streamline models is in a reasonably satisfactory state, though there are instances in Chapter V of differences of approach which can lead to somewhat different answers. These, however, are the exceptions in an area which after nearly forty years is, within its limitations, approaching finality.

The bulk of established interference theory is concerned with streamline flow. It is implicit that the wake is thin and that it can be taken to originate from the trailing edge of a wing or from the rearmost point of a body. However, there is a growing interest in flows which depart significantly from this classical pattern and also some evidence[1.33] to show that new, and sometimes surprising, interference effects may arise.

It is perhaps worth emphasising that high lift does not, in itself, imply a departure from the classical flow pattern. The principles of the classical interference theory of Chapter V can, therefore, remain valid, although wind-tunnel models may give rise to larger corrections than are strictly within the scope of current theories. High-order calculations of the interference field are straightforward in principle, but it may well be impossible to interpret such calculations usefully in terms of modified free-stream conditions. In any event, it is plainly dangerous to assume that large corrections can be estimated satisfactorily. To do so implies that the entire flow field could have been calculated with fair precision at the outset.

The extension of classical interference theory to a non-streamline flow is never straightforward, even though the appropriate corrections may be small. The distinguishing feature of a problem of this kind is that it requires, as a first step, the establishment of a suitable mathematical model of the given flow. The dominant physical characteristics of the flow must be described adequately by this model, but it must remain simple enough to admit of further analysis. Some typical examples are considered in Chapter VII, in particular Maskell's[1.33] theory of blockage effects on two-dimensional and three-dimensional bluff bodies and on stalled wings in a closed wind tunnel.

1.3.3 Ventilated Tunnels

The development of the ventilated-wall tunnel arose from the desire to exploit the opposing interference effects associated with closed and open boundaries; by combining these in some judicious manner zero wall interference might be obtained. The subsequent attainment of transonic test speeds seems to have been a most fortunate by-product, with its own rapid exploitation. The development of general theories for the calculation of wall interference stems from the concept of replacing the mixed boundary conditions by a single homogeneous condition valid over the entire wall, as discussed in Section 1.2 (Refs. 1.1 and 1.11). Baldwin et al.[1.34] have constructed a condition for inviscid or viscous flow at a ventilated boundary. The actual geometry of a slotted wall and the degree of porosity of a slotted or perforated wall appear as two parameters in the homogeneous condition. The validity of this simplification has been established by comparison with earlier and more exact calculations of Pistolesi[1.35] and Matthews[1.36] for a circular tunnel with discrete slots, and by examination of experimental data for the porosity parameter as in Reference 1.37. Thus the way is open for the calculation of the interference corrections due to lift and blockage; the latter assumes great importance as the Mach number approaches the region of high subsonic flow.

During the preparation of Chapter VI some calculations of two-dimensional lift interference have become available; Holder[1.38], using the boundary condition of Reference 1.34, evaluates the influence of slot geometry and porosity for a small two-dimensional model in a slotted rectangular tunnel. Two-dimensional blockage interference is covered fairly completely in References 1.29 and 1.34. A similar situation exists for small three-dimensional models in circular slotted tunnels (Refs. 1.40 and 1.37), but the more important cases of rectangular tunnels with slotted floor and roof are rather more difficult to calculate. Davis and Moore[1.40] give a few results for lift and blockage interference when there is inviscid flow near the slots, but important extensions to their analysis have appeared recently in References 1.41 and 1.42. Holder[1.41] has given analytical expressions and representative calculations of lift interference to satisfy the homogeneous condition including the porosity parameter. Acum[1.42] has simplifed the expression for the solid-blockage factor in Reference 1.40 and gives results for a wide range of rectangular cross-sections. The influence of viscous slot-flow on blockage interference does not seem to have been considered for this type of tunnel.

The theoretical approach to interference corrections in a rectangular tunnel with all four walls slotted is less satisfactory. Lift and blockage interference can be estimated from Chapter VI on the basis of limiting values for closed and completely open tunnels by allowing an analogy between the effect of slot geometry in circular and other tunnels. A similar basis might be used to estimate streamline curvature, but there is insufficient reliable information for any type of slotted tunnel. Solutions by electrical analogue should prove useful here, and a promising start has been made by Rushton in Reference 1.43 and the subsequent development of a three-dimensional network. Little experimental information exists on the value of the porosity parameter defining viscous effects near the slots, and in the absence of this the theoretical results cannot be applied with any precision. More experiments are essential, because estimates of both lift and blockage interference made for ideal wall conditions may be greatly in error.

The perforated wall has distinct characteristics, mentioned in Section 1.2 and discussed more fully in relation to experiment in Reference 1.1. The boundary condition is a limiting form of that used for a slotted wall with viscous flow as the slot spacing tends to zero. Parametric analysis suggests that the perforated tunnel behaves more and more like an open jet as sonic flow is approached. Theoretical calculations of interference corrections in terms of the porosity parameter are available for lifting and non-lifting two-dimensional models and fairly small wings in circular tunnels from the work of Goodman in References 1.44 and 1.45 and later developments given in Reference 1.46.

Blockage effects, however, have not been considered in a rectangular tunnel having two opposite or all four walls perforated. A lifting model may be treated as a special case of Reference 1.41 when the floor and roof are perforated. If the side-walls are perforated also, a graphical procedure in Chapter VI may be followed, but this is somewhat unsatisfactory as the square tunnel is considered by analogy with a circular tunnel.

1.3.4 Unsteady Interference

Most of Chapter IV is concerned with oscillatory problems, but some consideration is given to rotating models. Rolling wings of high aspect ratio can be treated fairly satisfactorily; for more slender wings only a quasi-steady theory is available, but the corrections are small. The interference corrections to propeller tests in Reference 1.4 have been standardized for many years.

There are rarely formulae or tables for corrections in oscillatory experiments, and Chapter IV is much more concerned with methods, some of which involve heavy computation. The subject is in a fairly satisfactory state numerically as regards two-dimensional closed tunnels. Timman[1.47] gives the basic theory for incompressible flow; compressibility introduces the phenomenon of acoustic resonance which is included in the general method of Runyan et al.[1.48]. For closed three-dimensional tunnels, also, there is a convenient theory, provided that the product of Mach number and frequency parameter is small; the basic idea stems from the work of Goodman[1.49], by which the unsteady interference upwash can be derived from its distribution upstream of the model in steady flow. The respective applications to closed rectangular and circular tunnels by Acum in References 1.50 and 1.51 suffice for incompressible flow. Chapter IV includes a generalization for subsonic Mach numbers and small frequency parameters. Acum[1.52] gives more explicit results for slowly oscillating slender wings, but even for slender wings there is no method when the Mach number and the frequency parameter are both fairly large, whatever the tunnel cross-section may be. Fortunately the frequency parameter is usually small for experiments on rigid models in subsonic compressible flow, but corrections to flutter tests pose a difficult problem.

The problems for ventilated tunnels are also difficult and perhaps more pressing. Wight[1.53] has reviewed experimental data obtained in slotted-wall tunnels with slots open and with slots sealed, which reveal some particularly large interference effects on damping derivatives. Unfortunately the steady interference upwash in ventilated tunnels has not yet been formulated in sufficient detail to be used on the basis of Reference 1.49. Nevertheless, a likely explanation of the observed differences in wall interference between closed and slotted tunnels is reported in Chapter IV through an extension of the classical theory of lift interference.

Further progress along the lines of investigation described in Chapter IV seems likely to lead to increased analytical, algebraic and computational complexity. One is tempted to wonder whether a better alternative would not be to use direct numerical solutions of the differential equations or analogue experiments, such as those envisaged in Reference 1.17 or in course of development as an extension to Reference 1.43.

1.3.5 High-Lift Systems

A common feature of the examples dealt with in Chapter VII is that they are concerned with flows differing materially from the essentially stream-line flow, with small lift, of the previous chapters. The flow past jet flaps or slender wings with leading-edge vortices can be regarded as an extension of the classical streamline flow. The appropriate mathematical model is still a vortex sheet, but one which includes novel features that require special attention when the effects of the interference field are to be interpreted. Maskell's[1.54] treatment of a three-dimensional jet-flap in a closed tunnel illustrates this group of problems. In others, for example bluff bodies and stalled wings (Ref. 1.33), a thick wake of uncertain structure is the dominant characteristic of the flow patterns. The main problem is to identify those properties of the wake that are most significant, and then to devise a mathematical model that reproduces them with sufficient accuracy.

A third group of problems is concerned with configurations for vertical or short take-off and landing, in which lifting rotors, fans or jets may be combined in various ways with wings and bodies to form systems in which the interference between the various constituent flows is fundamental to the performance of the system as a whole. Heyson has given linearized theories of tunnel-wall corrections for lifting rotors (Ref. 1.55) and other high-lift systems (Ref. 1.56). In the latter case there are serious unresolved difficulties, both in the construction of a suitable mathematical model of the flow and in the interpretation of the effects of wall constraint on the mutual interference between the different elements of the system. The subject is well reviewed by Templin in Reference 1.57 which is complementary to Chapter VII.

1.4 OUTSTANDING PROBLEMS FOR RESEARCH

There remain unresolved difficulties in subsonic wind-tunnel wall interference, only a few of which are likely to be overcome by mathematical analysis alone. In some instances the most promising method of solution may well be one of numerical analysis by a finite-difference technique: experiments by electrical analogue offer an alternative approach. In others, the primary handicap is the lack of a mathematical model or definitive boundary conditions, and progress may necessarily have to stem from experimental research. Apart from the thirteen general problems grouped below, there is scope for wind-tunnel investigations to check the applicability of existing theoretical methods of interference correction; notable examples are the non-linear two-dimensional theory of aerofoils with trailing-edge flaps at large angles of deflection[1.15], lifting slender wings in closed tunnels[1.27], hinge moments from three-dimensional control testing[1.29], and blockage interference on bluff models for non-aeronautical purposes[1.33].

Closed and open tunnels

1. Two-dimensional cambered aerofoils are often tested at high sub-critical Mach numbers. In such cases the effects of t/c and c/h on wall interference are aggravated by compressibility. It is desirable to seek a better solution to the non-linear mathematical problem than the relatively simple extension to Reference 1.13 suggested in Chapter II.

2. The conventional correction to yawing moment is calculated on the basis of lifting-line theory. In Chapter III this is shown to be problematical for wings of moderately small aspect ratio, and a precise treatment of the interference correction demands a reliable lifting-surface calculation of the spanwise distribution of leading-edge suction. Such a development for subsonic flow would have many applications.

3. For slender wings with leading-edge separation the correction to drag needs clarification; it is likely to be larger than in cases of attached flow. There is scope for a non-linear theoretical treatment of constrained flow with leading-edge vortices.

4. There exists no satisfactory method of applying residual interference corrections to, say, the pitching moment on a lifting wing-body combination; the theories discussed in Chapter III are thought to be of little help. As the corrections are unlikely to be very large, there may be justification for an adaption of slender-wing theory.

5. The uncertainties of blockage interference in open tunnels impose considerable restrictions on model size (Chapter V). The problem becomes more acute when bluff bodies have to be tested in open tunnels. It is important to establish whether the corrections for non-streamline flow increase as dramatically in open tunnels as in closed tunnels[1.33].

6. The discussion of Reference 1.56 in Chapter VII suggests that a convincing theory of wall interference on high-lift systems may require an improved mathematical model and further insight into the interpretation of corrections. This most novel aspect of wall interference may require inspiration from experimental sources.

Ventilated tunnels

7. There are insufficient numerical data on the streamline curvature induced by slotted walls. Even for rectangular tunnels there is no image system; the problem may best be solved by means of a three-dimensional electrical analogue (Chapter VI).

8. It has been demonstrated theoretically, and is illustrated in Chapter VI, that viscous effects near slots, represented by a constant porosity parameter, have large influence on lift and blockage interference. More experimental work is needed to establish an empirical formula for the porosity parameter appropriate to various Mach numbers and types of slot geometry, and to verify that its variation along the tunnel is small enough for the theory to apply.

9. There appears to be no information on three-dimensional solid-blockage interference in perforated rectangular tunnels. Each arrangement of perforated walls poses a distinct problem that should be amenable to mathematical analysis.

10. The problem of lift interference in rectangular tunnels with all four walls perforated is considered by a crude graphical procedure in Chapter VI. The interference upwash in the transverse plane of a lifting element is not expressible in terms of a two-dimensional flow, and solution by electrical analogue is recommended.

Unsteady interference

11. One mathematical definition of the linearized problem of an oscillating three-dimensional wing in a subsonic closed rectangular tunnel is given in Chapter IV, but

numerical analysis may well be prohibitive when neither Mach number nor frequency parameter is small. A new approach to this problem might be sought, say, for slender models.

12. As discussed in Chapter IV, there have been mathematical formulations of the interference on an oscillating model in a perforated tunnel, but the possibility of a phase difference between the pressure drop and the normal flow through the perforations has not been considered. This possibility is worth examination theoretically and experimentally in two-dimensional flow.

13. More theoretical work is needed to establish a method of evaluating the large interference effects on oscillating wings in slotted-wall tunnels[1.53]. It is desirable to examine experimentally whether or not the effects are smaller in perforated tunnels and how they can be minimized in existing ventilated tunnels.

1.5 ACKNOWLEDGEMENTS

The preparation of Chapters I to VI of the AGARDograph formed part of the research programme of the National Physical Laboratory. The authors wish to acknowledge the assistance of Mrs S.Lucas with the calculations and diagrams. Acknowledgements are due to the members of the Fluid Dynamics Panel of the Advisory Group for Aerospace Research and Development, and to Mr A.B.Haines and Dr R.C.Pankhurst who offered constructive criticism of the draft chapters.

REFERENCES

1.1 Goethert, B.H. *Transonic Wind Tunnel Testing.* AGARDograph 49. Pergamon Press, 1961.

1.2 Rogers, E.W.E. *A Background to the Problems of Wind-Tunnel Interference.* NPL paper presented at AGARD meeting on Interference Effects. AGARD Report 292, 1959.

1.3 Prandtl, L. *Tragflügeltheorie, Part II.* Nachrichten der K.Gesellschaft der Wissenschaften zu Göttingen, 1919. Reprinted in *Vier Abhandlungen zur Hydrodynamik und Aerodynamik* by L.Prandtl and A.Betz. Göttingen, 1927.

1.4 Glauert, H. *Wind Tunnel Interference on Wings, Bodies and Airscrews.* ARC R & M 1566, 1933.

1.5 von Kármán, T.
Burgers, J.M. *General Aerodynamic Theory – Perfect Fluids. Airfoils and Airfoil Systems of Finite Span. Aerodynamic Theory* (ed. W.F.Durand), Vol.II, Div.E, Chap.IV, Julius Springer, Berlin, 1935, pp.236-280.

1.6 Toussaint, A. — *Experimental Methods - Wind Tunnels. Influence of the Dimensions of the Air Stream. Aerodynamic Theory* (ed. W.F. Durand), Vol.III, Div.I, Chap.III, Julius Springer, Berlin, 1935, pp.280-319.

1.7 Riegels, F.W. — *Wind Tunnel Corrections for Incompressible Flow.* AVA Monographs (ed. A. Betz), Section $D_3$4.1. MAP Völkenrode VG-258. Reports and Trans. 958, 1947.

1.8 Katzoff, S. — *Wind-Tunnel-Wall Corrections.* NACA-University Conference on Aerodynamics. 21st - 23rd June, 1948. (NACA/TIB/1783).

1.9 Pankhurst, R.C.
Holder, D.W. — *Wind-Tunnel Technique,* Chap.8. *Tunnel Interference Effects.* Pitman, London, 1952. (Reprinted in 1965).

1.10 Pope, A. — *Wind-Tunnel Testing,* Chap.VI. *Wind-Tunnel-Boundary Conditions.* Second Edition. Wiley, New York, 1954.

1.11 Allen, H.J.
Spiegel, J.M. — *Wind Tunnel Measurements. Test-Section Flow Uniformity. High Speed Aerodynamics and Jet Propulsion,* Vol.VIII, *High Speed Problems of Aircraft and Experimental Methods, Part 2, Wind Tunnel Techniques,* Section K (ed. F.E. Goddard). Oxford University Press, 1951.

1.12 Molyneux, W.G. — *Wind Tunnel Interference in Dynamic Measurements.* RAE Tech. Report 64069. ARC Report 26,673, 1964. Presented at a short course on the Use of Flexible Models in Aeroelastic Research at the Von Kármán Institute of Fluid Dynamics, May 1964.

1.13 Goldstein, S. — *Two-Dimensional Wind-Tunnel Interference.* ARC R & M 1902, 1942.

1.14 Knechtel, E.D. — *Experimental Investigation of Two-Dimensional Tunnel-Wall Interference at High Subsonic Speeds.* NACA Tech. Note 3087, 1953.

1.15 Preston, J.H.
Manwell, A.R. — *Calculation of the Interference on a Thin Symmetrical Aerofoil with Hinged Flap Spanning a Closed Wind-Tunnel.* ARC R & M 2465, 1941.

1.16 de Jager, E.M.
van de Vooren, A.I. — *Tunnel-Wall Corrections for a Wing-Flap System between Two Parallel Walls.* NLR (Netherlands) Report W.7, 1961.

1.17 Katzoff, S. et al. — *Linear Theory of Boundary Effects in Open Wind Tunnels with Finite Jet Lengths.* NACA Report 976, 1950.

1.18 Batchelor, G.K. — *Interference in a Wind Tunnel of Octagonal Section.* Report ACA-1 (Australia), 1944.

1.19 Sivells, J.C.; Salmi, R.M. — *Jet-Boundary Corrections for Complete and Semispan Swept Wings in Closed Circular Wind Tunnels.* NACA Tech. Note 2454, 1951.

1.20 Davison, B.; Rosenhead, L. — *Wind Tunnel Correction for a Circular Open Jet Tunnel with a Reflexion Plate.* Proc. Roy. Soc. Series A, Vol. 177, 1941, pp. 366-382.

1.21 Silverstein, A.; White, J.A. — *Wind-Tunnel Interference with Particular Reference to Off-Centre Positions of the Wing and to the Downwash at the Tail.* NACA Report 547, 1935.

1.22 Brown, W.S. — *Wind Tunnel Corrections on Ground Effect.* ARC R & M 1865, 1938.

1.23 Sanders, J.; Pounder, J.R. — *Wall Interference in Wind Tunnels of Closed Rectangular Section.* NRC (Canada) Report AR-7, 1949.

1.24 Acum, W.E.A. — *Corrections for Symmetrical Swept and Tapered Wings in Rectangular Wind Tunnels.* ARC R & M 2777, 1950.

1.25 Katzoff, S.; Hannah, M.E. — *Calculation of Tunnel-Induced Upwash Velocities for Swept and Yawed Wings.* NACA Tech. Note 1748, 1948.

1.26 Garner, H.C.; Acum, W.E.A. — *Interference Corrections for Asymmetrically Loaded Wings in Closed Rectangular Wind Tunnels.* ARC R & M 2948, 1953.

1.27 Berndt, S.B. — *Wind Tunnel Interference Due to Lift for Delta Wings of Small Aspect Ratio.* KTH (Sweden) Tech. Note Aero TN 19, 1950.

1.28 Bryant, L.W.; Garner, H.C. — *Control Testing in Wind Tunnels.* ARC R & M 2881, 1950.

1.29 Knight, M.; Harris, T.A. — *Experimental Determination of Jet Boundary Corrections for Airfoil Tests in Four Open Wind Tunnel Jets of Different Shapes.* NACA Report 361, 1930.

1.30 Thom, A. — *Blockage Corrections in a Closed High-Speed Tunnel.* ARC R & M 2033, 1943.

1.31 Herriot, J.G. — *Blockage Corrections for Three-Dimensional Flow Closed-Throat Wind Tunnels, with Consideration of the Effect of Compressibility.* NACA Report 995, 1950.

1.32 Allen, H.J.; Vincenti, W.G. — *Wall Interference in a Two-Dimensional-Flow Wind Tunnel, with Consideration of the Effect of Compressibility.* NACA Report 782, 1944.

1.33 Maskell, E.C. — *A Theory of the Blockage Effects on Bluff Bodies and Stalled Wings in a Closed Wind Tunnel.* ARC R & M 3400, 1963.

1.34 Baldwin, B.S. et al. *Wall Interference in Wind Tunnels with Slotted and Porous Boundaries at Subsonic Speeds.* NACA Tech. Note 3176, 1954.

1.35 Pistolesi, E. (i) *On the Interference of a Wind Tunnel with a Mixed Boundary.* Pont. Accad. Sci. Vol.4, No.9, 1940. (Unpublished translation by Cornell Aero. Lab., 1949.)
(ii) *On the Interference of a Wind Tunnel with Mixed Contour.* Pont. Accad. Sci. Vol.7, No.5, 1943. (Unpublished translation by NACA, 1951.)

1.36 Matthews, C.W. *Theoretical Study of the Tunnel-Boundary Lift Interference Due to Slotted Walls in the Presence of the Trailing-Vortex System of a Lifting Model.* NACA Report 1221, 1955.

1.37 Reynolds, W.G. et al. *Boundary Interference Studies in the Slotted Test Section of the Southern California Cooperative Wind Tunnel for the Mach Number Range 0.4 to 1.3.* CWT Report P-29, 1959.

1.38 Holder, D.R. *Upwash Interference in a Rectangular Wind Tunnel with Closed Side Walls and Porous Slotted Floor and Roof.* ARC R & M 3322, 1962.

1.39 Maeder, P.F. *Theoretical Investigation of Subsonic Wall Interference in Rectangular Slotted Test Sections.* Brown Univ. Div. of Eng. Tech. Report WT-11, 1953.

1.40 Davis, D.D. Moore, D. *Analytical Study of Blockage – and Lift-Interference Corrections for Slotted Tunnels Obtained by the Substitution of an Equivalent Homogeneous Boundary for the Discrete Slots.* NACA RM L53E07b (NACA/TIB/3792), 1953.

1.41 Holder, D.R. *Upwash Interference on Wings of Finite Span in a Rectangular Wind Tunnel with Closed Side Walls and Porous-Slotted Floor and Roof.* ARC R & M 3395, 1963.

1.42 Acum, W.E.A. *Note on the Evaluation of Solid-Blockage Corrections for Rectangular Wind Tunnels with Slotted Walls.* ARC R & M 3297, 1961.

1.43 Rushton, K.R. *Studies of Slotted-Wall Interference Using an Electrical Analogue. Part II. Particular Examples of Slotted-Wall Tunnel Interference.* ARC R&M 3452, 1965.

1.44 Goodman, T.R. *The Porous Wall Wind Tunnel, Pt. V. Subsonic Interference. on a Lifting Wing between Two Infinite Walls.* Cornell Aero. Lab. Report AD-706-A-3, 1951.

1.45 Goodman, T.R. *The Porous Wall Wind Tunnel, Pt. IV. Subsonic Interference Problems in a Circular Tunnel.* Cornell Aero. Lab. Report AD-706-A-2, 1951.

1.46 Wright, R.H. *The Effectiveness of the Transonic Wind Tunnel as a Device for Minimizing Tunnel-Boundary Interference for Model Tests at Transonic Speeds.* NASA paper presented at AGARD meeting on Interference Effects. AGARD Report 294, 1959.

1.47 Timman, R. *The Aerodynamic Forces on an Oscillating Aerofoil between Two Parallel Walls.* App. sci. Res. A (Hague), Vol.3, 1951, pp.31-57.

1.48 Runyan, H.L. et al. *Theoretical and Experimental Investigation of the Effect of Tunnel Walls on the Forces on an Oscillating Airfoil in Two-Dimensional Subsonic Compressible Flow.* NACA Report 1262, 1956.

1.49 Goodman, T.R. *The Upwash Correction for an Oscillating Wing in a Wind Tunnel.* J. aero. Sci. Vol.20, 1953, pp.383-386,406.

1.50 Acum, W.E.A. *Wall Corrections for Wings Oscillating in Wind Tunnels of Closed Rectangular Section.* ARC R & M 3312, 1958.

1.51 Acum, W.E.A. Garner, H.C. *Approximate Wall Corrections for an Oscillating Swept Wing in a Wind Tunnel of Closed Circular Section.* ARC CP 184, 1954.

1.52 Acum W.E.A. *A Note on the Estimation of the Effect of Wind Tunnel Walls on the Forces on Slowly Oscillating Slender Wings.* ARC CP 707, 1963.

1.53 Wight, K.C. *A Review of Slotted-Wall Wind Tunnel Interference Effects on Oscillating Models in Subsonic and Transonic Flows.* J.Roy. aeron. Soc. Vol.68, 1964, pp.670-674.

1.54 Maskell, E.C. *The Interference on a Three-Dimensional Jet-Flap Wing in a Closed Wind Tunnel.* ARC. R & M 3219, 1959.

1.55 Heyson, H.H. *Jet-Boundary Corrections for Lifting Rotors Centered in Rectangular Wind Tunnels.* NASA Tech. Report R-71, 1960.

1.56 Heyson, H.H. *Linearized Theory of Wind-Tunnel Jet-Boundary Corrections and Ground Effect for VTOL-STOL Aircraft.* NASA Tech. Report R-124, 1962.

1.57 Templin, R.J. *The Choice of Working Section Size and Shape for V/STOL Wind Tunnels.* NRC (Canada) Quarterly Bulletin DME/NAE 1965 (4), 1965.

CHAPTER II

LIFT INTERFERENCE ON TWO-DIMENSIONAL WINGS

by

H. C. Garner

Aerodynamics Division, National Physical Laboratory,
Teddington, Middlesex, England

BLANK PAGE

CONTENTS

Page

LIST OF TABLES 24

LIST OF FIGURES 24

NOTATION 25

2.1 INTRODUCTION 29

2.2 WINGS OF ZERO THICKNESS IN CLOSED TUNNELS 31
  2.2.1 Corrections to Order $(c/h)^2$ 31
  2.2.2 Corrections to Order $(c/h)^4$ 34
  2.2.3 Non-Rectangular Tunnels 36

2.3 WINGS OF FINITE THICKNESS IN CLOSED TUNNELS 37
  2.3.1 Effect of One Wall 37
  2.3.2 Goldstein's Theory 37
  2.3.3 Allowance for Compressibility 42

2.4 AEROFOILS WITH HINGED FLAPS 44

2.5 OPEN-JET TUNNELS 46
  2.5.1 Boundary Conditions 46
  2.5.2 Fully Open Jets 47
  2.5.3 Two-Dimensional Tests 49
  2.5.4 Spillage Behind the Model 52

2.6 EXPERIMENTAL CONSIDERATIONS 53
  2.6.1 Viscous Effects 53
  2.6.2 Closed Tunnels 54
  2.6.3 Open-Jet Tunnels 56

REFERENCES 57

ADDITIONAL REFERENCES 59

TABLE 61

FIGURES 62

LIST OF TABLES

Page

TABLE 2.I Summary of Principal References, Figures and Formulae 61

LIST OF FIGURES

Fig. 2.1 Thin two-dimensional aerofoil and its image system for lift interference 62

Fig. 2.2 Spanwise distribution of lift and pitching moment on an aerofoil spanning a closed rectangular tunnel 63

Fig. 2.3 Closed-tunnel to free-stream ratios of lift and moment on a flat-plate aerofoil 64

Fig. 2.4 Wall corrections for an RAE 102 aerofoil 65

Fig. 2.5 Closed-tunnel to free-stream ratios of derivatives for aerofoils with hinged flaps (Ref. 2.14) 66

Fig. 2.6 Wall corrections to flap hinge moments 67

Fig. 2.7 Wall corrections due to flap setting 68

Fig. 2.8 Effect of large flap setting on lift interference ($M = 0$) 69

Fig. 2.9 Corrections to pitching moment due to a deflected flap ($M = 0$) 70

Fig. 2.10 Lift interference in rectangular open-jet tunnels 71

Fig. 2.11 Lift interference in circular open-jet tunnels 72

Fig. 2.12 Functions from equations (2.71) to (2.75) for closed-open-closed tunnels 73

Fig. 2.13 Experimental variation of C_L with M for various c/h 74

NOTATION

a	speed of sound
a_1	lift slope = $\partial C_L/\partial\alpha$
a_2	= $\partial C_L/\partial\xi$
A_n	coefficient in chordwise loading from Equation (2.12)
b	breadth of tunnel
b'	twice the horizontal projection of a corner fillet
b_1	= $\partial C_H/\partial\alpha$
b_2	= $\partial C_H/\partial\xi$
b_n	coefficient in spanwise loading from Equation (2.61)
c	chord of aerofoil
C	cross-sectional area of tunnel
C_D	drag coefficient = (drag per unit span)/$\frac{1}{2}\rho U^2c$
C_H	(hinge moment per unit span)/$\frac{1}{2}\rho U^2E^2c^2$
C_L	lift coefficient = $L/\frac{1}{2}\rho U^2c$
C_m	pitching-moment coefficient = $M/\frac{1}{2}\rho U^2c^2$
C_n	function of aerofoil profile in Equation (2.37) ($n = 0,1,2,\ldots.$)
d	distance of aerofoil from floor of tunnel (Fig. 2.1)
D_n	function of aerofoil camber line in Equation (2.34) ($n = 0,1,2,\ldots.$)
E	ratio of flap chord to aerofoil chord
G_0	function defined in Equation (2.73)
G_1	function defined in Equation (2.73)
h	height of tunnel
h'	twice the vertical projection of a corner fillet
h_e	equivalent height of tunnel (Section 2.2.3)
k	vortex strength per unit length

K	strength of vortex
l	non-dimensional aerodynamic loading in Equation (2.14)
l	length of open working section (Section 2.5)
L	lift per unit span
m_1	$= \partial C_m/\partial\alpha$
m_2	$= \partial C_m/\partial\xi$
M	Mach number
$\mathfrak{m}$	pitching moment per unit span about axis $x = \frac{1}{4}c$
$\mathfrak{m}_{\frac{1}{2}c}$	pitching moment per unit span about axis $x = \frac{1}{2}c$
p	pressure
R	radius of circular tunnel
S	area of planform of model
t	thickness of aerofoil
u	x-component of velocity
u′	perturbation in horizontal velocity at upper boundary of jet (Section 2.5.4
U	velocity of undisturbed stream
w	z-component of velocity
$w_{+\infty}$	value of w in distant wake
x	distance downstream of leading edge of aerofoil
$\bar{x}$	centre of pressure of aerofoil in Equation (2.8)
x_0	distance of model from entrance nozzle of open-jet tunnel
X	x in transformed plane
y	spanwise distance from centre of tunnel
z	distance upwards from leading edge of aerofoil
Z	transformed co-ordinate = βz
α	incidence of aerofoil (in radians unless otherwise stated)

β	$= (1 - M^2)^{\frac{1}{2}}$
Γ	circulation around aerofoil
Δ	prefix denoting increment due to wall correction
ζ	complex variable $= X + iZ$
θ	chordwise parameter defined in Equation (2.13)
λ	parameter $3b/\pi a_1 c$ used in Section 2.5.2
μ_a	viscous correction factor in Equation (2.77)
μ_b	viscous correction factor in Equation (2.78)
ξ	angle of flap setting (in radians)
ρ	density of undisturbed stream
Φ	velocity potential of two-dimensional flow
Ψ	stream function of two-dimensional flow

Subscripts

i	denotes quantity induced by tunnel walls.
o	denotes free-stream aerodynamic coefficient.
T	denotes theoretical value.

BLANK PAGE

LIFT INTERFERENCE ON TWO-DIMENSIONAL WINGS

H. C. Garner

2.1 INTRODUCTION

In any two-dimensional, steady, isentropic and irrotational compressible flow the velocity potential Φ satisfies the differential equation

$$\left(1-\frac{u^2}{a^2}\right)\frac{\partial^2\Phi}{\partial x^2}+\left(1-\frac{w^2}{a^2}\right)\frac{\partial^2\Phi}{\partial z^2}-\frac{2uw}{a^2}\frac{\partial^2\Phi}{\partial x\partial z} = 0 , \qquad (2.1)$$

where $u = \partial\Phi/\partial x$, $w = \partial\Phi/\partial z$ and a is the local speed of sound. The linearized form of this equation

$$(1-M^2)\frac{\partial^2\Phi}{\partial x^2}+\frac{\partial^2\Phi}{\partial z^2} = 0 \qquad (2.2)$$

follows from the simplifying assumption that terms of second order in the component perturbations of a uniform velocity $U = Ma$ are negligible throughout the field of flow.

The problem of wall interference arises because the differential equation is subject to outer boundary conditions dependent on the working section of the tunnel. For example, the flow must be tangential to the wall of a closed tunnel and of constant speed at the boundary of an open jet. More complicated boundary conditions are used in cases of ventilated tunnels which are treated separately in Chapter VI.

There are two distinct mathematical approaches to the problem. One is to obtain solutions for Φ for a particular model both with and without the boundary conditions imposed by the tunnel. Through neglect of viscous forces and many other approximations the potential solution that satisfies the extra boundary conditions cannot be identified with the real flow in the tunnel; large differences between these would cause major uncertainty in the interpretation of wall interference. The more realistic approach is to assume distributed doublets and vortices within the model compatible with its shape and the aerodynamic forces measured on it. The interference is then identified with the potential flow which, when added to the field of the model, satisfies the outer boundary conditions.

The lift interference is that associated with the circulation round the model. When the model is a thin aerofoil, its field can be represented by that of a distribution of vorticity along the length of the chord. The resulting potential flow within a closed tunnel thus corresponds to the infinite array of vortices partly illustrated in Figure 2.1. The interference will then depend on the height h of the tunnel, the Mach number M, the chord c and lift distribution of the aerofoil, and its incidence α and location d between the walls of the tunnel. When the aerofoil is thick, its field involves a chordwise distribution of doublets as well. The lift interference and blockage corrections (Chapter V) then interact.

When the linearized differential Equation (2.2) is used, the transformation

$$X = x, \qquad Z = z(1 - M^2)^{\frac{1}{2}} = \beta z \tag{2.3}$$

is made, so that the potential in the new co-ordinate system satisfies Laplace's equation for incompressible flow

$$\frac{\partial^2 \Phi}{\partial X^2} + \frac{\partial^2 \Phi}{\partial Z^2} = 0 . \tag{2.4}$$

It is convenient to regard the perturbation potential $(\Phi - Ux)$ as unchanged in the transformation. Thus chord and vortex strength are invariant, while the incidence of the aerofoil and all lateral dimensions are reduced by the factor β. The component perturbations of velocity in the (X, Z) plane are unchanged in the longitudinal direction and increased by the factor β^{-1} in the lateral direction. In accord with the linearized boundary condition the velocity ratio w/U on the aerofoil is reduced to match the inclination of the transformed surface $dZ/dX = \beta(dz/dx)$, so that in the (X, Z) plane the undisturbed velocity and the local upward component are respectively $\beta^{-2}U$ and $\beta^{-1}w$. Thus the linearized solution is readily expressed in terms of that of an equivalent incompressible flow. The problem involves the evaluation of $\beta^{-1}w_i$, the vertical velocity induced by the image system of Figure 2.1 with Γ, h, d and α replaced by $\beta^{-2}U$, βh, βd and βc respectively.

The tunnel-induced vertical velocity w_i has to be interpreted as a number of corrections to measured quantities, such as incidence, lift and pitching moment. The incremental correction to incidence is a somewhat arbitrary average value of w_i/U radians. After this correction has been applied, the residual upwash field is converted into "residual" incremental corrections to the aerodynamic forces. The evaluation of these corrections, which are as important as the incidence correction, is greatly simplified if the residual upwash field of the image system can be expressed as a uniform streamline curvature along the length of the model. When this is too approximate, a fuller mathematical treatment is necessary; further analysis is then required to isolate the individual corrections and to relate them to the measured quantities.

Provided that the incidence and aerofoil thickness are small enough and the whole flow field is subsonic, then linearized theory is valid and the problem of wall interference is relatively simple. When, however, the incidence of the aerofoil is no longer small, it is necessary to use conformal transformation of the general equations of inviscid flow, even though the aerofoil is thin (Section 2.2). Such applications are restricted to incompressible flow, for which Equation (2.1) reduces to Laplace's equation. Likewise the treatment of a thick aerofoil between parallel walls involves conformal transformation (Section 2.3); some allowance for compressibility may still be incorporated by means of the equivalent incompressible flow. The more difficult non-linear problem of compressible flow has received little attention.

Other instances of wall corrections on two-dimensional models arise with regard to control surfaces (Section 2.4) and open-jet tunnels (Section 2.5). Problems of interference on aerofoils with hinged flaps are treated either by means of the linearized equations or by a non-linear theory for incompressible flow. The linear treatment includes corrections to measured hinge moments, which may be subject to a semi-empirical factor to take account of large viscous effects. For very large flap deflections the non-linear theory shows a marked reduction, and even a reversal in sign, in the corrections to lift and pitching moment. An aerofoil spanning an open tunnel is strictly a three-dimensional configuration, since the lift falls to zero at the boundary of the jet; nevertheless, work on this problem is reviewed in Section 2.5. It is also necessary to consider the interference on an aerofoil mounted on solid side walls or large end plates for which it is usual to ignore any spanwise variation in lift distribution. The analytical solution and its physical interpretation are complicated by the finite length of open working section which is bounded by a closed entrance nozzle upstream and a collector downstream of the model.

The final Section 2.6 considers viscous effects and experimental approaches to the problems of two-dimensional wall corrections and the conclusions that may be drawn. It might be helpful to remark in advance that the boundary layers on the side walls do not have extensive influence on the pressure distribution. From their investigation Mendelsohn and Polhamus (Ref. 2.1; 1947) conclude that the loss of total load on an aerofoil spanning a closed rectangular tunnel is unlikely to exceed 1% at incidences below the stall. Figure 2.2, reproduced from Reference 2.1, shows that very close to the wall ($y = -\frac{1}{2}b$) the local lift is less than 10% below that at the centre of the tunnel ($y = 0$), while there is little effect on pitching moment. Large changes in side-wall boundary-layer thickness are found to produce only small changes in the loading. One may therefore have confidence in a purely two-dimensional theoretical analysis.

A summary of the principal references, figures and equations and their fields of application is contained in Table 2.I.

2.2 WINGS OF ZERO THICKNESS IN CLOSED TUNNELS

2.2.1 Corrections to Order $(c/h)^2$

The classical work of Glauert provides the basis on which two-dimensional wall interference is evaluated for thin aerofoils at small incidence and having moderately small chord. The lifting aerofoil can then be replaced by a single vortex of strength K at the centre of pressure to obtain the flow field induced by the walls. Batchelor (Ref. 2.2; 1944) considers the incompressible flow past a vortex situated at an arbitrary distance d from the floor of the tunnel. With allowance for compressibility (Section 2.1), the primary interference near the model then appears as a vertical velocity

$$w_i = \frac{\beta K}{2\pi}\left[\sum_{n=-\infty}^{\infty} \frac{x - \bar{x}}{(x - \bar{x})^2 + 4\beta^2(nh - d)^2} - 2\sum_{n=1}^{\infty} \frac{x - \bar{x}}{(x - \bar{x})^2 + 4\beta^2 n^2 h^2}\right] . \qquad (2.5)$$

which, at small streamwise distance $(x - \bar{x})$ from the vortex, becomes

$$w_i = \frac{\pi K(x - \bar{x})}{8\beta h^2}\left(\frac{2}{3} + \cot^2\frac{\pi d}{h}\right) + O(x - \bar{x})^3 \quad . \tag{2.6}$$

If the lift and pitching moment about the quarter-chord axis are

$$\left.\begin{aligned} L &= \rho U K = \tfrac{1}{2}\rho U^2 c C_L \\ M &= \tfrac{1}{2}\rho U^2 c^2 C_m \end{aligned}\right\} \quad , \tag{2.7}$$

then the centre of pressure is at a distance

$$\bar{x} = c\left(\frac{1}{4} - \frac{C_m}{C_L}\right) \tag{2.8}$$

downstream of the leading edge. From Equations (2.6) to (2.8) the induced upwash angle in radians is

$$\frac{w_i}{U} = \frac{\pi c^2}{16\beta h^2}\left\{\left(\frac{x}{c} - \frac{1}{4}\right)C_L + C_m\right\}\left(\frac{2}{3} + \cot^2\frac{\pi d}{h}\right) \quad . \tag{2.9}$$

Batchelor$^{2.2}$ also shows that there is an induced horizontal velocity

$$u_i = -\frac{K}{4\beta h}\cot\frac{\pi d}{h} = -\frac{UcC_L}{8\beta h}\cot\frac{\pi d}{h} \tag{2.10}$$

at the wing, which vanishes when the vortex is placed centrally ($d = \frac{1}{2}h$).

The aerofoil is usually taken to be in the central plane of the tunnel. This problem is considered by Allen and Vincenti (Ref. 2.3; 1944), who represent the field of the model by continuously distributed vortices and neglect terms in $(c/h)^4$. To carry out the analysis, points on the aerofoil are defined by the angular co-ordinate θ such that the distance from the leading edge

$$x = \tfrac{1}{2}c(1 - \cos\theta) \quad . \tag{2.11}$$

The vortex strength in the tunnel is expressed as

$$k = 2U\left\{A_0 \cot\tfrac{1}{2}\theta + \sum_{n=1}^{\infty} A_n \sin n\theta\right\} \tag{2.12}$$

per unit chordwise distance. From Equation (2.6) the vertical velocity induced by the system of images is

$$
\begin{aligned}
w_i &= \int_0^c \frac{\pi k(x - x_0)}{12\beta h^2}\,dx \\
&= \frac{\pi^2 c^2 U}{48\beta h^2}\left\{(A_0 + \tfrac{1}{2}A_2) - (2A_0 + A_1)\cos\theta\right\} \\
&= \frac{\pi c^2 U}{96\beta h^2}\left\{(C_L + 4C_m) - 2C_L\cos\theta\right\} \quad , \qquad (2.13)
\end{aligned}
$$

which varies linearly and confirms the accuracy of Equation (2.9) to order $(c/h)^2$ in the special case $d = \frac{1}{2}h$.

The non-dimensional aerodynamic loading is defined as

$$
l = \frac{p_l - p_u}{\frac{1}{2}\rho U^2} \qquad (2.14)
$$

where p_l and p_u are the respective pressures on the lower and upper surfaces of the aerofoil. To the approximation of linearized theory $l = 2k/U$, and the upwash in Equation (2.13) is equivalent to a theoretical increment

$$
l_i = \frac{\pi}{24}\left(\frac{c}{\beta h}\right)^2 \left\{(C_L + 4C_m)\cot\tfrac{1}{2}\theta + 2C_L\sin\theta\right\} \quad , \qquad (2.15)
$$

by which the loading in the tunnel would exceed that in the free stream. Allen and Vincenti argue that the data obtained in a wind tunnel should be corrected in such a way that the peak loading near the leading edge is unaltered. Accordingly

$$
\left.
\begin{aligned}
\Delta\alpha &= \frac{\pi c^2}{96\beta h^2}(C_L + 4C_m) \\
\Delta l &= -\frac{\pi}{12}\left(\frac{c}{\beta h}\right)^2 C_L\sin\theta
\end{aligned}
\right\} \qquad (2.16)
$$

are applied as corrections to the measured incidence α and loading l . $\Delta\alpha$ (rad) is precisely the value of w_i/U at mid-chord ($\theta = \frac{1}{2}\pi$), since the symmetrical streamline curvature equivalent to the second term of Equation (2.13) introduces no incremental singularity in the loading at the leading edge. The loading Δl leads to residual corrections

$$
\left.
\begin{aligned}
\Delta C_L &= -\frac{\pi^2}{48}\left(\frac{c}{\beta h}\right)^2 C_L \\
\Delta C_m &= \frac{\pi^2}{192}\left(\frac{c}{\beta h}\right)^2 C_L
\end{aligned}
\right\} \quad . \qquad (2.17)
$$

With the respective increments in Equation (2.17) the measured coefficients of lift and pitching moment relate to unconstrained flow of velocity U past the actual aerofoil at the corrected incidence $(\alpha + \Delta\alpha)$.

2.2.2 Corrections to Order $(c/h)^4$

In Reference 2.4 (1934) and Reference 2.5 (1938), Tomotika uses a series of conformal transformations to obtain the lift and pitching moment on a flat-plate aerofoil inclined at an arbitrary angle α to an incompressible stream between parallel walls. The mid-chord of the plate is assumed to lie on the centre line of the tunnel. His results as expansions in powers of c/h are

$$L = L_0 \left\{ 1 + \frac{\pi^2}{24}\left(\frac{c}{h}\right)^2 (1 + \sin^2\alpha) - \frac{\pi^4}{7680}\left(\frac{c}{h}\right)^4 (11 - 53 \sin^2\alpha - 22 \sin^4\alpha) + 0\left(\frac{c}{h}\right)^6 \right\} , \qquad (2.18)$$

where $L_0 = \frac{1}{2}\rho U^2 c(2\pi \sin\alpha)$, and the pitching moment about the mid-chord is

$$M_{\frac{1}{2}c} = (M_{\frac{1}{2}c})_0 \left\{ 1 + \frac{\pi^2}{48}\left(\frac{c}{h}\right)^2 (1 + 6 \sin^2\alpha) - \frac{\pi^4}{23040}\left(\frac{c}{h}\right)^4 (11 - 174 \sin^2\alpha - 170 \sin^4\alpha) + 0\left(\frac{c}{h}\right)^6 \right\} . \qquad (2.19)$$

where $(M_{\frac{1}{2}c})_0 = \frac{1}{2}\rho U^2 c^2(\frac{1}{2}\pi \sin\alpha \cos\alpha)$. The tunnel to free-air ratios L/L_0 and $M_{\frac{1}{2}c}/(M_{\frac{1}{2}c})_0$ are plotted against c/h for selected values of α in Figure 2.3. The broken curves for $\alpha = 0$ and $\alpha = 20^0$ are obtained when terms in $(c/h)^4$ are omitted. The discrepancies are apparent when $c = 0.3h$ and exceed $\frac{1}{2}\%$ when $c = 0.5h$; it should therefore be recognized that Equations (2.16) and (2.17) are subject to significant inaccuracy when $c > 0.45h$.

Havelock (Ref. 2.6; 1938) considers the same problem by treating the flat plate as the limiting case of an elliptical cylinder. He confirms Tomotika's[2.4] result in Equation (2.18) and derives Equation (2.19) independently. Havelock neglects terms of higher order than $(c/h)^2$ and gives formulae for L/L_0 and $M_{\frac{1}{2}c}/(M_{\frac{1}{2}c})_0$ for a plate whose midpoint is at an arbitrary distance d from the floor of the tunnel (Fig. 2.1). His results can be written as

$$L = L_0 \left[1 - \frac{\pi c}{2h} \cot\left(\frac{\pi d}{h}\right) \sin\alpha + \frac{\pi^2 c^2}{16h^2} \left\{ \left(\frac{2}{3} + \cot^2\frac{\pi d}{h}\right) + \left(\frac{2}{3} + 3\cot^2\frac{\pi d}{h}\right) \sin^2\alpha \right\} + 0\left(\frac{c}{h}\right)^3 \right] \qquad (2.20)$$

and

$$M_{\frac{1}{2}c} = (M_{\frac{1}{2}c})_0 \left[1 - \frac{\pi c}{2h} \cot\left(\frac{\pi d}{h}\right) \sin\alpha + \frac{\pi^2 c^2}{32h^2} \left\{ \left(\frac{2}{3} + \cot^2\frac{\pi d}{h}\right) + \left(4 + 10\cot^2\frac{\pi d}{h}\right) \sin^2\alpha \right\} + 0\left(\frac{c}{h}\right)^3 \right] . \qquad (2.21)$$

Equation (2.9) would lead to the ratios L/L_0 and $\mathfrak{M}_{\frac{1}{4}c}/(\mathfrak{M}_{\frac{1}{4}c})_0$ obtained by substituting $\alpha = 0$ in Equations (2.20) and (2.21). Havelock's values for $c = 0.2h$ and $\alpha = 0$ and 10° are compared below.

d/h	0.3	0.4	0.5	0.6	0.7
L/L_0 for $\alpha = 0$	1.028	1.019	1.016	1.019	1.028
L/L_0 for $\alpha = 10^\circ$	0.989	1.002	1.017	1.037	1.071
$\mathfrak{M}_{\frac{1}{4}c}/(\mathfrak{M}_{\frac{1}{4}c})_0$ for $\alpha = 0$	1.014	1.010	1.008	1.010	1.014
$\mathfrak{M}_{\frac{1}{4}c}/(\mathfrak{M}_{\frac{1}{4}c})_0$ for $\alpha = 10^\circ$	0.977	0.994	1.010	1.030	1.059

By contrast with Figure 2.3 the effect of incidence on wall interference can be of primary importance when the mid-chord is off the centre line. Moreover, a downward displacement of an aerofoil at positive incidence can change the sign of the interference. It should also be noted that, even for $c = 0.2h$, the terms in $(c/h)^4$ are becoming significant in the above table for $\alpha = 10^\circ$ and $d/h = 0.3$ and 0.7, when the series converges comparatively slowly.

We have already seen that Equations (2.16) and (2.17) represent a practical form of wall correction, but become inaccurate when $c > 0.4\beta h$; this condition is restrictive at the high Mach numbers. The theoretical ratios L/L_0 and $\mathfrak{M}_{\frac{1}{4}c}/(\mathfrak{M}_{\frac{1}{4}c})_0$ from Equations (2.18) and (2.19) must then be used to obtain terms in $(c/\beta h)^4$. The pitching-moment coefficient about the quarter-chord axis is

$$\begin{aligned} C_m &= \frac{\mathfrak{M}_{\frac{1}{4}c} - \frac{1}{4}cL\cos\alpha}{\frac{1}{2}\rho U^2 c^2} \\ &= \pi \sin\alpha \cos\alpha \left\{ -\frac{\pi^2}{96}\left(\frac{c}{h}\right)^2 (1 - 4\sin^2\alpha) + \right. \\ &\qquad\qquad \left. + \frac{\pi^4}{46080}\left(\frac{c}{h}\right)^4 (22 + 15\sin^2\alpha + 104\sin^4\alpha) \right\} . \end{aligned} \tag{2.22}$$

When α is small,

$$\left. \begin{aligned} C_L &= \frac{2\pi\alpha}{\beta}\left\{1 + \frac{\pi^2}{24}\left(\frac{c}{\beta h}\right)^2 - \frac{11\pi^4}{7680}\left(\frac{c}{\beta h}\right)^4\right\} \\ C_m &= \frac{\pi\alpha}{\beta}\left\{-\frac{\pi^2}{96}\left(\frac{c}{\beta h}\right)^2 + \frac{11\pi^4}{23040}\left(\frac{c}{\beta h}\right)^4\right\} \end{aligned} \right\} , \tag{2.23}$$

where the linearized compressibility factor β has been inserted.

It remains to convert the results in Equations (2.23) into incremental corrections to the measured incidence, lift and pitching moment. The previous discussion leaves no doubt that, to order $(c/h)^2$, Equation (2.16) is the best definition of $\Delta\alpha$. Although this could still be used, we prefer the definition

$$\Delta\alpha = \beta C_L \left\{ \frac{\pi}{96}\left(\frac{c}{\beta h}\right)^2 - \frac{41\pi^3}{92160}\left(\frac{c}{\beta h}\right)^4 + 0\left(\frac{c}{\beta h}\right)^6 \right\} . \qquad (2.24)$$

which conforms to that of Equation (2.36) in the following Section 2.3.2. Then

$$\Delta C_L = \left(\frac{2\pi}{\beta}\right)(\alpha + \Delta\alpha) - C_L ,$$

which by Equations (2.23) and (2.24) becomes

$$\Delta C_L = C_L \left\{ -\frac{\pi^2}{48}\left(\frac{c}{\beta h}\right)^2 + \frac{7\pi^4}{3072}\left(\frac{c}{\beta h}\right)^4 + 0\left(\frac{c}{\beta h}\right)^6 \right\} . \qquad (2.25)$$

Since C_m is zero in unconstrained flow, it follows from Equations (2.23) that

$$\Delta C_m = -C_m = C_L \left\{ \frac{\pi^2}{192}\left(\frac{c}{\beta h}\right)^2 - \frac{7\pi^4}{15360}\left(\frac{c}{\beta h}\right)^4 + 0\left(\frac{c}{\beta h}\right)^6 \right\} . \qquad (2.26)$$

An alternative and more practical form of Equation (2.24) is

$$\Delta\alpha = \frac{\pi c^2}{96\beta h^2}(C_L + 4C_m) - \frac{7\pi^3 c^4 C_L}{30720\beta^3 h^4} , \qquad (2.27)$$

and this should be used whenever C_m has been measured. In two-dimensional subsonic flow Equations (2.25) to (2.27) give the wall interference on a thin aerofoil with its mid-chord on the centre line of a closed tunnel as incremental corrections to the measured quantities α, C_L and C_m. If the aerofoil were displaced vertically, corresponding formulae could be derived from Reference 2.6 with neglect of $0(c/\beta h)^5$; these would include the effect of a non-uniform streamwise flow that is indicated by Equation (2.10).

2.2.3 Non-Rectangular Tunnels

There is no exact treatment of flat-plate aerofoils spanning closed tunnels of non-rectangular section. The mathematical difficulties involved in the case of a circular tunnel are well discussed and treated approximately by Vincenti and Graham (Ref. 2.7: 1946). Their assumption of uniform spanwise loading on a two-dimensional model is amply justified by experiment. Even with this simplification it only appears possible to obtain the interference upwash to order $(c/h)^2$ at the centre of the tunnel. To this approximation the first effect is that in a two-dimensional rectangular tunnel of height

$$h_e = 0.843 \times (\text{diameter of tunnel}) . \qquad (2.28)$$

A lower equivalent height would be expected, if it were possible to evaluate the average interference across the span. Nevertheless the result (2.28) should apply to pressure distributions at the centre section, which may be corrected by Equation (2.16).

For tunnels of octagonal section Batchelor[2.2] assumes that the flow in each plane normal to the span is two-dimensional, so that the interference has to be averaged across the span. His simple procedure leads to an equivalent height

$$h_e = h\left\{1 + \frac{b'h'}{b(h - h')}\right\}^{-\frac{1}{2}} , \qquad (2.29)$$

where $\frac{1}{2}b'$ and $\frac{1}{2}h'$ are the projections of each corner fillet on the horizontal and vertical walls respectively. Equation (2.29) must seriously underestimate h_e unless the fillets are fairly small. For balance measurements on a full-span model it may be safer to use, in place of Equations (2.28) and (2.29), an equivalent height C/b, where C is the cross-sectional area of the tunnel. Then respectively

$$\left.\begin{aligned} h_e &= 0.785 \times (\text{diameter of tunnel}) \\ h_e &= h - \tfrac{1}{2}b'h'/b \end{aligned}\right\} . \qquad (2.30)$$

2.3 WINGS OF FINITE THICKNESS IN CLOSED TUNNELS

2.3.1 Effect of One Wall

By way of introduction it is interesting to consider a thick aerofoil in the presence of one wall. Tomotika et al. (Ref. 2.8; 1951) investigate theoretically the forces acting on certain thick cambered aerofoils at incidence in a two-dimensional incompressible flow bounded by one plane wall which can be taken to represent the ground. The exact solution for the lift is derived as an intractable integral of an infinite series and is evaluated numerically. It can be said at once that corresponding exact solutions for flow in a straight channel are exceedingly laborious and that they defy numerical analysis if the fluid is compressible.

For positive incidences L/L_0, the ratio of lift with ground to the unconstrained lift, decreases at first from unity as c/d increases but later increases rapidly as the chord greatly exceeds the distance of the aerofoil from the ground. Then, by Figure 6 of Reference 2.8, both thickness and positive camber of the aerofoil can cause large reductions in L/L_0, although these reductions do not appear to exceed ½% for the values of c/d that normally occur in problems of wall interference corrections.

2.3.2 Goldstein's Theory

The general two-dimensional problem of a thick, cambered aerofoil at incidence in a low-speed closed tunnel has been solved by Goldstein (Ref. 2.9; 1942) as an algebraic power series in c/h. He first derives the transformation of the aerofoil into a circle and then considers the velocity-potential field at large distances from the aerofoil in a uniform free stream. Superposition of corresponding potential fields from the infinite system of images gives a first approximation to the non-uniform flow field generated by the walls of the tunnel. This flow is calculated in the neighbourhood of the aerofoil, and hence Goldstein evaluates a modified velocity distribution on the aerofoil by the theory described in the first paper of Reference 2.9. This provides a second approximation to the distant field of the aerofoil and hence to the non-uniform interference flow field from which the aerodynamic forces are obtained correct to the order $(c/h)^4$. The tedious algebra is restricted to cases in which the origin of the transformation close to the mid-chord point lies in the middle of the tunnel. Goldstein points out that, although simpler calculations such as those described in Section 2.2, are normally adequate for correcting lift and moment, his method allows us to decide whether this remains true in exceptional circumstances when c/h, thickness/chord ratio of the aerofoil, its camber or lift coefficient is larger than usual.

When all second-order terms in thickness, camber and incidence are neglected, the lift interference is independent of aerofoil thickness, just as the blockage corrections (Chapter V) are independent of aerofoil camber and incidence. Goldstein defines a correction to incidence to be the interference upwash angle at mid-chord. In the present notation Equations (76), (77) and (79) from the second paper of Reference 2.9 become

$$\Delta\alpha = \frac{\pi^2}{96}\left(\frac{c}{h}\right)^2 (2\alpha + D_2) + \frac{\pi^4}{92160}\left(\frac{c}{h}\right)^4 (-2\alpha + 20D_2 - 21D_4) , \qquad (2.31)$$

$$\Delta C_L = -\frac{\pi a_1 C_L}{96}\left(\frac{c}{h}\right)^2 + \frac{7\pi^3 a_1}{30720}\left(\frac{c}{h}\right)^4 \{3C_L + 2\pi(2\alpha - D_1 + D_2 + D_3)\} , \qquad (2.32)$$

and

$$\Delta C_m = -\tfrac{1}{4}\Delta C_L + \frac{7\pi^5}{61440}\left(\frac{c}{h}\right)^4 (2\alpha + D_2) \qquad (2.33)$$

respectively. Here a_1 is the two-dimensional lift slope and

$$D_n = \frac{4}{\pi}\int_0^{\pi} \frac{z_c}{c}\,\frac{\sin n\theta}{\sin\theta}\,d\theta , \qquad (2.34)$$

where z_c is the ordinate of the camber line of the aerofoil and θ is defined in Equation (2.11). Goldstein shows that

$$D_2 = \frac{4}{\pi}C_m + \frac{2}{a_1}C_L - 2\alpha + 0\left(\frac{c}{h}\right)^2 . \qquad (2.35)$$

Substitution of D_2 from Equation (2.35) and $a_1 = 2\pi$ in Equation (2.31) gives

$$\Delta\alpha = \frac{\pi}{96}\left(\frac{c}{h}\right)^2 (C_L + 4C_m) + 0\left(\frac{c}{h}\right)^4 \quad ;$$

therefore, to order $(c/h)^2$, Equations (2.[illegible]) to (2.27) for a flat plate aerofoil are not influenced by first-order effects of camber.

If the aerofoil is uncambered, i.e. $D_n = 0$, then with the aid of the relationship

$$(C_L + \Delta C_L) = a_1(\alpha + \Delta\alpha) = 2\pi(\alpha + \Delta\alpha)$$

Equations (2.31) to (2.33) reduce to

$$\left.\begin{aligned}\frac{\Delta\alpha}{C_L} &= \frac{\pi}{96}\left(\frac{c}{h}\right)^2 - \frac{41\pi^3}{92160}\left(\frac{c}{h}\right)^4\\ \frac{\Delta C_L}{C_L} &= -\frac{\pi^2}{48}\left(\frac{c}{h}\right)^2 + \frac{7\pi^4}{3072}\left(\frac{c}{h}\right)^4\\ \frac{\Delta C_m}{C_L} &= \frac{\pi^2}{192}\left(\frac{c}{h}\right)^2 - \frac{7\pi^4}{15360}\left(\frac{c}{h}\right)^4\end{aligned}\right\} . \tag{2.36}$$

These expressions are consistent with Equations (2.24) to (2.26).

For a symmetrical aerofoil it is straightforward to retain terms of second order in α , C_L and functions of the aerofoil profile

$$\left.\begin{aligned}C_0 &= \frac{2}{\pi}\int_0^\pi \frac{z_s/c}{\sin\theta}\,d\theta\\ C_n &= \frac{4}{\pi}\int_0^\pi \frac{z_s}{c}\,\frac{\cos n\theta}{\sin\theta}\,d\theta \ (n > 1)\end{aligned}\right\} , \tag{2.37}$$

where z_s is the ordinate of its upper surface. By Appendix 5 of the first paper of Reference 2.9 and Equations (69), (72) and (74) of the second paper with the appropriate theoretical lift slope $a_1 = 2\pi(1 + C_0)$, we have

$$\begin{aligned}\Delta\alpha = {} & \frac{\pi}{96}\left(\frac{c}{h}\right)^2\{2\pi\alpha(1 + C_2) + C_L C_1\} - \\ & - \frac{\pi^3}{92160}\left(\frac{c}{h}\right)^4\{2\pi\alpha(1 - 20C_0 - 9C_2 + 42C_4) + C_L(11C_1 + 31C_3)\} ,\end{aligned} \tag{2.38}$$

$$\begin{aligned}\Delta C_L = {} & -\frac{\pi^2}{96}\left(\frac{c}{h}\right)^2 C_L(2 + 14C_0 - 2C_1 - 5C_2) + \\ & + \frac{\pi^4}{92160}\left(\frac{c}{h}\right)^4\{2\pi\alpha(84 + 456C_0 - 120C_1 - 18C_2 + 120C_3) + \\ & + C_L(125 + 632C_0 - 70C_1 - 78C_2 - 14C_3 - 69C_4)\}\end{aligned} \tag{2.39}$$

and

$$\Delta C_m = -\tfrac{1}{4}\Delta C_L + \frac{\pi^2}{384}\left(\frac{c}{h}\right)^2\{2\pi\alpha(-8C_0 + 4C_2) + C_L(-3C_1 + 3C_3)\} +$$

$$+ \frac{\pi^4}{368640}\left(\frac{c}{h}\right)^4\{2\pi\alpha(42 + 212C_0 + 84C_1 + 20C_2 + 36C_4) +$$

$$+ C_L(156C_1 - 79C_3 - 35C_5)\} \quad . \qquad (2.40)$$

To determine the theoretical relationship between α and C_L, it is necessary to equate $(C_L + \Delta C_L)$ with $2\pi(1 + C_0)(\alpha + \Delta\alpha)$. Thus we substitute

$$2\pi\alpha = C_L\left[(1 - C_0)\frac{\pi^2}{96}\left(\frac{c}{h}\right)^2(4 + 10C_0 - 3C_2)\right] \qquad (2.41)$$

to give

$$\frac{\Delta\alpha}{C_L} = \frac{\pi}{96}\left(\frac{c}{h}\right)^2(1 - C_0 + C_1 + C_2) - \frac{\pi^3}{92160}\left(\frac{c}{h}\right)^4(41 + 79C_0 + 11C_1 + C_2 + 31C_3 + 42C_4) \ , \qquad (2.42)$$

$$\frac{\Delta C_L}{C_L} = -\frac{\pi^2}{96}\left(\frac{c}{h}\right)^2(2 + 14C_0 - 2C_1 - 5C_2) + \frac{\pi^4}{92160}\left(\frac{c}{h}\right)^4(210 + 1004C_0 - 190C_1 - 96C_2 + 106C_3 - 59C_4) \qquad (2.43)$$

and

$$\frac{\Delta C_m}{C_L} = \frac{\pi^2}{384}\left(\frac{c}{h}\right)^2(2 + 6C_0 - 5C_1 - C_2 + 3C_3) -$$

$$- \frac{\pi^4}{368640}\left(\frac{c}{h}\right)^4(168 + 514C_0 - 430C_1 + 44C_2 + 185C_3 - 105C_4 + 35C_5) \ . \qquad (2.44)$$

It is interesting to note that Equation (2.42) again reduces to

$$\Delta\alpha = \frac{\pi}{96}\left(\frac{c}{h}\right)^2(C_L + 4C_m) + 0\left(\frac{c}{h}\right)^4 \ ,$$

since, to first order in thickness, the theoretical centre of pressure occurs at a distance $\frac{1}{4}c(1 + C_0 - C_1 - C_2)$ behind the leading edge (Ref. 2.10).

Equations (2.42) to (2.44) have been evaluated for a 10-per-cent-thick RAE 102 aerofoil (Ref. 2.11). By Equations (27) of Reference 2.10, this aerofoil may be defined approximately by the coefficients

$$\left.\begin{array}{l} C_0 = 0.07728 \\ C_1 = 0.05343 \\ C_2 = -0.01512 \\ C_3 = 0.00089 \\ C_4 = 0.00065 \\ C_5 = 0 \end{array}\right\} , \qquad (2.45)$$

which lead to the curves of $2\pi\Delta\alpha/C_L$, $\Delta C_L/C_L$ and $\Delta C_m/C_L$ against $(c/h)^2$ in Figure 2.4. The terms in $(c/h)^4$ are seen to reduce the magnitude of each quantity and cannot safely be ignored unless $c \leqslant 0.3h$. The effect of thickness is especially important in the case of $\Delta C_L/C_L$ which is increased by 50% or more. Even for a 5-per-cent-thick aerofoil, $-\Delta C_L/C_L$ would be seriously underestimated by Equation (2.36) unless $c \leqslant 0.3h$.

Goldstein derives to order $(c/h)^4$ the residual corrections to the distribution of velocity on the aerofoil; his formulae in Equation (97) of Reference 2.9 can be of importance in special investigations, when the crude alternative, Δl in Equation (2.16), is unlikely to suffice. The problem of a thick aerofoil placed anywhere in the tunnel is solved to order $(c/h)^2$ in Reference 2.9, and the results are consistent with Equations (2.20) and (2.21) of Section 2.2. Unfortunately their usefulness is restricted by the rather slow convergence of the series in powers of c/h , when the aerofoil is far from the middle of the tunnel.

A method of conformal mapping has been applied by Moses (Ref. 2.12; 1949) to calculate the velocity distributions on an arbitrary aerofoil at incidence in a closed wind tunnel. The method provides a satisfactory numerical solution. If it were necessary to include terms of higher order than $(c/h)^4$, then it would appear to be more convenient to use Reference 2.12 than to extend the analysis of Reference 2.9. As an example Moses considers a 12-per-cent-thick aerofoil at $\alpha = 4^{\circ}$ and a ratio $c/h = 0.5$, which provides a severe test of the formulae (2.42) and (2.43). From the ordinates of the aerofoil in Table I of Reference 2.12, we obtain, by Reference 2.10,

$$\left.\begin{array}{l} C_0 = 0.090_5 \\ C_1 = 0.05\text{[illegible]} \\ C_2 = -0.0229 \\ C_3 = 0.0066_5 \\ C_4 = 0.0052_5 \end{array}\right\} \qquad (2.46)$$

and a theoretical value $(a_1)_T = 6.848$, which gives a free-stream $C_L = 6.848 \times 0.06981 = 0.478$ in agreement with the result in Reference 2.12. The value calculated by Moses for the aerofoil in the tunnel is $C_L = 0.537$, when $\alpha = 0.06981$ radians. When these values are corrected to free-stream conditions by Equations (2.42), (2.43) and (2.46), we have

$$\left.\begin{aligned} C_L + \Delta C_L &= 0.5922 \\ \alpha + \Delta\alpha &= 0.07340 \end{aligned}\right\}.$$

Hence $$a_1 = (C_L + \Delta C_L)/(\alpha + \Delta\alpha) = 6.842 \;,$$

which is virtually a perfect check. If $(c/h)^4$ is neglected in Equation (2.42) and (2.43), then the lift slope is over-corrected by nearly 3% to $a_1 = 6.65$: if, on the other hand, aerofoil thickness is ignored ($C_0 = 0$), then the corrected value $a_1 = 7.01$ is about 2½% too high.

2.3.3 Allowance for Compressibility

Solutions for the symmetrical compressible flow past aerofoils have yielded formulae for blockage corrections (Chapter V), but the difficult non-linear problem of a lifting aerofoil in a channel remains unsolved. Franke and Weinig (Ref. 2.13; 1939) use the transformed linearized differential Equation (2.4) and represent the aerofoil by its velocity-potential field at large distances

$$\Phi + i\Psi = i\lambda_1 \log \zeta - (\lambda_2 + i\lambda_3)\zeta^{-1} \;, \qquad (2.47)$$

where λ_1, λ_2 and λ_3 are real and $\zeta = X + iZ$. The accuracy of the resulting simple formulae is comparable with that of Reference 2.3.

Since there is no practicable alternative to the evaluation of the interference upwash by linearized subsonic theory, the recommended corrections are those of Equations (2.42) to (2.44) modified in accord with the remarks in Section 2.1. We first construct the solution for the equivalent incompressible flow of density ρ and velocity $\beta^{-2}U$ with boundary conditions set by the geometrical parameters listed below. The aerodynamic quantities so obtained can then be equated as follows.

Geometrical Parameters	*Aerodynamic Quantities*
Tunnel height $= \beta h$	Lift, Moment $= \beta^{-2}L, \beta^{-2}M$
Aerofoil chord $= c$	Force coefficients $= \beta^2 C_L, \beta^2 C_m$
Aerofoil incidence $= \beta\alpha$	Upwash velocity $= \beta^{-1}w$
Aerofoil thickness $= \beta t$	Upwash angle $= \beta\Delta\alpha$

where $h, t, C_L, C_m, \Delta\alpha$, etc. refer to the real compressible flow.

Thus

$$\left.\begin{aligned} \frac{\Delta\alpha}{C_L} = {} & \frac{\pi\beta}{96}\left(\frac{c}{\beta h}\right)^2 \{1 + \beta(-C_0 + C_1 + C_2)\} - \\ & - \frac{\pi^3\beta}{92160}\left(\frac{c}{\beta h}\right)^4 \{41 + \beta(79C_0 + 11C_1 + C_2 + 31C_3 + 42C_4)\} \end{aligned}\right\} \qquad (2.48)$$

$$\left.\begin{aligned}\frac{\Delta C_L}{C_L} &= -\frac{\pi^2}{96}\left(\frac{c}{\beta h}\right)^2\{2 + \beta(14C_0 - 2C_1 - 5C_2)\} + \\ &\quad + \frac{\pi^4}{92160}\left(\frac{c}{\beta h}\right)^4\{210 + \beta(1004C_0 - 190C_1 - 96C_2 + 105C_3 - 69C_4)\} \\ \frac{\Delta C_m}{C_L} &= \frac{\pi^2}{384}\left(\frac{c}{\beta h}\right)^2\{2 + \beta(6C_0 - 5C_1 - C_2 + 3C_3)\} - \\ &\quad - \frac{\pi^4}{368640}\left(\frac{c}{\beta h}\right)^4\{168 + \beta(514C_0 - 430C_1 + 44C_2 + 185C_3 - \\ &\qquad - 105C_4 + 35C_5)\}\end{aligned}\right\} \qquad (2.48)$$

where C_n is given by Equations (2.37) or may be identified with A_n in Equations (27) of Reference 2.10. In Figure 2.4 with abscissa relabelled $(c/\beta h)^2$ the appropriate curves will give $2\pi\Delta\alpha/(\beta C_L)$, $\Delta C_L/C_L$, $\Delta C_m/C_L$ for a typical symmetrical aerofoil of thickness $t = 0.1c/\beta$. The implicit assumption, that $a_1 = 2\pi(\beta^{-1} + C_0)$, must be recognized. In the absence of a more exact theory of two-dimensional wall interference there is some justification in that this lift slope will normally lie below the exact theoretical value and above the experimental one.

When Equations (2.16) and (2.17) will not suffice, the wall corrections for a thick cambered aerofoil should be obtained in two parts. If the measured lift coefficient is written as

$$C_L(\alpha) = C_L(0) + [C_L(\alpha) - C_L(0)] ,$$

then the contribution to interference from $C_L(0)$ is found by setting $\alpha = 0$ in Equations (2.31) to (2.33) as modified in accord with the above table. Thus

$$\left.\begin{aligned}\Delta\alpha &= \frac{\pi^2}{96}\left(\frac{c}{\beta h}\right)^2 D_2 + \frac{\pi^4}{92160}\left(\frac{c}{\beta h}\right)^4 (20D_2 - 21D_4) \\ \Delta C_L &= -\frac{\pi^2}{48}\left(\frac{c}{\beta h}\right)^2 C_L(0) + \frac{7\pi^4}{15360}\left(\frac{c}{\beta h}\right)^4 \left\{3C_L(0) + \frac{2\pi}{\beta}(-D_1 + D_2 + D_3)\right\} \\ \Delta C_m &= -\tfrac{1}{4}\Delta C_L + \frac{7\pi^5}{61440}\left(\frac{c}{\beta h}\right)^4 \frac{D_2}{\beta}\end{aligned}\right\} \qquad (2.49)$$

where D_n is given by Equation (2.34). To Equations (2.49) are added contributions from Equations (2.48) with the substitution $C_L = [C_L(\alpha) - C_L(0)]$. It may be necessary to reduce these corrections on account of the aerofoil boundary-layer; a simple semi-empirical procedure for this is discussed in Section 2.6.1.

2.4 AEROFOILS WITH HINGED FLAPS

Sections 2.2 and 2.3 have been concerned with lifting aerofoils without flaps; they apply to aerofoils with undeflected flaps, but an additional formula is needed for the residual correction ΔC_H to the hinge-moment coefficient. The interference on a thin symmetrical aerofoil with deflected trailing-edge flap spanning a closed two-dimensional tunnel has been obtained to order $(c/h)^4$ by Preston and Manwell (Ref. 2.14; 1941). Theoretical values of the non-dimensional derivatives of lift, quarter-chord pitching moment and hinge moment with respect to incidence α and flap setting ξ

$$a_1 = \partial C_L/\partial\alpha , \qquad a_2 = \partial C_L/\partial\xi ,$$

$$m_1 = \partial C_m/\partial\alpha , \qquad m_2 = \partial C_m/\partial\xi ,$$

$$b_1 = \partial C_H/\partial\alpha \quad \text{and} \quad b_2 = \partial C_H/\partial\xi$$

are given in the respective Equations (38), (39), (43a), (44a), (50) and (51) of Reference 2.14. The theory takes no account of finite thickness, and it is verified that the expressions for a_1 and m_1 are consistent with the full curves in Figure 2.3 for $\alpha = 0$. Ratios of the other derivatives to their free-stream values, $b_1/(b_1)_0$, $a_2/(a_2)_0$, $m_2/(m_2)_0$ and $b_2/(b_2)_0$ are plotted in Figure 2.5 as functions of $c/(\beta h)$ and $E = c_f/c$, where c_f is the chord of the flap. When $c = 0.5\beta h$ and $E = 0.3$, the inverted ratios are as follows.

Tunnel derivative	a_1	b_1	a_2	m_2	b_2
Correction factor	0.914	0.837	0.939	0.917	0.930

The correction factors to a_2, m_2 and b_2 decrease as E increases and are of the same order as that to a_1. The interference corrections to b_1 are comparatively large and much less dependent on E.

In conformity with Sections 2.2 and 2.3, we express the results of Reference 2.14 as theoretical incremental corrections to incidence and the aerodynamic coefficients. The corrected hinge moment on the undeflected flap is $\frac{1}{2}\rho U^2 c_f^2 (C_H + \Delta C_H)$ with

$$C_H + \Delta C_H = b_1\alpha + \Delta C_H = (b_1)_0(\alpha + \Delta\alpha) , \tag{2.50}$$

where b_1 and $(b_1)_0$ in Equation (50) of Reference 2.14 require the usual modification for compressibility, and $\Delta\alpha$ is defined in Equation (2.24) for a flat-plate aerofoil. Substituting

$$\alpha = \frac{\beta C_L}{2\pi}\left\{1 - \frac{\pi^2}{24}\left(\frac{c}{\beta h}\right)^2 + O\left(\frac{c}{\beta h}\right)^4\right\} \tag{2.51}$$

from Equation (2.23), we obtain

$$\frac{4E^2(\Delta C_H)}{C_L} = \frac{\pi}{288}\left(\frac{c}{\beta h}\right)^2 \{12(\pi - \theta_1)\cos\theta_1 + 9\sin\theta_1 + \sin 3\theta_1\} -$$

$$- \frac{7\pi^3}{921600}\left(\frac{c}{\beta h}\right)^4 \{-60(\pi - \theta_1) + 600(\pi - \theta_1)\cos\theta_1 + 520\sin\theta_1 -$$

$$- 20\sin 2\theta_1 + 25\sin 3\theta_1 - 5\sin 4\theta_1 + \sin 5\theta_1\} \, , \qquad (2.52)$$

where $E = c_f/c = \frac{1}{2}(1 + \cos\theta_1)$. In Figure 2.6(a) curves of $\Delta C_H/C_L$ against $c/\beta h$ are drawn for several fixed values of E. There is no reason to suppose that the effect of aerofoil thickness on these curves is any greater than on $\Delta C_m/C_L$ in Figure 2.4. However, the terms in $(c/\beta h)^6$ may become especially important in the case of $\Delta C_H/C_L$; it appears likely that for $c > 0.4\beta h$ these higher-order terms are more significant than thickness effect.

For the compressible flow past a thin aerofoil at zero incidence with deflected flap, we write

$$\left.\begin{aligned} C_L + \Delta C_L &= a_2\xi + \Delta C_L = (a_2)_0\xi + (a_1)_0\Delta\alpha \\ C_m + \Delta C_m &= m_2\xi + \Delta C_m = (m_2)_0\xi + (m_1)_0\Delta\alpha \\ C_H + \Delta C_H &= b_2\xi + \Delta C_H = (b_2)_0\xi + (b_1)_0\Delta\alpha \end{aligned}\right\} \, , \qquad (2.53)$$

where $(a_1)_0 = 2\pi/\beta$, $(m_1)_0 = 0$, $(b_1)_0$, $(a_2)_0$, $(m_2)_0$ and $(b_2)_0$ are β^{-1} times their values in Reference 2.14 for $M = 0$. The correction $\Delta\alpha$ to incidence is chosen from Equation (2.27), whence

$$\frac{2\pi\Delta\alpha}{\beta C_L} = \frac{\pi^2}{48}\left(\frac{c}{\beta h}\right)^2 \left\{1 + \frac{4m_2}{a_2}\right\} - \frac{7\pi^5}{15360}\left(\frac{c}{\beta h}\right)^4 \qquad (2.54)$$

By Equations (2.53) and (2.54)

$$\left.\begin{aligned} \frac{\Delta C_L}{C_L} &= \frac{1}{a_2}\{(a_2)_0 - a_2\} + \frac{2\pi\Delta\alpha}{\beta C_L} \, , \\ \frac{\Delta C_m}{C_L} &= \frac{1}{a_2}\{(m_2)_0 - m_2\} \\ \frac{\Delta C_H}{C_L} &= \frac{1}{a_2}\{(b_2)_0 - b_2\} + (b_1)_0\frac{\Delta\alpha}{C_L} \end{aligned}\right\} . \qquad (2.55)$$

These corrections are plotted as functions of $c/\beta h$ and E in Figures 2.6(b) and 2.7; $\Delta\alpha/C_L$ falls sharply as E decreases, and to order $(c/h)^2$ it tends to zero as $E \to 0$. To this order $\Delta C_L/C_L$ and $\Delta C_m/C_L$ are independent of E and $\Delta C_H/C_L$ is given by Equation (2.52); for large enough $c/\beta h$, however, all these corrections for a deflected flap are numerically larger than the corresponding values in Figures 2.4 and 2.5(a) for the lift interference due to aerofoil incidence.

In the case of a symmetrical aerofoil at incidence with deflected flap, $\Delta\alpha$ should first be evaluated directly from Equation (2.27). Then the residual corrections ΔC_L, ΔC_m and ΔC_H should be estimated both from Figures 2.4 and 2.6(a) and from Figures 2.6(b) and 2.7. Whenever these differ appreciably, a mean value should be weighted according to the contributions to C_L from aerofoil incidence and flap setting. Aerofoil camber should be treated separately as in Equation (2.49). Semi-empirical correction factors to ΔC_H will normally be required to take account of the boundary layer (Section 2.6.1).

The results in Figures 2.6 and 2.7 only apply to unbalanced two-dimensional flaps. To order $(c/h)^2$, Miss Lyon (Ref. 2.15; 1942) has extended the analysis to flaps with sealed shrouded balance on the supposition that the chordwise pressure distribution is that of an unbalanced flap of increased chord. The hinge moments are further modified, since the hinge is now set back from the nose of the flap. If required, the results for balanced flaps could be derived to order $(c/h)^4$ with the aid of Reference 2.14.

De Jager and van de Vooren (Ref. 2.16; 1961) have considered the non-linear problem of a hinged plate between parallel walls in incompressible flow. The forward portion of the plate lies along the centre of the channel, but the rear portion or flap is deflected through large angles ξ so that the vorticity may no longer be assumed to lie entirely in the central plane. Numerical solutions with six terms to represent the vorticity are obtained for a wide range of ξ when $E = 0.2, 0.25, 0.3$ and $c/h = 0.2, 0.3, 0.4$. Because of the non-linearity, the results cannot be presented as in Equations (2.53) to (2.55) with a correction $\Delta\alpha$, nor can any reliable allowance be made for compressibility. The corrections $\Delta C_L/C_L$ from Reference 2.16, reproduced in Figure 2.8, are therefore not comparable with those in Figure 2.7. The most striking feature of the results is the rapid decrease in the corrections as ξ increases above 30°; there is indeed a reversal in the sign of the correction near $\xi = 81^\circ, 70^\circ$ and 58° for $E = 0.2, 0.25$ and 0.3 respectively. With the aid of the graphical data in Figures 2, 3, 5 and 8 of Reference 2.16 it is simple to calculate the ratio

$$\frac{\Delta C_m}{C_L} = \frac{\Delta C_m}{C_m}\,\frac{(C_m)_0\{1 + (\Delta C_L/C_L)\}}{(C_L)_0\{1 + (\Delta C_m/C_m)\}}$$

to obtain the curves in Figure 2.9 for $E = 0.25$. In this case, since $(a_1)_0 = 0$, the results for small ξ are seen to be consistent with the corresponding Equation (2.55) and the curve in Figure 2.7 that is practically independent of E. For each value of c/h the correction is halved near $\xi = 40^\circ$ and vanishes near $\xi = 67^\circ$. It would be interesting to have experimental confirmation.

2.5 OPEN-JET TUNNELS

2.5.1 Boundary Conditions

At one time it was common practice to test two-dimensional aerofoils spanning an open jet; such models could be supported conveniently outside the stream. The problem of jet-boundary interference has to be considered from several points of view. The flow is far from two-dimensional, since the lift falls to zero where the aerofoil crosses the boundary; the wing therefore experiences a large downwash due to lift interference and also some lift-dependent drag which is absent in purely two-dimensional flow. In a flow of finite cross-section with free upper and lower boundaries, a finite lift on the aerofoil induces a finite downwash in the distant wake and a consequent interference at the model. Both of these considerations lead to large corrections $\Delta\alpha$ proportional to the chord of the aerofoil. Furthermore, the flow is accompanied by some distortion as well as the deflection of the jet, and these effects have never been incorporated in the boundary conditions. Therefore the interference corrections are not only larger but less soundly based than those for closed tunnels.

The boundary condition to be satisfied at the edge of a jet is that the pressure has a constant value equal to that of the surrounding air. Although linear velocity perturbations are hard to justify where the aerofoil emerges from the jet, this assumption is made; it then follows from Bernoulli's equation and the conditions of constant pressure, that $u = U$ over the entire boundary of the open jet. If it is further assumed that the jet is infinitely long and undistorted by the model, then on the boundary the velocity potential is $\Phi = Ux$ and the perturbations in velocity have zero tangential components.

2.3.2 Fully Open Jets

We first consider a lifting aerofoil spanning an incompressible jet of breadth $b(-\frac{1}{2}b \leqslant y < \frac{1}{2}b)$ and infinite height. Stüper (Ref. 2.17; 1932) has treated this problem as an application of the classical lifting-line theory to a wing of infinite span at incidence $\alpha(y) = (-1)^N$, where N is the integer nearest to y/b. This unit function of periodically changing sign is expanded as a Fourier series

$$\alpha(y) = \frac{4}{\pi}\sum_{n=0}^{\infty}\frac{(-1)^n}{2n+1}\cos\left\{\frac{\pi y}{b}(2n+1)\right\} . \tag{2.56}$$

Hence, for $|y| \leqslant \frac{1}{2}b$, the lift per unit span is $\rho U\Gamma(y)$ with

$$\Gamma(y) = \tfrac{1}{2}a_1 Uc\left[1 - \frac{4}{\pi}\sum_{n=0}^{\infty}\frac{(-1)^n}{2n+1+\lambda}\cos\left\{\frac{\pi y}{b}(2n+1)\right\}\right] , \tag{2.57}$$

where a_1 is the two-dimensional lift slope and

$$\lambda = 8b/(\pi a_1 c) = 4b/(\pi^2 c) \quad \text{when} \quad a_1 = 2\pi .$$

The total lift

$$\left.\begin{aligned} L &= \int_{-\frac{1}{2}b}^{\frac{1}{2}b} \rho U\Gamma(y)\, dy \\ &= L_0\left[1 - \frac{2}{\pi}\int_{-1}^{1}\sum_{n=0}^{\infty}\frac{(-1)^n}{2n+1+\lambda}\cos\{\tfrac{1}{2}\pi\eta(2n+1)\}\, d\eta\right] \end{aligned}\right\} \tag{2.58}$$

$$= L_0\left[1 - \frac{8}{\pi^2}\sum_{n=0}^{\infty}\frac{1}{(2n+1)(2n+1+\lambda)}\right]. \qquad (2.58)$$

This is easily summed when λ is a positive integer; in general

$$L = L_0\left[1 - \frac{4}{\pi^2\lambda}\left\{0.5772\cdots + 2\Psi(1+\lambda) - \Psi(1+\tfrac{1}{2}\lambda)\right\}\right], \qquad (2.59)$$

where $0.5772\cdots$ is Euler's constant and values of the psi function $\Psi(x)$ will be found in Reference 2.18. The boundary interference will depend on whether the experimental data are taken from measurements of total force or from pressure plotting at the centre section. In the former case L/L_0 is given by Equation (2.59) and is plotted in Figure 2.10(a) against $c/b = 4/(\pi^2\lambda)$; even for a small wing of chord $c = 0.1b$ the correction factor L_0/L is as high as 1.37.

Stüper[2.17] deals with open rectangular tunnels for which he obtains as a generalization of Equation (2.57),

$$\frac{\Gamma(y)}{\Gamma_0} = \frac{4}{\pi}\sum_{n=0}^{\infty}\frac{(-1)^n\cos\{(2n+1)\pi y/b\}}{(2n+1)\{1+F_n/\lambda\}}, \qquad (2.60)$$

where

$$\left.\begin{aligned} \Gamma_0 &= \tfrac{1}{2}a_1 Uc \\ F_n &= (2n+1)\coth\{(2n+1)\pi h/2b\} \end{aligned}\right\}.$$

He provides evidence from experimental pressure distributions for $h/b = \frac{1}{2}$ and 1 in support of the spanwise loadings predicted by Equation (2.60). Although there is less interference on the lift at the centre section than on the total lift, the curves of $\Gamma(0)/\Gamma_0$ against c/b in Figure 2.10(c) show that the correction factors for a wing of chord $0.1b$ are $\Gamma_0/\Gamma(0) = 1.18$, 1.20 and 1.35 for $h = \infty$, b and $\frac{1}{2}b$ respectively.

Another configuration that has received considerable attention is a rectangular wing spanning a circular open jet. In Reference 2.17 there appear to be errors on the left-hand sides of the final equations for the coefficients of the spanwise loading. Moreover, Squire (Ref. 2.19; 1939) points out that Stüper's form of solution misrepresents the mathematical singularity in downwash at the wing tips. Squire gives a more exact treatment of the lifting-line problem with a distribution of lift

$$\frac{\Gamma(y)}{\Gamma_0} = \frac{8\pi R}{a_1 c}\left[\frac{2}{\pi^2}\left\{2\log_e 2 - \left(1-\frac{y}{R}\right)\log_e\left(1-\frac{y}{R}\right) - \left(1+\frac{y}{R}\right)\log_e\left(1+\frac{y}{R}\right)\right\} - \right.$$

$$\left. - \sum_{n=0}^{\infty}\frac{b_n}{2n+2}\left\{1-\left(\frac{y}{R}\right)^{2n+2}\right\}\right]. \qquad (2.61)$$

where R is the radius of the jet. Equation (2.61) yields

$$\frac{L}{L_0} = \frac{8\pi R}{a_1 c}\left[\frac{2}{\pi^2} - \sum_{n=0}^{\infty} \frac{b_n}{2n+3}\right] , \tag{2.62}$$

where $b_n (n = 0, 1$ and $2)$ are obtained approximately by collocation. The numerical results are plotted in Figure 2.11(a) and are not greatly different from the values of $\Gamma(0)/\Gamma_0$ and L/L_0 for a square jet.

As a consequence of the non-uniform spanwise loading across the jet, the wing experiences lift-dependent drag which is absent in purely two-dimensional flow. Quite small errors in the spanwise loading are significant in the evaluation of this drag; it is not surprising, therefore, that Stüper's values are appreciably greater than those from Reference 2.19 which are used in Figure 2.11(b). Here the corrections to incidence and drag are given by

$$\frac{\Delta\alpha}{C_L} = -\frac{1}{a_1}\left(\frac{L_0}{L} - 1\right) \tag{2.63}$$

and by $\Delta C_D/C_L^2$, where ΔC_D is equal and of opposite sign to the theoretical drag coefficient of Reference 2.19 with $a_1 = 2\pi$; it is easily shown that the results are not sensitive to the choice of a_1.

The treatment by lifting-line theory ignores the effects of induced curvature of flow, which will be of the same order as the corrections for closed tunnels in Figure 2.4. By comparison with the positive values of $\Delta\alpha/C_L$ for closed tunnels, the quantity defined by Equation (2.63) in conjunction with either Figure 2.10(a) or Figure 2.11(a) is negative and of much higher magnitude. The likely accuracy of the interference corrections for open tunnels does not warrant allowance for induced curvature. Similarly there is little justification for applying lifting-surface theory, although Reference 2.20 (Rethorst, 1958) could be adapted for the purpose.

2.5.3 Two-Dimensional Tests

It is now supposed that the breadth of the tunnel is very large, or that with the aid of solid side-walls or end plates a two-dimensional flow is preserved. On the simple argument, that the interference downwash at the wing is half that in the distant wake, we have

$$\Delta\alpha = \frac{1}{2}\frac{w_{+\infty}}{U} = -\frac{1}{4}\frac{S}{C}C_L , \tag{2.64}$$

since from considerations of momentum the lift force $\frac{1}{2}\rho U^2 S C_L$ balances the rate of growth of downward momentum $-\rho U C w_{+\infty}$. An exact solution of the incompressible problem by Sasaki (Ref.2.21; 1928), quoted in Glauert's monograph, has given numerical values of L/L_0 for a flat plate placed midway between the boundaries of the jet at an incidence $\alpha = 10^\circ$. These are plotted against c/h in Figure 2.10(b), and for $c = 0.2h$ the correction factor L_0/L has reached 1.34. From consideration of Equation (2.64) alone we would have

$$\frac{L_0}{L} = 1 - \frac{2\pi(\Delta\alpha)}{C_L} \doteq 1 + \frac{\pi S}{2C} = 1 + \frac{\pi c}{2h} \doteq 1.31 \; , \qquad (2.65)$$

which is a fair approximation to the accurate theory.

We now suppose that the lifting aerofoil is of small chord and can be replaced by a single vortex at an arbitrary position between the upper and lower boundaries of the jet. Corresponding to Equations (2.6) and (2.10) for a closed tunnel, the induced upward and streamwise velocities for a tunnel with open roof and floor are

$$w_i = \frac{\pi K(x - \bar{x})}{8\beta h^2}\left(\frac{4}{3} + \cot^2\frac{\pi d}{h}\right) \qquad (2.66)$$

and

$$u_i = \frac{K}{4\beta h}\cot\frac{\pi d}{h} = \frac{UcC_L}{8\beta h}\cot\frac{\pi d}{h} \; . \qquad (2.67)$$

Equations (2.66) and (2.67) arise from an image system comprising a column of vortices, each of the same sense; these contribute a finite upwash $w_{-\infty}/U = + \frac{1}{4}cC_L/h$ upstream of the model and an equal and opposite downwash $w_{+\infty}/U = - \frac{1}{4}cC_L/h$ in the distant wake. In order to eliminate the undesired upstream upwash, a uniform downwash can be added to the solution in Equation (2.66) without violating the condition that the tangential velocity is unperturbed at the boundary of the jet. Hence, by Equations (2.7) and (2.8), the induced upwash angle in the neighbourhood of the model is

$$\frac{w_i}{U} = -\frac{1}{4}\frac{c}{h}C_L - \frac{\pi c^2}{16\beta h^2}\left\{\left(\frac{x}{c} - \frac{1}{4}\right)C_L + C_m\right\}\left(\frac{4}{3} + \cot^2\frac{\pi d}{h}\right) \; . \qquad (2.68)$$

Glauert has shown that this result with $\beta = 1$ and $d = 0$ is in very good agreement with the exact solution of Reference 2.21.

Vandrey (Ref. 2.22; 1942) has considered a small model in a two-dimensional open tunnel with a closed entrance nozzle, and he gives a physical discussion and mathematical solution of this mixed-boundary problem. The model is represented by a combined vortex and source, and the interference velocities are expressed in terms of lift and drag. The lift interference of Reference 2.22 can be regarded as a special case of the work of Gardner and Diesendruck in the second part of Reference 2.23 (1950). However far downstream the model may be, the closed entrance nozzle takes care of the upstream flow condition. One configuration of tunnel in Reference 2.23 has a closed entrance nozzle and a single lower exit lip, i.e. a roofless collector; for a lifting model midway between the roof and floor, the induced velocities at the model are

$$\left.\begin{aligned} u_i &= -\frac{K}{4\beta h}\, e^{\pi x_0/\beta h}\, F \\ w_i &= -\frac{K}{4h}\left[e^{\pi l/\beta h}\, F - 2(1 + e^{2\pi x_0/\beta h})^{-1}\right] \end{aligned}\right\} \; , \qquad (2.69)$$

where

$$F = \frac{(e^{2\pi l/\beta h} + e^{2\pi x_0/\beta h})^{\frac{1}{2}} + e^{\pi l/\beta h}}{e^{2\pi l/\beta h} + e^{2\pi x_0/\beta h}} ,$$

x_0 and l are the respective distances of the model and the exit lip downstream of the entrance nozzle. As $l \to \infty$, $u_i \to 0$ and

$$w_i \to -\frac{K}{2h}(1 + e^{-2\pi x_0/\beta h})^{-1} , \tag{2.70}$$

which is consistent with Reference 2.22.

Of greater practical interest is the two-dimensional closed-open-closed tunnel with an open working section of length l and a closed entrance nozzle and collector. In Reference 2.23 the interference velocity is derived for an arbitrarily placed vortex in such a tunnel. The streamwise component u_i vanishes when the vortex is in the horizontal plane of symmetry, and

$$w_i = -\frac{K}{2h}\left[G_0 + \frac{\pi(x - \bar{x})}{\beta h} G_1 + O(x - \bar{x})^2\right] , \tag{2.71}$$

where

$$G_0 = \frac{(e^{2\pi l/\beta h} - 1)e^{2\pi x_0/\beta h}}{(1 + e^{2\pi x_0/\beta h})(e^{2\pi l/\beta h} + e^{2\pi x_0/\beta h})} , \tag{2.72}$$

$$G_1 = -\frac{1}{6} + \frac{(e^{2\pi l/\beta h} - 1)e^{2\pi x_0/\beta h}}{(1 + e^{2\pi x_0/\beta h})^2(e^{2\pi l/\beta h} + e^{2\pi x_0/\beta h})} \times$$

$$\times \{e^{2\pi l/\beta h}(1 + \tfrac{1}{2}e^{2\pi x_0/\beta h}) - e^{2\pi x_0/\beta h}(\tfrac{1}{2} + e^{2\pi x_0/\beta h})\} \tag{2.73}$$

and $(x - \bar{x})$ denotes the distance downstream of the vortex. We substitute

$$\left.\begin{aligned} K &= \tfrac{1}{2}UcC_L \\ x - \bar{x} &= \tfrac{1}{4}c + cC_m/C_L \end{aligned}\right\}$$

to obtain the upwash angle at mid-chord

$$\Delta\alpha = -\frac{cC_L}{4h}\left[G_0 + \frac{\pi c}{\beta h}\left(\frac{1}{4} + \frac{C_m}{C_L}\right)G_1\right] . \tag{2.74}$$

Then the residual corrections to lift and moment are given by

$$\left.\begin{aligned} \frac{\Delta C_L}{C_L} &= -\frac{\pi c}{2\beta U}\frac{\partial w_i}{\partial x} = \frac{\pi^2 G_1}{8}\left(\frac{c}{\beta h}\right)^2 \\ \frac{\Delta C_m}{C_L} &= \frac{\pi c}{8\beta U}\frac{\partial w_i}{\partial x} = -\frac{\pi^2 G_1}{32}\left(\frac{c}{\beta h}\right)^2 \end{aligned}\right\} , \tag{2.75}$$

where G_1 is defined in Equation (2.73). If $x_0 \to \pm\infty$, $G_0 \to 0$ and $G_1 \to -1/6$ and we have the results for a closed tunnel in Equations (2.16) and (2.17). If $l \to \infty$ and then $x_0 \to \infty$, $G_0 \to 1$ and $G_1 \to +1/3$, so that for an open tunnel the residual corrections in Equation (2.75) are of twice the magnitude and of the opposite signs. The functions G_0 and G_1 are plotted in Figure 2.12. In a typical case $l = 1.5\beta h$, $x_0 = 0.5\beta h$, $G_0 = 0.96$ and $G_1 = 0.33$; such a closed-open-closed tunnel has interference characteristics very similar to those of a completely free jet.

2.5.4 Spillage Behind the Model

In the first part of Reference 2.23, Katzoff remarks that considerable uncertainty exists with regard to conditions at the exit and the mathematical equivalent of these conditions. Accordingly, certain compromises are justified when idealized downstream conditions are used in a determination of boundary interference. In the example $l = 1.5\beta h$, $x_0 = 0.5\beta h$ quoted above, it is found from integration of the vertical component of velocity at either free surface, that the downward displacement of the jet at the collector is $1.20\beta K/U = 0.60\beta c C_L$. The physical implications of this have been ignored; we may suppose, however, that the errors in the interference as given in Equations (2.74) and (2.75) would become serious, were the downward displacement of the jet to exceed $0.1\beta h$. Thus tests on an aerofoil of chord $c = 0.2\beta h$ would need to be restricted to incidences below 8°.

Katzoff also points out that the velocities at the two free boundaries need not be equal. If the space below the lower boundary is sealed off, the pressure at this free surface will adjust itself so that the jet attaches smoothly at the lower lip of the collector. By modifying the boundary conditions so that there are horizontal perturbation velocities $+u'$ on the upper free boundary and $-u'$ on the lower one, increments to the interference velocities are obtained in Reference 2.23. The downward components of induced velocity along the central axis and the free boundaries are given by simple functions of elliptic integrals. In the numerical example with $l = 1.5\beta h$ and $x_0 = 0.5\beta h$, the incremental upward displacement of the jet is $3.89\beta^2 u'h/U$; the original downward displacement $1.20\beta K/U$ is exactly cancelled if $u' = 0.31K/(\beta h)$. Now if the interference near the model is expressed in the form of Equation (2.71), the increment due to the unequal velocities at the free boundaries is

$$
\begin{aligned}
w_i &= 1.44\beta u' + 1.98u'(x - x_0)/h \\
&= \{0.45 + 0.61(x - x_0)/\beta h\}K/h \quad . \qquad (2.76)
\end{aligned}
$$

In other words, the increments to $G_0 = 0.96$ and $G_1 = 0.33$ are -0.90 and -0.39 respectively. This demonstrates theoretically that lift interference may be nearly eliminated if spillage at the collector is prevented by enclosing the space into which the spillage would normally occur.

On account of the large and unreliable interference corrections the use of a completely open tunnel for accurate testing of two-dimensional models is not recommended. The likely inaccuracies in the corrections predicted by Figures 2.10 and 2.11 set too low a limit on the chord of the model. If, however, two-dimensional flow is preserved by means of solid side walls or large end plates, then the chief uncertainty is the condition at the collector downstream of the jet. The linearized theoretical results in Equations (2.74) and (2.75) with Figure 2.12 ignore any effect of the jet deflection at the collector, though Reference 2.23 permits the evaluation of the vertical displacement of the jet. A condition that this should not exceed 0.1h, say, might restrict the tests to low incidences. Finally, there is the theoretical merit of a two-dimensional closed-open-closed tunnel with straight unflared collector and with self-adjusting unequal pressures at the free surfaces to prevent spillage.

2.6 EXPERIMENTAL CONSIDERATIONS

2.6.1 Viscous Effects

Unless there are extensive regions of separated flow, the theoretical interference corrections to lift and pitching moment can easily be modified to take some account of viscous effects; the correction to incidence would remain unchanged. From the semi-empirical reasoning in Section 4.2 of Reference 2.24 (Bryant and Garner, 1951), the incremental lift and pitching moment due to streamline curvature are influenced by boundary layers in roughly the same ratio as the lift slope. Viscous effects on two-dimensional wall interference can therefore be incorporated by applying to $\Delta C_L/C_L$ and $\Delta C_m/C_L$ the approximate correction factor

$$\mu_a = \frac{1}{(a_1)_T}\{\text{Corrected experimental } \partial C_L/\partial\alpha\} , \qquad (2.77)$$

where $(a_1)_T = 2\pi(\beta^{-1} + C_0)$ with $C_0 = 0$ unless aerofoil thickness has been taken into account (Section 2.3). The author (Ref. 2.25; 1957) has shown that this factor will become important at low Reynolds numbers, especially if the trailing-edge angle is large.

In the case of hinge moments, however, viscous effects will always be important and cause considerable uncertainty in the residual corrections $\Delta C_H/C_L$, as is discussed in detail in Reference 2.26 (1950). There is limited evidence that the hinge moment due to induced curvature of flow is influenced by boundary layers in the same ratio as the derivative b_1. It is advisable therefore to apply to $\Delta C_H/C_L$ the correction factor

$$\mu_b = \frac{1}{(b_1)_T}\{\text{Corrected experimental } \partial C_H/\partial\alpha\} , \qquad (2.78)$$

where, with $\cos\theta_1 = 2E - 1$,

$$4\beta E^2(b_1)_T = -2(\pi - \theta_1)(1 - 2\cos\theta_1) + 4\sin\theta_1 - \sin 2\theta_1 .$$

This factor may well reduce $\Delta C_H/C_L$ to less than one half of its value in Figure 2.6.

As discussed in Section 2.1, Mendelsohn and Polhamus[2.1] have shown experimentally that side-wall boundary layers can be ignored in problems of two-dimensional interference correction. Further evidence to this effect is given by Vincenti and Graham in Figures 6 and 7 of Reference 2.7. However, Barbieux (Ref. 2.27; 1955) has suggested that a reduced height of tunnel should be taken to allow for the displacement thickness of boundary layers on the roof and floor; such a correction would only become important if the ratio c/h were unusually large.

2.6.2 Closed Tunnels

Barbieux[2.27] has provided important experimental data on wall corrections in incompressible flow. An aerofoil (p.137 of Reference 2.27) was pressure plotted in a two-dimensional closed tunnel whose height was varied systematically in the range $c \leqslant h < 3c$. He applied an original theory of interference correction, which is described in Chapter I of the second part of Reference 2.27. This differs from Goldstein's theory in that the model is represented more simply by the combination of a streamwise doublet at its centroid, a finite vortex at its aerodynamic centre and a transverse doublet corresponding to the pitching moment at zero lift, each of which is assumed to lie midway between the walls of the tunnel. The resulting formulae, given as power series up to $(c/h)^6$, are summarized in Tables IX to XII of Reference 2.27. The lift interference is expressed as an incremental correction to incidence which is chosen such that there is a residual correction to pitching moment but not to lift. By following the sequence of Figures 62, 70, 76 and 79 (legend in Figure 82), it can be seen that Barbieux's results collapse on to a unique lift curve against incidence within about $\pm 2\%$; his fully corrected experimental pitching-moment curve in Figure 80 shows some small systematic residual effect of c/h . The results are remarkably good in view of the extensive range of c/h .

Nevertheless, the formulation of Goldstein's theory in Section 2.3 is preferable, since this involves a rigorous treatment of the first-order effects of aerofoil profile and a rigorous representation of the interference flow field to the order $(c/h)^4$. The resulting corrections in Equations (2.48) will now be considered in the light of viscous effects (Section 2.6.1) and an experimental investigation of Knechtel (Ref. 2.28; 1953) of two-dimensional wall interference in subsonic compressible flow on an NACA 4412 aerofoil. By varying the effective height of a closed tunnel, four ratios c/h in the range $0.119 \leqslant c/h \leqslant 0.595$ were obtained without change of Reynolds number. The two highest values $c/h = 0.357$ and 0.595 were obtained by using respectively two and four image aerofoils so as to simulate tunnels of 1/3 and 1/5 the true height. Tests were also carried out on the same model in a large two-dimensional open tunnel with $c/h = 0.026$ and negligible wall interference. The main conclusion from Figures 2(a) and 2(b) of Reference 2.28 is that wall corrections by the method of Allen and Vincenti[2.3] give satisfactory comparisons provided that $c < 0.15h$; for larger values of c/h , wall interference becomes progressively greater and results corrected by this method become increasingly questionable. The evidence on lift coefficient at $\alpha = 4^\circ$ is reproduced in Figures 2.13(a) and 2.13(b) for Mach numbers in the range $0.3 \leqslant M \leqslant 0.8$.

We now suppose that accurate blockage corrections and approximate lift interference from Equations (2.16) and (2.17)

$$\left.\begin{aligned} \Delta\alpha &= \frac{\pi c^2}{96\beta h^2}(C_L + 4C_m) \\ \Delta C_L &= -\frac{\pi^2}{48}\left(\frac{c}{\beta h}\right)^2 C_L \end{aligned}\right\} \qquad (2.79)$$

have been applied in Figure 2.13(b). It will be seen that the curve for $c/h = 0.595$ lies roughly 7% below the others. Equations (2.48) with the viscous correction factor μ_a from Equation (2.77) give more comprehensive corrections than Equation (2.79).

To estimate the effect of aerofoil thickness, we use the values of C_n from Equation (2.45) with a generalizing factor 10t/c to obtain the numerical formulae

$$\left.\begin{aligned} \Delta\alpha &= \frac{\pi c^2 C_L}{96\beta h^2}\left\{1 - 0.3897\frac{\beta t}{c}\right\} - \frac{\pi^3 c^4 C_L}{92160\beta^3 h^4}\left\{41 + 67.33\frac{\beta t}{c}\right\} \\ \Delta C_L &= \mu_a C_L\left[-\frac{\pi^2}{48}\left(\frac{c}{\beta h}\right)^2\left\{1 + 5.253\frac{\beta t}{c}\right\} + \frac{\pi^4}{92160}\left(\frac{c}{\beta h}\right)^4\left\{210 + 689.4\frac{\beta t}{c}\right\}\right] \end{aligned}\right\} . \quad (2.80)$$

We have seen in Section 2.3 that to order $(c/h)^2$ Equations (2.79) and (2.80) for $\Delta\alpha$ are identical, and we shall regard the term in $(c/h)^4$ in Equation (2.80) as an increment to the correction $\Delta\alpha$ given in Equation (2.79). This increment must be converted to an equivalent lift coefficient by means of the factor $-a_1$, since we wish to compare results at a fixed incidence $\alpha = 4^o$. Thus we apply as a further correction to C_L, as given in Figure 2.13(b), the increment

$$\begin{aligned} (\Delta C_L)' = {} & \frac{a_1\pi^3 c^4 C_L}{92160\beta^3 h^4}\left\{41 + 67.33\frac{\beta t}{c}\right\} + (1 - \mu_a)\frac{\pi^2}{48}\left(\frac{c}{\beta h}\right)^2 C_L + \\ & + \mu_a C_L\left[-\frac{\pi^2}{48}\left(\frac{c}{\beta h}\right)^2\left\{5.253\frac{\beta t}{c}\right\} + \frac{\pi^4}{92160}\left(\frac{c}{\beta h}\right)^4\left\{210 + 689.4\frac{\beta t}{c}\right\}\right], \quad (2.81) \end{aligned}$$

where

$$\mu_a = \frac{a_1}{2\pi(\beta^{-1} + C_0)} = \frac{\beta a_1}{2\pi}\left\{1 + 0.773\frac{\beta t}{c}\right\}^{-1}$$

and a_1 is estimated from experiment.

The four terms of Equation (2.81) may be described as

(i) the equivalent of the $(c/h)^4$ term in $\Delta\alpha$
(ii) the viscous correction to ΔC_L in Equation (2.79)
(iii) the thickness correction of order $(c/h)^2$
(iv) the $(c/h)^4$ term in ΔC_L in Equation (2.80) .

For the thickness to chord ratio $t/c = 0.12$ the correction factor $1 + (\Delta C_L)'/C_L$ has been evaluated with $c/h = 0.119, 0.156, 0.357, 0.595$ and $M = 0.30, 0.45, 0.60, 0.70, 0.80$; typical results are given in the following table, where the separate contributions (i) to (iv) often tend to cancel.

$\frac{c}{h}$	M	μ_a	Contributions to $(\Delta C_L)'/C_L$				$1 + \frac{(\Delta C_L)'}{C_L}$
			(i)	(ii)	(iii)	(iv)	
0.156	0.60	0.827	0.000	0.001	− 0.003	0.000	0.998
0.357	0.30	0.840	0.002	0.005	− 0.015	0.005	0.997
0.357	0.60	0.827	0.004	0.007	− 0.017	0.010	1.004
0.357	0.80	0.413	0.005	0.043	− 0.011	0.014	1.051
0.595	0.30	0.840	0.014	0.013	− 0.040	0.039	1.026
0.595	0.60	0.827	0.027	0.020	− 0.047	0.074	1.074
0.595	0.80	0.413	0.041	0.119	− 0.032	0.110	1.238

The results so corrected are plotted in Figure 2.13(c), where, for the four values of c/h and Mach numbers in the range $0.3 < M < 0.7$, the discrepancies appear to be random and never exceed ± 2%. Although the results for the interference-free case $c/h = 0.026$ are up to 4% higher, this discrepancy can be attributed to effects of extraneous flow in the large open-jet tunnel with side-walls installed[2.28].

It may be inferred from Figure 2.13 that effects of shock-induced separation on the NACA 4412 aerofoil at $\alpha = 4^0$ are felt at Mach numbers above 0.6. The theory of wall interference is based on the velocity-potential field at large distances from the aerofoil where the linearized equations continue to give a good approximation to the flow, and so to $\Delta\alpha$. Although the residual corrections ΔC_L and ΔC_m are less certain, the evaluation of wall interference remains justified until M approaches 0.8.

There can be general confidence in methods of applying two-dimensional interference corrections for tests in subsonic closed rectangular tunnels. The method of Reference 2.3 will normally be adequate for correcting lift and pitching moment; Equations (2.79) to (2.81) indicate some of the inaccuracies in such an approximation. When these are too large, Goldstein's theory[2.9], as formulated in Section 2.3, is recommended.

2.6.3 Open-Jet Tunnels

An experimental investigation by Adamson (Ref. 2.29; 1941) includes tests of two rectangular wings of different chord spanning an open-jet circular tunnel. The measurements of lift and drag have been corrected according to Squire's theory[2.19] as given here in Figure 2.11(b). These corrections are too small in magnitude on account of the approximate lifting-line theory. It is found that the corrected two-dimensional lift slopes a_1 from Figure 1 of Reference 2.29 are rather lower than would be predicted by Equation (22) of Reference 2.25. The following table shows that the inaccuracy in lifting-line theory is of the correct order of magnitude and sign to account for the discrepancies in a_1.

Aerofoil	$\frac{2R}{c}$	*Reynolds number*	*Value of* a_1		*Estimated inaccuracy*	
			Ref. 2.25	Ref. 2.29	a_1 (Ref. 2.29)	*l.-l.* theory
RAF 34	7.5	0.50×10^6	5.05	4.95	− 2%	+ 4%
RAF 48	5.0	0.75×10^6	5.29	4.88	− 8%	+ 7%

Nevertheless it would be unwise to expect a result to better accuracy than 5% from such experiments, whatever care were taken.

REFERENCES

2.1 Mendelsohn, R.A.
Polhamus, J.P. — *Effect of the Tunnel-Wall Boundary Layer on Test Results of a Wing Protruding from a Tunnel Wall.* NACA Tech. Note 1244, 1947.

2.2 Batchelor, G.K. — *Interference on Wings, Bodies and Airscrews in a Closed Tunnel of Octagonal Section.* Report ACA-5 (Australia), 1944.

2.3 Allen, H.J.
Vincenti, W.G. — *Wall Interference in a Two-Dimensional-Flow Wind Tunnel, with Consideration of the Effect of Compressibility.* NACA Report 782, 1944.

2.4 Tomotika, S. — *The Lift of a Flat Plate Placed in a Stream between Two Parallel Walls and Some Allied Problems.* Aero. Res. Inst. (Tokyo) Report 101, 1934.

2.5 Tomotika, S. — *The Moment of the Fluid Pressures Acting on a Flat Plate in a Stream between Two Parallel Walls and Some Allied Problems.* Aero. Res. Inst. (Tokyo) Report 170, 1938.

2.6 Havelock, T.H. — *The Lift and Moment on a Flat Plate in a Stream of Finite Width.* Proc. Roy. Soc., Series A, Vol.166, 1938, pp.178-196.

2.7 Vincenti, W.G.
Graham, D.J. — *The Effect of Wall Interference upon the Aerodynamic Characteristics of an Airfoil Spanning a Closed-Throat Circular Wind-Tunnel.* NACA Report 849, 1946.

2.8 Tomotika, S.
et al. — *The Forces Acting on an Aerofoil of Approximate Joukowski Type in a Stream Bounded by a Plane Wall.* Quart. J. Mech. appl. Math., Vol.4, 1951, pp.289-307.

2.9 Goldstein, S. *Two-Dimensional Wind-Tunnel Interference.* ARC R & M 1902, 1942.

2.10 Garner, H.C. *Simple Evaluation of the Theoretical Lift Slope and Aerodynamic Centre of Symmetrical Aerofoils.* ARC R & M 2847, 1951.

2.11 Pankhurst, R.C., Squire, H.B. *Calculated Pressure Distributions for the RAE 100 to 104 Aerofoil Sections.* ARC CP 80, 1950.

2.12 Moses, H.E. *Velocity Distributions on Arbitrary Airfoils in Closed Tunnels by Conformal Mapping.* NACA Tech. Note 1899, 1949.

2.13 Franke, A., Weinig, F. *Die Korrektur der Anströmgeschwindigkeit und des Anströmwinkels in einem Hochgeschwindigkeitskanal mit geschlossener Meßstrecke infolge der Verdrängungsströmung in Tragflügelmodellen.* Deutsche Luftfahrtforschung Forschungsbericht 1171, 1939. (Translated as MAP R & T 259. ARC Report 10,268.)

2.14 Preston, J.H., Manwell, A.R. *Calculation of the Interference on a Thin Symmetrical Aerofoil with Hinged Flap Spanning a Closed Wind-Tunnel.* ARC R & M 2465, 1941.

2.15 Lyon, H.M. *An Approximate Method of Calculating the Effect of the Interference of a Closed Tunnel on Hinge Moments of Control Surfaces.* ARC Report 5803, 1942.

2.16 de Jager, E.M., van de Vooren, A.I. *Tunnel-Wall Corrections for a Wing-Flap System between Two Parallel Walls.* NLR (Netherlands) Report W.7, 1961.

2.17 Stüper, J. *Der durch einen Freistrahl hindurchgesteckte Tragflügel.* Ing. Arch. Vol.3, 1932, pp.338-355. (Translated as NACA Tech. Memo.723.)

2.18 Davis, H.T. *Tables of the Higher Mathematical Functions.* Volume I. The Principal Press Inc., Indiana, USA. 1933.

2.19 Squire, H.B. *The Lift and Drag of a Rectangular Wing Spanning a Free Jet of Circular Section.* Phil. Mag., Vol.27, 1939, pp.229-239.

2.20 Rethorst, S. *Aerodynamics of Non-Uniform Flows as Related to an Airfoil Extending through a Circular Jet.* J. aero. Sci., Vol.25, 1958, pp.11-28.

2.21 Sasaki, T. *On the Effect of the Wall of a Wind Tunnel upon the Lift Coefficient of a Model.* Aero. Res. Inst. (Tokyo) Report 46, 1928.

2.22 Vandrey, F. *Der Düseneinfluss auf die Windkanalkorrekturen bei ebener Strömung.* Jahrbuch der Deutschen Luftfahrtforschung, 1942, pp. 1786-1793.

2.23 Katzoff, S. et al. *Linear Theory of Boundary Effects in Open Wind Tunnels with Finite Jet Lengths.* NACA Report 976, 1950.

2.24 Bryant, L.W.; Garner, H.C. *Control Testing in Wind Tunnels.* ARC R & M 2881, 1950.

2.25 Garner, H.C. *Charts for Low-Speed Characteristics of Two-Dimensional Trailing-Edge Flaps.* ARC R & M 3174, 1957.

2.26 Garner, H.C. *Note on Aerodynamic Camber.* ARC R & M 2820, 1950.

2.27 Barbieux, J. *Contribution a l'Étude de l'Effet de Paroi en Écoulement Plan Incompressible.* Publ. Sci. Tech. Min. Air France 304, 1955.

2.28 Knechtel, E.D. *Experimental Investigation of Two-Dimensional Tunnel-Wall Interference at High Subsonic Speeds.* NACA Tech. Note 3087, 1953.

2.29 Adamson, J.E. *An Experimental Investigation of Wind-Tunnel Interference in the RAE 5 ft Open-Jet Circular Tunnel.* ARC R & M 1897, 1941.

ADDITIONAL REFERENCES FOR CHAPTER II

Imai, I. *On the Deformation of Free Boundary Due to Line Vortices.* Aero. Res. Inst. (Tokyo) Report 183, 1939.

de Jager, E.M.; van Spiegel, E. *Calculated Tunnel-Wall Corrections for Two-Dimensional High-Lift Wings.* NLL (Netherlands) Report MP.181, 1959.

Katzoff, S. et al. *Interference Method for Obtaining the Potential Flow Past an Arbitrary Cascade of Airfoils.* NACA Tech. Note 1252, 1947.

Pankhurst, R.C.; Pearcey, H.H. *Camber Derivatives and Two-Dimensional Tunnel Interference at Maximum Lift.* ARC CP 28, 1950.

Preston, J.H. *Note on the Application of Interference Corrections for a Large-Chord Wing with Control Spanning a Closed Tunnel.* ARC Report 5802, 1942. (Unpublished.)

Sanders, J. — *Wall Corrections for a Two-Dimensional Electrical Tank.* NRL (Canada) Report MA-213, 1948.

Stüper, J. — *Beitrag zum Problem des durch einen Freistrahl hindurchgesteckten Tragflügels.* Luftfahrtforschung, Vol. 12, 1935, pp. 267-281. (Translated as NACA Tech. Memo., 796.)

Wijker, H. — *Experiments on the Two-Dimensional Flow over a NACA 0018 Profile at High Angles of Attack. Appendix II: Influence of Tunnel Walls on the Pressure Distribution.* NLL (Netherlands) Report A.1263, 1953.

TABLE 2.I

Summary of Principal References, Figures and Formulae

		Velocity u_i *or* w_i		Γ, L *or* $\mathfrak{M}$ *in tunnel*		*Correction* $\Delta\alpha$ *or* ΔC_L		*Correction* ΔC_m *or* ΔC_H	
Subject	*Ref.*	*Fig.*	*Eqn.*	*Fig.*	*Eqn.*	*Fig.*	*Eqn.*	*Fig.*	*Eqn.*
Thin aerofoil in closed tunnel	2.3 2.4 2.5 2.6		2.9 2.10	2.3	2.18 2.19 2.20 2.21		2.16 2.17 2.24 2.25 2.27		2.17 2.26
Thick aerofoil in closed tunnel	2.9 2.12 2.27 2.28			2.13		2.4	2.31 2.32 2.48 2.49 2.81	2.4	2.33 2.48 2.49
Aerofoil with flap in closed tunnel	2.14 2.15 2.16 2.24			2.5		2.7 2.8	2.54 2.55	2.6 2.7 2.9	2.52 2.55
Open-jet tunnel	2.17 2.21 2.22 2.23	2.12	2.67 2.68 2.69 2.71	2.10	2.60		2.74 2.75		2.75
Non-rectangular tunnel	2.2 2.7 2.19			2.11	2.61 2.62	2.11			

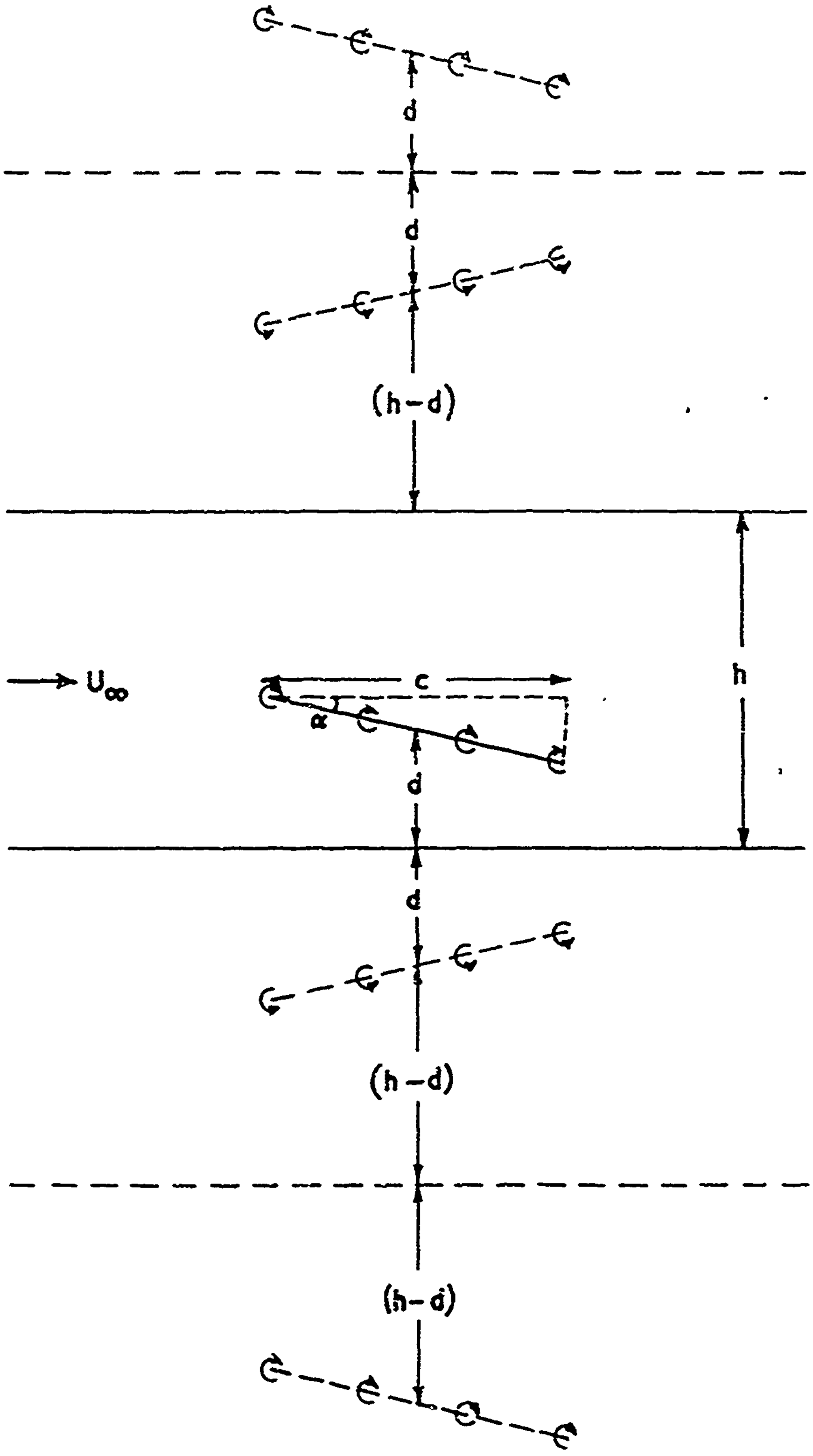
d
d
(h−d)
U∞
c
α
h
d
d
(h−d)
(h−d)

Fig. 2.1 Thin two-dimensional aerofoil and its image system for lift interference

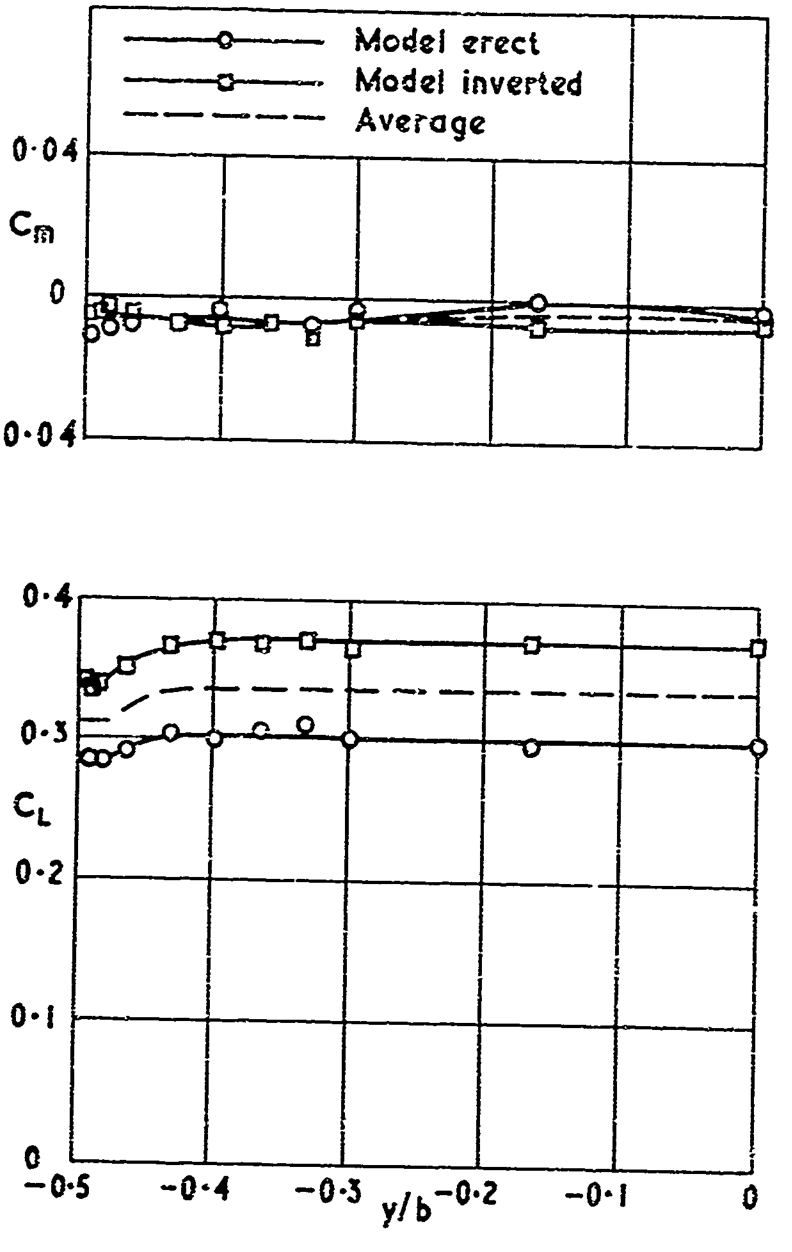

Reproduced from Fig. 6 of Ref. 2.1

Fig. 2.2 Spanwise distribution of lift and pitching moment on an aerofoil spanning a closed rectangular tunnel

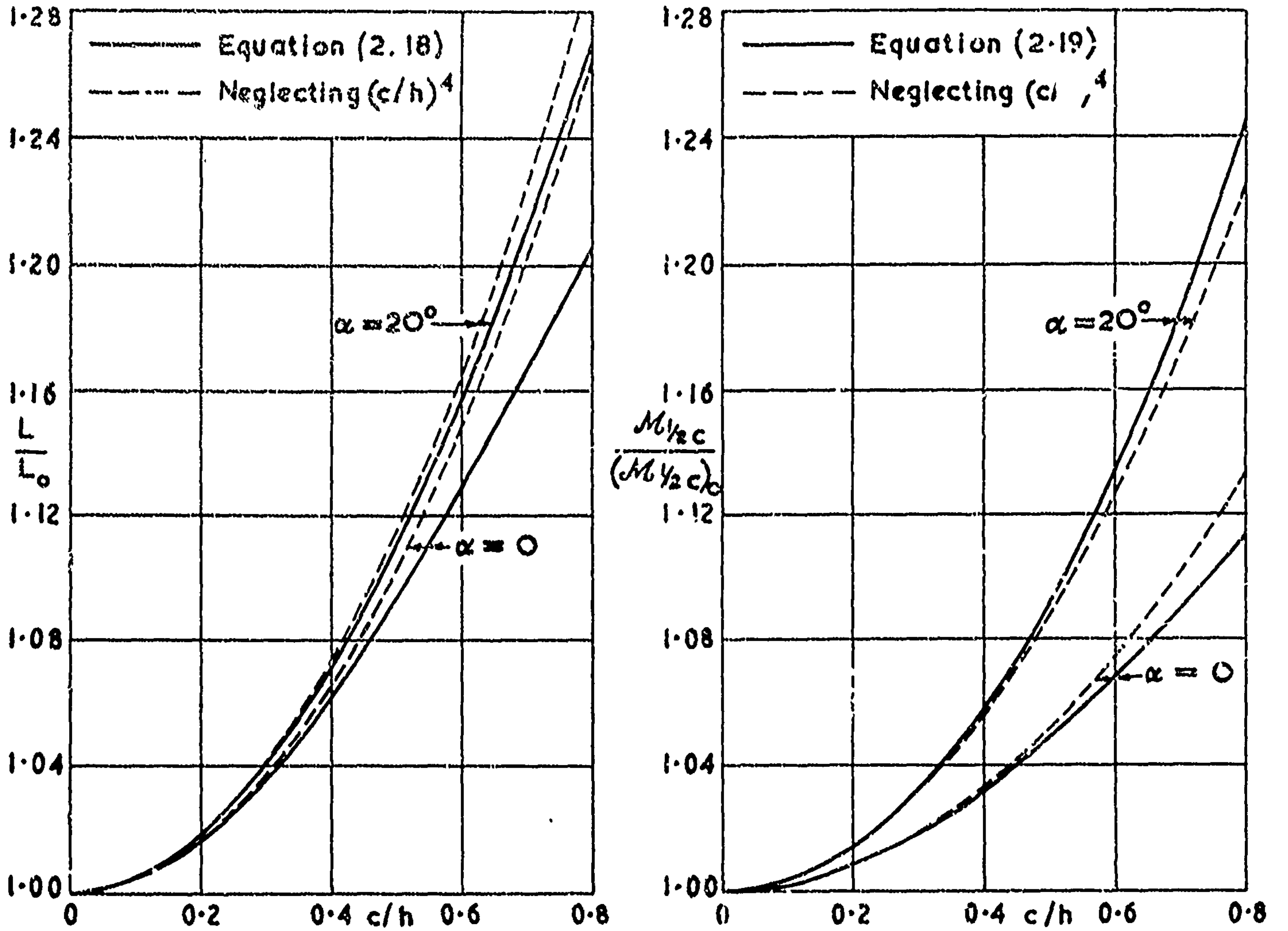

Fig. 2.3 Closed-tunnel to free-stream ratios of lift and moment on a flat-plate aerofoil

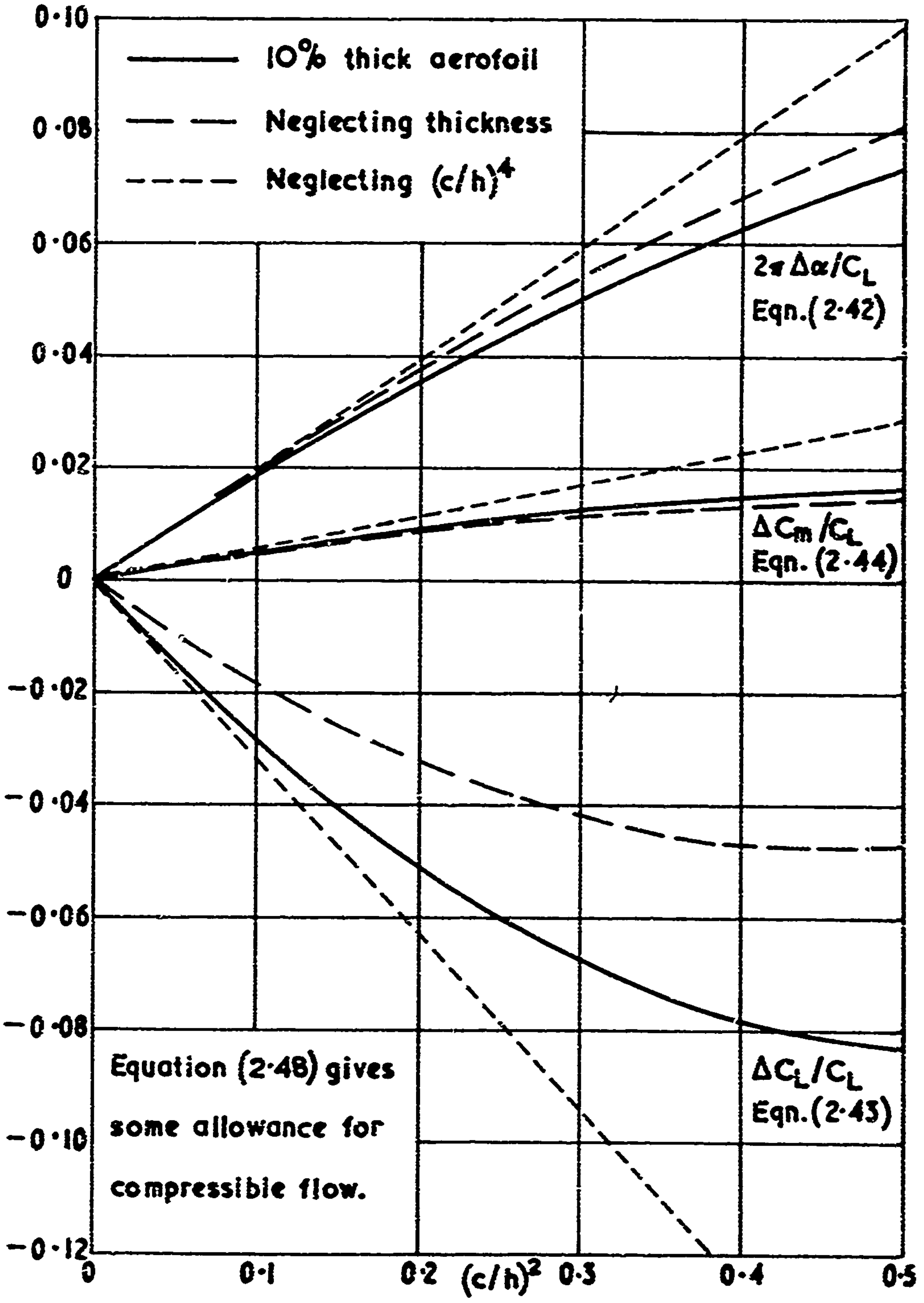

Fig. 2.4 Wall corrections for an RAE 102 aerofoil

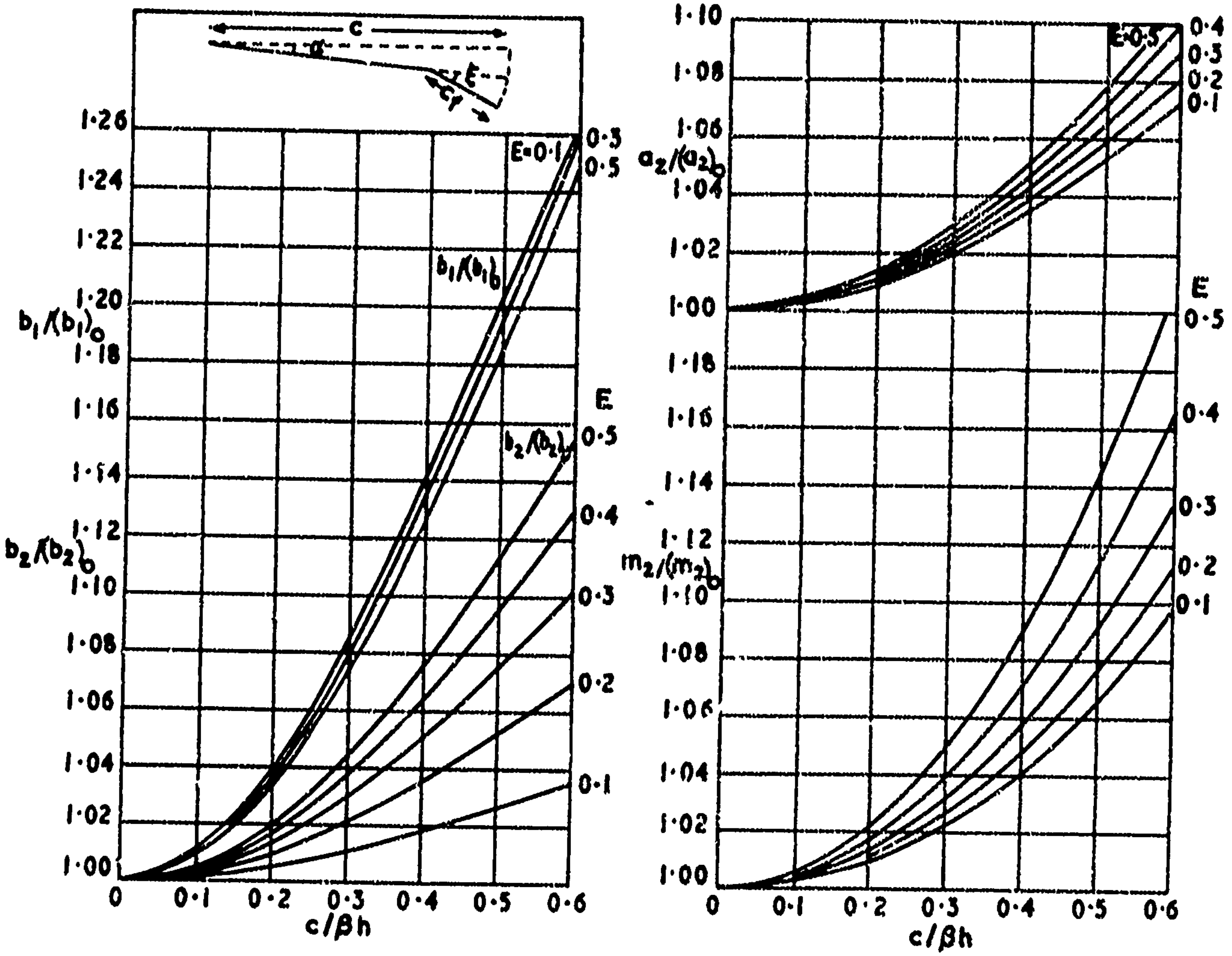

Fig. 2.5 Closed-tunnel to free-stream ratios of derivatives for aerofoils with hinged flaps (Ref. 2.14)

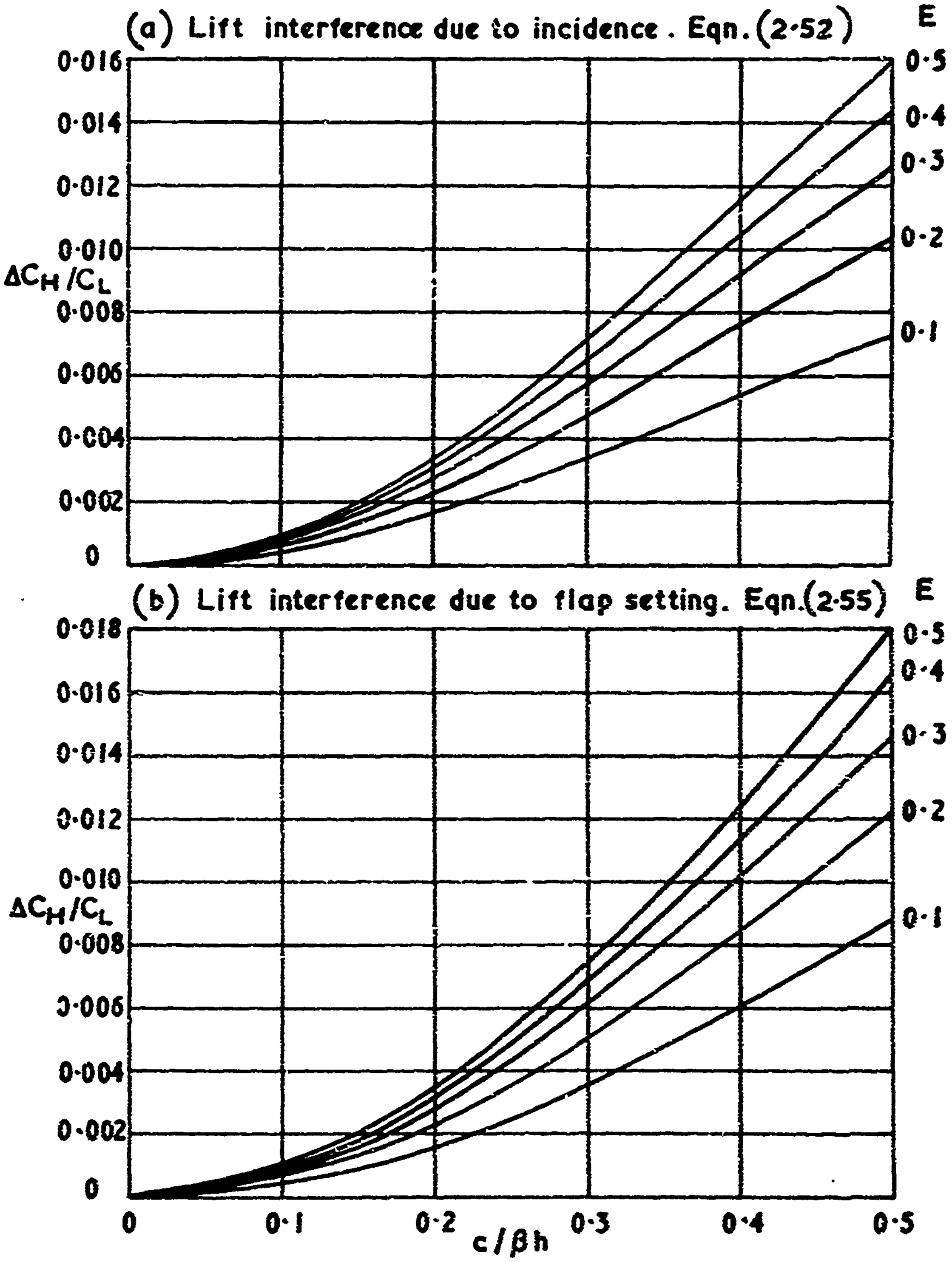

Fig.2.6 Wall corrections to flap hinge moments

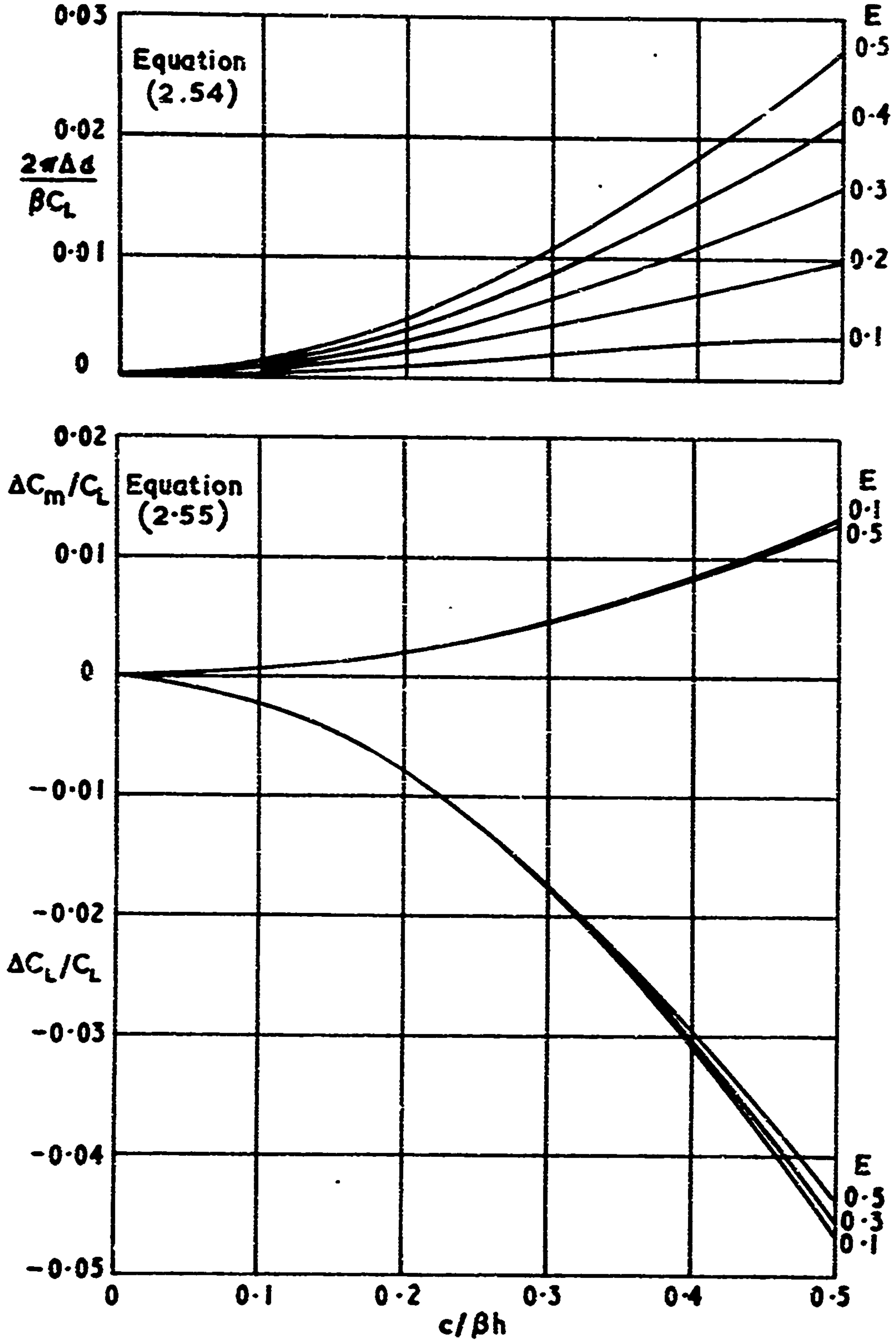

Fig. 2.7 Wall corrections due to flap setting

Based on Ref. 2.16

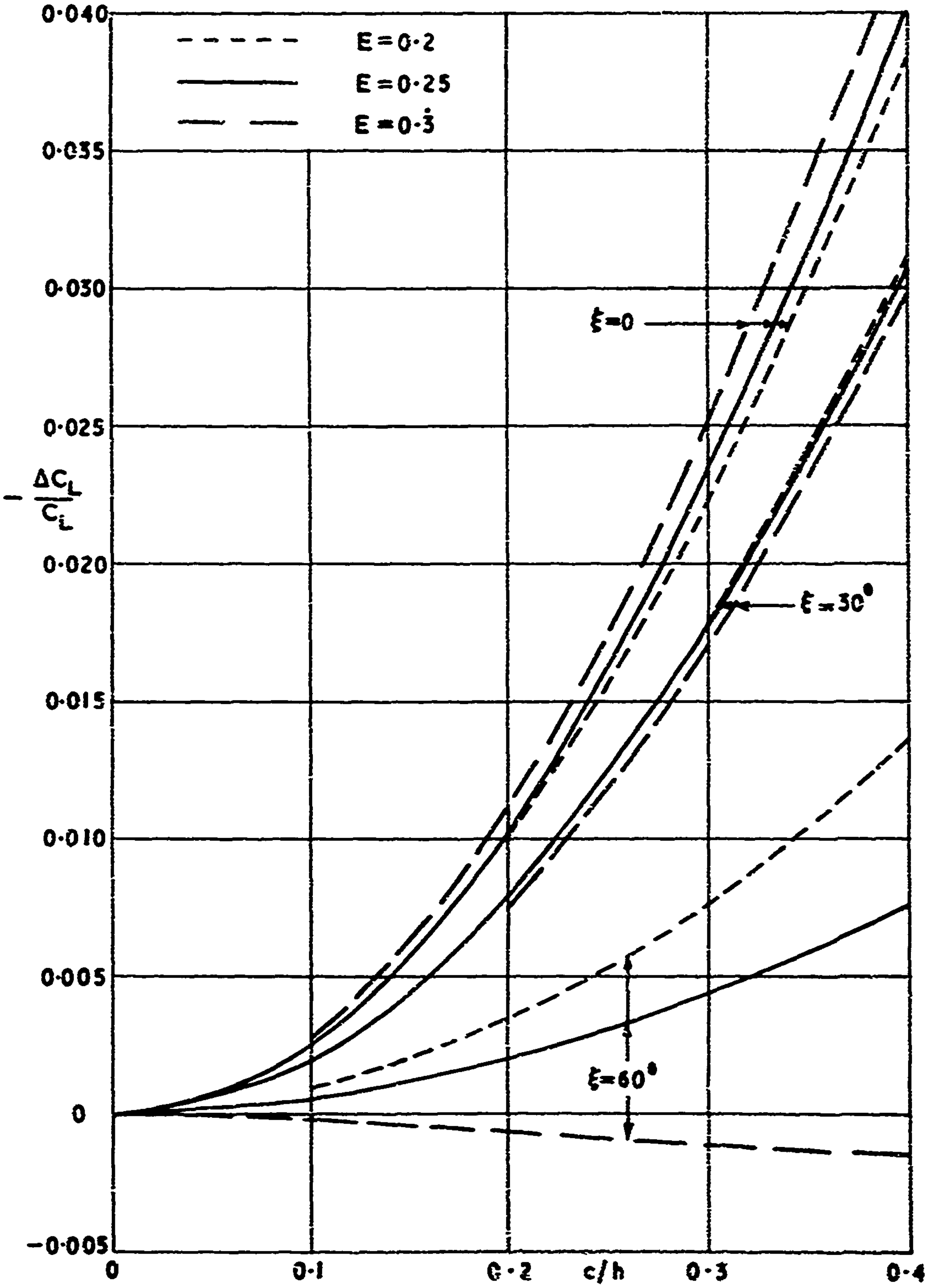

Fig. 2.8 Effect of large flap setting on lift interference (M = 0)

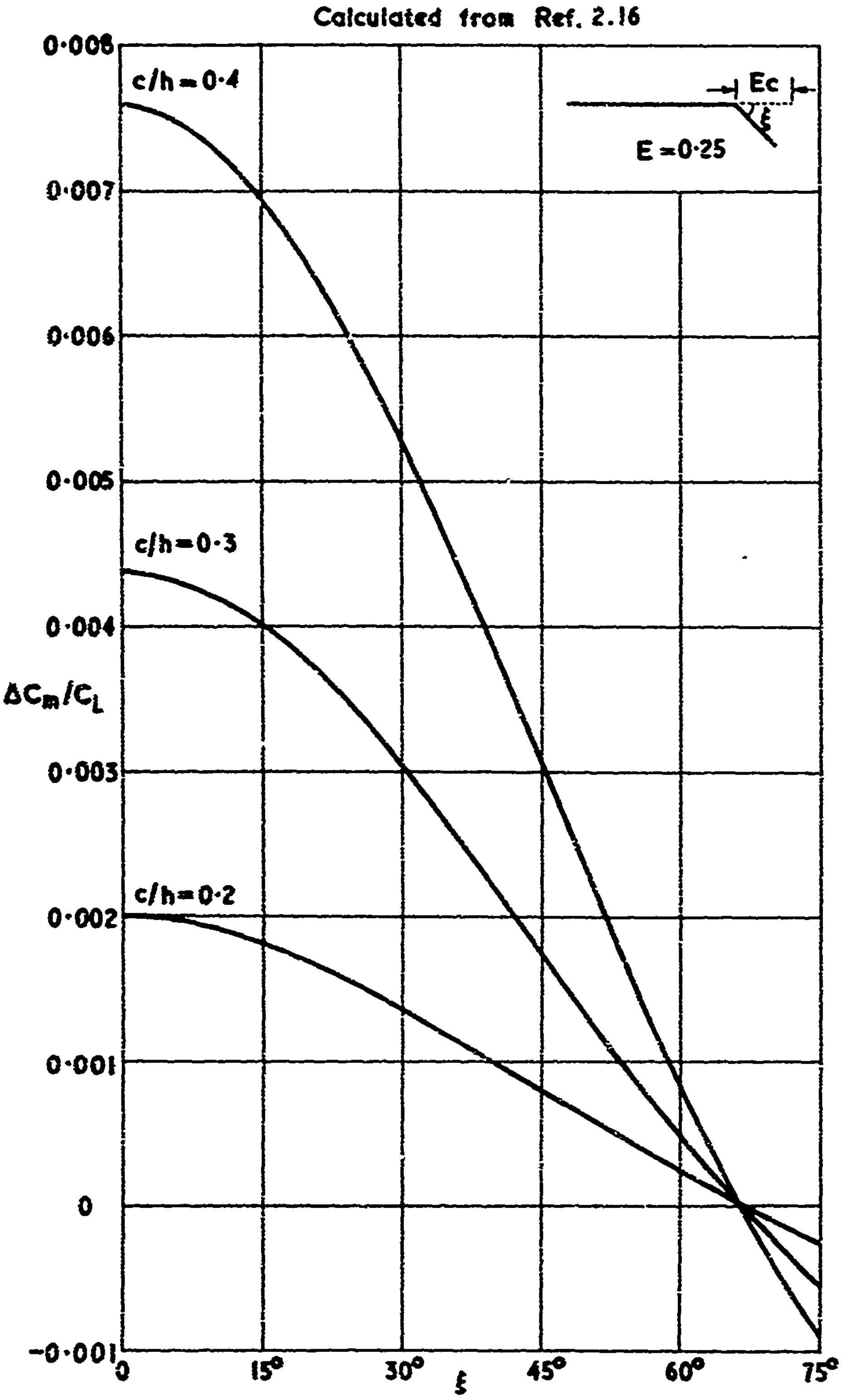

Fig. 2.9 Corrections to pitching moment due to a deflected flap (M = 0)

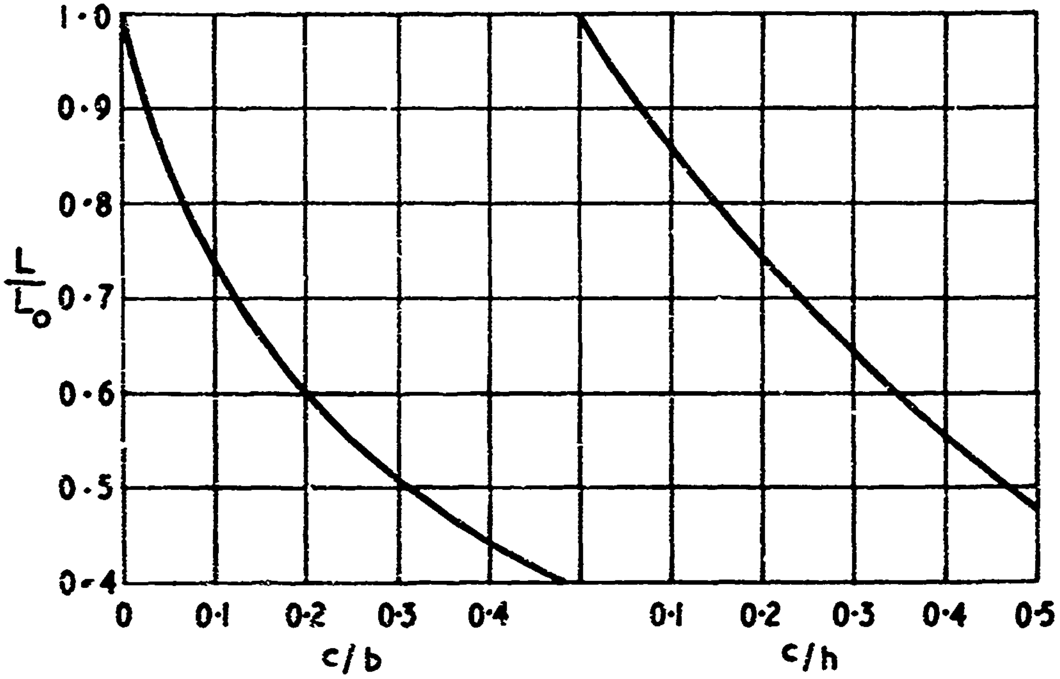

(a) h=∞. Equation (2·59)

(b) b = ∞. Ref. 2·21

(c) Centre section. Equation (2·60)

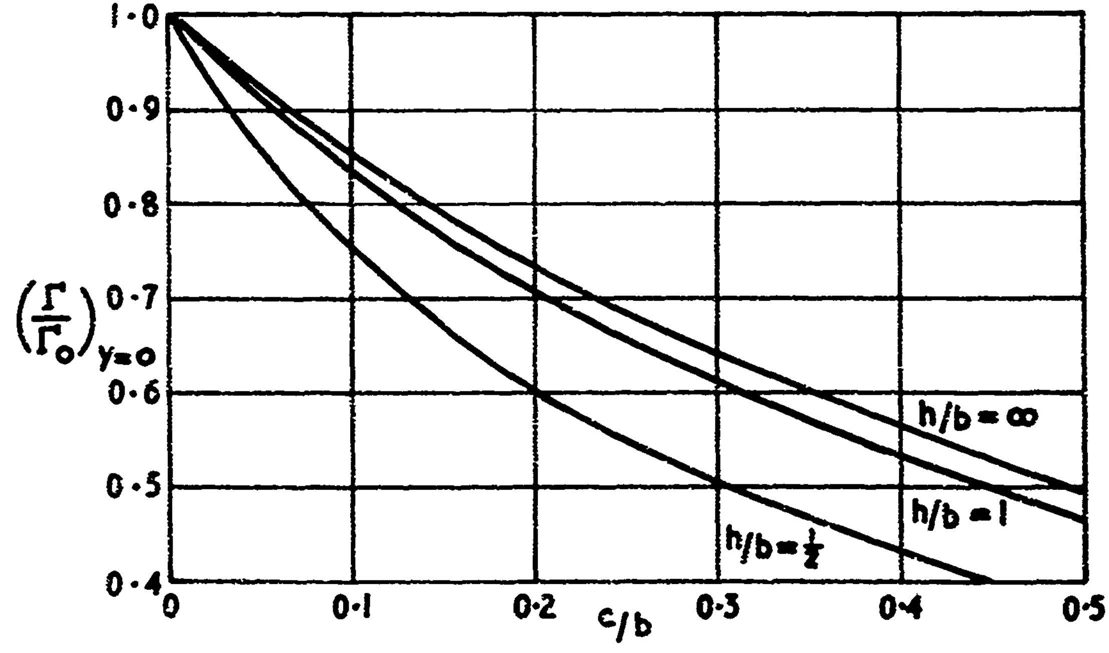

Fig. 2.10 Lift interference in rectangular open-jet tunnels

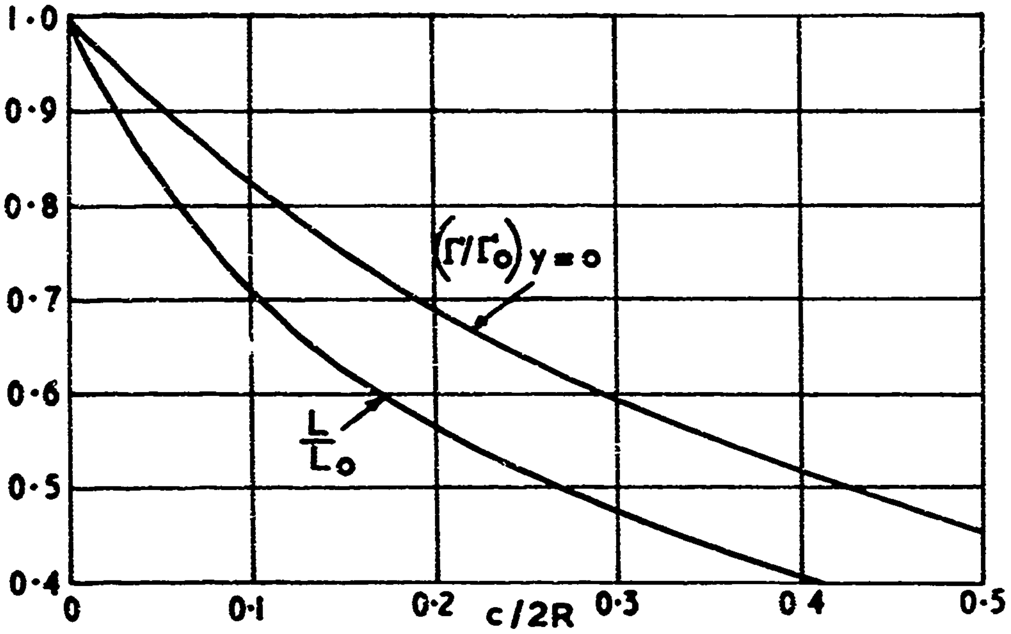
(a) Ratios of central and total lift. Ref. 2·19

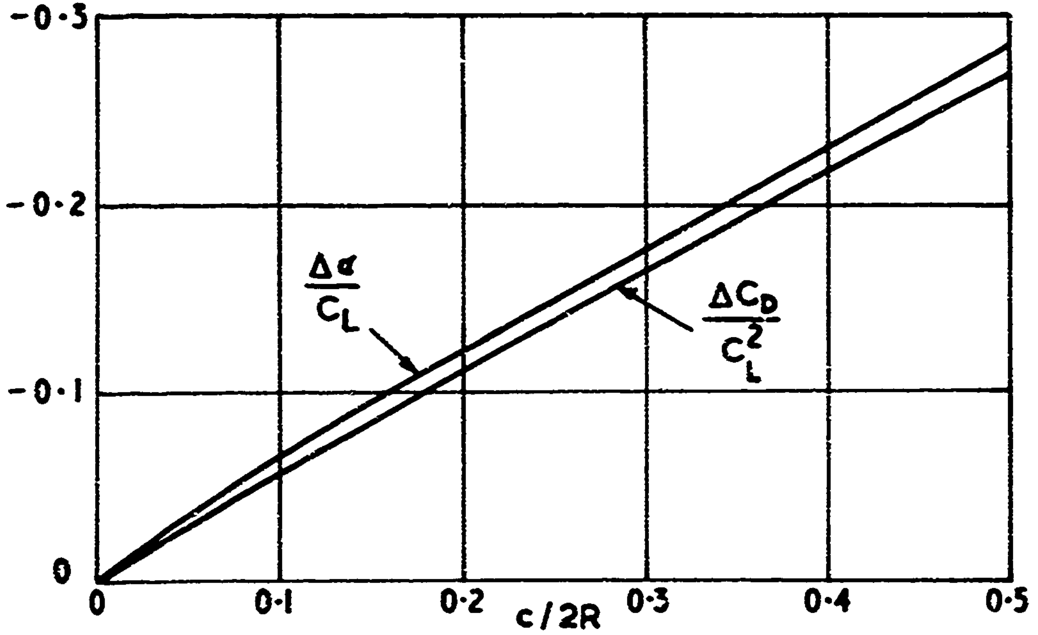
(b) Corrections to incidence and drag

Fig. 2.11 Lift interference in circular open-jet tunnels

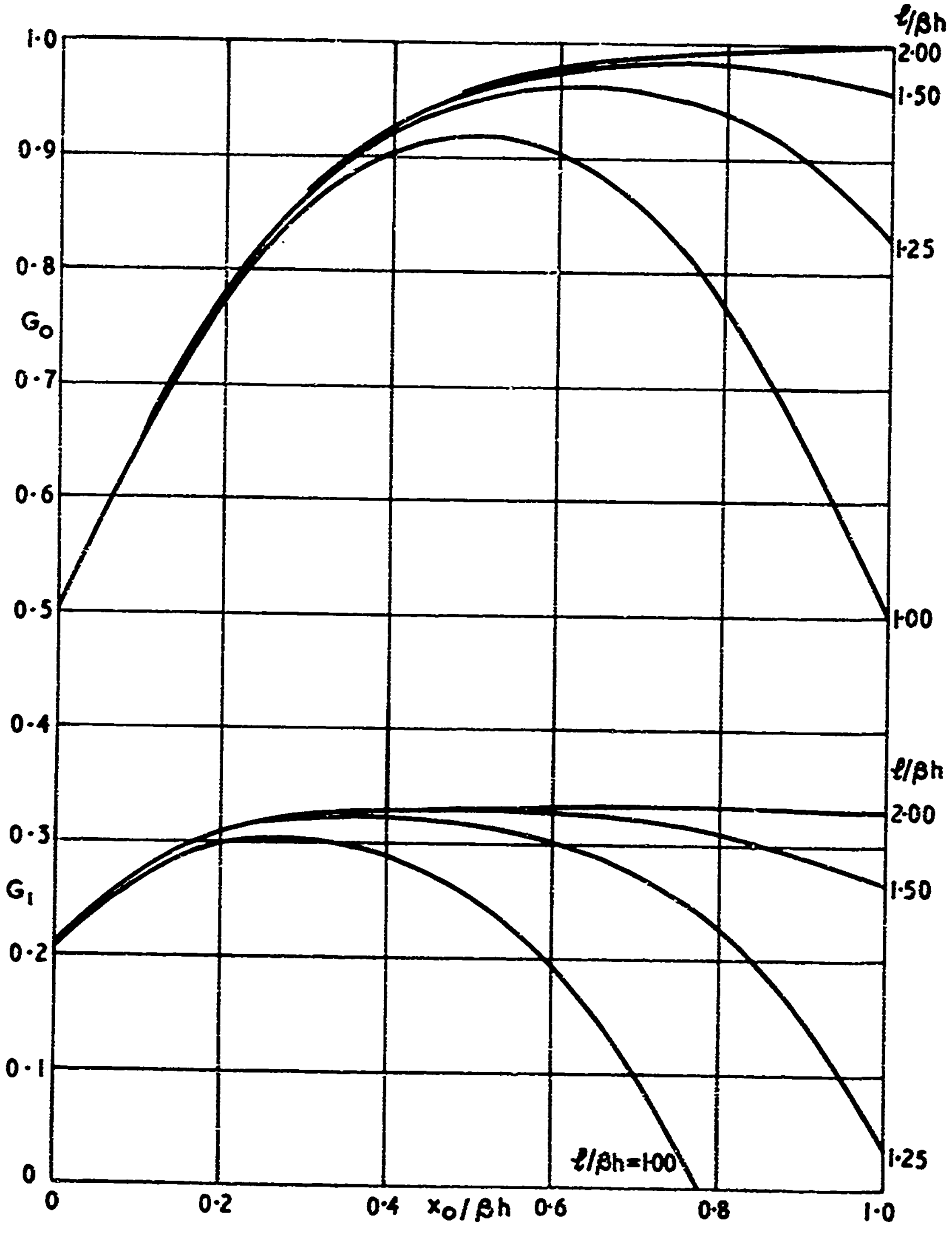

Fig. 2.12 Functions from Equations (2.71) to (2.75) for closed-open-closed tunnels

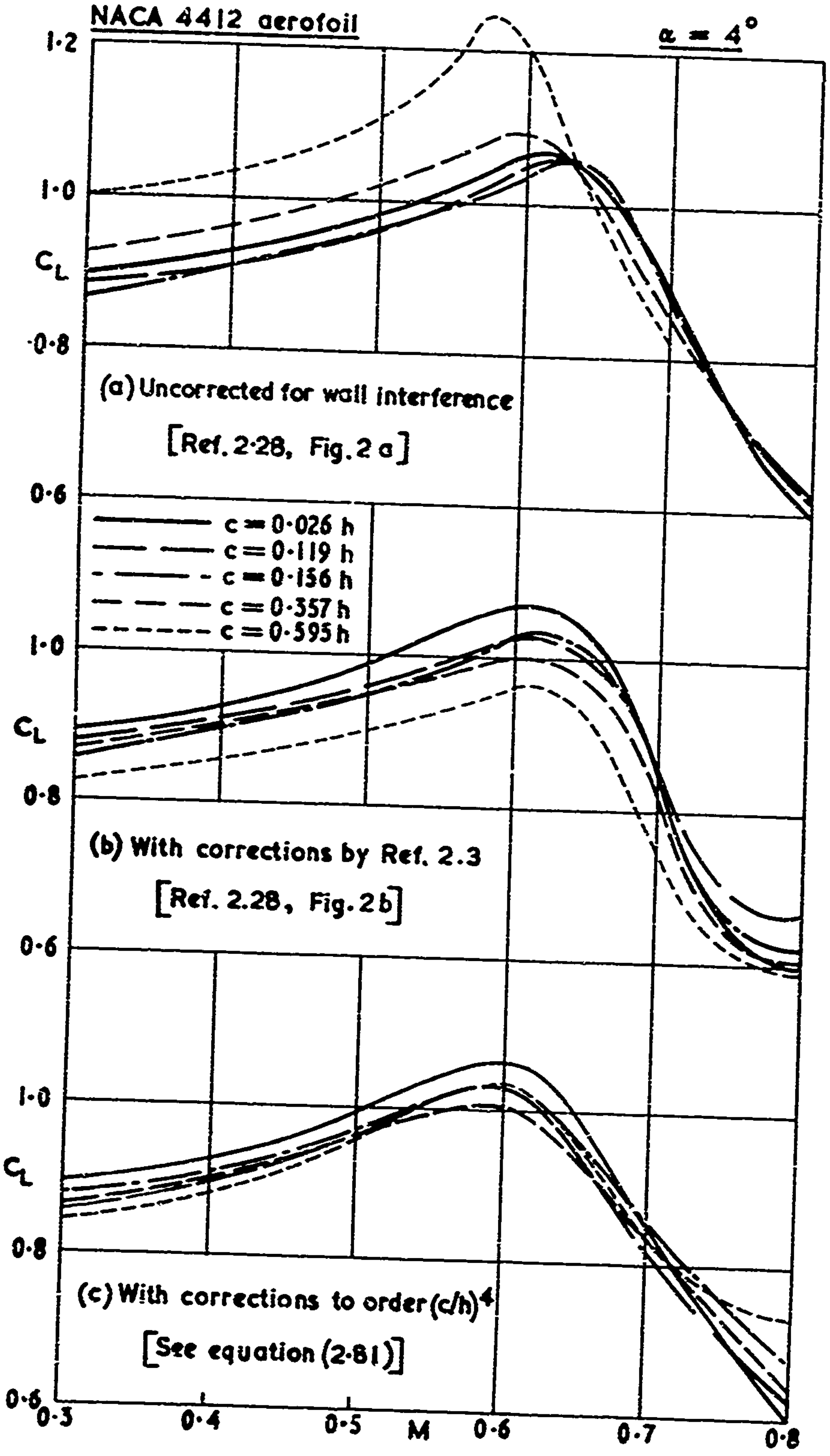

Fig. 2.13 Experimental variation of C_L with M for various c/h

CHAPTER III

LIFT INTERFERENCE ON THREE-DIMENSIONAL WINGS

by

H.C.Garner

Aerodynamics Division, National Physical Laboratory,
Teddington, Middlesex, England

BLANK PAGE

CONTENTS

Page

LIST OF TABLES 79

LIST OF FIGURES 79

NOTATION 81

3.1 INTRODUCTION 87

3.2 SMALL WINGS IN CLOSED AND OPEN TUNNELS 90
  3.2.1 Method of Images 91
  3.2.2 Rectangular Tunnels 92
  3.2.3 Non-Rectangular Tunnels 97
  3.2.4 Applications 100

3.3 GENERAL THEORY OF LIFT INTERFERENCE 103
  3.3.1 Representation of Model 103
  3.3.2 Basic Interference Parameters 105
  3.3.3 Corrections to Measured Quantities 108
  3.3.4 Complete Spanwise Symmetry 110
  3.3.5 Non-Symmetrical Spanwise Loading 112
  3.3.6 Asymmetrically Placed Wings 115

3.4 EVALUATION OF INTERFERENCE PARAMETERS 117
  3.4.1 Rectangular Tunnels 118
  3.4.2 Octagonal Tunnels 125
  3.4.3 Circular and Elliptical Tunnels 130
  3.4.4 Half-Wing Models 138

3.5 NUMERICAL INTERFERENCE CORRECTIONS 141
  3.5.1 Rectangular Tunnels 143
  3.5.2 Non-Rectangular Tunnels 147
  3.5.3 Comparisons of Methods 149

3.6 SPECIAL CONFIGURATIONS 153
  3.6.1 Slender Wings 154
  3.6.2 Wing-Body-Tail Combinations 157
  3.6.3 Interference on Ground Effect 163
  3.6.4 Models Spanning Closed Tunnels 165

3.7 EXPERIMENTAL CONSIDERATIONS 167
  3.7.1 High Lift 168
  3.7.2 Closed Tunnels 170
  3.7.3 Open Tunnels 171

Page

3.8 INDEX OF FORMULAE AND DATA 173
3.8.1 Simple or Approximate Interference Velocity 174
3.8.2 Elaborate or Accurate Interference Upwash 175
3.8.3 Corrections to Measured Quantities 176

REFERENCES 177

ADDITIONAL REFERENCES 182

TABLES 183

FIGURES 190

LIST OF TABLES

Page

TABLE 3.I Equivalent Incompressible Flow from Equation (3.5) when $M = (1-\beta^2)^{\frac{1}{2}}$ 183

TABLE 3.II Function S_1 from Equation (3.18) for the Evaluation of Streamline Curvature in Rectangular Tunnels 184

TABLE 3.III Values of λ and $\lambda x_1/\bar{c}$ from Lifting-Surface Theory and Strip Theory 185

TABLE 3.IV Summary of Numerical Data on Interference Upwash for Large Wings 186

TABLE 3.V Interference Parameters for a Closed Square Tunnel 187

TABLE 3.VI Interference Parameters ζ_0 and ζ_1 for Closed Rectangular Tunnels 188

TABLE 3.VII Comparative Calculations of $\Delta\alpha/C_L$ and $\Delta C_m/C_L$ for Wings in Closed Rectangular Tunnels 189

LIST OF FIGURES

Fig.3.1 Typical image systems 190

Fig.3.2 Lift interference on small wings in rectangular tunnels 191

Fig.3.3 Upwash and stream-velocity interference on a small lifting wing displaced vertically from the centre of a closed rectangular tunnel 192

Fig.3.4 Ratios δ_1/δ_c for small models in closed and open rectangular tunnels 193

Fig.3.5 Lift interference on small wings in elliptical tunnels 194

Fig.3.6 Axial distributions of interference upwash for several positions of a small lifting wing in a closed-open-closed circular tunnel 195

Fig.3.7 Lift-interference correction to measured incidence of small models of various planforms 196

Fig.3.8 Different vortex models of lifting wings 197

Fig.3.9 Lift interference on wings with elliptic spanwise loading in closed rectangular tunnels 198

Page

Fig.3.10 Approximate representations of doubly infinite arrays of doublets to evaluate W_A for rectangular tunnels 199

Fig.3.11 Lift interference on off-centre models in a closed duplex tunnel with and without ground simulation 200

Fig.3.12 Lift interference on wings with elliptic spanwise loading in closed octagonal tunnels 201

Fig.3.13 Interference parameter for elliptically loaded wings in elliptical tunnels 202

Fig.3.14 Vortex configurations defining Φ_m, $\Phi_1^{(1)}$ and $\Phi_1^{(2)}$ for circular tunnels 203

Fig.3.15 Lift interference on uniformly loaded half-wings in closed and open circular tunnels with variable reflection planes 204

Fig.3.16 Approximate interference corrections to incidence for wings of various spans and aspect ratios in three closed rectangular tunnels $(M = 0)$ 205

Fig.3.17 Interference corrections for wings of high aspect ratio in a closed rectangular tunnel $(b/h = 10/7)$ 206

Fig.3.18 Approximate curves of δ against b/h for wings of different area ratios in closed rectangular tunnels 207

Fig.3.19 Comparative calculations of residual corrections to pitching moment on wings in closed rectangular tunnels for a range of Mach number 208

Fig.3.20 Lift interference on slender delta wings in a closed duplex tunnel 209

Fig.3.21 Interference correction to tailplane incidence on models of varying size in a closed duplex tunnel $(M = 0)$ 210

Fig.3.22 Effect of wing span on lift interference with ground simulation in three closed rectangular tunnels 211

Fig.3.23 Lift interference on ground effect on uniformly loaded wings in three closed rectangular tunnels 212

Fig.3.24 Experiments on lift interference on models spanning closed tunnels 213

Fig.3.25 Lift curves for an elliptical wing in two closed circular tunnels 214

Fig.3.26 Comparison of aileron effectiveness of a complete model and a part-span model in a closed circular tunnel with reflection plane 215

Fig.3.27 Experimental determination of lift interference in two open tunnels 216

Fig.3.28 Interference corrections to drag on three similar delta wings in an open circular tunnel 217

NOTATION

a	speed of sound
a	length of corner fillet of octagonal tunnel
A	aspect ratio of wing $= 2s/\bar{c}$
b	breadth of tunnel
B	hinge moment parameter in Equation (3.77)
c	chord of wing
$\bar{c}$	geometric mean chord of wing $= S/2s$
$\bar{\bar{c}}$	aerodynamic mean chord of wing in Equation (3.60)
c_f	chord of control surface
c_r	root chord of wing
c_t	tip chord of wing
C	cross-sectional area of tunnel
C_D	drag coefficient $= D/\frac{1}{2}\rho U^2 S$
C_H	hinge moment coefficient
C_l	rolling moment coefficient $= \mathfrak{L}/\rho U^2 Ss$
C_L	lift coefficient $= L/\frac{1}{2}\rho U^2 S$
C_{LL}	(lift per unit span)$/\frac{1}{2}\rho U^2 c$
C_m	pitching moment coefficient $= \mathfrak{M}/\frac{1}{2}\rho U^2 S\bar{c}$
C_{mL}	(pitching moment per unit span)$/\frac{1}{2}\rho U^2 c^2$
C_n	yawing moment coefficient $= \mathfrak{N}/\rho U^2 Ss$
C_p	pressure coefficient
d	distance of wing from floor of tunnel
D	drag
E_1	complete elliptic integral

f	function defined in Equation (3.177) or (3.178)
f_q	functions ($q = 1, 2, 3, 4$) defined in Equations (3.90)
F	integral defined in Equation (3.177)
$\bar{g}_n$	function defined above Equation (3.121)
G	function defined in Equation (3.103)
h	height of tunnel
I_1	modified Bessel function of the first kind
j	sign according to the appropriate Equation (3.14)
J_n	Bessel function ($n = 1, 2, \ldots$)
K	strength of vortex
K_e	strength of equivalent horse-shoe vortex in Equations (3.41)
K_n	modified Bessel function of the second kind ($n = 1, 2$)
l	length of open working section
l	non-dimensional wing loading $= (p_l - p_u)\frac{1}{2}\rho U^2$
l	semi-focal distance of elliptical tunnel
L	lift
$L(x)$	lift ahead of position x
$\mathcal{L}$	rolling moment
m	integer defining column of images $y = mb$ (Fig. 3.1)
M	Mach number of undisturbed stream
$\mathfrak{M}$	nose-up pitching moment
n	outward normal distance from tunnel boundary
n	integer defining row of images $z = nh$ (Fig. 3.1)
$\mathfrak{N}$	yawing moment
p	pressure on upper or lower surface of wing
P	strength of doublet

r	radial distance
R	radius of circular tunnel
R_N	Reynolds number
s	semi-span of wing
$s(x)$	local semi-span of wing
s_e	semi-span of equivalent horse-shoe vortex in Equations (3.41)
S	area of planform of wing
S_q	functions ($q = 1,2,3$) in Equations (3.18), (3.19), (3.26)
t	thickness of wing
t	semi-span of elementary horse-shoe vortex
u	x-component of velocity perturbation
U	velocity of undisturbed stream
v	y-component of velocity
v_n	velocity component of image system in Figure 3.1(b) normal to fillet
w	z-component of velocity
w_i	interference upwash velocity
W	weight factor in Equation (3.55)
W	upwash function relating to horse-shoe vortex in Equation (3.79)
W_A	upwash function in Equations (3.96)
W_B	upwash function in Equations (3.96)
W_C	upwash function in Equation (3.97)
x	streamwise distance
$\bar{x}$	local centre of pressure
x_0	distance of model from entrance nozzle of open-jet tunnel
x_i	centre of lift defined below Equation (3.80)
x_L	ordinate of leading edge

$\bar{x}_L$	integral defined in Equation (3.60)
x_t	distance between three-quarter-chord points of wing and tail surfaces
X	x in transformed plane
y	spanwise distance from centre of tunnel
y_1	inboard end of aileron
y_2	outboard end of aileron
Y	transformed co-ordinate $= \beta y$
z	upward distance from centre of tunnel
Z	transformed co-ordinate $= \beta z$
α	incidence of wing (in radians unless otherwise stated)
α_t	incidence of tailplane
β	$= (1 - M^2)^{\frac{1}{2}}$
γ	non-dimensional circulation $= \Gamma/2sU$
Γ	circulation
δ	lift interference parameter in Equation (3.150)
δ'	incremental upwash interference in Equation (3.176)
δ_0	upwash interference at a lifting line
δ_1	upwash interference associated with streamline curvature
δ_ℓ	additional upwash interference downstream of wing
δ_D	drag interference parameter in Equation (3.215)
δ_w	upwash interference parameter at wing
δ_α	incidence interference parameter in Equation (3.215)
ϵ	non-dimensional correction to stream velocity
ζ_0	interference parameter in Equations (3.156)
ζ_1	interference parameter in Equations (3.156)
η, ζ	elliptical co-ordinates in Equation (3.113)

η_0	= $\tanh^{-1}(h/b)$ for elliptical tunnel ($b > h$)
θ	angular cylindrical polar co-ordinate
κ_0	antisymmetrical upwash interference at a lifting line
κ_1	effect of streamline curvature in Equation (3.49)
λ	planform parameter defined below Equation (3.60)
Λ	angle of sweepback
Λ_L	sweepback of leading edge
μ	planform parameter in Equation (3.62)
ξ	angle defined in Figure 3.15
ξ	angular deflection of aileron
ρ	density of undisturbed stream
σ	span ratio = $2s/b$
σ_e	equivalent span ratio = $2s_e/b$
Φ	velocity potential
Φ_1	velocity potential in Figure 3.14(b) or 3.14(c)
Φ_2	incremental velocity potential in Equation (3.119)
χ	function defined in Equation (3.104)
ψ	angle defined in Figure 3.15
Ψ	stream function in transverse plane
ω	complex (y,z) plane

Superscripts

(1)	closed tunnel
(2)	open tunnel

Subscripts

0.25	quarter-chord
0.5	mid-chord

0.75	three-quarter-chord
∞	wake ($x = \infty$)
A	antisymmetrical part
E	elliptic spanwise loading
F	free-stream
g	ground effect
i	induced by tunnel walls
l	from antisymmetrical loading
L	from symmetrical loading
m	model
N	point concentration of lift
R	rectangular tunnel
S	symmetrical part
t	tailplane
T	with tunnel constraint
U	uniform spanwise loading
v	vortex-induced

Prefixes

δ	contribution due to wall interference
Δ	increment due to wall correction
$\sum\sum_{-\infty}^{\infty}{}'$	denotes that (m,n) takes all possible integral pairs except $(0,0)$.
$'$(prime)	denotes differentiation unless otherwise stated.

LIFT INTERFERENCE ON THREE-DIMENSIONAL WINGS

H.C. Garner

3.1 INTRODUCTION

In Chapter II various aspects of lift interference on two-dimensional models have been covered. The wall interference corrections on three-dimensional lifting models are not only more numerous and greater in magnitude, but they involve considerably more geometrical parameters to represent the wind tunnel and the model. There is a corresponding diversity of mathematical techniques, and often the analysis demands simplifying assumptions that are unnecessary in two-dimensional flow. Glauert's classic monograph (Ref. 3.1; 1933) illustrates both these points and provides a comparative background for most subsequent developments.

The governing linearized equation for the velocity potential in three-dimensional steady ideal compressible flow is

$$(1 - M^2)\frac{\partial^2\Phi}{\partial x^2} + \frac{\partial^2\Phi}{\partial y^2} + \frac{\partial^2\Phi}{\partial z^2} = 0 \tag{3.1}$$

in rectangular co-ordinates; alternatively, in cylindrical co-ordinates,

$$(1 - M^2)\frac{\partial^2\Phi}{\partial x^2} + \frac{\partial^2\Phi}{\partial r^2} + \frac{1}{r}\frac{\partial\Phi}{\partial r} + \frac{1}{r^2}\frac{\partial^2\Phi}{\partial\theta^2} = 0 . \tag{3.2}$$

It is assumed that squares and products of the component perturbations of a uniform velocity $U = Ma$ are negligible throughout the field of flow. The differential Equation (3.1) or (3.2) is subject to outer conditions

$$\left.\begin{aligned} \partial\Phi/\partial n &= 0 \quad \text{at a closed boundary} \\ \partial\Phi/\partial x &= U \quad \text{at an open boundary} \end{aligned}\right\} ; \tag{3.3}$$

the former is exact, but the latter follows from the linearized approximation to constant pressure at an undistorted free boundary (Ref. 3.1, p.3). More complicated boundary conditions are used in cases of ventilated tunnels (Chapter VI). There are in addition the upstream and downstream conditions that the flow is undisturbed at $x = -\infty$ and independent of x for large positive values of x .

The first-order effects of compressibility can be obtained from solutions of the linearized differential Equation (3.1) with the aid of the transformation

$$X = x , \quad Y = \beta y , \quad Z = \beta z , \tag{3.4}$$

where $\beta = (1-M^2)^{\frac{1}{2}}$. In the new co-ordinate system the potential satisfies Laplace's equation for incompressible flow

$$\frac{\partial^2\Phi}{\partial X^2} + \frac{\partial^2\Phi}{\partial Y^2} + \frac{\partial^2\Phi}{\partial Z^2} = 0 . \tag{3.5}$$

It is convenient to regard the perturbation potential $(\Phi - Ux)$ as unchanged in the transformation. Then, by the argument in Section 2.1, the linearized solution in compressible flow is readily expressed in terms of an equivalent incompressible flow with the geometric and aerodynamic parameters listed in Table 3.I. That is to say, the equivalent incompressible flow gives an upwash velocity $\beta^{-1}w$ or an upwash angle $\beta w/U$ corresponding to a model of chord c , aspect ratio βA and thickness βt in a tunnel of breadth βb and height βh at an incidence $\beta\alpha$ to a stream of density ρ and velocity $\beta^{-2}U$. There are alternative methods of allowing for compressibility in Reference 3.2, where the free-stream velocity rather than the perturbation velocity potential is kept invariant. As Goldstein and Young point out, the linear perturbation theory of compressible flow is not intended to be applied when shock waves are present, and it must clearly fail in the neighbourhood of a stagnation point. Nevertheless, the theory of wall interference only involves the potential field at appreciable distances from the model, and the linearized equations can still be used to satisfy Equations (3.3) at fairly high subsonic Mach numbers. The effect of compressibility is obtained by substituting the generalized parameters of Table 3.I into any formulae or numerical data for wall interference in low-speed tunnels.

The classical approach due to Prandtl is to regard the model as a lifting line, when the problem of wall interference reduces to a solution of the two-dimensional Laplace equation in the transverse (y, z) plane containing the model (Ref.3.1, pp.3 to 5). The perturbation potential in this plane is exactly half that in the distant wake. For a given spanwise lift distribution and tunnel geometry, the interference upwash velocity $w_i(y)$ along the wing span can usually be obtained analytically; hence the simple corrections

$$\left.\begin{aligned} \Delta\alpha &= \delta_0 SC_L/C \\ \Delta C_D &= \delta_0 SC_L^2/C \end{aligned}\right\} \tag{3.6}$$

to the measured incidence and drag coefficient of the model are derived (Ref.3.1, pp.8 to 11). The interference parameter δ_0 is a non-dimensionalized mean value of w_i weighted proportionally to the spanwise lift distribution and given by

$$\delta_0 = \frac{1}{L}\int_{-s}^{s}\left(\frac{w_i}{U}\frac{C}{SC_L}\right)\frac{dL}{dy}\,dy . \tag{3.7}$$

Since the drag coefficient is determined by the conditions in the distant wake, the expression for ΔC_D in Equation (3.6) is usually regarded as exact according to linearized theory. The corresponding expression for $\Delta\alpha$ is often too approximate and underestimates the magnitude of the correction.

Unless the wing chord is small, it is necessary to consider the streamwise variation of w_i, which is interpreted as a curvature of the free stream due to wall constraint. For wings of fairly small span the results of Section 3.2 can often be used and the interference correction to incidence is approximately

$$\Delta\alpha = \left(\delta_0 + \frac{\bar{\bar{c}}}{2\beta h}\delta_1\right)\frac{SC_L}{C}\,. \tag{3.8}$$

where $\bar{\bar{c}}$ is the aerodynamic mean chord and δ_1 is independent of Mach number. Thus, as Göthert remarked (Ref.3.3; 1940), the streamline curvature correction is of growing importance in compressible flow. A more general treatment is necessary for sweptback wings of moderate span, which must be considered as lifting surfaces. Many different vortex representations of the model have been suggested (Section 3.3.1). For most purposes it is sufficient to regard $w_i(x,y)$ in the plane of the model as a linear function of x (Section 3.3.2). Indeed, with the exception of interference effects on long slender wings (Section 3.6.1) and tail planes (Section 3.6.2), a more detailed representation of the model than appears practicable would be required to justify a precise evaluation of the streamwise variation of the interference upwash.

There is a miscellany of literature concerning wall interference on lifting wings, ranging from the excessively numerical to the excessively mathematical. Some papers deal exclusively with one particular tunnel section and rely on extensive tables of interference upwash and approximate computations; the numerical results are only useful for the single tunnel shape, and it is often difficult to assess the ultimate accuracy. At the other extreme, it is not always expedient to carry the mathematical analysis so far that the complexity of the resulting formulae prohibits their use. An attempt is made in Section 3.3.2 to steer a middle course in presenting the basic interference parameters.

Broadly the cases to be considered fall into four categories

(a) complete spanwise symmetry, e.g., a wing at incidence,

(b) symmetrical planform but asymmetrical spanwise loading, e.g., a wing with deflected ailerons,

(c) asymmetrical planform relative to the tunnel, e.g., a yawed wing,

(d) special configurations to be considered in Section 3.6.

Even with complete spanwise symmetry there is no unique procedure for converting the tunnel-induced upwash distribution into corrections to the measured quantities. The incremental correction to incidence, such as Equation (3.8), is a somewhat arbitrary average value of w_i/U radians, and the subtraction of the residual upwash field is made equivalent to incremental corrections to the aerodynamic forces. The complication of asymmetry introduces residual corrections to the lateral moments (Section 3.3.5). The mathematical theories leading to the basic interference parameters for the various types of tunnel section are discussed in Sections 3.4.1 to 3.4.4, and some available sources of numerical data are listed in Table 3.IV. The final incremental corrections are considered numerically in Section 3.5, and in Section 3.5.3 an attempt is made to assess the accuracy of alternative methods where comparative calculations exist.

Experimental considerations of high lift and some practical confirmation of wall-interference theory are given in Section 3.7. The former is largely empirical and beyond the scope of linearized theoretical methods; the latter usually involves tests in different tunnels, on different models or at different or rather small Reynolds numbers and lacks firm conclusions. Unfortunately it is no easy matter to amalgamate the tunnel corrections for wall interference and Reynolds number. Sometimes large models or half models are tested to achieve the highest possible Reynolds number, since the uncertainties of scale effect exceed those of wall interference. In Reference 3.4, Bryant and the present author have suggested a scheme whereby the estimation of wall interference includes a correlation between experiment and an approximate wing-loading theory incorporating sectional wing characteristics dependent on Reynolds number. This ideal philosophy envisages corrections to full-scale conditions after wall interference has been taken into account.

There are many problems of lift interference, where a mathematical solution must involve simplifying assumptions regarding tunnel cross-section, wing thickness or location of model. In such cases the use of an electrical analogy is worth consideration. In particular, Reference 3.5 discusses the basic concepts of such analogies and their technical difficulties in relation to open wind tunnels of finite jet lengths.

Attention is drawn to the final Section 3.8 which serves as an index to the more important equations, tables and figures. It is intended as a preliminary guide firstly to the more approximate formulae and numerical data, and secondly to the more complicated and accurate formulae for the interference upwash. A third table lists the various expressions and results for the interference corrections themselves.

3.2 SMALL WINGS IN CLOSED AND OPEN TUNNELS

Useful estimates of lift interference can often be made when the model is assumed to be small. The interference upwash at the wing and the streamline curvature are given respectively by

$$\left.\begin{aligned}\delta_0 &= \frac{Cw_i}{USC_L}\\ \delta_1 &= \frac{\beta Ch}{USC_L}\frac{\partial w_i}{\partial x}\end{aligned}\right\} . \qquad (3.9)$$

Both parameters are readily evaluated for closed or open rectangular tunnels (Section 3.2.2). For more general cross-sections a method of conformal transformation will usually determine δ_0. When the analysis for δ_1 becomes intractable, an approximate formula may be used to relate δ_1/δ_0 to its known value for a rectangular tunnel (Section 3.2.3). Several types of semi-closed tunnel with mixed boundary conditions are also discussed.

The applications in Section 3.2.4 are restricted to wings of fairly small span; if accuracy within ±10% is necessary, then the wing span should not exceed half the tunnel breadth or half the tunnel height. For many purposes the formulae and graphs will give the order of magnitude of the interference corrections with a minimum of effort.

3.2.1 Method of Images

The small wing is represented as a semi-infinite vortex pair trailing from the origin of co-ordinates. The doublet strength is

$$\lim_{s\to 0}(2Ks) = \tfrac{1}{2}USC_L , \tag{3.10}$$

and the corresponding velocity potential is

$$\Phi_m = Ux + \frac{USC_L z}{8\pi(y^2 + z^2)}\left[1 + \frac{x}{(x^2 + \beta^2 y^2 + \beta^2 z^2)^{\frac{1}{2}}}\right] , \tag{3.11}$$

where x is in the horizontal direction of the undisturbed stream, y spanwise and z upwards. The boundary conditions (3.3) to be satisfied by the potential $\Phi = \Phi_m + \Phi_i$ are supposedly independent of x. Like Φ_m, the interference potential is then of the form

$$\Phi_i = f(y,z) + F(x,y,z) ,$$

where $F(x,y,z)$ is an odd function of x. From Prandtl's argument (Ref.3.1, pp.3 to 5), the solution for Φ_i in the plane $x = 0$ is given by the two-dimensional Laplace equation

$$\frac{\partial^2\Phi_i}{\partial y^2} + \frac{\partial^2\Phi_i}{\partial z^2} = 0 ;$$

by Equations (3.3) with the upstream condition and Equation (3.11) the boundary conditions on Φ_i are

$$\left.\begin{aligned} \frac{\partial\Phi_i}{\partial n} &= -\frac{\partial}{\partial n}\left\{\frac{USC_L z}{8\pi(y^2 + z^2)}\right\} && \text{at a closed boundary} \\ \Phi_i &= -\frac{USC_L z}{8\pi(y^2 + z^2)} && \text{at an open boundary} \end{aligned}\right\} , \tag{3.12}$$

where $\partial/\partial n$ denotes differentiation along the outward normal to solid portions of the tunnel boundary.

For special shapes and types of tunnel a convenient system of images can be constructed to give the required potential Φ_i in the plane $x = 0$, or a good approximation to it. Typical examples are illustrated in Figure 3.1. In the case of a closed circular tunnel the image system is particularly simple, but it is necessary to consider the wing as a uniformly loaded lifting line of finite span $2s$ and then take the limit as $s \to 0$ with the aid of Equation (3.10). The images for a closed rectangular tunnel are doubly infinite in number and are evenly distributed over the (y,z) plane; as will be seen in Section 3.2.2, image systems of this type are not always valid. When image systems fail or do not exist, special analytical treatment is sought. The third illustration of Figure 3.1 represents an incremental image system to the previous one, to give an approximate solution for an octagonal tunnel obtained by the addition of isosceles corner fillets (Section 3.2.3).

In general, the method of images can only be applied to the interference parameter δ_0 in Equation (3.9). For the important class of rectangular tunnels, however, the images can be regarded as semi-infinite vortex pairs trailing from the plane $x = 0$, which by symmetry provide a complete three-dimensional system from which Φ_i, and hence δ_1, can be evaluated. This is not true of the circular and octagonal tunnels.

3.2.2 Rectangular Tunnels

As early as 1931, Theodorsen[3.6] studied different types of rectangular tunnel from the standpoint of minimizing lift interference. Four particular types of breadth b and height h,

$$\left.\begin{array}{l}\text{(1) completely closed tunnel}\\ \text{(2) completely open tunnel}\\ \text{(3) open sides, closed floor and roof}\\ \text{(4) closed sides, open floor and roof}\end{array}\right\}\ ,$$

will be considered. In each case there is a complete image system comprising semi-infinite doublets of strength $\frac{1}{2}USC_L$ and the appropriate sign; for a central model they are situated at $(x,y,z) = (0,mb,nh)$ where m and n are integers. Thus, by Equation (3.11), the interference potential for a small lifting wing is

$$\Phi_i = \sum_{-\infty}^{\infty}\sum{}' (j)\,\frac{USC_L(z-nh)}{8\pi\{(y-mb)^2 + (z-nh)^2\}}\left[1 + \frac{x}{\{x^2 + \beta^2(y-mb)^2 + \beta^2(z-nh)^2\}^{\frac{1}{2}}}\right], \quad (3.13)$$

where $\sum_{-\infty}^{\infty}\sum{}'$ denotes that (m,n) takes all possible integral pairs except (0,0). Following Glauert (Ref.3.1, Figs.7 and 8, pp.21 to 24), we take

$$\left.\begin{array}{l} j = j^{(1)} = (-1)^n \\ j = j^{(2)} = (-1)^m \\ j = j^{(3)} = (-1)^{m+n} \\ j = j^{(4)} = 1 \end{array}\right\} \quad (3.14)$$

respectively for the four types of tunnel, the first of which is illustrated in Figure 3.1(b). From the definitions in Equations (3.9) the lift-interference parameters at the origin are obtained as

$$\delta_0 = \frac{bh}{USC_L}\frac{\partial\Phi_i}{\partial z} = \frac{bh}{8\pi}\sum_{-\infty}^{\infty}\sum{}' (j)\,\frac{m^2b^2 - n^2h^2}{(m^2b^2 + n^2h^2)^2} \quad (3.15)$$

and

$$\delta_1 = \frac{\beta bh^2}{USC_L}\frac{\partial^2\Phi_1}{\partial z\partial x} = \frac{bh^2}{8\pi}\sum_{-\infty}^{\infty}\sum{}' (j)\ \frac{m^2b^2 - 2n^2h^2}{(m^2b^2 + n^2h^2)^{5/2}}\ . \tag{3.16}$$

Theodorsen$^{3.6}$ derived expressions for the interference-upwash parameter δ_0 for the four types of rectangular tunnel. It was later remarked by Rosenhead (Ref.3.7; 1933) that the doubly infinite series of Equation (3.15) is not absolutely convergent. He therefore re-examined the problem rigorously and confirmed Theodorsen's result for types (1), (2) and (3), but not for type (4) having closed sides and open floor and roof. Van Schliestett (Ref.3.8; 1934) attempted to verify Theodorsen's values of δ_0 by experimental means and revealed serious discrepancies for a square tunnel of type (4); he likewise re-examined Theodorsen's work and gave a third expression for $\delta_0^{(4)}$ that differs from those of References 3.6 and 3.7, but is consistent with his experiment. A full theoretical discussion of this problem is given in Reference 3.9. An analytical treatment in Fourier series and an independent calculation by relaxation show that the correct result for $\delta_0^{(4)}$ is obtained when the summation (3.15) is carried out column by column (first with respect to n). However, Equations (3.13) and (3.15) are strictly divergent in this case. The image system fails, since the velocity gradient at the tunnel boundaries is satisfied, but not the upstream condition for undisturbed flow at $x = -\infty$. When this last condition is correctly applied, Rosenhead's rigorous analysis is reconciled with the others. Some expressions for δ_0 are given below.

For a completely closed rectangular tunnel

$$\delta_0 = \delta_0^{(1)} = \frac{\pi h}{24b} + \frac{\pi h}{b}\sum_{n=1}^{\infty}\frac{n}{e^{2\pi nh/b} + 1}\ .$$

For a completely open rectangular tunnel

$$\delta_0 = \delta_0^{(2)} = -\frac{\pi b}{24h} - \frac{\pi b}{h}\sum_{m=1}^{\infty}\frac{m}{e^{2\pi mb/h} + 1}$$

$$= -\frac{\pi h}{48b} - \frac{\pi h}{2b}\sum_{n=1}^{\infty}\frac{2n - 1}{e^{(2n-1)\pi h/b} - 1}\ . \tag{3.17}$$

For open sides, closed floor and roof

$$\delta_0 = \delta_0^{(3)} = -\frac{\pi h}{48b} + \frac{\pi h}{2b}\sum_{n=1}^{\infty}\frac{2n - 1}{e^{(2n-1)\pi h/b} + 1}\ .$$

For closed sides, open floor and roof

$$\delta_0 = \delta_0^{(4)} = -\frac{1}{4} + \frac{\pi h}{24b} - \frac{\pi h}{b}\sum_{n=1}^{\infty}\frac{n}{e^{2\pi nh/b} - 1}\ .$$

In Reference 3.9, Rosenhead's discrepancy in $\delta_0^{(2)}$ was resolved by the superposition of a uniform upwash velocity to restore undisturbed flow at $x = -\infty$ without violating the conditions (3.3). The streamline-curvature parameter δ_1 in Equation (3.16) is unaffected thereby; moreover, this doubly infinite series is seen to be absolutely convergent. To evaluate the series, we write

$$\delta_1 = \frac{h^2}{8\pi b^2}\left[2\sum_{m=1}^{\infty}(j)_{n=0}\left(\frac{1}{m^3}\right) + 2\sum_{n=1}^{\infty}\left\{\sum_{m=-\infty}^{\infty}(j)\,\frac{m^2 - 2(nh/b)^2}{[m^2 + (nh/b)^2]^{5/2}}\right\}\right]$$

and consider the summations in curly brackets. It can be shown that

$$\sum_{m=-\infty}^{\infty}\frac{m^2 - 2\lambda^2}{(m^2 + \lambda^2)^{5/2}} \quad \text{tends asymptotically to} \quad -\frac{2}{\lambda^2} \quad \text{when } \lambda \text{ is large.}$$

We therefore put

$$\begin{aligned} S_1(\lambda) &= \frac{2}{\lambda^2} + \sum_{m=-\infty}^{\infty}\frac{m^2 - 2\lambda^2}{(m^2 + \lambda^2)^{5/2}} \\ &= -16\pi^2\sum_{p=1}^{\infty}p^2K_0(2\pi p\lambda) - \frac{8\pi}{\lambda}\sum_{p=1}^{\infty}pK_1(2\pi p\lambda)^{*}, \qquad (3.18) \end{aligned}$$

which behaves like $-8\pi^2\lambda^{-\frac{1}{2}}e^{-2\pi\lambda}$ for large λ. Next we consider

$$\begin{aligned} S_2(\lambda) &= \sum_{m=-\infty}^{\infty}(-1)^m\frac{m^2 - 2\lambda^2}{(m^2 + \lambda^2)^{5/2}} \\ &= -S_1(\lambda) + \tfrac{1}{4}S_1(\tfrac{1}{2}\lambda), \qquad (3.19) \end{aligned}$$

which is identified with the derivative coefficient $f'(\lambda)$ of the function in Equation (A8) of the Appendix to Reference 3.10. When the appropriate values of j are substituted from Equations (3.14), δ_1 is obtained as follows.

For completely closed rectangular tunnels

$$\delta_1 = \delta_1^{(1)} = \frac{\pi}{24} + \frac{h^2}{4\pi b^2}\left[\sum_{m=1}^{\infty}\frac{1}{m^3} + \sum_{n=1}^{\infty}(-1)^n S_1\left(\frac{nh}{b}\right)\right].$$

For completely open rectangular tunnels

$$\delta_1 = \delta_1^{(2)} = \frac{h^2}{4\pi b^2}\left[\sum_{m=1}^{\infty}\frac{(-1)^m}{m^3} + \sum_{n=1}^{\infty}S_2\left(\frac{nh}{b}\right)\right]. \qquad (3.20)$$

---

[*] The functions K_0 and K_1 are defined and tabulated in "A Treatise on the Theory of Bessel Functions" by G.N.Watson (Cambridge University Press).

For open sides, closed floor and roof

$$\delta_1 = \delta_1^{(3)} = \frac{h^2}{4\pi b^2}\left[\sum_{m=1}^{\infty}\frac{(-1)^m}{m^3} + \sum_{n=1}^{\infty}(-1)^n S_2\left(\frac{nh}{b}\right)\right] . \qquad (3.20)$$

For closed sides, open floor and roof

$$\delta_1 = \delta_1^{(4)} = -\frac{\pi}{12} + \frac{h^2}{4\pi b^2}\left[\sum_{m=1}^{\infty}\frac{1}{m^3} + \sum_{n=1}^{\infty} S_1\left(\frac{nh}{b}\right)\right] .$$

Here

$$\sum_{m=1}^{\infty}\frac{1}{m^3} = 1.2020_5 \qquad \text{and} \qquad \sum_{m=1}^{\infty}\frac{(-1)^m}{m^3} = -0.9015_5 ;$$

$S_1(nh/b)$ from Equation (3.18) is evaluated in Table 3.II and $S_2(nh/b)$, given by Equation (3.19), is identically $f'(nh/b)$ from Table AI of Reference 3.10.

Glauert (Ref.3.1, pp.23 and 24) records numerous relationships between $\delta_0^{(1)}$, $\delta_0^{(2)}$, $\delta_0^{(3)}$ and $\delta_0^{(4)}$ regarded as functions of h/b, the most important of which is

$$\delta_0^{(1)}(h/b) + \delta_0^{(2)}(b/h) = 0 ; \qquad (3.21)$$

owing to the correction to Rosenhead's work, Equation (9.06) of Reference 3.1 becomes in the present notation

$$\delta_0^{(4)}(h/b) + \delta_0^{(4)}(b/h) = -0.25 \qquad (3.22)$$

with the corollary that $\delta_0^{(4)} = -0.125$ for a square tunnel. The following relationships between $\delta_1^{(1)}$, $\delta_1^{(2)}$, $\delta_1^{(3)}$ and $\delta_1^{(4)}$ are deduced from superposition of the image systems:

$$\left.\begin{aligned}
\delta_1^{(1)}(h/b) + \delta_1^{(3)}(h/b) &= \delta_1^{(1)}(\tfrac{1}{2}h/b)\\
\delta_1^{(1)}(h/b) + \delta_1^{(4)}(h/b) &= \tfrac{1}{2}\delta_1^{(4)}(2h/b)\\
\delta_1^{(2)}(h/b) + \delta_1^{(3)}(h/b) &= \tfrac{1}{2}\delta_1^{(2)}(2h/b)\\
\delta_1^{(2)}(h/b) + \delta_1^{(4)}(h/b) &= \delta_1^{(4)}(\tfrac{1}{2}h/b)
\end{aligned}\right\} . \qquad (3.23)$$

Special interest attaches to rectangular tunnels of types (2) and (4) in Chapter VI. The completely open tunnel is a limiting case of a tunnel with longitudinal slots on all four walls (Section 6.5.4): similarly, type (4) is a limiting case of rectangular tunnels with slotted floor and roof (Section 6.5.3). Figure 3.2 gives all the lift interference parameters of Equations (3.17) and (3.20) for the range of tunnel shape $0.5 \leq h/h \leq 2.0$.

If, however, a lifting model is displaced vertically from the centre of the tunnel, there arise both streamwise and upward interference velocities. For a completely closed tunnel with the model (and origin of co-ordinates) at a distance d from the floor, the interference potential corresponding to Equation (3.13) is

$$\Phi_i = \sum_{-\infty}^{\infty}\sum{}'(j)\,\frac{USC_L(z-\zeta)}{8\pi\{(y-mb)^2+(z-\zeta)^2\}}\left[1+\frac{x}{\{x^2+\beta^2(y-mb)^2+\beta^2(z-\zeta)^2\}^{\frac{1}{2}}}\right],$$

$$\left.\begin{aligned}\text{where}\quad j &= +1 \quad \text{with}\quad \zeta = 2nh \quad \text{and all integral pairs } (m,n) \text{ except } (0,0)\\ j &= -1 \quad \text{with}\quad \zeta = 2(nh-d) \quad \text{and all integral pairs } (m,n)\end{aligned}\right\}.$$

Then the upwash and stream-velocity interference at the model are respectively

$$\left.\begin{aligned}\delta_0 &= \frac{C}{USC_L}\frac{\partial\Phi_i}{\partial z} = \frac{bh}{8\pi}\sum_{-\infty}^{\infty}\sum{}'(j)\,\frac{m^2b^2-\zeta^2}{(m^2b^2+\zeta^2)^2}\\ \frac{C\epsilon}{SC_L} &= \frac{C}{USC_L}\frac{\partial\Phi_i}{\partial x} = \frac{bh}{8\pi\beta}\sum_{-\infty}^{\infty}\sum{}'(j)\,\frac{-\zeta}{(m^2b^2+\zeta^2)^{3/2}}\end{aligned}\right\}, \tag{3.24}$$

where in the latter equation the terms involving j = +1 cancel. Since

$$\sum_{m=-\infty}^{\infty}\frac{m^2-\lambda^2}{(m^2+\lambda^2)^2} = -\pi^2\,\mathrm{cosech}^2(\pi\lambda),$$

we obtain

$$\begin{aligned}\delta_0 = {} & \frac{\pi h}{24b}+\frac{\pi h}{8b}\,\mathrm{cosech}^2\left(\frac{2\pi d}{b}\right) + \\ & +\frac{\pi h}{8b}\sum_{n=1}^{\infty}\left\{\mathrm{cosech}^2\frac{2\pi(nh+d)}{b}+\mathrm{cosech}^2\frac{2\pi(nh-d)}{b}-2\,\mathrm{cosech}^2\frac{2\pi nh}{b}\right\}.\end{aligned} \tag{3.25}$$

Similarly to Equation (3.18), we put

$$S_3(\lambda) = -\frac{2}{\lambda}+\sum_{m=-\infty}^{\infty}\frac{\lambda}{(m^2+\lambda^2)^{3/2}} = 8\pi\sum_{p=1}^{\infty}pK_1(2\pi p\lambda). \tag{3.26}$$

It then follows from the second of Equations (3.24) that

$$\begin{aligned}\frac{\beta C\epsilon}{SC_L} &= \frac{h}{8\pi b}\left[\sum_{n=-\infty}^{\infty}\frac{b}{nh-d}+\sum_{n=-\infty}^{\infty}S_3\left(\frac{2(nh-d)}{b}\right)\right]\\ &= -\frac{1}{8}\cot\frac{\pi d}{h}+\frac{h}{8\pi b}\sum_{n=-\infty}^{\infty}S_3\left(\frac{2(nh-d)}{b}\right).\end{aligned} \tag{3.27}$$

Equations (3.25) and (3.27) with (3.26) have been evaluated for b/h = 0.5, 1.0 and 2.0, and both interference parameters are plotted against d/h in Figure 3.3. For example, if b/h = 2.0 and the model is displaced from the central position d = 0.5h to d = 0.625h, then the upwash interference is increased by 24%. The corresponding contribution to the stream velocity at the model is given by

$$\frac{\delta U}{U} = \epsilon = 0.095\,\frac{SC_L}{\beta C},$$

which could exceed the solid-blockage factor ϵ_s (Section 5.2.3).

3.2.3 Non-Rectangular Tunnels

Many closed working sections are of basic rectangular shape, but have triangular corner fillets. Batchelor (Ref.3.11; 1944) devised an image system to obtain δ_0 when the fillets are isosceles. As illustrated in Figure 3.1(c), the fillets and their images form a doubly infinite array of squares. To the image system for a closed rectangular tunnel in Figure 3.1(b) can be added an appropriate distribution of vorticity round the perimeter of each square, so as to cancel the normal velocity across the fillets and preserve the other boundaries as streamlines. Batchelor's method provides a good approximation to this, and his formulae for a particular tunnel have been generalized in Reference 3.12. By a conformal transformation, Gent (Ref.3.13; 1944) obtains δ_0 exactly for a closed tunnel of regular octagonal section. These theories are outlined in more detail in Section 3.4.2, where wings of finite span are considered. The interference upwash is increased by the presence of the fillets, but the increment is only about half that which would arise if w_i were inversely proportional to the cross-sectional area C The parameter δ_0 of Equation (3.9) is therefore reduced by the fillets. An approximate formula, suggested in Appendix II of Reference 3.4, gives

$$\delta_0 = \delta_0^{(1)}\,\frac{bh + C}{2bh}, \tag{3.28}$$

where $\delta_0^{(1)}$ is the value for a closed rectangular tunnel in the first of Equations (3.17). The results of References 3.11 to 3.13 indicate the likely accuracy of this formula as follows.

Tunnel	$\frac{C}{bh}$	*Theory*		$\delta_0^{(1)}$	*Equation (3.28)*
		Ref.	δ_0		
9 × 7 (Melbourne)	0.9028	3.11	0.1138	0.1204	0.1145
9 × 7 (NPL)	0.9048	3.12	0.1140	0.1204	0.1147
13 × 9 (NPL)	0.8932	3.12	0.1125	0.1191	0.1127
Regular octagon	0.8284	3.13	0.1262	0.1368	0.1251

The uncertainty in the decrement $(\delta_0^{(1)} - \delta_0)$ is of the order ±10%, but δ_0 itself is within ±1%. When the corner fillets are scalene, the squares of Figure 3.1(c) become rhombuses and Batchelor's approach is found to be less satisfactory. In such cases Equation (3.28) may continue to be a useful guide.

Conformal transformations from the (y,z) plane can simplify the boundary conditions (3.12) and in effect reduce the problem of evaluating δ_c to one having a simple image system. Examples are the Schwarz-Christoffel theorem whereby Gent[3.13] transforms the interior of the regular octagon into a half plane, the bipolar co-ordinates whereby Kondo[3.14] investigates tunnels with boundaries of circular arcs, and the simple transformation whereby Glauert (Ref.3.1, p.32) relates elliptical and rectangular boundaries.

In this last instance δ_0 for closed or open elliptical tunnels is reduced to double summations similar to Equation (3.15). In the present notation Glauert gives for a small wing in a closed elliptical tunnel

$$\left.\begin{aligned} \delta_0 &= \tfrac{1}{2} \sinh\theta \cosh\theta \sum_{p=1}^{\infty} \frac{2p-1}{e^{2\theta(2p-1)}+1} \\ &= \tfrac{1}{8} \sinh\theta \cosh\theta \left[\frac{\pi^2}{24\theta^2} + \frac{1}{6} - \frac{\pi^2}{\theta^2} \sum_{p=1}^{\infty} \frac{2p-1}{e^{(2p-1)\pi^2/2\theta}+1}\right] \end{aligned}\right\}, \qquad (3.29)$$

where b/h = coth $\theta \geqslant 1$; numerical values of δ_0 due to Sanuki are published in the Appendix to Reference 3.14. When the wing span lies along the minor axis of the ellipse, there are corresponding expressions from Equations (10.05) of Reference 3.1;

$$\left.\begin{aligned} \delta_0 &= \tfrac{1}{2} \sinh\theta \cosh\theta \sum_{p=1}^{\infty} \frac{2p-1}{e^{2\theta(2p-1)}-1} \\ &= \tfrac{1}{8} \sinh\theta \cosh\theta \left[\frac{\pi^2}{12\theta^2} - \frac{1}{6} + \frac{\pi^2}{\theta^2} \sum_{p=1}^{\infty} \frac{2p}{e^{p\pi^2/\theta}+1}\right] \end{aligned}\right\}, \qquad (3.30)$$

where b/h = tanh $\theta < 1$. The second of Equations (3.29) or (3.30) is rapidly convergent, unless the ellipse approaches very closely to a circle. In the limit as $\theta \to \infty$, the first of Equations (3.29) or (3.30) tends to the result $\delta_0 = 0.125$ for a closed circular tunnel and is consistent with the image system of Figure 3.1(a). Results for open elliptical tunnels follow from Glauert's interference theorem; as expressed in Equation (3.21), δ_0 has the same magnitude, but opposite sign, as that in a closed elliptical tunnel of height b and breadth h .

To the accuracy envisaged in Section 3.2.1 for fairly small models, it is considered satisfactory to assume that the ratio of $\beta \partial w_1/\partial x$ to $w_1/\sqrt{C}$ is the same as for a rectangular tunnel of the same breadth to height ratio, completely closed or completely open as the case may be. Thus we approximate to δ_1 by the formula

$$\delta_1 = \delta_0 \sqrt{\frac{bh}{C}} \frac{\delta_1^{(1)}}{\delta_0^{(1)}} \quad \text{or} \quad \delta_0 \sqrt{\frac{bh}{C}} \frac{\delta_1^{(2)}}{\delta_0^{(2)}} , \tag{3.31}$$

where $\delta_0^{(1)}$, $\delta_0^{(2)}$, $\delta_1^{(1)}$, $\delta_1^{(2)}$ are given in Equations (3.17) and (3.20). The ratios $\delta_1^{(1)}/\delta_0^{(1)}$ and $\delta_1^{(2)}/\delta_0^{(2)}$ are plotted against b/h in Figure 3.4. The values $\delta_1 = 0.248$ and -0.209 so obtained for closed and open circular tunnels are acceptably close to the respective exact values $\delta_1 = 0.2497$ and -0.1992 computed from Equations (3.136) and (3.137) of Section 3.4.3 and shown in Figure 3.5. The lift interference parameters δ_0 and δ_1 for closed and open elliptical tunnels can thus be calculated from Equations (3.29) to (3.31) and are given in Figure 3.5 for the range of shape $0.5 \leqslant b/h \leqslant 2.0$. Equations (3.28) and (3.31) combine to provide a rough formula

$$\delta_1 = \delta_1^{(1)} \frac{bh + C}{2\sqrt{bhC}} \approx \delta_1^{(1)} \tag{3.32}$$

for small wings in closed octagonal tunnels, $\delta_1^{(1)}$ being given by the full curve against b/h in the lower panel of Figure 3.2.

Generally speaking, the problem of lift interference in wind tunnels having partly closed and partly open boundaries is more complex. Tunnels with slotted walls (Chapter VI) and open-jet tunnels of finite length are cases in point. The latter problem is considered in Part III of Reference 3.5 by Eisenstadt, who gives a solution for a circular tunnel involving expansions in Bessel functions. In this particular problem the linearized condition in Equation (3.3) for constant pressure on the open boundary must in general be replaced by

$$\partial\Phi/\partial x = U + u \qquad (u \neq 0),$$

to achieve continuity of velocity at the lip of the closed entrance nozzle. However $u = 0$ in the special case of a small model situated on the axis of the tunnel, and numerical results are obtained by satisfying the boundary condition at ten points along the free surface. The distribution of interference upwash along the tunnel axis is reproduced in Figure 3.6 for a jet length $l = 3R$ with the wing at various distances x_0 downstream of the entrance nozzle, the broken portion of each curve corresponding to the extent of the open boundary. Provided $R \leqslant x_0 \leqslant (l - R)$, the corrections at the model $(x = 0)$ are essentially those for an infinitely long open jet, but the streamline-curvature parameter δ_1 may only apply over a restricted axial distance. As x_0 decreases below R, the upwash-interference parameter δ_0 changes rapidly towards the average (zero in this case) of that for an open tunnel and that for a closed tunnel. The greatest streamline curvature occurs in the region of the collector $x = (l - x_0)$.

For tunnels of infinite length, Kondo[3.18] has obtained exact values of δ_0 in two particular cases of mixed boundaries, namely semi-closed tunnels of circular and arch-shaped sections. Kondo's examples serve to illustrate an interesting general theorem proposed by Glauert[3.7]:

> "The interference on a very small aerofoil in a tunnel, whose boundaries are partly rigid walls and partly free surfaces, is of the same magnitude,

> but opposite in sign, as that on the same aerofoil rotated through a right angle in a tunnel of the same shape as the previous one but where rigid walls replace free surfaces, and free surfaces replace rigid walls."

Glauert has proved a corresponding theorem for completely open tunnels, of which Equation (3.21) is a special case. In the notation of Section 3.2.2, consequences of the general theorem are that

$$\left.\begin{aligned} \delta_0^{(3)}(h/b) + \delta_0^{(3)}(b/h) &= 0 \\ \delta_0^{(4)}(h/b) + \delta_0^{(4)}(b/h) &= 0 \end{aligned}\right\} ;$$

the former is true, but the latter conflicts with Equation (3.22) and is false. The present author[3.15] has recently proved the theorem for a wing arbitrarily placed in any tunnel having one closed portion and one open portion, as is true of Kondo's examples; apart from an additive constant, the interference velocity potential of the first half of the theorem can be identified with the interference stream function of the second half. With the exception of rectangular tunnels of type (3) having open side-walls and closed floor and roof, the proof cannot be extended to tunnels whose boundaries consist of two closed and two open portions.

3.2.4 Applications

The values of δ_0 and δ_1, discussed in Sections 3.2.2 and 3.2.3, will often suffice for the purpose of rapid estimates of tunnel wall interference. Equations (3.6) give the corrections to the measured incidence and drag of a small model. Although streamline curvature does not normally influence the latter correction, it does introduce a variation in the interference upwash

$$\frac{w_1}{U} = \left(\delta_0 + \frac{x}{\beta h}\delta_1\right)\frac{SC_L}{C} \qquad (3.33)$$

along the centre line of a wing. The first term of Equation (3.33) is equivalent to a lift coefficient

$$(\delta C_L)_0 = \delta_0 \frac{SC_L}{C}\frac{\partial C_L}{\partial \alpha} \quad \text{acting at the centre of lift} \quad x = 0 ;$$

the second term contributes an increment in lift coefficient

$$(\delta C_L)_1 = \frac{\lambda \bar{c}\delta_1}{2\beta h}\frac{SC_L}{C}\frac{\partial C_L}{\partial \alpha} \quad \text{acting at some position} \quad x = x_1 .$$

where λ and x_1 are to be determined.

The correction $\Delta\alpha$ is a somewhat arbitrary average value of w_1/U over the planform. We may simply take

$$\left.\begin{aligned}\Delta\alpha &= \delta_0\frac{SC_L}{C}\\ \Delta C_L &= -\frac{\lambda\bar{c}\delta_1}{2\beta h}\frac{SC_L}{C}\frac{\partial C_L}{\partial\alpha}\\ \Delta C_m &= \frac{\lambda x_1\delta_1}{2\beta h}\frac{SC_L}{C}\frac{\partial C_L}{\partial\alpha}\end{aligned}\right\} . \qquad (3.34)$$

where C_m is referred to an axis through the uncorrected centre of lift. But it is often more convenient to choose $\Delta\alpha$ such that there is no residual correction to lift. If

$$\Delta\alpha = \left(\delta_0 + \frac{\lambda\bar{c}}{2\beta h}\delta_1\right)\frac{SC_L}{C} , \qquad (3.35)$$

then the residual interference upwash $(w_1/U) - \Delta\alpha$ gives rise to increments in lift coefficient

$$\left.\begin{aligned}(\delta C_L)_c - \Delta\alpha\frac{\partial C_L}{\partial\alpha} &= -(\delta C_L)_1 \quad \text{acting at} \quad x = 0\\ (\delta C_L)_1 &= \frac{\lambda\bar{c}\delta_1}{2\beta h}\frac{SC_L}{C}\frac{\partial C_L}{\partial\alpha} \quad \text{acting at} \quad x = x_1\end{aligned}\right\} .$$

Together these give zero lift, but a pure couple or pitching moment coefficient

$$\delta C_m = -\frac{x_1}{\bar{c}}(\delta C_L)_1$$

which has to be subtracted from the measured C_m to give a residual correction

$$\Delta C_m = \frac{x_1}{\bar{c}}(\delta C_L)_1 = \frac{\lambda x_1\delta_1}{2\beta h}\frac{SC_L}{C}\frac{\partial C_L}{\partial\alpha} \qquad (3.36)$$

independent of pitching axis. As in the second of Equations (3.6) the correction to the drag coefficient is

$$\Delta C_D = \delta_0\frac{SC_L^2}{C} . \qquad (3.37)$$

Any residual correction to spanwise loading would involve a correction to drag, but this is usually ignored.

It is sometimes suggested, by analogy with two-dimensional models, that $\lambda = 1$ and $x_1 = (1/8)\bar{c}$. When the wing is regarded as a three-dimensional lifting surface, both λ and x_1 usually take larger values. On the approximate basis of strip theory, in which each streamwise section of a wing is treated as if the flow were two-dimensional,

$$\left.\begin{aligned} \lambda &= \int_0^1 \left(\frac{c}{\bar{c}}\right)^2 d\left(\frac{y}{s}\right) = \frac{\bar{\bar{c}}}{\bar{c}} \\ \frac{\lambda x_1}{\bar{c}} &= \frac{1}{8}\left(\frac{\bar{\bar{c}}}{\bar{c}}\right)^2 + \frac{1}{24}(A \tan \Lambda_{0.5})^2 \left(2 - \frac{\bar{\bar{c}}}{\bar{c}}\right) \end{aligned}\right\} ; \tag{3.38}$$

where $A = 2s/\bar{c}$ is the aspect ratio of the wing and $\Lambda_{0.5}$ is its midchord sweepback (assumed constant). Thus λx_1 would vary from $(1/8)\bar{c}$ for rectangular wings and $(1/3)\bar{c}$ for delta wings to larger values for some wings with sweptback trailing edges. The interference corrections resulting from Equations (3.35) to (3.38) are

$$\left.\begin{aligned} \Delta\alpha &= \left(\delta_0 + \frac{\bar{\bar{c}}\delta_1}{2\beta h}\right)\frac{SC_L}{C} \\ \Delta C_D &= \delta_0 \frac{SC_L^2}{C} \\ \Delta C_m &= \frac{\bar{c}\delta_1}{16\beta h}\left[\left(\frac{\bar{\bar{c}}}{\bar{c}}\right)^2 + \frac{1}{3}(A \tan \Lambda_{0.5})^2 \left(2 - \frac{\bar{\bar{c}}}{\bar{c}}\right)\right] \frac{SC_L}{C}\frac{\partial C_L}{\partial \alpha} \end{aligned}\right\} . \tag{3.39}$$

where $\bar{\bar{c}}$ is given in Equation (3.38); the terms involving δ_1 are approximate, the values of λ and x_1 from Equations (3.38) being poor substitutes for values from lifting-surface theory.

Typical theoretical values of λ and $\lambda x_1/\bar{c}$ are compared with the corresponding values from Equations (3.38) in Table 3.III. Apart from rectangular wings and some slender wings, $\bar{\bar{c}}/\bar{c}$ lies within 16% of the appropriate theoretical value of λ. The accuracy of strip theory for various planforms is illustrated for a range of leading-edge sweepback Λ_L in Figure 3.7, which suggests that $\bar{\bar{c}}/\bar{c}$ is likely to overestimate or underestimate λ according as $A \tan \Lambda_L$ is greater or less than about 3. Table 3.III shows the unreliability of the Equation (3.38) for $\lambda x_1/\bar{c}$; typically it is low by a factor of order 2 for wings without trailing-edge sweepback, whatever the taper parameter $c_r/\bar{c}$, but rather too large for wings of high trailing-edge sweepback. Whilst the residual correction ΔC_m is usually fairly small, it seems difficult to estimate without recourse to lifting-surface theory. Nevertheless, Table 3.III gives some guidance for uniformly tapered wings.

The interference upwash at the tail of a complete aircraft model may be estimated from Equation (3.33). This early application was made by Glauert and Hartshorn (Ref.3.16; 1924); after a correction $\Delta\alpha$ is made to incidence, there remains a residual correction to tailsetting

$$\Delta\alpha_t = \frac{x_t\delta_1}{\beta h}\frac{SC_L}{C} . \tag{3.40}$$

where x_t is approximately the distance between the centroids of the wing and tail surfaces. This will often be quite large and rather inaccurate. For example, in a closed circular tunnel with $x_t = R$ and $\beta = 1$, Equation (3.40) gives

$$\frac{\pi R^2}{SC_L}\Delta\alpha_t = 0.125$$

as compared with the correct value 0.099 from the full curve of Figure 3.6.

In practice the formulae (3.39) and (3.40) may be of more use in open than in closed tunnels, since it is inadvisable to test large models in open tunnels. The free boundaries of the jet will distort and spillage may occur at the collector downstream of the model (Section 2.5.4); for such reasons the more accurate interference corrections for large models become unreliable. In closed tunnels, however, the more accurate interference corrections will often be reliable and yet differ appreciably from those for small models on account of either large span or large chord. Present formulae for δ_0 will give accuracy within about 10%, provided that the wing span does not exceed half the tunnel height or breadth, i.e., $\sigma < \frac{1}{2}h/b$ and $\sigma < \frac{1}{2}$. These conditions will often be satisfied for slender models, when the chord length becomes a limiting factor. However, Equation (3.33) is a useful approximation to the more exact analysis considered in Section 3.6.1.

Half-models mounted on the side-wall of a tunnel are treated as complete wings in a tunnel of twice the area with the side-wall as reflection plane (Section 3.4.4). In view of the great difficulty in obtaining δ_1 for non-rectangular configurations, it may be expedient to use the simple formula of Equation (3.31) in conjunction with a mean value of δ_0 appropriate to the span of the model. The corrections to measured quantities in either Equations (3.34) or Equations (3.35) to (3.39) may then suffice.

3.3 GENERAL THEORY OF LIFT INTERFERENCE

In general the formulations of Section 3.2 will be too approximate. When the wing is large, there are many different approaches to the evaluation of interference upwash depending mainly on the representation of the model (Section 3.3.1). The choice of vortex model will be influenced by aspect ratio, sweepback and yaw of the wing, the symmetry or asymmetry of its spanwise lift distribution and by the availability of tabulated interference parameters for any particular tunnel (Section 3.4).

In Section 3.3.2, the interference parameters are defined for different basic types of model, irrespective of tunnel cross-section. General expressions for the distribution of interference upwash are then derived. The procedures for converting such distributions into corrections to measured quantities are far from standardized. Section 3.3.3 summarizes the general approach to this problem. The various cases are then classified according to the degree of symmetry about the centre line. Sections 3.3.4 to 3.3.6 summarize approximate formulae for the final lift interference corrections relating to complete and half-wing models.

3.3.1 Representation of Model

In problems of two-dimensional lift interference it may occasionally be desirable to represent the model precisely as a thin aerofoil is represented in classical theory. The same only remains true in three dimensions in the case of unswept wings of high aspect ratio to which the classical lifting-line theory applies. As illustrated in

Figure 3.8(a), an elementary strip of the wing (δy) having circulation Γ is represented by a trailing vortex element of strength $-(d\Gamma/dy)\delta y$. At the other extreme, a slender wing can be divided into elementary strips (δx) supporting a lift $\delta L = (dL/dx)\delta x$. The lift interference (Section 3.6.1) is regarded as that due to a distribution of trailing vortex pairs of doublet strength $\delta L/\rho U$ along the centre line; Figure 3.8(b) is the generalization of the representation of a small wing in Section 3.2.1. Thus even a slender wing is replaced by a simpler vortex model than that used in the corresponding free-stream theory.

This is still more evident for a general planform, as a complete vortex sheet is needlessly complicated. It is desirable to let the vortex model depend upon as many of the aerodynamic characteristics as are measured or can be estimated easily. Figure 3.8 includes three typical representations, but there is no universal opinion as to which is best. In Reference 3.17, Acum uses in effect a lifting line through the local chordwise centres of pressure with the appropriate trailing vorticity. The same model is used in Reference 3.18 for wings with asymmetrical spanwise loading, but it is then desirable to split the loading into its symmetrical and antisymmetrical parts, as indicated in Figures 3.8(c) and (d). Eisenstadt (Ref.3.19; 1947) uses discrete vortices in the form of swept uniformly loaded lifting lines, while Katzoff and Hannah (Ref.3.20; 1948) use point concentrations of lift, each representing a portion of the wing. These two vortex models, illustrated in Figures 3.8(e) and (f), are more adaptable, being readily applied to yawed wings.

It is sometimes sufficient to replace a trailing vortex sheet by a single vortex pair. By expanding the velocity field of the trailing vortex sheet in inverse powers of the lateral distance, Loos (Ref.3.21; 1951) derives the equivalent semi-span s_e and vortex strength K_e, such that

$$\left.\begin{aligned} K_e s_e &= -\int_0^s \frac{d\Gamma}{dy}\, y\, dy = \int_0^s \Gamma\, dy \\ K_e s_e^3 &= -\int_0^s \frac{d\Gamma}{dy}\, y^3\, dy = 3\int_0^s \Gamma y^2\, dy \end{aligned}\right\}. \qquad (3.41)$$

To a useful approximation a horse-shoe vortex of strength K_e and semi-span s_e gives the same interference upwash distribution as the unswept lifting line of Figure 3.8(a). For elliptic spanwise loading $s_e/s = \frac{1}{2}\sqrt{3}$. Since the interference upwash has to be averaged over the complete span, it may be expedient to replace the wing by a uniformly loaded one of semi-span slightly greater than s_e. In this respect Swanson and Toll (Ref.3.22; 1943) have suggested that for their particular application the effective span ratios $s_e/s = 0.93$, 0.88 and 0.83 may be used for wings of taper ratios $c_t/c_r = 1$, 0.5 and 0.25 respectively.

Certain types of model may require more complicated representation. Consideration of tail-plane interference and wing-body combinations will be deferred until Section 3.6.2. Wings with deflected control surfaces may be treated by the procedure suggested in Section 4.5 of Reference 3.4. Basically this amounts to the superposition of discrete elements of the type in Figure 3.8(e). The introduction of control surfaces affects the loci of the lifting lines in Figures 3.8(c) and (d), but otherwise leaves models (a) to (d) unchanged. Model (f) might well call for greater subdivision of the wing, but would serve for symmetrical and asymmetrical loading alike.

3.3.2 Basic Interference Parameters

In the first place the wing and its load distribution are supposed to be symmetrical about the vertical plane through the axis of the tunnel. The vortex models of the wing in Figures 3.8(a) and (c) can be constructed by superposition of symmetrically placed horse-shoe vortices of strength K and semi-span t. The interference upwash angle in the plane of the wing is then expressed as

$$\frac{w_i}{U} = \frac{4Kt}{UC}\left\{\delta_0(y,t) + \frac{x}{\beta h}\,\delta_1(y,t) + O\left(\frac{x}{\beta h}\right)^3\right\}, \qquad (3.42)$$

where, as in Acum's[3.17] theory, $\delta_0(y,t)$ and $\delta_1(y,t)$ are functions to be determined for a particular tunnel (Section 3.4) and terms involving the third and higher powers of $x/\beta h$ are neglected. Equation (3.42) is a generalization of Equation (3.33) for a small wing; both δ_0 and δ_1 may be regarded as also dependent on any vertical displacement of the wing from the tunnel axis.

The well known theorem of Prandtl shows that, in the limit as $x \to \infty$, Equation (3.42) becomes

$$\frac{w_i}{U} = \frac{4Kt}{UC}\{2\delta_0(y,t)\},$$

which may be calculated on a two-dimensional basis. Thus, if the chordwise extent of the model is small, as envisaged in Figure 3.8(a), δ_1 may be neglected and for certain tunnels the expressions for w_i/U are quite simple. Sanders and Pounder[3.23, 3.24] exploit this for closed rectangular tunnels on the basis of lifting-line theory. For an untwisted, uncambered wing at incidence, lifting-line theory yields the simple result in Equations (3.6) and (3.7) with the mean interference parameter

$$\delta_0 = \frac{1}{L_F}\int_{-s}^{s}\left(\frac{w_i}{U}\,\frac{C}{SC_L}\right)\frac{dL_F}{dy}\,dy, \qquad (3.43)$$

where dL_F/dy denotes the lift per unit span in free air. For a uniformly loaded wing it is particularly easy to obtain

$$(\delta_0)_U = \int_0^1 \delta_0(y,s)\,d\left(\frac{y}{s}\right). \qquad (3.44)$$

Alternatively $(\delta_0)_U$ is given directly by the two-dimensional solution in the transverse plane for the interference stream function Ψ_i corresponding to Φ_i, since

$$(\delta_0)_U = \frac{C}{sC_L}\int_0^1 \frac{w_i}{U}\, d\left(\frac{y}{s}\right) = -\frac{C}{sC_L}\int_0^1 \frac{1}{U}\frac{\partial\Psi_i}{\partial y}\, d\left(\frac{y}{s}\right)$$

$$= \frac{C}{UsC_L s}\,[\Psi_i]_{y=s}^{y=0} \; ; \tag{3.45}$$

in practice s would be replaced by a reduced effective semi-span, as discussed in Section 3.3.1. A better approximation is to assume that the spanwise loading is elliptic over the full span, when Equation (3.43) becomes

$$(\delta_0)_E = \frac{4}{\pi}\int_0^1 \left(\frac{w_i}{U}\frac{C}{sC_L}\right)\left\{1 - \left(\frac{y}{s}\right)^2\right\}^{\frac{1}{2}} d\left(\frac{y}{s}\right) , \tag{3.46}$$

where
$$\frac{w_i C}{UsC_L} = \frac{4}{\pi}\int_0^1 \delta_0(y,t)\left(\frac{t}{s}\right)^2\left\{1-\left(\frac{t}{s}\right)^2\right\}^{-\frac{1}{2}} d\left(\frac{t}{s}\right) .$$

This has been calculated for a wide range of tunnels (Section 3.4).

For sweptback wings of moderate aspect ratio the interference upwash due to the vortex model of Figure 3.8(c) is readily expressed in terms of $\delta_0(y,t)$ and $\delta_1(y,t)$. Following Reference 3.17, we replace the elementary vortices by a horseshoe vortex of strength Γ and semi-span $(t + \delta t)$ together with one of strength $-\Gamma$ and semi-span t . Hence

$$\frac{\delta w_i}{U} = \frac{4\Gamma}{UC}\left[\frac{\partial}{\partial t}\{t\delta_0(y,t)\} + \frac{x-\bar{x}}{\beta h}\frac{\partial}{\partial t}\{t\delta_1(y,t)\}\right]\delta t ,$$

where $x = \bar{x}(t)$ is the curve through the local centres of pressure. Integration over the span of the wing $-s \leqslant t \leqslant s$ gives

$$\frac{w_i}{U} = \int_0^1 \frac{4\Gamma s}{UC}\left[\frac{\partial}{\partial t}\{t\delta_0(y,t)\} + \frac{x-\bar{x}(t)}{\beta h}\frac{\partial}{\partial t}\{t\delta_1(y,t)\}\right] d\left(\frac{t}{s}\right) ; \tag{3.47}$$

for elliptic spanwise loading Equation (3.47) becomes

$$\frac{w_i}{U} = \frac{4sC_L}{\pi C}\int_0^1\left[\left[\frac{\partial}{\partial t}\{t\delta_0(y,t)\} + \frac{x-\bar{x}(t)}{\beta h}\frac{\partial}{\partial t}\{t\delta_1(y,t)\}\right]\right]\left\{1 - \frac{t^2}{s^2}\right\}^{\frac{1}{2}} d\left(\frac{t}{s}\right) , \tag{3.48}$$

as obtained in Equation (20) of Reference 3.4.

If the model remains symmetrically situated but its spanwise loading is asymmetrical, then the load distribution can be split into symmetrical and antisymmetrical portions represented by the vortex models (c) and (d) of Figure 3.8. In Reference 3.18 (Garner and Acum; 1953), the symmetrical part of the interference is obtained in the form of Equation (3.47). In addition to Equation (3.42) we now define

$$\frac{w_i}{U} = \frac{4Kt}{UC}\left\{\kappa_0(y,t) + \frac{x}{\beta h}\kappa_1(y,t) + O\left(\frac{x}{\beta h}\right)^2\right\} \qquad (3.49)$$

as the interference upwash angle due to a pair of asymmetrically placed horse-shoe vortices, one of strength $-K$ and span $-t < y < 0$ and the other of strength K and span $0 < y < t$. It then follows that, corresponding to Figure 3.8(d),

$$\frac{w_i}{U} = \int_0^1 \frac{4\Gamma s}{UC}\left[\frac{\partial}{\partial t}\{t\kappa_0(y,t)\} + \frac{x-\bar{x}(t)}{\beta h}\frac{\partial}{\partial t}\{t\kappa_1(y,t)\}\right] d\left(\frac{t}{s}\right), \qquad (3.50)$$

an antisymmetrical function of y in which Γ and $\bar{x}(t)$ refer to the antisymmetrical portion of the wing loading. This approach to wall interference demands the tabulation of the basic parameters

$$\frac{\partial}{\partial t}\{t\,\delta_0(y,t)\}, \quad \frac{\partial}{\partial t}\{t\delta_1(y,t)\}, \quad \frac{\partial}{\partial t}\{t\kappa_0(y,t), \quad \frac{\partial}{\partial t}\{t\kappa_1(y,t)\},$$

which can be evaluated fairly easily for rectangular tunnels (Section 3.4.1). There is no equivalent procedure for asymmetrically situated wings.

The more flexible method of Katzoff and Hannah in Reference 3.20 uses point sources of lift, which are considered to lie in the horizontal plane through the centre line of the tunnel. As indicated in Figure 3.8(f), it is necessary to segment the wing and to estimate the lift L_N and its centroid (x_N, y_N) on each segment. The total interference upwash is obtained as

$$\frac{w_i}{U} = \sum_N \frac{L_N}{\rho U^2 b^2}\, w_i\left(\frac{x-x_N}{\beta b}, \frac{y}{b}, \frac{y_N}{b}\right), \qquad (3.51)$$

where b is the breadth or some typical length of the tunnel cross-section. In general, charts of

$$w_i\left(\frac{x-x_N}{\beta b}, \frac{y}{b}\right)$$

must be constructed for a series of spanwise locations of the doublet $L_N/\rho U$. For rectangular tunnels, however, the function w_i can be defined by two charts independent of y_N/b.

Both the foregoing procedures for sweptback wings are economical as regards the basic computations for any particular tunnel cross-section. Both imply some knowledge of the lift distribution; Γ and $\bar{x}$ in Equation (3.47) or (3.50) are normally obtained by lifting-surface theory, while L_N and (x_N, y_N) in Equation (3.51) must be estimated likewise. The former procedure of Reference 3.18 neglects terms of order $[(x-\bar{x})/\beta h]^3$ and is restricted to unyawed wings. These limitations do not apply to that of Reference 3.20, which suffers from the inaccuracies of a graphical method and the poorer representation of the model. Between these two extremes are the intermediate schemes of References 3.19 and 3.25, which apply to closed circular and rectangular tunnels respectively. For each half of the vortex model of Figure 3.8(e) Eisenstadt tabulates, in the present notation,

$$\frac{4Cw_i}{Kt} \quad \text{as a function of} \quad \frac{2x}{\beta b}, \frac{2y}{b}, \frac{2t}{b} \quad \text{and} \quad \cot^{-1}(\beta \cot \Lambda) ,$$

the last parameter being the equivalent sweepback angle of the bound vortex line (Table 3.I). Swanson's approach in Reference 3.25 is for a particular model, but it would in general involve the non-dimensional interference upwash in terms of the same four parameters. These schemes are more cumbersome than the three-parameter system of Equation (3.51) or the two-parameter system of Equation (3.47). On the other hand Katzoff and Hannah have pointed out in Figure 9 of Reference 3.20, that a series of calculations for one sweep angle may suffice for computing the wall interference on a wing of different sweep.

3.3.3 Corrections to Measured Quantities

We first suppose that a suitable vortex model of the wing may be identified with some theoretical approximation to the non-dimensional wing loading $l_F(x,y)$ in the free stream. The basic interference parameters then determine an upwash angle $\delta\alpha(x,y)$ from which an equivalent incremental loading $\delta l(x,y)$ may be computed theoretically; this introduces additions to be superposed on the vortex model. The procedure may then be repeated to obtain the corresponding $\delta^2\alpha$ and $\delta^2 l$, and so on until the final theoretical picture gives distributions of load and interference upwash

$$\left.\begin{aligned} l_T &= l_F + \delta l + \delta^2 l + \dots \\ w_i/U &= \delta\alpha + \delta^2\alpha + \delta^3\alpha + \dots \end{aligned}\right\}$$

in the tunnel. For many reasons l_T will not be identical to the measured distribution l, and there will be inevitable discrepancies between the theoretical coefficients of lift and rolling moment C_{LT} and C_{lT} corresponding to l_T and the measured C_L and C_l. It becomes necessary to subdivide l_T into $l_S + l_A$, the sum of symmetrical and antisymmetrical functions of y, and to apply respective correction factors C_L/C_{LT} and C_l/C_{lT} to l_S and l_A and the appropriate parts of w_i/U.

The magnitude of the discrepancies, so removed, would be expected to be as great as that of δC_L or δC_l corresponding to δl. This would justify the minor simplifying assumption that δl is directly proportional to l_F, i.e.,

$$\delta l(x,y) \equiv k l_F(x,y) .$$

It then follows that

$$\left.\begin{aligned} l_T &= l_F(1 + k + k^2 + \dots) = l_F/(1 - k) \\ w_i/U &= \delta\alpha(1 + k + k^2 + \dots) = \delta\alpha/(1 - k) \end{aligned}\right\} .$$

The original vortex model, based on the aerodynamics of the free stream, will suffice, provided that it is separated into its symmetrical and antisymmetrical parts with adjustable factors to ensure consistency with the measured lift and rolling moment respectively. We therefore express

$$\frac{w_i}{U} = \left[\frac{(w_i)_L}{UC_L}\right] C_L + \left[\frac{(w_i)_l}{UC_l}\right] C_l \, . \tag{3.52}$$

For symmetrically placed wings $[(w_i)_L/UC_L]$ will be a symmetrical function of y and $[(w_i)_l/UC_l]$ antisymmetrical, but in general they will both be asymmetrical. The associated factors are the measured lift and rolling moment coefficients; the subscript T can now be omitted without ambiguity.

The distribution of incidence w_i/U has to be converted into corrections to measured quantities, both geometric and aerodynamic. In principle there is no difficulty in using lifting-surface theory to compute the aerodynamic coefficients δC_L , δC_l and δC_m corresponding to w_i/U and also the increments δC_{Dv} and δC_{nv} in the vortex-induced drag and yawing moment coefficients. Wall corrections could simply amount to the subtraction of these interference quantities from those measured; for example, in the notation of Equation (3.52) we could take

$$\Delta C_m = -\delta C_m = -\left[\frac{(\delta C_m)_L}{C_L}\right] C_L - \left[\frac{(\delta C_m)_l}{C_l}\right] C_l \, , \tag{3.53}$$

where the second term would vanish if the wing were symmetrically placed. An arbitrary correction may be applied to any measured geometric quantity, in particular a correction $\Delta\alpha$ to the incidence of the model. It is then necessary to calculate the appropriate free-stream derivatives $\partial C_L/\partial\alpha$, $\partial C_l/\partial\alpha$ and $\partial C_m/\partial\alpha$, and, for example, to add the quantity $\Delta\alpha(\partial C_m/\partial\alpha)$ to the right hand side of Equation (3.53). It is often convenient to choose $\Delta\alpha$ such that $\Delta C_L = 0$. Then Equation (3.53) would become

$$\Delta C_m = \left\{\frac{\partial C_m}{\partial C_L}\left[\frac{(\delta C_L)_L}{C_L}\right] - \left[\frac{(\delta C_m)_L}{C_L}\right]\right\} C_L + \left\{\frac{\partial C_m}{\partial C_L}\left[\frac{(\delta C_L)_l}{C_l}\right] - \left[\frac{(\delta C_m)_l}{C_l}\right]\right\} C_l \, . \tag{3.54}$$

The expressions in curly brackets are theoretical quantities dependent on the vortex model, the tunnel cross-section and the wing planform. Thus, like w_i/U , each interference correction becomes the product or sum of products of theoretically and experimentally determined quantities.

Difficulties arise when greater precision or, as is more often the case, rapid calculation is required. Reference 3.23 is an eminent example of the former; in effect Sanders and Pounder shun the use of Equation (3.52), for their treatment implies that the load distribution cannot be regarded as independent of wall interference apart from factors proportional to the measured C_L and C_l . Even within the framework of lifting-line theory their analysis becomes exceedingly complicated. The more common difficulty is that, because corrections are fairly small and therefore not required to great accuracy, the use of lifting-surface theory is considered to be an unwarranted computation. Section 3.2.4 has already illustrated the trouble. For a small symmetrical wing Equation (3.54) reduces to Equation (3.36), but the theoretical quantities λ and x_1 must be estimated. Figure 3.7 in conjunction with strip theory can perhaps give λ within ±10% and so $\Delta\alpha$ in

Equation (3.35) to a fair accuracy. However, Table 3.III suggests that in the absence of lifting-surface theory the residual correction ΔC_m , proportional to λx_1 , is liable to be excessively inaccurate. In the following Sections 3.3.4 to 3.3.6 suitable approximations are considered for different types of problem when the wing is not small.

3.3.4 Complete Spanwise Symmetry

For large wings having complete spanwise symmetry there are approximate methods by which rapid interference corrections may be estimated. It is usual to take $\Delta\alpha$ as a weighted mean of w_i/U along the three-quarter-chord line, such that the residual correction ΔC_L is negligible. Thus

$$\frac{\Delta\alpha}{C_L} = \int_0^1 \left(\frac{w_i}{UC_L}\right)_{0.75} W \, d\left(\frac{y}{s}\right) , \qquad (3.55)$$

where* from

$$\left.\begin{array}{rl}
\text{Reference 3.26, Equation (29),} & W = cC_{LL}/\bar{c}C_L \\[2ex]
\text{Reference 3.17, Equation (11),} & W = \dfrac{2.4}{\pi}\left\{1 - \left(\dfrac{y}{s}\right)^2\right\}^{\frac{1}{2}} + 0.4\,\dfrac{c}{\bar{c}} \\[2ex]
\text{elliptic loading} & W = \dfrac{4}{\pi}\left\{1 - \left(\dfrac{y}{s}\right)^2\right\}^{\frac{1}{2}} \\[2ex]
\text{strip theory} & W = c/\bar{c}
\end{array}\right\} .$$

The first weighting is the spanwise loading factor for the wing at uniform incidence; charts of $cC_{LL}/\bar{c}C_L$ are given in Figure 6 of Reference 3.26 for various sweep angles, aspect ratios and taper ratios. The second, equivalent to 0.6 times the elliptic weighting added to 0.4 times the chord weighting, can be evaluated when the factor $cC_{LL}/\bar{c}C_L$ is uncertain. In many cases the elliptic weighting is accurate enough, and the basic interference parameter $(\delta_0)_E$ in Equation (3.46) is useful. The chord weighting from strip theory has little to commend it.

---

* By application of the reverse-flow theorem C.R.Taylor$^{3.70}$ of the Aerodynamics Department of the Royal Aircraft Establishment has pointed out the precise result that

$$\Delta\alpha = \frac{1}{S}\iint_S \frac{w_i}{UC_L}\,\hat{l}\;dxdy ,$$

where $\hat{l}$ is the non-dimensional wing loading on the reversed planform at uniform incidence; the corresponding spanwise loading factor $c\hat{C}_{LL}/\bar{c}\hat{C}_L$ would therefore seem to be an appropriate choice of W in Equation (3.55).

The drag correction is usually taken to be consistent with lifting-line theory and Equations (3.6) and (3.7). If $(w_i/UC_L)_\infty$ denotes the value of w_i/UC_L in the distant wake, then

$$\frac{\Delta C_D}{C_L^2} = \frac{1}{2}\int_0^1 \left(\frac{w_i}{UC_L}\right)_\infty \frac{cC_{LL}}{\bar{c}C_L}\, d\left(\frac{y}{s}\right) , \qquad (3.56)$$

where $cC_{LL}/\bar{c}C_L$ now represents the actual spanwise loading that would be measured on the wing. As in Equation (3.37), a small term from a residual correction to spanwise loading is neglected.

Since $\Delta C_L = 0$, ΔC_m will be a pure couple independent of pitching axis. In both References 3.26 and 3.17 the residual correction may be written as

$$\Delta C_m = (\Delta C_m)_1 + (\Delta C_m)_2 , \qquad (3.57)$$

where $(\Delta C_m)_1$ results from the shift in spanwise centre of lift associated with the spanwise variation of $(w_i/UC_L)_{0.75}$, and $(\Delta C_m)_2$ arises from the streamline curvature. Alternative formulae for $(\Delta C_m)_1$ are given in References 3.26 and 3.17; the former is preferred as it avoids a calculation by lifting-line theory and in the present notation, gives directly

$$\frac{(\Delta C_m)_1}{C_L} = \frac{\frac{1}{2}\pi A^2(\partial C_L/\partial\alpha)\tan\Lambda_{0.25}}{\pi A + 2\partial C_L/\partial\alpha} \int_0^1 \left[\left(\frac{w_i}{UC_L}\right)_{0.75} - \frac{\Delta\alpha}{C_L}\right] w\,\frac{y}{s}\, d\left(\frac{y}{s}\right) , \qquad (3.58)$$

where A is the aspect ratio and $\Lambda_{0.25}$ is the sweepback of the quarter-chord line. $(\Delta C_m)_2$ is incorrectly derived in Reference 3.17: with allowance for compressibility Equation (35) of Reference 3.26 becomes

$$\frac{(\Delta C_m)_2}{C_L} = \frac{\pi\cos\Lambda_{0.5}}{4\sqrt{1 - M^2\cos^2\Lambda_{0.5}}} \int_0^1 \left[\left(\frac{w_i}{UC_L}\right)_{0.75} - \left(\frac{w_i}{UC_L}\right)_{0.25}\right]\left(\frac{c}{\bar{c}}\right)^2 d\left(\frac{y}{s}\right) . \qquad (3.59)$$

where $\Lambda_{0.5}$ is the half-chord sweepback.

Equations (3.58) and (3.59) are not applicable to planforms with curved or cranked edges. In place of Equation (3.57) strip theory would give the less accurate expression

$$\frac{\Delta C_m}{C_L} = \frac{\partial C_L}{\partial\alpha}\int_0^1 \left[\left(\frac{w_i}{UC_L}\right)_{0.75} (x_L - \bar{\bar{x}}_L + \tfrac{3}{8}c - \tfrac{1}{4}\bar{\bar{c}}) - \left(\frac{w_i}{UC_L}\right)_{0.25} (\tfrac{1}{8}c)\right] \frac{c}{\bar{c}^2}\, d\left(\frac{y}{s}\right) . \qquad (3.60)$$

where

$$\left.\begin{aligned} \bar{\bar{c}} &= \int_0^1 \frac{c^2}{\bar{c}}\, d\left(\frac{y}{s}\right) \\ \bar{\bar{x}}_L &= \int_0^1 x_L\left(\frac{c}{\bar{c}}\right) d\left(\frac{y}{s}\right) \end{aligned}\right\} .$$

It may sometimes be convenient to use Equation (3.60) with a correction factor based on lifting-surface theory. In the light of Equation (3.36) for a small model, it may be simple to evaluate the quantity $\lambda x_1/\bar{c}$ by both strip theory and lifting-surface theory. In general $\lambda \partial C_L/\partial\alpha$ is the lift coefficient and $x = x_1$ is the centre of lift corresponding to an incidence $2x/\bar{c}$, where x is measured from the theoretical aerodynamic centre. Thus a lifting-surface solution for the wing in steady pitching motion will suffice to determine an accurate value of $\lambda x_1/\bar{c}$. By strip theory

$$\left(\frac{\lambda x_1}{\bar{c}}\right)_{st} = 2\int_0^1 \left(\frac{x_L + \frac{1}{2}c}{\bar{c}}\right)^2 \frac{c}{\bar{c}}\, d\left(\frac{y}{s}\right) - 2\left(\frac{\bar{x}_L + \frac{1}{4}\bar{c}}{\bar{c}}\right)\left(\frac{\bar{x}_L + \frac{3}{4}\bar{c}}{\bar{c}}\right), \tag{3.61}$$

which reduces to the second of Equations (3.38) for straight tapered wings. The ratio $\lambda x_1/\bar{c}$ to $(\lambda x_1/\bar{c})_{st}$ may be inserted as a correction factor on the right hand side of Equation (3.60); typical values may be obtained from Table 3.III. The relative accuracy of this method and of Equations (3.57) to (3.59) is discussed in Section 3.5.3.

Other measured quantities may require interference corrections. Although control surfaces are considered under asymmetrical configurations in Section 3.3.6, the approximate residual correction to hinge moment in Equation (3.77) also applies when there is spanwise symmetry. To apply a residual correction to surface pressure, it is necessary to use lifting-surface theory and to replace C_m by C_p in Equation (3.54). Reference 3.26 includes expressions for the interference corrections to downwash angle and wake displacement. Swanson and Schuldenfrei[3.27] consider these corrections in the presence of a slipstream behind a powered model.

3.3.5 Non-Symmetrical Spanwise Loading

We next consider symmetrically placed wings with antisymmetrical spanwise loading. The case of deflected ailerons is treated approximately in References 3.26 and 3.28. Since Reference 3.28 is restricted to unswept wings, the expression from Equation (41) of Reference 3.26 is of greater generality. Hence

$$\frac{\Delta C_l}{C_l} = -\frac{\pi A \mu\, \partial C_L/\partial\alpha}{2(\pi A + \mu\, \partial C_L/\partial\alpha)} \int_c^1 \left(\frac{w_i}{UC_l}\right)_{0.75} W \frac{y}{s}\, d\left(\frac{y}{s}\right), \tag{3.62}$$

where

$$\mu = \frac{2 + \sqrt{A^2(\beta^2 + \tan^2\Lambda_{0.25}) + 4}}{2 + \sqrt{A^2(\beta^2 + \tan^2\Lambda_{0.25}) + 16}}$$

and W is the weighting factor in Equation (3.55) given by charts in Figure 6 of Reference 3.26. There will be a corresponding correction to the drag given by

$$\frac{\Delta C_D}{C_l^2} = \frac{1}{2}\int_0^1 \left(\frac{w_i}{UC_l}\right)_\infty \frac{cC_{LL}}{\bar{c}C_l}\, d\left(\frac{y}{s}\right). \tag{3.63}$$

It is now inappropriate to apply a correction to any measured geometric quantity such as aileron angle. In the case of a slowly rolling wing, however, the negative correction ΔC_l can be replaced by a positive correction to the rate of roll[3.29]. Similar considerations could apply to wings having smooth antisymmetrical modes of deformation.

Interference corrections for symmetrically placed, asymmetrically loaded wings are derived in Reference 3.18. In place of Equation (3.52) we may then write

$$\delta\alpha = \frac{w_i}{U} = \left(\frac{(w_i)_S}{UC_L}\right)C_L + \left(\frac{(w_i)_A}{UC_l}\right)C_l \; ; \tag{3.64}$$

likewise the spanwise distribution of circulation may be written as

$$\Gamma = 2sU\gamma = 2sU(\gamma_S + \gamma_A) \; , \tag{3.65}$$

where

$$\left.\begin{aligned} C_L &= 2A\int_0^1 \gamma_S\, d\left(\frac{y}{s}\right) \\ C_l &= A\int_0^1 \gamma_A \frac{y}{s}\, d\left(\frac{y}{s}\right) \end{aligned}\right\} . \tag{3.66}$$

By the application of lifting-surface theory the symmetrical interference upwash angle $(w_i)_S/U$ gives increments δC_L and δC_m to lift and pitching moment, and the antisymmetrical part $(w_i)_A/U$ gives an increment δC_l to the rolling moment coefficient. Hence

$$\left.\begin{aligned} \frac{\Delta\alpha}{C_L} &= \frac{\delta C_L}{(\partial C_L/\partial\alpha)\; 2A\int_0^1 \gamma_S\, d(y/s)} \\ \frac{\Delta C_m}{C_L} &= -\frac{\delta C_m}{2A\int_0^1 \gamma_S\, d(y/s)} + \frac{\Delta\alpha}{C_L}\,\frac{\partial C_m}{\partial\alpha} \\ \frac{\Delta C_l}{C_l} &= -\frac{\delta C_l}{A\int_0^1 \gamma_A (y/s)\, d(y/s)} \end{aligned}\right\} . \tag{3.67}$$

The second of Equations (3.67) is equivalent to Equation (3.54), since

$$(\delta C_L)_l = (\delta C_m)_l = 0$$

for symmetrically placed wings. Equations (3.55), (3.57) and (3.62) are working approximations to Equations (3.67) and are recommended whenever it is inexpedient to calculate the increments δC_L, δC_m and δC_l by lifting-surface theory.

The evaluation of the usual interference corrections to drag and yawing moment do not require calculations by lifting-surface theory, provided that the distributions of γ_S and γ_A can be estimated. These corrections are calculated on the principle* that the local lift per unit span acts at right angles to a local effective stream direction, and that wall interference causes this to deflect upwards through the angle $\frac{1}{2}(\delta\alpha)_\infty$. Under linear conditions this deflection does not influence the lift itself, but reduces the drag per unit span by an amount

$$\tfrac{1}{2}\rho U\Gamma(\delta\alpha)_\infty = \tfrac{1}{4}\rho U^2 S\left(\frac{A\gamma}{s}\right)(\delta\alpha)_\infty .$$

Thus there are increments

$$\left.\begin{aligned} \delta C_{Dv} &= -\frac{1}{2}A\int_{-1}^{1}\gamma(\delta\alpha)_\infty\, d\left(\frac{y}{s}\right) \\ \delta C_{nv} &= \frac{1}{4}A\int_{-1}^{1}\gamma(\delta\alpha)_\infty\frac{y}{s}\, d\left(\frac{y}{s}\right) \end{aligned}\right\} \qquad (3.68)$$

to the vortex-induced drag and yawing moment coefficients. When γ and $(\delta\alpha)_\infty$ are separated into their symmetrical and antisymmetrical parts, Equations (3.68) become

$$\left.\begin{aligned} \delta C_{Dv} &= -A\int_{0}^{1}\left[\gamma_S\left(\frac{(w_i)_S}{UC_L}\right)_\infty C_L + \gamma_A\left(\frac{(w_i)_A}{UC_l}\right)_\infty C_l\right] d\left(\frac{y}{s}\right) \\ \delta C_{nv} &= \frac{1}{2}A\int_{0}^{1}\left[\gamma_A\left(\frac{(w_i)_S}{UC_L}\right)_\infty C_L + \gamma_S\left(\frac{(w_i)_A}{UC_l}\right)_\infty C_l\right]\frac{y}{s}\, d\left(\frac{y}{s}\right) \end{aligned}\right\} . \qquad (3.69)$$

When γ is replaced by $cC_{LL}/4s$, it is seen that $-\delta C_{Dv}$ is equivalent to the sum of Equations (3.56) and (3.63). Only in the case of yawing moment do the symmetrical and antisymmetrical parts interact; the second of Equations (3.69) becomes

$$\frac{\delta C_{nv}}{C_L C_l} = \frac{1}{4}\int_{0}^{1}\left[\left(\frac{(w_i)_S}{UC_L}\right)_\infty \frac{c(C_{LL})_A}{\bar{c}C_l} + \left(\frac{(w_i)_A}{UC_l}\right)_\infty \frac{c(C_{LL})_S}{\bar{c}C_L}\right]\frac{y}{s}\, d\left(\frac{y}{s}\right) , \qquad (3.70)$$

where the right hand side is determined theoretically. It can easily be shown that δC_{Dv} and δC_{nv} are unaffected by the application of the interference correction $\Delta\alpha$, since the reductions in magnitude due to the substitution $[\frac{1}{2}(\delta\alpha)_\infty - \Delta\alpha]$ for $\frac{1}{2}(\delta\alpha)_\infty$ in Equations (3.68) exactly cancel the increases due to the change of wind axes. But the result of residual corrections to the load distribution needs to be considered. As $\Delta C_L = 0$, any correction to γ_S will have a negligible effect on vortex-induced drag and yawing moment. The correction ΔC_l implies a correction to γ_A, which may be regarded crudely as a factor $\{1 + (\Delta C_l/C_l)\}$; this will increase $(C_{Dv})_A$, the vortex drag corresponding to the antisymmetrical part of the spanwise loading, by the factor $\{1 + (\Delta C_l/C_l)\}^2$ and the total C_{nv} by the factor $\{1 + (\Delta C_l/C_l)\}$. The final corrections are therefore

---

* By consideration of the total energy of flow in the wake this principle can be justified in the case of drag. For yawing moment, however, the principle is not rigorous and numerical values of the interference correction are in some doubt (Section 3.5.3).

$$\left.\begin{aligned} \Delta C_D &= -\delta C_{Dv} + 2\frac{\Delta C_l}{C_l}(C_{Dv})_A \\ \Delta C_n &= -\delta C_{nv} + \frac{\Delta C_l}{C_l}C_{nv} \end{aligned}\right\} , \qquad (3.71)$$

where δC_{Dv} and δC_{nv} are given by Equations (3.69) and (3.70). The last terms in Equations (3.71) are approximate and relatively small and can usually be neglected, as in Equation (3.63). A full derivation of Equations (3.71) is found in Reference 3.18, but the latter is given incorrectly in Equation (8.13) of Reference 3.18. The magnitude of the corrections is discussed in Section 3.5.1.

References 3.23, 3.26 and 3.28 also consider the interference corrections for symmetrically placed, asymmetrically loaded wings. The rigorous treatment by lifting-line theory in Reference 3.23 is beyond the scope of rapid calculation. Like Reference 3.23, Graham's[3.26] method is restricted to lifting-line theory and unswept wings in closed rectangular tunnels, but with acceptable approximations he derives corrections to rolling and yawing moment in a practical form. For wings with sweepback or large chord the interference corrections derived by Sivells and Salmi[3.26] are practically consistent with those of the previous paragraph, except that w_i/U along the quarter-chord line replaces $\frac{1}{2}(\delta\alpha)_\infty$ in the formulae concerning drag and yawing moment.

3.3.6 Asymmetrically Placed Wings

More difficult is the case of yawed wings when Equation (3.52) applies in all its generality. The walls also induce an interference sidewash unless the wing is situated in the horizontal plane of symmetry, but this is usually ignored. Provided that the angle of yaw is fairly small, simple generalizations of Equations (3.67) to (3.71) are possible. Added to Equations (3.67) there will be contributions $\Delta\alpha/C_l$, $\Delta C_m/C_l$ and $\Delta C_l/C_L$, which may be estimated by inserting the symmetrical part of (w_i/UC_l) in place of (w_i/UC_L) in Equations (3.55), (3.58) and (3.59) and also the antisymmetrical part of (w_i/UC_L) in place of (w_i/UC_l) in Equation (3.62). Both ΔC_D and ΔC_n will contain contributions proportional to C_L^2, C_LC_l and C_l^2, since $(\delta\alpha)_\infty$ in Equation (3.68) must be written in four parts, viz.,

$$(\delta\alpha)_\infty = \left[\frac{\{(w_i)_L\}_S}{UC_L}\right]_\infty C_L + \left[\frac{\{(w_i)_L\}_A}{UC_L}\right]_\infty C_L + \left[\frac{\{(w_i)_l\}_S}{UC_l}\right]_\infty C_l + \left[\frac{\{(w_i)_l\}_A}{UC_l}\right]_\infty C_l . \qquad (3.72)$$

If, however, the angle of yaw is large, the information on lift distribution may be so scanty that a very simple vortex model will be adopted (Section 3.3.1). In Reference 3.25, Swanson represents the yawed wing as a number of skewed horse-shoe vortices corresponding to the equivalent wing semi-span of Equation (3.41) or the spanwise extent of the dihedral or aileron. Lengthy, but manageable, expressions are obtained for the interference corrections to incidence, drag, rolling and yawing moments, but it is hard to assess their accuracy for a typical sweptback wing. The uncertainty is such that there may be little point in applying corrections to the moment coefficients C_l and C_n. It may suffice to calculate the interference upwash angles $(\delta\alpha)_{0.75}$ and $\frac{1}{2}(\delta\alpha)_\infty$. Then, in place of Equation (3.55),

$$\Delta\alpha = \frac{1}{2}\int_{-1}^{1} (\delta\alpha)_{0.75}\, w\, d\left(\frac{y}{s}\right) , \qquad (3.73)$$

and in place of Equations (3.56), (3.63) and (3.68),

$$\left.\begin{aligned} \Delta C_D &= \frac{1}{US}\int_{-s}^{s} \Gamma(\delta\alpha)_\infty\, dy \\ \Delta C_n &= -\frac{1}{2USs}\int_{-s}^{s} \Gamma(\delta\alpha)_\infty y\, dy \end{aligned}\right\} , \qquad (3.74)$$

where the distribution of circulation $\Gamma = \Gamma(y)$ should be consistent with the measured lift and rolling moment. The extreme alternative is to calculate the distribution of $\delta\alpha = w_i/U$ over the yawed planform and then to apply the best available theory, as envisaged in Section 3.3.3; this would seldom be justified.

Half-wing or reflection-plane models introduce further types of interference correction. All corrections to be applied for symmetrically loaded conditions are precisely those for a complete model mounted in a wind tunnel of the same height as the original tunnel and twice the breadth (Section 3.4.4); Equations (3.55) to (3.59) remain just as valid. But, as discussed in Reference 3.22, there is a second group of corrections for antisymmetrically loaded conditions when the reflection would not be present on a complete model. In such cases there may be large corrections to

$$\left.\begin{aligned} \text{half-wing rolling moment} &= \tfrac{1}{2}\rho U^2(\tfrac{1}{2}S)2sC_l \\ \text{half-wing yawing moment} &= \tfrac{1}{2}\rho U^2(\tfrac{1}{2}S)2sC_n \end{aligned}\right\} . \qquad (3.75)$$

where $\frac{1}{2}S$ is the area of the half-wing planform and $2s$ is the span of the complete wing. The corrections are determined in two parts. Firstly, the model and its reflection are corrected for symmetrical interference effects on the half wing. This involves the main correction to incidence from Equation (3.55) and corrections to lateral coefficients

$$\left.\begin{aligned} \frac{\Delta C_l}{C_L} &= -\frac{\frac{1}{2}\pi A\, \partial C_L/\partial\alpha}{\pi A + 2\,\partial C_L/\partial\alpha}\int_0^1 \left[\left(\frac{w_i}{UC_L}\right)_{0.75} - \frac{\Delta\alpha}{C_L}\right] w\,\frac{y}{s}\, d\left(\frac{y}{s}\right) \\ \frac{\Delta C_n}{C_L^2} &= -\frac{1}{4}\int_0^1 \left(\frac{w_i}{UC_L}\right)_\infty \frac{cC_{LL}}{\bar{c}C_L}\,\frac{y}{s}\, d\left(\frac{y}{s}\right) \end{aligned}\right\} . \qquad (3.76)$$

Apart from the effects of streamline curvature, the residual spanwise loading is distributed along the quarter-chord line according to the assumptions of Reference 3.26. Since the corresponding moment on the half wing about an axis parallel to the quarter-chord line should vanish, Equations (3.58) and (3.76) are consistent in that

$$2s\Delta C_l = -\bar{c}(\Delta C_m)_1 \cot\Lambda_{0.25} .$$

Secondly and of greater importance, factors independent of the tunnel cross-section must be applied to the quantities $(C_l + \Delta C_l)$ and $(C_n + \Delta C_n)$ to account for the reflection plane, and these demand special theoretical calculations. Simplified treatments are discussed in References 3.4, 3.22 and 3.26.

Large half-wing models are often used to test control surfaces, for which the streamline curvature is particularly significant[3.x]. In the present notation the approximate residual correction to hinge moment becomes

$$\frac{\Delta C_H}{C_L} = -\frac{\partial C_H}{\partial \alpha}\,\frac{\displaystyle\int\left[B\left(\frac{w_i}{UC_L}\right)_{0.75} - (B-1)\left(\frac{w_i}{UC_L}\right)_{0.25} - \frac{\Delta\alpha}{C_L}\right] Wc_f^2\, d\left(\frac{y}{s}\right)}{\displaystyle\int Wc_f^2\, d\left(\frac{y}{s}\right)}\,, \qquad (3.77)$$

where the weighting* W is selected from Equation (3.55), the integrals are taken over the span of the control surface, $c_f(y)$ is the local control chord, and for unbalanced control surfaces B is tabulated below.

c_f/c	0	0.05	0.10	0.15	0.20	0.25	0.30	0.35	0.40	0.45	0.50
B	2.50	2.46	2.41	2.37	2.33	2.28	2.24	2.19	2.15	2.10	2.05

Values of B for balanced control surfaces having set-back hinges may be evaluated as $\frac{1}{2} + \frac{1}{4}(b'/b_1)$ from Table 2 in Section 4.2 of Reference 3.4. For antisymmetrically loaded conditions a factor should be applied to $(C_H + \Delta C_H)$ to account for the reflection plane. For outboard ailerons this will be less important than the corresponding factors for rolling and yawing moments, so that an estimate by lifting-line theory may suffice.

The interpretation of an interference correction may need adjustment if the lift or rolling moment is not measured. The uncertainty concerns which part of the expression is calculated theoretically and which part is determined experimentally. For example, Equation (3.77) envisages that C_L on the left hand side and $\partial C_H/\partial\alpha$ on the right hand side are measured, while the integrals are predetermined. If, however, only the control hinge moment is measured, it would be necessary to multiply both sides of the equation by an estimated value of C_L/C_H : then the ratio of $\Delta C_H/C_H$ to $\partial C_H/\partial\alpha$ is determined by calculation.

3.4 EVALUATION OF INTERFERENCE PARAMETERS

In order to apply the general methods of Section 3.3, it is necessary to obtain numerical data for the interference upwash w_i due to lifting elements in a particular tunnel. A wide range of tunnel cross-section has been employed in research centres, the most common shapes having closed rectangular boundaries (Section 3.4.1) or closed octagonal boundaries (Section 3.4.2); the latter are usually regarded as rectangular tunnels with small corner fillets. Much less attention has been given to open rectangular tunnels, as the rounded circular or elliptical shape is more appropriate for a free jet; these are considered as well as closed circular and elliptical tunnels in Section 3.4.3. As in the case of rectangular tunnels (Section 3.2.2), some curved shapes with mixed boundaries have been devised to reduce or eliminate the theoretical lift interference, but these semi-closed tunnels are of passing academic interest. Wind-tunnel testing of half models mounted on a reflection plane is common practice. Although this merely doubles the effective breadth to height ratio of rectangular tunnels and extends the practical upper limit of b/h, in the case of octagonal and circular tunnels Sections 3.4.2 and 3.4.3 no longer apply; in effect, the latter become bipolar tunnels (Section 3.4.4).

---

* Equation (3.77) gives a rough average value of the expression in square brackets. Although by strip theory the weighting W should be replaced by the two-dimensional $\partial C_H/\partial\alpha$ in each integrand, the major influence of boundary layers may override this consideration.

Table 3.IV summarizes the numerical data available for wings of moderate or large span. In many cases the information is limited to quantities such as $(\delta_0)_U$, $(\delta_0)_E$ and $\delta_0(y,t)$, as defined in Equations (3.44), (3.46) and (3.42), which are only sufficient if the wing can be regarded as an unswept lifting line. A tick in the final column of Table 3.IV indicates that the streamwise variation of w_i has been calculated, whether through the quantity $\delta_1(y,t)$ of Equation (3.42) or some more general tabulation or graph.

3.4.1 Rectangular Tunnels

The evaluation of upwash interference on large lifting models in closed rectangular tunnels is basically straightforward, since there is a complete image system corresponding to any vortex representation of the model. The upwash field of a horse-shoe vortex of strength K surrounding the area $x > 0$, $|y| < t$, $z = 0$ is

$$w = w_v(x,y,z,t) = \frac{K}{4\pi}\left[W(\beta^{-1}x,\ y+t,\ z) - W(\beta^{-1}x,\ y-t,\ z)\right], \qquad (3.78)$$

where

$$W(x,y,z) = -\frac{y}{y^2+z^2} - \left(\frac{1}{x^2+z^2} + \frac{1}{y^2+z^2}\right)\frac{xy}{(x^2+y^2+z^2)^{\frac{1}{2}}} \ . \qquad (3.79)$$

Its image system is a simple generalization of Figure 3.1(b), so that the interference upwash is

$$w_i = \frac{K}{4\pi}\sum_{-\infty}^{\infty}\sum{}'(-1)^n\left[W(\beta^{-1}x,\ y-mb+t,\ z-nh) - W(\beta^{-1}x,\ y-mb-t,\ z-nh)\right], \qquad (3.80)$$

where, as in Equation (3.13), $\sum_{-\infty}^{\infty}\sum{}'$ denotes that (m,n) takes all possible integral pairs except $(0,0)$.

If the wing is of large span $2s$ but of small chord, it may suffice to put $x = z = 0$ in Equation (3.80), so that in the notation of Equation (3.42)

$$w_i = \frac{4Kt}{bh}\,\delta_0(y,t)\ . \qquad (3.81)$$

where

$$\delta_0(y,t) = \frac{bh}{16\pi t}\sum_{-\infty}^{\infty}\sum{}' (-1)^n\left[-\frac{y-mb+t}{(y-mb+t)^2+n^2h^2}+\frac{y-mb-t}{(y-mb-t)^2+n^2h^2}\right]$$

$$= -\frac{bh}{16\pi t}\left[\frac{1}{y-t}-\frac{1}{y+t}\right]+\frac{b}{16t}\sum_{m=-\infty}^{\infty}\left[\operatorname{cosech}\frac{\pi(y-mb-t)}{h}-\operatorname{cosech}\frac{\pi(y-mb+t)}{h}\right] . \tag{3.82}$$

Hence the mean interference parameters $(\delta_0)_U$ and $(\delta_0)_E$ for uniform and elliptic spanwise loading in respective Equations (3.44) and (3.46) can be evaluated. As described in Section 9 of Reference 3.1, the early literature has shown that the results can be derived analytically, viz.,

$$(\delta_0)_U = \frac{h}{4\pi b\sigma^2}\log_e\frac{\pi\sigma}{\sin\pi\sigma}+\frac{\pi h}{b}\sum_{n=1}^{\infty}\frac{n}{e^{2\pi nh/b}+1}\left(\frac{\sin\pi n\sigma}{\pi n\sigma}\right)^2 \tag{3.83}$$

and

$$(\delta_0)_E = \frac{h}{2b}F(\sigma)+\frac{4\pi h}{b}\sum_{n=1}^{\infty}\frac{n}{e^{2\pi nh/b}+1}\left(\frac{J_1(\pi n\sigma)}{\pi n\sigma}\right)^2 . \tag{3.84}$$

where $\sigma = 2s/b$; numerical values of $F(\sigma)$ and $\{J_1(\pi\sigma)/\pi\sigma\}^2$ are found in Tables 4 and 5 of Reference 3.1. A good description of the mathematical analysis is given by Sanders and Pounder in Section 2.1 of Reference 3.23. They also give useful graphs of $(\delta_0)_U$ and $(\delta_0)_E$ against h/b for $\sigma = 0, 0.2, 0.4, 0.6, 0.8$ and 0.9; the latter is given in carpet form in Figure 3.9. The factor $(\delta_0)_E(\sigma)/(\delta_0)_E(0)$ provides a simple improvement on the corrections to incidence and drag coefficient for a small wing in Equations (3.39); thus

$$\left.\begin{aligned}\Delta\alpha &= (\delta_0)_E(\sigma)\left(1+\frac{\bar{c}\delta_1}{2\beta h\delta_0}\right)\frac{SC_L}{C}\\ \Delta C_D &= (\delta_0)_E(\sigma)\,\frac{SC_L^2}{C}\end{aligned}\right\} . \tag{3.85}$$

where $(\delta_0)_E(\sigma)$ is given in Figure 3.9, δ_1/δ_0 is given by the upper curve of Figure 3.4, and Figure 3.7 indicates a correction factor $\lambda\bar{c}/\bar{\bar{c}}$ to the term involving δ_1 .

It is often necessary to calculate the parameter $\delta_1(y,t)$ of Equation (3.42). By Equation (3.80) this is readily expressed as

$$\delta_1(y,t) = \frac{\beta ch^2}{4Kt}\left(\frac{\partial w_1}{\partial x}\right)_{x=0}$$

$$= \frac{bh^2}{16\pi t}\sum_{-\infty}^{\infty}\sum{}' (-1)^n\left[\frac{\partial w}{\partial x}(0,\ y-mb+t,\ -nh)-\frac{\partial w}{\partial x}(0,\ y-mb-t,\ -nh)\right] , \tag{3.86}$$

where

$$\frac{\partial W}{\partial x}(0, y, -nh) = -\frac{y(y^2 + 2n^2h^2)}{n^2h^2(y^2 + n^2h^2)^{3/2}} .$$

The singularity from $n = 0$ is illusory, since in the limit

$$\frac{\partial W}{\partial x}(0,\ y - mb + t,\ 0) - \frac{\partial W}{\partial x}(0,\ y - mb - t,\ 0) = \pm\frac{1}{2}\left[\frac{1}{(y - mb + t)^2} - \frac{1}{(y - mb - t)^2}\right]$$

according as m is positive or negative. The evaluation of w_1 for a duplex tunnel ($b = 2h$) was accomplished by Cowley and McMillan (Ref.3.30; 1934), who tabulated upwash angle at the tail of an elliptically loaded model without the approximation that W is linear in x. They obtained the equivalent of

$$\frac{4}{\pi}\int_0^1 \delta_1(0,t)\left(\frac{t}{s}\right)^2\left\{1 - \left(\frac{t}{s}\right)^2\right\}^{-\frac{1}{2}} d\left(\frac{t}{s}\right)$$

for a range of $\sigma = 2s/b$ by expanding $\delta_1(0,t)$ in even powers of t/s and neglecting contributions from $|m| > 3$ and from $|n| > 5$ in Equation (3.86). As it stands the double series converges slowly, but it can be transformed into the rapidly convergent expression in Equation (3.25) of Reference 3.23. Hence

$$\begin{aligned}\delta_1(y,t) = {} & \frac{\pi}{24} + \frac{2h^2}{bt}\sum_{p=1}^{\infty}\sum_{q=1}^{\infty}(-1)^{q-1}p\sin\frac{2\pi pt}{b}\cos\frac{2\pi py}{b}\chi\left(\frac{2\pi pqh}{b}\right) + \\ & + \frac{h^2}{32\pi bt}\left[\Psi'\left(1 + \frac{y-t}{b}\right) - \Psi'\left(1 + \frac{y+t}{b}\right) + \Psi'\left(1 - \frac{y+t}{b}\right) - \Psi'\left(1 - \frac{y-t}{b}\right)\right] .\end{aligned} \tag{3.87}$$

where $\Psi'(1 + \eta) = \sum_{m=1}^{\infty}\frac{1}{(\eta + m)^2}$ is the Trigamma function* and

$$\chi(\eta) = K_0(\eta) + \frac{1}{\eta}K_1(\eta)$$

in terms of modified Bessel functions of the second kind. It can be seen that Equation (3.87) reduces to the first of Equations (3.20) as both y and t tend to zero. A rigorous derivation of the rapidly convergent series has been given by Olver[3.31], who was responsible for the tabulation of $\delta_1(y,t)$ for $b/h = 1,\ 9/7,\ 2,\ 18/7$ in Reference 3.17.

When the interference upwash is to be calculated from Equation (3.47) or (3.48), it is convenient to tabulate the quantities

$$\frac{\partial}{\partial t}\{t\delta_0(y,t)\} \quad \text{and} \quad \frac{\partial}{\partial t}\{t\delta_1(y,t)\} .$$

---

* Ψ' has been tabulated by H.T.Davis in *Tables of the Higher Mathematical Functions*, Volume II (The Principal Press Inc., Indiana, USA, 1935).

It follows from Equations (3.82) and (3.87) that both quantities are even functions of y and t ; moreover, they are unaltered when y and t are interchanged. The diagonal symmetry is illustrated in Table 3.V, where both quantities are given for a closed square tunnel. Another account of the theory is given in Reference 3.18 by the present author and Acum. It is shown that

$$\frac{\partial}{\partial t}\{t\delta_0(y,t)\} = \frac{b}{16h}\left[\sum_{m=1}^{\infty}\left\{-f_1\left(\frac{y-t-mb}{h}\right) - f_1\left(\frac{y-t+mb}{h}\right) - f_1\left(\frac{y+t-mb}{h}\right) - f_1\left(\frac{y+t+mb}{h}\right)\right\} - f_2\left(\frac{y-t}{h}\right) - f_2\left(\frac{y+t}{h}\right)\right] \quad (3.88)$$

and

$$\frac{\partial}{\partial t}\{t\delta_1(y,t)\} = \frac{b}{16\pi h}\left[\sum_{m=1}^{\infty}\left\{-f_3\left(\frac{y-t-mb}{h}\right) - f_3\left(\frac{y-t+mb}{h}\right) - f_3\left(\frac{y+t-mb}{h}\right) - f_3\left(\frac{y+t+mb}{h}\right)\right\} - f_4\left(\frac{y-t}{h}\right) - f_4\left(\frac{y+t}{h}\right)\right], \quad (3.89)$$

where

$$\left.\begin{aligned} f_1(\lambda) &= \frac{d}{d\lambda}\{\operatorname{cosech}\pi\lambda\} \\ f_2(\lambda) &= \frac{d}{d\lambda}\left\{\operatorname{cosech}\pi\lambda - \frac{1}{\pi\lambda}\right\} \\ f_3(\lambda) &= \frac{1}{\lambda}f(\lambda) + \frac{d}{d\lambda}\{f(\lambda)\} \\ f_4(\lambda) &= \frac{1}{\lambda}f(\lambda) + \frac{d}{d\lambda}\{f(\lambda)\} + \frac{1}{|\lambda|^3} \\ \text{with}\quad f(\lambda) &= 4\pi\{K_1(\pi\lambda) + 3K_1(3\pi\lambda) + 5K_1(5\pi\lambda) + \ldots\} \end{aligned}\right\} \quad (3.90)$$

are found in Tables 1, 2 and 3 of Reference 3.18. The corresponding interference parameters from the antisymmetrical part of the spanwise loading are defined in Equation (3.49), viz.,

$$\frac{w_i}{U} = \frac{4Kt}{Ubh}\left\{\kappa_0(y,t) + \frac{x}{\beta h}\kappa_1(y,t) + O\left(\frac{x}{\beta h}\right)^3\right\}.$$

Then the antisymmetrical interference upwash in Equation (3.50) corresponding to the vortex model of Figure 3.8(d) involves the parameters

$$\frac{\partial}{\partial t}\{t\kappa_0(y,t)\} = \frac{b}{16h}\left[\sum_{m=1}^{\infty}(-1)^m\left\{-f_1\left(\frac{y-t-mb}{h}\right) - f_1\left(\frac{y-t+mb}{h}\right) + f_1\left(\frac{y+t-mb}{h}\right) + \right.\right.$$

$$\left.\left. + f_1\left(\frac{y+t+mb}{h}\right)\right\} - f_2\left(\frac{y-t}{h}\right) + f_2\left(\frac{y+t}{h}\right)\right] \qquad (3.91)$$

and

$$\frac{\partial}{\partial t}\{t\kappa_1(y,t)\} = \frac{b}{16\pi h}\left[\sum_{m=1}^{\infty}(-1)^m\left\{-f_3\left(\frac{y-t-mb}{h}\right) - f_3\left(\frac{y-t+mb}{h}\right) + f_3\left(\frac{y+t-mb}{h}\right) + \right.\right.$$

$$\left.\left. + f_3\left(\frac{y+t+mb}{h}\right)\right\} - f_4\left(\frac{y-t}{h}\right) + f_4\left(\frac{y+t}{h}\right)\right], \qquad (3.92)$$

which may be computed for any rectangular tunnel from Equations (3.90) for $f_1(\lambda)$ and $f_2(\lambda)$ and Table 3 of Reference 3.18 from which, with the use of second differences, $f_4(\lambda)$ may be obtained to four decimal places.

For models in the central horizontal plane $z = 0$, w_i can be evaluated quite easily from Equations (3.79) and (3.80) for a general value of x. The terms of order $(x/\beta h)^3$ will become significant if the model is of great streamwise extent, for example, a large sweptback wing or a complete aircraft. Moreover, the errors in assuming a linear upwash will increase nearly sevenfold as the Mach number increases from 0 to 0.85. Furthermore, the foregoing method cannot be applied to yawed or asymmetrical models. In such cases, or when higher order terms are required, it is convenient to replace the distributed vorticity by point concentrations as in Figure 3.8(f). Following Katzoff and Hannah[3.20], we replace Equation (3.78) by the upwash field due to a line doublet of strength

$$P = \lim_{t\to 0}(2Kt) = L/(\rho U)$$

extending along the x-axis from the origin to infinity. This upwash field is

$$w = \frac{P}{4\pi}\frac{\partial W(\beta^{-1}x,y,z)}{dy}, \qquad (3.93)$$

where, from Equation (3.79),

$$\frac{\partial}{\partial y}[W(x,y,z)] = \frac{y^2-z^2}{(y^2+z^2)^2} + \frac{x[(y^2+z^2)(x^2+y^2-2z^2) - 2x^2z^2]}{(y^2+z^2)^2(x^2+y^2+z^2)^{3/2}}. \qquad (3.94)$$

Now consider a number of lifting elements $L_N = \rho UP_N$ at positions $(x_N, y_N, 0)$ in a closed rectangular tunnel. In accord with the image system in Figure 2(a) of Reference 3.20, the interference upwash is expressed as

$$w_i(x,y,0) = \sum_N \frac{L_N}{4\pi\rho U} \left\{ \sum_{-\infty}^{\infty}\sum (-1)^n \frac{\partial}{\partial y}\left[W\left(\frac{x-x_N}{\beta}, y-2mb-b+y_N, -nh\right)\right] + \right.$$

$$\left. + \sum_{-\infty}^{\infty}\sum{}' (-1)^n \frac{\partial}{\partial y}\left[W\left(\frac{x-x_N}{\beta}, y-2mb-y_N, -nh\right)\right] \right\} .$$

This is conveniently written in non-dimensional form

$$\frac{w_i}{U} = \sum_N \frac{L_N}{\rho U^2 b^2}\left[W_A\left(\frac{x-x_N}{\beta b}, \frac{y-b+y_N}{b}\right) + W_A\left(\frac{x-x_N}{\beta b}, \frac{y-y_N}{b}\right) + W_B\left(\frac{x-x_N}{\beta b}, \frac{y-b+y_N}{b}\right)\right], \tag{3.95}$$

where

$$\left.\begin{aligned} W_A\left(\frac{x}{b}, \frac{y}{b}\right) &= \frac{b^2}{4\pi} \sum_{-\infty}^{\infty}\sum{}' (-1)^n \frac{\partial}{\partial y}\left[W(x, y-2mb, -nh)\right] \\ W_B\left(\frac{x}{b}, \frac{y}{b}\right) &= \frac{b^2}{4\pi}\frac{\partial}{\partial y}\left[W(x,y,0)\right] \end{aligned}\right\} . \tag{3.96}$$

Thus w_i/U may be evaluated from charts of the functions W_A and W_B. The former chart A is illustrated for ratios $b/h = 2/5$, $10/7$ and 2 respectively in Figures 7(b), 7(c) and 7(a) of Reference 3.20. The latter chart B in Figure 5 of Reference 3.20 is independent of tunnel shape. Katzoff and Hannah describe in detail their graphical procedure for the computation of w_i on a yawed lifting wing. They also give useful advice on the calculation and preparation of charts with particular reference to rectangular tunnels with one or more of their sides open. Any such configuration can be treated by means of chart A dependent on b/h and the floor and roof condition and the universal chart B, but there may be changes of sign in Equation (3.95). To expedite the calculation of chart A, a horizontal row of sufficiently distant image doublets ($|m| \geqslant 2$, say) may be replaced by a row of horse-shoe vortices of span $2b$, so that all the trailing vortices except the innermost ones cancel in pairs; for large enough n ($|n| \geqslant 2$, say) the upwash field from the complete row of doublets is approximately that of a two-dimensional bound vortex extending from $y = -\infty$ to $y = +\infty$, as illustrated in Figure 3.10(a). In the case of closed side-walls and open floor and roof (type (4) of Section 3.2.2), when all the images are of the same sign, Katzoff and Hannah suggest that, instead of being extended horizontally, the distant image doublets are extended vertically into a source line and a sink line at a distance h apart. The source and sink lines in any column cancel in pairs, and only those at a distance $\frac{1}{2}h$ above or below the inner group of doublets ($|m| < 1$, $|n| < 1$) remain, as illustrated in Figure 3.10(b). Although the image system for a rectangular tunnel of type (4) is not valid, the procedure adopted here amounts to an approximate summation column by column (first with respect to n); it follows from the discussion above Equation (3.17) that this leads to a correct approximation while the alternative array of Figure 3.10(c) would fail.

A further complication may arise when the displacement of the model from the central horizontal plane $z = 0$ can no longer be ignored. This can result from long models at high incidence or when the floor of the tunnel is used to simulate the ground. In the former case the interference corrections can be large and changes in the distance d of the lifting element from the floor can be significant, as has already been seen for a small wing in Figure 3.3. In the latter case $(\frac{1}{2}h - d)$ may be even larger, and the interference corrections, though smaller than usual because the principal image in the floor is not included, will again depend on d. Silverstein and White (Ref. 3.32; 1935) made an early contribution in this field, mainly with regard to interference effects on the downwash at a tail plane (Section 3.6.2). Brown[3.33] derives general formulae for $(\delta_0)_U$ and $(\delta_0)_{Ug}$, the corresponding corrections to wind-tunnel experiments in ground effect, and he gives results for $b/h = 2$ and 4. Some values for the duplex tunnel are reproduced in Figure 3.11. In a typical case $(d = 0.25h)$, the principal image in the floor accounts for a large proportion, $\{(\delta_0)_U - (\delta_0)_{Ug}\}/(\delta_0)_U$, of the interference, but the ratio $(\delta_0)_{Ug}/(\delta_0)_U$ increases from 0.036 to 0.118 as σ increases from 0 to 0.6. Provided that d/h is fairly small, crude estimates of $(\delta_0)_{Ug}$ should suffice (Section 3.6.3).

The quantities $\delta_0(y,t)$ and $\delta_1(y,t)$ for off-centre models are formulated in Appendix II of Reference 3.4, and a simple approximation to the double summation for $\delta_1(y,t)$, based on Reference 3.33, is included. A full mathematical discussion of $\delta_0(y,t)$ and interference effects at a lifting line displaced vertically from the centre line of the tunnel is given by Sanders and Pounder in References 3.23 and 3.24. They give expressions in Equations (1.51) and (1.52 to 1.57) of Reference 3.23 for the interference velocities v_i and u_i respectively. The effect of the sidewash v_i on the aerodynamic forces is unknown, but u_i will give a correction ΔU to the stream velocity akin to that in Figure 3.3(b).

In practice, the distance d between model and floor will depend on x, so that the complete evaluation of streamline curvature would involve displacements in z. This effect has been considered in References 3.32 and 3.27 in relation to the downwash field near a tail by introducing two extra parameters d/h and d'/h corresponding to the vertical locations of the lifting element and the required w_i. In the approximate representation of Figure 3.10(a), the odd rows would be lowered by the distance $(d - \frac{1}{2}h)$ and the even rows would be raised by the same amount. Although it is inadmissible so to split the image system in two parts, just as Figure 3.10(c) is incorrect, it is possible to construct the required upwash field from that of an isolated doublet and that of Figure 3.10(b) with double the vertical spacing. We need the complete upwash field of a doublet placed centrally in a rectangular tunnel of breadth $2b$, height $2h$, with closed sides but open roof and floor

$$W_c\left(\frac{x}{b}, \frac{y}{b}, \frac{z}{b}\right) = \frac{b^2}{4\pi}\sum_{-\infty}^{\infty}\sum \frac{\partial}{\partial y}\left[W(x,\ y-2mb,\ z-2nh)\right] , \qquad (3.97)$$

where $\partial W/\partial y$ is defined in Equation (3.94) and the summation is made first with respect to n. The final generalization of Equation (3.95) is

$$\frac{w_i}{U} = \sum_N \frac{L_N}{\rho U^2 b^2}\left\{-\frac{b^2}{4\pi}\frac{\partial}{\partial y}\left[W\left(\frac{x-x_N}{\beta},\ y-y_N,\ z-z_N\right)\right] + \right.$$

$$+ W_C\left(\frac{x-x_N}{\beta b},\ \frac{y-y_N}{b},\ \frac{z-z_N}{b}\right) - W_C\left(\frac{x-x_N}{\beta b},\ \frac{y-y_N}{b},\ \frac{z-h+z_N}{b}\right) +$$

$$\left. + W_C\left(\frac{x-x_N}{\beta b},\ \frac{y-b+y_N}{b},\ \frac{z-z_N}{b}\right) - W_C\left(\frac{x-x_N}{\beta b},\ \frac{y-b+y_N}{b},\ \frac{z-h+z_N}{b}\right)\right\}. \quad (3.98)$$

Since an approximation to Equation (3.97) may be made on the basis of Figure 3.10(b) with double the vertical spacing, it may well be practicable and desirable to use Equation (3.98) for a very long and slender model at high incidence with the simplification that $y = y_N = 0$, while $(z - z_N)/b$ may be far from small.

3.4.2 Octagonal Tunnels

Unlike rectangular tunnels, an octagonal tunnel has no exact image system. Any attempt to construct such a system for a closed boundary containing an obtuse angle is thwarted sooner or later by the demand for images within the boundary. The treatment of octagonal tunnels is necessarily approximate, and artificial methods have to be introduced.

In principle, the two-dimensional problem of obtaining $\delta_0(y,t)$ can be solved by transforming the interior of the octagon into the half plane; the Schwarz-Christoffel theorem achieves this, but the algebra is prohibitive for a general octagonal boundary. Gent[3.13] has derived the appropriate transformation for a regular octagon of breadth b,

$$\omega = 1.7191\ (\tfrac{1}{2}b) \int_0^{\Omega} \prod_{p=1}^{2} (\Omega_p^2 - \Omega^2)^{-\frac{1}{4}}\, d\Omega \qquad (3.99)$$

with $\Omega_1 = \Omega_4^{-1} = 0.1989$ and $\Omega_2 = \Omega_3^{-1} = 0.6682$, so that the real axis in the $\Omega = Y + iZ$ plane represents the octagon in the ω plane. A convenient alternative is to map the octagon on a unit circle by the related transformation

$$\omega = \frac{ib}{\kappa}\int_{-1}^{\Omega} \frac{d\Omega}{(1 + \Omega^8)^{\frac{1}{4}}}, \qquad (3.100)$$

where $\kappa = 1.9565$. This is written as a rapidly converging power series in Ω, which is inverted to give

$$\Omega = \left(\frac{\omega\kappa}{ib} - \frac{\kappa}{2}\right) + \frac{1}{36}\left(\frac{\omega\kappa}{ib} - \frac{\kappa}{2}\right)^9 - \frac{11}{4896}\left(\frac{\omega\kappa}{ib} - \frac{\kappa}{2}\right)^{17} + \ldots .$$

A vortex pair of strengths $\pm K$ at $\omega = i(\frac{1}{2}b \pm t)$ and a point $\omega = i(\frac{1}{2}b + y)$ transform into a vortex pair of strengths $\pm K$ at $\Omega = \pm T$ and a point $\Omega = Y$ in the plane of the unit circle. Hence the upwash interference parameter in the ω plane of the octagon becomes

$$\delta_0(y,t) = \frac{Cw_i}{4Kt} = \frac{C}{8\pi t}\left[\left\{-\frac{T}{T^2-Y^2}+\frac{T^{-1}}{T^{-2}-Y^2}\right\}\left|\frac{d\Omega}{d\omega}\right| + \frac{t}{t^2-y^2}\right] , \qquad (3.101)$$

where

$$\left.\begin{aligned}\left|\frac{d\Omega}{d\omega}\right| &= \frac{\kappa}{b}(1+Y^8)^{\frac{1}{4}} = \frac{\kappa}{b}\left(1+\frac{1}{4}Y^8-\frac{3}{32}Y^{16}+\ldots\right)\\ T &= \frac{\kappa t}{b}+\frac{1}{36}\left(\frac{\kappa t}{b}\right)^9-\frac{11}{4896}\left(\frac{\kappa t}{b}\right)^{17}+\ldots\\ Y &= \frac{\kappa y}{b}+\frac{1}{36}\left(\frac{\kappa y}{b}\right)^9-\frac{11}{4896}\left(\frac{\kappa y}{b}\right)^{17}+\ldots\end{aligned}\right\} .$$

It follows from Equations (3.100) and (3.101) that

$$\delta_0(0,0) = \frac{C\kappa^2}{8\pi b^2} = \frac{(\sqrt{2}-1)\kappa^2}{4\pi} = 0.1262 \ ,$$

consistent with the table in Section 3.2.3. Gent also derives this result from the transformation (3.99). The mean parameters $(\delta_0)_U$ and $(\delta_0)_E$ for uniform and elliptic loading are given in Tables 1 and 2 of Reference 3.13 for $\sigma = 2s/b$ up to 0.8. Larger values of σ would require an increasing number of terms in the power series. By a simple adjustment to Equation (3.100) a similar analysis could be developed for any regular polygonal tunnel; the result corresponding to Equation (3.101) would rapidly approach that for a circular tunnel (Section 3.4.3), if the number of sides were increased.

For a more general class of closed octagonal tunnels Batchelor[3.11] has supplemented the image system for the rectangular tunnel by superposing the doubly infinite system illustrated in Figure 3.1(c). Here each vortex represents a quadratic distribution of vorticity increasing from zero at each corner to a maximum k_s at the centre of each fillet. Each fillet of length a is assumed to be the hypotenuse of an isosceles triangle, so that their images form an array of squares. Batchelor's method exploits the fact that the image system for the rectangular tunnel in Figure 3.1(b) gives approximately an antisymmetric linear variation in normal velocity v_n across a fillet with distance along the fillet. The same is true of the corresponding normal velocity from the vorticity round the image square, and the mutual effect of any two squares can be ignored. The vorticity k_s is chosen to cancel the velocity v_n as best it can. Batchelor's formulae have been generalized for arbitrary a , b and h in Reference 3.12, and the result may be expressed as

$$\delta_0(y,t) = \frac{C}{bh}\,\delta_{0R}(y,t) - \frac{CG}{15.36P}\sum_{m=0}^{\infty}\left[\chi(S_m^+,\ T_m^+) + \chi(S_m^-,\ T_m^-)\right] , \qquad (3.102)$$

where the cross-sectional area $C = bh - a^2$, $\delta_{0R}(y,t)$ is $\delta_0(y,t)$ for a closed rectangular tunnel as given in Equation (3.82), P is the doublet strength 2Kt and the functions G and χ are defined below. G/P is a constant dependent on the tunnel geometry and is proportional to the gradient of v_n at the centre of the fillet due to a small wing* at the tunnel centre; from Equation (5) of Reference 3.12,

$$\frac{G}{P} = \frac{2\pi^2 a}{b^3}\sum_{n=-\infty}^{\infty}(-1)^n\left[\frac{(1+\cos 2\pi M\cosh 2\pi N+\sin 2\pi M\sinh 2\pi N)(\sin 2\pi M+\sinh 2\pi N)}{(\cos 2\pi M+\cosh 2\pi N)^3} - \frac{\sin 2\pi M\cosh 2\pi N}{(\cos 2\pi M+\cosh 2\pi N)^2}\right], \tag{3.103}$$

where

$$\left.\begin{aligned} 2\pi M &= \frac{\pi a}{b\sqrt{2}} \\ 2\pi N &= \frac{\pi a}{b\sqrt{2}} - \frac{(2n+1)\pi h}{b} \end{aligned}\right\} .$$

The function χ represents the upwash field of a column of image squares and is given by Equation (9) of Reference 3.12 plus an extra term, viz.,

$$\begin{aligned} \chi(S,T) = {} & \frac{2}{15}\left(\frac{\pi a}{h}\right)^3(-2S^3+S) + \\ & + \frac{\sqrt{2}}{15}\left(\frac{\pi a}{h}\right)^4(-6S^3+S)T + \\ & + \frac{1}{30}\left(\frac{\pi a}{h}\right)^5(24S^5-20S^3+S) + \\ & + \frac{\sqrt{2}}{180}\left(\frac{\pi a}{h}\right)^6(120S^5-60S^3+S)T + \\ & + \frac{8}{5670}\left(\frac{\pi a}{h}\right)^7(-720S^7+840S^5-182S^3+S) + \\ & + \frac{17\sqrt{2}}{113400}\left(\frac{\pi a}{h}\right)^8(-5040S^7+4200S^5-546S^3+S)T , \end{aligned} \tag{3.104}$$

where S and T take the values

$$\left.\begin{aligned} S_m^{\pm} &= \operatorname{sech}\frac{\pi(a\sqrt{2}+b\pm 2y+2mb)}{2h} \\ T_m^{\pm} &= \tanh\frac{\pi(a\sqrt{2}+b\pm 2y+2mb)}{2h} \end{aligned}\right\} .$$

---

* Note, however, the remarks above and below Equation (3.141), that G/P will depend on t when b/h is large.

The parameter $(\delta_0)_E$, as defined in Equation (3.46), has been derived approximately in References 3.11 and 3.12. For three particular octagonal tunnels $(\delta_0)_E$ as a function of σ may be identified with the quantity $\frac{1}{2}\delta$ from Table 4 of Reference 3.11 and from Tables 1 and 2 of Reference 3.12. $(\delta_0)_E$ for $\sigma = 0$ is given by Equations (3.102) to (3.104) with $y = t = 0$. This has been computed for the regular octagon $a = b(\sqrt{2} - 1)$, $b = h$. Equation (3.103) gives $Gb^2/P = -1.307$, so that Equation (3.102) becomes

$$\delta_0(0,0) = \frac{C}{b^2}\left[0.13678 - \frac{2 \times -1.307}{15.36}(0.0819 + 0.0053 + \ldots)\right]$$

$$= 0.82843 \times 0.15147 = 0.1255 ,$$

which is to be compared with the exact value $\delta_0(0,0) = 0.1262$ from Reference 3.13. The expansion in Equation (3.104) must fail if a/h is too large, but it appears to be satisfactory provided that $a < 0.35h$. The regular octagon and the NPL 13 x 9 tunnel have slightly larger fillets than this.

A more elegant, but less accurate method of dealing with the same problem has been formulated by Loos[3.21]. He replaces the distributed vorticity around Batchelor's image squares by a semi-infinite trailing quadrupole vortex at the centre of each square. The strength of the quadrupole is determined from the condition that there is zero flow across each half fillet. Unfortunately, no numerical results are given.

The accuracy to which v_E is cancelled by the squares of vorticity is discussed in Reference 3.12. With reference to Figure 5 of Reference 3.12, the accuracy deteriorates as wing span increases; for a typical span, $\sigma = 2/3$., it is found that the maximum uncertainty in G/P is of order 20%, and this can well be larger if the fillets no longer form isosceles triangles. In view of the consequent uncertainty in the second term of Equation (3.102) for wings of large span, it is pertinent to consider the following artifice. Equation (3.28) gives a good approximation to $(\delta_0)_E$ when σ is small; it may be rewritten as

$$(\delta_0)_E = (\delta_{0R})_E \frac{bh + C}{2bh} \quad \text{when} \quad \sigma = 0 . \tag{3.105}$$

When σ is very large, the fillets will have a negligible effect compared with those of the principal images in the side-walls, and we may write

$$(\delta_0)_E = (\delta_{0R})_E \frac{C}{bh} \quad \text{when} \quad \sigma = 1 , \tag{3.106}$$

since the influence of the fillets on w_i may be neglected. Since $(\delta_0)_E$ is an even function of σ, we combine Equations (3.105) and (3.106) to give

$$(\delta_0)_E = (\delta_{0R})_E \left[\left(\frac{1}{2} + \frac{C}{2bh}\right) - \left(\frac{1}{2} - \frac{C}{2bh}\right)\sigma^2\right] . \tag{3.107}$$

where $(\delta_{0R})_E$ is given by Equation (3.84) or Figure 3.9 for the rectangular tunnel of the same breadth and height. The success of Equation (3.107) is demonstrated in Figure 3.12 for the regular octagon of Reference 3.13 and the NPL 9 x 7 and 13 x 9 tunnels corresponding to the respective Tables 1 and 2 of Reference 3.12.

The treatment of rectangular tunnels in Section 3.4.1 includes an analysis of the streamline curvature through the parameter $\delta_1(y,t)$ of Equation (3.42). There is no corresponding theory for octagonal tunnels, and we can suggest nothing better than Equation (3.31), which is now written as

$$\delta_1(y,t) = \delta_0(y,t)\sqrt{\frac{bh}{C}}\,\frac{\delta_{1R}(y,t)}{\delta_{0R}(y,t)}\,, \qquad (3.108)$$

where $\delta_0(y,t)$ is given by Equation (3.102) and the parameters $\delta_{0R}(y,t)$ and $\delta_{1R}(y,t)$ are those for the basic rectangular tunnel from Equations (3.82) and (3.87). More simply than by Equation (3.108), it may suffice to evaluate the upwash interference as if the tunnel were rectangular and then to apply the correction factor

$$\left(\frac{bh}{C}\right)^{\frac{3}{2}}\frac{(\delta_0)_E}{(\delta_{0R})_E} \approx \left(\frac{bh}{C}\right)^{\frac{3}{2}}\left[\left(\frac{1}{2}+\frac{C}{2bh}\right)-\left(\frac{1}{2}-\frac{C}{2bh}\right)\sigma^2\right] \qquad (3.109)$$

to all contributions involving $\delta_1(y,t)$. With reference to Equation (3.55), it is suggested that the elliptic loading factor $\overline{W}$ be used, and that $\Delta\alpha/C_L$ be evaluated as if the fillets were not present and split into two parts

$$\left(\frac{\Delta\alpha}{C_L}\right)_R = \frac{S}{bh}(\delta_{0R})_E + \left[\left(\frac{\Delta\alpha}{C_L}\right)_R - \frac{S}{bh}(\delta_{0R})_E\right].$$

The first part would be replaced by the corresponding quantity for the octagonal tunnel, and the second multiplied by the factor (3.109). Thus

$$\frac{\Delta\alpha}{C_L} = \left(\frac{bh}{C}\right)^{\frac{3}{2}}\frac{(\delta_0)_E}{(\delta_{0R})_E}\left(\frac{\Delta\alpha}{C_L}\right)_R - \frac{S}{C}(\delta_0)_E\left\{\left(\frac{bh}{C}\right)^{\frac{1}{2}} - 1\right\}. \qquad (3.110)$$

The drag correction of Equation (3.56) does not involve $\delta_1(y,t)$ and would simply become

$$\frac{\Delta C_D}{C_L^2} = \frac{S}{C}(\delta_0)_E \qquad (3.111)$$

for elliptic spanwise loading. The principle of Equation (3.109) can be applied to the residual correction $\Delta C_m/C_L$ from Equations (3.57) to (3.59). $(\Delta C_m)_2$ depends only on streamline curvature, but $(\Delta C_m)_1$ has to be split into two parts

$$(\Delta C_m)_1 = (\Delta C_m)_{11} + (\Delta C_m)_{12}\,,$$

where $(\Delta C_m)_{11}$ corresponds to

$$\left[\left(\frac{w_i}{UC_L}\right)_{0.75} - \frac{\Delta\alpha}{C_L}\right] = \frac{4S}{\pi C}\int_0^1 \frac{\partial}{\partial t}\{t\delta_0(y,t)\}\left\{1-\frac{t^2}{s^2}\right\}^{\frac{1}{2}} d\left(\frac{t}{s}\right) - \frac{S}{C}(\delta_0)_E$$

in Equation (3.58). $(\Delta C_m)_{11}$ has to be evaluated for the octagonal tunnel as if $\delta_1(y,t) \equiv 0$, and the remainder $\Delta C_m - (\Delta C_m)_{11} = (\Delta C_m)_{12} + (\Delta C_m)_2$ for the rectangular tunnel. Thus

$$\frac{\Delta C_m}{C_L} = \frac{(\Delta C_m)_{11}}{C_L} + \left(\frac{bh}{C}\right)^{\frac{3}{2}} \frac{(\delta_0)_E}{(\delta_{0R})_E}\left[\frac{\Delta C_m}{C_L} - \frac{(\Delta C_m)_{11}}{C_L}\right]_R . \tag{3.112}$$

The principle can of course be used with arbitrary spanwise loading and with any method of correction to measured quantities suggested in Sections 3.3.3 to 3.3.6, provided that $\delta_0(y,t)$ is calculated from Equations (3.102) to (3.104) and the factor (3.109) is applied to all the upwash interference associated with streamline curvature.

Interference effects on off-centre models in a particular octagonal tunnel have been investigated by Batchelor in Reference 3.34. He has shown that fillets have a negligible effect on the incremental interference upwash due to a vertical displacement $(d - \frac{1}{2}h)$ of the model from the central position for all practical values of d. It therefore seems that Equation (3.102) may be used with $\delta_{0R}(y,t)$ as given in Appendix II of Reference 3.4. The extent to which this holds for values of d outside the range $0.4h < d < 0.6h$, say, could be checked by an extension of the analysis for the regular octagonal tunnel in Reference 3.13.

3.4.3 Circular and Elliptical Tunnels

While rectangular and octagonal tunnels are plentiful, there are not many elliptical tunnels in regular use today. Closed elliptical working sections are not particularly convenient, but the rounded shape is more appropriate for an open jet and a few open elliptical tunnels have survived. Only the simplest wall interference corrections are likely to be needed, and this may explain the lack of theoretical developments for elliptical tunnels in the past twenty years. On the other hand, the special case of a closed circular tunnel has received full development.

A brief description of the early work will suffice. Sanuki and Tani (Ref.3.35; 1932) use the transformation

$$y + iz = l \cosh (\eta + i\zeta) , \tag{3.113}$$

so that a segment of $\eta = \eta_0$ corresponds to an elliptical boundary of breadth $b = 2l \cosh \eta_0$ and height $h = 2l \sinh \eta_0$. They solve for the stream function in the (η, ζ) plane and evaluate the parameter $(\delta_0)_U$ for uniform spanwise loading from Equation (3.45). For a wing situated at

$$\left.\begin{aligned} |y| &< l \cosh \eta' \cos \zeta' \\ z &= l \sinh \eta' \sin \zeta' \end{aligned}\right\}$$

in a closed and open tunnel respectively

$$(\delta_0)_U = \frac{\sinh \eta_0 \cosh \eta_0}{2 \cosh^2\eta' \cos^2\zeta'}\left[\sum_{\substack{n=1 \\ \text{odd}}}^{\infty} \frac{\cosh^2 n\eta' \cos^2 n\zeta'}{n(e^{2n\eta_0} + 1)} + \sum_{\substack{n=2 \\ \text{even}}}^{\infty} \frac{\sinh^2 n\eta' \sin^2 n\zeta'}{n(e^{2n\eta_0} - 1)}\right] \tag{3.114}$$

$$(\delta_0)_U = -\frac{\sinh \eta_0 \cosh \eta_0}{2\cosh^2\eta' \cos^2\zeta'}\left[\sum_{\substack{n=1\\ \text{odd}}}^{\infty} \frac{\cosh^2 n\eta' \cos^2 n\zeta'}{n(e^{2n\eta_0} - 1)} + \sum_{\substack{n=2\\ \text{even}}}^{\infty} \frac{\sinh^2 n\eta' \sin^2 n\zeta'}{n(e^{2n\eta_0} + 1)}\right]\Bigg\} . \quad (3.114)$$

For a centrally placed wing $\eta' = 0$ and the summations in even n disappear. In the limiting case of small span, $\zeta' = \frac{1}{2}\pi$, the result for a closed tunnel may be identified with the first of Equations (3.29). Similarly the second of Equations (3.114) for an open tunnel reduces to the first of Equations (3.30) with a change of sign and $\theta = \eta_0 = \tanh^{-1}(h/b)$. For wings of finite span and $b/h < 1$ there would be a corresponding analysis with the transformation

$$y + iz = l \sinh (\eta + i\zeta) .$$

Curves* of $(\delta_0)_U$ against $\sigma = 2s/b = (\cosh \eta' \cos \zeta')/\cosh \eta_0$ are given in Figures 4 and 5 of Reference 3.35 for wings lying along the major axis of the elliptical section. It is found that the minimum interference parameter for small wings in a closed tunnel, $\delta_0 = 0.1147$, occurs when $b/h = \sqrt{2}$, as does the minimum $\delta_0 = 0.1190$ for closed rectangular tunnels; the corresponding minima in $-\delta_0$ for open tunnels occur when $b/h = 1/\sqrt{2}$. For any particular closed or open elliptical tunnel the minimum interference parameter occurs when the wing tips are situated at the foci of the ellipse, so that $\eta' = \zeta' = 0$ and

$$\sigma = 2l/b = \operatorname{sech} \eta_0 = (b^2 - h^2)^{\frac{1}{2}}/b .$$

This configuration is of particular interest when the wing has elliptic spanwise loading. Glauert has proved the remarkable result that the interference upwash is constant along the wing span, whether the tunnel is closed or open (Ref.3.1, pp.29 to 31); respectively

$$(\delta_0)_E = \frac{h}{4(b+h)} \quad \text{or} \quad -\frac{b}{4(b+h)} , \quad \text{when} \quad \sigma = \frac{(b^2 - h^2)^{\frac{1}{2}}}{b} . \quad (3.115)$$

The important general solution for $(\delta_0)_E$ has been obtained by Rosenhead (Ref.3.36; 1933) in terms of elliptic functions. The resulting formulae are rather complicated and comprise four expressions for $(\delta_0)_E$ according as $b > h$ or $h > b$ and the boundary is closed or open; his useful numerical data are presented in Figure 3.13. The special case of a circular tunnel gives a simple result for the parameter $\delta_0(y, t)$ of Equation (3.42); for closed and open tunnels respectively

$$\delta_0(y, t) = \pm \frac{R^4}{8(R^4 - t^2y^2)} , \quad (3.116)$$

where R is the radius (Ref.3.1, p.13). It can be shown (cf., Ref.3.4, Appendix II) that from Equations (3.46) and (3.116)

---

* Sanuki's tabulated values appear in the Appendix to Reference 3.14.

$$(\delta_0)_E = \frac{16}{\pi^2}\int_0^1\int_0^1 \delta_0(y,t)\left(\frac{t}{s}\right)^2\left\{1-\left(\frac{t}{s}\right)^2\right\}^{-\frac{1}{2}}\left\{1-\left(\frac{y}{s}\right)^2\right\}^{\frac{1}{2}} d\left(\frac{t}{s}\right)d\left(\frac{y}{s}\right)$$

$$= \pm\frac{1}{\pi\sigma^2}\left[\tfrac{1}{2}\pi - E_1(\sigma^2)\right] \; , \qquad (3.117)$$

where $\sigma = s/R$ and the complete elliptic integral

$$E_1(\sigma^2) = \int_0^{\frac{1}{2}\pi}(1-\sigma^4\sin^2\phi)^{\frac{1}{2}}\, d\phi \; .$$

There is the convenient expansion of Equation (3.117)

$$(\delta_0)_E = \pm\frac{1}{8}\left[1+\frac{3}{4^2}\sigma^4+\frac{3^2.5}{4^2.6^2}\sigma^8+\frac{3^2.5^2.7}{4^2.6^2.8^2}\sigma^{12}+\ldots\right] \; , \qquad (3.118)$$

positive for a closed and negative for an open circular tunnel, in agreement with Equation (6.8) of Reference 3.1.

Analytical expressions for $(\delta_0)_U$ have been obtained when the tunnel boundary is partly open and partly closed. Kondo$^{3.14}$ considers circular tunnels with a symmetrical closed portion below the wing by transforming the interior of the circle into an infinite strip with one straight boundary open and the other closed. For a small wing, zero lift interference is found when 36.4% of the circular boundary is closed, and the percentage increases slowly with wing span. Riegels$^{3.37}$ has extended Kondo's analysis to elliptical tunnels and gives numerical results for $b/h = \sqrt{2}$. For example, the closed portion can be chosen so that $|(\delta_0)_U| < 0.008$ for a range of span $0 \leqslant \sigma \leqslant 0.6$. Riegels also treats elliptical tunnels with closed portions above and below the wing by transforming the interior into a rectangular boundary with open sides and closed floor and roof; but this arrangement is a less effective means of minimizing lift interference for a range of wing span.

Before we consider further numerical results, it is convenient to outline the more elaborate mathematical methods that are needed to obtain the complete interference upwash field due to the lifting element. General theories for closed and open circular and elliptical tunnels are developed by Lotz (Ref.3.38; 1935). An independent treatment of the circular tunnels by Burgers$^{3.39}$ also appeared in 1935.

For the circular tunnels Lotz$^{3.38}$ solved the differential Equation (3.2) in cylindrical co-ordinates for

$$\Phi = \Phi_m + \Phi_i = \Phi_m + \Phi_1 + \Phi_2 \; , \qquad (3.119)$$

where Φ_m is the potential field of the horse-shoe vortex. Φ_1 corresponds to the image L-vortices of Figure 3.14 so that $(\Phi_m + \Phi_1)$ satisfies the boundary conditions at $x = 0$ and $\pm\infty$, and Φ_2 is to be determined. With allowance for compressibility the assumed series to satisfy the differential Equation (3.2) is

$$\Phi_2 = \frac{K}{4\pi}\sum_{n=1}^{\infty} \cos n\theta \sum_{k=1}^{\infty} D_{nk} \sin\left(\frac{k\pi x}{\beta pR}\right) J_n\left(\frac{ik\pi r}{pR}\right) . \qquad (3.120)$$

where $\beta^2 = 1 - M^2$, D_{nk} are unknown coefficients, J_n are Bessel functions of the first kind, and the periodicity in x will disappear as p is allowed to increase indefinitely. For the closed tunnel, zero normal velocity on the boundary $r = R$ gives the condition

$$\frac{\partial\Phi_2^{(1)}}{\partial r} = -\frac{\partial}{\partial r}(\Phi_n + \Phi_1^{(1)}) = -\frac{K}{4\pi R}\sum_{n=1}^{\infty} g_n\left(\frac{x}{\beta R}\right)\cos n\theta , \qquad \text{say,}$$

whence, by Equation (3.120),

$$D_{nk} = -\frac{1}{ik\pi J_n'(ik\pi/p)}\int_{-p}^{p} g_n\left(\frac{x}{\beta R}\right)\sin\left(\frac{k\pi x}{\beta pR}\right) d\left(\frac{x}{\beta R}\right) ; \qquad (3.121)$$

for the open tunnel, zero tangential velocity on the boundary gives the condition

$$\frac{\partial\Phi_2^{(2)}}{\partial x} = -\frac{\partial}{\partial x}(\Phi_n + \Phi_1^{(2)}) = -\frac{K}{4\pi\beta R}\sum_{n=1}^{\infty} l_n\left(\frac{x}{\beta R}\right)\cos n\theta , \qquad \text{say,}$$

whence, by Equation (3.120),

$$D_{nk} = -\frac{1}{k\pi J_n(ik\pi/p)}\int_{-p}^{p} l_n\left(\frac{x}{\beta R}\right)\cos\left(\frac{k\pi x}{\beta pR}\right) d\left(\frac{x}{\beta R}\right) . \qquad (3.122)$$

After the coefficients from Equation (3.121) or (3.122) have been substituted in Equation (3.120), the substitution $k\pi/p = q$ is made as $p \to \infty$, so that

$$\sum_{k=1}^{\infty}\frac{1}{k}F\left(\frac{k\pi\xi}{p}\right) \quad \text{is replaced by} \quad \int_0^{\infty}\frac{1}{q}F(q\xi)\,dq .$$

Thus the respective expressions for the upwash $w_2 = \pm(1/r)\partial\Phi_2/\partial\theta$ in the plane of the wing ($\theta = \pi/2$ or $3\pi/2$ in Figure 3.14) become

$$\left.\begin{aligned} w_2^{(1)} &= \pm\frac{K}{4\pi r}\sum_{n=1}^{\infty} n \sin n\theta \int_0^{\infty} \frac{\sin(qx/\beta R)\, J_n(iqr/R)}{i\pi q J_n'(iq)}\left[\int_{-\infty}^{\infty} g_n(\xi)\sin(q\xi)\,d\xi\right] dq \\ w_2^{(2)} &= \pm\frac{K}{4\pi r}\sum_{n=1}^{\infty} n \sin n\theta \int_0^{\infty} \frac{\sin(qx/\beta R)\, J_n(iqr/R)}{\pi q J_n(iq)}\left[\int_{-\infty}^{\infty} l_n(\xi)\cos(q\xi)\,d\xi\right] dq \end{aligned}\right\} . \qquad (3.123)$$

Along the axis of the tunnel $r = 0$ Equations (3.123) become relatively simple expressions, since

$$\frac{J_1(iqr/R)}{iqr/R} \to \tfrac{1}{2} \qquad \text{and, for } n > 1\,, \qquad \frac{J_n(iqr/R)}{iqr/R} \to 0\ ;$$

for closed and open circular tunnels respectively

$$\left.\begin{aligned} w_2^{(1)} &= \frac{K}{8\pi R}\int_0^\infty \frac{\sin(qx/\beta R)}{\pi J_1'(iq)}\left[\int_{-\infty}^{\infty} g_1(\xi)\sin(q\xi)\,d\xi\right]dq \\ w_2^{(2)} &= \frac{K}{8\pi R}\int_0^\infty \frac{i\sin(qx/\beta R)}{\pi J_1(iq)}\left[\int_{-\infty}^{\infty} l_1(\xi)\cos(q\xi)\,d\xi\right]dq \end{aligned}\right\}\,, \qquad (3.124)$$

where

$$\left.\begin{aligned} \frac{K}{8\pi R}\,g_1\!\left(\frac{x}{\beta R}\right) &= \frac{1}{\pi}\int_0^\pi \frac{\partial}{\partial r}\left(\Phi_m + \Phi_1^{(1)}\right)_{r=R}\cos\theta\,d\theta \quad \text{for the closed tunnel} \\ \frac{K}{8\pi R}\,l_1\!\left(\frac{x}{\beta R}\right) &= \frac{\beta}{\pi}\int_0^\pi \frac{\partial}{\partial x}\left(\Phi_m + \Phi_1^{(2)}\right)_{r=R}\cos\theta\,d\theta \quad \text{for the open tunnel} \end{aligned}\right\}.$$

Lengthy expressions for the velocity potentials Φ_m , $\Phi_1^{(1)}$ and $\Phi_1^{(2)}$ are defined by the vortex configurations in Figure 3.14. The equal and opposite interference upwashes corresponding to $\Phi_1^{(1)}$ and $\Phi_1^{(2)}$ are readily defined in terms of the function $W(x,y,z)$ of Equation (3.79), and the limit as $z \to 0$

$$w_1^{(1)} = -\,w_1^{(2)} = \frac{\partial\Phi_1^{(1)}}{\partial z} = \frac{Kt}{4\pi(R^2+yt)}\left[1 + \frac{xt/\beta}{R^2+yt+\{(R^2+yt)^2+(xt/\beta)^2\}^{\frac{1}{2}}}\right] +$$
$$+\frac{Kt}{4\pi(R^2-yt)}\left[1 + \frac{xt/\beta}{R^2-yt+\{(R^2-yt)^2+(xt/\beta)^2\}^{\frac{1}{2}}}\right]. \qquad (3.125)$$

The total interference upwashes in the plane of the wing are

$$\left.\begin{aligned} w_i^{(1)}(x,y) &= w_1^{(1)} + w_2^{(1)} \quad \text{for the closed tunnel} \\ w_i^{(2)}(x,y) &= w_1^{(2)} + w_2^{(2)} \quad \text{for the open tunnel} \end{aligned}\right\}. \qquad (3.126)$$

It will be observed that $w_2^{(1)}$ and $w_2^{(2)}$ in Equations (3.123) vanish when $x = 0$ and the whole interference upwash comes from Equations (3.125). On the other hand, for a small wing $(t \to 0)$ Equations (3.125) give zero upwash gradients $\partial w_i^{(1)}/\partial x$ and $\partial w_i^{(2)}/\partial x$ at $x = 0$, so that the streamline curvature comes entirely from Equations (3.123).

In Reference 3.39 Burgers considers point concentrations of lift at arbitrary positions in the tunnel; for an element of lift L_N at (x_N, y_N) in the plane $z = 0$ the upwash velocity in a closed circular tunnel is obtained as

$$\frac{\partial \Phi_N}{\partial z} = w_N^{(1)}(x,y) = \frac{L_N}{\pi\rho U}\sum_{n=1}^{\infty}\sum_{s}\frac{n^2 J_n(\kappa_s y)\, J_n(\kappa_s y_N)}{(\kappa_s^2 R^2 - n^2) y y_N [J_n(\kappa_s R)]^2}\, e^{\kappa_s (x-x_N)/\beta} \qquad (3.127)$$

when $(x - x_N) \leqslant 0$; here $\sum_s$ denotes that, for each n, s extends over all positive roots of $J_n'(\kappa_s R) = 0$. When $(x - x_N) > 0$

$$w_N(x,y) = w_N(\infty,y) - w_N(2x_N - x, y) \quad . \qquad (3.128)$$

The corresponding result for an open circular tunnel, when $(x - x_N) \leqslant 0$, is

$$w_N^{(2)}(x,y) = \frac{L_N}{\pi\rho U}\sum_{n=1}^{\infty}\sum_{s}\frac{n^2 J_n(\bar{\kappa}_s y)\, J_n(\bar{\kappa}_s y_N)}{(\bar{\kappa}_s R)^2 y y_N [J_n'(\bar{\kappa}_s R)]^2}\, e^{\bar{\kappa}_s (x-x_N)/\beta} \quad , \qquad (3.129)$$

where $\sum_s$ now denotes that, for each n, s extends over all positive roots of $J_n(\bar{\kappa}_s R) = 0$. Again Equation (3.128) holds for $(x - x_N) > 0$. The interference upwash velocity is obtained by subtracting from $w_N(x,y)$ the unconstrained upwash

$$w_{N0}(x,y) = \frac{L_N}{4\pi\rho U}\,\frac{\beta^2\{(x-x_N)^2 + \beta^2(y-y_N)^2\}^{-\frac{1}{2}}}{\{(x-x_N)^2 + \beta^2(y-y_N)^2\}^{\frac{1}{2}} - (x-x_N)} \qquad (3.130)$$

due to the lifting element. Thus for a number of lifting elements

$$w_i(x,y) = \sum_N [w_N(x,y) - w_{N0}(x,y)] \qquad (3.131)$$

in accordance with Equations (3.127) to (3.130).

An outline of the treatment of elliptical tunnels by Lotz[3.38] will complete the basic theory. She uses the elliptical co-ordinates of Equation (3.113), so that the differential Equation (3.2) becomes

$$\beta^2\frac{\partial^2\Phi}{\partial x^2} + \frac{1}{l^2(\cosh^2\eta - \cos^2\zeta)}\left(\frac{\partial^2\Phi}{\partial \eta^2} + \frac{\partial^2\Phi}{\partial \zeta^2}\right) = 0 \quad . \qquad (3.132)$$

The solution is again obtained in the form of Equation (3.119), where Φ_1 corresponds to Figure 14, 15 or 16 of Reference 3.38 and

$$\Phi_2 = -\frac{K}{4\pi}\sum_{\nu}\sum_{k} C_{\nu k}\sin\left(\frac{2k\pi x}{\beta p b}\right)\bar{M}_{\nu k}(\eta)\, M_{\nu k}(\zeta) \quad , \qquad (3.133)$$

where b , the tunnel breadth, is the major axis of the ellipse. By Equations (3.132) and (3.133), with separation of the variables η and ζ ,

$$\left.\begin{aligned} \frac{d^2\bar{M}_{\nu k}}{d\eta^2} - \left(\frac{2k^2\pi^2 l^2}{p^2 b^2}\cosh 2\eta + \nu\right)\bar{M}_{\nu k} &= 0 \\ \frac{d^2 M_{\nu k}}{d\zeta^2} + \left(\frac{2k^2\pi^2 l^2}{p^2 b^2}\cos 2\zeta + \nu\right) M_{\nu k} &= 0 \end{aligned}\right\} \quad , \qquad (3.134)$$

where ν is determined, for each k, so that the Mathieu function $\mathrm{me}_{\nu_k}(\zeta)$ is periodic in ζ. As for the circular tunnels, p is eventually allowed to tend to infinity so that $\sum_k$ is replaced by an integral. The final expressions for Φ_2 for closed and open elliptical tunnels respectively are found in the formidable Equations (73) and (50) of Reference 3.38. By Equations (3.113) and (3.119) the interference upwash becomes

$$w_i = \frac{\partial}{\partial z}(\Phi_1 + \Phi_2) = \frac{\partial \Phi_1}{\partial z} + \frac{\cosh \eta \sin \zeta}{l(\cosh^2\eta - \cos^2\zeta)} \frac{\partial \Phi_2}{\partial \eta} + \frac{\sinh \eta \cos \zeta}{l(\cosh^2\eta - \cos^2\zeta)} \frac{\partial \Phi_2}{\partial \zeta} \quad . \qquad (3.135)$$

Although Lotz gives graphs of w_i for both closed and open elliptical tunnels having $b = h\sqrt{2}$, the calculations only cover small span ($\sigma = 0$) and uniform loading when $\sigma = \frac{1}{2}\sqrt{2}$ and the wing tips lie at the foci of the ellipse. These difficult calculations (due to Riegels) illustrate a technique for handling Equations (3.133) to (3.135). Nevertheless, for general elliptical tunnels the data in Figures 3.5 and 3.13 may have to serve. The interference corrections $\Delta\alpha$ and ΔC_D must then be evaluated from Equations (3.85) with the aid of $(\delta_0)_E$ from Figure 3.13 and δ_1/δ_0 for a small wing from Figure 3.5 or Equation (3.31). For closed tunnels it seems better to invoke Equations (3.110) to (3.112), where now $bh/C = 4/\pi$. The quantities

$$\left(\frac{\Delta\alpha}{C_L}\right)_R \quad \text{and} \quad \left[\frac{\Delta C_m}{C_L} - \frac{(\Delta C_m)_{11}}{C_L}\right]_R$$

have to be evaluated for a closed rectangular tunnel of the same breadth and height as the elliptical tunnel. The ratio $(\delta_0)_E/(\delta_{0R})_E$ for arbitrary b/h and σ may be evaluated from Figures 3.13(a) and 3.9. Equation (3.112) for the residual correction to pitching moment involves the quantity $(\Delta C_m)_{11}/C_L$ which is to be calculated from Equation (3.58) as if $\delta_1(y,t) \equiv 0$, i.e. as if

$$\left[\left(\frac{w_i}{UC_L}\right)_{0.75} - \frac{\Delta\alpha}{C_L}\right] = \int_0^1 (1 - W)\left[\int_0^1 \frac{4\Gamma s}{UCC_L} \frac{\partial}{\partial t}\{t\delta_0(y,t)\}\, d\left(\frac{t}{s}\right)\right] d\left(\frac{y}{s}\right)$$

$$= \frac{S}{C}\left[\frac{4}{\pi}\int_0^1 \frac{\partial}{\partial t}\{t\delta_0(y,t)\}\left\{1 - \left(\frac{t}{s}\right)^2\right\}^{\frac{1}{2}} d\left(\frac{t}{s}\right) - (\delta_0)_E\right] ,$$

if the weighting factor W in Equation (3.55) and the circulation Γ in Equation (3.47) are both elliptic. This requires the knowledge of $\delta_0(y,t)$, which is formulated on the basis of Reference 3.38 in Equations (2) to (5) of Reference 3.40 by Gavin and Hensel; their function δ_0 requires the factor 0.125 to be consistent with Equation (3.42).

For circular tunnels, exact values of δ_1 are available for wings of small span. Von Baranoff[3.41] derives the result

$$\delta_1 = \frac{1}{4\pi}\int_0^\infty \frac{q^2K_2(q) - qK_1(q)}{I_1'(q)}\, dq$$

$$= -\frac{1}{4\pi}\int_0^\infty \frac{q^2K_1'(q)}{I_1'(q)}\, dq = 0.24975 \quad , \qquad (3.136)$$

when the tunnel is closed; for the open circular tunnel

$$\delta_1 = -\frac{1}{4\pi}\int_0^\infty \frac{q^2K_1(q)}{I_1(q)}\,dq = -0.19921 \ , \tag{3.137}$$

where $I_1(q) = -iJ_1(iq)$ and $K_1(q)$ are the modified Bessel functions. Lotz's calculations are consistent with the latter result, but overestimate the former. In Figure 8 of Reference 3.19 Eisenstadt gives further evidence to suggest that Lotz's calculations for the closed circular tunnel are incorrect while those of Burgers are reliable. The relative simplicity of Equations (3.127) and (3.130) as compared with Equations (3.123) and (3.125) commends the method of Burgers as a computational procedure. For the closed tunnel, however, both methods have received important development. While Eisenstadt[3.19] has extended Lotz's method to treat a swept lifting line, Sivells and Salmi[3.26] give extensive tables and charts based on Equation (3.127).

As a lifting element Eisenstadt takes a skew horse-shoe vortex with corners at an origin on the axis of the tunnel and at a point $(x, r, \theta) = (t \tan \Lambda,\ t \sec \Lambda,\ \tfrac{1}{2}\pi)$ in the co-ordinate system of Figure 3.14(a). Thus Λ is the angle of sweepback of the bound vortex, and t is the perpendicular distance between the trailing vortices. He chooses Φ_1 to correspond to the L-vortex of Figure 3.14(b) in the half plane $\theta = \tfrac{1}{2}\pi$, so that $\partial\Phi_1/\partial z$ is independent of Λ and is given by the second term of Equation (3.125). In an appendix he proves the validity of Lotz's method and discusses the convergence of the series for Φ_2 and its derivatives. In Reference 3.38, $\partial(\Phi_m + \Phi_1)/\partial r$ is even in y but not necessarily odd in z, but Eisenstadt's quantity

$$\frac{\partial\Phi_2}{\partial r} = -\frac{\partial}{\partial r}(\Phi_m + \Phi_1) = -\frac{K}{4\pi R}\sum_{n=1}^{\infty}\bar{g}_n\left(\frac{x}{\beta R}\right)\sin\{n(\theta - \tfrac{1}{2}\pi)\}$$

is odd in z but not necessarily even in y : moreover, Φ_2 is not in general odd in x. Therefore Equation (3.120) has to be modified and the first of Equations (3.123) is replaced by

$$\frac{\partial\Phi_2}{\partial z} = \mp\frac{K}{4\pi r}\sum_{n=1}^{\infty} n\cos\{n(\theta - \tfrac{1}{2}\pi)\}\int_0^\infty \frac{J_n(iqr/R)}{i\pi q J_n'(iq)}\left[\int_{-\infty}^{\infty}\bar{g}_n(\xi)\cos\left(q\xi - \frac{qx}{\beta R}\right)d\xi\right]dq \ , \tag{3.138}$$

where the negative sign corresponds to $y > 0$ $(\theta = \tfrac{1}{2}\pi)$ and the positive sign to $y < 0$ $(\theta = 3\pi/2)$. The integral in square brackets is expressed as

$$\int_{-\infty}^{\infty}\bar{g}_n(\xi)\cos\left(q\xi - \frac{qx}{\beta R}\right)d\xi = 2l_n(q)\sin\frac{qx}{\beta R} + 2k_n(q)\cos\frac{qx}{\beta R}$$

and the functions $l_n(q)$ and $k_n(q)$ are tabulated for $n = 1, 2, 3$. Finally in Table 4 of Reference 3.19

$$\frac{4\pi R^2 w_i}{Kt} = \frac{4\pi R^2}{Kt}\left(\frac{\partial\Phi_1}{\partial z} + \frac{\partial\Phi_2}{\partial z}\right) \tag{3.139}$$

is given as a function of four parameters; in the equivalent incompressible flow (Table 3.I) these parameters become

$$\frac{t}{R}\,(1+\beta^{-2}\tan^2\Lambda)^{\frac{1}{2}}\,, \qquad \cot^{-1}(\beta\cot\Lambda)\,, \qquad \frac{x}{\beta R} \qquad \text{and} \qquad \frac{y}{R}\,(1+\beta^{-2}\tan^2\Lambda)^{\frac{1}{2}}$$

which are somewhat inconvenient unless $M = 0$.

Sivells and Salmi[3.26] had found the results of Reference 3.19 for swept horse-shoe vortex elements difficult to apply and therefore, following Burgers, used point concentrations of lift. They have simply evaluated the quantity

$$F\left(\frac{y_N}{R}\,,\ \frac{x-x_N}{\beta R}\,,\ \frac{y}{R}\right) = \frac{\pi\rho U^2R^2}{L_N}\,[w_N(x,y) - w_{N0}(x,y)] \qquad (3.140)$$

from Equations (3.127), (3.128) and (3.130) and have given it in Tables 1(a) to 1(e) and Figures 2(a) to 2(e) for $y/R = 0$, 0.2 , 0.5 , 0.7 and 0.9 . The interference upwash can then be evaluated from Equations (3.131) and (3.140); illustrative calculations are given in Tables 3 to 9 of Reference 3.26.

Off-centre models above or below the plane $z = 0$ are covered by Equations (3.114) derived from Reference 3.35. The more elaborate theories do not preclude off-centre positions, but the numerical work is complicated further and no calculations appear to have been made. Silverstein and White have evaluated $(\delta_0)_U$ from Equations (3.114) for closed and open elliptical tunnels with $b/h = 1$ and 2 ; their curves in Figures 3, 4, 6 and 10 to 13 of Reference 3.32 indicate that the increased interference is quite as important as for rectangular tunnels (Fig.3.11). The vertical displacement gives a much greater correction factor to $(\delta_0)_U$ for small wings than for models of large span.

Full-span models are discussed in Section 3.6.4. In their treatment of this problem for a closed circular tunnel, Vincenti and Graham[3.42] consider a simplification of Equation (3.127) on the axis $y = 0$. In Equations (8) and (11) and Appendix A of Reference 3.42 they transform the series of Bessel functions into a convergent power series in $(x-x_N)$.

3.4.4 Half-Wing Models

When the model and the flow conditions have spanwise symmetry, only one half ($y > 0$, say) need be considered. In such cases there are many advantages in using half models mounted at the tunnel wall, which becomes a reflection plane of symmetry $y = 0$. Van der Bliek[3.43] has discussed the practical aspects, noting that half models are cheaper and easier to make and may be combined with shorter pressure leads or a test rig outside the tunnel so as to eliminate sting or strut interference. The Reynolds number can be doubled, and especially for control surfaces the larger size of model should ensure more accurate manufacture[3.4]. The use of half models introduces a number of interference effects. The modified upwash interference will be discussed in some detail; the other effects of tunnel-wall boundary layer and gap between model and tunnel wall are discussed in Reference 3.43.

Little need be said about rectangular tunnels. The formulae of Section 3.4.1 have simply to be applied to a complete model in a tunnel of the same height and twice the breadth. References 3.22 and 3.44 illustrate the procedure for unswept and swept models respectively.

Half models are frequently tested in octagonal tunnels. Batchelor's[3.11] method, outlined in Section 3.4.2, then requires the modification in Reference 3.45, where calculations are made for the tunnel in the middle diagram of Figure 3.12. The origin in Figure 1(c) is shifted one half breadth to the lift, and it is necessary to distinguish between the "corner fillets" at $y = \pm b$, $\pm 3b$, ... and the "central fillets" at $y = 0$, $\pm 2b$, ... In the first place it is convenient to re-define the quantity G/P in Equation (3.103), so that the gradient of v_n at the midpoint of the fillet is replaced by the mean gradient over its middle half. For the double tunnel of large breadth to height ratio $2b/h$, moreover, G/P is found to depend on the semi-span t of the horse-shoe vortex. For example, from the non-dimensional quantity

$$\Lambda' = 4\sqrt{2}\, bt\, G/P = 2\sqrt{2}\, b\, G/K = \bar{G}(t/b) \qquad (3.141)$$

in Table 2 of Reference 3.45 it is seen that G/P is more than doubled when t increases from 0 to 0.75b . The corresponding quantity for the central fillets is negative and may be identified with $-\bar{G}[1 - (t/b)]$. It follows that, in the special case $y = t = \frac{1}{2}b$, the contributions to the interference upwash from the corner and central fillets cancel each other. In principle, $\delta_0(y,t)$ is given by a simple extension of Equations (3.102) and (3.104). For the column of central fillets near the reflection plane

$$S = \operatorname{sech} \frac{\pi(a\sqrt{2} + y)}{2h} \quad .$$

Unfortunately the expansion for $\chi(S,T)$ in Equation (3.104) may converge too slowly when y is small, as shown in Table 3(a) of Reference 3.45; the alternative expansion of Equation (25) in the Appendix to Reference 3.45 is more accurate, and it is seen that relatively large negative values of χ are found for small y . The main conclusions are that the octagonal tunnel induces considerably more interference upwash near the reflection plane than does the corresponding rectangular tunnel, but that elsewhere the effect of the fillets, whether positive or negative, is likely to be much smaller than for complete models. No simple formula such as Equation (3.107) can be suggested, but it seems typical that $(\delta_0)_E/(\delta_{0R})_E > 1$ for small σ and is roughly equal to the area ratio C/bh for fairly small $(1-\sigma)$. For half-model testing σ is unlikely to be small; when $\sigma > \frac{1}{2}$, it is recommended that the fillets should be neglected for all but the most detailed experiments.

When a reflection plane is installed to test half models in a circular tunnel, the effective boundary is of bipolar cross section as illustrated in Figure 3.15. This configuration was first considered by Kondo (Ref.3.14; 1935), who used the transformation

$$y + iz = R \sin\psi \tan(\eta + i\zeta) \qquad (3.142)$$

to map the interior into the strip $|\eta| < \frac{1}{2}(\pi-\psi)$, where the angle ψ is indicated in Figure 3.15. By Equation (3.45), solutions for the interference stream function along a uniformly loaded lifting line give simple expressions

$$\left.\begin{aligned} (\delta_0)_U &= \frac{C}{16\pi t^2}\log_e \frac{\pi \sin 2\xi}{(\pi-\psi)\sin\left(\dfrac{2\pi\xi}{\pi-\psi}\right)} && \text{for closed tunnels} \\ (\delta_0)_U &= \frac{C}{16\pi t^2}\log_e \frac{\pi \sin 2\xi}{2(\pi-\psi)\tan\left(\dfrac{\pi\xi}{\pi-\psi}\right)} && \text{for open tunnels} \end{aligned}\right\}, \qquad (3.143)$$

where t is the half-wing span, $\tan\xi = t/(R\sin\psi)$ (Fig.3.15), and the bipolar area $C = 2R^2(\pi-\psi+\frac{1}{2}\sin 2\psi)$. Figure 4(b) of Reference 3.14 shows that a closed bipolar tunnel has values of $(\delta_0)_U$ remarkably close to those for the closed elliptical tunnel of the same breadth to height ratio $(1+\cos\psi)$; this is much less true of an open bipolar tunnel. Figure 3.15 shows how the interference on a half model of fixed span can be reduced from that on the corresponding complete model in a circular tunnel $(\psi = 90^\circ)$. The magnitude of the simple correction to incidence, given by

$$\frac{\pi R^2 \Delta\alpha}{SC_L} = \frac{\pi R^2}{C}(\delta_0)_U \quad . \qquad (3.144)$$

falls to a minimum as ψ decreases. For closed tunnels the minimum $\Delta\alpha$ is about one half that of a small complete wing or, when $t = 0.8R$, as little as one third of that for a complete wing. Less impressive reductions are found in the negative correction $\Delta\alpha$ when the boundary is open.

Davison and Rosenhead[3.46] have treated the open bipolar tunnel independently by the transformation

$$\pi\tan^{-1}\left(\frac{y+iz}{R\sin\psi}\right) = 2(\pi-\psi)\tan^{-1}(\eta+i\zeta) \qquad (3.145)$$

in place of Equation (3.142); Table 2 of Reference 3.46 gives precisely the quantity plotted in Figure 3.15. With an approximation they extend the analysis to obtain a convergent expansion for the corresponding quantity when the spanwise loading is elliptic.

Sivells and Deters[3.47] use the same transformation (3.145) for a closed bipolar tunnel to obtain the interference parameter

$$\delta_0(y,t) = \frac{C}{8\pi}\left[\frac{\pi R(1+\eta^2)\sin\psi}{2(\pi-\psi)(y^2+R^2\sin^2\psi)}\left\{\frac{\tau/t}{\eta^2-\tau^2}-\frac{\tau/t}{\eta^2\tau^2-1}\right\}-\frac{1}{y^2-t^2}\right] , \qquad (3.146)$$

where

$$\left.\begin{aligned} \tan^{-1}\tau &= \frac{\pi}{2(\pi-\psi)}\tan^{-1}\left(\frac{t}{R\sin\psi}\right) \\ \tan^{-1}\eta &= \frac{\pi}{2(\pi-\psi)}\tan^{-1}\left(\frac{y}{R\sin\psi}\right) \\ C &= 2R^2(\pi-\psi+\tfrac{1}{2}\sin 2\psi) \end{aligned}\right\} .$$

Values of $(4Rt/C)\ \delta_0(y,t) = w_i R/K$ at $x = 0$ are tabulated in Tables 1 and 2 of Reference 3.47 for two configurations $\psi = 43.09^0$ and 60.14^0 that are favourable in Figure 3.15. The streamwise variation of w_i is represented rather crudely by taking $h \simeq 2R$ and

$$\delta_1(y,t) \equiv 2.1\ \delta_0(y,t)$$

in Equation (3.42); the factor 2.1 was obtained from the incorrect calculations of Reference 3.38 for a closed circular tunnel, and from Equation (3.136) the value 1.998 might be preferred. Reference 3.47 also examines the consequences of replacing the reflection plane by an end plate; this tends to give a larger interference upwash and a spanwise lift distribution different from that of a complete wing. It is concluded that a reflection plane should be used wherever possible for half-model testing.

No rigorous method is available for determining the general interference upwash field $w_i(x,y)$ in the plane $z = 0$ of a closed bipolar tunnel. The best approximation appears to be that of Sivells and Salmi$^{3.26}$ using point concentrations of lift. If the element of lift L_N acts at a position (x_N, y_N), then following Reference 3.47 they obtain

$$w_N(x_N,y,y_N) = \frac{L_N}{4\pi\rho U}\left[\frac{\pi^2(1+\eta^2)(1+\eta_N^2)R^2\sin^2\psi}{4(\pi-\psi)^2(y^2+R^2\sin^2\psi)(y_N^2+R^2\sin^2\psi)}\left\{\frac{1}{(\eta-\eta_N)^2}+\frac{1}{(1-\eta\eta_N)^2}\right\} - \frac{1}{(y-y_N)^2}\right] , \tag{3.147}$$

where, as in Equation (3.146).

$$\tan^{-1}\eta_N = \frac{\pi}{2(\pi-\psi)}\tan^{-1}\left(\frac{y_N}{R\sin\psi}\right) .$$

The plausible assumption is then made that, for any fixed x and x_N, the ratio of $w_N(x,y,y_N)$ to $w_N(x_N,y,y_N)$ is equal to the corresponding ratio for the closed circular tunnel in the (η,ζ) plane; that is to say,

$$\frac{w_N(x,y,y_N)}{w_N(x_N,y,y_N)} = \frac{w_N^{(1)}(x,\eta) - w_{N0}(x,\eta)}{w_N^{(1)}(x_N,\eta) - w_{N0}(x_N,\eta)} , \tag{3.148}$$

where $w_N^{(1)}$ and w_{N0} are defined in Equations (3.127), (3.128) and (3.130) with y_N replaced by η_N. Hence the charts in Figure 5 of Reference 3.26 are derived for the particular bipolar tunnel of Reference 3.47 with $\psi = 60.14^0$ $(b/h = 1.49781)$. The interference corrections can then be obtained as simply as for the circular tunnel.

3.5 NUMERICAL INTERFERENCE CORRECTIONS

Various formulae for interference corrections to measured quantities have been derived earlier. Section 3.2.4 gives expressions suitable for small wings, while more general formulae are discussed in Sections 3.3.3 to 3.3.6. The application of these formulae to a particular tunnel requires knowledge of the appropriate interference parameters from Sections 3.4.1 to 3.4.4. We consider in Sections 3.5.1 and 3.5.2 the relative importance of the various corrections from available numerical data for rectangular and non-rectangular tunnels respectively. In Section 3.5.3 an attempt is made to assess the accuracy of the simpler methods of estimation.

In the first place the measured quantities that often require interference correction can be divided into three groups.

Geometrical quantity	α
Force coefficients affecting the interference upwash	C_L , C_l . C_m
Other force coefficients	C_D , C_n , C_H

Although the vortex representation of the model may be governed partly by the theoretical lift distribution, the reliability of interference corrections must also depend on the amount of experimental information in the second group. In half-model tests all three coefficients may be measured, so that the spanwise and streamwise centres of pressure may be known. For complete models there will be separate fields of interference upwash from the symmetrical loading (C_L and C_m) and antisymmetrical loading (C_l); the latter, though smaller, will be less well defined, since the streamwise centre of pressure associated with C_l is unknown. There will be varying degrees of uncertainty in the absence of one or more of these coefficients, especially when only the control hinge moment C_H or a restricted pressure distribution is measured. An independent appeal to the theoretical lift distribution or an empirical estimate of C_L or C_l is then essential.

The more common interference corrections can be grouped as in the following table.

Principal corrections	$\Delta\alpha$, ΔC_l
Zero correction	ΔC_L
Residual corrections to longitudinal moments	ΔC_m , ΔC_H ΔC_l (half-model)
Residual corrections to vortex-induced coefficients	ΔC_D , ΔC_n

The principal corrections are the easiest to estimate quickly; $\Delta\alpha$ is usually much more important than ΔC_l . It is convenient to choose $\Delta\alpha$ such that $\Delta C_L = 0$. The residual corrections ΔC_m and ΔC_H are rather difficult to estimate at all accurately; the latter can be especially important. The vortex-induced coefficients C_{DV} and C_{nV} are only part of the measured quantities, but are subject to large percentage interference corrections. It will be assumed that ΔC_n is governed by the principles of lifting-line theory, but it is suggested in Section 3.5.3 that the resulting formulae are somewhat unreliable.

A different category of correction arises when lateral aerodynamic characteristics are to be deduced from tests of half-span or part-span models. After the interference corrections, including ΔC_l, have been applied to give conditions of unconstrained flow with a reflection plane $y = 0$, there remains a lifting-surface problem independent of the tunnel shape. The precise details of such a calculation are not discussed, but the resulting correction factor to $(C_l + \Delta C_l)$ is of major importance.

3.5.1 Rectangular Tunnels

Attention is now given to specific calculations of wall interference on lifting wings in rectangular tunnels. An attempt is made by illustrative charts or formulae or inequalities to indicate the likely magnitude of the various principal and residual corrections relevant to wing models. Brief discussions of the numerical corrections for slender wings, complete aircraft models and other special configurations will be deferred until the appropriate subsections of Section 3.6.

Figure 3.2 has already provided the order of magnitude of the correction $\Delta\alpha$ for various types of rectangular tunnel. For closed rectangular tunnels Equation (3.55) with some weighting W has been used to calculate the influence of wing span over a wide range of planforms. Polhamus[3.88] has evaluated the mean interference upwash along a swept lifting line with the weighting $W = c/\bar{c}$; this indicates very little influence of sweep angle $(-60^\circ \leqslant \Lambda \leqslant 60^\circ)$ for planforms of moderate taper and span ratios $\sigma = 2s/b \leqslant 0.8$ in a tunnel of effective shape $b/h = 1.4$. Acum[3.17] used the weighting

$$W = \frac{2.4}{\pi}\left\{1 - \left(\frac{y}{s}\right)^2\right\}^{\frac{1}{2}} + 0.4\,\frac{c}{\bar{c}}.$$

in Equation (3.55) to evaluate the mean interference upwash at three-quarter chord. It is found to a useful approximation that, for any particular breadth to height ratio,

$$\delta = \left(\frac{bh}{SC_L}\right)\Delta\alpha \tag{3.149}$$

can be regarded as a function of σ and aspect ratio $A = (2s)^2/S$ in incompressible flow. Not only is δ largely independent of sweepback and wing taper, but it is practically insensitive to spanwise loading, as Appendix I of Reference 3.4 illustrates convincingly for a square tunnel. For elliptic spanwise loading carpets of δ are reproduced from Reference 3.17 with allowance for compressibility by plotting against a horizontal scale of $\sigma + 3(\beta A)^{-1}$ in Figure 3.16; the three diagrams for $b/h = 1$, $9/7$ and 2 show δ within the range $0.11 < \delta < 0.22$ for $\beta A \leqslant 8$, $\sigma \leqslant 0.8$ and $\sigma + 3(\beta A)^{-1} \leqslant 2$. For fixed b/h and σ, δ is represented as a linear function of $(\beta A)^{-1}$; we may therefore write

$$\frac{\Delta\alpha}{C_L} = \frac{S}{bh}\,\delta(\beta A)\,, \tag{3.150}$$

where

$$\delta(\beta A) = \delta(6)\left[2 - \frac{6}{\beta A}\right] + \delta(3)\left[\frac{6}{\beta A} - 1\right].$$

There is a tendency for Equation (3.150) to underestimate $\Delta\alpha$ for highly tapered wings when b/h is large (Fig. 12 of Ref. 3.17) and to overestimate $\Delta\alpha$ when $\beta A < 2$, say.

Independent calculations of $\Delta\alpha$ by the method of Reference 3.22 for $b/h = 10/7$ are included in Reference 3.48. The results take the form

$$\frac{\Delta\alpha}{C_L} = \frac{S}{bh}\left[\delta_{ll} + \delta_{sc}\right] , \tag{3.151}$$

where the 'lifting line' contribution δ_{ll} corresponds to $A = \infty$ and the 'streamline curvature' contribution δ_{sc} is roughly inversely proportional to βA, as in Equation (3.150). The curves against σ, reproduced in the top two diagrams of Figure 3.17, show δ_{ll} for three values of d/h, the non-dimensional distance from model to floor, and the quantity $\beta A \delta_{sc}$ subject to the restriction $\beta A \geqslant 2$, say. In Figure 3.18 we try to piece together the approximate information on δ, as defined in Equation (3.149), for wings and Mach numbers such that $\beta A = 2.5$, i.e.,

$$\sigma^2 = \frac{AS}{b^2} = \frac{2.5h}{b}\left(\frac{S}{\beta bh}\right) .$$

The curves of δ against b/h for constant area ratios $S/(\beta bh)$ show how the minimum interference shifts from $b/h = \sqrt{2}$ for small wings to broader shapes of tunnel as the area ratio increases. Thus the variation in δ from tunnel to tunnel is likely to increase with the relative size of model.

Whereas the momentum at right angles to the stream direction is influenced by normal pressures at the tunnel boundary, the streamwise momentum is virtually uninfluenced by external forces. The vortex-induced drag is therefore determined by the spanwise loading on the wing and the cross-section of the tunnel. When an elliptically loaded lifting line can be assumed, a good approximation to the interference correction is given by

$$\Delta C_D = \frac{SC_L^2}{bh}(\delta_0)_E , \tag{3.152}$$

where for closed rectangular tunnels $(\delta_0)_E$ is given as a function of b/h and σ in Figure 3.9. Minor contributions due to residual effects and asymmetrical spanwise loading are noted in Equations (3.63) and (3.71). The parameter δ_{ll} at the top of Figure 3.17 illustrates approximately the increase in $(\delta_0)_E$ with off-centre models. The uncorrected vortex drag of a lifting line with elliptic loading is simply

$$C_{Dv} = \frac{SC_L^2}{4\pi s^2} . \tag{3.153}$$

By Equations (3.152) and (3.153) the ratio

$$\frac{\Delta C_D}{C_{Dv}} = \frac{\pi b\sigma^2}{h}(\delta_0)_E , \tag{3.154}$$

which can be large, e.g., 26% when $b/h = 1.6$, $\sigma = 0.7$ and $(\delta_0)_E = 0.105$. This may appear slightly exaggerated, since C_{D_V} does not represent the total drag.

The residual correction to pitching moment, as defined in Equation (3.36) or Equations (3.57) to (3.59) or more generally in the second of Equations (3.67), is independent of pitching axis. The accuracy of the different methods of estimating ΔC_m will be discussed in Section 3.5.3. As far as can be judged from a few lifting-surface calculations by the Equation (3.67), the correction is likely to lie within the range

$$0.03 \frac{\sigma^2 b}{\beta A h} < \frac{\Delta C_m}{C_L} < 0.05 \frac{\sigma^2 b}{\beta A h} \tag{3.155}$$

for fairly large models in closed rectangular tunnels; Equation (3.36) with Table 3.III would have suggested a much wider variation.

The principal correction ΔC_l to rolling moment is never very large. It appears in the form of Equation (3.62) or the last of Equations (3.67). For unswept wings of high aspect ratio, in particular, there are other simple procedures. With a change of sign, Equation (9) of Reference 3.28, with charts for $b/h = 10/7$ and $3/2$, gives $-\Delta C_l/C_l$ for wings with deflected ailerons; Equation (3.62) may be regarded as a generalization of this. Equation (3) of Reference 3.48, based on Reference 3.25, gives the result in the third panel of Figure 3.17 and incorporates the factor $(2.5 \cos \psi - 1.5)$ for wings yawed through the angle ψ. We now examine the behaviour of the interference upwash in Equation (3.50). When the wing is small, it can be shown that

$$\left.\begin{aligned} \frac{\partial}{\partial t}\{t\kappa_0(y,t)\} &= \frac{bty}{8h^3}\zeta_0 \\ \frac{\partial}{\partial t}\{t\kappa_1(y,t)\} &= \frac{bty}{8\pi h^3}\zeta_1 \end{aligned}\right\} , \tag{3.156}$$

where, by Equations (3.91) and (3.92),

$$\left.\begin{aligned} \zeta_0 &= f_2''(0) + 2\sum_{m=1}^{\infty}(-1)^m f_1''(mb/h) \\ \zeta_1 &= f_4''(0) + 2\sum_{m=1}^{\infty}(-1)^m f_3''(mb/h) \end{aligned}\right\} ; \tag{3.157}$$

the second derivatives f_n'' may be evaluated from Reference 3.18. The antisymmetric spanwise loading is taken such that in Equation (3.50)

$$\frac{4s\Gamma}{UC} = \frac{2scC_{LL}}{C} = \frac{32SC_l}{\pi bh}\frac{t}{s}\left(1 - \frac{t^2}{s^2}\right)^{\frac{1}{2}} . \tag{3.158}$$

By Equations (3.50), (3.156) and (3.158),

$$\frac{w_l}{U} = \frac{4sySC_l}{\pi h^4}\int_0^1\left[\zeta_0 + \frac{x-\bar{x}(t)}{\pi\beta h}\,\zeta_1\right]\left(\frac{t}{s}\right)^2\left(1-\frac{t^2}{s^2}\right)^{\frac{1}{2}} d\left(\frac{t}{s}\right) . \qquad (3.159)$$

For larger wings it may be appropriate to evaluate ζ_0 and ζ_1 in the special case $y = t = \frac{1}{4}h$, when there are simple formulae

$$\left.\begin{aligned}\zeta_0 &= \frac{8h^2}{b^2}\left[-f_2(0) + f_2\left(\frac{b}{2h}\right) - f_1\left(\frac{b}{2h}\right) - 2\sum_{m=1}^{\infty}(-1)^m f_1\left(\frac{mb}{h}\right)\right]\\ \zeta_1 &= \frac{8h^2}{b^2}\left[-f_4(0) + f_4\left(\frac{b}{2h}\right) - f_3\left(\frac{b}{2h}\right) - 2\sum_{m=1}^{\infty}(-1)^m f_3\left(\frac{mb}{h}\right)\right]\end{aligned}\right\} . \qquad (3.160)$$

Values of ζ_0 and ζ_1 from Equations (3.157) and (3.160) are listed in Table 3.VI. To obtain a rough estimate of ΔC_l for wings of high aspect ratio, we omit the second term in the square bracket of Equation (3.159) and use Equations (3.62) and (3.159) to give

$$-\frac{\Delta C_l}{C_l} = \frac{\pi A\mu\partial C_L/\partial\alpha}{2(\pi A + \mu\partial C_L/\partial\alpha)}\,\frac{s^2S\zeta_0}{4h^4}\int_0^1 W\left(\frac{y}{s}\right)^2 d\left(\frac{y}{s}\right) .$$

With the further approximations

$$\mu = 1 , \qquad \frac{\partial C_L}{\partial\alpha} = \frac{2\pi A}{\beta A + 2} , \qquad W = \frac{4}{\pi}\left(1 - \frac{y^2}{s^2}\right)^{\frac{1}{2}} ,$$

this becomes

$$-\frac{\Delta C_l}{C_l} = \frac{\pi s^4\zeta_0}{4h^4(\beta A + 4)} , \qquad (3.161)$$

which has formal similarity with Equation (9) of Reference 3.28. A typical correction to C_l would be -2.2%, when $b/h = 1.6$, $\zeta_0 = 2.9$, $\sigma = 0.7$ and $\beta A = 6$. For wings of small span $\Delta C_l/C_l$ is negligible, being porportional to σ^4. Equation (3.161) with ζ_0 from Table 3.VI will determine whether the correction can be ignored safely.

The vortex-induced yawing moment involves interaction between symmetrical and antisymmetrical parts of the spanwise loading. Even for unyawed wings, the evaluation of the interference correction ΔC_n from Equations (3.70) and (3.71) includes three terms, and further subdivision of the symmetrical part may be needed when control surfaces are deflected. This is illustrated in the methods of Swanson[3.25] and Graham[3.28]. To obtain a rough estimate of ΔC_n, we assume a spanwise load distribution

$$\frac{cC_{LL}}{\bar{c}} = \frac{4C_L}{\pi}\left(1 - \frac{y^2}{s^2}\right)^{\frac{1}{2}} + \frac{32C_l y}{\pi s}\left(1 - \frac{y^2}{s^2}\right)^{\frac{1}{2}} \qquad (3.162)$$

and an interference upwash

$$\frac{1}{2}\left(\frac{w_i}{U}\right)_\infty = \left(\frac{SC_L}{bh}\right)\delta_0 + \left(\frac{\eta y S C_l}{4h^3}\right)\zeta_0 \, . \qquad (3.163)$$

where the last term is derived from Equation (3.159). The parameters δ_c and ζ_0 here denote suitable mean values dependent on b/h and σ. Then Equation (3.70) gives

$$\frac{\delta C_{nv}}{C_L C_l} = \frac{S}{bh}\left[\delta_0 + \left(\frac{bs^2}{32h^3}\right)\zeta_0\right] \, . \qquad (3.164)$$

From the lifting-line integral it is found that the vortex-induced incidence is

$$\begin{aligned} \alpha_v &= \frac{1}{4\pi A}\int_{-1}^{1} \frac{s}{y'-y}\,\frac{d}{d(y/s)}\left[\frac{cC_{LL}}{\bar{c}}\right]_{y=y'} d\left(\frac{y'}{s}\right) \\ &= -\frac{1}{\pi A}\,[C_L + 16(y/s)\ C_l] \ , \end{aligned}$$

whence

$$C_{nv} = \frac{1}{4}\int_{-1}^{1} \alpha_v \frac{cC_{LL}}{\bar{c}}\,\frac{y}{s}\, d\left(\frac{y}{s}\right) = -\frac{3C_L C_l}{\pi A} \, . \qquad (3.165)$$

By Equations (3.71), (3.164) and (3.165),

$$\frac{\Delta C_n}{C_{nv}} = \frac{\pi b \sigma^2}{3h}\left[\delta_0 + \left(\frac{\sigma^2 b^3}{128h^3}\right)\zeta_0\right] + \frac{\Delta C_l}{C_l} \, . \qquad (3.166)$$

This lies between the corresponding ratios $\Delta C_D/C_{Dv}$ and $\Delta C_l/C_l$ from Equations (3.154) and (3.161), e.g., 10% when $b/h = 1.6$, $\sigma = 0.7$, $\delta_0 = 0.105$ and $\zeta_0 = 2.9$. In practice, ΔC_n can be a larger proportion of the measured C_n (Section 9 of Ref. 3.18). It is noted that the second term of Equation (3.164) largely explains the difference between δ_{ll} and $-(C/S)(\Delta C_n/C_L C_l)$ in the top and bottom panels of Figure 3.17.

Hypothetical cases of swept and unswept half-models with control surface in a closed square tunnel are considered in Section 9 and Figures 6 and 7 of Reference 3.4. The residual correction to hinge moment from Equation (3.77) is seen to be important for large models. Further discussion of wall interference on control hinge moments with aerodynamic balance is found in Reference 3.49; Miss Lyon has pointed out that uncorrected wind-tunnel results may be misleading in the design of closely balanced elevators.

3.5.2 Non-Rectangular Tunnels

There is evidence in Reference 3.40 of a small effect of spanwise loading on $\Delta\alpha$ for unswept wings of aspect ratio $A = 8$ in a closed elliptical tunnel of ratio $b/h = 1.37$. Given total lift and wing span, the wall interference is less for lift distributions that are more concentrated towards the centre line. But Figure 8 of Reference 3.40 shows that $\Delta\alpha$ is only slightly less for highly tapered than for untapered wings. Even smaller changes would be expected of sweptback wings and those of lower aspect ratio; for most purposes elliptic spanwise loading may be assumed. There should be little difficulty in preparing approximate charts for octagonal and elliptical tunnels similar to those for rectangular tunnels in Figure 3.16.

Once the principal correction $\Delta\alpha/C_L$ is known for rectangular tunnels, the corresponding correction for octagonal or elliptical tunnels can be estimated quickly from Equation (3.110). This only requires the further knowledge of the parameter $(\delta_0)_E$ for the appropriate value of σ, which is given in Figure 3.12 or 3.13; otherwise Equation (3.107) is available to give a rough estimate for closed octagonal tunnels. Although $(\delta_0)_E$ will be smaller than the corresponding quantity $(\delta_{0R})_E$ for a closed rectangular tunnel of the same breadth and height, the interference correction will be larger for the same model. By contrast the bipolar shape, appropriate to a half-model in a closed circular tunnel with reflection plane, can give a much smaller interference (Fig. 3.15) than the half-model in a rectangular tunnel of the same breadth and height.

Equation (3.152) with bh replaced by C will continue to give a good approximation to ΔC_D. The inequality (3.155) should again indicate whether ΔC_m is negligible; if not, Equation (3.112) is available. Likewise Equation (3.161) with an appropriate value of ζ_0 will give the order of magnitude of the correction ΔC_l. A crude estimate of δC_{nv} then follows from Equation (3.164), but this correction will seldom be negligible under conditions of asymmetrical spanwise loading. For a closed circular tunnel it can be shown that ζ_0, as defined in Equation (3.156), is

$$\zeta_0 = \frac{32R^2}{ty}\frac{\partial}{\partial t}\left\{\frac{R^2t^2y}{8(R^8-t^2y^2)}\right\} = \frac{8R^8}{(R^8-t^2y^2)^2} ; \qquad (3.167)$$

for the present purpose this is not appreciably different from the quantity for a closed square tunnel, especially if it is adjusted in the ratio of the parameters δ_0 for the respective tunnels. In other words, a change in tunnel shape from rectangular to octagonal or elliptical is likely to influence all the corrections by roughly the same factor

$$\frac{bh(\delta_0)_E}{C(\delta_{0R})_E} .$$

For wings of high aspect ratio with part-span ailerons in a closed circular tunnel the correction to yawing moment is conveniently evaluated by means of Reference 3.50. In the present notation

$$-\Delta C_n = (\delta C_{nv})_1 + (\delta C_{nv})_2 + (\delta C_{nv})_3 . \qquad (3.168)$$

where

$$\left.\begin{aligned}
(\delta C_{nv})_1 &= \frac{SR^2(C_L)_1C_l}{4s^2(y_2^2-y_1^2)}\left\{F_1\left(\frac{sy_2}{R^2}\right) - F_1\left(\frac{sy_1}{R^2}\right)\right\}\\
(\delta C_{nv})_2 &= \frac{S(C_L)_1C_l}{y_2^2-y_1^2}\left\{F_2\left(\frac{sy_2}{R^2}\right) - F_2\left(\frac{sy_1}{R^2}\right)\right\}\\
(\delta C_{nv})_3 &= \frac{SR(C_L)_2C_l}{4\pi(y_2^2-y_1^2)(y_2-y_1)}F_3\left(\frac{y_2}{R}, \frac{y_1}{y_2}\right)
\end{aligned}\right\} .$$

$(C_L)_1$ and $(C_L)_2$ denote the contributions to C_L from the wing incidence and the deflected ailerons respectively, and $y_1 < |y| < y_2$ denotes the spanwise extent of the ailerons; the functions F_1, F_2 and F_3 are formulated and plotted in Reference 3.50. Stewart states that the total correction is likely to be a large percentage of the uncorrected C_n and may even exceed it when s/R is as large as 0.8.

Special reference must be made to the illustrative computation for a complete swept-back model with tailplane in a closed circular tunnel admirably set out in Tables III to XIII of Reference 3.26. The spanwise distributions of interference upwash at quarter chord, three-quarter chord and the tail are shown in Figures 7 and 8 of Reference 3.26. The corrections to incidence, drag, pitching-moment, rolling-moment and yawing-moment coefficients resemble* those in Equations (3.55) to (3.59), (3.62) and (3.70), and are evaluated in simple stages with the aid of the charts in Figures 2 and 6 of Reference 3.26, so that similar calculations for other models are reduced to a straightforward routine.

3.5.3 Comparisons of Methods

We first consider four methods of calculating the principal correction to incidence, viz.,

$$\left.\begin{array}{rl} \text{(i)} & \text{Small-wing method. Equation (3.35)} \\ \text{(ii)} & \text{Charts of Reference 3.17. Figure 3.16} \\ \text{(iii)} & \text{Reference 3.26. Equation (3.55) with } W = cC_{LL}/\bar{c}C_L \\ \text{(iv)} & \text{Lifting-surface theory. Equation (3.67)} \end{array}\right\} .$$

The results are compared in Table 3.VII for fairly large models of various planforms in closed rectangular tunnels. The wings are uncambered and without control surfaces. For method (i) the factor λ is taken from lifting-surface theory, as given in Table 3.III. Whether these or the more approximate values $\lambda = \bar{\bar{c}}/\bar{c}$ are used, it is only when $\sigma \leqslant 0.5$ and $\sigma \leqslant 0.5h/b$ that the method can always be trusted within ±10%; for nearly square tunnels, however, these conditions on σ can be relaxed a little. In most of the examples one of these limits is violated and larger errors are found. There is little reason to use so crude a calculation when the simple methods (ii) and (iii) exist. In method (ii) extrapolation has been used to cover $b/h = 0.911$: in method (iii) $W = cC_{LL}/\bar{c}C_L$ has been taken from lifting-surface theory and, as for method (iv), Equation (3.47) is used to determine w_i/U. Method (iii) gives marginally better over-all accuracy and a root-mean-square deviation from method (iv) of 0.0011 in $\Delta\alpha/C_L$ (0.3 degrees when $C_L = 0.5$); $\Delta\alpha$ tends to be underestimated by method (iii), but in the present examples the error does not exceed 0.5% of the measured incidence.

A comparison of $\Delta\alpha/C_L$ for a non-rectangular tunnel is made by applying Equation (3.110) to the illustrative example defined in Table III of Reference 3.26. With $\sigma = s/R = 0.656$,

$$\left.\begin{array}{rcll} (\delta_0)_E & = & 0.129_5 & \text{for a closed circular tunnel from Figure 3.13} \\ (\delta_{0R})_E & = & 0.150_5 & \text{for a closed square tunnel from Figure 3.9} \\ \delta & = & 0.169_5 & \text{for } b = h \text{ and } \beta A = 5.11 \text{ from Figure 3.16} \end{array}\right\} .$$

---

* In Reference 3.26, $(w_i/U)_{0.25}$ replaces $\frac{1}{2}(w_i/U)_\infty$ in Equations (3.56) and (3.70).

Therefore for the square tunnel

$$\left(\frac{\Delta\alpha}{C_L}\right)_R = \frac{S}{bh}\delta = 0.0842 \times 0.169_5 = 0.0143 \ ,$$

and for the circular tunnel Equation (3.110) becomes

$$\frac{\Delta\alpha}{C_L} = \left(\frac{4}{\pi}\right)^{\frac{3}{2}} \frac{0.129_5 \times 0.0143}{0.150_5} - 0.107 \times 0.129_5\left(\sqrt{\frac{4}{\pi}} - 1\right)$$

$$= 0.0177 - 0.0018 = 0.0159 \ ,$$

which is in excellent agreement with the value $\Delta\alpha/C_L = 0.0158$ in Table X of Reference 3.28.

We next consider four methods of calculating the residual correction to pitching moment coefficient, viz.,

(i) Small-wing method. Equation (3.36)
(ii) Strip theory. Equation (3.60) with factor
(iii) Reference 3.28. Equations (3.57) to (3.59)
(iv) Lifting-surface theory. Equation (3.67) .

The results are compared in Table 3.VII for the eleven examples of wings at uniform incidence in closed rectangular tunnels. Method (i) is by far the simplest and uses values of the quantity $\lambda x_1/\bar{c}$ from lifting-surface theory* in Table 3.III. As would be expected from the behaviour of $(\delta_0)_g$ against σ in Figure 3.9, both $\Delta\alpha/C_L$ and $\Delta C_m/C_L$ are seriously underestimated when $b/h < 1.0$ and σ is large and seriously overestimated when $b/h > 1.8$ and σ is moderately large. For many cases Equation (3.36) will suffice to show the order of magnitude of the residual correction. $\Delta C_m/C_L$ amounts to a forward movement of the aerodynamic centre as a fraction of the mean chord $\bar{c}$ and may not be required to better accuracy than ±0.002, say. Method (ii) uses the formula

$$\frac{\Delta C_m}{C_L} = \frac{(\lambda x_1/\bar{c})_{ls}}{(\lambda x_1/\bar{c})_{st}} \frac{\partial C_L}{\partial\alpha} \int_0^1 \left[\left(\frac{w_i}{UC_L}\right)_{0.75} (x_L - \bar{\bar{x}}_L + \tfrac{3}{8}c - \tfrac{1}{4}\bar{\bar{c}}) - \left(\frac{w_i}{UC_L}\right)_{0.25} (\tfrac{1}{8}c)\right] \frac{c}{\bar{c}^2}\, d\left(\frac{y}{s}\right) \ . \tag{3.169}$$

where $\bar{\bar{c}}$ and $\bar{\bar{x}}_L$ are defined in Equation (3.60), $(\lambda x_1/\bar{c})_{ls}$ and $(\lambda x_1/\bar{c})_{st}$ are taken from the last two columns of Table 3.III. The latter is formulated in Equation (3.61) and the former is defined above that equation; their ratio is an essential correction factor in Equation (3.169). Except for the very broad tunnels $b/h \geqslant 2$, method (ii) gives quite as good accuracy as method (iii); furthermore, unlike method (iii), it is not restricted to wings of constant sweepback from root to tip. However, method (iii) does not require the quantity $(\lambda x_1/\bar{c})_{ls}$ and involves only slightly more computation. Its root-mean-square deviation from method (iv) is as small as 0.0010. Finally, from Table 3.VII, with the exception of Case 11 $(\Delta C_m/C_L = 0.054\,\sigma^2 b/\beta Ah)$ all the calculations in the last column by method (iv) satisfy the inequality (3.155). The effect of compressibility on $\Delta C_m/C_L$ tends to be greater than the factor β^{-1} ; typical comparisons of methods (iii) and (iv) over the Mach number range $0.4 \leqslant M \leqslant 0.9$ are shown in Figure 3.19.

---

* Note that Equation (3.38) from strip theory seriously underestimates $\lambda x_1/\bar{c}$ for unswept wings of moderate or small aspect ratio.

Turning to antisymmetrical spanwise loading, we now consider three examples of the principal correction to rolling moment coefficient in closed tunnels, viz.,

(a) b/h = 10/7 . Figure 3.17 based on Reference 3.48
(b) b/h = 2 . Tables A3 to A7 of Reference 3.18
(c) Circular. Tables III and XIII of Reference 3.26

For example (a) the wings are unswept and of high aspect ratio; the quantity

$$-\frac{\beta A + 4}{\beta A}\,\frac{\beta c\Delta C_l}{SC_l}$$

is calculated by Equation (3.161), by Graham's method[3.28] and from Figure 3.17. Equation (3.161) gives

$$-\frac{(\beta A + 4)c\Delta C_l}{4s^2C_l} = \frac{\pi b^3\zeta_0\sigma^2}{64h^3} = 0.1431\zeta_0\sigma^2 \ ,$$

where, by Table 3.VI, $\zeta_0 = 5.0$ and 4.0 for $y = t = 0$ and $\frac{1}{4}b$ respectively. When the latter is used, the following comparisons are obtained with results from Figure 3.17 for large values of βA .

σ	0.5	0.6	0.7	0.8
Figure 3.17	0.19	0.23	0.30	0.42
$0.572\sigma^2$	0.14	0.21	0.28	0.37

By Equation (9) of Reference 3.28 with taper parameter $K_1 = 0.8\bar{c}/\bar{\bar{c}}$ and section lift-curve slope 2π

$$-\frac{(\beta A + 4)c\Delta C_l}{4s^2C_l} = \frac{0.8h}{2\sigma b}\,\frac{F_1(y_2/b) - F_1(y_1/b)}{(y_2/b)^2 - (y_1/b)^2} \ , \qquad (3.170)$$

where $y_1 < y < y_2$ denotes the span of an aileron and F_1 is plotted for $b/h = 10/7$ and $\sigma = 0.68\ (0.04)\ 0.92$ in Figure 5 of Reference 3.28. Equation (3.170) has been evaluated for $\sigma = 0.8$ to investigate the dependence of the interference correction on aileron span

y_1/s	y_2/s	Equation (3.170)
0.4	0.8	0.402
0.4	1.0	0.430
0.6	1.0	0.438
0.8	1.0	0.444

The results only vary within ±6% of the value 0.42 from Figure 3.17.

Examples (b) and (c) are for swept wings. In example (b) Equation (3.62) is evaluated with $(w_1/U)_{0.75}$ from Table A4 of Reference 3.18 and the lift slope $\partial C_L/\partial\alpha = 2.80$ and weighting W from lifting-surface theory. With $A = 2.64$, $\beta = 1$ and $\tan\Lambda_{0.25} = 1$, it follows that $\mu = 0.835$; hence Equation (3.62) gives

$$-\frac{\Delta C_l}{C_l} = \frac{0.912 \times 0.00315}{0.1413} = 0.0203$$

in excellent agreement with the value 0.0202 from Table A7 of Reference 3.18 by lifting-surface theory. The rough Equation (3.161) gives

$$-\frac{\Delta C_l}{C_l} = \frac{\pi s^* \zeta_c}{4h^*(\beta A+4)} = 0.01426\ \zeta_0 \ .$$

when $\beta A = 2.64$, $b = 2h$ and $s = 0.589h$. For the broader rectangular tunnels ζ_0 varies greatly with wing span. The value $\zeta_0 = 1.637$ from Table 3.VI(b) gives $-\Delta C_l/C_l = 0.023$ of the correct order. In view of the crudity of the approximations leading to Equation (3.161) and the difficulty in assigning a mean value to ζ_0 , errors of ±20% are likely. But the interference correction ΔC_l is often so small that such errors can be tolerated. When applied to example (c) for a closed circular tunnel, Equations (3.161) and (3.167) with $t = y = s_e$ give

$$-\frac{\Delta C_l}{C_l} = \frac{\pi\sigma^*}{8(\beta A+4)(1-\sigma_e^*)^2} = \frac{0.00798}{(1-\sigma_e^*)^2} \ .$$

when $\sigma = 0.656$, $\beta A = 5.11$ and $\sigma_e = s_e/R$. This agrees with the reliable value 0.01007 from Table XIII of Reference 3.26 when $\sigma_e = 0.575$; the ratio $\sigma_e/\sigma = 0.88$ is reminiscent of the effective span ratios s_e/s discussed below Equation (3.41).

Finally we examine the interference corrections to yawing moment coefficient corresponding to the same three examples. The simple expression in Equation (3.164) is evaluated with $\delta_0 = (\delta_0)_E$ and ζ_0 from Table 3.VI(b).

Example	*Tunnel*	σ	$(\delta_0)_g$	ζ_0	g/c	$-\Delta C_n/C_L C_l$	
						Eq.(3.164)	*Original*
(a)	b/h = 10/7	0.600	0.1117	4.00	0.0857	0.0124	0.0118
(b)	b/h = 2	0.589	0.0980	1.64	0.2631	0.0351	0.0435
(c)	Circular	0.656	0.1295	10.08	0.1072	0.0175	0.0216

The table compares the approximate values of $-\Delta C_n/C_L C_l$ with the original values from Figure 3.17, Equation (9.8) of Reference 3.18 and Table XIII of Reference 3.26 respectively. The discrepancies are as much as 20% for both the swept wings. It is instructive to calculate example (c) by the method of Reference 3.50 set out in Equation (3.168) with $\sigma = 0.656$ and $(C_L)_2 = 0$.

y_1/s	y_2/s	$-\Delta C_n/C_L C_l$
0.4	0.8	0.0173
0.4	1.0	0.0178
0.6	1.0	0.0181
0.8	1.0	0.0185

The values lie closer to that from Equation (3.164) than to the result in Reference 3.26. A likely explanation is that the latter uses the interference upwash $(w_i/U)_{0.25}$ in place of $\frac{1}{2}(w_i/U)_\infty$ in Equation (3.70), while the quantity in Equation (3.163), and also in Reference 3.50, is an approximation to $\frac{1}{2}(w_i/U)_\infty$. There is no reason for preferring either, and the uncertainty of about ±10% in ΔC_n may be fundamental. This is demonstrable in example (b). The original calculations from Table 8b of Reference 3.18 used Equation (3.70), except that $(\bar{w}_i)_g$ and $(w_i)_A$ were taken respectively at the local centres of pressure of the antisymmetrical and symmetrical portions of the loading. The calculation has been repeated for the particular aileron considered in Tables A3 to A7 of Reference 3.18, not only with Equation (3.70) as it stands but with $\frac{1}{2}(w_i/U)_\infty$ replaced by $(w_i/U)_{0.25}$.

w_i/U	*Local c.p.*	*0.25 chord*	*Half* $x=\infty$	*Eq.(3.164)*
$-\Delta C_n/C_L C_l$	0.0437	0.0376	0.0331	0.0351

The results convey the necessary warning, that ΔC_n is rather unreliable.

3.6 SPECIAL CONFIGURATIONS

Two important aspects of lift interference have not yet been considered. The first of these concerns slender wings, whose span is small compared with the tunnel breadth and whose length is of the same order as the tunnel height (Section 3.6.1). The second important configuration is that of wing-body combinations treated in Section 3.6.2 which includes tail-plane interference. Finally there are some remarks on three-dimensional interference effects when the tunnel floor is used to simulate the ground (Section 3.6.3) and when models span the tunnel (Section 3.6.4).

3.6.1 Slender Wings

The vortex model of a slender wing is represented in Figure 3.8(b) as a distribution of lifting elements along a portion of the x-axis. Let $L(x_0)$ denote the lift on the portion of the wing $0 < x < x_0$, so that

$$\frac{1}{\rho U}\frac{dL}{dx_0}\,\delta x_0$$

defines the doublet strength of the semi-infinite vortex pair trailing from $x = x_0$. Then by Equation (3.13) the interference potential in a rectangular tunnel is

$$\Phi_i(x,y,z) = \frac{1}{4\pi\rho U}\int \psi(x_0,x,y,z)\,\frac{dL}{dx_0}\,dx_0 \,, \tag{3.171}$$

where

$$\psi(x_0,x,y,z) = \sum_{-\infty}^{\infty}\sum{}' (j)\,\frac{z-nh}{(y-mb)^2+(z-nh)^2}\left[1+\frac{x-x_0}{\{(x-x_0)^2+\beta^2(y-mb)^2+\beta^2(z-nh)^2\}^{\frac{1}{2}}}\right] \tag{3.172}$$

and the integral is taken along the length of the wing. It follows from Equation (3.171) and integration by parts that the interference upwash along the axis of the tunnel is

$$w_i(x) = \left(\frac{\partial\Phi_i}{\partial z}\right)_{y=z=0} = \frac{L}{4\pi\rho U}\int\left(\frac{\partial^2\psi}{\partial z\partial x_0}\right)_{y=z=0}\left[1-\frac{L(x_0)}{L}\right]dx_0 \,. \tag{3.173}$$

provided that $L(0) = 0$: Equation (3.172) yields

$$\left(\frac{\partial^2\psi}{\partial z\partial x_0}\right)_{y=z=0} = -\beta^2\sum_{-\infty}^{\infty}\sum{}' (j)\,\frac{(x-x_0)^2+\beta^2(m^2b^2-2n^2h^2)}{\{(x-x_0)^2+\beta^2(m^2b^2+n^2h^2)\}^{5/2}} \,. \tag{3.174}$$

Berndt[3.51] gives the theory for uncambered wings with unswept trailing edges in closed rectangular tunnels. His result for w_i/U follows from Equations (3.173) and (3.174) with $j = (-1)^n$ by Equation (3.14) and with the theoretical slender-wing loading

$$\frac{L(x_0)}{L} = \left[\frac{s(x_0)}{s(c_r)}\right]^2 \,, \tag{3.175}$$

where $s(x_0)$ is the local semi-span and it is assumed that $s(0) = 0$ and $ds/dx_0 \geqslant 0$ for $0 \leqslant x_0 \leqslant c_r$. In his final expression

$$\frac{w_i}{U} = \frac{SC_L}{C}\,[\delta_0 + \delta'(x)] \ , \qquad (3.176)$$

δ_0 is the parameter $\delta_0^{(1)}$ as defined for a small wing in Equation (3.17) and

$$\delta'(x) = \int_0^{c_r}\left[\frac{s(x_0)}{s(c_r)}\right]^2 f\left(\frac{x-x_0}{\beta\sqrt{C}}\right)\frac{dx_0}{\beta\sqrt{C}} - F\left(\frac{c_r-x}{\beta\sqrt{C}}\right) \ , \qquad (3.177)$$

where

$$f(\xi) = \frac{1}{8\pi}\sum_{-\infty}^{\infty}\sum{}' (-1)^n\,\frac{\xi^2 + (b/h)m^2 - 2(h/b)n^2}{\{\xi^2 + (b/h)m^2 + (h/b)n^2\}^{5/2}}$$

and

$$F(\xi) = \int_0^{\xi} f(\xi)\,d\xi \ .$$

Berndt gives graphs of both $f(\xi)$ and $F(\xi)$ $(0 \leqslant \xi \leqslant 1)$ for the four tunnel cross-sections $b/h = \frac{1}{2}\sqrt{2}$, 1 , $\sqrt{2}$ and 2 . It may be noted that $F(\infty) = \delta_0^{(1)}$; there is a critical value of b/h above which $F(\xi)$ ceases to be monotonic. Equations (3.176) and (3.177) also hold for a closed circular tunnel, when $\delta_0 = 0.125$ and

$$f(\xi) = \frac{1}{8\sqrt{\pi}}\int_0^{\infty}\int_0^{\infty}\frac{(2-t^2)\cos ut\cos(u\xi\sqrt{\pi})}{(1+t^2)^{5/2}\,I_1'(u)}\,dt\,du \ , \qquad (3.178)$$

where I_1' is the derivative of the modified Bessel function I_1 . The interference corrections corresponding to the upwash angle of Equation (3.176) are easily formulated from slender-wing theory. In the present notation Berndt's expressions for the incremental corrections to incidence and pitching moment are

$$\left.\begin{aligned} \Delta\alpha &= \frac{SC_L}{C}\,[\delta_0 + \delta'(c_r)] \ , \\ \Delta C_m &= \frac{SC_L}{C}\,\frac{\partial C_L}{\partial\alpha}\int_0^{c_r}[\delta'(c_r) - \delta'(x)]\left[\frac{s(x)}{s(c_r)}\right]^2\frac{dx}{\bar{c}} \end{aligned}\right\} \ . \qquad (3.179)$$

A useful approximation to Berndt's theory is to replace $f(\xi)$ by a constant $f(0) = \delta_1\sqrt{C}/h$ given in Equation (3.16). Then Equation (3.177) becomes

$$\delta'(x) = \frac{\delta_1}{\beta h}\left[\int_0^{c_r}\left[\frac{s(x_0)}{s(c_r)}\right]^2 dx_0 - (c_r - x)\right] \ . \qquad (3.180)$$

To this approximation Equation (3.176) can be rewritten as

$$\frac{w_i}{U} = \frac{SC_L}{C}\left[\delta_0 + \frac{x-\bar{x}}{\beta h}\,\delta_1\right] \ . \qquad (3.181)$$

where $x = \bar{x}$ denotes the centre of lift; it may be noted that Equation (3.181) would apply to cambered slender wings with swept trailing edges when Equation (3.175) is invalid. Equations (3.179) are replaced by the approximations

$$\left.\begin{aligned}\Delta\alpha &= \frac{SC_L}{C}\left[\delta_0 + \frac{c_r - \bar{x}}{\beta h}\,\delta_1\right]\\ \Delta C_m &= \frac{SC_L}{C}\,\frac{\partial C_L}{\partial\alpha}\,\delta_1\int_0^{c_r}\frac{c_r - x}{\beta h}\left[\frac{s(x)}{s(c_r)}\right]^2\frac{dx}{\bar{c}}\end{aligned}\right\}\,, \qquad (3.182)$$

where δ_0 and δ_1 are the interference parameters discussed in Sections 3.2.2 and 3.2.3 for all practical tunnel cross-sections; the expression for ΔC_m is subject to the same restrictions on planform as Equation (3.175).

The numerical examples in Reference 3.51 concern triangular wings of aspect ratio $A = 1$ in a low-speed closed duplex tunnel ($b = 2h$), and Berndt concludes that the corrections do not differ very much from the lifting-line quantities given by Equations (3.182) with $\delta_1 = 0$. This is largely a consequence of the corrections being fairly small. Naturally Equations (3.182) as they stand should be even closer to Berndt's values corresponding to Equations (3.179) with $\delta'(x)$ from Equation (3.177) and

$$\beta = 1\,, \quad b = 2h\,, \quad \frac{s(x_0)}{s(c_r)} = \frac{x_0}{c_r}\,, \quad \frac{S}{C} = \frac{1}{8}\left(\frac{c_r}{h}\right)^2, \quad \bar{c} = \tfrac{1}{2}c_r\,, \quad \frac{\partial C_L}{\partial\alpha} = 1.3\,.$$

Equations (3.182) with $\delta_0 = 0.1368$, $\delta_1 = 0.2927$ and $\bar{x} = (2/3)c_r$ give the broken curves of $\Delta\alpha/C_L$ and $\Delta C_m/C_L$ against c_r/h in Figure 3.20, which lie very near the full curves obtained from Berndt's calculations. Even when $c_r/h = 1$, the discrepancy in $\Delta\alpha$ is only 0.3% of the measured incidence and the discrepancy in corrected aerodynamic centre is less than $0.001c_r$. It seems worth remarking that at $\alpha = 10$ degrees, when the discrepancy in $\Delta\alpha$ is 0.03 degrees, the vertical displacement of the wing from apex to trailing edge is $c_r \sin\alpha = 0.174h$ and is beginning to be significant. That is to say, in rare instances when Equations (3.182) cease to be accurate enough because c_r/h is large, Equations (3.179) may well be inaccurate through the assumption that the lifting elements are situated in the plane $z = 0$. The latter defect would require the unattractive remedy of replacing z in Equations (3.171) and (3.172) by $z - z_0(x_0)$ where z_0 is linear in x_0.

When the effects of compressibility are calculated, there is greater restriction on the accuracy of Equations (3.182) without prejudice to Equations (3.179). The function $f(\xi)$ in Equation (3.177) is required over the wider range $|\xi| < c_r/(\beta/C)$ and the approximation in Equation (3.180) fails for a smaller value of c_r/h. If the compressibility factors of Table 3.I are applied at very high subsonic Mach numbers, then both the wing and the tunnel may be regarded as slender[3.52]. It is easily shown that, in place of Equation (3.176),

$$\frac{w_i}{U} = \frac{2L(x)}{\rho U^2 C}\,[2\delta_0]\,.$$

When $(1 - M)$ is small, the interference corrections are therefore

$$\left.\begin{aligned}\Delta\alpha &= \frac{SC_L}{C}\,[2\delta_0]\\ \Delta C_m &= \Delta\alpha\,\frac{\partial C_L}{\partial\alpha}\int_0^{c_r}\left\{1 - \left[\frac{s(x)}{s(c_r)}\right]^2\right\}\left[\frac{s(x)}{s(c_r)}\right]^2\frac{dx}{\bar{c}}\end{aligned}\right\}\,. \qquad (3.183)$$

Nevertheless it is difficult to envisage practical situations in which Equations (3.183) may be used confidently.

Berndt gives the drag correction

$$\Delta C_D = \delta_0 \frac{SC_L^2}{C} . \qquad (3.184)$$

This can be justified either by considering the momentum flux across a transverse plane in the distant wake, with the corollary that the vortex drag is independent of any changes in the chordwise load distribution. Alternatively, Taylor[3.70] has shown that Equation (3.184) is compatible with the concept of normal pressures and a suction force distributed along the leading edge. The assumptions of linearized theory are essential to both these arguments.

Unfortunately slender wings usually involve flow separation along the whole leading edge. Such flows, with a free vortex sheet rolling up into concentrated vortices, are beyond the scope of linearized theory; the results in Equations (3.179) or (3.182) and in Equation (3.184) therefore need reconsideration. In the absence of a suitable non-linear theory the expressions for $\Delta\alpha$ in Equations (3.179) and (3.182) will be retained, but it is doubtful whether those for ΔC_m are worth applying. Equation (3.184) needs to be modified, since the leading-edge suction force disappears and the whole lift acts normal to the planform. Even if the wing is cambered, it seems reasonable to neglect the redistribution of lift associated with the residual interference correction ΔC_m ; then the principal correction $\Delta\alpha$ to incidence is accompanied by a correction

$$\Delta C_D = C_L \Delta\alpha = \frac{SC_L^2}{C} [\delta_0 + \delta'(c_r)] \qquad (3.185)$$

by the first of Equations (3.179). Equation (3.185) should therefore replace Equation (3.184) whenever there is extensive leading-edge flow separation.

3.6.2 Wing-Body-Tail Combinations

Many fundamental aerodynamic experiments requiring accurate wall interference correction are carried out on wing models, but the majority of wind-tunnel tests are made on more complete aircraft models. Although rather lower accuracy may often be sought, models of wing-body-tail configurations tend to have larger dimensions relative to the tunnel, so that wall interference remains important. The evaluation of interference corrections becomes more complicated in each of its phases, vortex representation, interference upwash field, principal corrections and residual corrections.

In the first place there are more unknowns in the vortex model, as the wing, body and tail may all carry lift and only the total forces may be measured. The usual approximation is to ignore the body lift and to take the theoretical spanwise loading along the quarter-chord lines of the wing and tail so as to be consistent with the measured lift and pitching moment. A more detailed representation is of course desirable, but is only practicable when there are additional theoretical or experimental loading data. Next, the interference upwash field involves large streamwise displacements between the lifting elements and the various parts of the model, so that it is inadmissible to suppose that the upwash is linear in x ; this particular complication is aggravated by the effect of compressibility. Furthermore, vertical displacements from the tunnel axis may no longer be negligible.

Then there are corrections to measured quantities to consider, and in this respect it is usual to treat the wing, body and tail quite separately. The principal interference correction $\Delta\alpha$ is still calculated from Equation (3.55) where $(w_i/U)_{0.75}$ now includes a small contribution proportional to $(C_L)_t$ the lift coefficient of the tail plane. It is also necessary to calculate a mean value of the interference upwash along the three-quarter-chord line of the horizontal tail surface

$$\delta\alpha_t = \int_0^1 \left(\frac{w_i}{U}\right)_t \frac{U}{U_t} W_t \, d\left(\frac{y}{s_t}\right) , \tag{3.186}$$

where U_t is the local streamwise velocity at the tail, s_t is its semi-span, and W_t is the weighting appropriate to the planform of the tail surface. Then the correction

$$\Delta\alpha_t = \delta\alpha_t - \Delta\alpha \tag{3.187}$$

may be applied to the incidence of the tail plane. Alternatively Equation (3.187) may be replaced by corrections

$$\left.\begin{aligned} \Delta C_L &= -\frac{\partial C_L}{\partial \alpha_t}(\delta\alpha_t - \Delta\alpha) \\ \Delta C_m &= -\frac{\partial C_m}{\partial \alpha_t}(\delta\alpha_t - \Delta\alpha) \end{aligned}\right\} , \tag{3.188}$$

where $\partial C_L/\partial\alpha_t$ and $\partial C_m/\partial\alpha_t$ are the experimentally determined aerodynamic derivatives with respect to tail setting. A further correction must be applied to the vertical location of the vortex wake or positions at which the local flow is measured. The wake displacement is obtained as

$$\Delta z = \int_{TE}^{x} \left(\frac{w_i}{U}\right) \frac{U}{U'} \, dx . \tag{3.189}$$

where U' denotes the local streamwise velocity and the integration is from the trailing edge to the position concerned. This correction can be particularly important when the aerodynamic characteristics of the tail are strongly influenced by body vortices or trailing vortices from the wing. Difficulties arise from the lack of a suitably simple lifting-surface theory for wing-body-tail configurations. Because the interference upwash is interpreted separately for each component, the residual corrections are liable to be larger than usual and less predictable. This is certainly the case when wall interference effects at the body are considered in isolation, as will be discussed later.

In the earlier theories the effect of the body was neglected. Glauert and Hartshorn (Ref.3.16; 1924) were the first to evaluate Equation (3.187) from the simple result in Equation (3.40), viz.,

$$\Delta\alpha_t = \frac{x_t\delta_1}{\beta h}\frac{SC_L}{C} ,$$

where x_t is the length of the tail arm from the three-quarter-chord point and δ_1 is the interference parameter for a small wing. They assume that the tail arm is of the same order of magnitude as the wing semi-span and that the dimensions of the wing are small relative to those of the tunnel. Their correction to tail setting $\Delta\alpha_t$ and tunnel-induced downwash at the tail

$$-\left(\frac{w}{U}\right)_t = -\left(\delta_0 + \frac{x_t\delta_1}{\beta h}\right)\frac{SC_L}{C} \tag{3.190}$$

are well confirmed by experiments on the same model in closed square tunnels of different sizes, as shown in Figures 3 to 6 of Reference 3.16 (Figs. 17 and 18 of Ref. 3.1). Towards the end of Section 3.2.4 with reference to Figure 3.6, it is shown that so simple a theory fails when the tail arm x_t is as much as half the tunnel height. The following discussion explains the apparent success of this theory when applied to square tunnels.

A more general theory is described in Reference 3.30, where Cowley and McMillan calculate $\Delta\alpha_t$ with allowance for wing span and the non-linear variation in interference upwash with streamwise distance. For uniform spanwise loading w_1 is obtained from Equation (3.80) without the terms $|m| > 3$ and $|n| > 5$, and the correction may be written as

$$\Delta\alpha_t = \frac{SC_L}{C}(\delta_t')_U = \frac{SC_L}{C}\left[\delta_0(0,s) + \delta'(\beta^{-1}x_t,0,s) - (\delta_0)_U\right] , \tag{3.191}$$

where $\delta_0(y,t)$ and $(\delta_0)_U$ are given by Equations (3.82) and (3.83) and $\delta'(\beta^{-1}x_t,0,s)$ corresponds to the increment in w_1 along the tail arm. For elliptic spanwise loading they evaluate

$$\Delta\alpha_t = \frac{SC_L}{C}(\delta_t')_E , \tag{3.192}$$

where

$$(\delta_t')_E = \frac{4}{\pi}\int_0^1 \left[\delta_0(0,t) + \delta'(\beta^{-1}x_t,0,t) - \{\delta_0(t)\}_U\right]\left(\frac{t}{s}\right)^2\left\{1 - \left(\frac{t}{s}\right)^2\right\}^{-\frac{1}{2}} d\left(\frac{t}{s}\right) .$$

Cowley and McMillan showed that their results for a low-speed duplex tunnel differed greatly from the simpler theory of Reference 3.16 when $\sigma > 0.5$. The comparisons between $(\delta_t')_U$, $(\delta_t')_E$ and the linear quantity $x_t\delta_1/h$ against σ are reproduced in Figure 3.21 for the particular configuration $x_t = 0.8s$. The additional mixed-broken curve of

$$\frac{C}{SC_L}\Delta\alpha_t = \delta'(\beta^{-1}x_t,0,0) = F\left(\frac{x_t}{\beta\sqrt{C}}\right) \tag{3.193}$$

by Equation (3.177) shows that for large models more than half the error from Reference 3.16 is attributable to the approximation that $\Delta\alpha_t$ is linear in x_t. Now for square tunnels, in which the experiments of Reference 3.16 were made, the effects of non-linearity in x_t and of wing span are in opposition. This cancellation of errors must have played an important part in the otherwise perfect experimental confirmation of the simpler theory mentioned above.

The most comprehensive calculations of $\Delta\alpha_t$ for rectangular tunnels are those of Silverstein and White (Ref. 3.32; 1935). The body and the tail loadings are ignored and the wing is assumed to have uniform spanwise loading. The interference upwash in the central plane $y = 0$ is calculated as

$$\frac{w_i}{U} = \frac{SC_L}{C}\,\delta_w\left(1 + \frac{\delta_A}{\delta_w}\right) , \tag{3.194}$$

where δ_w is a function of $\sigma = 2s/b$ and the vertical location of the wing and the ratio δ_A/δ_w is obtained to a good approximation as a function of σ, $x_t/\beta b$ and the vertical locations of wing and tail. In effect Equation (3.80) is evaluated exactly where $|m|$ and $|n|$ are both less than 3, but the remainder of the double series is calculated to first order in x and $t = s$. Extensive results are available for four different rectangular tunnels in the following charts of Reference 3.32.

Boundary	b/h	δ_w	δ_A/δ_w
Closed	1	Figure 10	Figures 15 to 17
Open	1	Figure 11	Figures 18 to 20
Closed	2	Figure 12	Figures 21 to 23
Open	2	Figure 13	Figures 24 to 26

It is suggested that the values of δ_A/δ_w for rectangular tunnels may suffice for elliptical tunnels of the same breadth to height ratio and type of boundary, provided that the correct δ_w is used in Equation (3.194). For circular tunnels Figure 6 of Reference 3.32 would be used in place of Figure 10 or 11 for δ_w, and likewise for elliptical tunnels ($b = 2h$) Figures 3 and 4 would replace Figures 12 and 13.

A different method of calculation has been given by Brown[3.33]. The wing loading is again represented by a horse-shoe vortex, and the complete expression for the interference upwash at the tail in a closed rectangular tunnel is given by

$$\begin{aligned}\frac{16\pi s}{SC_L}\,\Delta\alpha_t(y) = {} & \sum_{-\infty}^{\infty}\sum{}'\,[W(\beta^{-1}x_t, y-mb+s, d_t-d-2nh) - W(\beta^{-1}x_t, y-mb-s, d_t-d-2nh)] - \\ & - \sum_{-\infty}^{\infty}\sum{}'\,[W(\beta^{-1}x_t, y-mb+s, d_t+d-2nh) - W(\beta^{-1}x_t, y-mb-s, d_t+d-2nh)] - \\ & - [W(\beta^{-1}x_t, y+s, d_t+d) - W(\beta^{-1}x_t, y-s, d_t+d)] \ .\end{aligned} \tag{3.195}$$

where, as usual, $\sum\sum_{-\infty}^{\infty}{}'$ denotes that (m,n) takes all possible integral pairs except (0,0), $W(x,y,z)$ is defined in Equation (3.79), x_t is the length of the tail arm, y is the spanwise distance along the tail, d and d_t denote the respective distances of the wing and horizontal tail surface from the tunnel floor. Brown writes each double summation in the form

$$\sum\sum_{-\infty}^{\infty}{}' = \sum_{m=-M}^{M}\sum_{n=-N}^{N}{}' + R_{MN}$$

and the remainder R_{MN} is evaluated on the basis that $W(x,y,z)$ is a nearly linear function of y when y and z are not both small; thus

$$W(x,\ y+s,\ z) - W(x,\ y-s,\ z) \approx \frac{2s}{b}\left[W(x,\ y+\tfrac{1}{2}b,\ z) - W(x,\ y-\tfrac{1}{2}b,\ z)\right] \ ,$$

so that

$$\begin{aligned} R_{MN} &= \left(\sum\sum_{-\infty}^{\infty}{}' - \sum_{-M}^{M}\sum_{-N}^{N}{}'\right)\left[W(x,\ y-mb+s,\ z-2nh) - W(x,\ y-mb-s,\ z-2nh)\right] \\ &= \frac{2s}{b}\left[2\sum_{n=-\infty}^{\infty}W(x,\infty,z-2nh) - \sum_{n=-N}^{N}W(x,\ Mb+\tfrac{1}{2}b+y,\ z-2nh) - \sum_{n=-N}^{N}W(x,\ Mb+\tfrac{1}{2}b-y,\ z-2nh)\right] . \end{aligned} \tag{3.196}$$

When $y = 0$, Equations (3.195) and (3.196) simplify to give

$$\begin{aligned} \frac{C}{SC_L}\,\delta\alpha_t = \delta_t = \frac{bh}{16\pi s}\Bigg[\sum_{-M}^{M}\sum_{-N}^{N}{}'\{W(\beta^{-1}x_t,\ mb+s,\ z-2nh) - W(\beta^{-1}x_t,\ mb-s,\ z-2nh)\} \ + \\ + \frac{4s}{b}\left\{\sum_{-\infty}^{\infty}W(\beta^{-1}x_t,\ \infty,\ z-2nh) - \sum_{-N}^{N}W(\beta^{-1}x_t,\ Mb+\tfrac{1}{2}b,\ z-2nh)\right\}\Bigg]_{z=d_t+d}^{z=d_t-d} - \\ - 2W(\beta^{-1}x_t,\ s,\ d_t+d) \ , \end{aligned} \tag{3.197}$$

where the square bracket notation indicates that, as in the case of an integrated function, the value for $z = d_t + d$ is to be subtracted from that for $z = d_t - d$. A few calculations for horizontal models ($d_t = d$) in two closed rectangular tunnels $b = 2h$ and $b = 4h$ are found in Table 8 of Reference 3.33. A more elaborate method of computation for closed rectangular tunnels is suggested by Sanders and Pounder in Section 3.4 of Reference 3.23. When the tail span is appreciable, an average value of $\delta\alpha_t$ is required so that the correction to tail setting becomes

$$\Delta\alpha_t = \int_0^1 \delta\alpha_t(y)\ d(y/s_t) - \Delta\alpha \ . \tag{3.198}$$

Batchelor[3.34], following the method of Reference 3.32 for a centrally placed wing ($d = \frac{1}{2}h$) in a closed rectangular tunnel ($b/h = 9/7$), has devised a rough procedure for estimating the incremental effect of superimposed fillets to form an octagonal tunnel. As an alternative estimate, the assumption of Equation (3.108) may be generalized, so that for octagonal tunnels Equation (3.194) is replaced approximately by

$$\frac{w_i}{U} = \frac{SC_L}{C}\,\delta_w\left[1 + \left(\frac{\delta_A}{\delta_w}\right)_R\sqrt{\frac{bh}{C}}\right] , \tag{3.199}$$

in which $(\delta_A/\delta_w)_R$ corresponds to the rectangular tunnel. The parameter δ_w for a centrally placed wing is identified with $\delta_0(0,s)$ from Equations (3.102) to (3.104). For off-centre wings it is shown in Reference 3.34 that the fillets have negligible effect on the variation of $SC_L\,\delta_w/C$ with the vertical location of the wing. Therefore the result for closed rectangular tunnels from Reference 3.33[*]

$$\delta_w = \frac{b}{16s}\left[\frac{2h}{\pi s} - \sin^2\frac{\pi d}{h}\sum_{m=-\infty}^{\infty}\frac{\coth\dfrac{\pi(bm+s)}{2h}}{\sinh^2\dfrac{\pi(bm+s)}{2h} + \sin^2\dfrac{\pi d}{h}}\right] \tag{3.200}$$

provides the increment

$$\delta_w - \delta_0(0,s) = \frac{C}{bh}\,\frac{b}{16s}\left[\sum_{m=-\infty}^{\infty}\frac{\coth\dfrac{\pi(bm+s)}{2h}}{\sinh^2\dfrac{\pi(bm+s)}{2h} + 1} - \sin^2\frac{\pi d}{h}\sum_{m=-\infty}^{\infty}\frac{\coth\dfrac{\pi(bm+s)}{2h}}{\sinh^2\dfrac{\pi(bm+s)}{2h} + \sin^2\dfrac{\pi d}{h}}\right]$$

$$= \frac{C}{16hs}\cos^2\frac{\pi d}{h}\sum_{m=-\infty}^{\infty}\frac{\tanh\dfrac{\pi(bm+s)}{2h}}{\cosh^2\dfrac{\pi(bm+s)}{2h} - \cos^2\dfrac{\pi d}{h}} \tag{3.201}$$

to apply to the value of $\delta_0(0,s)$ from Equations (3.102) to (3.104) for use in Equation (3.199). The quantity $(\delta_A/\delta_w)_R$ may be evaluated as $(\delta_t/\delta_w) - 1$, where δ_t and δ_w are defined in Equations (3.197) and (3.200). The factor $\sqrt{(bh/C)}$ in Equation (3.199) is rather speculative when x_t is large, and indeed is not required in the limit as $x_t \to \infty$ when $\delta_A = \delta_w$ whatever the tunnel section. However, it may be noted from the results in Table 3 of Reference 3.34 and Table 4 of Reference 3. that the fillets appear to have greater percentage influence on w_i at the tail than on w_i at the wing, so that the factor $\sqrt{(bh/C)}$ greater than unity is compatible.

Several papers have been published on tunnel-wall corrections for wing-body combinations. Smith[3.53] considers a circular body concentric with a closed circular tunnel, represents the lifting wing by a horse-shoe vortex, and solves the two-dimensional problem in the plane of the bound vortex $x = 0$ subject to tangential flow at the two circular boundaries. The resulting infinite sequence of image vortices is shown to give rise to an interference upwash that may be up to twice as great as for the wing alone. Gorgui[3.54] gives closed expressions for the series in Reference 3.53 by a method of conformal transformation and also derives analytical results when the circular body is symmetrically placed in any closed rectangular tunnel. In most of his numerical examples the interference upwash at the wing-body junction is practically twice what it would have been in the absence of the body. Loos[3.21] has treated the same problem for a closed octagonal tunnel with an elegant approximation to the influence of the fillets, and he points out that the interference effects have to be interpreted as a principal correction to lift in respect of the vortex pairs added within the body on account of the tunnel boundary. In consequence there is the excessive residual interference upwash at the wing that would be likely to disturb the stalling characteristics of the model. Smith and Gorgui conclude wrongly that their results cast considerable doubt on the practice of applying the corrections, such as Equations (3.186) to (3.188) to measurements on wing-body combinations. There may be uncertainty as to the interference flow field associated with body lift, but this merely requires a few point concentrations of lift distributed along the body and the uncertainty is purely one of representation. From knowledge of the interference field it is a retrograde step to treat the body in isolation. The principal correction to lift in respect of the added vortex pairs is illusory or at least highly undesirable. Instead the principal corrections $\Delta\alpha$ and $\Delta\alpha_t$ should be applied, and the difficulties of interpretation may then be confined to the much smaller residual interference upwash $(w_i/U) - \Delta\alpha$ in the presence of the complete model.

---

[*] $\delta_w = \frac{1}{2}\delta_T$ from the bottom equation on p.4 of Reference 3.33, since the lift coefficient $k_L = \frac{1}{2}C_L$ was used in the definition of δ_T.

3.6.3 Interference on Ground Effect

The discussion of off-centre models towards the end of Section 3.4.1 includes a brief reference to ground effect. Figure 3.11 shows some results from Reference 3.33 for uniformly loaded wings in a closed duplex tunnel as the model is displaced towards the floor of the tunnel. The primary effect on the mean interference parameter $(\delta_0)_U$ is the increasing contribution from the principal image in the floor. When the floor is used to simulate the ground, this effect ceases to be part of the wall interference and the remainder $(\delta_0)_{Ug}$ falls rapidly to zero as the model approaches the ground $(d = 0)$ and the other images tend to cancel out. The effect is illustrated by the removal of the contribution from the principal image in Equation (3.200). The remainder represents the upwash interference parameter at the centre $y = 0$ of the uniformly loaded wing with ground simulation

$$\delta_{wg} = \frac{b}{16s}\left[\frac{3hd^2}{\pi s(s^2+4d^2)} - \sin^2\frac{\pi d}{h}\sum_{m=-\infty}^{\infty}\frac{\coth\dfrac{\pi(bm+s)}{2h}}{\sinh^2\dfrac{\pi(bm+s)}{2h}+\sin^2\dfrac{\pi d}{h}}\right] . \qquad (3.202)$$

which is seen to be $O(d^2)$ as $d \to 0$. Typically, with $d = 0.25h$ in Figure 3.11, $(\delta_0)_{Ug}$ is smaller than $(\delta_0)_U$ by an order of magnitude and is not required to great accuracy. Even for wings in the centre of oblong tunnels ($h = 0.25b$ and $h = 0.50b$), Brown calculates small maximum values of $|(\delta_0)_{Eg} - (\delta_0)_{Ug}|$ in Figures 2 and 3 of Reference 3.33 (0.013 and 0.005 respectively), so that it should be unnecessary to consider elliptic spanwise loading when d/h is fairly small.

Sanders[3.55] has derived a fairly simple expression for the mean upwash interference along a uniformly loaded lifting-line model in a closed rectangular tunnel. The correction to incidence with ground simulation is

$$\Delta\alpha_g = \frac{SC_L}{C}(\delta_0)_{Ug} , \tag{3.203}$$

where

$$(\delta_c)_{Ug} = [(\delta_0)_U]_{d=\frac{1}{2}h} + \frac{\pi h}{b}\sum_{n=1}^{\infty}\frac{n \sinh^2\dfrac{\pi n(h-2d)}{b}}{\sinh(2\pi nh/b)}\left(\frac{\sin \pi n\sigma}{\pi n\sigma}\right)^2 - \frac{h}{8\pi b\sigma^2}\log_e\left(1+\frac{b^2\sigma^2}{4d^2}\right)$$

and the first term on the right hand side is identified with Equation (3.83). Values of $(\delta_0)_{Ug}$ are available in Tables 5 and 6 of Reference 3.33 which require the factor $\frac{1}{2}$, and in Figure 3 of Reference 3.55 where the ordinate is ten times too large. Some of the results are collected in Figures 3.22 and 3.23 for the three shapes of tunnel, $h/b = 0.25$, 0.35 and 0.50. Figure 3.22 shows the effect of model span for two height ratios $d/h = 0.5$ and 0.2, and Figure 3.23 shows the effect of model height for $\sigma = 0$ and 0.6. The series in Equation (3.203) only converges rapidly when $(h-2d)$ is small, but the alternative expression, derived in Equation (A-3) of Appendix A of Reference 3.55, is quite suitable for the smaller values of d. Sanders also formulates the sidewash interference with alternative expressions suitable for the two ranges of d. The images of the bound vortex induce a velocity parallel to the tunnel axis, and the average value of this stream-velocity correction over the span of the wing is obtained as

$$\left(\frac{\Delta U}{U}\right)_g = \epsilon_{Ug} = \frac{SC_L}{C}\frac{h}{8\pi\beta b\sigma^2}\sum_{-\infty}^{\infty}\sum{}'\frac{1}{2nh-2d}\left[\{(2nh-2d)^2+(m+\sigma)^2b^2\}^{\frac{1}{2}} + \right.$$

$$\left. + \{(2nh-2d)^2+(m-\sigma)^2b^2\}^{\frac{1}{2}} - 2\{(2nh-2d)^2+m^2b^2\}^{\frac{1}{2}}\right] . \tag{3.204}$$

The slow convergence of this double series is discussed fully in Appendix A of Reference 3.55 where Equation (3.204) is reformulated for computation in the two cases when $(2h-d)$ or d is small. The calculations for $h = 0.35b$ indicate that $(C/SC_L)\epsilon_{Ug}$ can be considerably larger than $(\delta_0)_{Ug}$. Equation (3.204) shows that $\epsilon_{Ug} = O(d)$ as the model approaches the simulated ground. For the larger values of d, however, ϵ_{Ug} can be quite as important as the usual blockage corrections discussed in Chapter V. But the compressibility factor is only β^{-1} as compared with β^{-3} for solid blockage.

As regards interference on ground effect at the tail, the parameter $\delta\alpha_{tg}(y)$ is given by Equation (3.195) with the last term omitted. Since W is an even function of z, it follows that $\delta\alpha_{tg}$ is unaltered if the vertical locations of the wing and tail are interchanged. However, the interference at the wing is different in the two cases, and so therefore is the correction to tail setting

$$\Delta\alpha_{tg} = \int_0^1 \delta\alpha_{tg}(y)\, d(y/s_t) - \Delta\alpha_g . \tag{3.205}$$

The evaluation of $\Delta\alpha_{tg}$ is discussed further in Reference 3.33.

Irrespective of tunnel shape, the interference corrections on ground effect are readily deduced from those for off-centre models. The remark on closed octagonal tunnels involving Equations (3.199) and (3.201) may be helpful, but it is more straightforward to estimate the correction to incidence as

$$\Delta\alpha_g = \frac{SC_L}{C}\lambda_g(\delta_0)_g \, , \qquad (3.206)$$

where

$$\lambda_g = (\delta_0)_{Ug}/[(\delta_0)_U]_{d=\frac{1}{2}h}$$

is defined by Equation (3.203) for the basic rectangular tunnel and the parameter $(\delta_0)_g$ for an octagonal tunnel is found from the approximate Equation (3.107). When the original working section is circular, experiments on ground effect require the insertion of a ground plate and the tunnel is effectively of bipolar shape. The parameter $(\delta_0)_{Ug}$ has been derived for open and closed circular tunnels. In Section 12 of Reference 3.14, Kondo has given the general expression (δ_u') and tabulated results in Table IX in particular cases when the model lies along the horizontal diameter of the open circular boundary. Albritton and Huber$^{3.56}$ give an analytical expression for the distribution $[\delta_0(y,s)]_g$ along the span of a horse-shoe vortex in a closed circular tunnel with ground plate. The results in Figure 9 of Reference 3.56 for $s = 0.62R$ and $0.11 < d/s < 0.41$ correspond to the range $0.002 < (\delta_0)_{Ug} < 0.026$ based on the area of the complete circular section. Again $(\delta_0)_{Ug}$ is an order of magnitude smaller than the contribution from the ground plate

$$\frac{C}{32\pi s^2}\log_e\left(1+\frac{s^2}{d^2}\right) = 0.082\log_e\left(1+\frac{s^2}{d^2}\right) .$$

3.6.4 Models Spanning Closed Tunnels

We shall consider two investigations in which two-dimensional models have been tested under conditions when wall interference is three-dimensional. The first configuration of an unswept wing in a closed circular tunnel$^{3.42}$ has already been mentioned in Section 2.2.8 and at the end of Section 3.4.3. The other configuration is of a swept wing spanning a closed rectangular tunnel$^{3.57}$. In each case the practical problem is to determine whether pressure measurements at the centre section can be corrected to two-dimensional values.

The analysis of Vincenti and Graham is based on their manipulation of Equation (3.127) with $y = 0$ in Appendix A of Reference 3.42. Hence

$$w_N^{(1)}(x,0) = \frac{L_N}{4\pi\rho UR}\left[\frac{R^2+y_N^2}{Ry_N^2} + \frac{Rx}{y_N^2(x^2+\beta^2y_N^2)^{\frac{1}{2}}} - \right.$$

$$\left. - \sum_{q=0}^{\infty}\sum_{p=0}^{\infty}\frac{(-1)^p\mu'_{2(p+q+1)}y_N^{2q}(x/\beta)^{2p+1}}{q!\,(q+1)!\,(2p+1)!\,2^{2q}R^{2(p+q+1)}}\right] . \qquad (3.207)$$

where

$$\mu'_{2f} = -\frac{1}{(2f+1)\pi}\int_0^\infty \frac{t^{2f-2}(1+t^2)}{[I_1'(t)]^2}\,dt$$

$$= -0.999 \, , \quad -1.627 \, , \quad -9.78 \, , \quad -120.8 \quad \text{for} \quad f = 1,2,3,4.$$

Since the spanwise loading is approximately constant, L_N is replaced by elements $\frac{1}{2}\rho U^2 l(x_N)\ \delta x_N\ \delta y_N$ in Equation (3.207) and the total downwash along the centre line becomes

$$\frac{w(x)}{U} = \int_0^c \frac{l(x_N)}{8\pi R} \int_{-R}^{R} \frac{4\pi\rho U R}{L_N} w_N^{(1)}(x - x_N,\ 0)\ dy_N dx_N$$

$$= \int_0^c \frac{l(x_N)}{8\pi R} \left[-\frac{2\{\beta^2 R^2 + (x - x_N)^2\}^{\frac{1}{2}}}{x - x_N} - \sum_{q=0}^{\infty} \sum_{p=0}^{\infty} \frac{(-1)^p \mu'_{2(p+q+1)}}{q!\,(q+1)!\,(2p+1)!\,(2q+1)2^{2q-1}} \left(\frac{x - x_N}{\beta R}\right)^{2p+1} \right] dx_N \ ; \qquad (3.208)$$

special care has been taken with the integration across $y_N = 0$ (Ref. 3.42). In general the integral equation (3.208) would have to be solved for the chordwise load distribution $l(x_N)$ with $w(x)/U$ corresponding to the camber line of the wing. But the approximation is made that terms of order $[(x - x_N)/\beta R]^3$ and higher are negligible, so that only $p = 0$ is retained and Equation (3.208) reduces to

$$-\frac{w(x)}{U} = \frac{\beta}{4\pi} \int_0^c l(x_N) \left\{ \frac{1}{x - x_N} + \frac{x - x_N}{\beta^2 R^2} \left(\frac{1}{2} + \sum_{q=0}^{\infty} \frac{\mu'_{2(q+1)}}{q!\,(q+1)!\,(2q+1)2^{2q}} \right) \right\} dx_N$$

$$= \frac{\beta}{4\pi} \int_0^c l(x_N) \left\{ \frac{1}{x - x_N} - \frac{0.579(x - x_N)}{\beta^2 R^2} \right\} dx_N \ . \qquad (3.209)$$

To this approximation the wall interference is precisely that which would arise in a two-dimensional tunnel of height 1.686R. By a corresponding treatment the interference to the stream velocity is precisely the solid blockage of the same model in a two-dimensional tunnel of height 1.558R. The interference corrections are thus

$$\left.\begin{aligned} \Delta\alpha &= \frac{0.289}{8\pi\beta} \left(\frac{c}{R}\right)^2 (C_{LL} + 4C_{mL}) \\ \Delta C_{LL} &= -\frac{0.289 c^2 C_{LL}}{4\beta^2 R^2} \\ \Delta C_{mL} &= \frac{0.289 c^2 C_{LL}}{16\beta^2 R^2} \end{aligned}\right\} \qquad (3.210)$$

where C_{LL} and C_{mL} are the local lift coefficient and pitching moment coefficient about the quarter-chord axis and there are additional terms to account for blockage effects in Equations (51) and (52) of Reference 3.42.

The analysis for the swept wing spanning a rectangular tunnel in incompressible flow is more straightforward. Again the spanwise loading is taken to be uniform, but it is represented simply by a bound vortex along the quarter-chord line. Dannenberg[3.57] gives the interference upwash at the centre section in the form

$$\frac{w_i}{U} = \frac{SC_{LL}}{8\pi b^2} \sum_{-\infty}^{\infty}\sum{}' \frac{(-1)^{m+n} m \tan\Lambda}{m^2\sin^2\Lambda + (nh/b)^2}\left[\frac{m\cos^2\Lambda + \frac{1}{2}}{\{\frac{1}{4}\tan^2\Lambda + (m+\frac{1}{2})^2 + (nh/b)^2\}^{\frac{3}{2}}} - \right.$$

$$\left. - \frac{m\cos^2\Lambda - \frac{1}{2}}{\{\frac{1}{4}\tan^2\Lambda + (m-\frac{1}{2})^2 + (nh/b)^2\}^{\frac{3}{2}}}\right] . \qquad (3.211)$$

As a result of the swept lifting line the interference velocity also has streamwise and sidewash components which are formulated. The final correction to incidence at $y = 0$ is

$$\Delta\alpha = \frac{k_1 C_{LL}}{1 + k_2 C_{LL}} , \qquad (3.212)$$

where $k_1 = 0.43^\circ$ and $k_2 = -0.084$ for the sweepback $\Lambda = 45^\circ$.

Figures 3.24(a) and 3.24(b) show the uncorrected and corrected curves of C_{LL} against α from the respective investigations. In Reference 3.42 the corrections of Equations (3.210) are applied with further allowance for solid blockage to measurements on two sizes of model, $c/R = 0.71$ and 1.25 , in low-speed flow. The corrected results in Figure 3.24(a) collapse on to a single curve apart from uncertainties near maximum lift, and Vincenti and Graham also find satisfactory agreement between the two corrected curves of C_{mL} against C_{LL} . In Reference 3.57 the experimental lift curve is corrected by Equation (3.212) and compared with that for an unswept wing of the same NACA 63_1-012 aerofoil section normal to the leading edge with the simple sweep factor $\cos\Lambda$. The agreement in Figure 3.24(b) is remarkably good, and the corrected experiments in Reference 3.57 also give satisfactory comparisons with the pitching moment and wake drag of the unswept aerofoil. Both configurations can be justified as means of estimating two-dimensional flow.

3.7 EXPERIMENTAL CONSIDERATIONS

Although the study of wind-tunnel wall interference arose directly from experiment, it rapidly became a source of absorbing mathematical problems. In some respects the ensuing theoretical developments have outstripped the needs of many experimenters to whom wall interference is one of several corrections to be applied; these and other factors set a limit to the accuracy of the investigation. Moreover, there are types of experiment in which the air flow is so complicated that only the principal interference corrections are likely to have significance. Flow separation due to high incidence, leading-edge sweepback, strong shock waves or bluffness of the model occur in most programmes of wind-tunnel testing. Any one of these may cause serious violation of the linear assumptions implicit in the preceding formulae. The remarks in Section 3.7.1 concern the experimental evidence of wall interference at the stalling incidence. Other aspects of separated flow form the subject of Chapter VII.

Naturally the precision of calculated interference parameters is far greater than that of any experimental verification of the underlying theory. The available information for closed and open tunnels is summarized in Sections 3.7.2 and 3.7.3 respectively. Although much of the material is inconclusive, the results have some practical interest. It is pertinent that, especially for open tunnels, there is more evidence of underestimation than overestimation of interference effects. Neglect of streamline curvature is perhaps more prevalent than it should be. Simple approximations cover this and other refinements, and there can be little justification for ignoring them.

3.7.1 High Lift

There are many factors to complicate wall interference on wings at high lift. The attitude of the model may introduce off-centre effects due to vertical displacement. If the chord of the wing is large, the wing and its principal image in a closed roof will represent a divergent passage and so tend to cause flow separation from the upper surface of the wing. The high lift will increase the magnitude of spanwise variations in interference upwash and the chordwise variation known as streamline curvature. The residual effects of these on the stalling characteristics of the wing are usually unpredictable, but could be important. Furthermore, the trailing-vortex system may suffer pronounced distortion at high incidence, and so may the boundary of an open jet. All these uncertainties leave little confidence in the standard interference corrections.

Glauert (Ref.3.1, p.38) gives a clear qualitative picture of the effect of spanwise variation of interference upwash on the stalling of lifting-line models of large span. A wing of elliptical planform, having a constant effective incidence throughout the span, can be expected to develop a tip stall in a closed tunnel and a root stall in an open tunnel. A rectangular wing normally stalls at the root where the effective incidence is greatest; in a closed tunnel the interference upwash at the root will often be less than the weighted mean $\Delta\alpha$ so that the corrected stalling incidence is strictly too high, and the reverse is true in an open tunnel. Conversely, with the correction $\Delta\alpha$, a highly tapered wing of large span in a closed tunnel should exhibit conservative stalling characteristics, while tests in an open tunnel should be unduly optimistic.

In the derivation of the interference corrections in Section 3.3.3 it is mentioned that the correction to incidence $\Delta\alpha$ is in a sense quite arbitrary. It is convenient to choose it so that $\Delta C_L = 0$; if some other value of $\Delta\alpha$ were taken, the residual corrections would be different, but within the framework of linearized theory the corrected aerodynamic data would be consistent. Such considerations no longer apply near the stall, and the theory of wall interference is incapable of determining the effect of wall constraint on maximum lift. Therefore Bradfield, Clark and Fairthorne[3.58] carried out an experimental investigation of $(C_L)_{max}$ on rectangular wings of various sections in different sizes of tunnel. Their results in closed rectangular tunnels satisfy the empirical negative correction

$$\Delta(C_L)_{max} = -0.76\ S/b^2 \qquad (3.213)$$

within ±0.005, but there is no systematic evidence of any corresponding correction in an open circular tunnel. Although Equation (3.213) would appear to be consistent with the expected higher stalling incidence in a closed tunnel, a further series of experiments by Adamson, Piper and Brown[3.59] on rectangular wings revealed no evidence of systematic wall interference on maximum lift. They suggest that, if full account of wake blockage were taken in Reference 3.58, the correction to $(C_L)_{max}$ would practically disappear. Furthermore, tests in Reference 3.59 with off-centre models show little effect on $(C_L)_{max}$. Since wake blockage can usually be neglected in open tunnels (Section 5.5.3), the results of Reference 3.58 for closed and open tunnels become compatible.

A convincing quantitative study of the effect of spanwise variation of interference upwash has been published by Stewart (Ref.3.60; 1941), who considers a large lifting-line model with elliptic spanwise loading in two closed circular tunnels. The interference upwash at the wing root on the tunnel axis

$$(w_i/U)_r = \frac{SC_L}{8C}$$

is independent of $\sigma = s/R$, and it is supposed that this incremental correction has been applied to the incidence. Stewart obtains the residual interference at the wing tip

$$(w_i/U)_t - (w_i/U)_r = \frac{SC_L}{C}\left[\frac{1}{4\sigma^4}\{(1-\sigma^4)^{-\frac{1}{2}} - 1\} - \frac{1}{8}\right] \qquad (3.214)$$

which gives

$$\frac{(w_i/U)_t - (w_i/U)_r}{SC_L/C} = 0.047 \text{ and } 0.207$$

for $\sigma = 0.77$ and 0.93 respectively. In the two corresponding experiments on an elliptical planform of aspect ratio 5.88 the tip stall was observed carefully with tufts to occur suddenly at corrected incidences $\alpha = 17.3^\circ$ and 15.1° respectively. Figure 3.25 shows the results and indicates how perfectly Equation (3.214) accounts for the difference in stalling angle. It also illustrates two important conclusions, that the correction to stalling angle is unlikely to be large unless $\sigma > 0.8$, and that no deductions about $(C_L)_{max}$ can be made; the larger observed $(C_L)_{max}$ corresponds to the lower stalling angle. Some additional information for a closed elliptical tunnel (b/h = 1.37) is found in Reference 3.40.

Davis and Sweberg[3.61] have studied interference effects in an open circular tunnel by comparisons of full-scale tunnel and flight measurements of maximum lift for a complete aircraft. The experiments are complicated by the large size of the aircraft and the high $(C_L)_{max} = 1.99$ obtained in flight with flaps and landing gear extended. With these retracted, $(C_L)_{max} = 1.36$ and 1.39 are deduced from tunnel and flight respectively, when allowance is made for Reynolds number and time rate of change of incidence. In the landing condition, however, the corresponding tunnel result $(C_L)_{max} = 1.80$ is as much as 0.19 below the value in flight. Half this discrepancy has been explained by two unusual corrections. The first is associated with a large spanwise variation in dynamic pressure ahead of the aircraft due to a distortion of the circular jet; weighted in accordance with the spanwise loading, this gives a large negative correction to the dynamic pressure and an increment of 0.05 in $(C_L)_{max}$. A second correction of $\Delta(C_L)_{max} = 0.05$ is stated to arise from the negative camber associated with streamline curvature; a corresponding increment of 0.03 eliminates the small discrepancy in $(C_L)_{max}$ with flaps and landing gear retracted. The only firm conclusion is that the area ratio S/C of the planform to the jet should be well below 0.2. It would be realistic to impose restrictions $S/C < 0.10$ for open tunnels, $S/C < 0.15$ for closed tunnels, and never to assume better accuracy than ±0.02 in $(C_L)_{max}$.

3.7.2 Closed Tunnels

Much of the theory of wall interference in closed tunnels is now accepted without question. Nevertheless, experimental checks on the theoretical formulae for $\Delta\alpha$ and ΔC_D for wings of high aspect ratio are important in the historical development of the subject. In Figures 11 and 12 of Reference 3.1, Glauert summarizes the experiments of Cowley and Jones[3.62] on a biplane model of span 3 ft, tested in closed square tunnels of side 4 ft and 7 ft. Glauert applied the corrections of Equation (3.6) with $\delta_0 = (\delta_0)_E$ to bring the lift and drag curves from the two tunnels into satisfactory agreement. He also describes the results of experiments by Higgins[3.63] on three rectangular wings of aspect ratio 6 $(\sigma \leqslant 0.6)$ at constant Reynolds number in a closed circular tunnel; after trying several empirical corrections without success, Higgins concluded that the theoretical formulae $(\delta_0 = 0.125)$ gave the best correlation.

In later experiments the method of analysis is to determine empirically the corrections

$$\left.\begin{aligned} \Delta\alpha &= \delta_\alpha\, SC_L/C \\ \Delta C_D &= \delta_D\, SC_L^2/C \end{aligned}\right\} \qquad (3.215)$$

that reconcile the measurements. It is instructive to compare the results with the theoretical values from Equations (3.65), whence

$$\left.\begin{aligned} \delta_\alpha &= (\delta_0)_E \left(1 + \frac{\delta_1}{\delta_0}\,\frac{\bar{\bar{\varepsilon}}}{2\beta h}\right) \\ \delta_D &= (\delta_0)_E \end{aligned}\right\} . \qquad (3.216)$$

where δ_1/δ_0 is given in Figure 3.4 for rectangular tunnels. Three examples are taken for square tunnels.

Source	σ	A	*Experiment*		*Theory*	
			δ_α	δ_D	δ_α	δ_D
Reference 3.8, Case I	0.40	4	0.140	0.140	0.152	0.140
Reference 3.8, Case I	0.60	6	0.142	0.125	0.160	0.147
Reference 3.64, Test 20	0.75	6	0.170	0.1_7?	0.175	0.158

In the last example the experimental δ_D varied from 0.15 to 0.19. The tabulated results represent a reasonable confirmation of the theory.

The investigation of Sivells and Deters[3.47] justifies the use of part-span models in a closed circular tunnel with a reflection plane. Figure 3.15 illustrates the reduction in lift interference when a half-wing model is used. The rolling moments due to aileron deflection ξ will also have to be corrected to conditions of antisymmetrical spanwise loading, as discussed briefly in Section 3.3.6. Furthermore, if a part-span model is used, there will be a third correction to allow for the change in planform. In the example of Reference 3.47, sketched in Figure 3.26, these corrections are respectively

$$\Delta C_l = -0.0816 \, C_l$$

and factors 0.949 and 0.934, which combine to give a free-stream rolling moment coefficient

$$(C_l)_F = 0.814 \, C_l \; .$$

The success of this large correction is illustrated in Figure 3.26, where corrected results (+) from the part-model test at a Reynolds number $R_N = 8.9 \times 10^6$ are compared with the full curve against ξ from experiments on a complete model at $R_N = 4.7 \times 10^6$.

Reference 3.4 sets out to put wall interference and scale effect into perspective. Table 5B (Ref. 3.4, p. 45) illustrates how the two corrections may often oppose each other when the tunnel boundary is closed. It may be typical that the wall interference corrections to aerodynamic forces and moments due to incidence are as important as corrections to full-scale Reynolds number. On the other hand, the characteristics of deflected control surfaces are likely to be influenced less by wall interference than by scale effect; the case of rolling moment on a part-span or half model is a notable exception.

3.7.3 Open Tunnels

Because open tunnels were used extensively during the period in which the theory of wall interference was developed, more attention has been given to the experimental verification of the theory for open and semi-closed tunnels than for completely closed tunnels. Knight and Harris[3.65] have tested three rectangular wings of aspect ratio 5 with span ratios $\sigma = 0.45$, 0.60 and 0.75 in four open tunnels of circular, rectangular ($b = h\sqrt{2}$) and oval section ($b = h\sqrt{2}$ and $b = h$ with circular sides). Their analysis follows Equations (3.215) on the assumption that the results in the circular tunnel can be extrapolated to zero interference. In the present theoretical analysis Equation (3.216) is used, but δ_1/δ_0 is now defined by Equation (3.31) with $\delta_1^{(2)}/\delta_0^{(2)}$ from Figure 3.4. The comparisons in Figure 3.27(a) for the open circular tunnel are reasonably satisfactory. There is further experimental confirmation of the theoretical lift interference in open circular tunnels published by Tani and Taima[3.66]; in Figure 3 of Reference 3.66 they make allowance for streamline curvature and obtain consistent lift and drag curves for three rectangular wings ($\sigma = 0.5$, 0.6, 0.7) of aspect ratio 5. The results of Reference 3.65 are less convincing for the rectangular and oval sections, but experimentally $-\delta_\alpha$ tends to be larger than $-\delta_D$ and the difference indicates the order of magnitude of the streamline-curvature correction. Figure 3.27(b) compares the experimental results for the oval tunnel ($b = h\sqrt{2}$) with calculations based on Equations (3.216) and the approximate theory of Sanuki and Tani in Section III of Reference 3.35 for the particular open boundary.

The investigation of van Schliestett[3.8] is particularly interesting. Not only does he give a satisfactory confirmation of the theoretical interference parameters for an open square tunnel, but obtains experimental results that contradict the theory of

Reference 3.6 for a square jet with solid side-walls (type (4) in Section 3.2.2) and a square jet with one solid horizontal boundary. The double achievement of detecting two theoretical errors by experimental means and correcting both successfully deserves special mention. Other results for semi-closed tunnels are found in the experiments described by Tani and Taima in the second part of Reference 3.66 for a circular boundary having a symmetrical closed portion below the model. The related theory is discussed briefly in the fourth paragraph of Section 3.4.3; Kondo has applied his theory to the experiments of Reference 3.66 and obtains very consistent lift and drag curves in Figures 13(a) and 13(b) of Reference 3.14 for three sizes of model and five amounts of closed portion. For $\sigma = 0.5$ he confirms the elimination of lift interference when the lower 38.5% of the circle is closed.

In Reference 3.67, Silverstein and Katzoff describe tests on rectangular wings in a full-scale open circular tunnel and in a 1/15-scale model of the tunnel. The assumption that the free jet is of infinite length is shown to be adequate for the purpose of obtaining interference upwash at the lifting line. Traverses of downwash behind the wings have confirmed that it is essential to consider the finite length of the open tunnel in relation to interference corrections at a tail plane, and qualitative agreement is found with a theory of Weinig (Ref.3.68; 1936). The experiments in Reference 3.67 led presumably to the theoretical developments in Reference 3.5, discussed in Section 3.2.3 and illustrated in Figure 3.6.

Finally we consider tests on three equilateral delta wings ($A = 2.31$) by Jones and Miles[3.69] in a low-speed open circular tunnel, to which were applied the simple corrections in Equation (3.6) with $\delta_0 = -0.125$. For each of the span ratios $\sigma = s/R = 0.361$, 0.500 and 0.664 the interference corrections to incidence based on Equation (3.35) are now calculated from the formula

$$\Delta\alpha = (\delta_0)_E \left[1 + \frac{\lambda\bar{c}}{4\beta R}\frac{\delta_1}{\delta_0}\right]\frac{SC_L}{C} \tag{3.217}$$

with $\delta_1/\delta_0 = 1.594$ and $\lambda = 1.25$ interpolated from Table 3.III. The application of this correction in place of the first of Equations (3.6) increases the lift slope by the approximate factor

$$F = 1 - \frac{S}{C}\frac{\partial C_L}{\partial\alpha}\left[(\delta_0)_E\left(1 + 0.498\frac{\bar{c}}{R}\right) + 0.125\right] \tag{3.218}$$

which is calculated below with the experimental $\partial C_L/\partial\alpha = 2.66$.

Model	σ	S/C	$-(\delta_0)_E$	$\bar{c}/R$	F
A	0.361	0.072	0.1255	0.312	1.004
B	0.500	0.138	0.1267	0.453	1.011
C	0.664	0.243	0.1302	0.575	1.027

It is stated in Reference 3.69 that respective empirical factors 1.01 and 1.05 were applied to C_L on the models B and C to give consistent lift curves. Allowance for streamline curvature through the factor F is now seen to account for half the effect of these empirical factors. As regards drag, consideration is given to the remarks at the end of Section 3.6.1 and we examine the consequences of applying the correction in Equation (3.185),

$$\Delta C_D = C_L \Delta\alpha \ , \qquad (3.219)$$

at the higher values of C_L when there is flow separation along the whole leading edge. When this speculative correction is used in place of the second of Equations (3.6) for the largest model C, the solid circles are obtained in place of the open circles in Figure 3.28. The results for the three models are seen to be in acceptable agreement while C_L is fairly small, but the correction in Equation (3.219) reduces the scatter for $C_L > 0.4$. Unfortunately $R_H = 0.59 \times 10^6$ is the highest Reynolds number at which all three models were tested over the full range of C_L. The results in Figure 3.28 are far from conclusive, but they are included as a warning that the standard corrections to C_D are too small when leading-edge vortices are present.

3.8 INDEX OF FORMULAE AND DATA

The process of evaluating the interference velocity field depends primarily on the tunnel section, but the requirements are influenced greatly by the configuration of the model, by the aerodynamic quantities to be measured and above all by the accuracy of the experiments. When small inaccuracies can be tolerated, many of the simpler formulae for interference parameters are most useful. These are grouped according to tunnel section for various purposes in the first table below; although this includes reference to the numerical data in the present tables and figures, there are important additional sources listed in Table 3.IV. The second table concerns the more elaborate formulae that define more detailed calculations of the distribution of interference upwash for the three main types of tunnel. When the basic numerical data relating to these two tables are known, many useful approximate and more accurate formulae for the corrections to measured quantities are available without explicit reference to the type of tunnel. These and more special formulae are listed in the third table together with calculated results.

Each table gives the relevant equations and related tables and figures. For example the entries in the first table under rectangular tunnels for a small wing associate Equation (3.17) with Figure 3.2, Equation (3.20) with Table 3.II and also with Figure 3.2.

3.8.1 Simple or Approximate Interference Velocity

	Rectangular tunnels		*Octagonal tunnels*		*Elliptical and bipolar*	
	Eqn	T & F	Eqn	T & F	Eqn	T & F
Small wing	17	F2	28		29	F5
	20	T2	32		30	F5
	20	F2			31	F4
					31	F5
					136	
					137	
Lifting line	83	F11	107	F12	115	F13
	84	F9			117	F13
	156	T6			118	
					143	F15
Lifting surface	156	T6	109			
Slender wing	176				176	
	177				178	
Tail plane	191	F21	199			F6
	192		201			
	194					
Ground effect		F11	206			
	203	F22				
	203	F22				
	204					
	205					
Off-centre wing	25	F3	201		114	
	27	F3				
	200					

3.3.2 Elaborate or Accurate Interference Upwash

	Rectangular tunnels		*Octagonal tunnels*	*Circular and bipolar*		*Any*
	Eqn	**T & F**	**Eqn**	**Eqn**	**T & F**	**Eqn**
Lifting line	82		101	116		43
	88	T5	102	146		44
	91		103	167		48
			104	214	F25	
Lifting surface	87		108	138		42
	89	T5		139		47
	92					50
Complete model	95			124 to 126		51
	96					186
	93			127 to 131		189
	195					
	196			140		
	197			147		
				148		

3.8.3 Corrections to Measured Quantities

	$\Delta\alpha$		ΔC_m		ΔC_l		ΔC_D & ΔC_n	
	Eqn	T & F	Eqn	T & F	Eqn	T & F	Eqn	T & F
General and approximate	6		34		161		6	
	8		36				37	
	34		60				164	
	35		182	F20			166	
	182	F20	183				185	
	183		188					
General and more accurate	55		57		62		56	
	67		58		67		63	
	73		59		76		70	
	179	F20	67				71	
			179	F20			74	
							76	
Rectangular tunnels	85		155		170	F17	85	
	150	F16		F19			154	
	151	F17		T7				F17
		F18						
		T7						
Octagonal	110		112				111	
Circular	215	F27					168	
							215	F27
								F28
Bipolar	144	F15				F26		

There are also general formulae for ΔC_H in Equation (3.77) and $\Delta\alpha_t$ in Equation (3.198).

REFERENCES

3.1 Glauert, H. — *Wind Tunnel Interference on Wings, Bodies and Airscrews.* ARC R & M 1566, 1933.

3.2 Goldstein, S.
Young, A.D. — *The Linear Perturbation Theory of Compressible Flow, with Applications to Wind-Tunnel Interference.* ARC R & M 1909, 1943.

3.3 Göthert, B.H. — *Windkanalkorrekturen bei hohen Unterschallgeschwindigkeiten unter besonderer Berücksichtigung des geschlossenen Kreiskanals.* Deutsche Luftfahrtforschung Forschungsbericht 1216, 1940. (Translated as NACA Tech. Memo. 1300.)

3.4 Bryant, L.W.
Garner, H.C. — *Control Testing in Wind Tunnels.* ARC R & M 2881, 1950.

3.5 Katzoff, S. et al. — *Linear Theory of Boundary Effects in Open Wind Tunnels with Finite Jet Lengths.* NACA Report 976, 1950.

3.6 Theodorsen, T. — *The Theory of Wind-Tunnel Interference.* NACA Report 410, 1931.

3.7 Rosenhead, L. — *Interference Due to Walls of a Wind-Tunnel.* Proc. Roy. Soc., Series A, Vol.142, 1933, pp.308-320.

3.8 van Schliestett, G. — *Experimental Verification of Theodorsen's Theoretical Jet-Boundary Correction Factors.* NACA Tech. Note 506, 1934.

3.9 Garner, H.C. et al. — *An Anomaly in the Theory of Tunnel-Wall Interference on a Lifting Wing.* Aeron. Quart. Vol.14, 1963, pp.31-40.

3.10 Acum, W.E.A.
Garner, H.C. — *Approximate Wall Corrections for an Oscillating Swept Wing in a Wind Tunnel of Closed Circular Section.* ARC CP 184, 1954.

3.11 Batchelor, G.K. — *Interference in a Wind Tunnel of Octagonal Section.* Report ACA-1 (Australia), 1944.

3.12 Garner, H.C. — *Note on Interference in a Wind-Tunnel of Octagonal Section.* ARC Report 6659, 1943. (Unpublished).

3.13 Gent, B.L. — *Interference in a Wind Tunnel of Regular Octagonal Section.* Report ACA-2 (Australia), 1944.

3.14 Kondo, K. — *The Wall Interference of Wind Tunnels with Boundaries of Circular Arcs.* Aero. Res. Inst. (Tokyo) Report 126, 1935.

3.15 Garner, H.C. — *Some Remarks on Glauert's General Interference Theorem.* Aeron. Quart. Vol.14, 1963, pp.41-44.

3.16 Glauert, H. Hartshorn, A.S.	*The Interference of Wind Channel Walls on the Downwash Angle and the Tail-Setting to Trim.* ARC R & M 947, 1924.
3.17 Acum, W.E.A.	*Corrections for Symmetrical Swept and Tapered Wings in Rectangular Wind Tunnels.* ARC R & M 2777, 1950.
3.18 Garner, H.C. Acum, W.E.A.	*Interference Corrections for Asymmetrically Loaded Wings in Closed Rectangular Wind Tunnels.* ARC R & M 2948, 1953.
3.19 Eisenstadt, B.J.	*Boundary-Induced Upwash for Yawed and Swept-Back Wings in Closed Circular Wind Tunnels.* NACA Tech. Note 1265, 1947.
3.20 Katzoff, S. Hannah, M.E.	*Calculation of Tunnel-Induced Upwash Velocities for Swept and Yawed Wings.* NACA Tech. Note 1748, 1948.
3.21 Loos, H.G.	*Tunnelwall Interference for Aerofoils and Aerofoil-Fuselage Combinations in a Tunnel with an Octagonal Section for Incompressible Flow.* NLL (Netherlands) Report A 1024, 1951.
3.22 Swanson, R.S. Toll, T.A.	*Jet-Boundary Corrections for Reflection-Plane Models in Rectangular Wind Tunnels.* NACA Report 770, 1943.
3.23 Sanders, J. Pounder, J.R.	*Wall Interference in Wind Tunnels of Closed Rectangular Section.* NRC (Canada) Report AR-7, 1949.
3.24 Sanders, J. Pounder, J.R.	*Wall Interference in Wind Tunnels of Closed Rectangular Section. Development of Equations.* NRC (Canada) Report AR-11, 1951.
3.25 Swanson, R.S.	*Jet-Boundary Corrections to a Yawed Model in a Closed Rectangular Wind Tunnel.* NACA ARR (WR-L-603), 1943.
3.26 Sivells, J.C. Salmi, R.M.	*Jet-Boundary Corrections for Complete and Semispan Swept Wings in Closed Circular Wind Tunnels.* NACA Tech. Note 2454, 1951.
3.27 Swanson, R.S. Schuldenfrei, M.J.	*Jet-Boundary Corrections to the Downwash behind Powered Models in Rectangular Wind Tunnels with Numerical Values for 7- by 10- Foot Closed Wind Tunnels.* NACA ARR (WR-L-711), 1942.
3.28 Graham, D.J.	*Tunnel-Wall Corrections to Rolling and Yawing Moments Due to Aileron Deflection in Closed Rectangular Wind Tunnels.* NACA ARR 4F21 (WR-A-14), 1945.
3.29 Evans, J.M.	*Stability Derivatives. Wind Tunnel Interference on the Lateral Derivatives l_p, l_r, and l_v with Particular Reference to l_p.* Report ACA-33 (Australia), 1947.

3.30 Cowley, W.L.
McMillan, G.A.
Effect of Wind Tunnel Wall Interference on the Pitching Moments of Large Models in the Duplex Tunnel. ARC R & M 1639, 1934.

3.31 Olver, F.W.J.
Transformation of Certain Series Occurring in Aerodynamic Interference Calculations. Quart. J. Mech. appl. Math., Vol.2, 1949, pp.452-457.

3.32 Silverstein, A.
White, J.A.
Wind-Tunnel Interference with Particular Reference to Off-Centre Positions of the Wing and to the Downwash at the Tail. NACA Report 547, 1935.

3.33 Brown, W.S.
Wind Tunnel Corrections on Ground Effect. ARC R & M 1865, 1938.

3.34 Batchelor, G.K.
Interference on Wings, Bodies and Airscrews in a Closed Tunnel of Octagonal Section. Report ACA-5 (Australia), 1944.

3.35 Sanuki, M.
Tani, I.
The Wall Interference of a Wind Tunnel of Elliptic Cross Section. Proc. Phys. Math. Soc. Japan, Vol.14, 1932, pp.592-603.

3.36 Rosenhead, L.
The Aerofoil in a Wind Tunnel of Elliptic Section. Proc. Roy. Soc., Series A, Vol.140, 1933, pp.579-604.

3.37 Riegels, F.
Korrekturfaktoren für Windkanäle elliptischen Querschnitts mit teilweise offener und teilweise geschlossener Meßstrecke. Luftfahrtforschung, Vol.16, 1939, pp.26-30. (Translated as NACA Tech. Memo. 1310.)

3.38 Lotz, I.
Korrektur des Abwindes in Windkanälen mit kreisrunden oder elliptischen Querschnitten. Luftfahrtforschung, Vol.12, 1935, pp.250-264. (Translated as NACA Tech. Memo. 801.)

3.39 von Kármán, T.
Burgers, J.M.
General Aerodynamic Theory - Perfect Fluids. Airfoils and Airfoil Systems of Finite Span. "Aerodynamic Theory" (ed. W.F. Durand), Vol.II, Div. E, Chap.IV, Sect.42-44. Julius Springer, Berlin, 1935.

3.40 Gavin, J.G.
Hensel, R.W.
Elliptic Tunnel-Wall Corrections on Drag and Stall. J. aero. Sci., Vol.9, 1942, pp.533-537.

3.41 von Baranoff, A.
Zur Frage der Kanalkorrektur bei kompressibler Unterschallströmung. Jahrbuch der Deutschen Luftfahrtforschung, 1941, pp.I672-I677.

3.42 Vincenti, W.
Graham, D.
The Effect of Wall Interference upon the Aerodynamic Characteristics of an Airfoil Spanning a Closed-Throat Circular Wind-Tunnel. NACA Report 849, 1946.

3.43 van der Bliek, J.A. *Notes on Half Model Testing in Wind Tunnels.* AGARD Report 298, 1959. Canadian Aeronautical Journal, Vol.6, 1960, pp.59-68.

3.44 Polhamus, E.C. *Jet-Boundary-Induced-Upwash Velocities for Swept Reflection-Plane Models Mounted Vertically in 7- by 10- Foot, Closed, Rectangular Wind Tunnels.* NACA Tech. Note 1752, 1948.

3.45 Garner, H.C. *Note on the Interference on a Part-Wing Mounted Symmetrically on One Wall of a Wind Tunnel of Octagonal Section.* ARC CP 5, 1947.

3.46 Davison, B. Rosenhead, L. *Wind Tunnel Correction for a Circular Open Jet Tunnel with a Reflexion Plate.* Proc. Roy. Soc., Series A, Vol.177, 1941, pp.366-382.

3.47 Sivells, J.C. Deters, O.J. *Jet Boundary and Plan-Form Corrections for Partial-Span Models with Reflection Plate, End Plate or no End Plate in a Closed Circular Wind Tunnel.* NACA Report 843, 1946.

3.48 Gillis, C.L. et al. *Charts for Determining Jet-Boundary Corrections for Complete Models in 7- by 10- Foot Closed Rectangular Wind Tunnels.* NACA ARR L5G31 (WR-L-123), 1945.

3.49 Lyon, H.M. *An Approximate Method of Calculating the Effect of the Interference of a Closed Tunnel on Hinge Moments of Control Surfaces.* ARC Report 5803, 1942. (Unpublished).

3.50 Stewart, H.J. *A Correction to the Yawing Moment Due to Ailerons for Circular Wind Tunnels.* J. aero. Sci., Vol.6, 1939, pp.329-331.

3.51 Berndt, S.B. *Wind Tunnel Interference Due to Lift for Delta Wings of Small Aspect Ratio.* KTH (Sweden) Tech. Note Aero TN 19, 1950.

3.52 Tirumalesa, D. *Lift Interference for Low Aspect Ratio Wings in Transonic Wind Tunnels.* J. aero. Soc. India, Vol.11, 1959, pp.79-82.

3.53 Smith, C.B. *Wind-Tunnel Wall Corrections for Wing-Body Combinations.* J. aero. Sci., Vol.16, 1949, pp.237-242.

3.54 Gorgui, M.A. *Wind-Tunnel Interference for Wing-Body Combination.* J. aero. Sci., Vol.28, 1961, pp.823-825.

3.55 Sanders, J. *Wind Tunnel Corrections on Ground Effect Tests.* NRC (Canada) Report AR-5, 1948.

3.56 Albritton, J.P. Huber, P.J.A. *Wall Corrections for a Wing near a Ground Plate in a Circular Cross Section Wind Tunnel.* Wright Air Development Center Tech. Report 55-280, 1955.

3.57 Dannenberg, R.E. *Measurements of Section Characteristics of a 45° Swept Wing Spanning a Rectangular Low-Speed Wind Tunnel as Affected by the Tunnel Walls.* NACA Tech. Note 2160, 1950.

3.58 Bradfield, F.B. et al. *Measurement of Maximum Lift in Closed Tunnels of Different Sizes, and in an Open Jet Tunnel.* ARC R & M 1363, 1930.

3.59 Adamson, J.E. et al. *The Effect of Tunnel Size on Maximum Lift Coefficients.* ARC Report 5436, 1942. (Unpublished).

3.60 Stewart, H.J. *The Effect of Wind Tunnel Wall Interference on the Stalling Characteristics of Wings.* J. aero. Sci. Vol.8, 1941, pp.426-428.

3.61 Davis, D.D. Sweberg, H.H. *Investigation of Some Factors Affecting Comparisons of Wind-Tunnel and Flight Measurements of Maximum Lift Coefficients for a Fighter-Type Airplane.* NACA Tech. Note 1639, 1948.

3.62 Cowley, W.L. Jones, L.J. *An Experimental Test of the Prandtl Correction for Tunnel Wall Interference.* ARC R & M 898, 1924.

3.63 Higgins, G.J. *The Effect of the Walls in Closed Type Wind Tunnels.* NACA Report 275, 1927.

3.64 Theodorsen, T. Silverstein, A. *Experimental Verification of the Theory of Wind-Tunnel Boundary Interference.* NACA Report 478, 1934.

3.65 Knight, M. Harris, T.A. *Experimental Determination of Jet Boundary Corrections for Airfoil Tests in Four Open Wind Tunnel Jets of Different Shapes.* NACA Report 361, 1930.

3.66 Tani, I. Taima, M. *Two Notes on the Boundary Influence of Wind Tunnels of Circular Cross Section.* Aero. Res. Inst. (Tokyo) Report 121, 1935.

3.67 Silverstein, A. Katzoff, S. *Experimental Investigation of Wind-Tunnel Interference on the Downwash behind an Airfoil.* NACA Report 609, 1937.

3.68 Weinig, F. *Der Strahleinfluss bei offenen Windkanälen.* Luftfahrtforschung, Vol.13, 1936, pp.210-213.

3.69 Jones, R. Miles, C.J.W. *Tests on Three Equilateral Triangular Plates in the Compressed Air Tunnel.* ARC R & M 2518, 1945.

3.70 Taylor, C.R. *Private Communication.* 1966.

ADDITIONAL REFERENCES FOR CHAPTER III

Adamson, J.E. *An Experimental Investigation of Wind Tunnel Interference in the RAE 5 ft Open Jet Circular Tunnel.* ARC R & M 1897, 1941.

Bradfield, F.B. (editor) *Notes on the Technique Employed at the RAE in Low-Speed-Wind-Tunnel Tests in the Period 1939-1945.* ARC R & M 2556, 1947.

Garner, H.C. Halliday, A.S. *An Investigation of a Part-Wing Test on an Aileron and Methods of Computing Aileron Characteristics.* ARC Report 8922, 1945. (Unpublished).

Halliday, A.S. Cox, D.K. *Note on the Effect of Size and Position of End Plates on the Lift of a Rectangular Wing in a Wind Tunnel.* ARC CP 305, 1955.

Malavard, L. *Étude de Quelques Problèmes Techniques Relevant de la Théorie des Ailes. Application a Leur Solution de la Méthode Rhéoélectrique.* Chaps. IV and V. Publ. Sci. Tech. Min. Air France 153, 1939.

Muttray, H. *Über die Grösse der Berichtigungsbeiwerte für Widerstand und Anstellwinkel bei Freistrahlen von elliptischem Querschnitt.* Luftfahrtforschung, Vol.12, 1935, pp.265-266. (Translated as ARC Report 2492.)

Narayana, B.L. *Interference Effects in an Infinite Cascade of Wings of Finite Span.* J. Roy. aeron. Soc., Vol.66, pp.460-461, 1962.

Patraulea, N.N. Dumitrescu, L. *Influence of Walls on the Results of Tests on Annular Wings in Tunnels of Circular Cross-Section.* Stud. Cercet. Mec. apl. (Rumania), Vol.8, 1957, pp.703-710.

Recant, I.G. *Wind-Tunnel Investigation of Ground Effect on Wings with Flaps.* Appendix: *Tunnel-Wall Corrections for Test Installation Used.* NACA Tech. Note 705, 1939.

Silverstein, A. Katzoff, S. *Design Charts for Predicting Downwash Angles and Wake Characteristics behind Plain and Flapped Wings.* NACA Report 648, 1939.

TABLE 3.I

Equivalent Incompressible Flow from Equation (3.5) when $M = (1-\beta^2)^{\frac{1}{2}}$

Geometric Parameters	
Wing chord	c
Wing semi-span	βs
Wing area	βS
Aspect ratio	βA
Wing thickness	βt
Incidence	$\beta\alpha$
Aileron setting	$\beta\xi$
Tunnel breadth	βb
Tunnel height	βh
Tunnel area	$\beta^2 C$
Distance from floor	βd

The equivalent angle of sweepback is $\cot^{-1}(\beta\cot\Lambda)$.

Aerodynamic Parameters	
Stream density	ρ
Stream velocity	$\beta^{-2}U$
Velocity perturbations	$u,\ \beta^{-1}v,\ \beta^{-1}w$
Upwash angle	$\beta(\Delta\alpha)$
Circulation	Γ
Vortex strength	K
Pressure difference	$\beta^{-2}(p_u - p_l)$
Lift	$\beta^{-1}L$
Vortex-induced drag	D_v
Pitching moment	$\beta^{-1}\mathfrak{M}$
Rolling moment	$\mathfrak{L}$
Lift coefficient	$\beta^2 C_L$
Moment coefficients	$\beta^2 C_m, \beta^2 C_l$
Drag coefficient	$\beta^3 C_{Dv}$

TABLE 3.II

Function S_1 from Equation (3.18) for the Evaluation of Streamline Curvature in Rectangular Tunnels

$\frac{nh}{b}$	$-S_1\left(\frac{nh}{b}\right)$
0.25	94.1122
0.30	50.1543
0.35	28.8239
0.40	17.4569
0.45	10.9781
0.50	7.0976_5
0.55	4.6851
0.60	3.1419
0.65	2.1329
0.70	1.4618
0.75	1.0095
0.80	0.7014
0.85	0.4897_5
0.90	0.3433_5
0.95	0.2415
1.00	0.1704
1.05	0.1205
1.10	0.0854
1.15	0.0606
1.20	0.0431
1.25	0.0307
1.30	0.0219
1.35	0.0156
1.40	0.0111_5
1.45	0.0080
1.50	0.0057
1.55	0.0041
1.60	0.0029
1.65	0.0021
1.70	0.0015
1.75	0.0011
1.80	0.0008
1.85	0.0005_5
1.90	0.0004
1.95	0.0003
2.00	0.0002
2.05	0.0001_5
2.10	0.0001
2.15	0.0001
2.20	0.0000_5
2.25	0.0000_5
2.30	0.0000

TABLE 3.III

Values of λ and $\lambda x_1/\bar{c}$ from Lifting-Surface Theory and Strip Theory

βA	$c_r/\bar{c}$	$A \tan \Lambda_{0.5}$	λ		$\lambda x_1/\bar{c}$	
			L-S Th.	$\bar{\bar{c}}/\bar{c}$	L-S Th.	Eqn. (3.38)
0.624	1	0	1.48	1	0.54	0.12_5
1	1	0	1.33	1	0.42	0.12_5
2	1	0	1.16	1	0.28	0.12_5
4	1	0	1.06	1	0.20	0.12_5
2	1	2	1.04	1	0.33	0.29
4	1	4	0.84	1	0.57	0.79
0.66	1.44	0.88	1.37	1.06	0.49	0.17
1.32	1.44	0.88	1.26	1.06	0.39	0.17
1.98	1.44	0.88	1.20	1.06	0.33	0.17
2.64	1.44	0.88	1.16	1.06	0.29	0.17
0.66	1.44	2.2	1.12	1.06	0.44	0.33
1.32	1.44	2.2	1.11	1.06	0.42	0.33
1.98	1.44	2.2	1.10	1.06	0.39	0.33
2.64	1.44	2.2	1.08	1.06	0.37	0.33
0.667	1.44	3.567	0.95	1.06	0.57	0.64
1.334	1.44	3.567	0.95	1.06	0.55	0.64
2.001	1.44	3.567	0.96	1.06	0.54	0.64
2.668	1.44	3.567	0.96	1.06	0.53	0.64
1.352	1.58	0	1.30	1.11	0.40	0.15
2.598	1.58	0	1.20	1.11	0.30	0.15
4.329	1.58	0	1.12	1.11	0.24	0.15
1.2	1.75	1.5	1.22	1.19	0.44	0.25
1.8	1.75	1.5	1.20	1.19	0.40	0.25
3	1.75	1.5	1.17	1.19	0.35	0.25
0.654	2	2	1.31	1.33	0.59	0.33
1	2	2	1.28	1.33	0.56	0.33
1.5	2	2	1.26	1.33	0.52	0.33
4	2	2	1.22	1.33	0.42	0.33
1	Gothic wing		1.31	1.12		
1	Ogee wing		1.26	1.24		

TABLE 3.IV

Summary of Numerical Data on Interference Upwash for Large Wings

Tunnel	*Ref.*	*Table(s)*	*Fig(s)*	b/h	$(\delta_0)_U$	$(\delta_0)_g$	$\delta_0(y,t)$	$w_i(x,y,t)$
Rectangular closed	3.1	6	10	1,2	✓	✓		
	3.17	1 to 8	-	1,2			✓	✓
	3.17	9 to 16	-	9/7, 18/7			✓	✓
	3.18	4 to 7	-	2			✓	✓
	3.20	-	5,7	2/5, 10/7, 2				✓
	3.22	2	3,4	20/7			✓	✓
	3.23	-	3,4	0.91 to 2.63	✓	✓		
	3.27	-	3	10/7	✓			
	3.30	2*, 3, 9	1,2,3	2				$y=0$
	3.32	-	15, 21	1,2				$y=0$
	3.33	5,6	4, 5, 12, 13	2,4	✓	✓		
	3.44	-	4	7/5			✓	✓
Octagonal closed	3.11	4	10	9/7		✓		
	3.12	1,2	6,7	9/7, 13/9		✓		
	3.13	1,2	-	regular	✓	✓		
	3.45	4,5	-	9/7**			✓	
Elliptical closed	3.1	1	5	1	✓	✓		
	3.1	10	15	½ to 2		✓		
	3.14	Appendix	-	½ to 1	✓			
	3.19	4	3 to 7	1				✓
	3.26	1	2	1				✓
	3.35	1	-	$\sqrt{2}$, 2	✓			
	3.35	-	4	1 to 2	✓			
	3.36	2	2	$\frac{1}{3}$ to 3		✓		
	3.38	-	32 to 34	$\sqrt{2}$				✓
	3.39	15	-	1				$y=0$
	3.40	-	2	1.37			✓	
Elliptical open	3.1	11	16	½ to 2		✓		
	3.14	Appendix	-	½ to 1	✓			
	3.35	2	-	$\sqrt{2}$, 2	✓			
	3.35	-	5	1 to 2	✓			
	3.36	3	3	$\frac{1}{3}$ to 3		✓		
	3.38	-	22 to 24	$\sqrt{2}$				✓
	3.39	14	-	1				$y=0$
Bipolar closed	3.14	1	4	1 to 5/3	✓			
	3.26	-	5	1.50				✓
	3.47	1,2	2,3	1.50, 1.73			✓	
Bipolar open	3.14	2	6	1 to 5/3	✓			
	3.46	2,3	3,4	1 to 2	✓	✓		
Semi-closed								
circular	3.14	3	10	1	✓			
arch-shaped	3.14	7	16	<1	✓			
elliptical	3.37	-	6,7	$\sqrt{2}$	✓			

* corrected in Table 7 of Reference 3.33

** half model

TABLE 3.V

Interference Parameters for a Closed Square Tunnel

(a) Values of $\frac{\partial}{\partial t}\{t\delta_0(y,t)\}$

2t/b \ 2y/b	0	0.1	0.2	0.3	0.4	0.5	0.6	0.7	0.8
0	0.1368	0.1371	0.1383	0.1404	0.1437	0.1488	0.1561	0.1664	0.1807
0.1	0.1371	0.1375	0.1387	0.1410	0.1446	0.1499	0.1576	0.1684	0.1835
0.2	0.1383	0.1387	0.1402	0.1429	0.1472	0.1534	0.1622	0.1746	0.1919
0.3	0.1404	0.1410	0.1429	0.1464	0.1518	0.1595	0.1704	0.1857	0.2071
0.4	0.1437	0.1446	0.1472	0.1518	0.1588	0.1688	0.1830	0.2029	0.2313
0.5	0.1488	0.1499	0.1534	0.1595	0.1688	0.1822	0.2013	0.2286	0.2687
0.6	0.1561	0.1576	0.1622	0.1704	0.1830	0.2013	0.2278	0.2671	0.3276
0.7	0.1664	0.1684	0.1746	0.1857	0.2029	0.2286	0.2671	0.3269	0.4259
0.8	0.1807	0.1835	0.1919	0.2071	0.2313	0.2687	0.3276	0.4259	0.6065

(b) Values of $\frac{\partial}{\partial t}\{t\delta_1(y,t)\}$

2t/b \ 2y/b	0	0.1	0.2	0.3	0.4	0.5	0.6	0.7	0.8
0	0.2401	0.2407	0.2428	0.2462	0.2525	0.2627	0.2785	0.3024	0.3379
0.1	0.2407	0.2413	0.2435	0.2476	0.2545	0.2655	0.2826	0.3082	0.3464
0.2	0.2426	0.2435	0.2463	0.2517	0.2605	0.2743	0.2952	0.3266	0.3737
0.3	0.2462	0.2476	0.2517	0.2593	0.2715	0.2902	0.3183	0.3607	0.4253
0.4	0.2525	0.2545	0.2605	0.2715	0.2890	0.3156	0.3557	0.4171	0.5140
0.5	0.2627	0.2655	0.2743	0.2902	0.3156	0.3544	0.4143	0.5090	0.6659
0.6	0.2785	0.2826	0.2952	0.3183	0.3557	0.4143	0.5077	0.6631	0.9394
0.7	0.3024	0.3082	0.3266	0.3607	0.4171	0.5090	0.6631	0.9381	1.4778
0.8	0.3379	0.3464	0.3737	0.4253	0.5140	0.6659	0.9394	1.4778	2.6943

TABLE 3.VI

Interference Parameters ζ_0 and ζ_1 for Closed Rectangular Tunnels

(a) $y \to 0$, $t \to 0$. *Equations (3.157)*

$\frac{b}{h}$	ζ_0	ζ_1	$\frac{b^2\zeta_0}{h^2}$	$\frac{b\zeta_1}{h\zeta_0}$
0.8	14.746	108.34	9.44	5.88
1.0	9.028	56.24	9.03	6.23
1.3	5.688	33.42	9.61	7.64
1.6	4.426	26.73	11.33	9.66
2.0	3.847	24.16	15.39	12.56

(b) $y = t = \frac{1}{2}b$. *Equations (3.160)*

$\frac{b}{h}$	ζ_0	ζ_1	$\frac{b^2\zeta_0}{h^2}$	$\frac{b\zeta_1}{h\zeta_0}$
0.8	19.389	180.98	12.41	7.47
1.0	10.186	74.58	10.19	7.32
1.3	5.059	30.55	8.55	7.85
1.6	2.934	16.49	7.51	8.99
2.0	1.637	9.07	6.55	11.08

TABLE 3.VII

Comparative Calculations of $\Delta\alpha/C_L$ and $\Delta C_m/C_L$ for Wings in Closed Rectangular Tunnels

Case	$\frac{b}{h}$	σ	Wing			M	$\frac{\partial C_L}{\partial\alpha}$	$\frac{\bar{c}}{\beta h}$	$\frac{S}{C}$
			A	$c_r/\bar{c}$	$A \tan \Lambda_{0.5}$				
1	0.911	0.500	2.00	1.00	0	0.8	2.83	0.379	0.1138
2	0.911	0.714	4.00	1.00	0	0.8	4.62	0.271	0.1162
3	0.911	0.684	4.33	1.58	0	0.6	4.33	0.180	0.0983
4	0.911	0.684	4.33	1.58	0	0.8	4.95	0.240	0.0983
5	1	0.450	1.50	2.00	2.00	0	1.83	0.300	0.1350
6	1	0.450	1.50	2.00	2.00	0.8	2.02	0.500	0.1350
7	1.286	0.611	2.64	1.44	2.20	0	2.80	0.298	0.1819
8	2	0.393	2.64	1.44	2.20	0	2.80	0.298	0.1170
9	2	0.589	2.64	1.44	2.20	0	2.80	0.446	0.2631
10	18/7	0.473	2.64	1.44	2.20	0	2.80	0.460	0.2175
11	16/7	0.361	3.00	1.75	1.50	0.8	3.70	0.479	0.1036

Case	$\Delta\alpha/C_L$				$\Delta C_m/C_L$			
	$\sigma \to 0$ Eqn. (3.35)	Ref. 3.17 Fig. 3.16	Ref. 3.26 Eqn. (3.55)	L-S Th. Eqn. (3.67)	$\sigma \to 0$ Eqn. (3.36)	Eqn. (3.169)	Ref. 3.26 Eqn. (3.57)	L-S Th. Eqn. (3.87)
1	0.0238	0.0240	0.0253	0.0253	0.0058	0.0064	0.0078	0.0063
2	0.0216	0.0249	0.0259	0.0257	0.0048	0.0062	0.0068	0.0072
3	0.0171	0.0184	0.0193	0.0194	0.0026	0.0038	0.0035	0.0037
4	0.0181	0.0202	0.0203	0.0205	0.0045	0.0063	0.0061	0.0056
5	0.0246	0 0244	0.0241	0.0255	0.0047	0.0051	0.0056	0.0054
6	0.0289	-	0.0274	0.0298	0.0093	0.0100	0.0111	0.0098
7	0.0285	0.0283	-	0.0283	0.0063	-	-	0.0065
8	0.0215	0.0176	0.0176	0.0179	0.0052	0.0027	0.0034	0.0036
9	0.0546	0.0388	0.0386	0.0397	0.0177	0.0072	0.0098	0.0103
10	0.0569	0.0372	0.0366	0.0376	0.0188	0.0052	0.0090	0.0076
11	0.0286	0.0212	0.0224	0.0238	0.0136	0.0073	0.0120	0.0100

(a) Closed circular tunnel

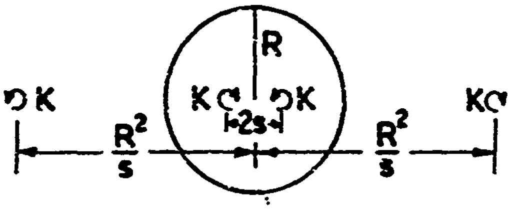
R
K
K
K
K
K
2s
R²/s
R²/s

(b) Closed rectangular tunnel

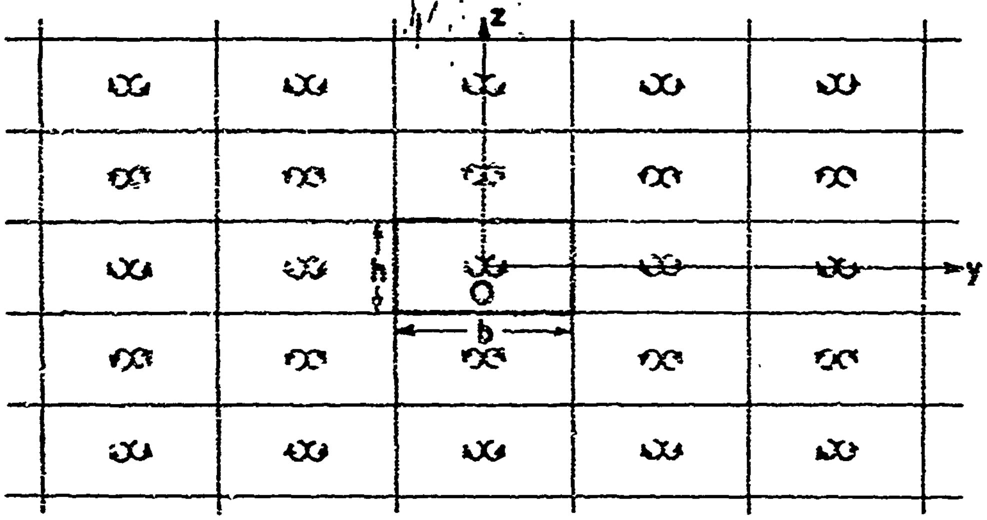

(c) Corner fillets (Ref. 3.11)

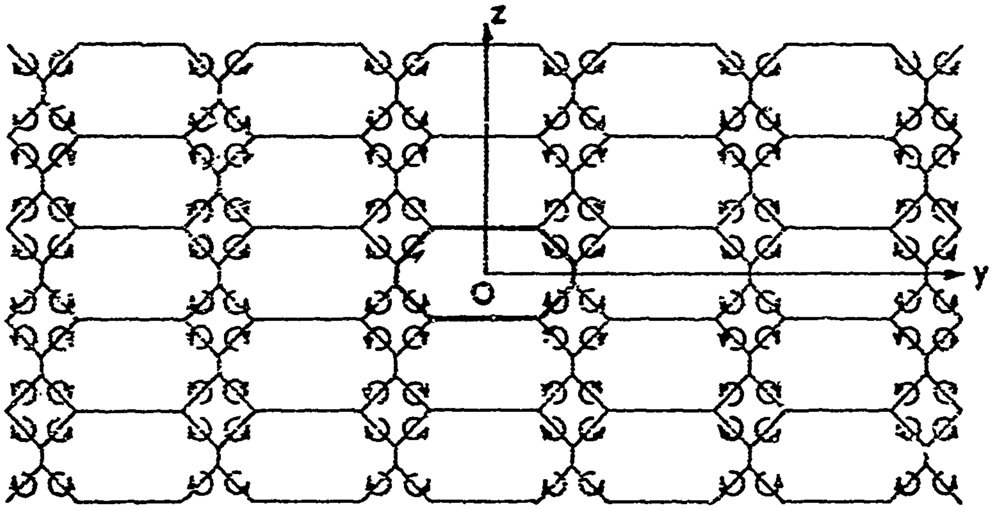

Fig. 3.1 Typical image systems

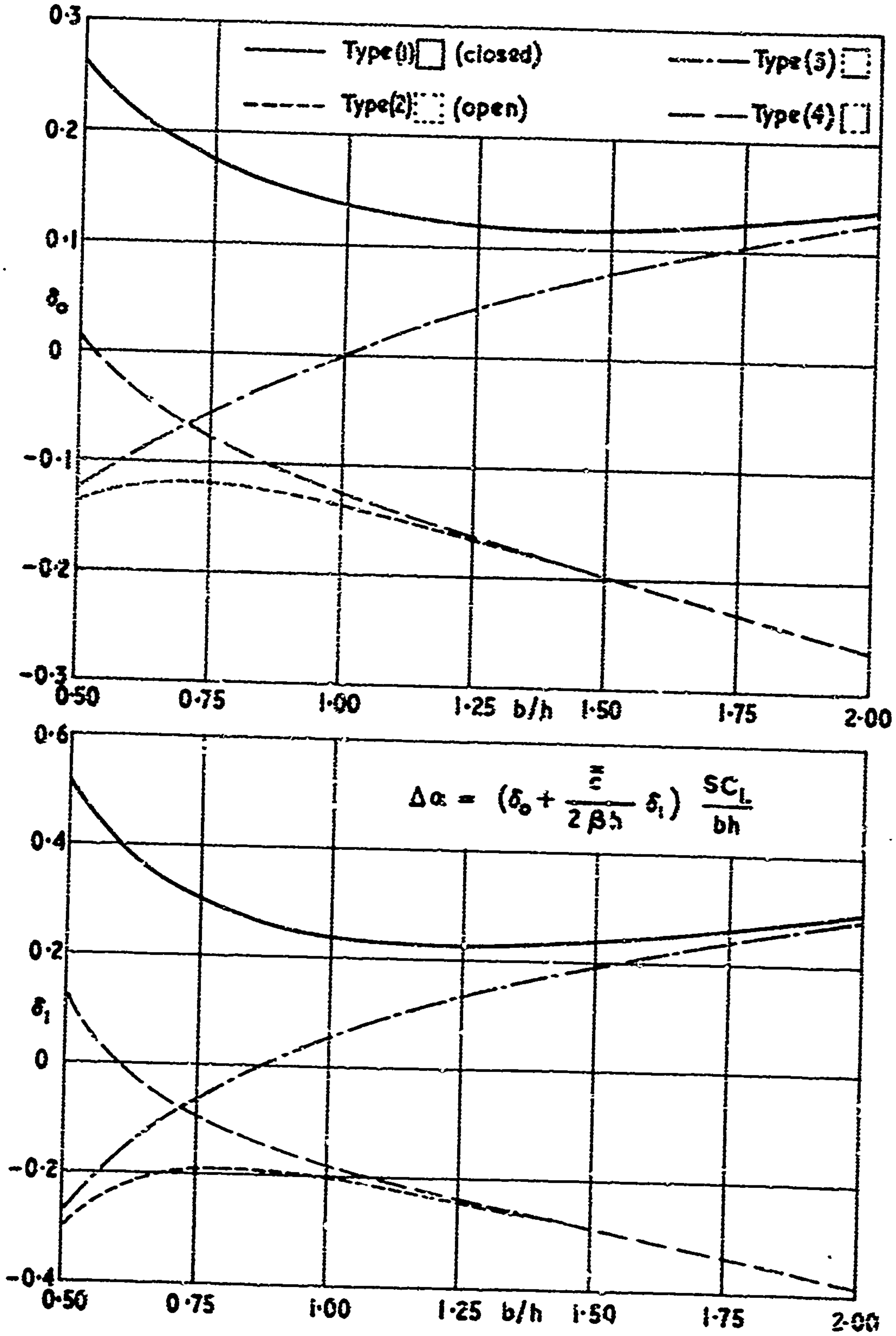

Fig. 3.2 Lift interference on small wings in rectangular tunnels

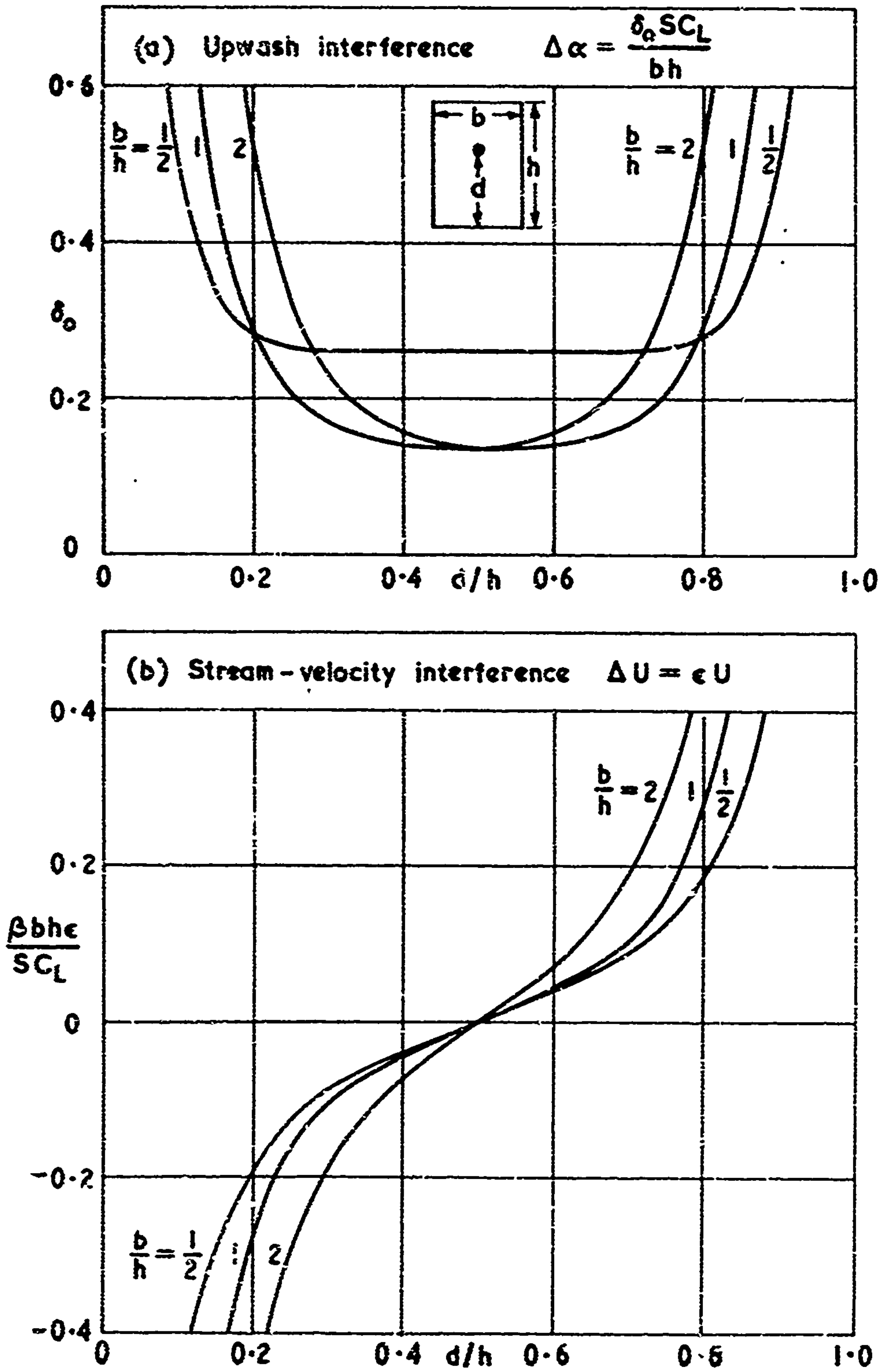

Fig. 3.3 Upwash and stream-velocity interference on a small lifting wing displaced vertically from the centre of a closed rectangular tunnel

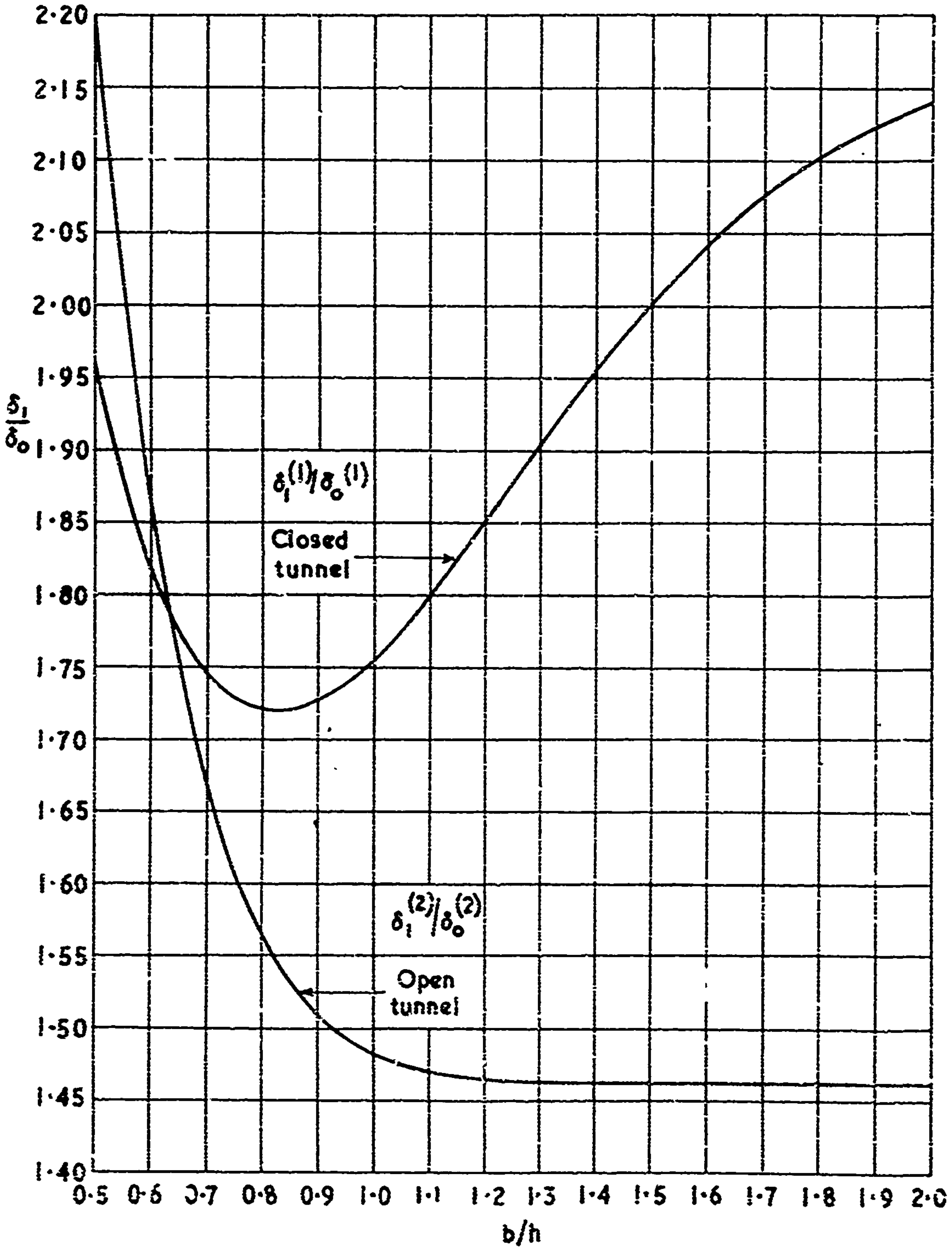

Fig. 3.4 Ratios δ_1/δ_0 for small models in closed and open rectangular tunnels

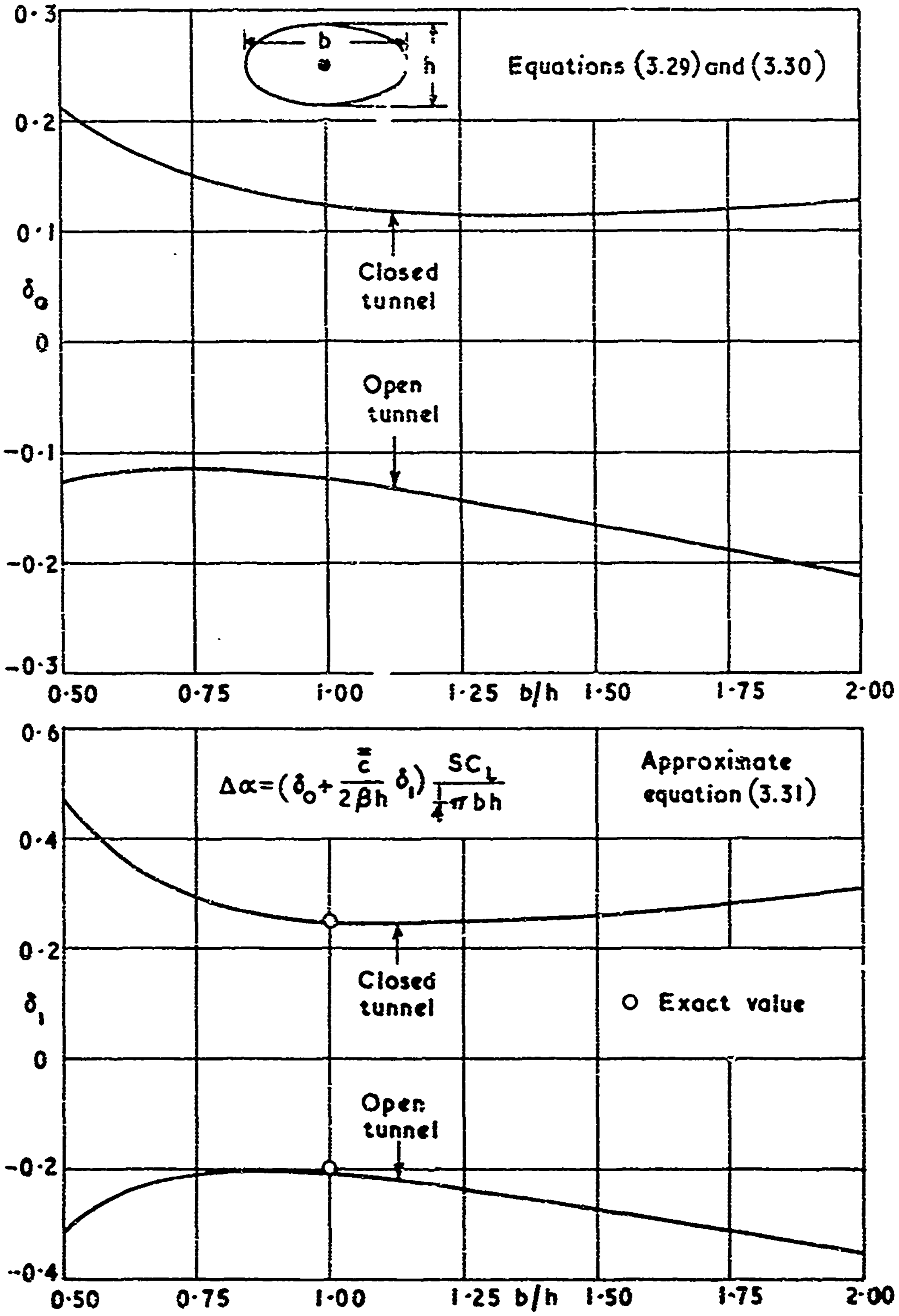

Fig. 3.5 Lift interference on small wings in elliptical tunnels

FIG. 3.6

Reproduced from Fig. 24 of Ref. 3.5

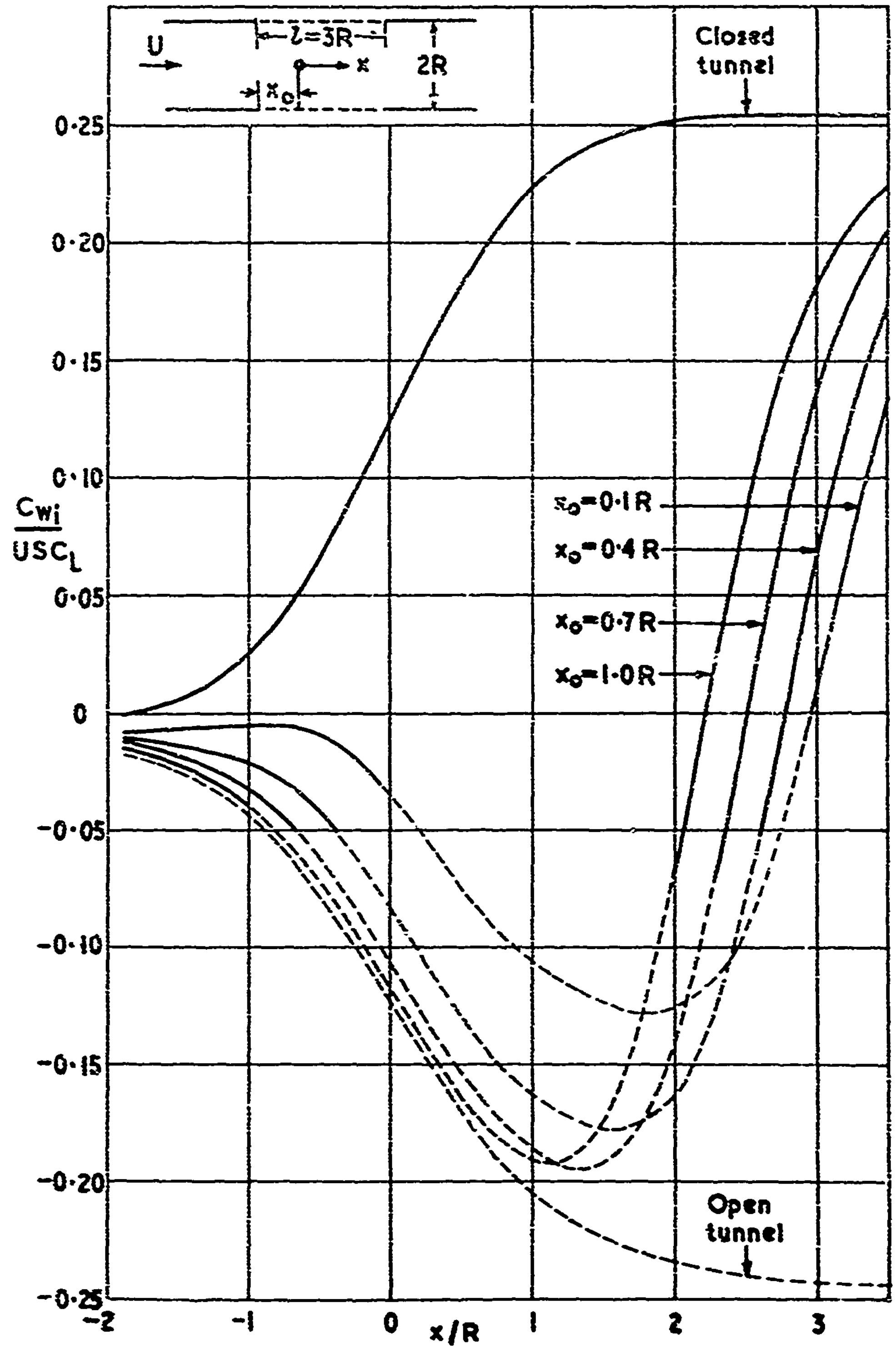

Fig. 3.6 Axial distributions of interference upwash for several positions of a small lifting wing in a closed-open-closed circular tunnel

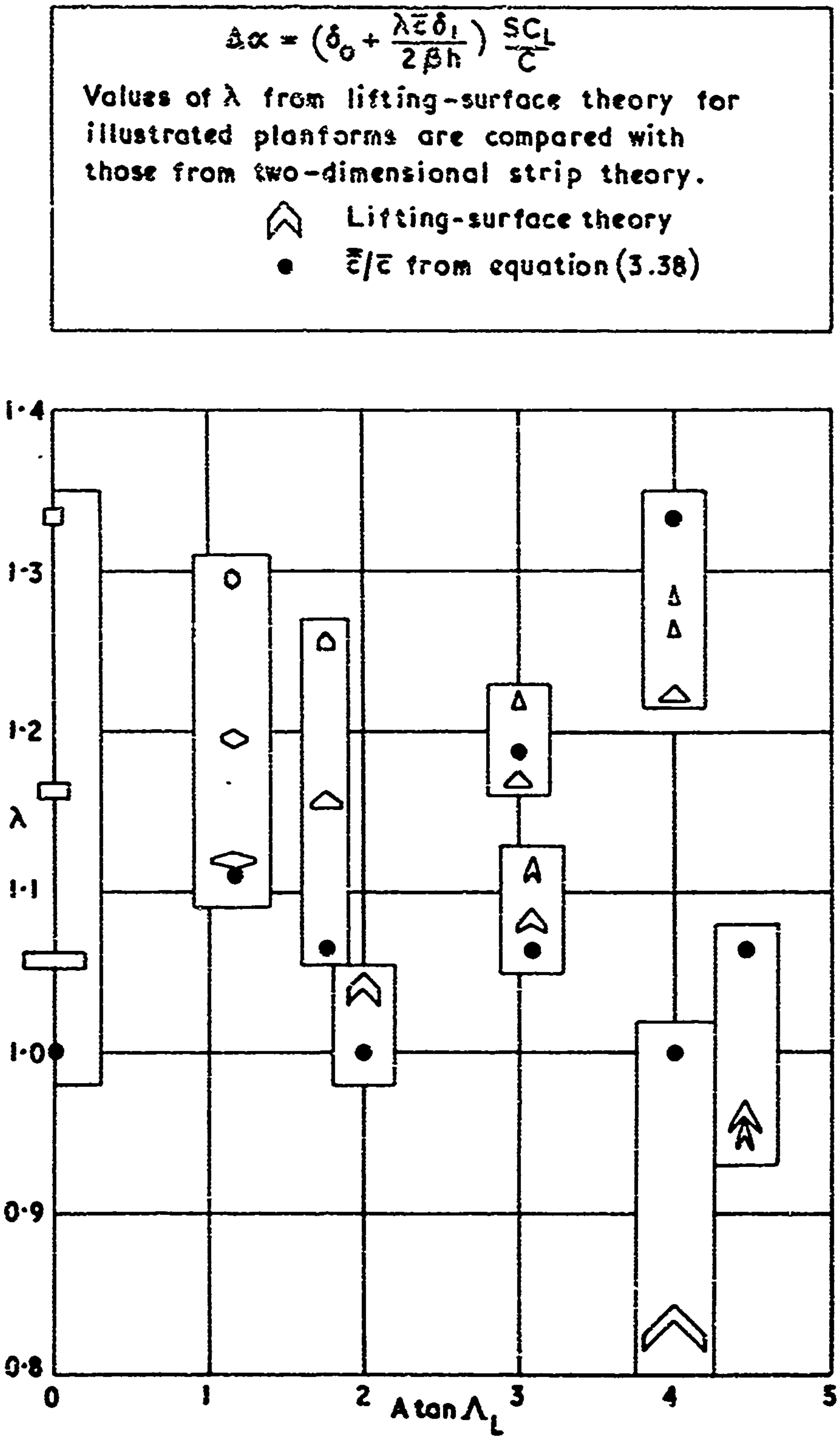

$$\Delta\alpha = \left(\delta_0 + \frac{\lambda\bar{\bar{c}}\delta_1}{2\beta h}\right)\frac{SC_L}{C}$$

Values of λ from lifting-surface theory for illustrated planforms are compared with those from two-dimensional strip theory.

Lifting-surface theory

● $\bar{\bar{c}}/\bar{c}$ from equation (3.38)

Fig.3.7 Lift-interference correction to measured incidence of small models of various planforms

FIG. 3.8

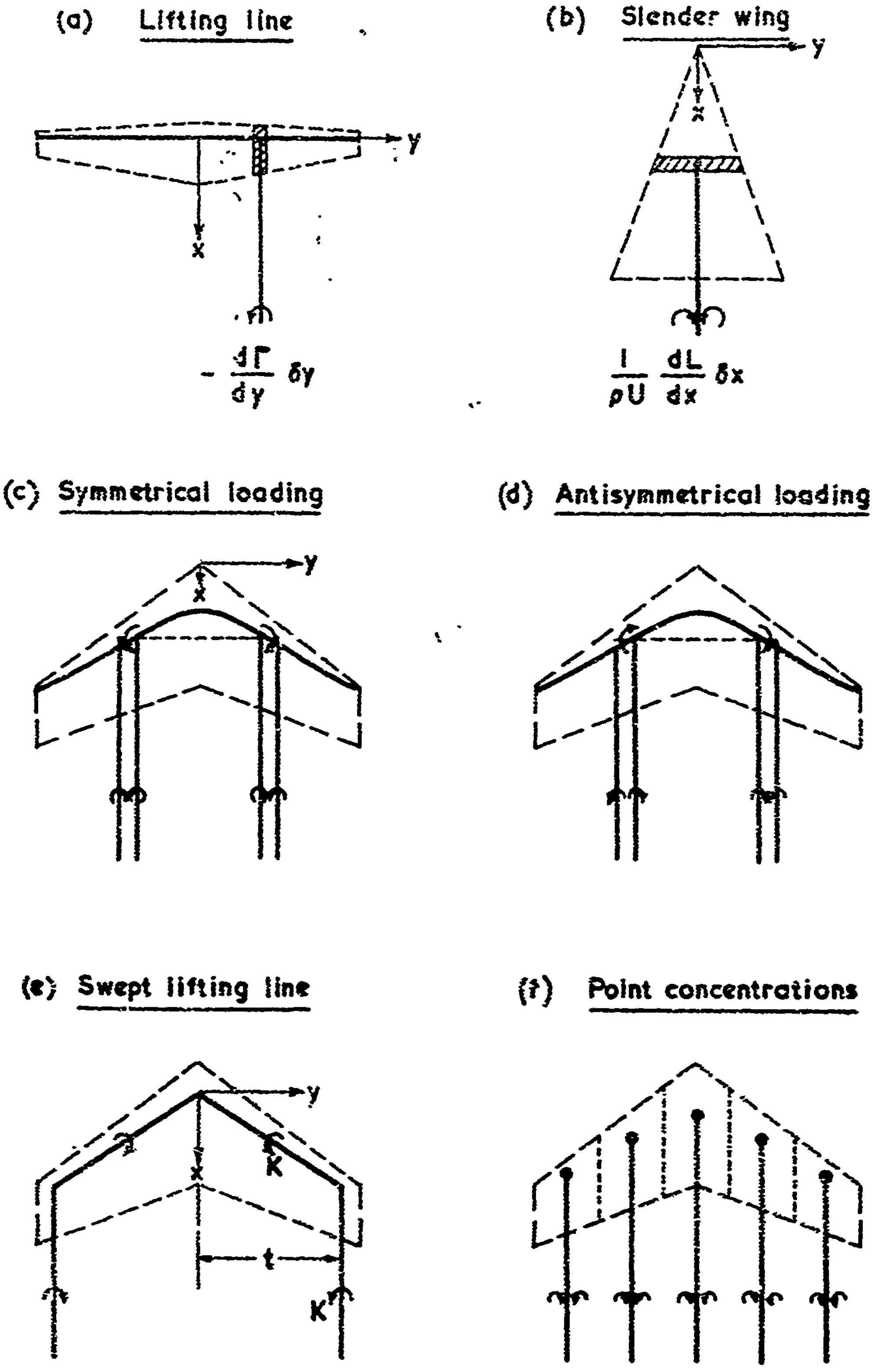

(a) Lifting line

(b) Slender wing

(c) Symmetrical loading

(d) Antisymmetrical loading

(e) Swept lifting line

(f) Point concentrations

y
x
$-\frac{d\Gamma}{dy}\delta y$
y
x
$\frac{1}{\rho U}\frac{dL}{dx}\delta x$
y
x
y
x
K
t
K'

Fig.3.8 Different vortex models of lifting wings

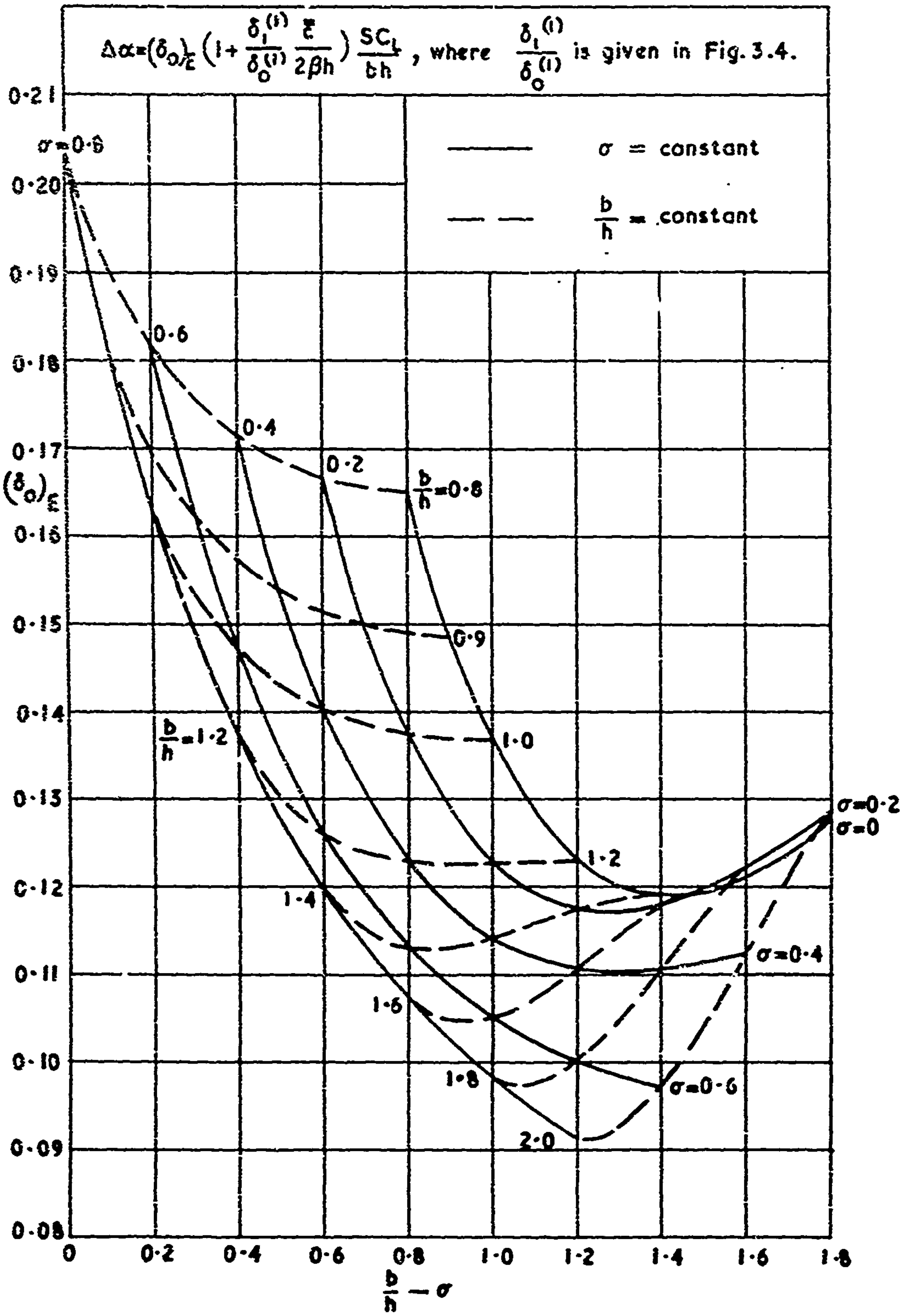

Fig. 3.9 Lift interference on wings with elliptic spanwise loading in closed rectangular tunnels

Based on Fig.6 of Ref.3.20

(a) Closed rectangular tunnel

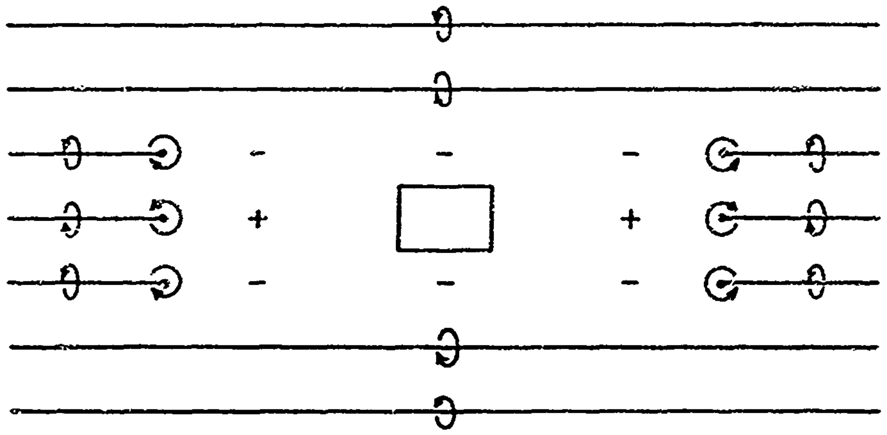

(b) Closed sides, open floor and roof. Correct

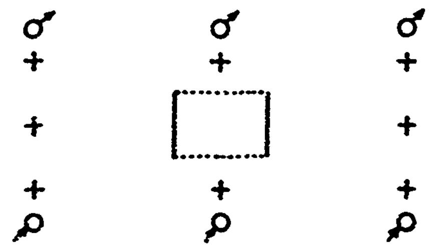

(c) Closed sides, open floor and roof. Incorrect

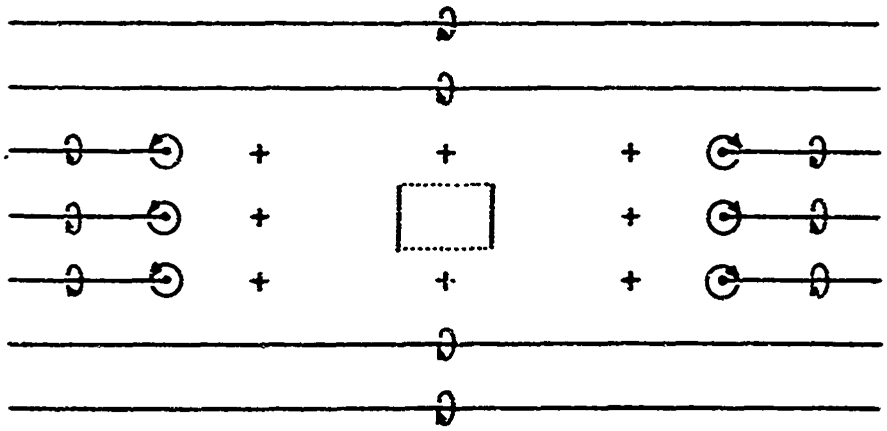

Fig.3.10 Approximate representations of doubly infinite arrays of doublets to evaluate W_A for rectangular tunnels

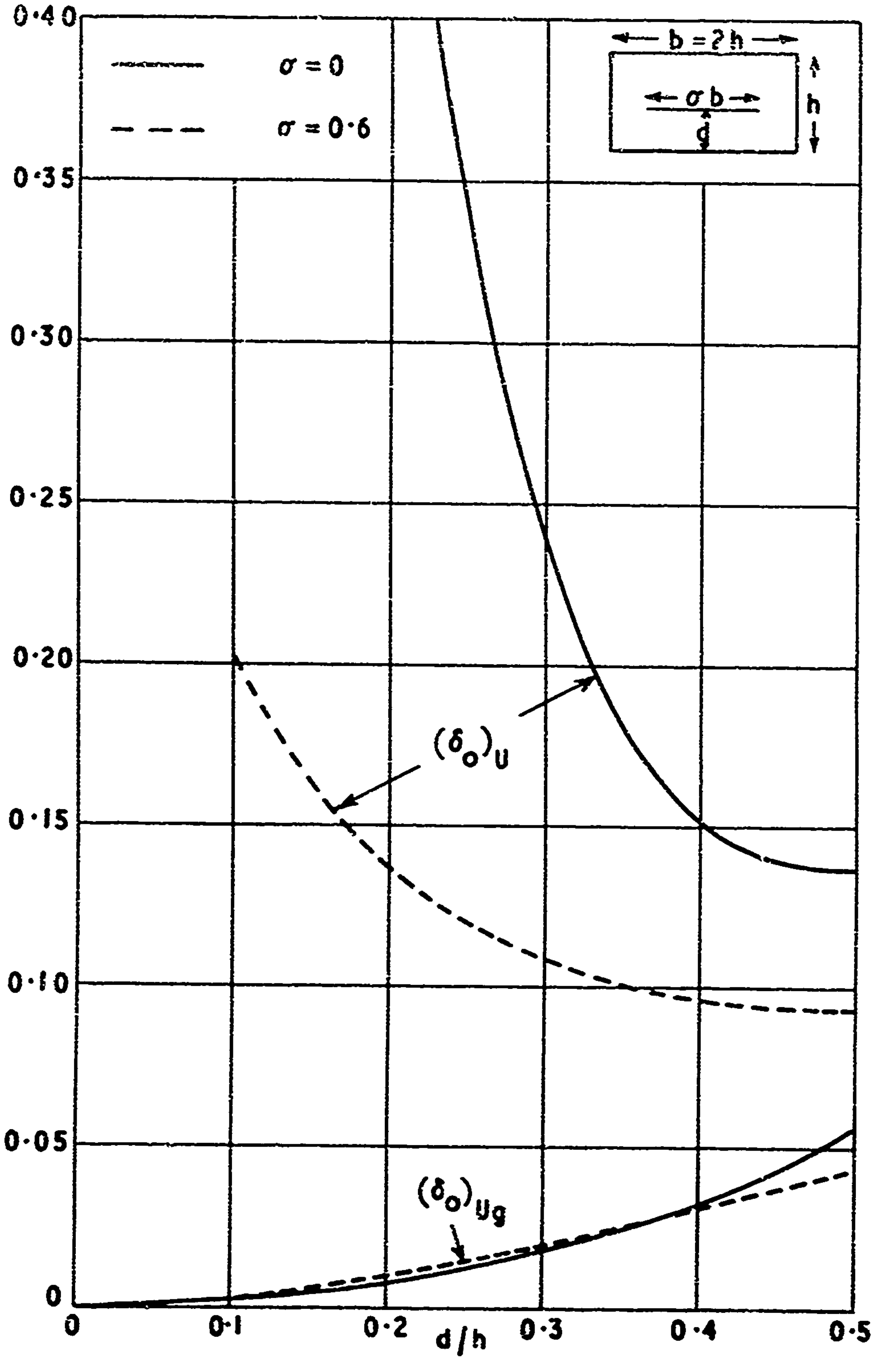

Fig. 3.11 Lift interference on off-centre models in a closed duplex tunnel with and without ground simulation

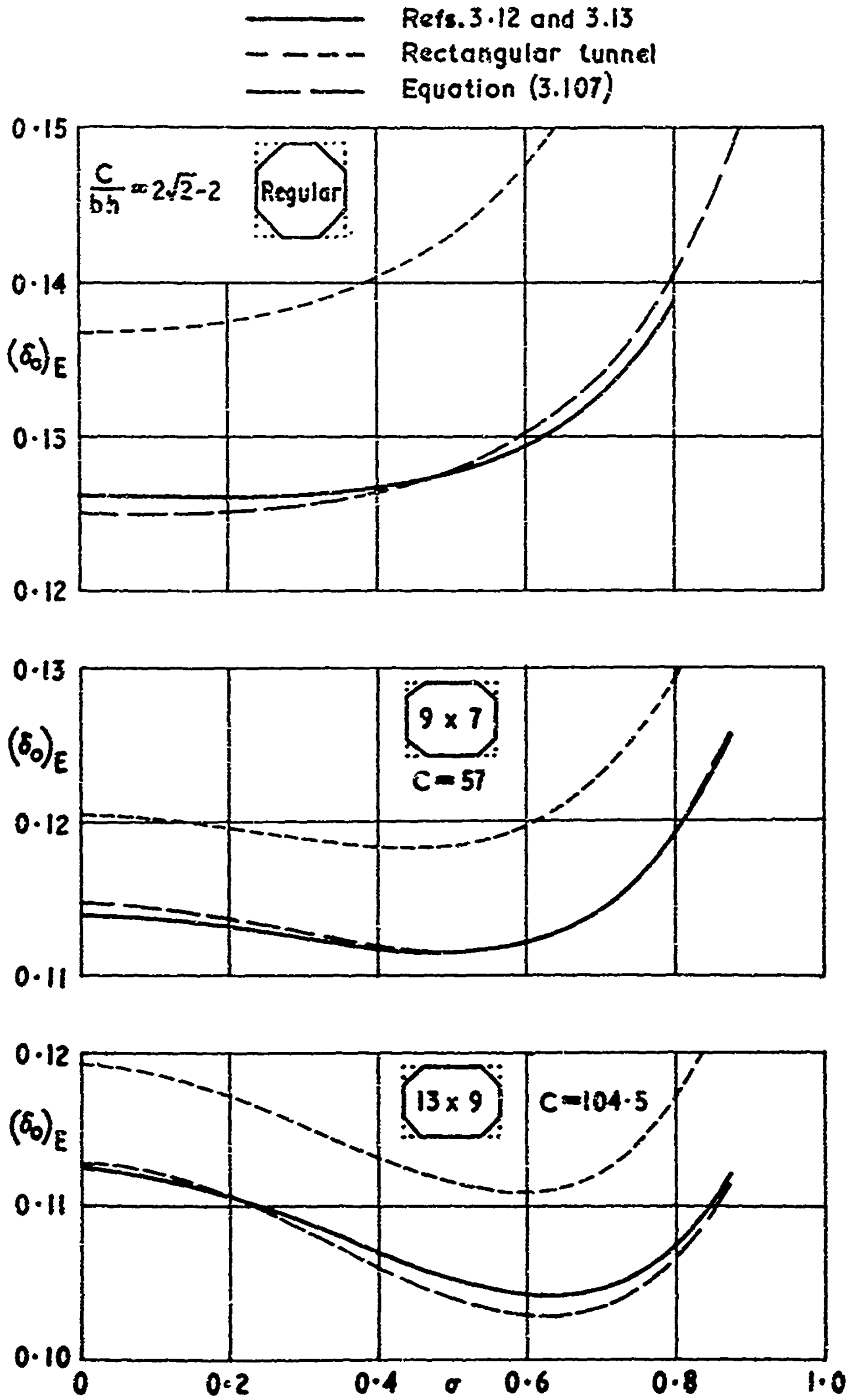

Fig. 3.12 Lift interference on wings with elliptic spanwise loading in closed octagonal tunnels

Reproduced from Tables 10 and 11 of Ref. 3·1

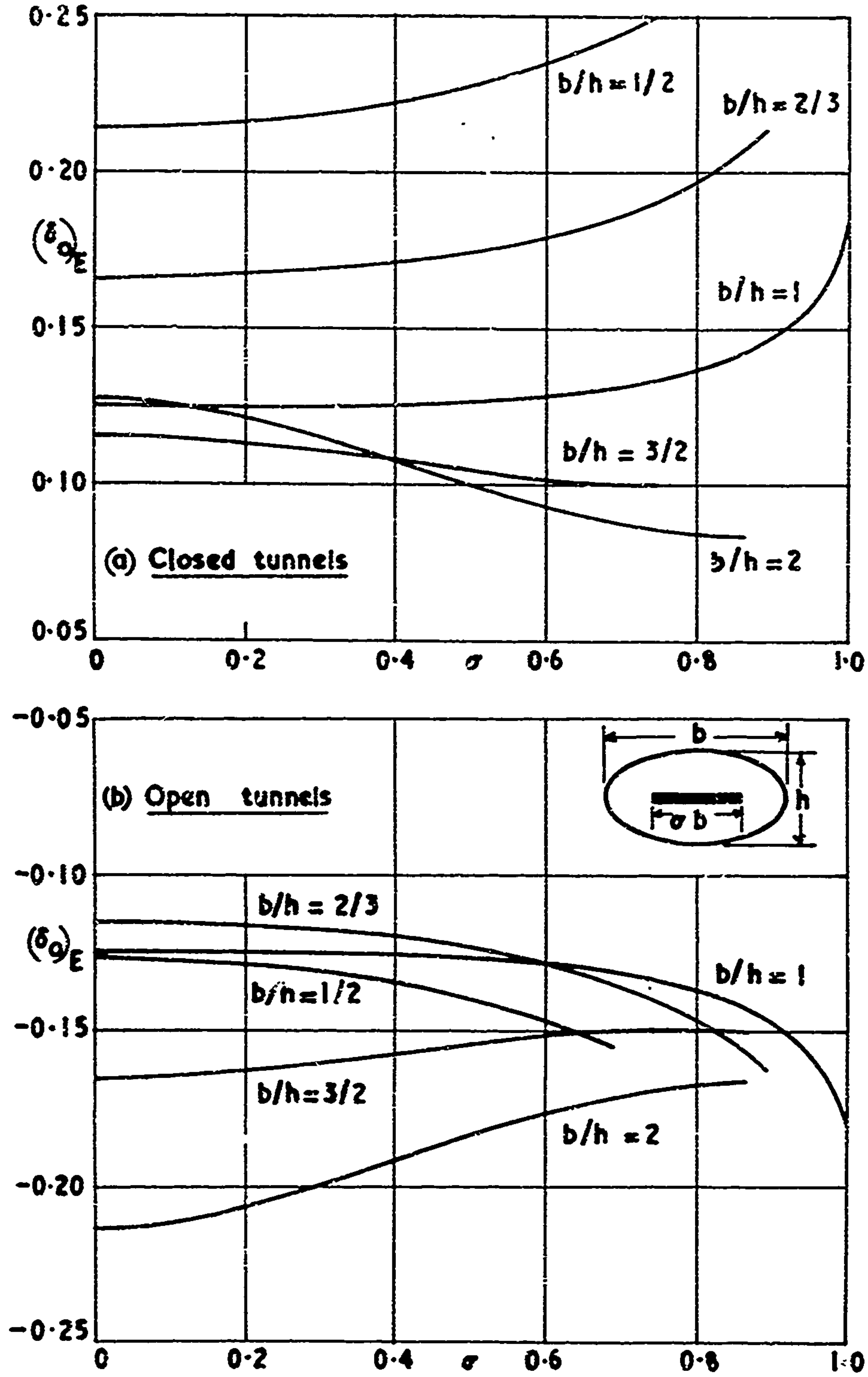

Fig. 3.13 Interference parameter for elliptically loaded wings in elliptical tunnels

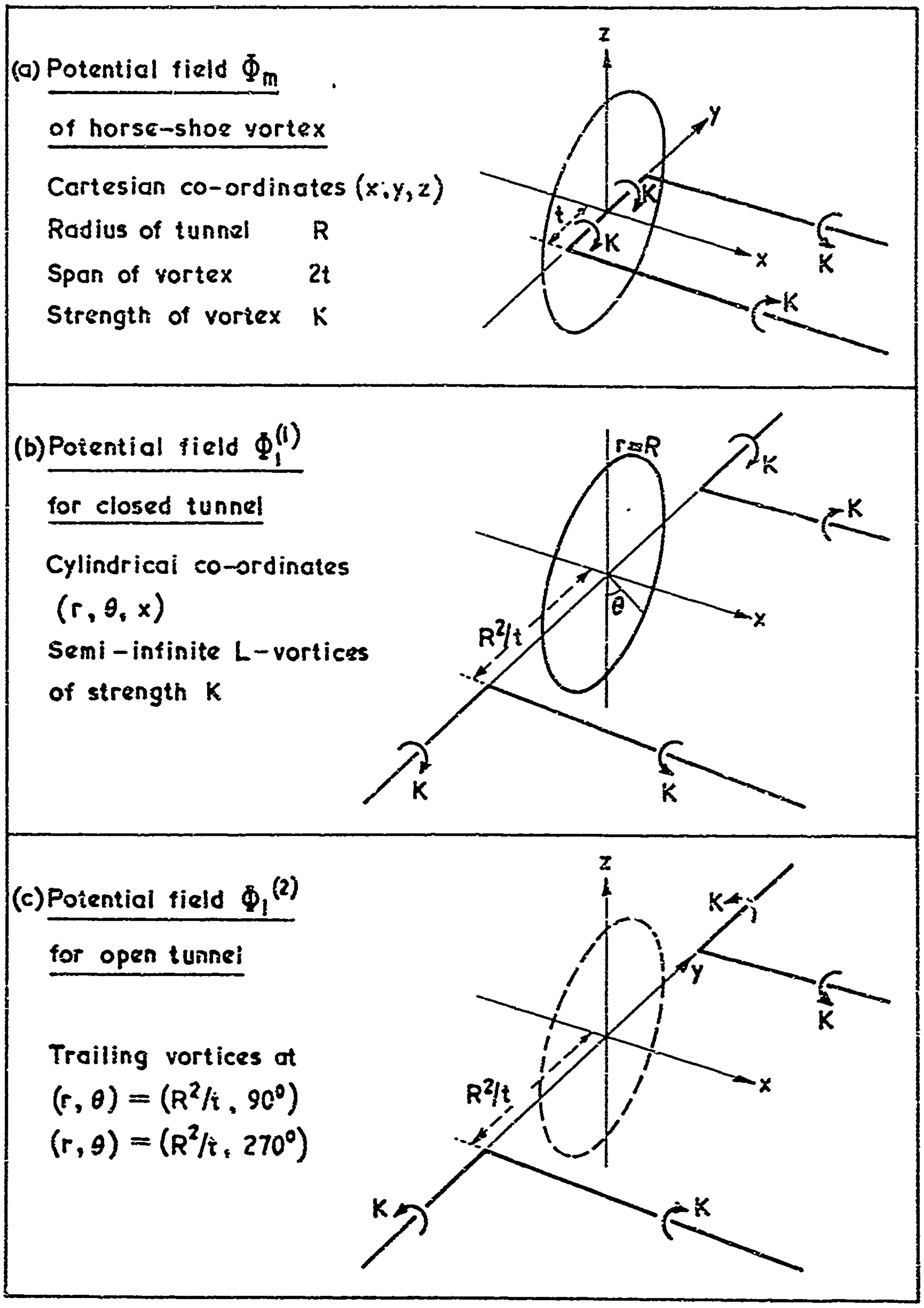
(a) Potential field Φ_m
of horse-shoe vortex
Cartesian co-ordinates (x,y,z)
Radius of tunnel R
Span of vortex 2t
Strength of vortex K
z
y
x
t
K
K
K
K
(b) Potential field $\Phi_1^{(1)}$
for closed tunnel
Cylindrical co-ordinates
(r, θ, x)
Semi-infinite L-vortices
of strength K
r=R
θ
x
R^2/t
K
K
K
K
(c) Potential field $\Phi_1^{(2)}$
for open tunnel
Trailing vortices at
$(r, \theta) = (R^2/t, 90^\circ)$
$(r, \theta) = (R^2/t, 270^\circ)$
z
y
x
R^2/t
K
K
K
K

Fig. 3.14 Vortex configurations defining Φ_m, $\Phi_1^{(1)}$ and $\Phi_1^{(2)}$ for circular tunnels

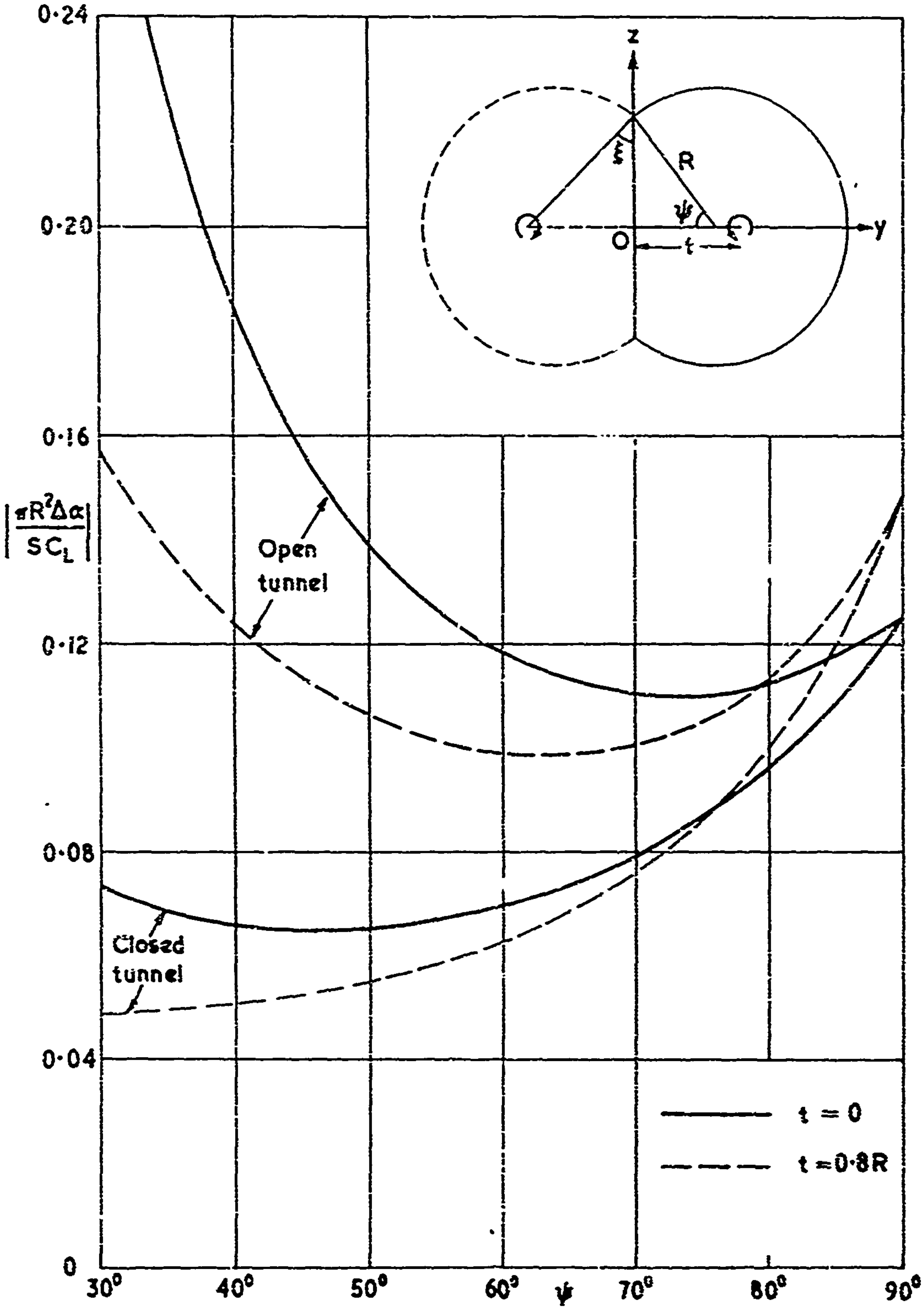

Fig. 3.15 Lift interference on uniformly loaded half-wings in closed and open circular tunnels with variable reflection planes

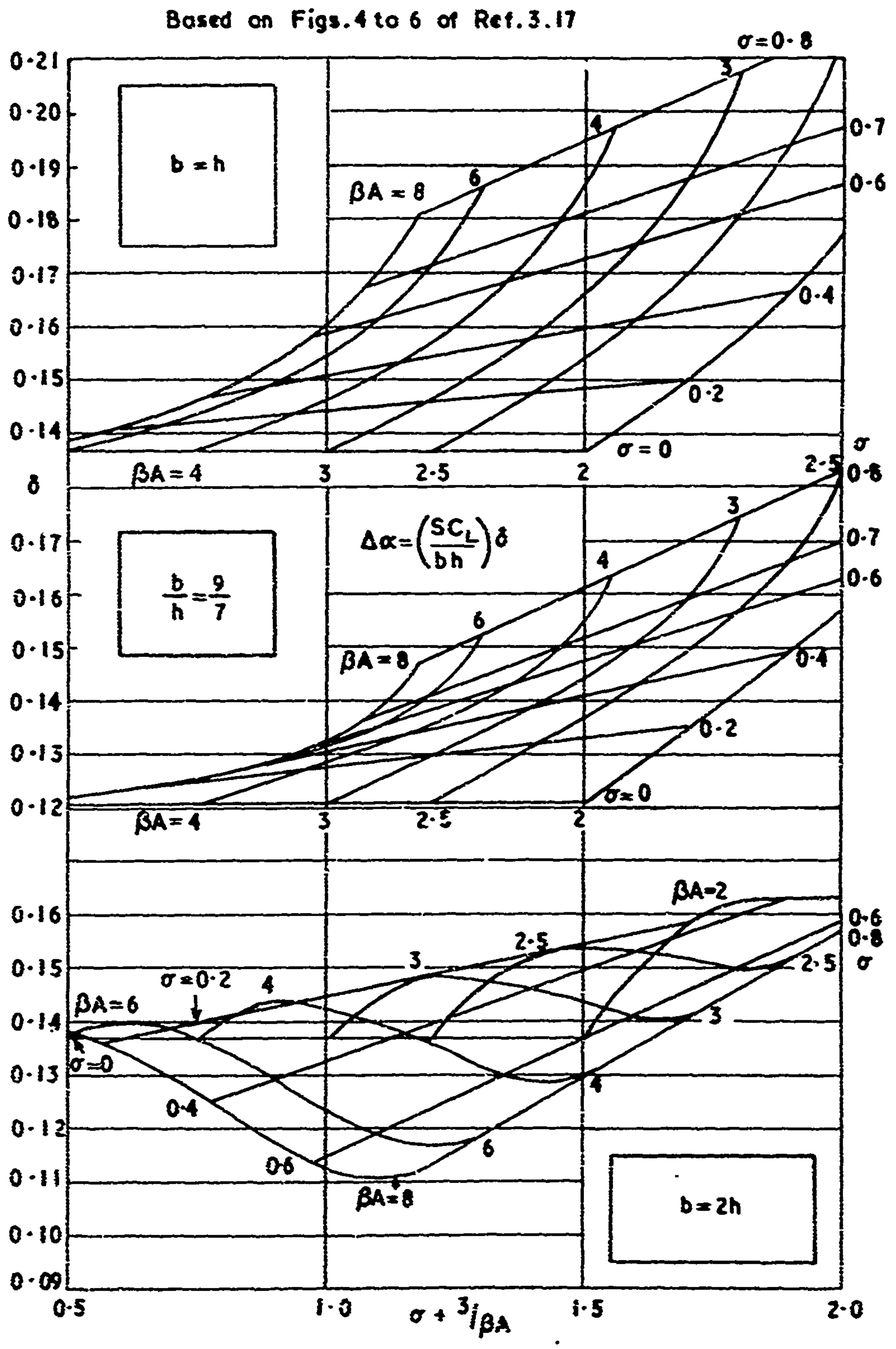

Fig.3.16 Approximate interference corrections to incidence for wings of various spans and aspect ratios in three closed rectangular tunnels (M = 0)

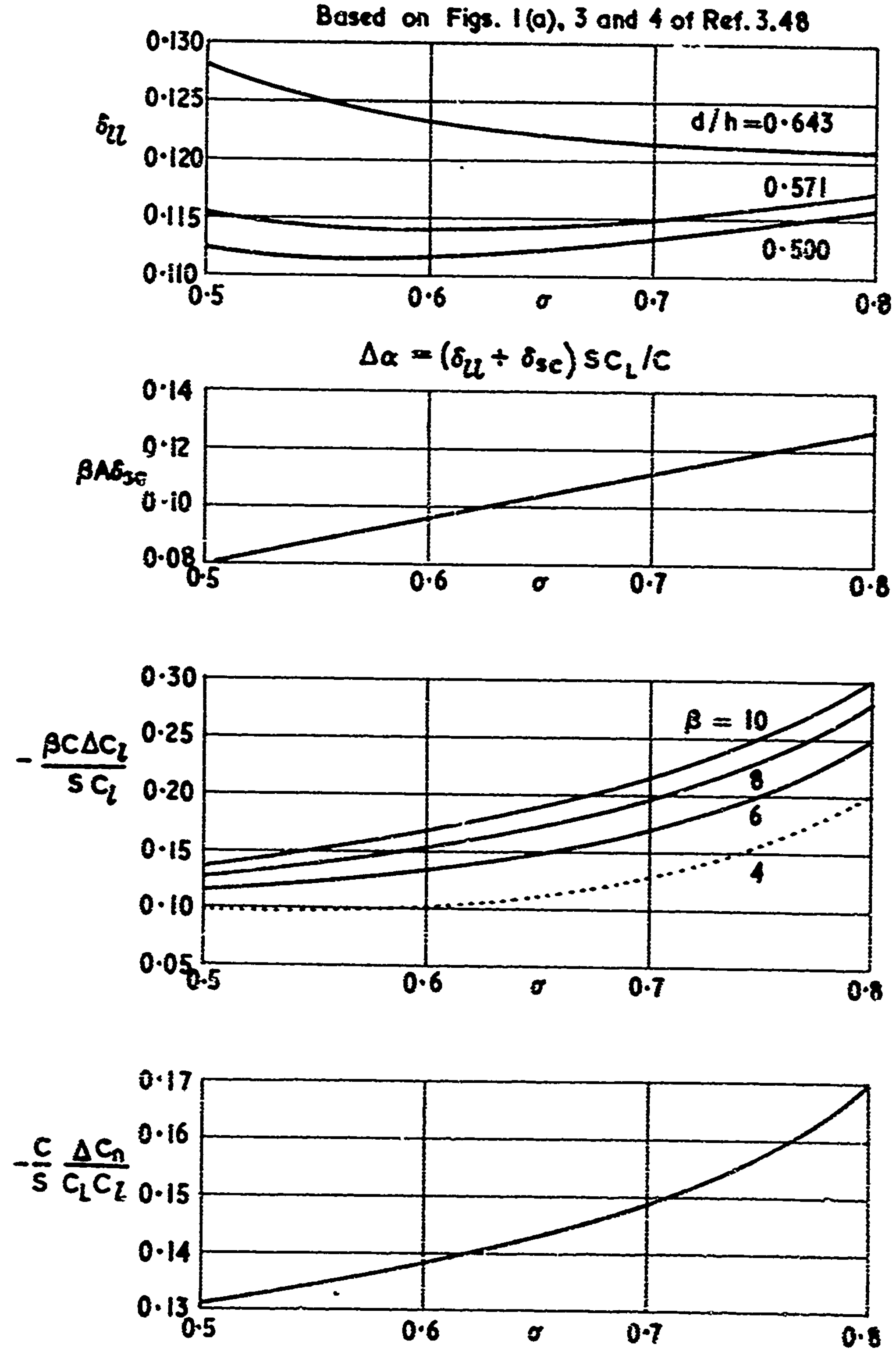

Fig. 3.17 Interference corrections for wings of high aspect ratio in a closed rectangular tunnel (b/h = 10/7)

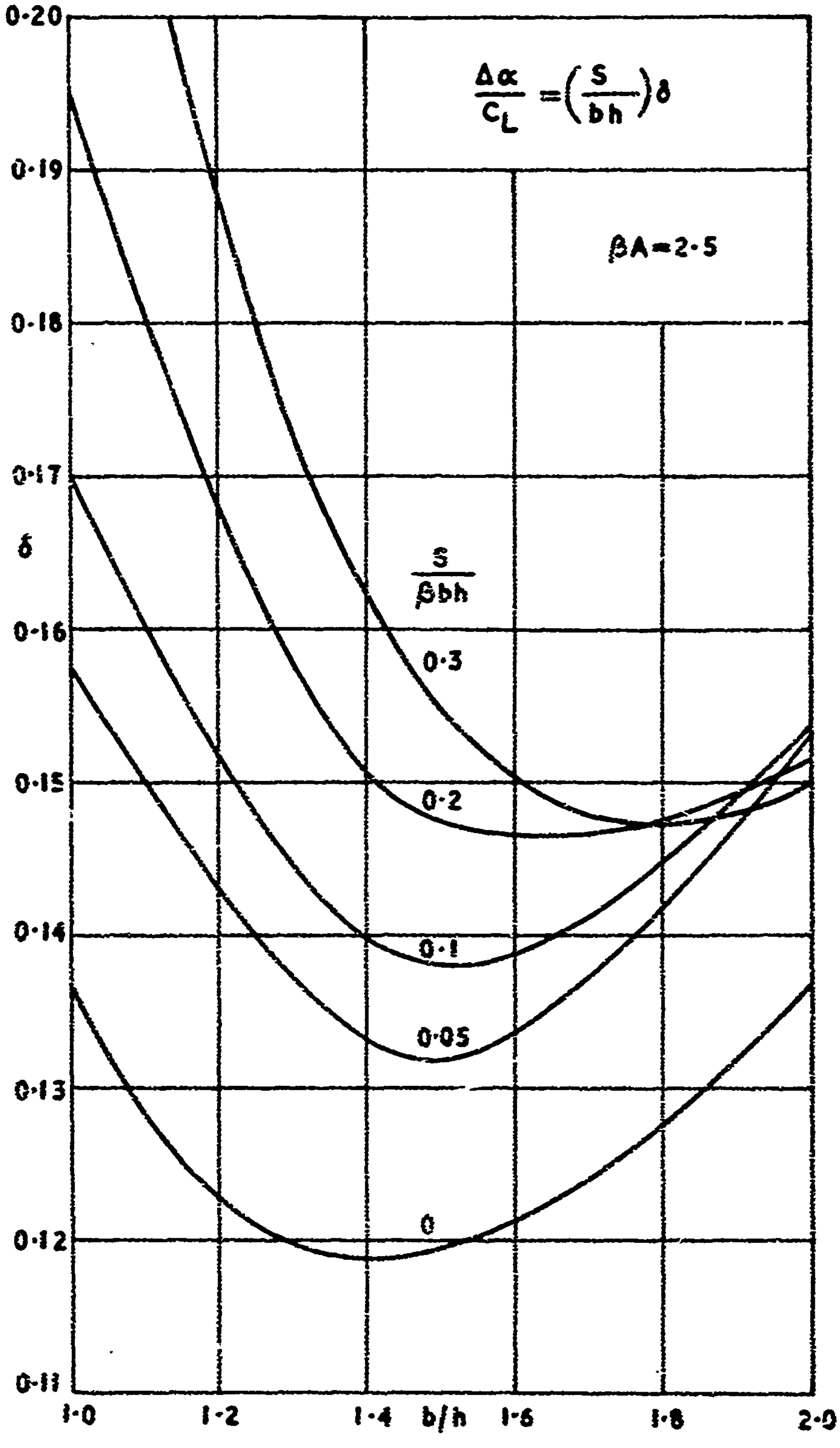

Fig. 3.18 Approximate curves of δ against b/h for wings of different area ratios in closed rectangular tunnels

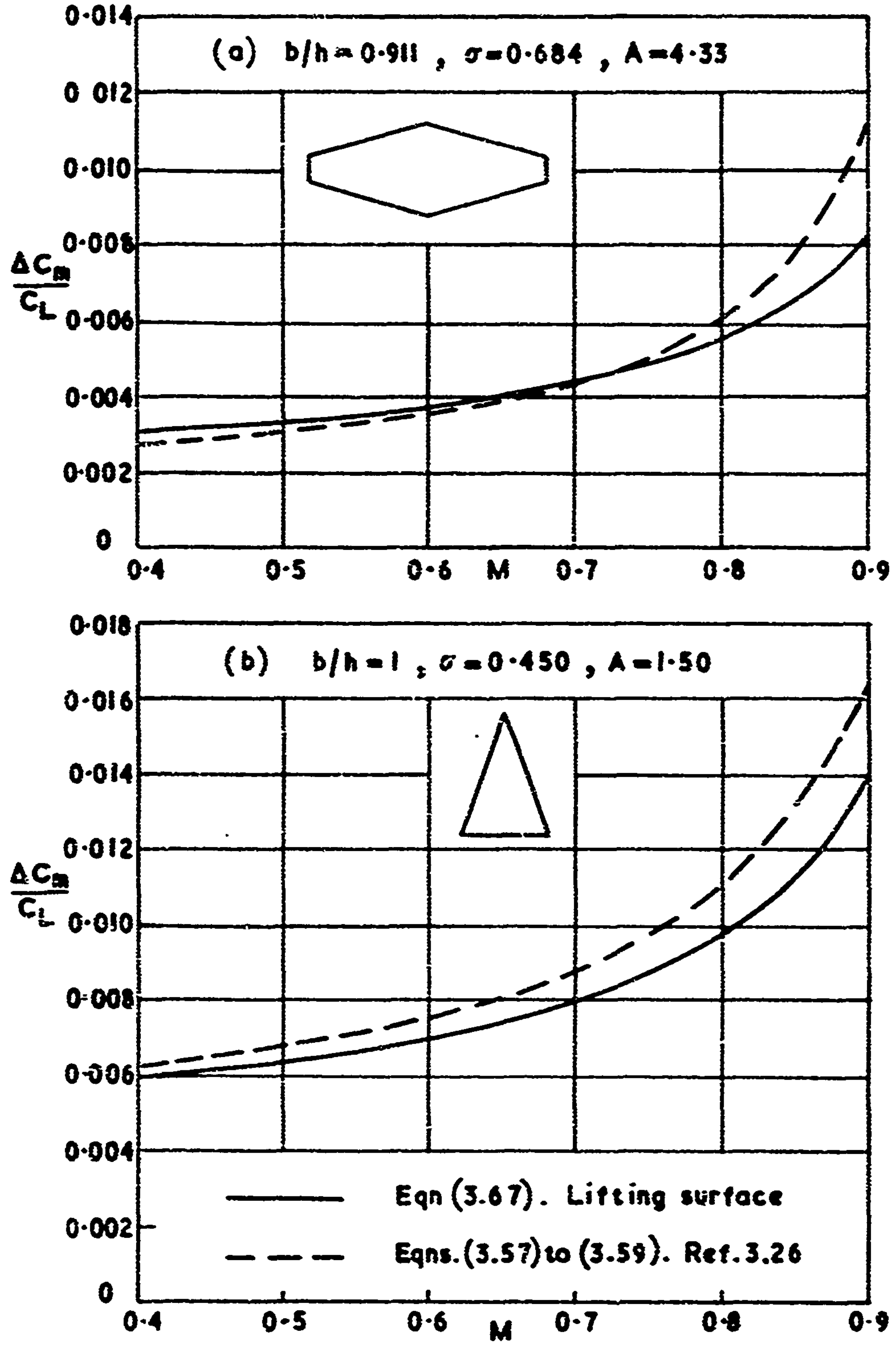

Fig. 3.19 Comparative calculations of residual corrections to pitching moment on wings in closed rectangular tunnels for a range of Mach number

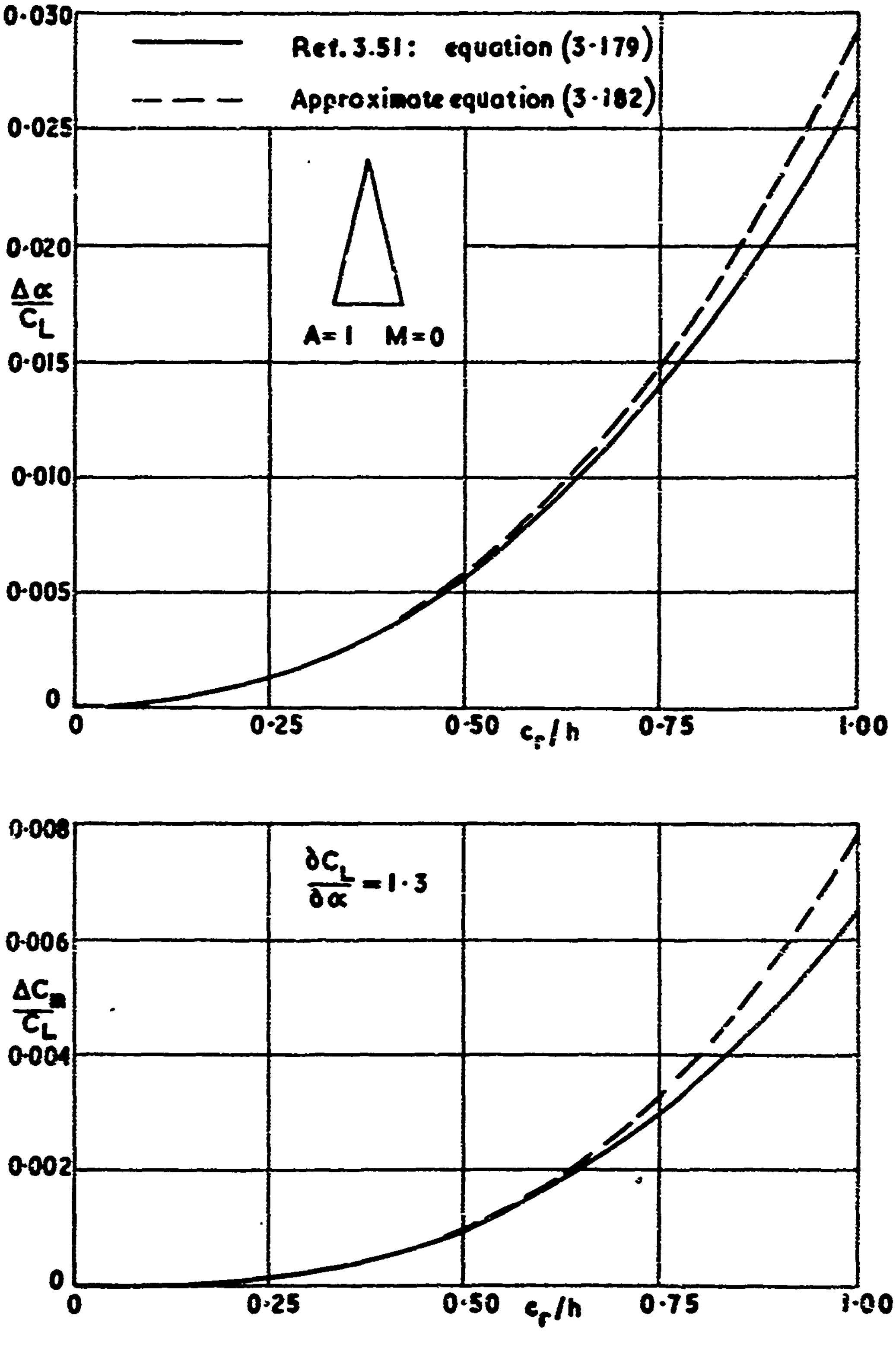

Fig. 3.20 Lift interference on slender delta wings in a closed duplex tunnel

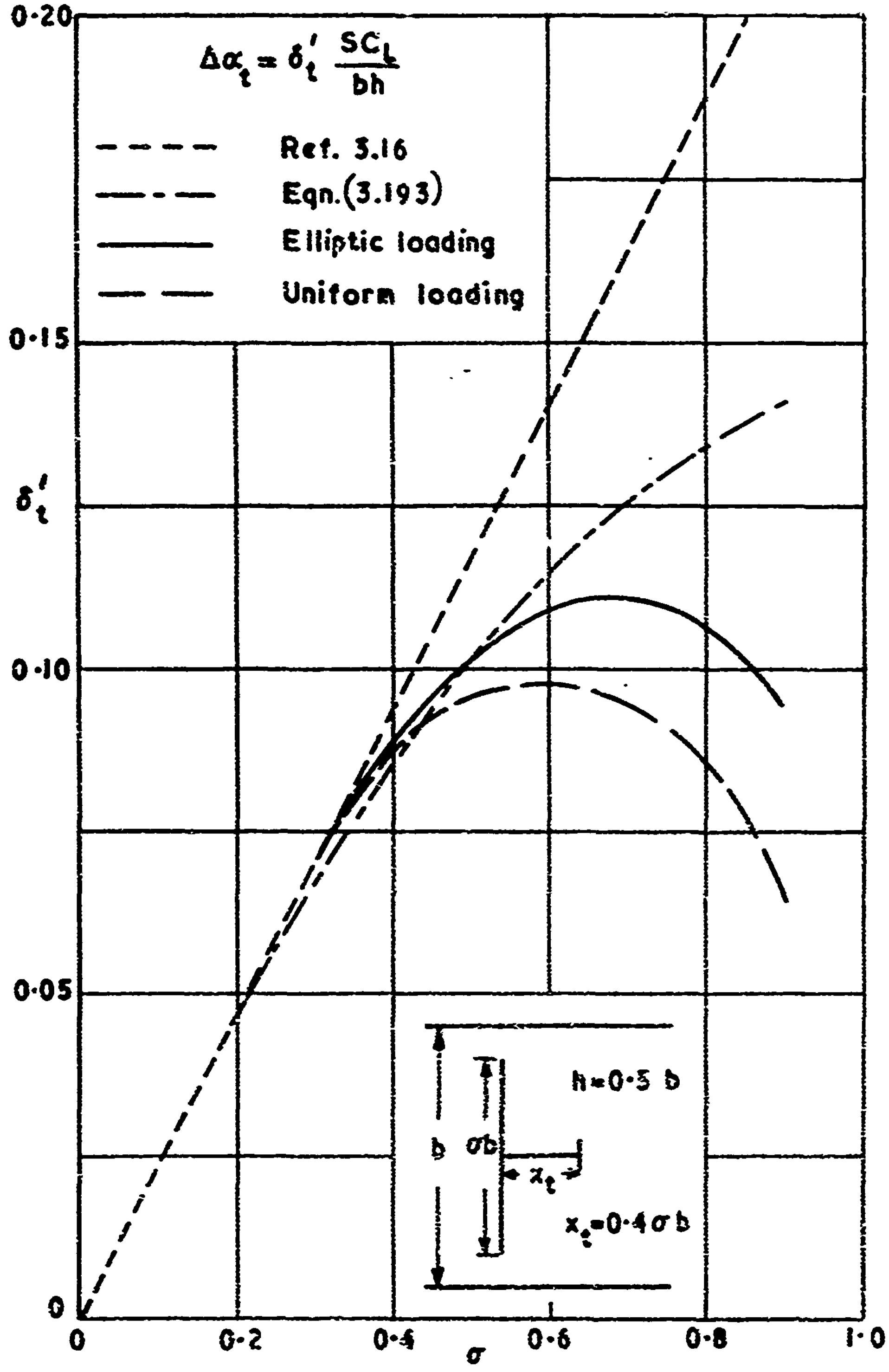
Partly reproduced from Fig. 3 of Ref.3.30

Fig.3.21 Interference correction to tailplane incidence on models of varying size in a closed duplex tunnel (M = 0)

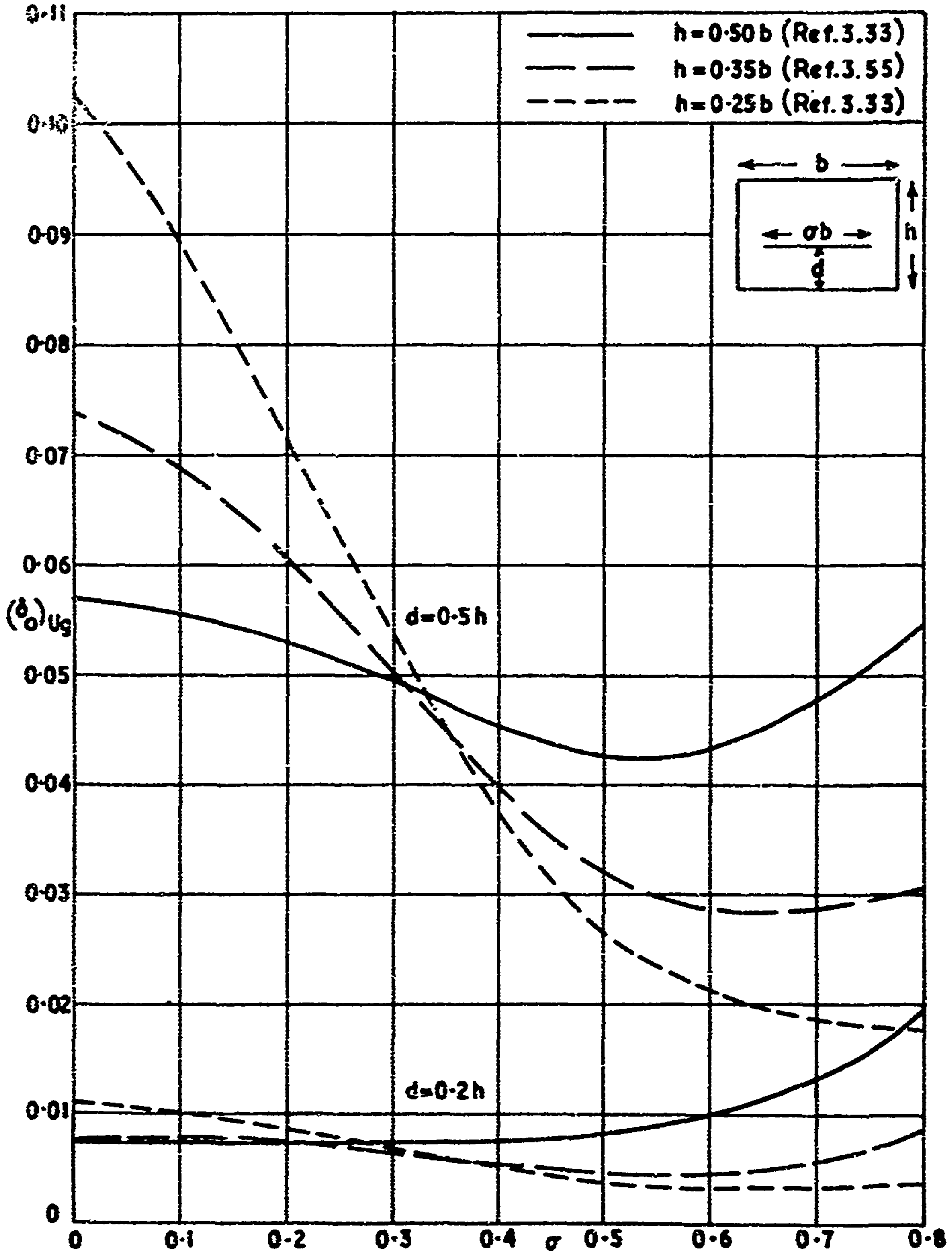

Fig.3.22 Effect of wing span on lift interference with ground simulation in three closed rectangular tunnels

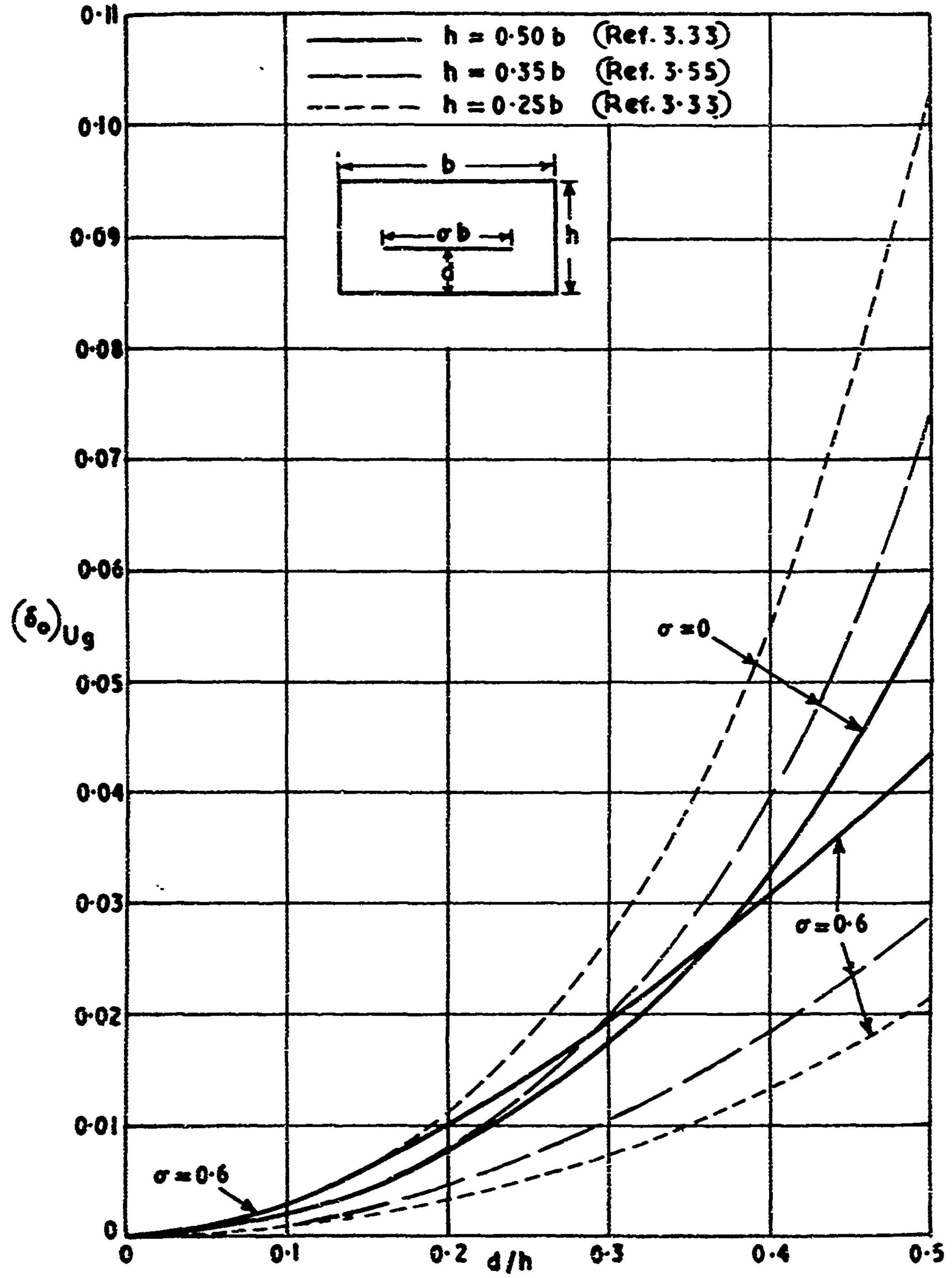

Fig. 3.23 Lift interference on ground effect on uniformly loaded wings in three closed rectangular tunnels

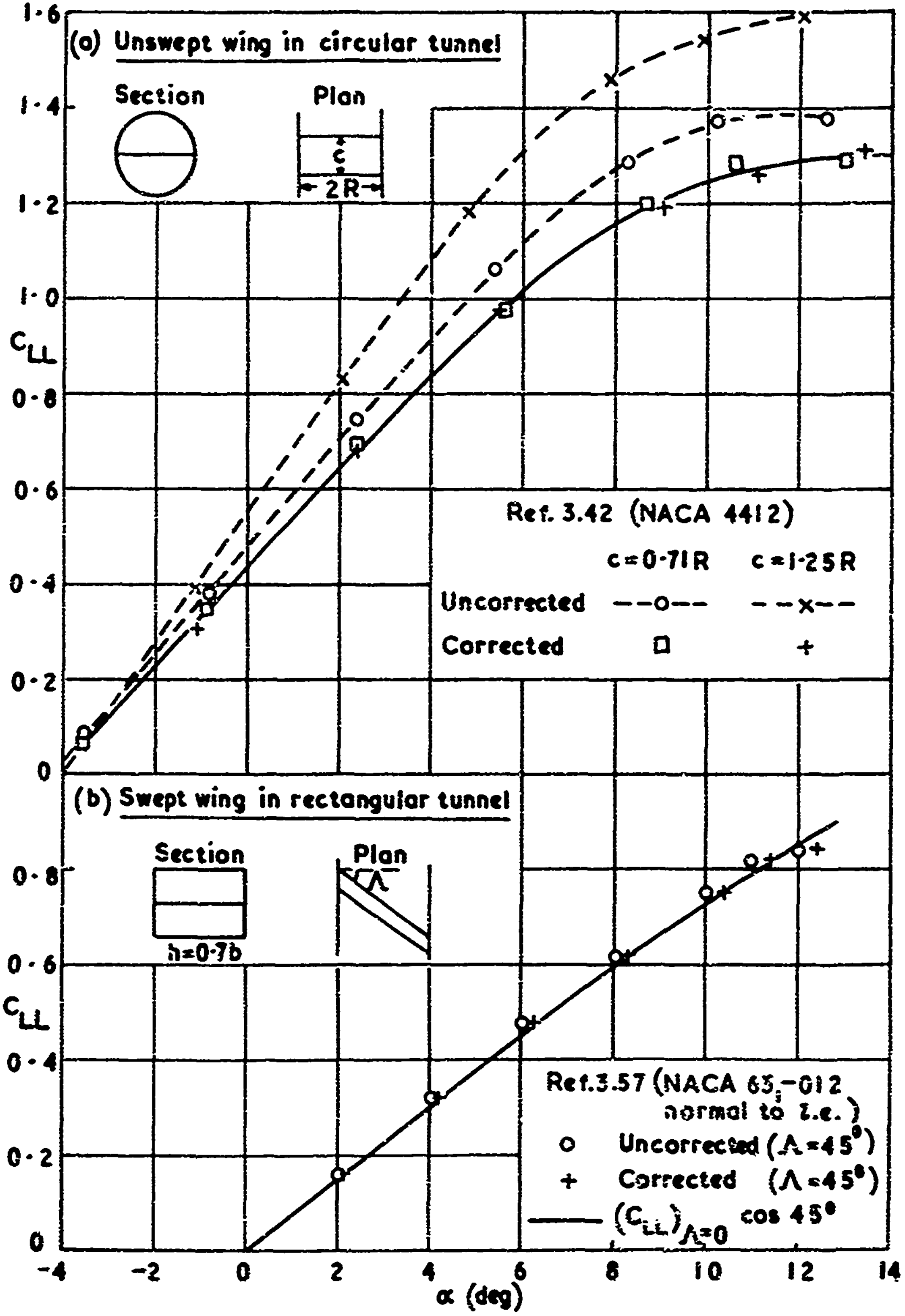

Fig.3.24 Experiments on lift interference on models spanning closed tunnels

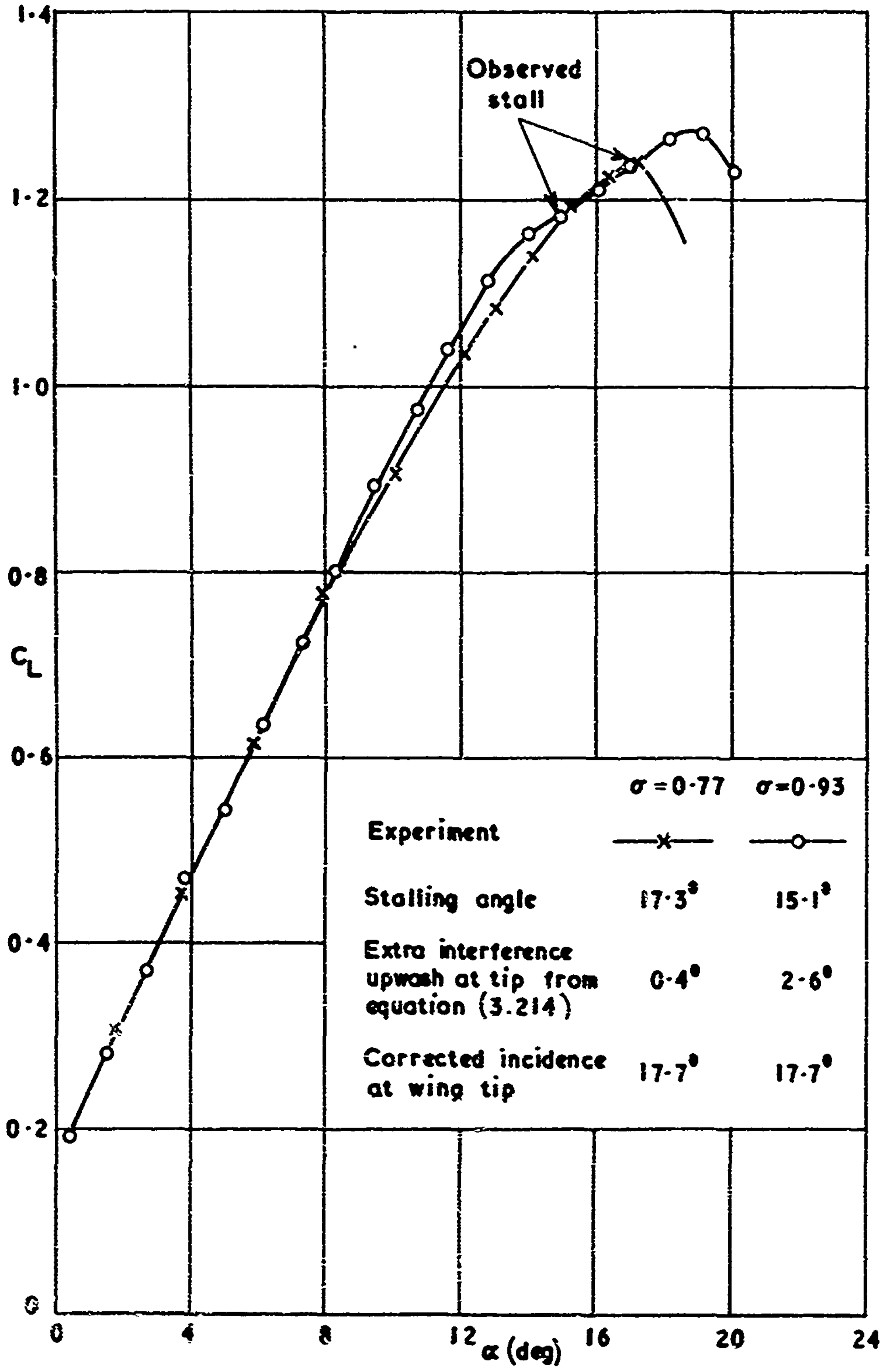
Reproduced from Fig.4 of Ref.3.60

Fig.3.25 Lift curves for an elliptical wing in two closed circular tunnels

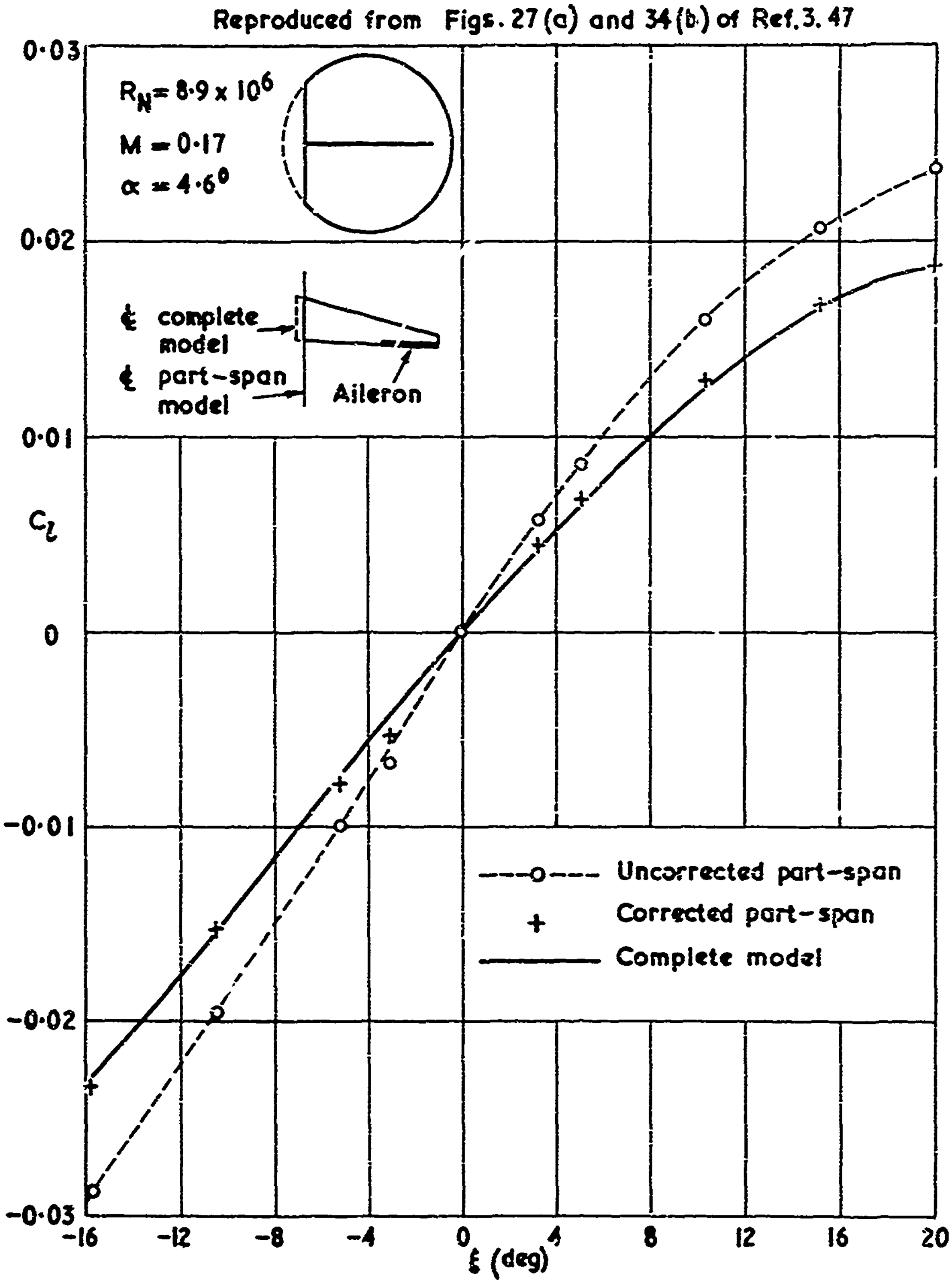

Fig. 3.26 Comparison of aileron effectiveness of a complete model and a part-span model in a closed circular tunnel with reflection plane

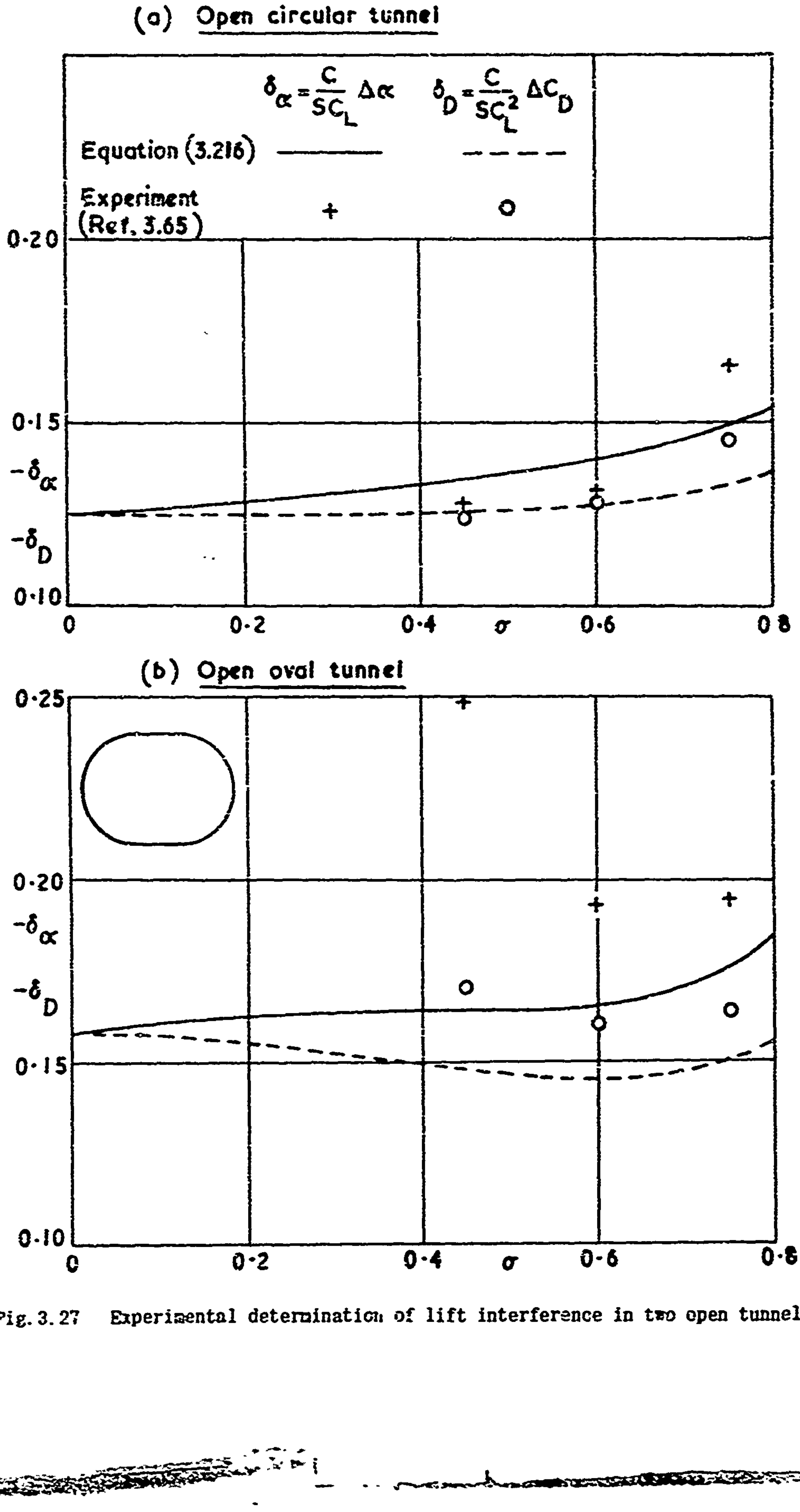

Fig. 3.27 Experimental determination of lift interference in two open tunnels

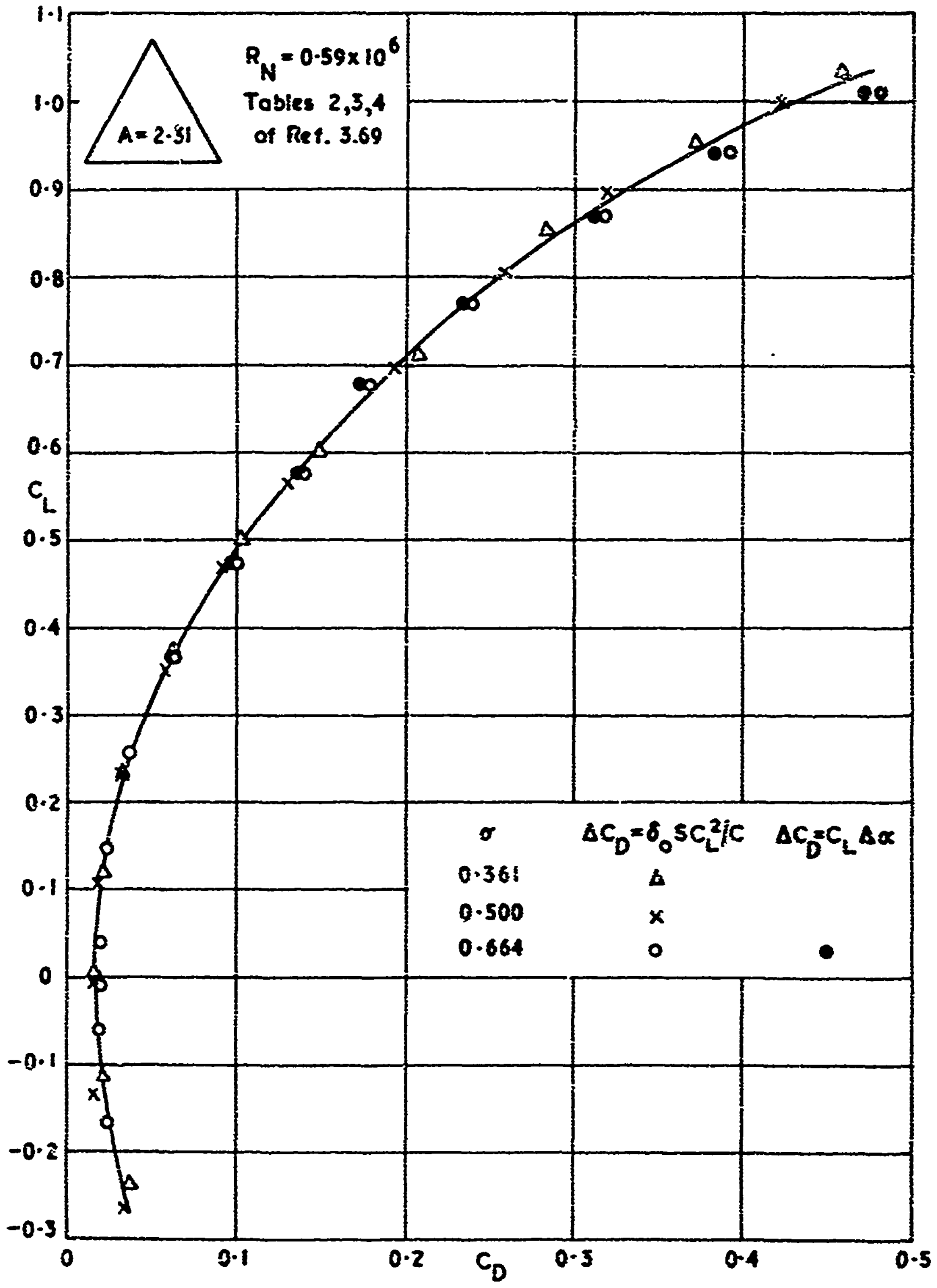

Fig. 3.28 Interference corrections to drag on three similar delta wings in an open circular tunnel

CHAPTER IV

INTERFERENCE EFFECTS IN UNSTEADY EXPERIMENTS

by

W.E.A. Acum

Ship Division, National Physical Laboratory,
Feltham, Middlesex, England

CONTENTS

Page

LIST OF FIGURES 222

NOTATION 223

DEFINITIONS 227

4.1 INTRODUCTION 229

4.2 TWO-DIMENSIONAL WINGS IN INCOMPRESSIBLE FLOW 232

4.3 TWO-DIMENSIONAL WINGS IN COMPRESSIBLE FLOW 236

4.4 GENERAL THEORY FOR THREE-DIMENSIONAL WINGS 239
- 4.4.1 Tunnel Resonance 240
- 4.4.2 Relations Between Steady and Unsteady Interference 241
- 4.4.3 General Interference Corrections 244

4.5 APPLICATION TO THREE-DIMENSIONAL WINGS IN CLOSED TUNNELS 247
- 4.5.1 Rectangular Tunnels 247
- 4.5.2 Circular Tunnels 250
- 4.5.3 Small Wings 250
- 4.5.4 Slender Wings 253
- 4.5.5 Numerical Examples 254

4.6 PERFORATED AND SLOTTED WALLS 256

4.7 STEADILY ROTATING MODELS 258
- 4.7.1 General Theory for Circular Tunnels 259
- 4.7.2 Slowly Rolling Wings 262
- 4.7.3 Propellers 263

4.8 APPLICATIONS TO COMMON EXPERIMENTAL SITUATIONS 264
- 4.8.1 Incompressible Flow 264
- 4.8.2 Compressible Flow 265

REFERENCES 266

ADDITIONAL REFERENCES 269

FIGURES 270

LIST OF FIGURES

		Page
Fig.4.1	Boundary conditions for oscillating wing in two-dimensional closed tunnel	270
Fig.4.2	Tunnel corrections for wing pitching about its mid-chord point	271
Fig.4.3	The effect of resonance on lift in a two-dimensional tunnel at $M = 0.7$	272
Fig.4.4	Interference parameters for small wings in closed rectangular wind tunnels	273
Fig.4.5	Planform of model wing used as an example in Section 4.5.5	274
Fig.4.6	Effect of frequency on the interference upwash due to a horse-shoe vortex in a closed 9 x 7 tunnel	275
Fig.4.7	Effect of number of slots on the pitching damping of an M-wing ($\bar{\nu} \simeq 0.05$)	277
Fig.4.8	Boundary conditions far downstream of a rolling wing	278

NOTATION

a	width of slot
a_n	constants defining the lift distribution in Equation (4.34)
A_n	constants defined by Equations (4.26)
b	breadth of tunnel
c	chord of aerofoil
$\bar{c}$	mean chord of wing (S/2s)
c_r	root chord
c_t	tip chord
C	Theodorsen's lift function, defined in Equation (4.23)
C_l	rolling moment coefficient = (rolling moment)/($\rho U^2 Ss$)
C_L	$= \bar{C}_L e^{i\omega t}$, lift coefficient = (lift)/($\frac{1}{2}\rho U^2 S$)
C_m	$= \bar{C}_m e^{i\omega t}$, pitching moment coefficient = (pitching moment)/($\frac{1}{2}\rho U^2 S\bar{c}$)
C_n	constants in Equation (4.19)
d	representative length of tunnel cross-section
$\tilde{E}$	free vorticity defined in Equations (4.13)
$\bar{E}$	function defined in Equations (4.35)
f, f_1	functions defined in Equations (4.75) and (4.76)
F	function defined in Equation (4.27)
F_1, F_2	functions defined in Equations (4.74) and (4.79)
G	function defined in Equation (4.80)
h	height of a tunnel of rectangular cross-section
Im	prefix denoting imaginary part of
K	kernel of integral Equation (4.39), defined in Equations (4.40) and (4.41)
K	geometric slot parameter in Equation (4.98)

$\tilde{K}$	kernel of integral equation, defined in Equation (4.72)
l	= $\bar{l}e^{i\omega t}$, non-dimensional wing loading = $(p_l - p_u)/(\frac{1}{2}\rho U^2)$
$l_z, l_{\dot{z}}$	direct heaving derivatives (see Definitions)
$l_\alpha, l_{\dot{\alpha}}$	derivatives of lift due to pitching (see Definitions)
L	lift force on wing
L(x)	lift per unit length in the streamwise direction
L_R, L_I	spanwise lift distributions defined in Equation (4.62)
$m_z, m_{\dot{z}}$	derivatives of pitching moment due to heaving (see Definitions)
$m_\alpha, m_{\dot{\alpha}}$	direct pitching derivatives (see Definitions)
M	Mach number of undisturbed stream
n	outward normal distance from tunnel boundary
N	number of slots in roof (or floor) of tunnel
p	pressure
p(x,y)	shape of a general mode of oscillation in Equation (4.65)
p_∞	pressure of undisturbed stream
p_c	pressure in plenum chamber
p_n	weighting function for generalized force P_n
P	wall porosity parameter defined in Equation (4.7)
P_n	generalized force $(n = 1, 2, \ldots)$ in Equation (4.66)
q	= $q_0e^{i\omega t}$, amplitude of a general mode [illegible] Equation (4.65)
r	radial cylindrical polar co-ord [illegible] in Equations (4.101)
$\bar{r}$	non-dimensional radial distance = $\omega r/U$
R	radius of circular tunnel
$\bar{R}$	non-dimensional radius = $\omega R/U$
R_β	see Equation (4.41)
Re	prefix denoting real part of

s		semi-span of wing
$s(x)$		local span of wing
$\bar{s}$		non-dimensional semi-span $= \omega s/U$
S		area of wing planform
t		time
T		tunnel slot parameter in Equation (4.99)
U		velocity of undisturbed stream
w	$=$	$\bar{w}e^{i\omega t}$, component of velocity in z direction
w_i	$=$	$\bar{w}_i e^{i\omega t}$, part of w induced by tunnel walls
x		streamwise distance
x_0		value of x at pitching axis
y		spanwise distance
z		upward distance
$\bar{z}$		wing mode shape defined by $z = \mathrm{Re}\{\bar{z}(x,y)e^{i\omega t}\}$
z_0		non-dimensional amplitude of heaving mode (see Definitions)
α		incidence of wing (in radians)
α_0		amplitude of pitching oscillation defined by $\alpha = \alpha_0 e^{i\omega t}$
α_E		effective angle of incidence of a rotating wing
β	$=$	$(1-M^2)^{\frac{1}{2}}$
$\tilde{\Gamma}$		bound vorticity in Equations (4.13)
Γ	$=$	$\bar{\Gamma}e^{i\omega t}$, strength of vortex; circulation in Section 4.7
$\tilde{\Gamma}_n$		functions defined in Equation (4.20)
$\bar{\Gamma}_R$, $\bar{\Gamma}_I$		vortex strengths defined in Equation (4.64)
δ		prefix denoting contribution due to wall interference
Δ		prefix denoting increment due to wall correction
δ		non-dimensional interference upwash defined in Equation (4.55)

δ_0, δ_1 δ_0', δ_1'	interference upwash parameters for a small wing defined in Equations (4.86) or (4.90)
η	$= y/d$
θ	angular chordwise parameter in Equation (4.22)
θ	angular cylindrical polar co-ordinate in Equations (4.101) (Section 4.7.1)
λ	eigenvalue in Equation (4.37)
μ	frequency parameter $= \omega d/U$
ν	frequency parameter $= \omega c/U$
$\bar{\nu}$	frequency parameter $= \omega \bar{c}/U$
ξ	$= x/d$
ξ_R, ξ_I	local chordwise centres of pressure corresponding to L_R, L_I
ρ	density of undisturbed stream
σ	$= s/d$
Φ	$= \bar{\Phi}e^{i\omega t}$, perturbation velocity potential in Equation (4.2)
Φ_v	velocity potential of a steady horse-shoe vortex in Equation (4.43)
Φ_n	components of Φ for a rolling wing in Equation (4.105)
Ψ_n	see Equation (4.107)
ω	angular frequency of oscillation
ω	angular velocity of steadily rolling wing
ω_r	critical angular frequency for tunnel resonance in Equations (4.28) and (4.38)

Subscripts

F	denotes flow in free air.
i	denotes quantity induced by tunnel walls.
l, u	denotes lower, upper surface of wing.
L, T	denotes leading, trailing edge of wing.

DEFINITIONS

If the wing is performing oscillations such that its surface has the equation

$$z = -[z_0 c + \alpha_0(x - x_0)]e^{i\omega t} ,$$

the derivative coefficients are defined by

$$\left.\begin{aligned} \text{Lift} &= \rho U^2 S\, e^{i\omega t}[(l_z + i\bar{\nu} l_{\dot{z}})z_0 + (l_\alpha + i\bar{\nu} l_{\dot{\alpha}})\alpha_0] \\ \text{Pitching moment} &= \rho U^2 S\bar{c}\, e^{i\omega t}[(m_z + i\bar{\nu} m_{\dot{z}})z_0 + (m_\alpha + i\bar{\nu} m_{\dot{\alpha}})\alpha_0] \end{aligned}\right\} .$$

The pitching moment about $x = x_0$ is reckoned as positive if it tends to raise the leading edge and depress the trailing edge.

For two-dimensional wings $\bar{c}$ is the (constant) chord, and then $\bar{\nu} = \nu = \omega c/U$.

The usual convention about the interpretation of complex quantities in sinusoidal oscillations is assumed; each of the three equations above should be interpreted as having the prefix $\Re$ in its right-hand side, and similarly throughout the whole chapter.

INTERFERENCE EFFECTS IN UNSTEADY EXPERIMENTS

W.E.A.Acum

4.1 INTRODUCTION

As might be expected, the calculation of unsteady interference effects on wings oscillating in wind tunnels is considerably more complicated than for steady flow; as a result not all cases of practical importance are covered by theory. Moreover, since it is possible for an oscillating model and a wind tunnel to form a resonating system, a new phenomenon not occurring in steady flow must be considered. Interference effects can, however, be calculated for many cases of practical interest, although here again a difference arises in that the calculation may be quite lengthy, and simple formulae cannot usually be given.

For the most part this chapter will be concerned with wings performing oscillations sinusoidal in time, but steadily rotating models will be dealt with in Section 4.7.

In most theoretical methods the equations, which have to be solved in order to determine the tunnel interference, are basically those of the small perturbation theory for oscillating thin wings in a free stream, but with modifications to the usual boundary conditions to account for the tunnel walls. The basis of linearized wing theory is set out in Reference 4.1. Thus for thin wings the perturbation velocity potential, $\Phi(x,y,z,t)$, is assumed to satisfy the linearized differential equation

$$\frac{\partial^2\Phi}{\partial x^2} + \frac{\partial^2\Phi}{\partial y^2} + \frac{\partial^2\Phi}{\partial z^2} = \frac{M^2}{U^2}\left(U^2\frac{\partial^2\Phi}{\partial x^2} + 2U\frac{\partial^2\Phi}{\partial x\partial t} + \frac{\partial^2\Phi}{\partial t^2}\right) . \tag{4.1}$$

Since the flow is oscillating with angular frequency ω , we take

$$\Phi = \mathrm{Re}\{\bar{\Phi}(x,y,z)e^{i\omega t}\} , \tag{4.2}$$

and obtain

$$(1 - M^2)\frac{\partial^2\bar{\Phi}}{\partial x^2} + \frac{\partial^2\bar{\Phi}}{\partial y^2} + \frac{\partial^2\bar{\Phi}}{\partial z^2} - \frac{2i\omega M^2}{U}\frac{\partial\bar{\Phi}}{\partial x} + \frac{\omega^2M^2}{U^2}\bar{\Phi} = 0 . \tag{4.3}$$

The linearized expression for the pressure corresponding to Φ is

$$\begin{aligned} p - p_\infty &= -\rho\left(U\frac{\partial\Phi}{\partial x} + \frac{\partial\Phi}{\partial t}\right) \\ &= -\rho\,\mathrm{Re}\left\{\left(U\frac{\partial\bar{\Phi}}{\partial x} + i\omega\bar{\Phi}\right)e^{i\omega t}\right\} . \end{aligned} \tag{4.4}$$

As is customary in the theory of sinusoidal oscillations, the symbol Re for "the real part of" will be omitted unless there is any risk of ambiguity.

On the wing the vertical velocity of the fluid is determined by the wing motion. In the linearized theory this condition becomes

$$\frac{\partial\bar{\Phi}}{\partial z} = U\frac{\partial\bar{z}}{\partial x} + i\omega\bar{z} \tag{4.5}$$

on that part of the plane occupied by the planform, where the wing surface is assumed to be defined by $z = \bar{z}(x,y)e^{i\omega t}$, and the plane $z = 0$ is chosen so that $\bar{z}$ is always small. At infinity Φ must represent outgoing waves; in the presence of tunnel walls this condition can be applied only in the upstream and downstream directions. The wake is assumed to lie in the strip, downstream of the trailing edge, defined by $x > x_T$, $|y| < s$, $z = 0$; the pressure must be continuous across the wake, so that, provided $\bar{\Phi}$ is an odd function of z, its distribution over either side of the wake satisfies*

$$U\frac{\partial\bar{\Phi}}{\partial x} + i\omega\bar{\Phi} = 0 \ . \tag{4.6}$$

At the trailing edge it is assumed that both $\bar{\Phi}$ and $\partial\bar{\Phi}/\partial x$ are continuous, so as to satisfy the Kutta-Joukowski condition.

On solid tunnel walls the normal velocity, $\partial\Phi/\partial n$, must be zero. In an open jet the pressure must be continuous at the edge of the jet and the boundary condition follows from Equation (4.4). These two cases are the limits of the boundary condition which is sometimes applied to represent a porous wall, that is, that the velocity normal to the wall is proportional to the pressure difference across it. This may be written

$$p - p_c = \frac{\rho U}{P}\frac{\partial\Phi}{\partial n} \ , \tag{4.7}$$

where P is the porosity parameter, p is the pressure on the inside of the wall, and p_c the pressure on the outside. This p_c is normally the pressure in a plenum chamber. Solid walls correspond to $P = 0$ and free surfaces to $P \to \infty$†. The application of Equation (4.7) to steady flow is discussed in Section 6.7.

---

* By symmetry $\bar{\Phi}$ is an odd function of z for free-stream flow, and for most practical tunnel arrangements. If $\bar{\Phi}$ is not an odd function of z, then the condition for the continuity of pressure across the wake becomes

$$\left(U\frac{\partial}{\partial x} + i\omega\right)(\bar{\Phi}_u - \bar{\Phi}_l) = 0 \ ;$$

it does not follow that either $\bar{\Phi}_u$ or $\bar{\Phi}_l$ separately satisfies Equation (4.6).

† Where free surfaces are concerned these remarks apply only to wind tunnels. If a water tunnel has a free surface, the effect of gravity may have to be taken into consideration.

In the theory it is usually assumed that $p_c = p_\infty$ and that Equation (4.7) may be linearized by using Equation (4.4). It is conceivable that, to give a good representation of the conditions for an oscillating flow, P might have to be a complex number.

Equation (4.3) is valid for thin wings provided M is not too near to one. It is, however, not the only differential equation which can be used; for example, the approximation

$$\frac{\partial^2\bar{\Phi}}{\partial y^2} + \frac{\partial^2\bar{\Phi}}{\partial z^2} = 0 \tag{4.8}$$

may be used for very slender wings, while near $M = 1$ the unsteady transonic equation

$$\frac{\partial^2\bar{\Phi}}{\partial y^2} + \frac{\partial^2\bar{\Phi}}{\partial z^2} - \frac{2i\omega M^2}{U}\frac{\partial\bar{\Phi}}{\partial x} + \frac{\omega^2 M^2}{U^2}\bar{\Phi} = 0 \tag{4.9}$$

is more applicable. In fact little use has so far been made of them for problems of unsteady wall interference. Miles[4.1] gives a summary of the parameter ranges in which Equations (4.3), (4.8) and (4.9) are valid, and an account of their derivations. For two-dimensional flow Equation (4.3) still holds, but the derivative with respect to y vanishes.

In most theoretical treatments the tunnel is assumed to be cylindrical and to extend to infinity upstream and downstream, so that the determination of tunnel interference is equivalent to solving Equation (4.3) with boundary conditions such as those shown in Figure 4.1, which represents a wing in a closed two-dimensional tunnel. Jordan (Ref.4.2; 1953) has considered the effect of a two-dimensional vortex wake of finite length, but in general it seems essential to assume that the wake is infinite if a mathematical treatment is to be feasible.

For rectangular or two-dimensional tunnels the method of images, which is exactly analogous to that employed in steady flow, may be used. As in free-stream theory, it is then often possible to replace the differential equation by an equivalent integral equation. For the general cylindrical tunnel, with that of circular section as the most important example, it is not possible to construct an image system, and present methods of solution are restricted to the special cases of incompressible flow or low frequency.

Wind-tunnel experiments involving force measurements may be of two kinds. The object of the first is the determination of some force acting on a model, and the correction is applied to obtain a value appropriate to free-stream conditions. In such cases it is desirable that as much as possible of the measured data should be used in computing the interference corrections, in order to offset the inaccuracies of linearized theory. In particular, the calculation of a correction by taking the difference between

(i) free-stream linearized theory

and (ii) linearized theory modified to include the presence of the walls,

is not likely to be satisfactory unless the theory represents the experimental situation with an unusual degree of accuracy. The second kind of experiment has as its objective an assessment of the accuracy of a theory. If this theory is the same in principle for both the free-stream and tunnel cases, then it is sufficient to compare (ii) with the uncorrected experiments.

Section 4.8 summarizes the methods recommended for typical configurations in incompressible and in compressible flow. There are difficult cases where no method of solution exists, and others where the numerical work might well be considered prohibitive.

4.2 TWO-DIMENSIONAL WINGS IN INCOMPRESSIBLE FLOW

Consider first an aerofoil of chord c on the centre line of a two-dimensional tunnel with solid walls distant h apart. Suppose that the motion of the aerofoil may be described by the equation

$$z = -[z_0 c + \alpha_0(x-x_0)]e^{i\omega t} , \tag{4.10}$$

so that the motion is rigid pitching of amplitude α_0 about an axis $x = x_0$, superimposed on a rigid heaving motion of amplitude $z_0 c$. If α_0 is not zero, Equation (4.10) also represents a rigid pitching motion about the axis $x = x_0 - z_0 c/\alpha_0$.

Since the fluid is incompressible, Equation (4.3) reduces to

$$\nabla^2\bar{\Phi} = 0 , \tag{4.11}$$

with boundary conditions (Fig. 4.1)

$$\left.\begin{aligned} \frac{\partial\bar{\Phi}}{\partial z} &= -U\alpha_0 - i\omega[z_0 c + \alpha_0(x-x_0)] && \text{on } z = 0 ,\ x_L < x < x_T \\ \frac{\partial\bar{\Phi}}{\partial x} + \frac{i\omega\bar{\Phi}}{U} &= 0 && \text{on } z = 0 ,\ x > x_T \\ \frac{\partial\bar{\Phi}}{\partial z} &= 0 && \text{on } z = \pm\tfrac{1}{2}h ,\ -\infty < x < \infty \end{aligned}\right\} ; \tag{4.12}$$

furthermore at $x = x_T$, $\bar{\Phi}$ and $\partial\bar{\Phi}/\partial x$ must be continuous with respect to x. For a general mode of oscillation the first of Equations (4.12) has to be replaced by Equation (4.5).

The alternative to the solution of the differential Equation (4.11) lies in the formulation of the corresponding integral equation. In this approach the vorticity distribution over the wing and wake is regarded as being the sum of two parts, $\tilde{\Gamma}e^{i\omega t}$, the "bound" vorticity, which is proportional to the local lift, and $\tilde{\Xi}e^{i\omega t}$, the "free" vorticity. $\tilde{\Xi}$ and $\tilde{\Gamma}$ are defined by

$$\left.\begin{aligned}\tilde{\Gamma}+\tilde{E} &= \frac{\partial}{\partial x}(\bar{\Phi}_u-\bar{\Phi}_l)\\ \tilde{\Gamma} &= \left(\frac{\partial}{\partial x}+\frac{i\omega}{U}\right)(\bar{\Phi}_u-\bar{\Phi}_l)\end{aligned}\right\} \quad . \tag{4.13}$$

so that, by Equation (4.4), the local loading per unit area is

$$l = \frac{p_l - p_u}{\frac{1}{2}\rho U^2} = \frac{2\tilde{\Gamma}}{U}e^{i\omega t} \quad , \tag{4.14}$$

and, by Equations (4.13),

$$\tilde{E}(x) = -\frac{i\omega}{U}\exp\left(-\frac{i\omega x}{U}\right)\int_{x_L}^{x}\tilde{\Gamma}(x')\exp\left(\frac{i\omega x'}{U}\right)dx' \quad . \tag{4.15}$$

In the wake, $x > x_T$, $\tilde{\Gamma}$ is zero, so that for $x > x_T$ the upper limit of integration in Equation (4.15) is x_T .

Now in the unbounded free stream the upwash corresponding to the vorticity distribution $(\tilde{\Gamma}+\tilde{E})$ would be given by

$$\bar{w}(x,z) = -\frac{1}{2\pi}\int_{x_L}^{\infty}\frac{(\tilde{\Gamma}+\tilde{E})(x-x')}{(x-x')^2+z^2}\,dx' \quad ; \tag{4.16}$$

this relation is a straightforward extension of that arising in the treatment of two-dimensional thin wings in steady incompressible flow, for example that given in Chapter VIII of Reference 4.3.

In the wind-tunnel case it is necessary to modify this by including the contributions of the images which are assumed to be present in a way analogous to that for the corresponding steady flow (Chapter II). Then for a closed tunnel the upwash on $z = 0$ is that due to an infinite column of vortex sheets, of alternating sign, lying on $z = \pm nh$, $n = 1,2,3,\ldots$. Equation (4.16) is then replaced by

$$\bar{w}(x,0) = -\frac{1}{2\pi}\int_{x_L}^{\infty}[\tilde{\Gamma}(x')+\tilde{E}(x')]\left\{\frac{1}{x-x'}+2\sum_{n=1}^{\infty}(-1)^n\frac{x-x'}{(x-x')^2+n^2h^2}\right\}dx' \quad ,$$

or, with the known sum of the infinite series,

$$\bar{w}(x,0) = -\frac{1}{2\pi}\int_{x_L}^{\infty}[\tilde{\Gamma}(x')+\tilde{E}(x')]\,\frac{\pi}{h}\,\mathrm{cosech}\,\frac{\pi(x-x')}{h}\,dx' \quad . \tag{4.17}$$

The singularity at $x' = x$ is accounted for by taking the Cauchy principal value. Since $\bar{w}(x,0)$ is known from Equation (4.12) for $x_L < x < x_T$, Equation (4.17) is the required integral equation for $(\tilde{\Gamma} + \tilde{E})$.

Explicit analytical solutions of Equation (4.17) are available covering most cases of practical interest. However, it may be remarked that for experiments of the first type discussed at the end of Section 4.1 such solutions are not essential.

The equation for the interference upwash, due to the images only, is

$$\bar{w}_i(x,0) = -\frac{1}{2\pi}\int_{x_L}^{\infty}[\tilde{\Gamma}(x') + \tilde{E}(x')]\left\{\frac{\pi}{h}\operatorname{cosech}\frac{\pi(x-x')}{h} - \frac{1}{x-x'}\right\}dx' . \qquad (4.18)$$

Now if l were known, $(\tilde{\Gamma} + \tilde{E})$ could be calculated from Equations (4.14) and (4.15) and $\bar{w}_i$ evaluated numerically using Equation (4.18). Unless c/h were large, $\bar{w}_i$ would be obtained sufficiently accurately if l were given its free-stream theoretical value, modified by a factor to make it consistent with the measured forces. The interference forces could then be calculated from free-stream theory.

Some progress towards a solution of Equation (4.17) may be made by the modification of the "vortex sheet" theory for two-dimensional oscillating wings in Reference 4.4 which is itself an extension of the simple theory for steady wings[4.3]. For the oscillating free-stream case, the bound vorticity is expanded in the form

$$\tilde{\Gamma} = U\sum_{n=0}^{\infty} C_n\tilde{\Gamma}_n , \qquad (4.19)$$

with

$$\left.\begin{aligned} \tilde{\Gamma}_0 &= 2[C(\tfrac{1}{2}\nu)\cot\tfrac{1}{2}\theta + \tfrac{1}{2}i\nu\sin\theta] \\ \tilde{\Gamma}_1 &= -2\sin\theta + \cot\tfrac{1}{2}\theta + \tfrac{1}{2}i\nu[\sin\theta + \tfrac{1}{2}\sin 2\theta] \\ \tilde{\Gamma}_n &= -2\sin n\theta + \tfrac{1}{2}i\nu\left[\frac{\sin(n+1)\theta}{n+1} - \frac{\sin(n-1)\theta}{n-1}\right] \quad (n \geq 2) \end{aligned}\right\} . \qquad (4.20)$$

Here

$$\nu = \omega c/U , \qquad (4.21)$$

$$x = x_L + \tfrac{1}{2}c(1 - \cos\theta) , \qquad (4.22)$$

and $C(\frac{1}{2}\nu)$ is Theodorsen's lift function

$$C(\tfrac{1}{2}\nu) = H_1^{(2)}(\tfrac{1}{2}\nu)/\{H_1^{(2)}(\tfrac{1}{2}\nu) + iH_0^{(2)}(\tfrac{1}{2}\nu)\} . \qquad (4.23)$$

where $H_0^{(2)}$ and $H_1^{(2)}$ are Hankel functions. The upwash distribution is then given by

$$\bar{w} = -U\left[C_0 + \tfrac{1}{2}C_1 + \sum_{n=1}^{\infty} C_n \cos n\theta\right] , \qquad (4.24)$$

and the unknown coefficients C_n may be determined by comparison with the first of Equations (4.12).

Now, if tunnel walls are present, Equation (4.19) will not lead to Equation (4.24) but to a modified form of it. There appears to be no simple method of working out what this is for general values of the ratio c/h, but Jones (Ref. 4.4; 1950) has given a method for small c/h. Equation (4.24) is replaced by

$$\bar{w} = -U\left[(C_0 + \tfrac{1}{2}C_1 + A_0) + \sum_{n=1}^{\infty} (C_n + A_n)\cos n\theta\right] , \qquad (4.25)$$

where

$$\left.\begin{aligned} A_0 &= -\frac{\pi^2 c^2}{24h^2}\left[C_0\left(\tfrac{1}{2} - \frac{2iC}{\nu}\right) + \frac{C_1 - C_2}{4}\right] + J_0(\tfrac{1}{2}\nu)FC_0 \\ A_n &= 2i^n J_n(\tfrac{1}{2}\nu)FC_0 \qquad (n \geqslant 1) \end{aligned}\right\} . \qquad (4.26)$$

Here

$$F = \{CJ_0(\tfrac{1}{2}\nu) + i(1-C)J_1(\tfrac{1}{2}\nu)\}\left\{\frac{\pi^2 c^2}{24h^2}\exp(-\tfrac{1}{2}i\nu)\left(1 - \frac{2i}{\nu}\right) - \right.$$
$$\left. - \tfrac{1}{2}i\nu\int_{\frac{1}{2}\nu}^{\infty}\left[\frac{\exp(-iy)}{y} - \frac{\pi c}{\nu h}\,\frac{\exp(-iy)}{\sinh(\pi cy/\nu h)}\right]dy\right\} . \qquad (4.27)$$

$C = C(\tfrac{1}{2}\nu)$ is given by Equation (4.23) and J_n is the Bessel function in the usual notation.

Lilley (Ref. 4.5; 1952) has transformed Equation (4.18) into one of a type having known solutions, but unfortunately the result for general c/h ratio is too long and complicated to reproduce here, although some simplification occurs if c/h is of order one or larger. Certain modes of oscillation of cascades cause flows like those considered in tunnel interference; for example, the flow through an unstaggered cascade in which consecutive elements are oscillating in antiphase is the same as that past an aerofoil in a closed wind tunnel, as may be seen by considering the image system. Reference 4.6 could be applied in this way.

The alternative to an approach via vortex-sheet theory is the solution of the differential Equation (4.11) and associated boundary conditions. This has been carried out by Rosenblat (Ref. 4.7; 1957) by a method involving conformal transformation of the interior of the tunnel, and also by Timman (Ref. 4.8; 1951) by a modification of Theodorsen's free-stream theory. The analytical expressions are too lengthy for inclusion, but de Jager has presented Timman's results in Reference 4.9.

algebraically and as graphs, for a rigid aerofoil with or without a trailing-edge control. It should be noted that, contrary to the statement made by Rosenblat in Reference 4.7, his results do in fact agree with Timman's*.

It is likely that in most experiments c/h will be small enough for Equations (4.25) to (4.27) to apply. A comparison of the results from Reference 4.4 with the graphs of Reference 4.9 indicates that this may be expected to be good enough for $c/h < 0.25$. Figure 4.2 shows the variation with ν of Δm_α and $\nu \Delta m_{\dot{\alpha}}$ (where the prefix Δ denotes free-stream value minus tunnel value) for a wing pitching about the mid-chord axis. The results from Equations (4.25) to (4.27) (Ref. 4.4) for $c/h = 0.21$ fit in very well. Alternatively the tunnel corrections may be estimated from the graphs of Reference 4.9. A method of applying the theoretical quantities such as Δm_α to practical situations is set out in Section 4.4.3.

A further simplification occurs when both the frequency parameter and c/h are small. If this is so, there are explicit expressions for the lift and pitching moment[4.8]; these will not be given here as they are merely special cases, with $M = 0$ and $\beta = 1$, of the corresponding expressions for compressible flow in Equations (4.35).

4.3 TWO-DIMENSIONAL WINGS IN COMPRESSIBLE FLOW

Before considering the possibility of calculating the tunnel interference it is necessary to recognise that, if the fluid is compressible, the phenomenon of "tunnel resonance" is possible. It has been shown in References 4.10 and 4.11 that, according to linearized theory, the interference upwash due to a small oscillating model wing in a two-dimensional closed tunnel will become infinite for certain critical frequencies, the smallest of which is given by

$$\frac{\omega_r h}{U} = \frac{\pi\beta}{M} . \tag{4.28}$$

The physical significance of this particular frequency may be seen by considering the possibility of perturbation flows of the form

$$\Phi = e^{ikx} \sin(\pi z/h) , \tag{4.29}$$

where k is a constant, as yet undetermined. This Φ automatically satisfies the condition of no flow through the tunnel walls at $z = \pm\frac{1}{2}h$, but unless k is real Φ will not remain finite at large distances upstream and downstream. Substitution of Equation (4.29) into Equation (4.3) gives

$$\left(\frac{\omega M}{U} + Mk\right)^2 = k^2 + \frac{\pi^2}{h^2} , \tag{4.30}$$

---

* The second equation in Section 14 (p.271) of Reference 4.7 should read

$$q = \frac{1}{16}k^2[1 + \tfrac{1}{4}k^2 + O(k^4)] .$$

and the smallest value of ω for which Equation (4.30), considered as an equation for k, has real roots, is in fact ω_r as given by Equation (4.28). The lowest critical frequency for resonance is therefore the smallest for which a disturbance of the type Equation (4.29) can remain of finite amplitude at all large distances from the model.

According to Equation (4.28) the critical frequency is small if M is near to one, and measurements at high subsonic speeds are most likely to be affected. It might also appear that ω_r should be small for a very large tunnel, but it must be borne in mind that Equation (4.28) is deduced on the assumptions that the tunnel is of infinite length and that viscosity is negligible, and it can therefore only roughly represent actual experiments. There is, nevertheless, strong experimental evidence, such as that in Figure 4.3, that the result is approximately correct.

The evaluation of the forces on a thin wing in a wind tunnel requires either the solution of Equation (4.1) with the appropriate boundary conditions, or else a solution of one of the equivalent integral equations. In free-stream flow the lift and upwash distributions are related by Possio's equation

$$\frac{\bar{w}(x)}{U} = \frac{i}{8\beta}\lim_{z\to 0}\int_{x_L}^{x_T}\bar{l}(x')\int_{-\infty}^{x-x'}\exp\{-i\omega(x-x')\}\exp\left(\frac{i\omega\xi}{U\beta^2}\right)\times$$

$$\times\frac{\partial^2}{\partial z^2}H_0^{(2)}\left(\frac{\omega M}{U\beta^2}\sqrt{\xi^2+\beta^2 z^2}\right)d\xi\,dx' \quad , \qquad (4.31)$$

where $H_0^{(2)}(z)$ is a Hankel function of argument z ; the velocity potential on the upper surface and the upwash are related by

$$\frac{\bar{w}(x)}{U} = -\frac{i}{2\beta U}\lim_{z\to 0}\int_{x_L}^{\infty}\bar{\Phi}_u(x')\exp\left(-\frac{i\omega M^2(x-x')}{U\beta^2}\right)\frac{\partial^2}{\partial z^2}H_0^{(2)}\left(\frac{\omega M}{U\beta^2}\sqrt{(x-x')^2+\beta^2 z^2}\right)dx' \ .$$

$$(4.32)$$

These relations can be obtained from the corresponding three-dimensional integral equations by integrating spanwise with respect to y .

In the case of the closed wind tunnel the simulation of the walls by images introduces sums of the form

$$\sum_{-\infty}^{\infty}(-1)^n H_0^{(2)}\left(\frac{\omega M}{U\beta^2}\sqrt{(x-x')^2+\beta^2(z-nh)^2}\right) \ . \qquad (4.33)$$

No analytical solutions of the integral equations modified in this way seem to be known, and calculations have to be made by approximate and numerical methods. Nevertheless, by analytical treatment of the series Equation (4.33), it was shown in References 4.10 and 4.11 that the sum is infinite when $\omega h/U = (2m-1)\pi\beta/M$, $(m = 1,2,3\ldots.)$; obviously ω_r corresponds to $m = 1$.

In Reference 4.12 the integral equation corresponding to Equation (4.31) is studied and a numerical collocation method of solution is outlined, in which the usual expansion

$$\bar{l} = a_0 \cot\tfrac{1}{2}\theta + \sum_{n=1}^{\infty} a_n \sin n\theta \tag{4.34}$$

is assumed and the upwash evaluated at a number of control points on the aerofoil. Three points were found to be enough for $h/c = 3.8$, and frequencies $\omega < \omega_r$. In this approach the aerofoil in a free stream is merely a particular case. Figure 4.3 refers to a wing pitching about the mid-chord axis and shows how the lift varies with frequency, in particular the marked effect as resonance is approached. The experimental phase angle agrees very well with the calculated value but the amplitude of the lift tends to be overestimated by theory. This behaviour is typical for the pitching moment also at Mach numbers from 0.35 to 0.70 (Ref.4.12). Evidently this method of calculation is reasonably satisfactory, provided the numerical work can be tolerated.

Molyneux (Ref.4.39; 1964) has pointed out that the range of frequency for which the forces on the model are strongly affected by resonance becomes narrower if the size of the model is reduced while the height of the tunnel remains constant. This favours the use of small models. Molyneux also observes that the sharpness of the resonance decreases as M increases, particularly as regards changes in phase angle.

If the frequency is well below critical, the method described in Reference 4.10 may be used. This again is a collocation treatment, based on the modified form of Equation (4.32), and involving an expansion of the kernel in powers of frequency; it is accordingly restricted in frequency range. When the frequency parameter is small and c/h is not large, the heaving and pitching derivatives for reference axis at the mid-chord (Fig.4.1) are

$$\left.\begin{aligned}
l_z &= 0\,, & l_{\dot z} &= \frac{\pi}{\beta}\left(1 + \frac{\pi^2c^2}{24\beta^2h^2}\right)\\
m_z &= 0\,, & m_{\dot z} &= \frac{\pi}{4\beta}\left(1 + \frac{\pi^2c^2}{48\beta^2h^2}\right)\\
l_\alpha &= l_{\dot z}\,, & l_{\dot\alpha} &= \frac{\pi}{2\beta^3}\left[\left(1 + \frac{\pi^2c^2}{48\beta^2h^2}\right)\left(\frac{3\beta^2-1}{2}\right) - \bar{E}\left(1 + \frac{\pi^2c^2}{12\beta^2h^2}\right)\right]\\
m_\alpha &= m_{\dot z}\,, & m_{\dot\alpha} &= -\frac{\pi}{8\beta^3}\left[\left(1 + \frac{\pi^2c^2}{16\beta^2h^2}\right)\bar{E} + \frac{\pi^2c^2M^2}{32\beta^2h^2}\right]
\end{aligned}\right\} \,. \tag{4.35}$$

where

$$\bar{E} = \log_e\left\{2\coth\left(\frac{\pi c}{4\beta h}\right)\right\} \,.$$

According to Equations (4.35) $l_{\dot\alpha}$ and $m_{\dot\alpha}$ tend to infinity when h tends to infinity for a fixed c . This agrees with the fact that in a free stream

$(l_{\dot{\alpha}})_F$ and $(m_{\dot{\alpha}})_F$ do become infinitely large for very small ν. Although the tunnel corrections are theoretically infinite, the forces in quadrature with the pitching motion are in fact proportional to $\nu(l_{\dot{\alpha}})_F$ and $\nu(m_{\dot{\alpha}})_F$, which remain finite.

Tabulated tunnel corrections for the compressible case are few in number, and in the nature of illustrative examples only, but enough evidence is available to show that the corrections can be significant in practice. For example, the following table, taken from Reference 4.10, refers to a wing for which h/c = 4.75 oscillating about its mid-chord axis in a stream with $M = 0.7$.

ν	$(l_\alpha)_F$	l_α	$(l_{\dot{\alpha}})_F$	$l_{\dot{\alpha}}$	$(-m_\alpha)_F$	$-m_\alpha$	$(-m_{\dot{\alpha}})_F$	$-m_{\dot{\alpha}}$
0	4.399	4.556	$-\infty$	-8.882	-1.100	-1.119	∞	3.012
0.04	4.066	4.510	-12.981	-8.715	-1.015	-1.106	4.030	2.969
0.08	3.757	4.339	- 8.903	-7.979	-0.933	-1.061	2.981	2.778
0.20	3.117	3.657	- 3.877	-5.084	-0.759	-0.880	1.669	2.023
0.40	2.638	2.975	- 1.274	-2.026	-0.617	-0.694	0.976	1.236

The values $l_\alpha/(l_\alpha)_F$ and $\tan^{-1}(\nu l_{\dot{\alpha}}/l_\alpha)$ have been used to plot a series of points in Figure 4.3. These agree quite well with the trend of variation predicted by Reference 4.12, although the magnitude of the correction is different since the value of c/h is different.

4.4 GENERAL THEORY FOR THREE-DIMENSIONAL WINGS

In this section the calculation of tunnel interference for three dimensions will be considered from a general viewpoint; corrections for tunnels with rectangular and circular sections will be left until Sections 4.5.1 and 4.5.2.

It will be assumed that the tunnel is a cylinder of infinite length with generators parallel to the x axis, and that linearized inviscid theory may be used. The model will be assumed to lie in the plane $z = 0$.

At the outset it may be pointed out that, even if the wing is represented by a lifting line, Prandtl's theorem relating the flow at the wing to that far downstream does not apply to oscillatory flow.

Three-dimensional lifting-surface theory has now reached the stage where the calculation of wing loading can be carried out with an accuracy sufficient for application to tunnel interference by one or other of the versions of the "kernel function" or "collocation" theory, for example References 4.13, 4.14 or 4.15. The success of free-stream lifting-surface theory depends on replacing the differential Equation (4.1) by an equivalent integral equation. With the added boundary conditions at the tunnel walls this integral equation becomes extremely complicated. In the absence of special simplifying features an analytical solution of the differential equation is not possible; although a numerical finite-difference treatment might conceivably be attempted with a high-speed computer, no programme for doing so seems to exist. In practice, therefore, we are largely confined to tunnels for which the method of images is possible, or to flow conditions ($M\bar{\nu} \ll 1$) for which the method suggested in Section 4.4.2 is available.

Even when the flow is such that the lifting-surface theory is of doubtful applicability, having for example local supersonic regions or separation from the leading edge of the wing, the theory may be used to estimate the far flow field. Provided that the measured derivatives are available to adjust the predictions of linearized theory, the conditions at the tunnel boundary, and hence the interference upwash, can be established fairly accurately.

4.4.1 Tunnel Resonance

This phenomenon has already been discussed in connection with two-dimensional tunnels, but it seems reasonable to suppose that something similar will occur in three dimensions also.

In Reference 4.16 arguments are put forward to show that for a three-dimensional tunnel the critical frequency for resonance is given by

$$\frac{\omega_r}{U} = \frac{\beta\lambda}{M} , \qquad (4.36)$$

where λ is the smallest eigenvalue of the equation

$$\frac{\partial^2\phi}{\partial y^2} + \frac{\partial^2\phi}{\partial z^2} + \lambda^2\phi = 0 . \qquad (4.37)$$

This equation is to be satisfied inside the empty tunnel cross-section, with the boundary conditions that $\partial\phi/\partial n = 0$ at a solid wall and $\phi = 0$ at an open boundary. Modes for which the derivative of ϕ normal to the plane of the wing is zero, may be ignored. Reference 4.16 includes some calculations for open and closed three-dimensional tunnels and for three-dimensional slotted tunnels. Some experimental evidence supporting the view that resonance effects occur in three dimensions may be found in Reference 4.17.

For a rectangular tunnel with solid roof and floor the relevant critical frequency turns out to be the same as for the two-dimensional tunnel of the same height. If the tunnel has open roof and floor the critical frequency is doubled. For a closed circular tunnel of radius R the critical frequency is given by

$$\frac{\omega_r R}{U} = 1.84\frac{\beta}{M} , \qquad (4.38)$$

where $x = 1.84$ is the first zero of the Bessel function $J_1'(x)$.

For other cross-sections the ease or difficulty of finding the critical resonance frequency is simply that of determining the eigenvalue λ of Equation (4.37); in general this will have to be done numerically.

4.4.2 Relations Between Steady and Unsteady Interference

The basic idea underlying the method given below is due to Goodman (Ref. 4.18; 1953), but the development differs from his.

Let it be assumed that the wing and its wake lie in the plane $z = 0$. Then according to linearized theory[4.13] in an unbounded stream $\bar{\Phi}$ is antisymmetric with respect to z , and

$$\bar{\Phi}(x,y,z) = -\frac{1}{2\pi}\iint \bar{\Phi}(x',y',+0)\,K(x-x',y-y',z)\,dx'dy' \; , \qquad (4.39)$$

where

$$K = \exp\left(\frac{i\omega M^2(x-x')}{U\beta^2}\right)\frac{\partial}{\partial z}\left[\exp\left\{-\frac{i\omega MR_\beta}{U\beta^2}\right\}\Big/R_\beta\right] \qquad (4.40)$$

with

$$R_\beta = [(x-x')^2+\beta^2(y-y')^2+\beta^2z^2]^{\frac{1}{2}} \; . \qquad (4.41)$$

The region of integration in Equation (4.39) is that part of the plane $z = 0$ in which $\bar{\Phi}(x',y',+0) \neq 0$, that is the wing and its wake. If the interference effect can be represented by an image system, Equation (4.39) provides formally a method of calculating the interference flow field due to the images, but the computation would be formidable. Nevertheless a practical procedure can be developed provided ωM is small.

Consider first a steady horse-shoe vortex of circulation $\bar{\Gamma}$ and span $2s$ in an incompressible flow. This may be represented by

$$\left.\begin{aligned}\bar{\Phi}(x,y,+0) &= \tfrac{1}{2}\bar{\Gamma} \quad \text{for} \quad x>0\,, \quad |y|<s\\ &= 0 \quad \text{for} \quad x<0 \quad \text{or} \quad |y|>s\end{aligned}\right\} . \qquad (4.42)$$

Then by Equation (4.39) the associated flow field is given by

$$\Phi = \Phi_v(x,y,z) = -\frac{1}{2\pi}\int_{x'=0}^{\infty}\int_{y'=-s}^{s}\tfrac{1}{2}\bar{\Gamma}\,\frac{(-z)}{[(x-x')^2+(y-y')^2+z^2]^{3/2}}\,dx'dy' \; . \qquad (4.43)$$

Hence

$$\Phi_v = \frac{\bar{\Gamma}z}{4\pi}\int_{-\infty}^{x}\frac{1}{\xi^2+z^2}\left[\frac{(s-y)}{[\xi^2+(s-y)^2+z^2]^{\frac{1}{2}}}+\frac{(s+y)}{[\xi^2+(s+y)^2+z^2]^{\frac{1}{2}}}\right]d\xi \; , \qquad (4.44)$$

so that

$$\frac{\partial\Phi_v}{\partial x} = \frac{\bar{\Gamma}z}{4\pi}\,\frac{1}{x^2+z^2}\left[\frac{(s-y)}{[x^2+(s-y)^2+z^2]^{\frac{1}{2}}}+\frac{(s+y)}{[x^2+(s+y)^2+z^2]^{\frac{1}{2}}}\right] \; . \qquad (4.45)$$

Now consider an oscillatory horse-shoe vortex of the same span with circulation $\Gamma = \bar{\Gamma}e^{i\omega t}$, so that

$$\left.\begin{aligned} \bar{\Phi}(x', y', +0) &= \tfrac{1}{2}\bar{\Gamma}\exp\left(-\frac{i\omega x'}{U}\right) \quad \text{for} \quad x' > 0 , \quad |y'| < s \\ &= 0 \qquad\qquad\qquad\qquad \text{for} \quad x' < 0 \quad \text{or} \quad |y'| > s \end{aligned}\right\} . \tag{4.46}$$

Hence, if the flow is incompressible,

$$\bar{\Phi} = -\frac{\bar{\Gamma}}{4\pi}\int_{x'=0}^{\infty}\exp\left(-\frac{i\omega x'}{U}\right)\int_{y'=-s}^{s}\frac{(-z)}{[(x-x')^2 + (y-y')^2 + z^2]^{3/2}}\,dx'dy' \tag{4.47}$$

$$= \frac{\bar{\Gamma}z}{4\pi}\int_{-\infty}^{x}\exp\left(\frac{i\omega(\xi - x)}{U}\right)\frac{1}{\xi^2 + z^2}\left[\frac{(s-y)}{[\xi^2 + (s-y)^2 + z^2]^{\frac{1}{2}}} + \frac{(s+y)}{[\xi^2 + (s+y)^2 + z^2]^{\frac{1}{2}}}\right]d\xi$$

$$= \int_{-\infty}^{x}\exp\left(\frac{i\omega(\xi - x)}{U}\right)\frac{\partial\Phi_v(\xi, y, z)}{\partial\xi}\,d\xi \quad . \tag{4.48}$$

Alternatively Equation (4.48) may be written

$$\bar{\Phi} = \Phi_v(x, y, z) - \frac{i\omega}{U}\exp\left(-\frac{i\omega x}{U}\right)\int_{-\infty}^{x}\exp\left(\frac{i\omega\xi}{U}\right)\Phi_v(\xi, y, z)\,d\xi \quad . \tag{4.49}$$

Equation (4.49) refers to the free-stream values of $\bar{\Phi}$ and Φ_v. If Φ_v is taken to represent the potential of a horse-shoe vortex in the presence of a tunnel, a function $\bar{\Phi}$ may still be calculated from it by Equation (4.49). Now $\nabla^2\Phi_v = 0$ and it follows from Equation (4.48) and the vanishing of Φ_v and its derivatives at $x = -\infty$ that $\nabla^2\bar{\Phi} = 0$. Moreover, if on the walls $\partial\Phi_v/\partial n = 0$, it follows from Equation (4.48) or (4.49) that $\partial\bar{\Phi}/\partial n = 0$; similarly if $\Phi_v = 0$ at the tunnel boundary, then $\bar{\Phi} = 0$. Thus $\Phi = \bar{\Phi}e^{i\omega t}$ is the oscillatory velocity potential in the presence of the tunnel walls. Since both the free-stream and wind-tunnel values of $\bar{\Phi}$ and Φ_v are related by Equations (4.48) and (4.49), it follows that the interference fields satisfy the same relations.

The foregoing argument is based on the assumption that $M = 0$. If M is not zero then $\bar{\Phi}$ is found by substituting from Equation (4.46) into Equation (4.39). This yields

$$\bar{\Phi}(x, y, z) = -\frac{1}{2\pi}\int_{x'=0}^{\infty}\int_{y'=-s}^{s}\tfrac{1}{2}\bar{\Gamma}\exp\left(-\frac{i\omega x'}{U}\right)K(x-x', y-y', z)\,dx'dy' \quad .$$

that is, by Equations (4.40) and (4.41)

$$\bar{\Phi} = \frac{1}{2\pi}\int_{x'=0}^{\infty}\int_{y'=-s}^{s} \tfrac{1}{2}\bar{\Gamma}\exp\left(-\frac{i\omega x'}{U}\right)\exp\left(\frac{i\omega M^2(x-x')}{U\beta^2}\right)\exp\left(-\frac{i\omega MR_\beta}{U\beta^2}\right)\frac{\beta^2 z}{R_\beta^3}\left(1+\frac{i\omega MR_\beta}{U\beta^2}\right)dx'dy' \, . \tag{4.50}$$

Then by an argument similar to that in Appendix I of Reference 4.19 it can be shown that for small ω Equation (4.50) may be replaced by

$$\bar{\Phi} = \frac{\beta^2\bar{\Gamma}z}{4\pi}\int_{x'=0}^{\infty}\int_{y'=-s}^{s} \exp\left(-\frac{i\omega x'}{U}\right)\exp\left(\frac{i\omega M^2(x-x')}{U\beta^2}\right)\frac{1}{R_\beta^3}\,dx'dy' + 0(\omega^2\log\omega) \, . \tag{4.51}$$

If the integration with respect to y' is performed it follows from Equation (4.45) that

$$\bar{\Phi} = \int_{-\infty}^{x/\beta} \exp\left(-\frac{i\omega x}{U}\right)\exp\left(\frac{i\omega\xi}{U\beta}\right)\frac{\partial\Phi_v(\xi,y,z)}{\partial\xi}\,d\xi + 0(\omega^2\log\omega) \, . \tag{4.52}$$

By virtue of the fact that $\nabla^2\Phi_v = 0$ it follows that $\bar{\Phi}$, as given by the integral in Equation (4.52), satisfies

$$\beta^2\frac{\partial^2\bar{\Phi}}{\partial x^2} + \frac{\partial^2\bar{\Phi}}{\partial y^2} + \frac{\partial^2\bar{\Phi}}{\partial z^2} - \frac{2i\omega M^2}{U}\frac{\partial\bar{\Phi}}{\partial x} - \frac{\omega^2 M^2}{U^2\beta^2}\bar{\Phi} = 0 \, , \tag{4.53}$$

so that, provided ω^2 is negligible, $\bar{\Phi}$ satisfies Equation (4.5). Moreover as for incompressible flow $\bar{\Phi}$ represents flow in the tunnel, or in a free stream, according as Φ_v does so; hence, if Φ_v represents the interference in steady incompressible flow, then $\bar{\Phi}$ is the interference in oscillatory compressible flow with an error of order $\omega^2\log\omega$. An alternative form of Equation (4.52) is

$$\bar{\Phi} = \exp\left(\frac{i\omega M^2 x}{U\beta^2}\right)\Phi_v\left(\frac{x}{\beta}, y, z\right) - \frac{i\omega}{U\beta}\exp\left(-\frac{i\omega x}{U}\right)\int_{-\infty}^{x/\beta}\exp\left(\frac{i\omega\xi}{U\beta}\right)\Phi_v(\xi, y, z)\,d\xi \, , \tag{4.54}$$

which reduces to Equation (4.49) if $M = 0$.

The interference upwash angle due to an oscillatory horse-shoe vortex of span $2s$ and circulation $\Gamma = \bar{\Gamma}e^{i\omega t}$ will be written in the form

$$\frac{w_i}{U} = \frac{\bar{w}_i}{U}e^{i\omega t} = \frac{\bar{\Gamma}e^{i\omega t}}{Ud}\,\delta\left(\frac{x}{d}, \frac{y}{d}, \frac{s}{d}, \frac{\omega d}{U}\right) , \tag{4.55}$$

where d is a representative length of the tunnel cross-section. Then Equation (4.54) becomes

$$\begin{aligned}\delta(\xi\,,\eta\,;\sigma\,,\mu) &= \exp\left(\frac{i\mu M^2\xi}{\beta^2}\right)\delta\left(\frac{\xi}{\beta}\,,\eta\,;\sigma\,,0\right) - \\ &\quad - \frac{i\mu}{\beta}\exp\,(-i\mu\xi)\int_{-\infty}^{\xi/\beta}\exp\left(\frac{i\mu\theta}{\beta}\right)\delta(\theta\,,\eta\,;\sigma\,,0)\;d\theta \\ &= \exp\,(-i\mu\xi)\int_{-\infty}^{\xi/\beta}\frac{\partial}{\partial\theta}[\delta(\theta\,,\eta\,;\sigma\,,0)]\exp\left(\frac{i\mu\theta}{\beta}\right)d\theta\;, \end{aligned} \tag{4.56}$$

where

$$\left.\begin{aligned}\xi &= x/d \\ \eta &= y/d \\ \sigma &= s/d \\ \mu &= \omega d/U\end{aligned}\right\}\;. \tag{4.57}$$

4.4.3 General Interference Corrections

In order to apply the theory of Section 4.4.2, it is necessary to know the interference upwash due to a steady horse-shoe vortex, and moreover this must be known for all points upstream of the model. It is then necessary to express the potential distribution round the oscillating model in terms of those of horse-shoe vortices.

Consider first a steady lift distribution symmetrical with respect to y . It may be shown[4.20] that the interference upwash is given by

$$\begin{aligned}\frac{w_i\,(x,y)}{U} &= \frac{1}{2d}\int_{y'=0}^{s}\int_{x'=x_L(y')}^{x_T(y')}\bar{l}(x'\,,y')\,\frac{\partial}{\partial y'}\left[\delta\left(\frac{x-x'}{d}\,,\;\frac{y}{d}\,;\;\frac{y'}{d}\,,\;\frac{\omega d}{U}\right)\right]dx'dy' \\ &= \frac{1}{2}\int_{\eta'=0}^{\sigma}\int_{\xi'=\xi_L(\eta')}^{\xi_T(\eta')}\bar{l}(\xi'\,,\eta')\,\frac{\partial}{\partial\eta'}\,[\delta(\xi-\xi'\,,\eta\,;\eta'\,,\mu)]\;d\xi'd\eta'\;,\end{aligned} \tag{4.58}$$

where δ is given by Equation (4.56). The planes $y = 0$ and $\eta = 0$ need not be symmetrically situated in the tunnel, indeed the tunnel need not have any symmetry at all provided that it is cylindrical, but δ must refer to a horse-shoe vortex lying in $z = 0$ and symmetrical about $y = 0$.

For a distribution of lift antisymmetrical with respect to $y = 0$, Equation (4.58) will still hold[4.20], provided $\delta(\xi\,,\eta\,;\sigma\,,0)$ now defines the interference upwash angle due to the distribution of potential on $z = +0$ given by

$$\left.\begin{aligned}\Phi &= \frac{y}{2|y|}\,\bar{\Gamma} \quad \text{for} \quad x > 0 \quad \text{and} \quad |y| < s \\ &= 0 \qquad\quad\ \text{for} \quad x < 0 \quad \text{or} \quad |y| > s\end{aligned}\right\} . \tag{4.59}$$

The arguments of Section 4.4.2 apply to such a distribution; in particular Equation (4.56) still holds. Since any lift distribution may be split into symmetrical and antisymmetrical parts, the corresponding interference upwash may be calculated.

Of course in most experiments $\bar{l}$ will not be measured in sufficient detail to apply Equation (4.58) directly. Generally one or more derivatives will be found, that is to say there will be available weighted integrals of $\bar{l}$ over the planform. A possible simplification is to assume that the real and imaginary parts of $\bar{l}$ may be concentrated on the curves passing through their respective theoretical centres of pressure at each spanwise position. Suppose the centres of pressure are defined by

$$\xi' = \xi_R(\eta') \quad \text{and} \quad \xi' = \xi_I(\eta') . \tag{4.60}$$

Then Equation (4.58) becomes

$$\frac{w_i(\xi,\eta)}{U} = \frac{1}{2}\int_0^{\sigma} \left\{ L_R(\eta')\frac{\partial}{\partial\eta'}\,[\delta(\xi_1, \eta; \eta', \mu)] + \right.$$

$$\left. + \, iL_I(\eta')\frac{\partial}{\partial\eta'}\,[\delta(\xi_2, \eta; \eta', \mu)] \right\} d\eta' , \tag{4.61}$$

where

$$L_R(\eta') + iL_I(\eta') = \int_{\xi_L(\eta')}^{\xi_T(\eta')} \bar{l}(\xi', \eta')\, d\xi' , \tag{4.62}$$

and after the differentiation we put

$$\xi_1 = \xi - \xi_R(\eta') , \qquad \xi_2 = \xi - \xi_I(\eta') . \tag{4.63}$$

This should be a valid approximation provided the chord of the wing is small compared with the dimensions of the tunnel.

An alternative method may be found by observing that the circulation round any section of the wing is given by

$$\bar{\Gamma} = \bar{\Gamma}_R + i\bar{\Gamma}_I = \frac{Ud}{2}\int_{\xi_L(\eta')}^{\xi_T(\eta')} \bar{l}(\xi', \eta') \exp\{i\mu[\xi - \xi_T(\eta')]\}\, d\xi' . \tag{4.64}$$

and then regarding $\bar{\Gamma}_R$ and $\bar{\Gamma}_I$ as being concentrated into vortices along the curves $\xi' = \xi_R(\eta')$ and $\xi' = \xi_I(\eta')$. Then in Equation (4.61) L_R must be replaced by

$2\bar{\Gamma}_R/Ud$ and L_I by $2\bar{\Gamma}_I/Ud$. Provided that the chord is small, the difference in the calculated values of w_I/U will be small. If the chord is large neither form will be accurate, but fortunately fairly crude representations of the model are usually satisfactory for interference calculations.

A further approximation is obtained by assuming that the span of the wing, as well as its chord, is small relative to the tunnel. This will be dealt with in Section 4.5.3.

The calculation is very much facilitated when a theoretical treatment by one of the available lifting-surface theories for oscillating wings (e.g. Refs.4.13 to 4.15) is carried out in conjunction with the experiments. If such a calculation has been performed, there are available a theoretical lift distribution and the required theoretical derivatives. Suppose that the wing is oscillating in some mode

$$z = q_0 e^{i\omega t} p(x,y) = q p(x,y) , \qquad (4.65)$$

and that measurements are made of the amplitude q and the generalized forces

$$P_n = \iint_S \bar{l}(x,y) p_n(x,y)\, dx dy \quad (n = 1,2,\ldots.) , \qquad (4.66)$$

where p_n is a weighting function. The theoretical free-stream lift distribution and derivatives $(\partial P_n/\partial q)_F$ may be calculated, and hence the corresponding theoretical interference upwash $\bar{w}_I$ is evaluated from Equation (4.58). Again by lifting-surface theory the distribution $\bar{w}_I$ may be converted into theoretical increments $(\partial P_n/\partial q)_I$ due to wall interference. A linear factor $(P_1/q)/(\partial P_1/\partial q)_F$ is applied to the theoretical free-stream loading, so that it becomes consistent with the measured generalized force P_1 . Then the contribution to P_n due to wall interference is

$$\delta P_n = \frac{P_1 (\partial P_n/\partial q)_I}{(\partial P_1/\partial q)_F} . \qquad (4.67)$$

The wall interference can be regarded as a correction Δq to be applied to the measured amplitude q and residual corrections

$$\Delta P_n = -\delta P_n + \Delta q (\partial P_n/\partial q)_F . \qquad (4.68)$$

It may be convenient to choose

$$\left.\begin{aligned} \frac{\Delta q}{P_1} &= \frac{(\partial P_1/\partial q)_I}{(\partial P_1/\partial q)_F^2} , \\ \text{so that} \quad \Delta P_1 &= 0 \\ \frac{\Delta P_n}{P_1} &= \frac{1}{(\partial P_1/\partial q)_F^2} \left[\left(\frac{\partial P_n}{\partial q}\right)_F \left(\frac{\partial P_1}{\partial q}\right)_I - \left(\frac{\partial P_1}{\partial q}\right)_F \left(\frac{\partial P_n}{\partial q}\right)_I \right] \quad (n \geq 2) \end{aligned}\right\} . \qquad (4.69)$$

The right-hand sides of Equations (4.69) are theoretically determined complex numbers, so that in general Δq involves a phase shift as well as a change in amplitude.

If only one force has been measured there is no choice in the above procedure, but if several have been measured some care must be taken. For example, if P_n is a control hinge moment giving no information about $\bar{l}(x,y)$ off the control surface, then it is probably best to take P_1 to be the overall lift, if this is measured or can be estimated.

4.5 APPLICATION TO THREE-DIMENSIONAL WINGS IN CLOSED TUNNELS

The general theory of Section 4.4 is now applied to closed rectangular and circular tunnels (Sections 4.5.1 and 4.5.2). There are great simplifications for small wings (Section 4.5.3), and these form the basis of an approximate treatment of wall interference for oscillating slender wings (Section 4.5.4). Some numerical examples are given in Section 4.5.5.

4.5.1 Rectangular Tunnels

Before applying the theory developed above we observe that, since the interference in a rectangular tunnel may be represented by an image system, expressions for the interference potential may be written down at once by a simple extension of free-stream subsonic lifting-surface theory. For a wing symmetrically placed in a closed rectangular tunnel the kernel function in Equation (4.39) has to be replaced by

$$\sum_{m=-\infty}^{\infty}\sum_{n=-\infty}^{\infty}(-1)^n K(x-x',\, y-y'-mb,\, z-z'-nh) \quad , \tag{4.70}$$

where b is the breadth of the tunnel and h its height. The interference upwash for a given $\bar{\Phi}(x',\, y',\, +0)$ is obtained by omitting the term $m = n = 0$ from the double summation; alternatively Equation (4.39) as modified by Equation (4.70) may be regarded as an integral equation for $\bar{\Phi}(x',\, y',\, +0)$. The same remarks apply to an alternative form of lifting-surface theory such as Reference 4.15 which uses the loading $\bar{l}$ as the unknown instead of $\bar{\Phi}$. For the wing symmetrically situated in a rectangular tunnel this gives

$$\frac{\bar{w}(x,y,0)}{U} = \lim_{z\to 0}\left[-\frac{1}{8\pi}\iint_S \bar{l}(x',\, y')\sum_{m=-\infty}^{\infty}\sum_{n=-\infty}^{\infty}(-1)^n\tilde{K}(x-x',\, y-y'-mb,\, z-nh)\, dx'dy'\right] \; . \tag{4.71}$$

where

$$\tilde{K}(x-x',\, y-y',\, z) = \frac{\partial^2}{\partial z^2}\int_{-\infty}^{x-x'}\frac{\exp\left\{-\frac{i\omega}{U}\left[(x-x')-\frac{\tilde{\xi}}{\beta^2}+\frac{M}{\beta^2}\sqrt{\tilde{\xi}^2+\beta^2(y-y')^2+\beta^2z^2}\right]\right\}}{\sqrt{\tilde{\xi}^2+\beta^2(y-y')^2+\beta^2z^2}}\, d\tilde{\xi} \; . \tag{4.72}$$

Unfortunately both of the expressions Equations (4.70) and (4.71) are too unwieldy for practical computation, except in special cases. Moreover, in view of the remarks on tunnel resonance in Section 4.4.1, it may be expected that the sums will become infinite for critical values of ω.

In order to apply the method proposed in Section 4.4.2 it is necessary to consider first the interference in the steady case. From Equation (4.55) and Equation (7) of Reference 4.20 it may be shown that*

$$\delta(\xi,\eta;\sigma,0) = \frac{d}{b}\left\{F_1\left(\frac{x}{b},\frac{y-s}{b}\right) - F_1\left(\frac{x}{b},\frac{y+s}{b}\right)\right\} . \tag{4.73}$$

where

$$\begin{aligned} F_1(\kappa,\lambda) = \frac{1}{4\pi}\frac{b}{h}\Bigg\{ & f_1\left(\frac{b\kappa}{h},\frac{b\lambda}{h}\right) + \pi\,\mathrm{cosech}\frac{\pi b\lambda}{h} - \frac{h}{b\lambda} + \\ & + \sum_{m=1}^{\infty}\left[f\left(\frac{b\kappa}{h},\frac{b(\lambda+m)}{h}\right) + f\left(\frac{b\kappa}{h},\frac{b(\lambda-m)}{h}\right) + \right. \\ & \left. + \pi\,\mathrm{cosech}\frac{\pi b(\lambda+m)}{h} + \pi\,\mathrm{cosech}\frac{\pi b(\lambda-m)}{h}\right]\Bigg\} , \end{aligned} \tag{4.74}$$

$$f(x,y) = \sum_{n=-\infty}^{\infty}(-1)^n\frac{xy}{\sqrt{x^2+y^2+n^2}}\left\{\frac{1}{x^2+n^2}+\frac{1}{y^2+n^2}\right\} , \tag{4.75}$$

and

$$f_1(x,y) = f(x,y) - \frac{xy}{\sqrt{x^2+y^2}}\left\{\frac{1}{x^2}+\frac{1}{y^2}\right\} . \tag{4.76}$$

Tables of $f(x,y)$ may be found in Reference 4.20.

Then by Equations (4.73) and (4.56)

$$\begin{aligned} \delta(\xi,\eta;\sigma,\mu) = \exp(-i\mu\xi)\int_{-\infty}^{\xi/\beta} & \frac{d}{b}\frac{\partial}{\partial\theta}\left[F_1\left(\frac{\theta d}{b},\frac{d(\eta-\sigma)}{b}\right) - \right. \\ & \left. - F_1\left(\frac{\theta d}{b},\frac{d(\eta+\sigma)}{b}\right)\right]\exp\left(\frac{i\mu\theta}{\beta}\right)d\theta . \end{aligned} \tag{4.77}$$

---

* In Reference 4.20 the typical length d was taken to be the tunnel breadth b ; in the present exposition d will be left general until numerical examples are given in Section 4.5.5.

No difficulty arises in these calculations since the series in Equation (4.74) is rapidly convergent, and the infinite integral in Equation (4.77) converges by virtue of the fact that $F_1 = O(\xi^{-2})$ as $\xi \to \infty$.

If μ is small,

$$\delta(\xi,\eta;\sigma,\mu) = \frac{d}{b}\left(1+\frac{i\mu M^2\xi}{\beta^2}\right)\left[F_1\left(\frac{\xi d}{\beta b}, \frac{d}{b}(\eta-\sigma)\right) - F_1\left(\frac{\xi d}{\beta b}, \frac{d}{b}(\eta+\sigma)\right)\right] -$$

$$- \frac{i\mu d}{\beta b}\int_{-\infty}^{\xi/\beta}\left[F_1\left(\frac{\theta d}{b}, \frac{d(\eta-\sigma)}{b}\right) - F_1\left(\frac{\theta d}{b}, \frac{d(\eta+\sigma)}{b}\right)\right] d\theta \ . \qquad (4.78)$$

Further, it follows from Equation (4.77) that δ tends to zero as μ tends to infinity.

The function required for the calculation of the interference upwash by Equation (4.58) or (4.61) is $\partial[\delta(\xi,\eta;\eta',\mu)]/\partial\eta'$. If we put

$$F_2(\kappa,\lambda) = -\frac{\partial F_1(\kappa,\lambda)}{\partial\lambda} \qquad (4.79)$$

and

$$G(\xi,\eta;\mu) = \frac{d^2}{b^2}\exp\left(\frac{i\mu M^2\xi}{\beta^2}\right)F_2\left(\frac{\xi d}{\beta b}, \frac{\eta d}{b}\right) -$$

$$- \frac{i\mu d^2}{\beta b^2}\exp(-i\mu\xi)\int_{-\infty}^{\xi/\beta}\exp\left(\frac{i\mu\theta}{\beta}\right)F_2\left(\frac{\theta d}{b}, \frac{\eta d}{b}\right) d\theta \ , \qquad (4.80)$$

then

$$\frac{\partial}{\partial\eta'}[\delta(\xi,\eta;\eta',\mu)] = G(\xi,\eta-\eta';\mu) + G(\xi,\eta+\eta';\mu) \ , \qquad (4.81)$$

and, by Equation (4.58), for a symmetrical lift distribution,

$$\frac{w_i(\xi,\eta)}{U} = \frac{1}{2}\int_{\eta'=-\sigma}^{\sigma}\int_{\xi'=\xi_L(\eta')}^{\xi_T(\eta')} \bar{l}(\xi',\eta')G(\xi-\xi', \eta-\eta';\mu)\, d\xi' d\eta' \ . \qquad (4.82)$$

The interference upwash will be required at whatever set of points is employed in the lifting-surface theory used to estimate $\bar{l}$. This fixes the set of values of (ξ,η) in Equation (4.82), and hence the region in which $G(\xi,\lambda;\mu)$ has to be determined. The tabulation of $G(\xi,\lambda;\mu)$ in this region is the main part of the computation involved, and has to be followed by integration over the planform. This method involves too much numerical work to be generally practicable.

The approximate Equation (4.61) may be written

$$\frac{\bar{w}_1(\xi,\eta)}{U} = \frac{1}{2}\int_{\eta'=-\sigma}^{\sigma} \{L_R(\eta')G[\xi-\xi_R(\eta'),\, \eta-\eta';\, \mu] + $$

$$+ iL_I(\eta')G[\xi-\xi_I(\eta'),\, \eta-\eta';\, \mu]\}\, d\eta' \quad . \qquad (4.83)$$

This still involves the tabulation of $G(\xi, \eta; \mu)$ for one or more values of μ, although only a single integration is necessary after that. A few examples of calculations by this method are given in Reference 4.20.

For routine use it is desirable to represent the vorticity distribution over the wing by discrete horse-shoe vortices, as few in number as possible. The calculation then reduces to the determination of δ for each of them. By Equation (4.77) this involves the calculation of $F_1(\xi,\lambda)$ for several specified values of λ and all points, ξ, upstream of the model.

The calculation for antisymmetrical lift distributions is formally similar; the basic equations may be found in Reference 4.20.

4.5.2 Circular Tunnels

Just as for the rectangular tunnel, the first point which arises is the availability of the interference upwash of a horse-shoe vortex in steady flow. In Reference 4.21 expressions are obtained for the interference upwash due to an elementary horse-shoe vortex arbitrarily situated in the tunnel, but they are rather complicated infinite series and only a few numerical values are given. Eisenstadt (Ref. 4.22; 1947) has given tables of interference upwash for horse-shoe vortices covering a range of spans and upwash positions which should be adequate for the majority of wings. Eisenstadt's tables include the interference upwash for horse-shoe vortices with swept cross-stream parts and can moreover be used for antisymmetrical as well as symmetrical lift distributions.

Once the required steady data have been obtained, the procedure of Reference 4.23 can be applied; this is almost identical to that for a rectangular tunnel, and it is unnecessary to elaborate on it here. The results of a typical calculation are given in Section 4.5.5.

4.5.3 Small Wings

If the overall chord and span are both small compared with the tunnel dimensions, the lift may be regarded as being concentrated at a single point. Consider first a closed rectangular tunnel and suppose the small wing is at the origin. Equation (4.82) then becomes

$$\frac{\bar{w}_1}{U} = \frac{S\bar{C}_L}{2d^2}\, G(\xi, \eta; \mu) \quad . \qquad (4.84)$$

Since the wing is small, only small values of ξ and η need be included. Take $\eta = 0$ and suppose that ξ^2 is negligibly small. Then by Equations (4.80) and (4.84),

$$\frac{\bar{w}_1(\xi,0)}{U} = \frac{S\bar{C}_L}{2b^2}\left[F_2(0,0) + \frac{\xi d}{\beta b} F_2'(0,0) - \right.$$

$$- i\mu\xi\, F_2(0,0) - \frac{i\mu}{\beta}\int_{-\infty}^{0} F_2\left(\frac{\theta d}{b},\, 0\right) \exp\left(\frac{i\mu\theta}{\beta}\right) d\theta -$$

$$\left. - \mu^2 \frac{\xi}{\beta}\int_{-\infty}^{0} F_2\left(\frac{\theta d}{b},\, 0\right) \exp\left(\frac{i\mu\theta}{\beta}\right) d\theta\right] . \qquad (4.85)$$

where

$$F_2'(0,0) = \left[\frac{\partial F_2(\kappa,\lambda)}{\partial \kappa}\right]_{\kappa=\lambda=0} .$$

If also μ is small, Equation (4.85) may be written as

$$\frac{\bar{w}_1(\xi,0)}{U} = \frac{S\bar{C}_L}{bh}\left\{\delta_0 + \frac{x}{h}\,\delta_1 + i\,\frac{\omega h}{U}\left(\delta_0' + \frac{x}{h}\,\delta_1'\right) + 0\left(\frac{x^2}{h^2}\right)\right\} , \qquad (4.86)$$

where

$$\left.\begin{aligned} \delta_0 &= \frac{h}{2b}\,F_2(0,0) \\ \delta_1 &= \frac{h^2}{2\beta b^2}\,F_2'(0,0) \\ \delta_0' &= -\frac{1}{2\beta}\int_{-\infty}^{0} F_2(\kappa,0)\,d\kappa \\ \delta_1' &= -\,\delta_0 \end{aligned}\right\} . \qquad (4.87)$$

By Equations (4.74), (4.75), (4.76) and (4.79), and by virtue of the fact that

$$\pi\,\mathrm{cosech}\,\pi y = \frac{1}{y} + 2\sum_{n=1}^{\infty} (-1)^n \frac{y}{y^2 + n^2} . \qquad (4.88)$$

it follows that

$$F_2(0,0) = \frac{b^2}{4\pi}\sum_{m=-\infty}^{\infty}\sum_{n=-\infty}^{\infty}(-1)^n \frac{m^2b^2 - n^2h^2}{(m^2b^2 + n^2h^2)^2} , \quad (m,n \neq 0,0) . \tag{4.89}$$

so that we recover the usual expression for steady interference (cf. $\delta_0^{(1)}$ in Section 3.2.2). A more straightforward method of tabulating $\delta_0 , \delta_1 , \delta_0' , \delta_1'$ is described in Reference 4.23, which includes a table of their values. They are plotted in Figure 4.4.

Reference 4.23 also gives, for incompressible flow, the interference upwash for a small wing in a closed circular tunnel of radius R ; by Equation (4.56) the compressibility factors are the same as in Equations (4.87), and hence

$$\frac{\bar{w}_1}{U} = \frac{S\bar{C}_L}{\pi R^2}\left[\delta_0 + \frac{x}{2R}\delta_1 + \frac{i\omega R}{U}\left(\delta_0' + \frac{x}{2R}\,\delta_1'\right)\right] , \tag{4.90}$$

where

$$\left.\begin{aligned} \delta_0 &= 0.125 , & \delta_1 &= 0.25\,\beta^{-1} \\ \delta_0' &= -0.07\,\beta^{-1} , & \delta_1' &= -0.25 \end{aligned}\right\} . \tag{4.91}$$

Goodman[4.18] has given an analysis by a method basically that of Section 4.4.2 for the small wing in the circular tunnel, but without assuming that x and $\omega R/U$ are small. The results are presented in the form of a chart which, apart from a number of misprints, appears to be consistent with Equations (4.91).

For a tunnel of any cross-section the quantities $\delta_0 , \delta_1 , \delta_0'$ and δ_1' may be found from Equation (4.56) provided $\delta(\xi , \eta ; \sigma , 0)$ is known.

An alternative approach, valid when $M = 0$, has been given by W.P.Jones (Ref.4.24; 1943). His method may be illustrated by referring to Equation (4.71) which, for $M = 0$, leads to the following expression for the interference upwash

$$\frac{\bar{w}_1}{U} = -\frac{1}{8\pi}\iint_S \bar{l}(x',y') \int_{-\infty}^{x-x'} \exp\left(-\frac{i\omega(x-x')}{U}\right)\exp\left(\frac{i\omega\xi}{U}\right) \times$$

$$\times \sum_{m=-\infty}^{\infty}\sum_{n=-\infty}^{\infty}(-1)^n \frac{[2n^2h^2 - (y' + mb)^2 - \xi^2]}{[\xi^2 + (y' + mb)^2 + n^2h^2]^{5/2}}\, d\xi\, dx'\, dy' , \quad (m,n \neq 0,0) , \tag{4.92}$$

where it is assumed that w_1/U is independent of y . When it is also assumed that the wing is small, Equation (4.92) leads to

$$\frac{\bar{w}_i}{U} = -\frac{1}{8\pi}\iint\limits_S \bar{l}(x',y')\,dx'dy'\left\{\left(1-\frac{i\omega x}{U}\right)\int_{-\infty}^{0}\exp\left(\frac{i\omega\xi}{U}\right)\sum_{m=-\infty}^{\infty}\sum_{n=-\infty}^{\infty}{}'(-1)^n\frac{(2n^2h^2-m^2b^2-\xi^2)}{[\xi^2+m^2b^2+n^2h^2]^{5/2}}d\xi\,+\right.$$

$$\left.+\,x\sum_{m=-\infty}^{\infty}\sum_{n=-\infty}^{\infty}{}'(-1)^n\frac{2n^2h^2-m^2b^2}{(m^2b^2+n^2h^2)^{5/2}}+o(x)\right\}\qquad (m,n\neq 0,0)\ . \qquad (4.93)$$

The second summation is that encountered as $\delta_1^{(1)}$ in the treatment of steady interference given in Section 3.2.2. The integrals in Equation (4.93) are studied in Reference 4.24 and reduced to tractable expressions.

4.5.4 Slender Wings

If the model is very slender, it may be regarded as made up of a number of small wings arranged in the streamwise direction. Consider a slender wing oscillating with small frequency parameter in a closed rectangular tunnel. It follows from Equation (4.86) that the interference upwash is given by[4.25]

$$\frac{\bar{w}_i}{U}(x,0) = \frac{1}{bh}\iint\limits_S \bar{l}(\xi,y)\left[\delta_0+\frac{x-\xi}{h}\delta_1+\frac{i\omega h}{U}\left(\delta_0'+\frac{x-\xi}{h}\delta_1'\right)\right]d\xi dy$$

$$= \frac{S}{bh}\left\{\bar{C}_L\left[\delta_0+\frac{x}{h}\delta_1+\frac{i\omega h}{U}\left(\delta_0'+\frac{x}{h}\delta_1'\right)\right]+\frac{\bar{c}}{h}\bar{C}_m\left[\delta_1+\frac{i\omega h}{U}\delta_1'\right]\right\}\ , \qquad (4.94)$$

where δ_0, δ_1, δ_0' and δ_1' are given in Equations (4.87), and $\bar{C}_m$ refers to the nose-up pitching moment about the axis $x = 0$. A similar formula may be constructed for any tunnel for which δ_0, δ_1, δ_0' and δ_1' are known.

The interference upwash may be used to calculate the overall corrections to forces and moments as for general wings, but since the wing is slender the aerodynamics are considerably simplified, especially because $\bar{w}_i$ may be regarded as independent of y. From the formula of unsteady slender-wing theory[4.26] the correction to lift per unit length in the streamwise direction corresponding to $\bar{w}_i$ is

$$\Delta L(x) = -\pi\rho U^2\left\{s(x)^2\left[\frac{\partial}{\partial x}+\frac{i\omega}{U}\right]\frac{\bar{w}_i}{U}+2s(x)\,\frac{ds(x)}{dx}\,\frac{\bar{w}_i}{U}\right\}\ , \qquad (4.95)$$

where $s(x)$ is the local span.

An example of the application of Equations (4.94) and (4.95) may be found in Reference 4.25.

4.5.5 Numerical Examples

Only a small amount of numerical data on the numerical corrections to three-dimensional wings has been published, and this is entirely confined to incompressible flow. The reason is obviously the fact that heavy computation is involved unless drastic simplifying assumptions are made. The earliest attempt on the problem seems to be that by W.P.Jones (Ref.4.24; 1943) described in Section 4.5.3. It is assumed that the wing is small although the frequency is left general. Some numerical values are given for the corrected and uncorrected pitching derivatives of rectangular wings in a tunnel of square cross-section.

An example of calculation for which the wing was not assumed to be small is given in Reference 4.23. A model with the swept planform shown in Figure 4.5 was assumed to be performing low-frequency pitching oscillations in the closed circular tunnel shown there. Two pitching axes were considered, as shown in Figure 4.5. The theoretical pitching derivatives, as determined by the method of Reference 4.19, are given in the following table.

x_0/c_r	l_α	$l_{\dot\alpha}$	$-m_\alpha$	$-m_{\dot\alpha}$
0.613	0.852	0.892	0.055	0.301
0.738	0.852	0.738	−0.099	0.159

It was assumed that the parts of the circulation in phase and in quadrature with the incidence could be regarded as concentrated in horse-shoe vortices with their finite parts swept through 60° and semi-span equal to 0.35 of the tunnel radius. The position and strength of these vortices are then easily calculated from the pitching derivatives given above, and are plotted in Figure 4.5. Since the interference for steady horse-shoe vortices of this planform is tabulated in Reference 4.22, it is a straightforward matter to calculate the required oscillatory interference upwash distribution by Equation (4.56). Since the interference forces were also calculated by the method of Reference 4.19 with 2 chordwise and 5 spanwise stations, these upwashes were in fact required at only six points on the half wing. The overall interference increments to the derivatives for the two pitching axes are given below.

x_0/c_r	$\delta(l_\alpha)$	$\delta(l_{\dot\alpha})$	$\delta(-m_\alpha)$	$\delta(-m_{\dot\alpha})$
0.613	0.051	0.004	0.008	0.001
0.738	0.051	−0.005	−0.001	0.009

It is interesting to compare these values with those obtained by the "small-wing" method of Section 4.5.3, which gives

x_h/c_r	$\delta(l_\alpha)$	$\delta(l_{\dot\alpha})$	$\delta(-m_\alpha)$	$\delta(-m_{\dot\alpha})$
0.613	0.051	0.013_5	0.009	0.003
0.738	0.051	0.004	−0.001	0.001

The differences between the values computed by the two methods are negligible except for $\delta l_{\dot\alpha}$ when it is of order 0.01. Even this is only marginally significant compared with the accuracy of present experimental techniques. The inference is that, for wings up to the size shown in Figure 4.5, the small-wing approximation is probably adequate, when the frequency parameter is small.

The small-wing theories of Jones[4.24] and Goodman[4.18] both predict that the interference effects decrease rapidly to zero when the frequency parameter becomes large, but nevertheless remain significant over much of the practical range. This effect may be illustrated by Figures 4.6(a) and (b) which show respectively the in-phase and quadrature components of interference upwash in a closed 9 x 7 rectangular tunnel due to a horse-shoe vortex with $2s/b = 0.4$. Note how, for positive ξ, the in-phase part decreases as μ increases, while the part in quadrature at first increases but eventually starts to decrease.

The effect of model size and frequency may be illustrated by some calculations from Reference 4.20. A cropped delta wing of aspect ratio $2s/\bar{c} = 1.8$ and taper ratio, $c_t/c_r = 1/7$ is assumed to be performing pitching oscillations about an axis through its apex in a closed rectangular 9 x 7 tunnel. The load distributions are calculated by the lifting-surface theories of References 4.19 and 4.27 for the low and finite frequency cases respectively, and the interference upwash is obtained from Equation (4.31) with the lift replaced by the circulation as suggested after Equation (4.64). The results obtained may be summarized as in the following table in the notation of Section 4.4.3.

$\dfrac{\omega b}{U}$	$\dfrac{2s}{b}$	$\dfrac{\Delta\alpha_0}{\bar{C}_L}$	$\dfrac{\Delta\bar{C}_m}{\bar{C}_L}$
→ 0	0.25	$0.006 - i\mu\ 0.003$	$0.001 - i\mu\ 0.001$
→ 0	0.50	$0.029 - i\mu\ 0.027$	$0.006 - i\mu\ 0.008$
→ 0	0.75	$0.076 - i\mu\ 0.103$	$0.020 - i\mu\ 0.025$
1.6	0 50	$0.009 - i\mu\ 0.008$	$-0.001 - i\mu\ 0.002$

These corrections are given as a correction to α_0 and a residual correction to $\bar{C}_m$. The complex value of $\bar{C}_L$ would be determined from wind-tunnel measurements. We may note the rapid increase in the corrections as $2s/b$ increases, and that the correction to incidence involves a change of phase as well as magnitude. Indeed it is obvious that for $2s/b = 0.75$ the model would be too large for measurements to be satisfactory. The effect of taking the frequency to be no longer small is a large reduction in the corrections, as might be expected from the results of Reference 4.10 and Figure 4.6. Of course these remarks apply only to this particular configuration, and it would be rash to generalize them.

4.6 PERFORATED AND SLOTTED WALLS

The use of ventilated tunnels is essential, if a fixed wall geometry is to be preserved for measurements in transonic flow. The usual way of achieving this is to use either a perforated tunnel, having a large number of small holes in one or more of its sides, or a slotted tunnel, usually with the slots parallel to the direction of flow.

In practice, tunnels with perforated walls are the less common, but most of the available oscillatory theories are in fact concerned with them and relate to the boundary condition in Equation (4.7). It is assumed that the perturbation velocities are small, so that Equation (4.7) is taken in its linearized form

$$\frac{\partial\bar{\Phi}}{\partial n} + P\left[\frac{\partial\bar{\Phi}}{\partial x} + \frac{i\omega}{U}\bar{\Phi}\right] = 0 \quad . \tag{4.96}$$

For perforated tunnels to be amenable to these theories, it is necessary to find a constant value of P to use in Equation (4.96), which then becomes a simple homogeneous boundary condition. The parameter P for steady flow in perforated tunnels is discussed in Section 6.7. It is not known whether the parameter should remain unchanged for oscillatory flow; possibly P should then be complex, and results obtained using Equation (4.96) should not be trusted if the frequency is large.

The two-dimensional problem of a slowly oscillating aerofoil symmetrically situated between perforated walls has been investigated by Drake[4.28,4.29], using the boundary condition Equation (4.96). He derives an integral equation expressing the known upwash distribution on the aerofoil as a weighted integral of the lift distribution $\bar{l}$, and obtains solutions by expanding $\bar{l}$ in a series similar to that in Equation (4.34) with coefficients assumed to be linear functions of frequency. Unfortunately the expressions for the derivatives given in Reference 4.29 are incorrect.

There is an alternative treatment due to Rosenblat[4.30], which is restricted to low-frequency oscillations in incompressible flow. The derivatives are given as complicated analytical expressions and have not been evaluated.

Drake[4.31] has also treated some transonic flow problems involving perforated tunnels by solving Equation (4.9) for the following three cases

(i) two-dimensional wing midway between two perforated walls,

(ii) slender wing midway between infinite perforated roof and floor,

(iii) slender wing in a rectangular tunnel with solid side-walls and perforated roof and floor.

In all these cases mathematical difficulties require that the frequency parameter is small, and in (ii) and (iii) that the porosity parameter is small. The use of Equation (4.9) also imposes the restriction[4.32] that the thickness has to be very small. Drake's formulae for the derivatives are too lengthy to be given here, but are for the most part fairly straightforward to evaluate numerically.

The homogeneous boundary condition for steady flow in slotted tunnels is given in Chapter VI as Equation (6.7). The corresponding condition for oscillatory flow is not known with certainty, but from the analysis of Reference 4.40 it seems plausible to assume that it should be

$$\left(\frac{\partial}{\partial x} + \frac{i\omega}{U}\right)\left(\bar{\Phi} + K\frac{\partial\bar{\Phi}}{\partial n}\right) + \frac{1}{P}\frac{\partial\bar{\Phi}}{\partial n} = 0 \ , \tag{4.97}$$

where, for rectangular tunnels with solid side-walls and the roof and floor each having N equally spaced slots of width a,

$$K = \frac{b}{\pi N}\log_e \operatorname{cosec}\frac{\pi N a}{2b} \ . \tag{4.98}$$

Equation (4.97) is perhaps harder to apply than the boundary condition for the perforated tunnel in Equation (4.96), while its validity is possibly even more dubious if the frequency is large.

It is now necessary to enquire if the steady and unsteady interference flow fields in ventilated tunnels are related by the simple Equation (4.56). This depends on whether or not the unsteady potential $\bar{\Phi}$, defined by Equation (4.48) or (4.52), satisfies the unsteady boundary condition when Φ_v satisfies the steady boundary condition. It may be deduced that this is not true for tunnels with boundary condition (4.96) or (4.97), because these both contain additional terms in ω when the flow is oscillatory. Nevertheless, when viscosity is negligible so that $P \to \infty$, Equation (4.97) becomes

$$\bar{\Phi} + K\frac{\partial\bar{\Phi}}{\partial n} = 0 \ ,$$

and it follows that the oscillatory and steady interference fields do satisfy Equation (4.56). Alternatively, if the boundary of a longitudinally slotted tunnel may be regarded as a finite number of solid and open portions on which the boundary conditions are $\partial\bar{\Phi}/\partial n = 0$ and $\bar{\Phi} = 0$ respectively, then the argument following Equation (4.48) remains valid and Equation (4.56) is applicable.

There is experimental evidence that the interference in slotted-wall tunnels may be very large for some unsteady experiments. References 4.33 and 4.34 describe some measurements of pitching derivatives made in various rectangular tunnels with longitudinally slotted roof and floor. As shown in Figure 4.7, it has been found that by varying the number of slots very large changes are caused in the pitching damping derivative of a half-model M-wing in the NPL 25 in. by 20 in. Wind Tunnel. The parameter T is defined by

$$T = \frac{h - K}{h + K} , \qquad (4.99)$$

so that $T = -1$ corresponds to a completely closed tunnel and $T = +1$ to a tunnel with solid side-walls and open roof and floor. Remarkably similar results have been obtained for an unswept tapered half-model in the same tunnel; in both cases the presence of slots reduces $-m_{\dot\alpha}$ by the order of 25% at $M = 0.80$ to 40% or more at high subsonic Mach numbers. These large effects are not characteristic of all slotted tunnels and apparently do not occur on oscillating half-models in the NPL 36 in. by 14 in. Wind Tunnel. Nevertheless unsteady interference effects in ventilated tunnels pose an important problem. Unfortunately no satisfactory theoretical solutions for slotted tunnels are yet available.

Garner and Moore[4.41*] have found some explanation of the large interference effects in Figure 4.7 by considering the limiting case $T = +1$. The small-wing theory of Section 4.5.3, in particular Equation (4.86), may in principle be applied to any tunnel for which δ_0, δ_1, δ_0' and δ_1' are known. A half model in the NPL 25 in. by 20 in. Tunnel corresponds closely to a complete model in a duplex tunnel $(b = 2h)$; for such a tunnel with solid side-walls and open floor and roof it is calculated that $\delta_0' = +0.159\,\beta^{-1}$ as compared with $\delta_0' = -0.004\,\beta^{-1}$ for a completely closed tunnel of the same cross-section. The term in δ_0' in Equation (4.86) is particularly important, as it is inversely proportional to a linear dimension of the tunnel while the next terms are inversely proportional to tunnel area. It is now possible to make a theoretical estimate of the difference between $-m_{\dot\alpha}$ for $T = -1$ and for $T = +1$ on the hypothesis that the wing is small. Computations for the M-wing at Mach numbers 0.6 and 0.8 for the pitching axis indicated in Figure 4.7 give respective differences

$$[-m_{\dot\alpha}]_{T=+1} - [-m_{\dot\alpha}]_{T=-1} = -0.55 \quad \text{and} \quad -0.81 \; ;$$

these are consistent with Figure 4.7. The calculated effect of compressibility is slightly greater than the factor β^{-1} in δ_0'; this appears to explain the larger differences observed at $M = 0.8$ and above. The same conclusions are derived for the unswept tapered wing tested in the same tunnel.

4.7 STEADILY ROTATING MODELS

Suppose that a wing of symmetrical planform has its line of symmetry in the direction of the airflow while rotating with a constant angular velocity ω about the line of symmetry. It will be assumed that the vorticity shed at the trailing edge is convected downstream in a direction parallel to the velocity of the undisturbed fluid

---

[*] Reference 4.41 is superseded by the fully theoretical and experimental study in the following paper:

Garner, H.C. et al. *The Theory of Interference Effects on Dynamic Measurements in Slotted-Wall Tunnels at Subsonic Speeds and Comparison with Experiment.* NPL Aero. Report 1211, ARC Report 28,339, 1966.

flow, so that each element of the trailing vortex sheet will be a helix with pitch inversely proportional to ω. Obviously the theory of the rolling wing may be expected to be closely related to that of the screw propeller[4.35]; in fact the treatment of the circular tunnel given in Section 4.7.1 is an extension by Mandl and Pounder (Ref.4.36; 1951) of Goldstein's theory (Ref.4.37; 1929).

The assumption that the trailing vortices are exactly helical implies that the circulation is small, and therefore that the induced drag is small, and hence, in most cases, that the total drag is also small. By the momentum theory of wall interference on propellers (Ref.4.3, Chap.XVII), if the thrust coefficient is small and negative, then the correction to the tunnel stream velocity may be neglected even in closed tunnels.

If the rotation is sufficiently slow, the helical nature of the vortex sheet will be negligible and the tunnel interference may be calculated by the theory for steady wings with antisymmetrical loading. However, in order to establish the range of ω for which this method would be sufficiently accurate, it is necessary to consider the effect of non-zero angular velocity. Only for a circular tunnel cross-section is such an investigation practicable.

4.7.1 General Theory for Circular Tunnels

The following analysis is essentially that of Reference 4.36* with different notation and sign conventions. Both the flow in the tunnel and that in the free stream will be assumed to have a velocity potential satisfying Laplace's equation

$$\nabla^2\Phi = \frac{\partial^2\Phi}{\partial r^2} + \frac{1}{r}\frac{\partial\Phi}{\partial r} + \frac{1}{r^2}\frac{\partial^2\Phi}{\partial\theta^2} + \frac{\partial^2\Phi}{\partial x^2} = 0 \qquad (4.100)$$

in cylindrical polar co-ordinates (x, r, θ) where

$$\left.\begin{aligned} y &= r\cos\theta \\ z &= r\sin\theta \end{aligned}\right\} , \qquad (4.101)$$

such that the angular rolling velocity ω is in the sense of θ increasing. Far downstream the flow field will have helical symmetry so that Φ must satisfy

$$\Phi(r, \theta + \omega\delta t, x + U\delta t) = \Phi(r, \theta, x) ,$$

where δt is an arbitrary increment of time. Thus

$$\omega\frac{\partial\Phi}{\partial\theta} = -U\frac{\partial\Phi}{\partial x} , \qquad (4.102)$$

and Equation (4.100) becomes

---

* This paper contains several errors of sign.

$$\frac{\partial^2\Phi}{\partial r^2} + \frac{1}{r}\frac{\partial\Phi}{\partial r} + \left(\frac{\omega^2}{U^2} + \frac{1}{r^2}\right)\frac{\partial^2\Phi}{\partial\theta^2} = 0 \ . \tag{4.103}$$

The boundary conditions are $\partial\Phi/\partial r = 0$ on a solid wall, $\Phi = 0$ at the boundary of an open jet, and for the free stream $\Phi \to 0$ as $r \to \infty$.

Now consider Φ at a time when the wing is in the position $\theta = \pm\frac{1}{2}\pi$. Let the circulation on the upper half $(\theta = \frac{1}{2}\pi)$ be $\Gamma(r)$. Then the boundary conditions to be satisfied by Φ on the line $\theta = \pm\frac{1}{2}\pi$ are shown in Figure 4.8. Let the wing be a lifting line in the plane $x = 0$. By considerations analogous to those used in steady flow it follows that at the wing the normal velocity induced by the vortex system is

$$\frac{1}{2}\left(\frac{1}{r}\frac{\partial\Phi}{\partial\theta}\right)_{\theta=\frac{1}{2}\pi} \ ,$$

where Φ has its value in the helical wake far downstream. Thus the problem of finding the interference velocity is reduced to solving Equation (4.103) subject to the boundary conditions in Figure 4.8. The first step in obtaining a solution is the removal of the discontinuities across the line $\theta = \pm\frac{1}{2}\pi$. From the theory of Fourier series it follows that

$$\frac{\Gamma(r)}{\pi}\sum_{n=1}^{\infty}\frac{(-1)^n}{n}\sin 2n\theta$$

has the required discontinuities, although it will not satisfy either Equation (4.103) or the other boundary conditions.

It is now convenient to change to the non-dimensional variables

$$\left.\begin{aligned} \bar{r} &= \omega r/U \\ \bar{s} &= \omega s/U \\ \bar{R} &= \omega R/U \end{aligned}\right\} \ . \tag{4.104}$$

Then Equation (4.103) becomes

$$\frac{\partial^2\Phi}{\partial\bar{r}^2} + \frac{1}{\bar{r}}\frac{\partial\Phi}{\partial\bar{r}} + \left(1 + \frac{1}{\bar{r}^2}\right)\frac{\partial^2\Phi}{\partial\theta^2} = 0 \ .$$

Now put

$$\Phi = \frac{\Gamma(\bar{r})}{\pi}\sum_{n=1}^{\infty}\frac{(-1)^n}{n}\sin 2n\theta + \sum_{n=1}^{\infty}\Phi_n(\bar{r})\sin 2n\theta \ , \tag{4.105}$$

and it is found that the functions $\Phi_n(\bar{r})$ must satisfy*

---

* The first summation in Equation (4.105) has a linear variation between discontinuities and therefore contributes nothing to $\partial^2\Phi/\partial\theta^2$.

$$\frac{d^2\Phi_n}{d\bar{r}^2} + \frac{1}{\bar{r}}\frac{d\Phi_n}{d\bar{r}} - 4n^2\left(1 + \frac{1}{\bar{r}^2}\right)\Phi_n + \frac{(-1)^n}{n\pi}\left(\frac{d^2\Gamma}{d\bar{r}^2} + \frac{1}{\bar{r}}\frac{d\Gamma}{d\bar{r}}\right) = 0 \quad . \qquad (4.106)$$

If we put

$$\Psi_n(\bar{r}) = \Phi_n(\bar{r}) + \frac{(-1)^n}{n\pi}\Gamma(\bar{r}) \quad , \qquad (4.107)$$

then

$$\frac{d^2\Psi_n}{d\bar{r}^2} + \frac{1}{\bar{r}}\frac{d\Psi_n}{d\bar{r}} - 4n^2\left(1 + \frac{1}{\bar{r}^2}\right)\Psi_n = -\frac{4n}{\pi}(-1)^n\left(1 + \frac{1}{\bar{r}^2}\right)\Gamma(\bar{r}) \quad . \qquad (4.108)$$

This last step removes any difficulty associated with infinities in the derivatives of Γ at the wing tips.

When its right-hand side is zero, Equation (4.108) has the two fundamental solutions

$$\Psi_n = I_{2n}(2n\bar{r}) \quad \text{and} \quad \Psi_n = K_{2n}(2n\bar{r})$$

in the usual notation for Bessel functions of imaginary argument. The solution for arbitrary $\Gamma(\bar{r})$ may be obtained by the method of "variation of parameters". It follows eventually that for an open-jet tunnel the increment to Φ due to the tunnel boundaries is

$$\Phi_i = -\frac{4}{\pi}\sum_{n=1}^{\infty}(-1)^n n \sin 2n\theta \, \frac{K_{2n}(2n\bar{R})}{I_{2n}(2n\bar{R})} \, I_{2n}(2n\bar{r}) \int_0^{\bar{s}} \frac{1+\xi^2}{\xi} I_{2n}(2n\xi)\Gamma(\xi)\, d\xi \quad , \qquad (4.109)$$

while for a closed tunnel the factor

$$\frac{K_{2n}(2n\bar{R})}{I_{2n}(2n\bar{R})} \quad \text{has to be replaced by} \quad \frac{K'_{2n}(2n\bar{R})}{I'_{2n}(2n\bar{R})} \quad .$$

The interference velocity at the wing is thus

$$w_i = \frac{1}{2r}\left(\frac{\partial\Phi_i}{\partial\theta}\right)_{\theta=\frac{1}{2}\pi} \quad . \qquad (4.110)$$

This result only applies to an unswept wing of small chord. There appears to have been no development of a theory capable of dealing with rolling wings of significant streamwise extent.

It is now necessary to assess the effect of the interference velocity on the rolling moment. Mandl and Pounder[4.36] use simple strip theory as applied to wings of fairly high aspect ratio. Thus an element dr of the wing at a distance r from the tunnel axis is regarded as being at an incidence $-\tan^{-1}(\omega r/U)$ to a free stream of speed $\sqrt{(U^2 + \omega^2 r^2)}$. The circumferential component of the interference velocity opposes ωr , so that the effective angle of incidence

$$\alpha_g = -\tan^{-1}\left(\frac{\omega r - w_i}{U}\right) = -\tan^{-1}\left(\frac{\omega r}{U}\right) + \frac{U w_i}{U^2 + \omega^2 r^2} \quad . \tag{4.111}$$

when terms in w_i^2 are neglected. Then the rolling moment coefficient is defined* by

$$C_l = (C_l)_p + \delta C_l = \frac{2}{\rho U^2 S s} \int_0^s r \frac{dL}{dr} dr \quad , \tag{4.112}$$

where the element of lift dL corresponds to the local incidence α_g.

From the initial assumption that the circulation is $\Gamma(r)$, a factor

$$\frac{U S s C_l}{2 \int_0^s r\Gamma(r)\, dr}$$

must be applied to the right-hand side of Equation (4.112), so that the assumed rolling moment is consistent with the measured C_l. To the first order in w_i the interference correction to C_l is given by

$$\frac{\Delta C_l}{C_l} = -\frac{\delta C_l}{C_l} = -\frac{\delta C_l}{(C_l)_p} \quad . \tag{4.113}$$

Alternatively the correction

$$\Delta\omega = -\frac{\omega(\Delta C_l / C_l)}{1 + (\Delta C_l / C_l)} \tag{4.114}$$

may be applied to the measured angular velocity.

4.7.2 Slowly Rolling Wings

If the angular velocity is small enough, the helical nature of the wake may be neglected; the calculation of the interference then reduces to that for an anti-symmetrically loaded wing in steady flow. This topic is treated in Section 3.3.5, and needs no further consideration here.

Evans (Ref.4.38; 1947) has treated the rolling wing in a circular tunnel by another method in which the trailing vorticity is convected downstream along straight lines. He assumes that the spanwise distribution of circulation is

---

* Mandl and Pounder apparently include an axial component of interference velocity, which is taken to be $\frac{1}{2}\partial\Phi_i/\partial x$ as given by Equations (4.102) and (4.109). The justification for this is obscure. Moreover, the effective stream velocity would appear to include a contribution of order $\omega r w_i/U$. These considerations do not influence the results for $\omega = 0$, but the calculated frequency effect in Reference 4.38 is regarded with suspicion.

$$\Gamma(\bar{r}) = \sum_{m=0}^{\infty} \Gamma_m(\bar{r}/\bar{s})^m \quad , \tag{4.115}$$

and evaluates δC_l by strip theory for wings of arbitrary taper ratio. At first sight his formula for δC_l is inconsistent with the limiting result from Reference 4.36 as $\omega \to 0$. However, Evans has implicitly assumed that the circulation at the wing tip is zero; in Appendix A of Reference 4.36, Mandl and Pounder have shown that the discrepancy disappears provided that

$$\Gamma(\bar{s}) = \sum_{m=0}^{\infty} \Gamma_m = 0 \quad . \tag{4.116}$$

4.7.3 Propellers

Rolling wings might be expected to lead on to corrections for airscrews in wind tunnels, but in fact this subject seems to have made relatively little progress since a method of correcting the longitudinal velocity for a model propeller in a closed circular wind tunnel was devised by McKinnon Wood and Harris[4.42] as long ago as 1920. This method appears to be satisfactory. The correction to free-stream velocity is presented in various standard works either graphically (as in Reference 4.43) or in a table (as in Reference 4.44). In practice it is sufficiently accurate to use the approximate formula

$$\frac{\Delta U}{U} = -\frac{\pi D^2}{8C}\,\frac{\tau}{(1+2\tau)^{\frac{1}{2}}} \quad , \tag{4.117}$$

where D is the diameter of the propeller disc, C is the cross-sectional area of the tunnel and τ is the thrust coefficient defined by

$$\text{Thrust} = \tfrac{1}{4}\pi\rho U^2 D^2 \tau \quad . \tag{4.118}$$

Young (Ref.4.45; 1944) gives a correction for compressibility in which τ is replaced by τ/β^2 in Equation (4.117).

Equation (4.117) is obtained by an extension of the axial momentum theory[4.44] and is normally used only when τ is positive, so that the propeller has a slip-stream of the usual type and the closed tunnel gives a negative correction to free-stream speed. In the terminology of Chapter V it might be said that a positive thrust is equivalent to a negative drag and therefore produces a negative wake-blockage factor. The applicability of Equation (4.117) to other propeller operating conditions depends on how well the assumptions of momentum theory are satisfied. Presumably windmills ($\tau < 0$) would be covered.

Alternatively the correction to free-stream velocity may be found by measuring the axial velocity near the tunnel wall[4.44]. This method has the advantage that it is applicable when the propeller is mounted on a body.

Theory points to the conclusion that the interference effect on a propeller in a circular open jet is negligible, and this is confirmed by experiment in Reference 4.44. Some recent empirical work by Berry and Whiting[4.36] on models of marine screw propellers in water suggests that the interference is much reduced in tunnels having longitudinally slotted walls.

4.8 APPLICATIONS TO COMMON EXPERIMENTAL SITUATIONS

It is generally advisable to estimate the tunnel corrections before the experiments are carried out. The lift or vorticity distribution should be represented as simply as possible. The recommended procedures for oscillatory measurements in incompressible flow are summarized in Section 4.8.1. The availability of methods for compressible flow is indicated in Section 4.8.2. For numerical data or formulae reference should always be made to the original papers.

4.8.1 Incompressible Flow

(i) Two-dimensional closed tunnel

For c/h small, use Equations (4.19) and (4.25).

For c/h not small, estimate l from free-stream theory, then use Equations (4.14), (4.15) and (4.18) to compute $\bar{w}_i$.

Corrections for rigid modes may be obtained from Equation (4.35) if $\nu \ll 1$ and c/h is small, or may be estimated from graphs in Reference 4.9.

(ii) Closed rectangular tunnel

In general, represent the vorticity distribution as simply as possible and apply the theory of Section 4.5.1 (Ref.4.20).

A rough estimate of the interference upwash may be obtained from Equation (4.86) and Figure 4.4 by assuming that the wing is small, or from Equation (4.94) for slender wings.

(iii) Closed circular tunnel

Apply the theory outlined in Section 4.5.2 (Ref.4.23).

Rough estimates may be made, as if the wing were small or slender.

(iv) Tunnels of other cross sections

The method of Section 4.4.2 may be applied, provided that the distribution of interference upwash can be estimated for steady incompressible flow.

Simplified formulae for small or slender wings then follow from Equations (4.56) and (4.58).

(v) Longitudinally slotted tunnels

When viscous effects at the slots are ignored, the slotted tunnel becomes a particular case of (iv).

Unfortunately the steady interference upwash (Chapter VI) has not yet been calculated in sufficient detail to be used in this way.

4.8.2 Compressible Flow

In all the following applications the experimental frequency should be kept below that for tunnel resonance (Sections 4.3 and 4.4.1).

(i) Two-dimensional closed tunnel

In general, the interference may be evaluated by summing over the images the upwashes as given by Equation (4.31) or (4.32).

The chordwise loading $\bar{l}$ may either be assumed to have its free-stream value, or the integral Equation (4.31) may be solved numerically[4,12].

If the chord is small and ν is small, then Equations (4.35) may be used for rigid modes.

(ii) Three-dimensional tunnels

There is no general method for three-dimensional tunnels. If the frequency is low, the method of Section 4.4.2 may be used provided that the steady interference upwash is known.

(iii) Closed rectangular tunnel

In general, the evaluation of Equation (4.71) is required. For low frequency the theory of Sections 4.4.2 and 4.5.1 may be used.

For small or slender wings and low frequency the theory of Sections 4.5.3 and 4.5.4 may be used.

(iv) Closed circular tunnel

For low frequency the theory of Sections 4.4.2 and 4.5.2 may be used.

For small or slender wings and low frequency, use Section 4.5.3 or 4.5.4 and Equations (4.90) and (4.91).

REFERENCES

4.1 Miles, J.W. — *The Potential Theory of Unsteady Supersonic Flow.* Cambridge University Press, 1959.

4.2 Jordan, P.F. — *The Harmonically Oscillating Wing with Finite Vortex Trail.* ARC R&M 3038, 1953.

4.3 Glauert, H. — *The Elements of Aerofoil and Airscrew Theory.* Second Edition. Cambridge University Press, 1948.

4.4 Jones, W.P. — *Wing Tunnel Interference Effects on Measurements of Aerodynamic Coefficients for Oscillating Aerofoils.* ARC R&M 2786, 1950.

4.5 Lilley, G.M. — *An Investigation of the Flexure-Torsion Flutter Characteristics of Aerofoils in Cascade.* Coll. Aero. (Cranfield) Report 60. ARC Report 14,952, 1952.

4.6 Mendelson, A.
Carroll, R.W. — *Lift and Moment Equations for Oscillating Airfoils in an Infinite Unstaggered Cascade.* NACA Tech. Note 3263, 1954.

4.7 Rosenblat, S. — *The Aerodynamic Forces on an Aerofoil in Non-Uniform Unsteady Motion in a Closed Tunnel.* Phil. Trans. Roy. Soc. A, Vol.250, 1957, pp.247-278.

4.8 Timman, R. — *The Aerodynamic Forces on an Oscillating Aerofoil between Two Parallel Walls.* App. sci. Res. A (Hague), Vol.3, 1951, pp.31-57.

4.9 de Jager, E.M. — *The Aerodynamic Forces and Moments on an Oscillating Aerofoil with Control-Surface between Two Parallel Walls.* NLL (Netherlands) Report F.140, 1953.

4.10 Jones, W.P. — *Wind-Tunnel Wall Interference Effects on Oscillating Aerofoils in Subsonic Flow.* ARC R&M 2943, 1953.

4.11 Runyan, H.L.
Watkins, C.E. — *Considerations on the Effect of Wind-Tunnel Walls on Oscillating Air Forces for Two-Dimensional Subsonic Compressible Flow.* NACA Report 1150, 1953.

4.12 Runyan, H.L. et al. — *Theoretical and Experimental Investigation of the Effect of Tunnel Walls on the Forces on an Oscillating Airfoil in Two-Dimensional Subsonic Compressible Flow.* NACA Report 1262, 1956.

4.13 Acum, W.E.A. — *Theory of Lifting Surfaces Oscillating at General Frequencies in a Stream of High Subsonic Mach Number.* ARC Report 17,824, 1955. (To be ARC R&M.)

4.14 Richardson, J.R. *A Method for Calculating the Lifting Forces on Wings (Unsteady Subsonic and Supersonic Lifting-Surface Theory).* ARC R&M 3157, 1955.

4.15 Watkins, C.E. et al. *A Systematic Kernel Function Procedure for Determining Aerodynamic Forces on Oscillating or Steady Finite Wings at Subsonic Speeds.* NASA Tech. Report R-48, 1959.

4.16 Acum, W.E.A. *A Simplified Approach to the Phenomenon of Wind-Tunnel Resonance.* ARC R&M 3371, 1962.

4.17 Widmayer, E. et al. *Some Measurements of Aerodynamic Forces and Moments at Subsonic Speeds on a Rectangular Wing of Aspect Ratio 2 Oscillating about the Midchord.* NACA Tech. Note 4240, 1958.

4.18 Goodman, T.R. *The Upwash Correction for an Oscillating Wing in a Wind Tunnel.* J. aero. Sci., Vol.20, 1953, pp.383-386, 406.

4.19 Garner, H.C. *Multhopp's Subsonic Lifting-Surface Theory of Wings in Slow Pitching Oscillations.* ARC R&M 2885, 1952.

4.20 Acum, W.E.A. *Wall Corrections for Wings Oscillating in Wind Tunnels of Closed Rectangular Section.* ARC R&M 3312, 1958.

4.21 von Kármán, T. Burgers, J.M. *General Aerodynamic Theory - Perfect Fluids. Airfoils and Airfoil Systems of Finite Span.* "Aerodynamic Theory" (Ed. W.F.Durand), Vol.II, Div.E, Chapter IV, Sect.42 to 44. Julius Springer, Berlin, 1935.

4.22 Eisenstadt, B.J. *Boundary-Induced Upwash for Yawed and Swept-Back Wings in Closed Circular Wind Tunnels.* NACA Tech. Note 1265, 1947.

4.23 Acum, W.E.A. Garner, H.C. *Approximate Wall Corrections for an Oscillating Swept Wing in a Wind Tunnel of Closed Circular Section.* ARC CP 184, 1954.

4.24 Jones, W.P. *Wind Tunnel Interference Effect on the Values of Experimentally Determined Derivative Coefficients for Oscillating Aerofoils.* ARC R&M 1912, 1943.

4.25 Acum, W.E.A. *A Note on the Estimation of the Effect of Wind Tunnel Walls on the Forces on Slowly Oscillating Slender Wings.* ARC CP 707, 1963.

4.26 Garrick, I.E. *Some Research on High-Speed Flutter.* Anglo-American Aeronautical Conference, Brighton, 1951, pp.419-446. (Royal Aero. Soc.)

4.27 Lehrian, Doris, E. *Calculation of Stability Derivatives for Oscillating Wings.* ARC R&M 2922, 1953.

4.28 Drake, D.G. *The Oscillating Two-Dimensional Aerofoil between Porous Walls.* Aero. Quart., Vol.8, 1957, pp.226-239.

4.29 Drake, D.G. *Quasi-Steady Derivatives for the Subsonic Flow past an Oscillating Aerofoil in a Porous Wind Tunnel.* Aero. Quart., Vol.10, 1959, pp.211-229.

4.30 Rosenblat, S. *The Aerodynamic Forces on an Aerofoil in Unsteady Motion between Porous Walls.* Quart. J. Mech. appl. Math., Vol.12, 1959, pp.151-174.

4.31 Drake, D.G. *Wind-Tunnel Interference for Oscillating Wings at Transonic Speeds.* ARC Report 21,489, 1959 (unpublished).

4.32 Landahl, M.T. *Unsteady Transonic Flow.* Pergamon Press, 1961.

4.33 Acum, W.E.A.
Garner, H.C. *The Estimation of Oscillatory Wing and Control Derivatives.* AGARD Report 340, 1961.

4.34 Wight, K.C. *A Review of Slotted-Wall Wind Tunnel Interference Effects on Oscillating Models in Subsonic and Transonic Flows.* J. Roy. aeron. Soc., Vol.68, 1964, pp.670-674.

4.35 Theodorsen, Th. *Theory of Propellers.* McGraw-Hill, 1948.

4.36 Mandl, P.
Pounder, J.R. *Wind Tunnel Interference on Rolling Moment of a Rotating Wing.* NRC (Canada) Aeronautical Report AR-10, 1951.

4.37 Goldstein, S. *On the Vortex Theory of Screw Propellers.* Proc. Roy. Soc., Series A, Vol.123, 1929, pp.440-465.

4.38 Evans, J.M. *Stability Derivatives. Wind Tunnel Interference on the Lateral Derivatives* l_p, l_r *and* l_v *with Particular Reference to* l_p. Report ACA-33 (Australia), 1947.

4.39 Molyneux, W.G. *Wind Tunnel Interference in Dynamic Measurements.* RAE Tech. Report 64069, ARC Report 26,673, 1964. Presented at a short course on the Use of Flexible Models in Aeroelastic Research, Von Kármán Institute of Fluid Dynamics, May 1964.

4.40 Davis, D.D.
Moore, D. *Analytical Study of Blockage- and Lift-Interference Corrections for Slotted Tunnels Obtained by the Substitution of an Equivalent Homogeneous Boundary for the Discrete Slots.* NACA RM L53E07b (NACA/TIB/3792), 1953.

4.41 Garner, H.C. Moore, A.W. — *Notes on Unsteady Slotted-Wall Tunnel Interference.* NPL Aero. Note 1039, ARC Report 27,486, 1965.

4.42 Wood, R.McK. Harris, R.G. — *Some Notes on the Theory of an Airscrew Working in a Wind Channel.* ARC R&M 662, 1920.

4.43 Pankhurst, R.C. Holder, D.W. — *Wind-Tunnel Technique.* Pitman, London, 1952 (reprinted in 1965).

4.44 Glauert, H. — *Airplane Propellers. The Experimental Study of Propellers.* "Aerodynamic Theory" (Ed. W.F.Durand), Vol.IV, Div.L, Chap.IX, Julius Springer, Berlin, 1935. pp.293-310.

4.45 Young, A.D. — *Note on the Application of the Linear Perturbation Theory to Determine the Effect of Compressibility on the Wind Tunnel Constraint on a Propeller.* ARC R&M 2113, 1944.

4.46 Berry, L.W. Whiting, D. — *Channel Speed Correction for No.1 Tunnel.* NPL Ship Division Tech. Memo. 71, 1964 (unpublished).

ADDITIONAL REFERENCES FOR CHAPTER IV

Drake, D.G. — *The Motion of an Oscillating Aerofoil in a Compressible Free Jet.* J. Roy. aeron. Soc., Vol.60, 1956, pp.621-623.

Meller, A.G. Berton, A. — *Étude des Vibrations Aéro-Elastiques des Gouvernes en Subsonique Élevé.* Rech. aeron. No.47, September/October 1955, pp.27-35.

Miles, J.W. — *The Compressible Flow past an Oscillating Airfoil in a Wind Tunnel.* J. aero. Sci., Vol.23, 1956, pp.671-678.

Reissner, E. — *Wind Tunnel Corrections for the Two-Dimensional Theory of Oscillatory Airfoils.* Cornell Aero. Lab. Report SB-318-S-3, 1947.

Whitehead, D.S. — *The Vibration of Air in a Duct with a Subsonic Mean Flow.* Aero. Quart., Vol.12, 1961, pp.34-40.

Woods, L.C. — *The Aerodynamic Forces on an Oscillating Aerofoil in a Free Jet.* Proc. Roy. Soc., Series A, Vol.229, 1955, pp.235-250.

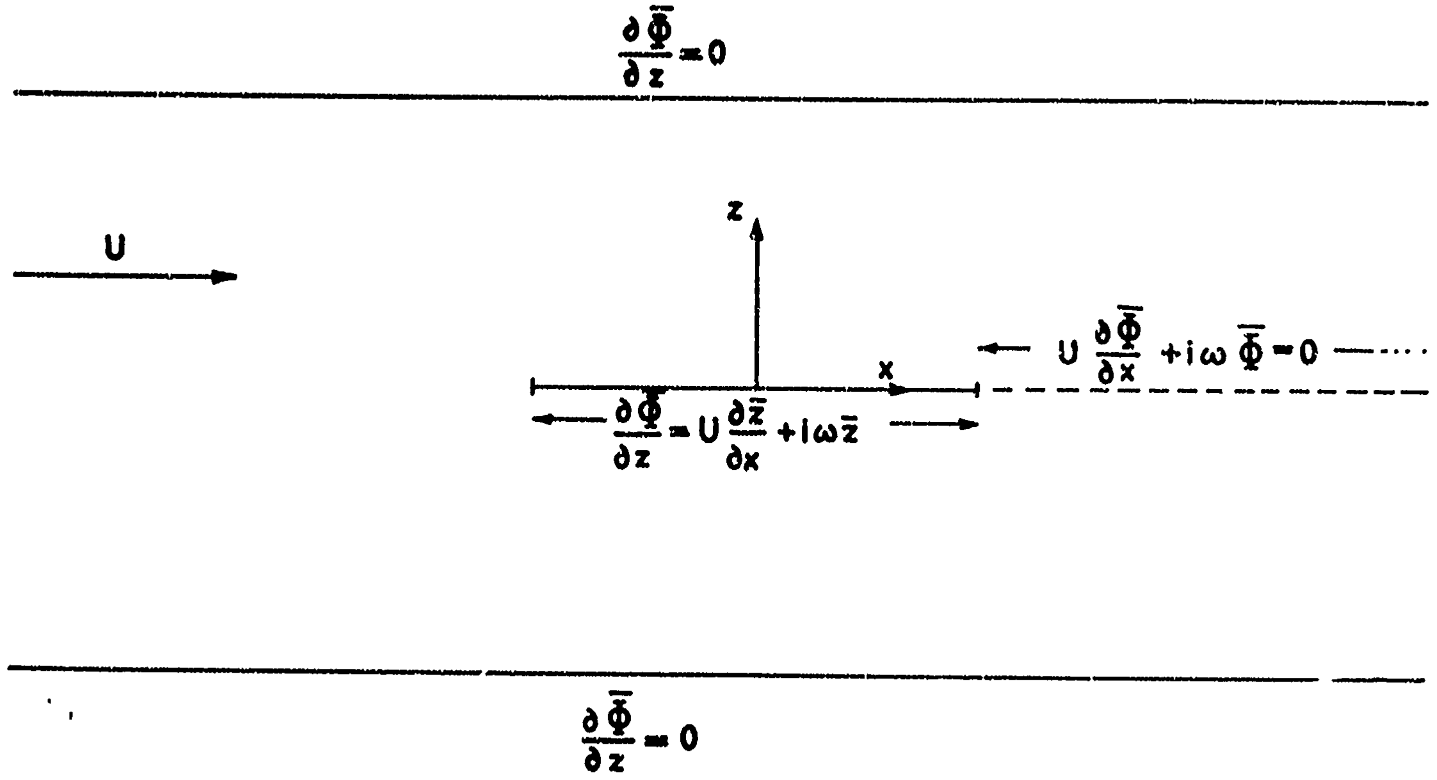
$\frac{\partial \bar{\Phi}}{\partial z} = 0$
U
z
x
$\frac{\partial \bar{\Phi}}{\partial z} = U \frac{\partial \bar{z}}{\partial x} + i\omega \bar{z}$
$U \frac{\partial \bar{\Phi}}{\partial x} + i\omega \bar{\Phi} = 0$
$\frac{\partial \bar{\Phi}}{\partial z} = 0$

Fig.4.1 Boundary conditions for oscillating wing in two-dimensional closed tunnel

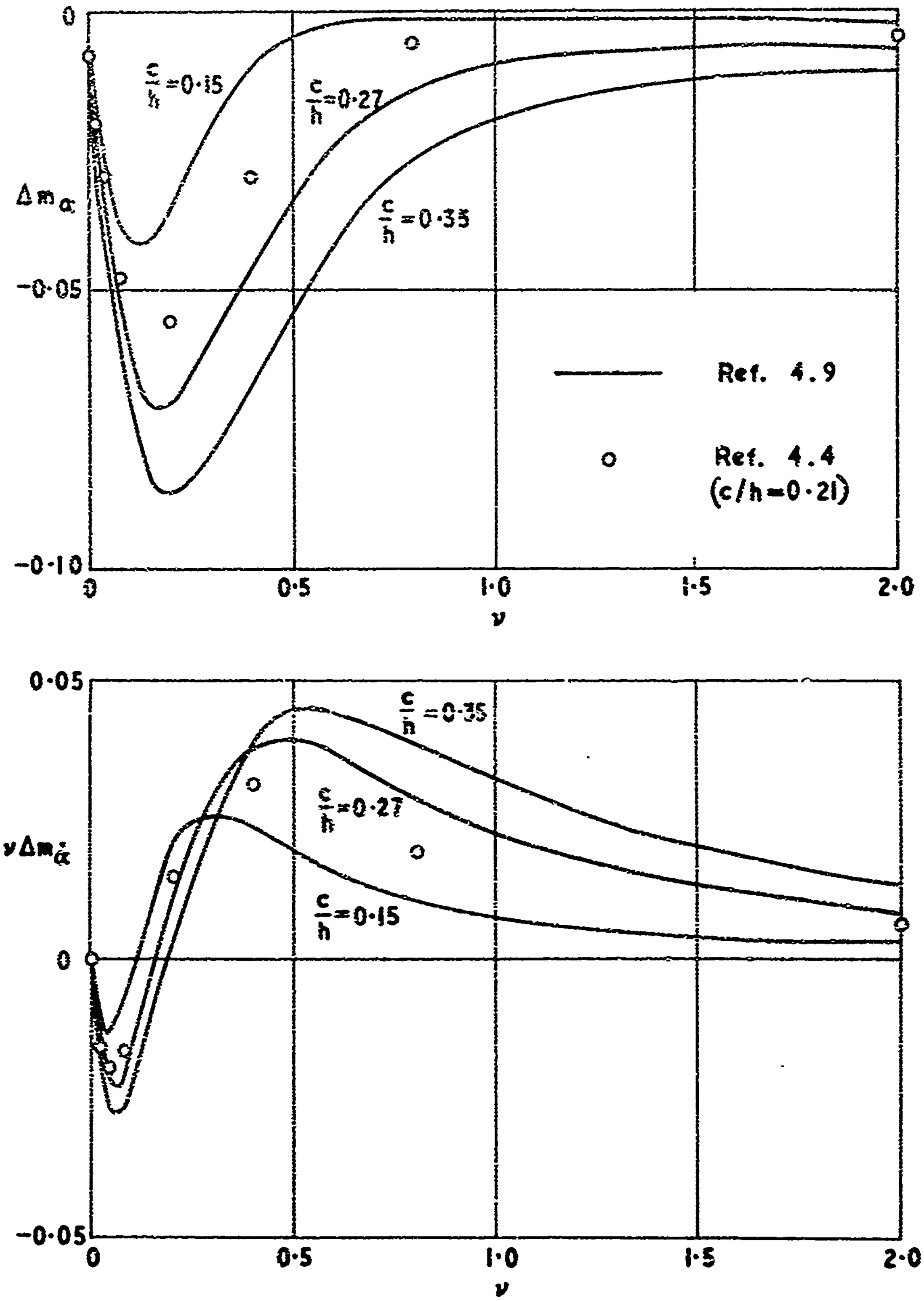

Fig.4.2 Tunnel corrections for wing pitching about its mid-chord point

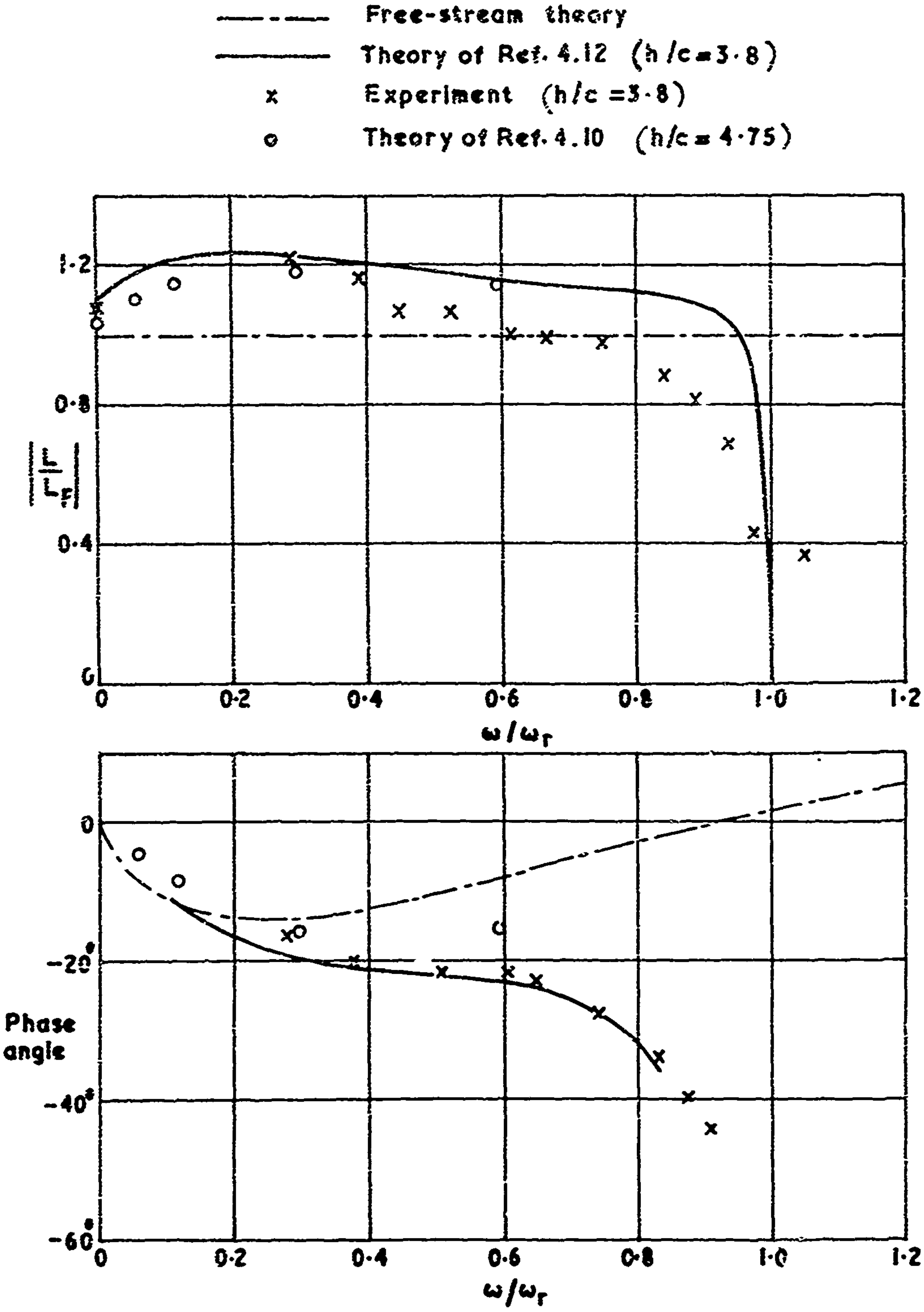
Based on Fig.4 of Ref. 4.12

Fig.4.3 The effect of resonance on lift in a two-dimensional tunnel at M = 0.7

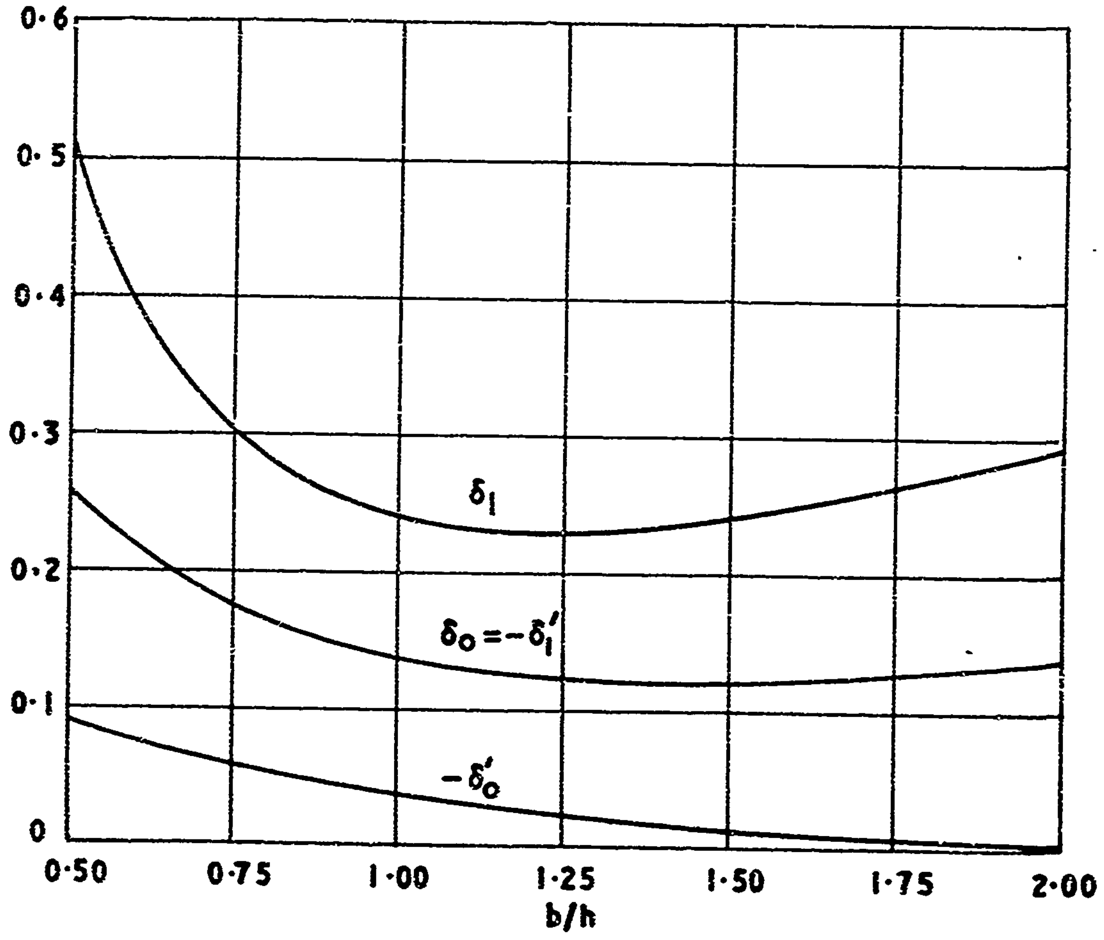

Fig. 4.4 Interference parameters for small wings in closed rectangular wind tunnels

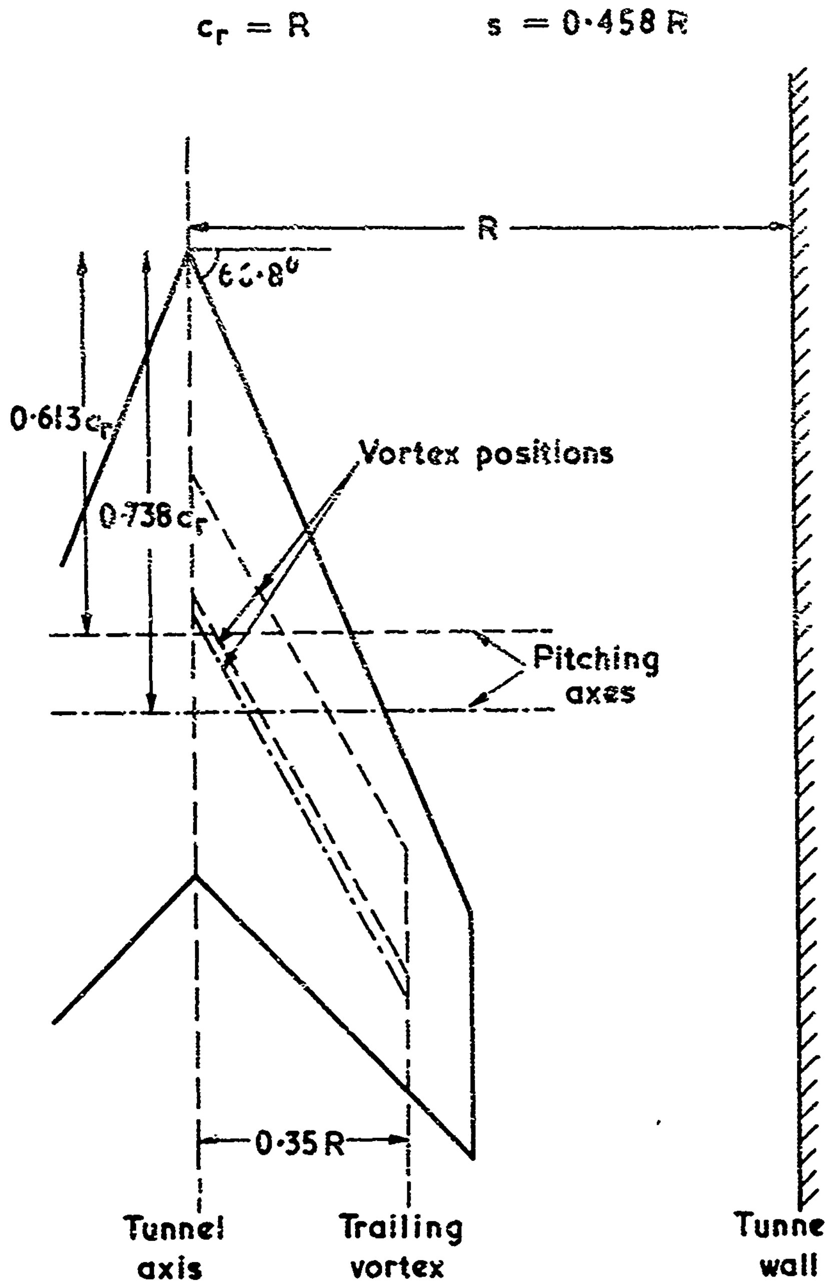
$c_r = R$
$s = 0{\cdot}458R$
R
60·8°
0·613c_r
0·738c_r
Vortex positions
Pitching axes
0·35R
Tunnel axis
Trailing vortex
Tunnel wall

Fig.4.5 Planform of model wing used as an example in Section 4.5.5

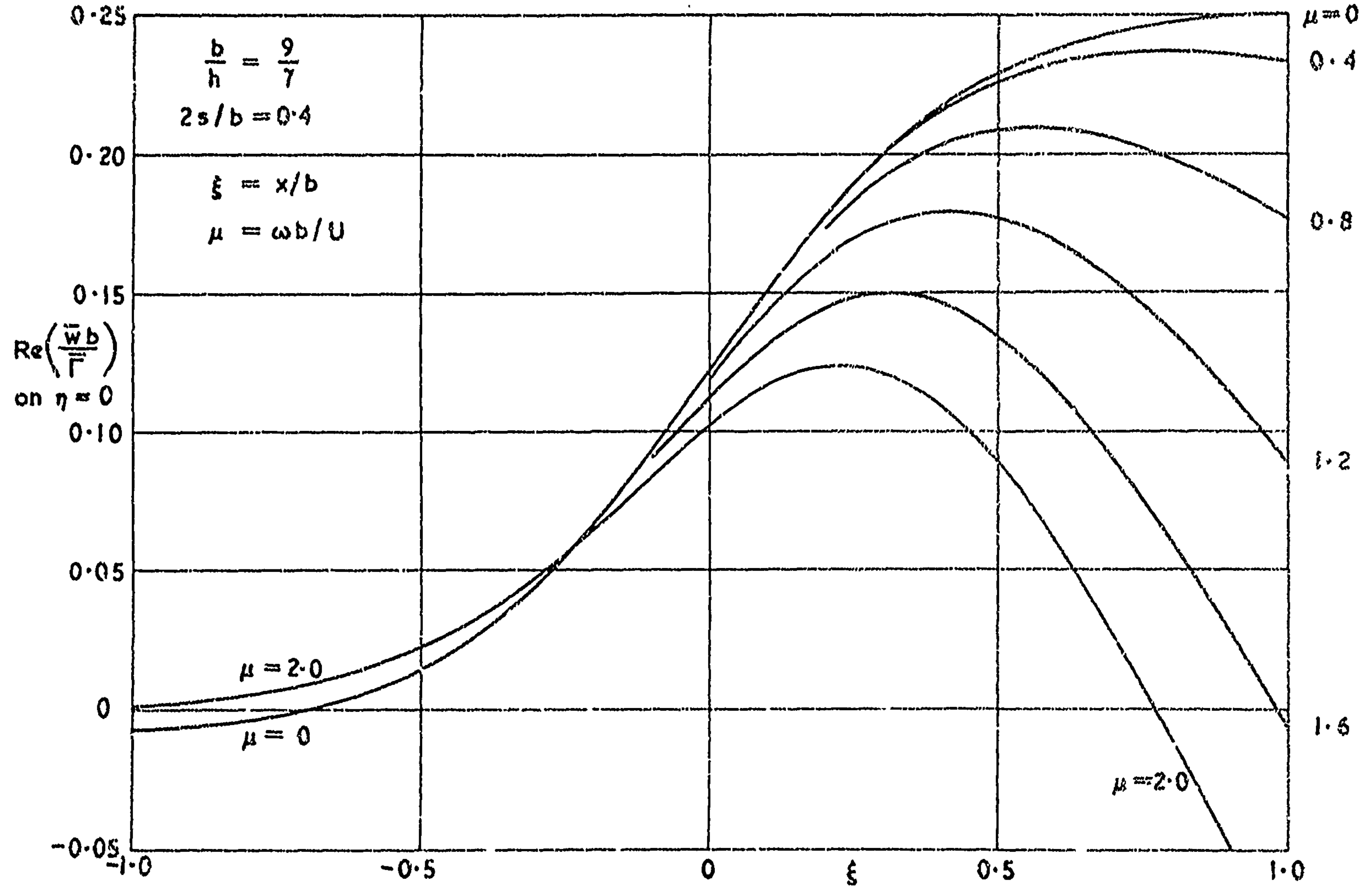

Fig. 4.8(a) Effect of frequency on the interference upwash due to a horse-shoe vortex in a closed 9 × 7 tunnel

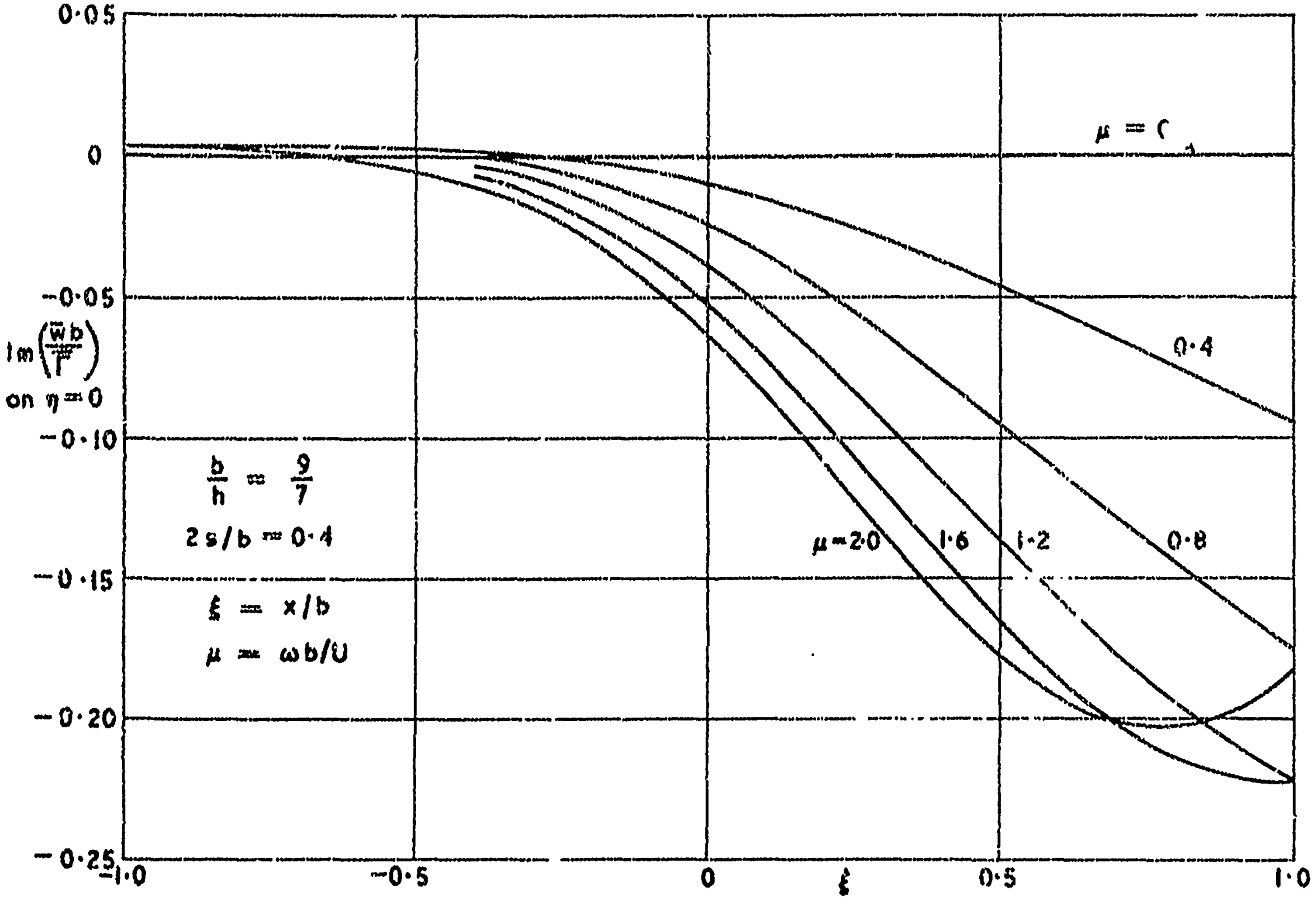

Fig. 4.6(b) Effect of frequency on the interference upwash due to a horse-shoe vortex in a closed 9 × 7 tunnel

Reproduced from Fig.3 of Ref. 4·34

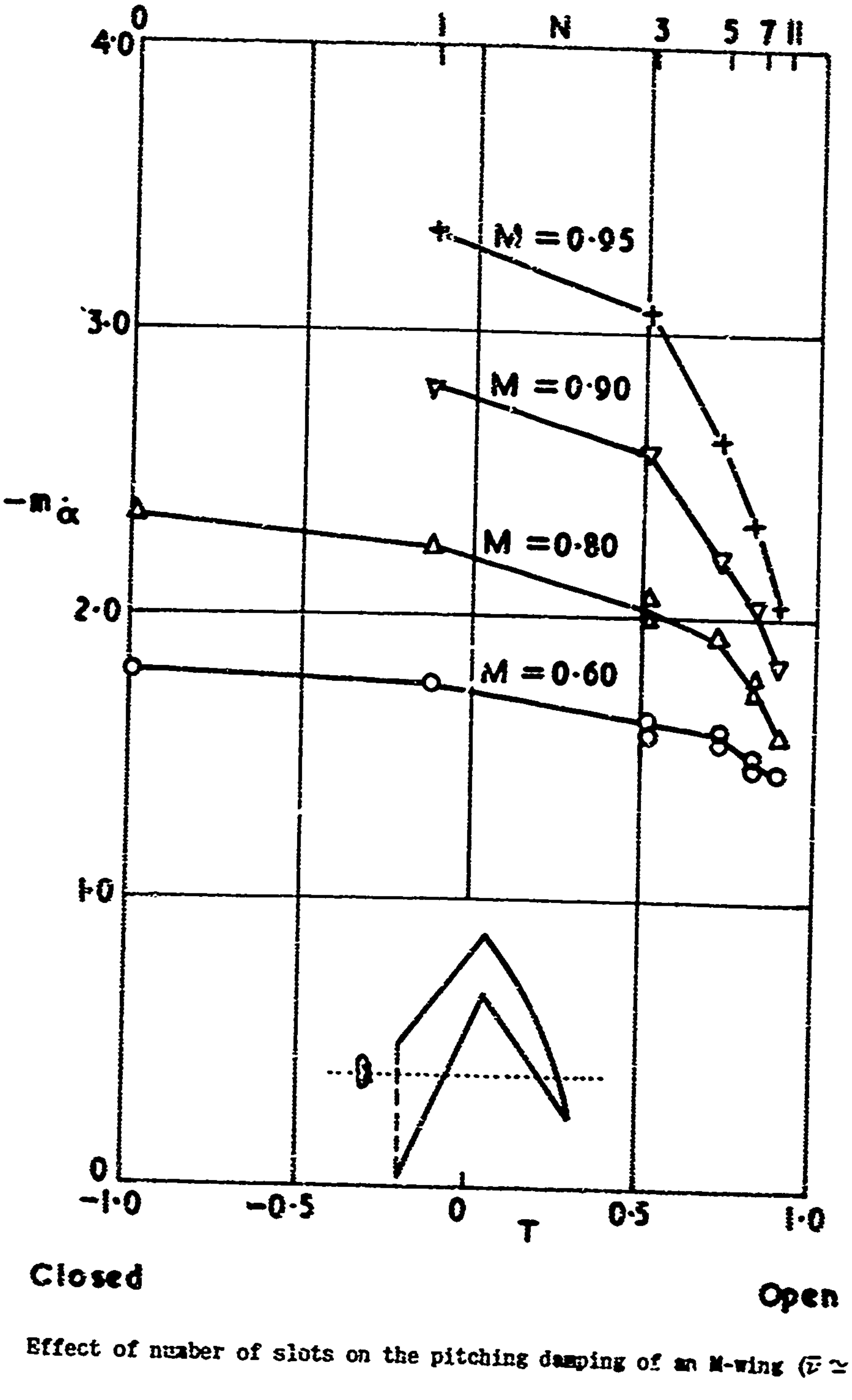

Fig.4.7 Effect of number of slots on the pitching damping of an M-wing ($\bar{\nu} \simeq 0.05$)

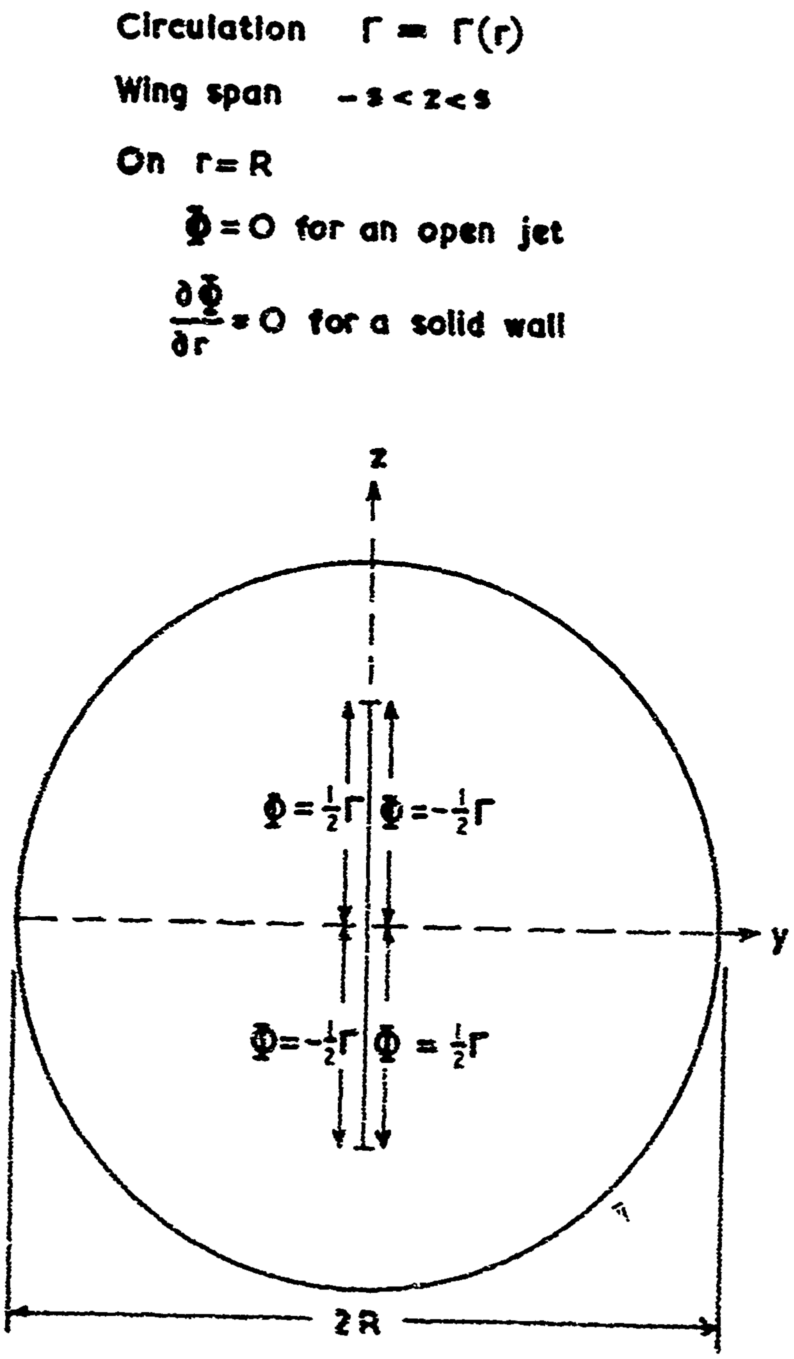

Circulation $\Gamma = \Gamma(r)$
Wing span $-s < z < s$
On $r = R$
$\Phi = 0$ for an open jet
$\frac{\partial \Phi}{\partial r} = 0$ for a solid wall
z
$\Phi = \frac{1}{2}\Gamma$
$\Phi = -\frac{1}{2}\Gamma$
y
$\Phi = -\frac{1}{2}\Gamma$
$\Phi = \frac{1}{2}\Gamma$
2R

Fig.4.6 Boundary conditions far downstream of a rolling wing

CHAPTER V

BLOCKAGE EFFECTS IN CLOSED OR OPEN TUNNELS

by

E.W.E.Rogers

Aerodynamics Division, National Physical Laboratory,
Teddington, Middlesex, England

BLANK PAGE

CONTENTS

Page

LIST OF TABLES 283

LIST OF FIGURES 283

NOTATION 284

5.1 INTRODUCTION 287

5.2 SOLID BLOCKAGE FACTORS IN CLOSED RECTANGULAR TUNNELS 289
- 5.2.1 Two-Dimensional Aerofoil 289
- 5.2.2 Body of Revolution 294
- 5.2.3 Wings and Wing-Body Combinations 297

5.3 SOLID BLOCKAGE FACTORS IN CLOSED NON-RECTANGULAR TUNNELS 299
- 5.3.1 Octagonal Tunnels 299
- 5.3.2 Circular and Elliptical Tunnels 300

5.4 WAKE BLOCKAGE FACTORS IN CLOSED TUNNELS 304
- 5.4.1 Two-Dimensional Aerofoil in a Rectangular Tunnel 304
- 5.4.2 Three-Dimensional Models in a Rectangular Tunnel 306
- 5.4.3 Closed Non-Rectangular Tunnels 308
- 5.4.4 Wake Blockage Gradient 308

5.5 BLOCKAGE FACTORS IN OPEN-JET TUNNELS 308
- 5.5.1 Solid Blockage for Models Spanning the Tunnel 308
- 5.5.2 Three-Dimensional Solid Blockage 309
- 5.5.3 Wake Blockage Effects 311

5.6 ESTIMATION OF BLOCKAGE FROM WALL MEASUREMENTS 311
- 5.6.1 Two-Dimensional Aerofoil 312
- 5.6.2 Three-Dimensional Models 313

5.7 BLOCKAGE CORRECTIONS AT VERY HIGH SUBSONIC SPEEDS IN CLOSED TUNNELS 315
- 5.7.1 Modification of Simple Compressibility Theory 315
- 5.7.2 Regions of Local Supersonic Flow 316

Page

5.8 USE OF BLOCKAGE FACTORS IN CORRECTING MEASURED QUANTITIES 317
5.8.1 Corrections to Stream Quantities 317
5.8.2 Corrections to Model Quantities 319

5.9 SUMMARY OF PRINCIPAL BLOCKAGE FORMULAE 321
5.9.1 Closed Rectangular Tunnel 321
5.9.2 Closed Non-Rectangular Tunnels 322
5.9.3 Open-Jet Tunnels 323
5.9.4 Corrections to Stream Quantities 323
5.9.5 Corrections to Model Quantities 324

REFERENCES 324

ADDITIONAL REFERENCES 329

TABLE 330

FIGURES 331

LIST OF TABLES

Page

TABLE 5.I Functions Giving the Distribution of Solid Blockage along Bodies in Circular Tunnels (Ref.5.33) 330

LIST OF FIGURES

Fig.5.1 Aerofoil-shape parameter 331

Fig.5.2 Body-shape parameter 331

Fig.5.3 Tunnel-shape parameter for small models 332

Fig.5.4 Tunnel-shape parameter from various formulae 332

Fig.5.5 Tunnel-shape parameter for large-span models 333

Fig.5.6 Effect of model span on T for various closed tunnels 333

Fig.5.7 Distribution of solid blockage along bodies in closed circular tunnel 334

Fig.5.8 Approximate values of tunnel-shape parameters for long bodies in closed circular tunnels 334

Fig.5.9 Blockage factors for semi-infinite bodies of revolution in circular tunnels 335

Fig.5.10 Blockage at centre section of wing spanning an elliptical tunnel 335

Fig.5.11 Glauert's two-dimensional wake-blockage factor 336

Fig.5.12 Simple compressibility factors used in blockage equations 336

Fig.5.13 Tunnel-shape parameters for small models in open rectangular tunnels 337

Fig.5.14 Effect of model span and sweepback on wall-velocity ratio $Z_s(b/h = \sqrt{2})$ 338-339

Fig.5.15 Examples of calculated and experimental Mach number increments at side-wall of 10 ft × 7 ft tunnel 340

NOTATION

a	distance between source and sink
a^*	critical speed of sound
A	cross-sectional area of aerofoil
A_m	maximum transverse cross-section of model
b	breadth of tunnel
c	chord of aerofoil
C	cross-sectional area of tunnel
C_D	drag coefficient $= D/\frac{1}{2}\rho U^2 S$
C_{Do}	drag coefficient at zero lift
C_p	pressure coefficient $= (p - p_\infty)/\frac{1}{2}\rho U^2$
d	distance of model from floor of tunnel
D	drag of model
f	fineness ratio $= l/t$
h	height of tunnel
H, I	functions given in Table 5.I
$k(x)$	moment of inertia of aerofoil about chordwise position $x = \text{constant}$
k_x	moment of inertia about x axis
k_2	$= A/tc$
k_3	$= V/t^2 l$
l	length of body
m	major axis of elliptical tunnel
M	Mach number of undisturbed stream
M^*	$= U/a^*$
n	minor axis of elliptical tunnel

p	local static pressure
p_∞	static pressure of undisturbed stream
P	strength of doublet
q	local surface velocity
Q	strength of source
R	radius of circular tunnel
R_N	Reynolds number
s	distance along body contour (Section 5.2.1)
s	semi-span of wing
S	reference area of model
t	maximum thickness of model
T	shape parameter of tunnel (cf. Figures 5.3 to 5.6)
u	x-component of velocity
U	velocity of undisturbed stream
V	volume of model
x	distance downstream (origin at leading edge of aerofoil or centre of body axis)
y	spanwise distance normal to body axis
z	distance upwards from body axis
Z	$= (\Delta U)/(u - U)_{wall}$
α	incidence of model
β	$= (1 - M^2)^{\frac{1}{2}}$
γ	ratio of specific heats (taken as 1.400 for air)
Δ	prefix denoting increment due to wall correction
ϵ	blockage factor $= (\Delta U)/U$
η	Glauert's two-dimensional wake-blockage factor

η'	Glauert's three-dimensional wake-blockage factor
θ	chordwise parameter of aerofoil = $\cos^{-1}\left(1 - \dfrac{2x}{c}\right)$
Θ	static temperature of undisturbed stream
λ_2	shape parameter of aerofoil (Fig. 5.1)
λ_3	shape parameter of body (Fig. 5.2)
Λ	angle of sweepback
ρ	density of undisturbed stream
τ	shape parameter of tunnel (cf. Figures 5.8 and 5.13)

Subscripts

B	denotes effect of blockage.
c	denotes corrected value.
e	denotes equivalent value.
g	denotes effect of velocity gradient (buoyancy).
s	denotes solid blockage.
w	denotes wake blockage.

BLOCKAGE EFFECTS IN CLOSED OR OPEN TUNNELS

E.W.E. Rogers

5.1 INTRODUCTION

In the preceding chapters, the boundary interference arising from the model lift has been discussed in some detail. There exists, however, an additional interference effect associated with the fact that the model and its wake occupy a certain volume within the finite tunnel stream. The streamline pattern about the model is thereby distorted compared with free-air conditions, and this distortion exists even at zero model lift. The magnitude of the streamline displacement will depend, amongst other things, on the relative sizes of the model and tunnel working section, and on their cross-sections; the direction of the distortion (and hence the sign of the ensuing correction) depends on whether the tunnel boundaries are of the fixed-wall or open-jet type.

This interference is said to arise from the "blockage" of the model and its wake, that associated with the model itself being called "solid blockage", and that due to the wake "wake blockage". For most purposes it is sufficiently accurate to assume that the two blockage components are independent both of each other and of the model lift. This simplifies the analysis and enables corrections for blockage effects to be evaluated at zero lift. Such a procedure implies that the model is small compared to the tunnel working section and that the lift is not too large; moreover it is assumed that the blockage only influences the longitudinal component of the flow about the model, and this is true only if the model is mounted in the centre of the tunnel.

In the simplest case, the flow about a small model in a tunnel corresponds to that about the same model in free air, but at a corrected velocity $U + \Delta U_S$, where U is the nominal velocity of the tunnel stream and ΔU_B is the sum of velocity increments associated with the solid and wake blockages. For streamline flow it is convenient to express the ratio $\Delta U_B/U$ by the blockage factor ϵ_B, which is then the sum of corresponding solid and wake blockage factors

$$\epsilon_B = \epsilon_S + \epsilon_W . \tag{5.1}$$

For bluff bodies this subdivision of blockage effects is not applicable. The principle of correspondence between the observed flow and some free-air flow at a different velocity is valid for a wide range of flow conditions. Sometimes, however, it may be necessary to determine the variation of the blockage factor along the model length, as for example in the case of a long slender body, or perhaps to consider whether the model blockage is affected by changes in the model incidence. These more complex analyses are usually less general in application than those concerned simply with some average correction applied over the whole volume occupied by the model.

The present chapter will be concerned with blockage effects in tunnels with either completely closed or completely open boundaries. Related problems for ventilated tunnels, having a combination of open and closed boundaries, are discussed in Chapter VI.

The walls of a completely closed tunnel impose a constraint on the flow about the model such that the flow near the wall follows that surface. The stream tubes surrounding the model do not take up their free-air shape but are compressed together, causing a corresponding increase in the local fluid velocities. A similar conclusion may be reached by equating the mass flow well upstream of the model to that at the model position. The velocity correction, and hence the solid-blockage factor, will therefore be positive in a closed tunnel.

The conditions at the boundary of an open jet are less easy to define precisely, but it is usual to assume that the jet boundary is one of constant pressure, equal to that of the surrounding motionless air. In practice, the edge of the jet may be difficult to specify because of mixing between the stream and the surrounding fluid and moreover it may be distorted by the presence of the model. Such difficulties are frequently overcome by assuming that the constant pressure condition may always be applied at the undisturbed boundary and that mixing effects can be ignored.

The assumption of a constant-pressure boundary also implies that the perturbation velocities, particularly the streamwise component, are small at the edge of the jet, since Bernouilli's equation may be applied to a boundary streamline extending from well upstream to a position opposite the model. Since the model induces supervelocities at this position, the constant-pressure condition may only be preserved by a reduction in the effective stream velocity approaching the model. Thus for the open-jet tunnel the solid-blockage factor will be negative.

Glauert (Ref. 5.1; 1933) has pointed out an additional matter which makes the treatment of the open-jet tunnel less precise than its closed counterpart. In the latter case there is usually a considerable length of working section of almost constant cross-section upstream and downstream of the model. A free jet on the other hand frequently issues from a nozzle placed at a relatively short distance upstream of the model and flows into a collector not far downstream. The assumption of an infinitely long jet inherent in much of the analysis is therefore violated[5.47] and the validity of the simple theoretical corrections must rest largely on experimental evidence. The boundary conditions appropriate to finite-length open-jet tunnels have been discussed by Katzoff et al. (Ref. 5.48; 1950) and in more general terms by Vandrey (Ref. 5.49; 1942), but up to the present the simple constant-pressure condition has been most widely used in the theory of wall interference.

It should perhaps be pointed out that the reasons for using short working sections are entirely practical. It is, for example, difficult to obtain a stable jet longer than about two jet diameters. In effect this imposes a restriction on the model size, since the ends of the model must be a moderate distance from both nozzle and collector, and the model length is hence unlikely to exceed about 0.8 jet diameters. In turn the small model size implies that the corrections will not be excessively large.

The simple boundary conditions of the open-jet tunnel suggest that the flow behind the model can enlarge to allow for the presence of a wake of reduced velocity. This is not the case in a closed tunnel of constant cross-section where, to satisfy continuity upstream and downstream of the model, the flow velocity outside the wake must be greater than in the free stream ahead of the model. The effect of the wake in the closed tunnel is to increase the effective stream velocity, so as to introduce the wake-blockage factor ϵ_w at the model position and to impose a longitudinal pressure gradient along the model. The latter buoyancy effect is equivalent to a boundary-induced drag force on the model, for which a correction is required. In the open-jet tunnel, the wake-blockage velocity increment is absent, but there is still a buoyancy correction.

When the flow departs significantly from the classical streamline flow, it becomes necessary to reconsider the mathematical model of the flow. The representation must incorporate the essential features of the separated flow and still remain simple enough to leave a tractable problem when there are closed boundaries. Such a theory for a non-lifting bluff body is developed in Chapter VII. The relatively large blockage factor for a bluff body is confirmed by experiment.

In the following sections methods of estimating the solid-blockage and wake-blockage factors will be discussed for a variety of tunnel cross-sections. The two important methods of determining the blockage factors are from theoretical calculations involving the model and tunnel geometry, tunnel Mach number and model drag (Sections 5.2 to 5.5), and from pressure measurements made at the tunnel wall (Section 5.6).

At high subsonic stream Mach numbers, shock waves may be present in the flow about the model, and some change in the form of the blockage factors discussed earlier may be required. In addition modifications may be necessary to the simple linear theory used to estimate the effect of stream compressibility. Matters of this kind are considered in Section 5.7.

The use of the blockage factors in correcting the measured quantities is discussed in Section 5.8, whilst the final Section 5.9 sets out the more important formulae used in the text.

5.2 SOLID BLOCKAGE FACTORS IN CLOSED RECTANGULAR TUNNELS

5.2.1 Two-Dimensional Aerofoil

We will consider here an aerofoil of chord c , maximum thickness t , spanning centrally a rectangular tunnel of height h . An early method of calculating the solid blockage of this configuration was given by Lock (Ref.5.29; 1929: see also Reference 5.1). He represented the aerofoil by an equivalent doublet and the effect of the tunnel walls by an infinite array of doublet images extending above and below the model and spaced at the tunnel height h . The additional velocity induced by the images at the model position may then be calculated and this is the velocity increment due to the solid blockage. The solid-blockage factor ϵ_s in incompressible flow is then given by

$$\epsilon_s = \frac{\Delta U_s}{U} = \frac{\pi^2}{12}\left(\frac{c}{h}\right)^2\left(\frac{t}{c}\right)^2\lambda_2 . \qquad (5.2)$$

where λ_2 is a parameter related to the profile thickness such that the model is replaced in the analysis by a cylinder of radius $t\sqrt{\lambda_2}$. Lock calculated λ_2 for four typical body shapes (Fig.5.1), but a simple formula is obtained in only a few cases, e.g., ellipse[5.1] and Rankine oval[5.2]. An accurate determination of λ_2 can be made if the surface pressure distribution about the model is known, so that the local surface velocity q can be found. Then for a symmetrical aerofoil

$$\lambda_2 = \frac{4}{\pi}\int \frac{q}{U}\,\frac{z(s)}{t^2}\,ds\,, \tag{5.3}$$

where s is the distance along the body contour from the leading edge and $z(s)$ is the surface ordinate from the chordline at s. The integral is taken along the curved surface from leading to trailing edge. For a cambered profile it is sufficient to consider only the thickness distribution of the section.

Allen and Vincenti (Ref.5.3; 1944) use the blockage factor

$$\Lambda = 4\left(\frac{t}{c}\right)^2\lambda_2 \tag{5.4}$$

so that

$$\epsilon_s = \frac{\pi^2}{48}\left(\frac{c}{h}\right)^2\Lambda\,. \tag{5.5}$$

Values of Λ for various basic aerofoil profiles will be found in References 5.3 and 5.27, and λ_2 may easily be obtained from these sources. As Figure 5.1 shows, values of λ_2 for typical families of NACA 6-series aerofoils are close to those for Joukowski-type profiles. The solid blockage of an aerofoil in an incompressible stream has also been considered by Toussaint (see Reference 5.54) using a complex potential method. His equation is similar to (5.2) but tends to give somewhat smaller values of ϵ_s.

In a compressible fluid when the stream Mach number is subsonic and not too near the choking value, the effect of compressibility may be allowed for sufficiently accurately by small-perturbation theory[5.3,5.30,5.44]. The velocity increment at the model position is then β^{-1} times the appropriate increment for an incompressible fluid in a tunnel of height βh; the model thickness and chord are assumed to remain unchanged. Thus Equations (5.2) and (5.5) must be multiplied by a factor β^{-3}. Lock's original equation then becomes

$$\epsilon_s = \frac{\pi^2}{12}\left(\frac{c}{h}\right)^2\left(\frac{t}{c}\right)^2\frac{1}{\beta^3}\lambda_2\,. \tag{5.6}$$

Sometimes however a more direct relationship between the blockage factor and model geometry is convenient. Thom (Ref.5.4; 1943) replaced the single doublet of Lock's method by a series of sources and sinks distributed along the model chord. For a thin aerofoil the distribution need not be very complex and leads to the relationship

$$\epsilon_s = \frac{\pi A}{6\beta^3 h^2} = 0.524\,\frac{A}{\beta^3 h^2}\,, \tag{5.7}$$

where A is the cross-sectional area of the profile, related by some numerical factor to the product ct . If this factor is known, Equation (5.7) may be rearranged to a form similar to (5.6). For thin aerofoils the two equations yield similar blockage factors. Von Baranoff (Ref. 5.39; 1940) had earlier derived an expression for the solid-blockage factor identical with Equation (5.7).

Alternatively, use may be made of a simple formula developed by Young and Squire (Ref. 5.5; 1945), which is equivalent to

$$\epsilon_s = 0.62 \frac{A}{\beta^3 h^2} . \tag{5.8}$$

The numerical factor is higher than in Equation (5.7) and Reference 5.5 suggests that Equation (5.8) may be preferable for thick sections. The effect of profile thickness has in fact been allowed for empirically by Thompson (Ref. 5.6; 1948), whose work suggests an equation of the form (see Reference 5.25*)

$$\epsilon_s = 0.524 \left[1 + 1.2\beta\left(\frac{t}{c}\right)\right] \frac{A}{\beta^3 h^2} \tag{5.9}$$

which agrees with Thom's relation for very thin aerofoils and with Young and Squire's equation when the thickness/chord ratio is about 0.2. An equation similar to (5.9) is probably the best simple approximation for the solid-blockage factor provided c/h is not too large, say about 0.25 for moderate subsonic Mach numbers.

It is interesting to note that, if $A = k_2 ct$ and the aerofoil is replaced by an ellipse of the same area and thickness (but smaller chord), Equation (5.6) may be written in a similar form to Equation (5.9) but with the numerical factor 1.2 replaced by $\frac{1}{4}\pi/k_2$. If $k_2 = 0.65$, a typical value, then $\frac{1}{4}\pi/k_2 = 1.21$. This correspondence suggests that a more general form of Equation (5.9), or of Equation (5.6) is possible; in the latter case λ_2 must be replaced by $\frac{1}{2}[1 + (4k_2/\pi)(c/t)]$.

It is obviously possible to extend the preceding analyses to include terms up to the fourth power in (c/h); this was done in incompressible flow by Goldstein (Ref. 5.7; 1942) who derived an equation which must be solved for each aerofoil. Allen and Vincenti$^{5.3}$ show that the first term in this is identical with Equation (5.7), so that Goldstein's relation becomes

$$\epsilon_s = \frac{\pi A}{6h^2} + \frac{\pi^3}{360}\left(\frac{c}{h}\right)^4 \int_0^{\pi} \frac{z(x)}{c} \frac{\cos 4\theta}{\sin\theta}\, d\theta . \tag{5.10}$$

where , with x measured from the leading edge, θ is defined by

$$x = \tfrac{1}{2}c(1 - \cos\theta) . \tag{5.11}$$

---

[*] The compressibility factor applied to the aerofoil thickness in Equation (5.9) was omitted in Thompson's original paper, and later inserted by Evans. Though not strictly in accord with Goldstein's theory in Equation (5.14) below, it is partially justified by experimental data and is recommended by the present author.

The more complex solid-blockage corrections have also received considerable attention from Woods. In Reference 5.8 (1954), for example, he shows that the distribution of solid blockage along a thin aerofoil may be written as

$$\epsilon_s(x) = \frac{\pi A}{6\beta^3 h^2}\left[1 + \frac{N}{\beta} - \frac{k(x)}{5A}\left(\frac{\pi}{\beta h}\right)^2\right], \qquad (5.12)$$

where $k(x)$ is the moment of inertia of the section about the position x . The parameter N is given by

$$N = -\frac{2}{\pi A}\int_0^c\int_0^c \frac{dz(x')}{dx'}\,\frac{z(x)}{x' - x}\,dx'dx\ . \qquad (5.13)$$

This topic is also discussed in Section 7.8 of Woods's book (Ref. 5.22; 1961). To the first approximation $\epsilon_s(x)$ is constant along the chord and has the value calculated by Thom in Equation (5.7). This variation of ϵ_s may be used to determine some mean value over the length of model, particularly if balance measurements have been made. In correcting the measured pressure distribution along the model, the local value of ϵ_s may be used; care is required if ϵ_s changes greatly along the model, as this may indicate that the pressure distribution itself may be distorted by the tunnel walls, thus reducing the validity of applying a blockage factor of the type contained in Equation (5.12). More complicated methods of calculating the blockage may then be required; some of these are discussed below.

To illustrate a particular application of Equation (5.12), an elliptical profile may be considered. Then

$$\epsilon_s(x) = \frac{\pi A}{6\beta^3 h^2}\left[1 + \frac{1}{\beta}\left(\frac{t}{c}\right)\right] - \frac{\pi^3}{1920}\left(\frac{c}{h}\right)^4\frac{1}{\beta^5}\left(\frac{t}{c}\right)[1 + 4\cos^2\theta]\ . \qquad (5.14)$$

The solid blockage is therefore a maximum at the mid-chord of the profile and falls off towards the leading and trailing edges. The first term is in fact similar to that derived by Thompson in Equation (5.9) apart from the compressibility factor for thickness effect. The second term of Equation (5.14) in incompressible flow might be expected to agree with that derived from Equation (5.10) for an ellipse. At the mid-chord position, Woods' equation has a term of magnitude $-(\pi^4/1920)(c/h)^4(t/c)$, whereas Goldstein's equation has a $(c/h)^4$ term of zero value. Similar discrepancies occur for a biconvex profile.*

Knechtel (Ref. 5.32; 1953) has made an experimental investigation in which the ratio of aerofoil chord to tunnel height was varied progressively. Near zero-lift conditions at Mach numbers up to 0.85 satisfactory corrections can be made for boundary-interference effects with only terms in $(c/h)^2$ unless $c > 0.15h$. For larger models the simple corrections become increasingly questionable.

In allowing for the effect of compressibility Woods uses hodograph-type equations to avoid the limitations of simple small-perturbation theory. Considerations of this type have led Klunker and Harder (Ref. 5.9; 1951) to use the so-called Prandtl-Busemann iteration method for small disturbances to calculate a second approximation to the blockage corrections for a thin symmetrical body at zero incidence. It is assumed that the potential function of the non-linear equations of motion may be expanded in a series form where each successive term is small compared with its predecessor. It is possible in this way to calculate the blockage effect over the complete model surface and to estimate the errors which may arise, when $c/\beta h$ is large, from ignoring the chordwise changes in induced velocity.

---

* At present the reason for this disagreement is not apparent.

The occasional need for more precise solid-blockage corrections than result from the simple theories has given rise to several diverse approaches, a few of which may be mentioned briefly. Thom and Klanfer (Refs. 5.10 and 5.11; 1946-47) have developed a "squares" method for solving the complete field about an aerofoil in a wind tunnel. A similar relaxation technique has been used by Emmons (Ref. 5.12; 1948) and by Epstein and Albers (Ref. 5.13; 1948). In the latter case a 10-per-cent-thick symmetrical aerofoil of two sizes, $c = \frac{1}{2}h$ and $c = h$, was considered at stream Mach numbers of zero and 0.5. Tsien and Lees (Ref. 5.45; 1945) have combined linear perturbation theory with a representation of the aerofoil by a source-sink distribution and consider the correction to the maximum surface velocity on a 10-per-cent-thick parabolic-arc profile for two different heights of tunnel. Whitehead (Ref. 5.17; 1950) gives an additional method for calculating the solid blockage of very large bodies, and the effect of the tunnel walls on the critical Mach number of a circular cylinder spanning a tunnel is discussed in a paper by Suzuki (Ref. 5.53; 1941) who uses the hodograph method.

These examples perhaps serve to illustrate that in seeking more accurate corrections for a large model much simplicity is lost and extensive calculation may be needed for each case. It is unlikely therefore that use of such techniques for routine test work will be wide-spread. With large models indeed it may no longer be sufficient to calculate the distribution of blockage along the model and assume that this is independent of model lift. What may then be required is the distortion of the surface pressure distribution due to the presence of the wind-tunnel walls.

A process of conformal mapping is valuable for obtaining this information. No general expressions can be derived and a fresh calculation must be made for each aerofoil and test incidence. Both the symmetrical aerofoil at zero lift and the arbitrary lifting aerofoil have been discussed by Perl and Moses in References 5.15 and 5.16; the results, obtained by a series of flow transformations, are compared with those obtained from image methods of Lock$^{5.1}$ and Goldstein$^{5.7}$. At incidence the solid blockage is calculated as well as the modified surface pressures. It is claimed that the conformal mapping method is very convenient to use if more exact corrections are required than would be given by equations using terms up to $(c/h)^4$. A similar though less complicated method of mapping was developed some years earlier by Franke and Weinig (Ref. 5.20; 1939). A full discussion of the use of a complex potential method for determining the combined lift and blockage interference of a two-dimensional aerofoil is given by Barbieux (Ref. 5.54; 1955), where comparison is made with the simple equations derived by Lock, Thom, Allen and Vincenti and others. Barbieux gives results from which the distribution of blockage along the profile may be calculated.

Though the advanced general methods deal adequately with the lifting aerofoil, it is possible to adapt the simple theory to deal with the solid blockage of an aerofoil at an incidence α. This was done for incompressible flow by Batchelor (Ref. 5.21; 1944), who showed that the solid-blockage factor must be increased by an amount proportional to α^2. The relationship between the new blockage factor and that appropriate at zero incidence may be written approximately as

$$\epsilon_s(\alpha) = \epsilon_s\left[1 + 1.1\left(\frac{c}{t}\right)\alpha^2\right], \qquad (5.15)$$

where α is measured in radians. For $c/t = 10$ and $\alpha = 10^0$ the blockage factor is about one-third greater than at $\alpha = 0^0$. This order of increase is near that derived from semi-empirical corrections to large models at incidence based on the measurement of wall pressures. One such approach is discussed in Reference 5.19 where the velocities at the walls of the tunnel close to the model position were measured and then averaged to remove the lift effect. The increase in this average value with model incidence was related to changes in the blockage. Such a technique can, of course, be regarded as an extension of more normal methods for estimating the solid blockage from the pressures on the tunnel walls, a subject discussed further in Section 5.6. For compressible flow, Equation (5.15) may still be used, though presumably with the additional factor β in the term in α^2.

In all the foregoing discussion it has been assumed that the model is placed midway between the two tunnel walls. If the model is offset from the centre line by a distance $(\frac{1}{2}h - d)$, so that d is the distance of the aerofoil from the tunnel wall, a small increase in the solid-blockage factor occurs. This effect has been estimated for low-speed flow by Batchelor[5.21] and the relationship between the off-centre and centre-line blockage factors may be written as

$$\epsilon_s(d) = \epsilon_s\left[1 + \tfrac{3}{4}\cot^2\frac{\pi d}{h}\right]; \qquad (5.16)$$

this equation is also valid in subsonic compressible flow. Thus, a model offset from the tunnel centre line by 0.1h will be subject to about 8% increase in solid blockage. It should be pointed out that, when the model is offset, the transverse component of the velocity induced by the images of the model is no longer zero; strictly therefore there should be an incidence (and camber) correction due to solid blockage. This is usually very small, especially when compared with the corresponding correction due to the lift on the model. The aerofoil displaced from the tunnel centre line is also discussed in Reference 5.7.

5.2.2 Body of Revolution

The analysis for a body of revolution, though more complex, is in many ways similar to that for an aerofoil. In the early work Lock (Refs. 5.1; 5.29) replaced a small body by a doublet whose strength was related to [illegible] e-stream velocity by a factor λ_3, analogous to λ_2 in the preceding sectic [illegible] ody was then effectively represented by an equivalent sphere of diameter $(4A_m/\pi)^{\frac{1}{2}}\lambda_3$, where A_m is the maximum cross-section of the body normal to the stream and, corresponding to Equation (5.3),

$$\lambda_3 = 4\int\frac{q}{U}\,\frac{[z(s)]^2}{t^3}\,ds\,. \qquad (5.17)$$

The images of this doublet persist to infinity on all sides of the model, so that a doubly-infinite summation is required to obtain the solid-blockage factor. For a model centrally placed in a tunnel of height h and breadth b

$$\epsilon_s = \tau\left(\frac{A_m}{bh}\right)^{3/2}\lambda_3 \,, \tag{5.18}$$

where

$$\tau = \frac{1}{2\pi^{3/2}}\sum_{-\infty}^{\infty}\sum{}' \left(\frac{bh}{m^2b^2 + n^2h^2}\right)^{3/2} .$$

Here $\sum_{-\infty}^{\infty}\sum{}'$ indicates that (m,n) takes all integral pairs except (0,0). τ is a numerical coefficient which must be determined for each ratio of tunnel height to breadth; for a square tunnel $\tau = 0.809$ (Ref.5.1). Lock calculated λ_3 for a Rankine ovoid and a spheroid and this work was later extended by Borden (Ref.5.2; 1954) and Herriot (Ref.5.23; 1950). The latter reference contains tables from which λ_3 can be estimated for many shapes of body. The variation of λ_3 with body fineness ratio is shown in Figure 5.2.

Young (Ref.5.5; 1945) has also estimated λ_3 for bodies having pointed tails, for a range of maximum-thickness position. If the fineness ratio of the body is denoted by f , the equation

$$\lambda_3 = 0.4 + 0.49f \tag{5.19}$$

approximately represents Young's results (Fig.5.2) and gives a rather lower value than for symmetrical bodies of the same fineness ratio. A more recent discussion of Lock's method, which includes an approximate method of deriving λ_3 for streamline bodies has been given by Vasy (Ref.5.24; 1957).

Despite the existence of fairly extensive data for estimating λ_3 for any given body, many authors have adopted the alternative approach whereby the blockage factor is related to the body volume V . This is analogous to the use of the cross-sectional area A in the case of a two-dimensional aerofoil. It can be shown that

$$2\lambda_3 A_m^{3/2} \fallingdotseq \sqrt{\pi}V \,, \tag{5.20}$$

and that the strength P of the doublet representing the model is given by the product VU . Thus Equation (5.18) may be rewritten

$$\epsilon_s = \left(\tau\frac{\sqrt{\pi}}{2}\right)\left(\frac{1}{bh}\right)^{3/2} V = T\left(\frac{1}{bh}\right)^{3/2} V \,, \tag{5.21}$$

where the tunnel shape factor

$$T = \frac{1}{4\pi}\sum_{-\infty}^{\infty}\sum{}' \left(\frac{bh}{m^2b^2 + n^2h^2}\right)^{3/2} .$$

Small perturbation theory allows the effect of compressibility to be estimated in the same way as for an aerofoil*. Thus

$$\epsilon_s = T\left(\frac{1}{bh}\right)^{3/2}\frac{V}{\beta^3}\,. \tag{5.22}$$

Evans[5.25], using some earlier work of Thompson[5.5], includes an additional term to allow for the effect of body fineness ratio, so that Equation (5.22) becomes**

$$\epsilon_s = T\left(\frac{1}{bh}\right)^{3/2}\frac{V}{\beta^3}(1 + 0.4\beta/f)\,. \tag{5.23}$$

If it is assumed that $V = k_3 l t^2$, where l is the length of the body and t its maximum diameter, this modification is equivalent to putting in Equation (5.16)

$$\lambda_3 = \frac{4}{\pi}k_3[f + 0.4]\,, \tag{5.24}$$

which, for a typical value $k_3 = 0.45$, gives values of λ_3 close to those derived more directly.

In Section 5.2.1 it was suggested that the solid-blockage factor of an aerofoil could be determined readily if the model was replaced by an equivalent ellipse. Similarly, the body of revolution may be replaced by a spheroid having the same volume and maximum thickness; the length of the equivalent spheroid will usually be less than l, and the equivalent fineness ratio will be

$$f_e = \frac{6k_3}{\pi}f\,. \tag{5.25}$$

The value of λ_3 for the body may now be found directly from Figure 5.2. As an example, consider a body of actual fineness ratio 10, where the equivalent-spheroid approach yields the value $\lambda_3 = 5.91$ in close agreement with $\lambda_3 = 5.96$ from Equation (5.24).

So far we have considered the contribution of the model geometry to the blockage factor. The tunnel shape also influences ϵ_s through the parameter T or τ and values for specific tunnel cross-sections are given in several papers (e.g., References 5.1, 5.4, 5.23). The most complete calculations for the tunnel-shape parameter are probably those by Herriot[5.23], covering values of b/h between 0.29 and 3.5 with corresponding changes in τ from 0.81 to 1.73. These results are replotted in Figures 5.3 and 5.4 in terms of T, where use is made of the fact that for a small model the value of τ is independent of the orientation of the model with respect to the walls. Approximate formulae for T have been suggested as an alternative to the more precise calculations. Thus, for $\frac{1}{2} < b/h < 2$, Thompson[5.6] recommends

---

* In some early papers there was confusion about the precise form of the boundary conditions at the model and hence of the compressibility factor. It is now generally accepted that β^{-3} is correct.

** The remarks contained in the footnote, indicated just before Equation (5.9), about the compressibility factor for thickness effect of two-dimensional profiles apply to three-dimensional bodies also.

$$T = 0.36\left[\frac{b}{h} + \frac{h}{b}\right]. \tag{5.26}$$

As Figure 5.4 shows, this lies very close to Herriot's curve. For $1.2 < b/h < 2.0$ Young and Squire[5.5] have suggested the following formula

$$T = 0.65\left(\frac{b}{h}\right)^{\frac{1}{2}}, \tag{5.27}$$

which, though far less satisfactory, leads to a very simple form of Equation (5.22),

$$\epsilon_s = 0.65\,\frac{V_m}{\beta^3 h^2 b}. \tag{5.28}$$

It is claimed that this gives the blockage correction to within ±5% for any three-dimensional model. For a body of revolution specifically, Young and Squire suggest that the numerical factor is taken as 0.68. There would seem to be little to be saved in using their form in place of the more exact relation (5.22) or (5.23), combined with (5.26).

As in the case of the two-dimensional aerofoil, it is sometimes necessary to use more complex expressions for the solid blockage, if the body is long compared with the tunnel dimensions. This problem has been considered, for example, by Evans (Ref.5.25; 1949), whose method is essentially a development and extension of the earlier papers by Thom and Thompson. A thin body of revolution may be represented approximately by a distribution of sources and sinks along the body axis, and the walls by an infinite array of images. The variation of the blockage factor along the body may now be calculated; this is done by Evans for a tunnel where $b/h = 1.43$. The method, though more complex than the simple analyses discussed earlier, may easily be applied to any value of b/h so that the validity of the simple equation can be checked in any particular case.

A model mounted off the tunnel axis is considered in Reference 5.57.

5.2.3 Wings and Wing-Body Combinations

For the purpose of calculating the solid-blockage effects the small wing or wing-body combination of finite span may be regarded as identical to a body of revolution of the same volume. This implies, however, that the wing is replaced by an equivalent sphere or spheroid, and not, as one might feel is more appropriate, by an equivalent cylinder. A rectangular wing of 6 ft (1.83 m) span, 1 ft (0.305 m) chord with $t/c = 0.125$ would be replaced in the analysis by a sphere of diameter about 11.8 ins (0.30 m); the equivalent spheroid, having the same frontal area as the wing, would not be greatly different from this sphere.

Though precision is not possible in such matters a "small" wing may conveniently be regarded as one in which the ratio of the wing span (2a) to the tunnel breadth (b) is below about 0.5. Within this range, Equation (5.22) may be used and Equation (5.23) modified to become

$$\epsilon_s = T\left(\frac{1}{C}\right)^{3/2} \frac{V}{\beta^3}\left[1 + 1.2\beta\left(\frac{t}{c}\right)\right], \qquad (5.29)$$

where $C = bh$. It is assumed in this equation that the wing effects will be more important than those arising from the body.

When the model is no longer small compared with the tunnel dimensions, its representation by a doublet becomes invalid. For a slender delta planform a distribution of sources and sinks lying along the model axis should be used and the calculation made as for a long body of revolution[5.25]. In practice, a single source-sink arrangement is often sufficient. If the wing is unswept or only moderately swept, it may be better to represent it by a series of finite line sources and sinks running either parallel to the span, or parallel to the leading edge. Such an approach was made by Thom[5.4], who chose to keep the strength of the sources and sinks constant along the span despite the fact that this arrangement strictly entails some distortion of the planform and a reduction in wing thickness near the tip. The axial velocity induced in the tunnel by the images of the distribution representing the model may now be found, though in some cases the calculation may be complex.

The representation of the wing by line sources and sinks was also adopted by Herriot[5.23], whose results cover a wide range of tunnel shape ($0.29 < b/h < 3.5$) and model span ($0 < 2s/b < 1$) in compressible flow. Herriot's results may be expressed in terms of the tunnel-shape parameter τ and the body-shape parameters λ_2 and λ_3. In the notation of the present text his equation for the solid-blockage factor at the centre of a finite wing of frontal area A_a may be written as

$$\epsilon_s = \frac{\pi^{3/2}\tau A_a t\lambda_2}{4\beta^3(bh)^{3/2}}, \qquad (5.30)$$

where τ now depends on $2s/b$.

Equation (5.30) may be transformed to yield equations similar to (5.22) and (5.29) above, but where T is now a function of b/h and $2s/b$, as shown in Figures 5.5* and 5.6 which are based on Reference 5.23; when $2s/b < 0.5$, T does not vary greatly with $2s/b$. The general forms of Equations (5.23) and (5.29) may be applied to wing-body combinations as well as simple wings, since the effect of the wing is generally of greatest importance in determining the blockage. In cases where this is less obvious, the contributions of the wing and body separately may be estimated and their effects added.

When the wing is sweptback, and perhaps tapered, the lines of sources and sinks may no longer be normal to the stream and the infinite summations are less easy. Evans[5.25] has shown that most wings may be represented by a uniform non-tapered wing, having the

---

* For $2s/b = 1$, a comparison can be made with two-dimensional results by putting $V = Ab$ in Equation (5.22). In this case

$$T = \frac{\pi}{6}\left(\frac{b}{h}\right)^{\frac{1}{2}} + \frac{1}{\pi}\left(\frac{h}{b}\right)^{3/2}.$$

where the first term corresponds to Equation (5.7) and the second term arises from the side-wall images.

same volume, mean sweep and thickness-chord ratio as the original wing, but with a span equal to $2\sqrt{3}\,k_x$, where k_x is the radius of gyration of the original wing about the x axis. In Reference 5.25, Evans is concerned with a tunnel with b/h = 1.43 and carries out summations for various mean sweeps, so that ϵ_s may be calculated over the model. The method, however, is of very general application.

When a half-span model, mounted directly on to the tunnel side-wall, is being tested, the solid blockage at the model position is approximately that due to a complete model in a tunnel of twice the breadth.

It may sometimes be necessary to calculate the solid-blockage effects of model supports, such as struts and stings. Some care is required, because the strut is roughly equivalent to a half-wing model and the sting to a very long solid of revolution; moreover the corrections to stream velocity are required at the model position and not at the centre of the support. It is sometimes preferable to attempt to measure directly this velocity increment associated with the support gear in the absence of the model.

5.3 SOLID BLOCKAGE FACTORS IN CLOSED NON-RECTANGULAR TUNNELS

5.3.1 Octagonal Tunnels

Many wind tunnels, though basically of rectangular cross-section, have corner fillets to form what may be described as an octagonal working section. The effect of the corner fillets in modifying the results presented in Section 5.2 is therefore of some importance, though it is likely that significant differences will only arise if the fillets are large. The analysis for an octagonal tunnel is less straightforward than for a rectangular tunnel and only very approximate methods are at present available. Batchelor[5.21], considering incompressible flow, uses the fact that the tunnel height varies along the span of a two-dimensional aerofoil and argues that there is a consequent spanwise variation in ϵ_s which locally is given by Equation (5.2). This means that when the overall force on the wing is measured the interference must be averaged across the span to give an equivalent height, as defined by Equation (2.29) of Chapter II. Details of the results for the Melbourne 9 ft x 7 ft tunnel will be found in Reference 5.21; some care is required if the forces are measured on only part of the wing span. Batchelor's approach probably overestimates the interference present on a full-span model, and it would seem safer to adopt the alternative equivalent height suggested in Equation (2.30) of Chapter II. The fillets can probably be ignored in relation to measurements of pressure at the mid-span position.

Batchelor also discusses the interference likely to arise from three-dimensional models within the octagonal working section. It is assumed that the solid blockage is the sum of that due to the basic rectangular section and a contribution from the corner fillets. The condition of zero flow across the fillet boundary is only approximately satisfied by the chosen distribution of sources and sinks because of the complexity of the analysis. Working in terms of the tunnel-shape parameter τ and the three-dimensional model-shape parameter λ_3, Batchelor estimates the blockage factor from the following equation

$$\epsilon_s = \tau_0 \left(\frac{A_m}{bh}\right)^{3/2} \lambda_3 + \tau_1 \left(\frac{A_m}{C}\right)^{3/2} \lambda_3 . \qquad (5.31)$$

where τ_0 is the value for the basic rectangular tunnel, τ_1 is the calculated increment due to the fillets, and C is the cross-sectional area of the octagonal working section. Equation (5.31) may be rewritten as

$$\epsilon_s = \left[\tau_0 \left(\frac{C}{bh}\right)^{3/2} + \tau_1\right] \left(\frac{A_m}{C}\right)^{3/2} \lambda_3 . \qquad (5.32)$$

which is in an analogous form to Equation (5.18). For the Melbourne tunnel $\tau_0 = 0.83$, and the first term in the square bracket has a value of 0.71. τ_1 is estimated to be about 0.04 which is sufficiently small to suggest that, for moderately small fillets, a sufficiently good answer may be obtained by simply calculating the blockage factor appropriate to the basic rectangular tunnel, i.e., by putting $\tau_1 = 0$ in Equation (5.32). If this procedure is valid, then any of the formulae in Section 5.2 may be used and the effect of compressibility is allowed for by the factor β^{-3}.

The lift interference on a model in an octagonal tunnel was also discussed by Batchelor in Reference 5.21, and this approach was later extended by Loos (Ref. 5.51; 1951), who represented the tunnel walls in a simpler but rather more approximate fashion. It seems possible that a similar analysis could be made for the blockage correction.

5.3.2 Circular and Elliptical Tunnels

Tunnels having a closed circular cross-section are now less widely employed than in the past; as a consequence there is less literature on blockage effects than for the rectangular working section.

The calculation of the solid blockage attributable to an aerofoil spanning a closed circular tunnel is far from easy and seems first to have been discussed by Vincenti and Graham (Ref. 5.27; 1946); they pointed out that the interference cannot be found by the image method, since no system of images satisfies the appropriate conditions at the tunnel boundary. The flow field of the non-lifting two-dimensional model was represented by a distribution of horse-shoe vortex elements of infinitesimal span for which the interference field in a circular tunnel is known[5.55]. In the present notation, these authors obtained, for the solid-blockage factor at the tunnel centre,

$$\epsilon_s = 1.356 \left(\frac{c}{2R}\right)^2 \left(\frac{t}{c}\right)^2 \frac{1}{\beta^3} \lambda_2 , \qquad (5.33)$$

where R is the radius of the tunnel. This is identical to Equation (5.6) for an aerofoil spanning a two-dimensional rectangular tunnel of height 1.558R. It follows that, provided this transformation of tunnel height and diameter is made, the several blockage equations of Section 5.2.1 may be used. Thompson's Equation (5.9) becomes, for example,

$$\epsilon_s = 0.216 \left[1 + 1.2\beta \left(\frac{t}{c}\right)\right] \frac{A}{\beta^3 R^2} . \qquad (5.34)$$

Vincenti and Graham show that, because of the symmetry of the system, no vertical velocity is induced at any position along the span of the aerofoil, nor is there a streamwise pressure-gradient associated with the solid blockage.

The blockage effect of a body of revolution inside a circular tunnel was one of the earliest problems of this type to be discussed. Lamb (Ref.5.26; 1926) considered a Rankine ovoid. The series of Bessel functions which arise in the analysis were subsequently reduced to a more usable form by Watson (Ref.5.28; 1930). Glauert[5.1] and Lock[5.29] derived the solid-blockage factor for incompressible flow in the simple form

$$\epsilon_s = 0.797\left(\frac{A_m}{C}\right)^{3/2}\lambda_3 . \qquad (5.35)$$

where $C = \pi R^2$. Hence

$$\epsilon_s = 0.144\left(\frac{A_m}{R^2}\right)^{3/2}\lambda_3 ; \qquad (5.36)$$

λ_3 may be derived for a wide range of bodies from the tables in Reference 5.23, or alternatively estimated from Figure 5.2. The numerical factor in Equation (5.35) is, of course, a tunnel-shape parameter analogous to τ ; its value is close to that for a square tunnel (0.81).

Once again it is sometimes convenient to use the model volume V and a tunnel-shape parameter corresponding to $T(=\frac{1}{4}\sqrt{\pi}\tau)$. With allowance for compressibility, Equations (5.35) and (5.36) then become

$$\epsilon_s = 0.706\left(\frac{1}{C}\right)^{3/2}\frac{V}{\beta^3} \qquad (5.37)$$

and

$$\epsilon_s = 0.128\,\frac{V}{\beta^3 R^3} . \qquad (5.38)$$

The tunnel parameter T thus has a value of 0.706 for circular tunnels. Equations of this type have been derived by several authors[5.23,5.30-5.32] for small bodies of revolution, small wings or wing-body combinations. Thompson's thickness modification may also be applied by multiplying the equations by either $[1 + 1.2\beta(t/c)]$ or $(1 + 0.4\beta/f)$.

When the model span is no longer small compared with the tunnel breadth, the numerical constants in Equations (5.35) and (5.37) must be modified[5.23] as shown in the following table and Figure 5.6.

2s/b	0	0.25	0.50	0.75
τ	0.797	0.812	0.828	0.859
T	0.706	0.720	0.734	0.761

The actual variation in T with model size is very close to that for a square tunnel. Herriot's theory is not really applicable at the limit $2s/b = 1$, but a similar difference to that noted for rectangular tunnels (footnote in Section 5.2.3) occurs if his limiting results are compared with the quasi-two-dimensional Equation (5.34).

Fuchshuber (Ref.5.59; 1961) gives a mathematical solution of the axisymmetrical problem without numerical results. The solid-blockage corrections associated with a body of revolution at incidence in the centre of a circular tunnel has been considered in general terms by Cremer and Kolberg (Ref.5.58; 1960). Even the expression for the velocity increment at the centre-line of the tunnel is quite complicated, and the authors suggest the use of a computer in any applications.

The distribution of solid blockage along a body of length l placed at the axis of a circular tunnel has been discussed by Vandrey (Ref.5.33; 1951) in a paper which may be regarded as the counterpart of Borden's analysis$^{5.2}$ for rectangular tunnels. Vandrey replaces the body by a Rankine ovoid having the same volume and maximum cross-section and obtains an expression for the solid-blockage factor at a distance x from the body centre

$$\epsilon_s(x) = [H(\xi_1)] - H(\xi_2)] \frac{A_m}{C} , \qquad (5.39)$$

where

$$\left.\begin{aligned} \xi_1 &= \frac{x + \frac{1}{2}a}{R} \\ \xi_2 &= \frac{x - \frac{1}{2}a}{R} \end{aligned}\right\}$$

and $H(\xi)$ is given in Table 5.I. Distributions of $\epsilon_s(x)$ for bodies of different lengths are illustrated in Figure 5.7.

The maximum blockage factor is reached at the centre of the body $(x = 0)$, where

$$\epsilon_s(0) = 2\left[H\left(\frac{a}{2R}\right)\right] \frac{A_m}{C} , \qquad (5.40)$$

where a is the distance between the source and the sink that represent the body. For a Rankine ovoid the shape parameter λ_3 is approximately equal to the body fineness ratio$^{5.2}$. Equation (5.40) may be rewritten as

$$\begin{aligned} \epsilon_s(0) &= \left\{\frac{4R}{\ell f} H\left(\frac{a}{2R}\right)\right\} \lambda_3 \left(\frac{A_m}{C}\right)^{3/2} \\ &= \tau \left(\frac{A_m}{C}\right)^{3/2} \lambda_3 , \qquad (5.41) \end{aligned}$$

which is formally similar to Equation (5.18). The parameter τ will now vary with the ratio of the body length to tunnel diameter (Fig.5.8). For a very small body τ

approaches Lock's value of 0.797. It is at once apparent that use of this small-body value for long bodies will seriously overestimate the maximum solid-blockage correction.

Though the analysis is strictly only applicable to Rankine ovoids, it should also apply approximately to bodies of rather similar shape. Thus Equation (5.41) may be rewritten as

$$\epsilon_s(0) = T\left(\frac{1}{C}\right)^{3/2}\frac{V}{\beta^3}\,. \qquad (5.42)$$

where $T(=\frac{1}{2}\sqrt{\pi}\,\tau)$ is also given in Figure 5.8. It is interesting to note the marked similarity between Vandrey's work and an earlier discussion by Lock and Johansen (Ref.5.34; 1931). The value of $\epsilon_s(0)$ is by definition the maximum achieved on the body and not the average over its length. It may be argued that for many purposes, such as the determination of critical flow conditions, it is this maximum value which is of greatest importance; in other cases, such as the correction of drag and pressure measurements, the mean blockage may well be used.

Vandrey's method may also be applied to find the solid-blockage factor for a semi-infinite body; the variation ahead of, and along, the body is shown in Figure 5.9. The maximum value of ϵ_s has almost been reached by one tunnel diameter from the nose of the body. For this case the origin can conveniently be changed to the source position near the body nose. If x_1 is the distance from this origin, then Equation (5.39) reduces to

$$\epsilon_s(x_1) = [0.5 + H(\xi_3)]\left(\frac{A_m}{C}\right). \qquad (5.43)$$

where $$\xi_3 = x_1/R\,.$$

Since the velocity gradient at the origin due to a source corresponds in magnitude to the velocity induced by a doublet, the tangent to the curve shown in Figure 5.9 may be regarded as equivalent to Lock's small-body Equation (5-35) if the fineness ratio is assumed to equal λ_3.

Though several authors have considered the lift interference associated with a model mounted in a tunnel of elliptical cross-section, the corresponding blockage problem seems to have been neglected. To estimate the solid-blockage factor at the centre section of a two-dimensional aerofoil spanning an elliptical tunnel, it would seem possible to apply rectangular-tunnel corrections for an effective tunnel height h_e. If m and n are the major (spanwise) and minor axes of the tunnel, then h_e will be in the range between the values for circular and rectangular tunnels $0.779 < h_e/n < 1$; in the absence of other evidence, a simple linear relationship between h_e/n and n/m is suggested in Figure 5.10. For balance measurements on the full aerofoil span, h_e may be taken as equal to $\frac{1}{4}\pi n$.

For a small three-dimensional model the tunnel-shape parameter T or τ for a circular tunnel is within 2% of that for a square tunnel, and Figure 5.6 shows that the variation of the tunnel-shape parameter with increasing model size is similar for the two shapes of working section. In the absence of direct information it is suggested that, for three-dimensional models, the approximate value of T or τ for an elliptical tunnel may be taken as that for a rectangular tunnel of breadth to height ratio m/n . It is important to remember that, in adapting the formulae of Sections 5.2.2 and 5.2.3, the cross-sectional area of the elliptical tunnel $C(=\frac{1}{4}\pi mn)$ should be used in place of bh .

5.4 WAKE BLOCKAGE FACTORS IN CLOSED TUNNELS

5.4.1 Two-Dimensional Aerofoil in a Rectangular Tunnel

An early attempt to allow for the wake blockage of a two-dimensional aerofoil in incompressible flow was made by Page (Ref.5.35; 1929) and Lock (Ref.5.29; 1929), who introduced an empirical factor based on the effective width of the wake, into the solid-blockage correction. Later Glauert[5.1] drew an analogy with the discontinuous flow behind a bluff body in a constricted stream and suggested that the effect of the wake-induced longitudinal velocity increment on the measured drag force (D) could be represented by

$$D_C = D\left[1 - \frac{\eta t}{h}\right]^2 , \qquad (5.44)$$

where D_C is the corrected drag; ηt is the effective width of the wake some distance downstream of the model and is assumed to vary with thickness/chord ratio in the manner shown in Figure 5.11. This curve is based on the experimental evidence available when Reference 5.1 was written (1933). Equation (5.44) corresponds to a wake-blockage factor

$$\epsilon_w = \eta\left(\frac{t}{c}\right)\left(\frac{c}{h}\right). \qquad (5.45)$$

if terms in η^2 are neglected.

Subsequent authors have felt that the use of the factor η was in many ways unsatisfactory, particularly for aerofoils and slender bodies and it is now usual to relate ϵ_w to the measured body drag when this is known or can be estimated. Use has often been made of Prandtl's suggestion that the wake can be represented by an equivalent source situated at some point on the aerofoil (say, mid-chord or trailing edge). The strength of this source Q is related to the aerofoil drag by

$$Q = \frac{D}{\rho U} . \qquad (5.46)$$

A sink of equal strength must be placed far downstream. The velocity increment due to wake blockage may then be calculated as that effectively induced at the model position by the infinite array of source and sink images. The appropriate wake-blockage factor in incompressible flow

$$\epsilon_w = \frac{1}{4}\left(\frac{c}{h}\right)C_D \qquad (5.47)$$

has been derived by many authors. For modern aerofoil sections, Equation (5.47) gives a lower value of ϵ_w than Equation (5.45) and is to be preferred.

Equation (5.47) is derived in slightly different ways in the literature, mainly because of inherent difficulties in satisfying the conditions well downstream of the model*. These differences are of little importance in incompressible flow, but may affect the compressibility factor that is applied. Thom[5.4] and Göthert[5.31] recommend multiplying Equation (5.47) by β^{-2} to give

$$\epsilon_w = \frac{1}{4}\left(\frac{c}{h}\right)\frac{1}{\beta^2} C_D . \qquad (5.48)$$

Allen and Vincenti[5.3] consider that the source representing the model wake should give the same pressure drop far downstream and not, as in Reference 5.4, the same drag as the model in the tunnel. Allen and Vincenti obtain a different compressibility factor which, for the ratio of specific heats $\gamma = 1.4$, gives

$$\epsilon_w = \frac{1}{4}\left(\frac{c}{h}\right)\frac{1 + 0.4M^2}{\beta^2} C_D . \qquad (5.49)$$

This compressibility factor lies between β^{-2} and β^{-3} (Fig. 5.12). Thompson[5.6] doubts whether this more complex factor is theoretically better than the simpler form, because the representation of the wake by a source is in any case difficult to justify rigorously. The use of Equation (5.49) sometimes leads to better agreement with experiment at high subsonic Mach numbers than does Equation (5.48), since in practice the compressibility factor β^{-2} often underestimates the effect of stream Mach number; for this reason alone, Equation (5.49) would seem to be preferable.

Goldstein[5.7] has also considered the wake-blockage effect in incompressible flow and concludes that the source-image system of representing the wake and walls is valid if C_D is small, even though c/h is comparatively large. In such cases, however, terms up to $(c/h)^3$ may be required. Although no direct expression for a wake-blockage factor is contained in Reference 5.7, the correction is implicit in the equations derived for finding the stream velocity from measurements made at the tunnel wall.

Equation (5.48) is the first term of an equation due to Woods[5.8], who gives a somewhat different approach both in allowing for stream compressibility and for representing the wake. This is replaced by a sting of thickness g attached to the trailing edge of the model and extending to infinity downstream. In an unbounded stream

$$g = \tfrac{1}{2} c C_D , \qquad (5.50)$$

and this remains true in the tunnel provided terms in C_D^2 can be neglected. Woods shows that ϵ_w may vary along the model chord and derives the expression, valid in the neighbourhood of the aerofoil,

$$\epsilon_w(x) = \frac{1}{4}\left(\frac{c}{h}\right)\frac{1}{\beta^2} C_D \left[1 + \frac{\pi}{3\beta h}(x - c)\right] . \qquad (5.51)$$

---

* Compare, for example, the methods of References 5.3 and 5.4. Thom, in the latter paper, discusses the position of the sink and concludes that it need not be at infinity provided it is further away from the model than 5h : at smaller distances ϵ_w is affected.

The largest value of ϵ_w along the chord of the model occurs at the trailing edge ($x = c$) and is that given by Equation (5.48). Equation (5.51) may be used to calculate an approximate mean wake-blockage factor for a large model, for say, the correction of balance results. If the variation of ϵ_w along the model is large this may indicate that the pressure field around the model is distorted and does not correspond to some free-air pressure field. The validity of using the local value of ϵ_w to correct the measured pressure distribution then seems doubtful. As far as is known, the distortion of the model surface pressures due to the presence of a large wake has not been considered.

5.4.2 Three-Dimensional Models in a Rectangular Tunnel

Originally Glauert[5.1] suggested that his empirical wake-blockage factor η might be applied in a modified form for three-dimensional bodies, particularly solids of revolution. A new factor

$$\eta' = \eta^2 \tag{5.52}$$

was suggested, η being obtained from an equivalent two-dimensional body of the same fineness ratio. Equation (5.52) implies that the wake-blockage effect is far less important for small three-dimensional models than for aerofoils. Such arguments are less forceful for a large wing, and later authors have once more preferred to relate the wake-blockage factor to the model drag. As in two-dimensional flow, the wake is replaced by a source at the model position. The corresponding equation to (5.48) above is

$$\epsilon_w = \frac{1}{4}\left(\frac{S}{bh}\right)\frac{1}{\beta^2}C_D , \tag{5.53}$$

where S is the model area on which the aerodynamic coefficients are based (e.g., the planform area of a wing). Alternatively, following Allen and Vincenti[5.3] and Herriot[5.23], we have

$$\epsilon_w = \frac{1}{4}\left(\frac{S}{bh}\right)\frac{1 + 0.4M^2}{\beta^2} C_D . \tag{5.54}$$

These equations are usually held to apply to any three-dimensional model but some care is needed if this is a lifting wing; the drag is then partly due to the trailing-vortex system and partly to surface friction and incomplete pressure recovery over the after part of the model. It seems reasonable to ignore the influence of the vortex drag on the wake blockage, so that in Equations (5.53) and (5.54), C_{D_0}, the zero-lift drag should be used. Such an approach is of course consistent with the general assumption that the blockage is independent of lift, provided the latter is not large. With separated flow, however, an alternative method is required and this is discussed in Chapter VII.

Methods so far discussed have largely ignored the actual structure of the wake. This matter was considered by Evans[5.25] who, starting from the momentum and continuity equations of the flow, showed that the form of the velocity distribution within the wake had little influence on the velocity increment experienced by the flow outside the wake. The velocity inside the wake can therefore be considered as constant at Ω times the uncorrected free-stream velocity U . The velocity increment sufficiently far downstream from the model (where the wake blockage will be higher than at the model position) may be written as

$$(\delta u)_{wake} = \left[\frac{1}{4}\left(\frac{S}{bh}\right)\frac{1}{\beta^2}C_D\right]2UW , \qquad (5.55)$$

where

$$W = \frac{1}{\Omega}\left[1 + \frac{1+\Omega}{2}(\gamma - 1)M^2\right] .$$

A source of strength Q placed on the tunnel axis at the model position gives an increment

$$(\delta u)_{wake} = \frac{Q}{\beta^2 bh} . \qquad (5.56)$$

Thus the source strength equivalent to Equation (5.55) is

$$Q_e = \tfrac{1}{2}WSC_D U . \qquad (5.57)$$

Now Ω is about 0.9 in the region downstream of the model and hence as the stream Mach number increases from zero to unity W changes from 1.1 to about 1.5. Evans in fact suggests that a value of 1.4 is appropriate for most high-speed tunnel tests, if no more exact information is available. Thom[5.8] and others, using Equation (5.46), may be regarded as putting W equal to unity in Equation (5.57).

The form of Equation (5.53) advocated by Evans then becomes

$$\epsilon_W = \frac{1}{4}\left(\frac{S}{bh}\right)\left[\frac{1 + 0.2(1+\Omega)M^2}{\Omega\beta^2}\right]C_D . \qquad (5.58)$$

If Ω is taken as unity for all stream Mach numbers, this equation reduces to a form identical with Equation (5.54) above.

For a long body, Evans suggests that the source be placed at the model centre-of-volume and the wake-blockage velocity increment calculated not only along the length of the body but along the tunnel walls as well. As Section 5.6 shows, the latter information is valuable in providing a method of checking the validity of blockage-correction theory. Although Reference 5.25 is concerned with a tunnel where $b/h = 1.43$, the method is of general application.

As in the case of the solid blockage, the wake blockage for a half-span model mounted directly on the side-wall of a rectangular tunnel should be calculated from the value appropriate to a complete model in a tunnel of twice the breadth. The wake blockage of struts supporting a model may sometimes be significant and these should be regarded as equivalent to half-wings mounted on the tunnel floor. It is usually sufficient to assume that the velocity increment calculated from present techniques may be applied at the actual model position.

5.4.3 Closed Non-Rectangular Tunnels

Batchelor[5.21] and Vincenti and Graham[5.27] discuss the appropriate wake-blockage factors for two-dimensional aerofoils spanning octagonal and circular tunnels respectively; they recommend, as for solid blockage (Sections 5.3.1 and 5.3.2), that a similar formula should be used to that for a rectangular tunnel, but with an equivalent height h_e in place of h. At the centre section it seems best to ignore corner fillets, to take $h_e = 1.558R$ for a circular tunnel, and to use Figure 5.10 for an elliptical tunnel. When balance results on a full-span model have been obtained and require correction, it would seem best to put

$$h_e = \frac{C}{b}, \tag{5.59}$$

as suggested in Equation (2.30) of Chapter II; this would give a slightly larger value $h_e = 1.571R$ for a circular tunnel, or generally for an elliptical tunnel $h_e = 0.785h$ in place of Figure 5.10. The relevant wake-blockage equation in all cases will be

$$\epsilon_W = \frac{1}{4}\left(\frac{c}{h_e}\right)\left(\frac{1 + 0.4M^2}{\beta^2}\right)C_{D0} . \tag{5.60}$$

where C_{D0} is the zero-lift drag.

For bodies of revolution, wings and wing-body combinations, it is suggested that Equation (5.54) be used to determine the wake-blockage factor, but with the tunnel cross-sectional area C in place of bh. If the wake characteristics are known, Equation (5.58), similarly modified, may be employed.

5.4.4 Wake Blockage Gradient

In the preceding sections, the discussion has mainly been concerned with the calculation of the effective velocity increment at the model position caused by the images of the source and sink, that simulate the walls of the tunnel. This velocity increment varies along the tunnel axis, and hence along the model length, but the calculated value at the source position usually represents an average increment over the model unless this is very long.

Unlike the solid-blockage velocity increment, the wake-blockage effect is not symmetrical about the model but increases continuously from nose to tail. The model is therefore subject to a longitudinal velocity gradient. This buoyancy effect imposes a drag force on the model which, since it would be absent in free air, must be corrected for. The method of doing this is discussed in Section 5.8.2.

5.5 BLOCKAGE FACTORS IN OPEN-JET TUNNELS

5.5.1 Solid Blockage for Models Spanning the Tunnel

For an open jet of rectangular shape the method of images may be used to represent the model and the jet boundaries. The doublet images are no longer of the same sign, but alternate with distance from the model. The induced velocity is therefore smaller at the model position than for a closed tunnel and of opposite sign, as shown by the equation (Refs. 5.1, 5.29)

$$\epsilon_s = -\frac{\pi^2}{24}\left(\frac{c}{h}\right)^2\left(\frac{t}{c}\right)^2 \lambda_2 \, . \qquad (5.61)$$

where λ_2 is given in Figure 5.1. In magnitude this is half the blockage correction appropriate to a closed tunnel; accordingly the equations of Section 5.2.1 may be modified simply. Equation (5.9), for example, becomes

$$\epsilon_s = -0.262\left[1 + 1.2\beta\left(\frac{t}{c}\right)\right]\frac{A}{\beta^3 h^2} \, . \qquad (5.62)$$

In Reference 5.22, Section 7.21, Woods has considered the distribution of blockage factor along the axis of an open-jet tunnel due to the presence of a two-dimensional aerofoil. At the centre of the model the value obtained is identical to that given by the simple theories.

The blockage effect on an aerofoil spanning a circular jet seems to have received little consideration. By analogy with Equation (5.62) one possible assumption is that the blockage factor is half that of the corresponding closed tunnel, and of opposite sign, so that in place of Equation (5.34)

$$\epsilon_s = -0.108\left[1 + 1.2\beta\left(\frac{t}{c}\right)\right]\frac{A}{\beta^3 R^2} \, . \qquad (5.63)$$

A similar assumption may be made for elliptical working sections.

5.5.2 Three-Dimensional Solid Blockage

The boundary conditions for a small model at the centre of a rectangular free jet may be represented by a doubly-infinite set of images, as for a closed tunnel. As in the two-dimensional case the signs of the doublets alternate, this time in rows and columns, so that the velocity induced at the model position is smaller than if the boundaries were closed. Lock[5.29] evaluated the blockage factor for a square jet; the equation is similar to (5.18) above

$$\epsilon_s = \tau\left(\frac{A_m}{h^2}\right)^{3/2}\lambda_3 \, , \qquad (5.64)$$

but now $\tau = -0.238$ compared with its value 0.809 for a closed square section. The magnitude of blockage effect in a square open jet is thus only about 0.29 of that present in a closed tunnel. In terms of the model volume, with allowance for compressibility effects, a simple equation for the square jet tunnel is

$$\epsilon_s = -0.211\frac{V}{\beta^3 h^3} \, . \qquad (5.65)$$

The general case of a rectangular jet has only recently been considered, both at the NPL and by Wuest[5.57]. In the former work, values of τ were evaluated from the double summation in the notation of Equation (5.18)

$$\tau = \frac{1}{2\pi^{3/2}} \sum_{-\infty}^{\infty}\sum{}' (-1)^{m+n} \left(\frac{bh}{m^2b^2 + n^2h^2}\right)^{3/2} \tag{5.66}$$

and are given, together with $T(=\frac{1}{2}\sqrt{\pi}\,\tau)$ in the following table:

$\frac{b}{h}$	2.00 0.50	1.80 0.55_6	1.66_7 0.60	1.60 0.62_5	1.40 0.71_4	1.25 0.80	1.10 0.90_9	1.0
τ	−0.461	−0.397	−0.357	−0.339	−0.289	−0.260	−0.242	−0.238
T	−0.409	−0.352	−0.316	−0.300	−0.256	−0.231	−0.214	−0.211

The results are plotted in Figure 5.13. The percentage increase in the tunnel-shape factor in the range $1 < b/h < 2$ is much larger than for similar closed rectangular tunnels (see Figure 5.4), but the actual change in value in this range is little different for the two types of boundary.

Wuest has also considered the effects of displacing the model from the tunnel centre line.

The circular open jet containing a small model was discussed in Lock's original paper[5.29] and led to a similar equation to that for the closed tunnel but with a different numerical factor, and of opposite sign,

$$\epsilon_S = -\,0.206\left(\frac{A_m}{C}\right)^{3/2} \lambda_3\,, \tag{5.67}$$

where λ_3 is given in Figure 5.2. The ratio of solid blockage in open and closed circular tunnels is therefore −0.26, a value close to that for square tunnels. A simple equation in terms of the stream Mach number, tunnel diameter, and model volume is

$$\epsilon_s = -\,0.0333\left(\frac{V}{R^2}\right)\frac{1}{\beta^3}\,. \tag{5.68}$$

Cremer and Kolberg (Ref.5.58; 1960) have considered the solid-blockage effects due to a body of revolution placed at incidence in a circular open jet. General expressions are given for the velocity increments induced in the vicinity of the model and for the deformation of the streamlines. These expressions are very complicated, however, and are not readily evaluated without mechanized computation.

Vandrey[5.33] has considered the solid-blockage correction for long Rankine ovoids in circular open jets and obtains an analogous expression to Equation (5.39)

$$\epsilon_s(x) = [I(\xi_1) - I(\xi_2)]\,\frac{A_m}{C}\,. \tag{5.69}$$

where ξ_1 and ξ_2 are defined, and values of $I(\xi)$ listed, in Table 5.I. It is interesting to note that the largest value of $\epsilon_s(x)$ is reached at the centre of the body only if the body length is less than 6R. For longer bodies $\epsilon_s(x)$ is larger near the ends of the body than at the centre and on a semi-infinite body this maximum is achieved at a distance 1.2R downstream from the nose of the body (Fig.5.9). Fuchshuber (Ref.5.59; 1961) gives a complete axisymmetrical mathematical solution and has evaluated the flow along the boundary of the jet. For body lengths greater than about 1.5R the maximum velocity increment is obtained at two positions fore and aft of the centre; these maxima sharpen and their positions approach the ends of the body as its length increases. Because of the difficulties of obtaining long stable jets it seems that these results will seldom be needed.

Many open-jet tunnels are of elliptical cross-section and some simple blockage correction may therefore be required. In the absence of more direct information it is suggested that an equation of the form

$$\epsilon_s = (T_R + 0.029)\left(\frac{1}{C}\right)^{3/2}\frac{V}{\beta^3}\,. \qquad (5.70)$$

may be used, where T_R is that for a rectangular open jet of breadth/height ratio equal to m/n (Fig.5.13) and $C = \frac{1}{4}\pi mn$.

5.5.3 Wake Blockage Effects

It is often stated that wake interference effects are zero in open-jet tunnels, but this is true only in a restricted sense. If the model wake is represented by a source, the effect of the tunnel boundaries may be simulated by an array of images alternating in sign with the original. The velocity increment associated with the wake blockage due to the presence of these images is zero, because the alternately positive and negative infinite sets of images produce zero velocity increment at the model position and at infinity downstream or upstream. The velocity gradient along the model length is not zero, however, and is opposite in sign to, and smaller than, that in the corresponding closed tunnel. Thus for a small model one may conclude that $\epsilon_w = 0$, but for a long model a distribution of ϵ_w corresponding to the velocity gradient, will exist. A correction must therefore be applied to the measured drag to allow for the wall-induced horizontal buoyancy. This is discussed in Section 5.8.2.

The distribution of the wake-blockage factor along the chord of a two-dimensional aerofoil spanning a two-dimensional open jet is discussed by Woods in Section 7.21 of Reference 5.22. At the mid-chord position the blockage factor becomes zero, though the gradient is finite.

5.6 ESTIMATION OF BLOCKAGE FROM WALL MEASUREMENTS

In the preceding sections we have been concerned with the calculation of the blockage effects from the geometry of the model and tunnel, and from the state of the tunnel stream. The existing theory may also be used to estimate the incremental blockage velocities anywhere within the working section, for example, at the tunnel-speed hole. The changes in stream velocity induced by the model and wake and their images may also be calculated at the tunnel wall immediately opposite, say, the midpoint of the model. The ratio (Z) of the velocity induced at the model position by the images alone, to the total induced velocity at this wall position is important, since, if this is known on theoretical grounds, the blockage of the model may be found very simply from measurements at the wall. An approach of this kind is therefore most valuable and has special advantages. It is of course of greatest application to tunnels having closed boundaries and these will be mainly considered in relation to two-dimensional (Section 5.6.1) and three-dimensional (Section 5.6.2) models.

In discussing the methods of estimating blockage from wall measurements it will be assumed that the model is at zero lift. If this is not the case, the lift effect on the wall pressures must be removed by averaging the pressures obtained above and below the model.

5.6.1 Two-Dimensional Aerofoil

For a small aerofoil placed at the centre of a closed rectangular tunnel the solid-blockage velocity increment at the wall immediately above or below a non-lifting model is about 1.78* times that at the model position. The velocity increment at the wall deduced from pressure measurements will, however, include the increase in velocity due to the model itself, as well as that due to the images. The velocity ratio (Z_s) for this case is exactly 1/3; that is to say, the solid-blockage factor at the model will be given by

$$Z_s = \frac{U\epsilon_s}{(u - U)_{max}} = \frac{1}{3}, \tag{5.71}$$

where $(u - U)_{max}$ is the maximum supervelocity at the tunnel wall opposite the model and may be estimated from the wall pressure distribution.

The value of Z_s is unaffected by compressibility of the tunnel stream (Refs. 5.4, 5.29), but at high Mach numbers the velocity peak on the wall tends to move downstream from a position opposite the maximum thickness of the model. For large models Z_s may fall below 1/3; Woods[5.8] has considered the relation between the distribution of ϵ_s along the model and the velocity increments along the wall.

As the distance upstream or downstream of the model increases, the supervelocity at the wall due to the solid blockage becomes smaller and finally vanishes. At infinity downstream, however, a velocity increment will be recorded which is due entirely to the wake blockage and is found to be twice $\epsilon_w U$. If $(u - U)_\infty$ is estimated from the wall pressures well downstream, then

$$Z_w = \frac{U\epsilon_w}{(u - U)_\infty} = \frac{1}{2}. \tag{5.72}$$

---

* Thom[5.4] discusses the variation across the tunnel and gives this ratio as $3(\pi^2 - 4)/\pi^2$. See also Reference 5.54.

Goldstein[5.7] gives a general expression for the velocity at the wall in incompressible flow

$$\left(\frac{u}{U}\right)_{wall} = 1 + \frac{\pi}{2}\frac{A}{h^2}\,\mathrm{sech}^2\chi + \frac{1}{4}\left(\frac{c}{h}\right)C_D[1 + \tanh\chi] \,, \qquad (5.73)$$

where

$$\chi = \frac{\pi(x - \frac{1}{2}c)}{h} \,.$$

In terms of the solid and wake blockage factors this expression becomes

$$\left(\frac{u}{U}\right)_{wall} = 1 + (3\,\mathrm{sech}^2\chi)\epsilon_s + (1 + \tanh\chi)\epsilon_w \,, \qquad (5.74)$$

thus enabling the solid and wake blockage to be estimated from measurements made at any two stations; one of these should preferably be close to the model and one downstream. Because $\tanh\chi$ rapidly approaches its asymptotic value as x increases, whilst $\mathrm{sech}^2\chi$ decreases, the latter station need not be further downstream than about 1.5 tunnel heights in order to make an accurate estimate of ϵ_w. This is of great convenience in view of the limited length of tunnel working sections. The solid-blockage contribution at this position will be less than 1% of the total.

The values of Z_s and Z_w for an aerofoil spanning a circular tunnel have only been discussed in a limited manner[5.36]; it seems likely that the methods of Reference 5.27 could be extended to cover this case.

5.6.2 Three-Dimensional Models

For a rectangular tunnel containing a three-dimensional model small enough to be represented by a doublet, the value of Z_s is different on the roof and side-walls, unless the tunnel cross-section is square. In an early paper Thom[5.8] showed that Z_s was respectively 0.28 and 0.56 for the roof and side-walls of a tunnel with $b/h = 1.43$, when the model was represented by a simple doublet. For a wing composed of line sources and sinks, whose span is 0.6 of the tunnel breadth, these values become 0.36 and 0.32. A body of revolution in a square tunnel gives $Z_s = 0.43$; in a circular tunnel $Z_s = 0.45$ (Ref. 5.30).

Thom's work for a rectangular tunnel was later extended by Hensel (Ref. 5.40; 1951), who represented a finite-span wing by a distribution of line sources and sinks, and a body of revolution by a distribution of point sources and sinks. The finite swept wing however presents certain analytical difficulties, and discrete doublets were used in this case. Hensel's method is quite general and can be applied to any closed rectangular tunnel. The numerical computation is however complicated, and in Reference 5.40 results are given only for $b/h = \sqrt{2}$. The effect of sweep on Z_s for both the side-walls and roof is shown in Figures 5.14(a) and (b). Although Z_s is larger for swept than for unswept wings, it should be remembered that the actual wall velocity increments are smaller in the latter case, so that the trend in Z_s with sweep is not necessarily that of ϵ_s. The value of Z_s at the roof for an unswept finite wing almost completely spanning the tunnel exceeds that for a two-dimensional wing. A similar effect occurs in the direct calculation of the solid blockage (see footnote in Section 5.2.3).

For compressible flow Hensel recommends the use of an equivalent sweep angle Λ_e related to the geometric sweep angle Λ by

$$\beta \tan \Lambda_e = \tan \Lambda \; ; \tag{5.75}$$

Λ_e can then be used in the charts or equations of Reference 5.40.

Hensel's analysis assumes that the body length or wing chord is small compared with the tunnel dimensions. This will often be the case for models tested in high-speed wind tunnels. Exceptionally long bodies of revolution may be investigated and then the method developed by Evans[5.25] seems preferable, though the calculations and experiments described in the reference are primarily concerned with a tunnel where $b/h = 1.43$. Evans shows that Z_s is not constant for large models but depends on the length of the model and the Mach number of the stream.

Hensel points out that, for larger wings, the velocity ratio should be related to the mean blockage increment over the wing span and not to a local value on the centre section. This mean is comparatively easy to calculate for a straight wing, but for a sweptback planform each spanwise position lies in a different longitudinal position and this complicates the analysis. The effect of wing taper on both swept and unswept wings cannot readily be obtained by Hensel's approach, though he suggests that the effects of ignoring both wing taper and spanwise variation of Z_s tend to cancel each other. Evans considers that any wing, unless of most unorthodox shape, may be represented by a non-tapered swept wing of equal volume, mean angle of sweep and thickness/chord ratio, but with a span $2\sqrt{3}k_x$, where k_x is the radius of gyration of the original wing about the x axis. Slender delta wings are best replaced by an equivalent body of revolution.

Evans also suggests an allowance for the effect of small supersonic flow regions adjacent to the model surface, an effect likely to be present at high subsonic stream speeds. This aspect is briefly discussed in Section 5.8.2. In general Reference 5.25 shows that very good agreement may be obtained between the calculated and observed wall pressures, and that the latter may be used reliably to estimate the solid-blockage factor.

The wake-blockage factor for small three-dimensional models may be found from the velocity increments far downstream in the same way as for a two-dimensional aerofoil by Equation (5.72).

The velocity-ratio method of obtaining blockage factors for models in circular closed tunnels has been discussed by Göthert[5.30] and Schmitz[5.36]. As was mentioned earlier, the value of Z_s for a small wing or body is 0.45, which is close to the value for a square tunnel. For an unswept wing whose span is equal to the tunnel radius, Z_s equals 0.50.

References 5.36 and 5.59 both consider the case of an open-jet tunnel containing a body of revolution, though it seems unlikely that the velocity-ratio method will be used to find the solid-blockage factor in this type of tunnel.

5.7 BLOCKAGE CORRECTIONS AT VERY HIGH SUBSONIC SPEEDS IN CLOSED TUNNELS

The effects of compressibility have been allowed for in the earlier sections by means of a small perturbation theory which essentially becomes less valid as flow Mach numbers approach unity. This means that the compressibility factors become unreliable as the tunnel Mach number reaches high subsonic values. Moreover, in such flows, supersonic velocities may be reached locally about the model and the associated shock waves violate the assumption that the flow is everywhere isentropic. Unfortunately it is just in this region of stream Mach number that the model characteristics show the greatest sensitivity and a precise value of equivalent free-air Mach number (and hence of the appropriate blockage correction) is important. The magnitude of the blockage corrections will in any case be larger than at lower stream Mach numbers because of the form of the simple compressibility factors (Fig. 5.12), and also because the model drag used in the wake-blockage correction factor may increase very rapidly with M . The highest Mach number obtainable in a closed-wall tunnel is that achieved when the tunnel chokes; no additional mass flow can then be passed through the working section by increasing the fan speed or tunnel power. The exact value of the choking Mach number depends on the geometry of the model and the tunnel, but a simple one-dimensional consideration often gives a useful guide to this limiting speed (see Reference 5.56, for example).

The presence of a maximum Mach number, the clash between the increasing magnitude and importance of the blockage corrections and the uncertainties inherent in their determination, led to the development of wind tunnels having slotted or perforated walls. The choking effect was completely overcome and the blockage effects could be considerably reduced (see Chapter VI). The success of these ventilated working sections has been such as to reduce the demand for more accurate blockage corrections at high subsonic speeds. Nevertheless such corrections will be required occasionally, and a short discussion of some available techniques is justified.

5.7.1 Modification of Simple Compressibility Theory

Experimental evidence suggests that by using the simple compressibility factors given by small perturbation theory the true compressibility effect on blockage is frequently underestimated; some modification of the factors may therefore be considered, or alternatively a new theoretical approach attempted. Blockage corrections applicable near the choking condition have been put forward by Thom and Jones (Ref. 5.18; 1947: Ref. 5.41; 1946); a noticeable feature is a new term in the solid-blockage relation proportional to β^{-5} . This method is not easy to apply in general, and perhaps the most valuable and simple suggestion was made by Evans[5.25]: that the *corrected* Mach number should be used in calculating the factors β^{-2} and β^{-3} of the simple theory. This implies, of course, that the final value of the corrected stream Mach number is reached by successive approximations; usually two or three iterations are sufficient. This technique is amply justified by the experimental evidence of Evans's paper, which considers both the calculated blockage and the use of the wall-velocity increments. Examples illustrating agreement between theory and experiment are given in Figure 5.15.

Drougge (Ref. 5.14; 1951) has developed an approximation (due to Oswatitsch and valid near $M = 1$) useful for analysing the transonic flow past an aerofoil, and from which a transonic similarity law relating the aerofoil pressure drag and a free-stream

Mach number (M^*) based on the critical velocity of sound (a^*) may be derived. Drougge suggests that this law may be applied to the blockage problem at high transonic speeds, if tests results are available on two similar models of different sizes. An extrapolation to zero model size* valid at transonic speeds may then be made.

5.7.2 Regions of Local Supersonic Flow

The presence of regions of local supersonic flow on the model further complicates the problem of blockage corrections at high subsonic speeds. Thompson[5.6] considers that potential theory can still be used to calculate the velocity increment at the model position due to blockage from an array of simple doublet images, but that the theory is no longer valid for finding the strength of the equivalent doublet for the model. This suggests that the effect may be simulated by an increase in the effective volume of the model in the solid-blockage equations. Evans[5.25] in fact argues that the influence of the supersonic regions on the induced velocity at some distant point is similar to that produced by a local bulge on the model surface. The extra volume may be related roughly to the increase in drag coefficient (δC_D) that occurs after the drag rise has begun. From an analysis of experimental results on three unswept wings in the RAE 10 ft x 7 ft High Speed Tunnel, Evans deduced an equation for high subsonic speeds which may be rewritten, in a form analogous to Equation (5.29) above,

$$\epsilon_s = T\left(\frac{1}{bh}\right)^{3/2} \frac{V}{\beta_c^3}\left[1 + 1.2\beta_c\left(\frac{t}{c}\right) + 14\delta C_D\right]. \qquad (5.76)$$

where $\beta_c = (1 - M_c^2)^{\frac{1}{2}}$ corresponds to the corrected Mach number M_c. The actual value of the numerical factor in the last term is rather uncertain and is best determined directly for each tunnel and class of model. Slender bodies of revolution develop extensive supersonic flow fields only at test Mach numbers close to the choking condition and for this limited speed range an equation similar to Equation (5.23) above, but with β_c in place of β, is probably sufficient.

The growth of the supersonic region and the lateral extension of shock waves will widen the wake behind the body, thus increasing the wake-blockage effect. The usual wake-blockage equations contain the model drag, which increases rapidly with stream Mach number in this region, but in certain cases they may seriously underestimate the true wake blockage[5.42]. The wall pressure downstream of the model is then more reliable. If the theoretical wake-blockage equations are used, the corrected value of the stream Mach number should be used in the compressibility factor.

The use of the wall-velocity increments to deduce solid and wake blockage is very valuable at these high subsonic speeds, because, though small perturbation theory may no longer apply at the model, it may still be valid at some distance away. Göthert[5.39] indeed considers that the velocity-ratio method may be employed up to the choking speed of the tunnel for this very reason.

---

* Drougge also considers the more simple case of extrapolation to zero model size at moderate subsonic Mach numbers. The technique has also been discussed by Ackeret, Degen and Rott (Ref.5.43; 1950) for both straight and swept wings, and by Petersohn (Ref.5.50; 1948) for two-dimensional models spanning a circular tunnel.

5.8 USE OF BLOCKAGE FACTORS IN CORRECTING MEASURED QUANTITIES

We have so far been concerned with the estimation of the blockage factors ϵ_s and ϵ_w associated with the presence of the model and its wake within the tunnel. It is now necessary to consider how these factors are used to correct the measured quantities. Once more it is assumed that the model is small enough for the blockage effects to be additive; in addition the stream Mach number must not be so high as to invalidate the simple linear-perturbation theory.

The quantities to be corrected fall conveniently into two main groups; those, such as velocity and density, associated with the working fluid (Section 5.8.1), and the forces, moments and surface pressures measured on the model (Section 5.8.2).

5.8.1 Corrections to Stream Quantities

It is one of the important assumptions of blockage theory that the model behaves within the tunnel as it would in free air at some speed slightly different from the nominal tunnel velocity. It is the purpose of the theory to establish means of estimating the necessary increment ΔU_B which must be applied to the tunnel velocity U . The latter is of course that appropriate to the model position in the empty tunnel and must itself contain any corrections required by the tunnel calibration. Thus the corrected stream velocity is given by

$$U_C = U + \Delta U_B \, . \tag{5.77}$$

In terms of the solid and wake blockage factors this becomes

$$U_C = (1 + \epsilon_s + \epsilon_w)U \, . \tag{5.78}$$

Usually, however, the tunnel speed is determined from the pressure at some reference hole on the tunnel wall upstream of the model position. In some cases this pressure may itself be influenced by the presence of the model, so that the undisturbed free-stream velocity will be unknown; the effects of both the model lift and the blockage must then be considered. The influence of the lift can, in principle, be removed by averaging the pressures on the top and bottom walls of the tunnel, or its magnitude may be calculated by replacing the model by a vortex of the appropriate strength. The solid-blockage influence on the tunnel-speed hole has been considered by Goldstein[5.7] and Thom[5.8] amongst others. The latter shows that, for a small two-dimensional wing at zero lift in free air, a small negative velocity would be induced at positions ahead of the wing and the magnitude of this perturbation decreases with distance from the wing. When the model is in a tunnel with closed rectangular boundaries the effect is counterbalanced by the influence of the images which induce a small positive velocity. Ahead of about 1.5 tunnel heights from the model centre the two effects almost cancel out, and a wall hole upstream of this position should similarly indicate a velocity very close to the postulated undisturbed free-stream value U . Goldstein shows that the effect of the wake blockage is negligible beyond about one tunnel height upstream of the model.

Schmitz[5.36] has also considered the corrections required in a rectangular tunnel, and his results are in general agreement with earlier authors. In addition, he discusses the closed circular tunnel containing a body of revolution and shows that the correction is very small at more than one tunnel diameter ahead of the model. Open-jet tunnels of rectangular and circular cross-section are considered in References 5.36 and 5.59 and it is interesting to note that in these cases the velocity increments induced at a position on the edge of the jet corresponding to the tunnel-speed hole in a closed tunnel may be positive and thus of opposite sign to that induced at the model position. This effect is probably of little practical importance, since the stream velocity in open-jet tunnels is often determined from readings of wall pressure within the nozzle, a calibration having been made with the tunnel empty. If, however, a direct measurement of tunnel velocity is made in the stream ahead of the model, then this may be subject to blockage interference.

For compressible flow the stream velocity is of rather less importance than the stream Mach number M. The correction to M can be obtained very simply by differentiating the adiabatic isentropic flow equations. For $\gamma = 1.4$ the correction to the nominal Mach number is given by

$$\Delta M = (1 + 0.2M^2)M\epsilon_B . \tag{5.79}$$

Then

$$M_C = M + \Delta M , \tag{5.80}$$

where ΔM takes the sign of ϵ_B, which is positive for closed tunnels and negative for open tunnels.

Once the blockage factors are known, corrections may also be made to the stream static pressure (p), density (ρ) and static temperature (θ) on the assumption that the flow is isentropic and adiabatic. For $\gamma = 1.4$,

$$\Delta p_\infty = -1.4M^2p_\infty\epsilon_B , \tag{5.81}$$

$$\Delta\rho = -M^2\rho\epsilon_B , \tag{5.82}$$

$$\Delta\theta = -0.4M^2\theta\epsilon_B . \tag{5.83}$$

In incompressible flow, Equation (5.81) will be replaced by

$$\Delta p_\infty = -\rho U^2\epsilon_B . \tag{5.84}$$

It follows that the correction to the stream kinetic pressure is given by

$$\Delta(\tfrac{1}{2}\rho U^2) = (2 - M^2)(\tfrac{1}{2}\rho U^2)\epsilon_B . \tag{5.85}$$

The test Reynolds number (R_N) is also modified by the blockage effects. Usually such changes can be ignored, but a correction may be calculated from a knowledge of the changes in stream velocity, density and temperature. If a suitable, but simple, relationship between fluid viscosity and temperature is used, a simple correction equation may be obtained. For example, if it is assumed that the viscosity is proportion to $\theta^{3/4}$, then

$$\Delta R_N = (1 - 0.7M^2)R_N\epsilon_B . \tag{5.86}$$

5.8.2 Corrections to Model Quantities

The lift interference discussed in Chapters II and III gives rise to corrections to the measured model incidence, forces and moments, but not to the stream velocity at the model position unless this is off the tunnel centre line. The correction to the stream velocity, because of the solid and wake blockage effects, has already been discussed, together with the change in stream kinetic pressure. In forming the non-dimensional coefficients from the measured forces and moments, use can be made directly of the corrected kinetic pressure; the resulting coefficients will then be corrected for blockage effects. Alternatively, it is sometimes convenient to form these coefficients using the uncorrected values of stream density and velocity and then to apply a correction to the coefficient itself. Thus if C_A is a typical non-dimensional coefficient, the corrected value will be

$$C_A + \Delta C_A \ = \ C_A[1 - (2 - M^2)\epsilon_B] \ , \qquad (5.87)$$

if squares of small quantities are neglected. Equation (5.87) is obtained by using Equation (5.85) above and may be applied to any measured force or moment coefficient, provided due regard is paid to the restrictions implicit in the derivation of ϵ_B .

An extra correction is required to the drag coefficient, because, as was mentioned in Sections 5.4.4 and 5.5.3, the images of the source representing the wake impose a longitudinal pressure gradient along the tunnel and hence a longitudinal buoyancy force on the model. The measured drag is higher than the free-air value in a closed tunnel, and lower in an open tunnel. The pressure gradient may conveniently be regarded as linear along the length of the model. The buoyancy force D_g may then be taken as the product of the pressure gradient and the effective volume of the model V_e , where this is the sum of the actual volume and a virtual volume V_v corresponding to the virtual mass of the body in the accelerated flow along the tunnel axis. Thus

$$D_g \ = \ -\left(\frac{dp}{dx}\right)_B V_e \ = \ -\left(\frac{dp}{dx}\right)_B (V + V_v) \ . \qquad (5.88)$$

Now V_v may be related to the shape parameter λ_2 or λ_3 and to the doublet strength P representing the potential flow past the body (see References 5.1, 5.23, for example). Thus for a slender body of revolution in incompressible f'~

$$P \ = \ V_e U \ = \ \tfrac{1}{4}\pi\lambda_3 t^3 U \ . \qquad (5.89)$$

On the basis of linear theory the pressure gradient may be written as

$$\left(\frac{dp}{dx}\right)_B \ = \ -\rho U \frac{\partial U_B}{\partial x} \ = \ -\rho U^2 \frac{\partial \epsilon_w}{\partial x} \ . \qquad (5.90)$$

If ΔU_s denotes the solid-blockage effect of a doublet of strength P , then the gradient $(\partial/\partial x)(\epsilon_w U)$ due to a source of strength Q is precisely $Q(\Delta U_s)/P$ (References 5.37 and 5.38). Moreover the source strength used in the wake-blockage analysis is equal to $D/\rho U$. Thus

$$\left(\frac{dp}{dx}\right)_B \ = \ -\frac{DU\epsilon_s}{P} \ . \qquad (5.91)$$

With the substitution of V_e and (dp/dx) from Equations (5.89) and (5.91), Equation (5.88) gives a simple expression for $-D_g$, which can be rewritten non-dimensionally as a correction to drag coefficient

$$(\Delta C_D)_g \doteq -C_D\epsilon_S \, . \tag{5.92}$$

This equation is independent of corrections to the kinetic pressure if second-order terms in ϵ_s are neglected. Goldstein[5.7] derives a more complex relation for the wake-buoyancy correction in incompressible flow, but shows that Equation (5.92) is valid if the square of the drag coefficient is small enough to be neglected.

The influence of compressibility on the wake buoyancy correction has sometimes caused difficulty. Equation (5.88) is unaffected by simple compressibility theory, and some authors have argued that no compressibility factor is required in Equation (5.91) other than that inherent in ϵ_s itself. Others[5.3, 5.23] consider that a compressibility correction to the source strength should be included, as in Equation (5.49), so that in place of Equation (5.92)

$$(\Delta C_D)_g = -C_D(1 + 0.4M^2)\epsilon_S \, . \tag{5.93}$$

Ludwieg[5.37], moreover, points out that the virtual volume is also modified slightly by compressibility and Herriot[5.23] considers it worthwhile allowing for this in the drag correction. For most wind tunnels and models this particular effect will be small even at high Mach numbers.

The sign of the buoyancy force follows that of ϵ_S and hence is different in open and closed tunnels. For a two-dimensional rectangular section the magnitude of the open-jet correction is half that of the closed tunnel: for three-dimensional models this ratio is about one-quarter.

The full correction to the measured drag coefficient is obtained by combining the corrections obtained in Equations (5.37) and (5.92) or (5.93). Thus, in two-dimensional flow, either

$$\Delta C_D = -[\epsilon_S + (2-M^2)\epsilon_B]C_D \tag{5.94}$$

or

$$\Delta C_D = -[(1+0.4M^2)\epsilon_S + (2-M^2)\epsilon_B]C_D \, . \tag{5.95}$$

In three dimensions C_D is replaced by C_{D0} in Equations (5.92) and (5.93) and there is corresponding adjustment to the first terms in Equations (5.94) and (5.95).

Allen and Vincenti[5.3] remark that it is not at once apparent that these equations apply to drag coefficients determined by the wake-traverse method[5.46] and, after discussing the matter, they suggest that, for normal-sized aerofoil models, the error in using Equation (5.95) is about the same order as the experimental error. This view has sometimes been questioned. The matter is extremely complex and each term in the formulae used in calculating the aerofoil drag from the experimental data needs to be considered with great care. Moreover the physical significance of the formula must be clear; for example the final calculated drag need not be the force actually experienced by the model in the tunnel, and the final drag coefficient may be obtained in a way which allows for some wall-interference effects. In the opinion of the present author no wake-buoyancy correction should be applied to a drag coefficient obtained from wake-traverse measurements if these are reduced in the usual way.

The pressure coefficient C_p on the body will also require correction because of changes in both the static and kinetic pressures of the tunnel stream. The requisite correction may be written as

$$\Delta C_p = \frac{p - (p_\infty + \Delta p_\infty)}{\frac{1}{2}\rho U^2 + \Delta(\frac{1}{2}\rho U^2)}$$

$$= [2 - (2 - M^2)C_p]\epsilon_s \, . \qquad (5.96)$$

Such an expression assumes that the observed pressures are those which would be obtained in the corrected free-air conditions. That is to say, the use of Equation (5.96) is equivalent to the use of Equations (5.81) and (5.84) before the pressure is non-dimensionalized. The actual distortion of the pressure distribution about the body because of buoyancy effects and other higher-order wall corrections cannot be obtained in this manner. Methods such as the conformal mapping of References 5.15 and 5.16 or the higher-order calculations of Goldstein[5.7] must be used. Provided that the model is not too large, the stream Mach number is not near unity and the model incidence is moderate, then the distortion will be small.

5.9 SUMMARY OF PRINCIPAL BLOCKAGE FORMULAE

It is convenient to list together the simple formulae which may be most frequently required in calculating the blockage effects and which seem most satisfactory in use. Only those which give explicit answers will be presented; for more complicated expressions requiring extensive calculations the text of this report and the appropriate references should be consulted.

5.9.1. Closed Rectangular Tunnel

For two-dimensional aerofoils

$$\epsilon_s = \frac{\pi^2}{12}\left(\frac{c}{h}\right)^2\left(\frac{t}{c}\right)^2\frac{1}{\beta^3}\lambda_2 \qquad \text{(see Figure 5.1)}$$

or

$$\epsilon_s = \frac{\pi}{6}\left[1 + 1.2\beta\left(\frac{t}{c}\right)\right]\frac{A}{\beta^3 h^2}$$

and

$$\epsilon_w = \frac{1}{4}\left(\frac{c}{h}\right)\left(\frac{1 + 0.4M^2}{\beta^2}\right)C_D \, .$$

If incidence effects must be allowed for, put

$$\epsilon_s(\alpha) = \epsilon_s\left[1 + 1.1\beta\left(\frac{c}{t}\right)\alpha^2\right] .$$

If the model is at a distance d from the wall, put

$$\epsilon_s(d) = \epsilon_s\left[1 + \frac{3}{4}\cot^2\frac{\pi d}{h}\right].$$

For three-dimensional models

$$\left.\begin{aligned} \epsilon_s &= \tau\left(\frac{A_m}{bh}\right)^{3/2}\frac{1}{\beta^3}\lambda \\ \text{or} \qquad \epsilon_s &= T\left(\frac{1}{bh}\right)^{3/2}\frac{1}{\beta^3}VG \end{aligned}\right\},$$

where for wings

$$\left.\begin{aligned} \lambda &= \lambda_2 \qquad \text{(Fig. 5.1)} \\ G &= 1 + 1.2\beta\left(\frac{t}{c}\right) \end{aligned}\right\}$$

and for bodies

$$\left.\begin{aligned} \lambda &= \lambda_3 \qquad \text{(Fig. 5.2)} \\ G &= 1 + 0.4\beta/f \end{aligned}\right\}.$$

Values of $\tau(=2T/\sqrt{\pi})$ and T depend on ratios b/h and 2s/b (Figures 5.5 and 5.6). For large wing-body combinations, it may be better to add the separate contributions of the wing and body.

$$\epsilon_w = \frac{1}{4}\left(\frac{S}{bh}\right)\left(\frac{1 + 0.4M^2}{\beta^2}\right)C_{D0}.$$

If the wake structure is known, use Equation (5.58) instead. For lifting wings, use zero-lift drag coefficient.

5.9.2 Closed Non-Rectangular Tunnels

For two-dimensional aerofoils, use the solid-blockage equations for the rectangular tunnel of an equivalent height (h_e). The value of h_e depends on both the tunnel shape and whether a correction is required at the mid-span position or as an average over the complete span.

Tunnel Shape	*Value of* h_e	
	At Mid-Span	*Average*
Circular	1.558R	1.571R
Octagonal	h (at centre)	C/b
Elliptical	Fig. 5.10	0.785h

For the wake-blockage factor, in all cases use

$$\epsilon_w = \frac{1}{4}\left(\frac{c}{h_e}\right)\left(\frac{1 + 0.4M^2}{\beta^2}\right)C_D \ ,$$

where h_e is the value used in calculating the solid-blockage. For lifting wings, use zero-lift drag coefficient.

For three-dimensional models, use equations for rectangular tunnel, with appropriate values of τ or T and with bh replaced by the tunnel cross-sectional area C .

5.9.3 Open-Jet Tunnels

For a two-dimensional aerofoil in a rectangular jet

$$\epsilon_s = -\frac{\pi^2}{24}\left(\frac{c}{h}\right)^2\left(\frac{t}{c}\right)^2\frac{1}{\beta^3}\lambda_2 \qquad \text{(see Figure 5.1)}$$

or

$$\epsilon_s = -\frac{\pi}{12}\left[1 + 1.2\beta\left(\frac{t}{c}\right)\right]\frac{A}{\beta^3 h^2}$$

and

$$\epsilon_w = 0 \ .$$

For three-dimensional models, use equations for ϵ_s for closed rectangular tunnels, but with values of T and τ given in the table in Section 5.5.2. For non-rectangular tunnels, replace bh in these equations by C : for a circular tunnel $T = -0.182$ and $\tau = -0.206$: for an elliptical tunnel take $T_R + 0.029$ (or $\tau_R + 0.032$) where T_R (or τ_R) corresponds to a rectangular open jet of breadth/height ratio equal to a/b . The wake-blockage factor

$$\epsilon_w = 0 \ .$$

5.9.4 Corrections to Stream Quantities

For $\gamma = 1.4$,

$$\left.\begin{aligned}
\Delta U &= (\epsilon_s + \epsilon_w)U = \epsilon_B U \\
\Delta M &= (1 + 0.2M^2)M\epsilon_B \\
\Delta p_\infty &= -\,1.4M^2 p_\infty \epsilon_B \\
\Delta\rho &= -\,M^2\rho\epsilon_B \\
\Delta\theta &= -\,0.4M^2\theta\epsilon_B \\
\Delta(\tfrac{1}{2}\rho U^2) &= (2 - M^2)(\tfrac{1}{2}\rho U^2)\epsilon_B \\
\Delta R_N &\doteqdot (1 - 0.7M^2)R_N\epsilon_B
\end{aligned}\right\} \ .$$

For incompressible flow

$$\Delta p_\infty = -\rho U^2\epsilon_B \ .$$

5.9.5 Corrections to Model Quantities

$$\Delta C_A = -(2-M^2)C_A\epsilon_B \ .$$

where C_A is a non-dimensional force or moment coefficient other than drag coefficient C_D .

For two-dimensional aerofoils

$$\Delta C_D = -\left[(1+0.4M^2)\epsilon_S + (2-M^2)\epsilon_B\right]C_D \ .$$

For three-dimensional models

$$\Delta C_D = -(1+0.4M^2)\epsilon_S C_{D0} - (2-M^2)\epsilon_B C_D \ .$$

In both cases

$$\Delta C_p = \left[2-(2-M^2)C_p\right]\epsilon_B \ .$$

These corrections only apply if the uncorrected stream quantities (Section 5.9.4) are used in obtaining the non-dimensional coefficients.

REFERENCES

5.1	Glauert, H.	*Wind Tunnel Interference on Wings, Bodies and Airscrews.* ARC R & M 1566, 1933.
5.2	Borden, A.	*Wall Corrections for Flow about Two- and Three-Dimensional Symmetrical Bodies in Rectangular Channels of Infinite and Finite Lengths.* David W.Taylor Model Basin, Report 864, 1954.
5.3	Allen, H.J. Vincenti, W.G.	*Wall Interference in a Two-Dimensional-Flow Wind Tunnel, with Consideration of the Effect of Compressibility.* NACA Report 782, 1944.
5.4	Thom, A.	*Blockage Corrections in a Closed High-Speed Tunnel.* ARC R & M 2033, 1943.
5.5	Young, A.D. Squire, H.B.	*Blockage Corrections in a Closed Rectangular Tunnel.* ARC R & M 1984, 1945.
5.6	Thompson, J.S.	*Present Methods of Applying Blockage Corrections in a Closed Rectangular High Speed Wind Tunnel.* ARC Report 11,385, 1948. (Unpublished.)
5.7	Goldstein, S.	*Two-Dimensional Wind-Tunnel Interference.* ARC R & M 1902, 1942.

5.8 Woods, L.C. *The Second Order Terms in Two-Dimensional Tunnel Blockage.* Aeron. Quart. Vol.IV, 1954, pp.361-372.

5.9 Klunker, E.B.
Harder, K.C. *On the Second-Order Tunnel-Wall-Constriction Corrections in Two-Dimensional Compressible Flow.* NACA Tech. Note 2350, 1951.

5.10 Thom, A. *The Method of Influence Factors in Arithmetical Solutions of Certain Field Problems. Part I.* ARC R & M 2440, 1946.

5.11 Klanfer, L. *The Method of Influence Factors in Arithmetical Solutions of Certain Field Problems. Part II* ARC R & M 2440, 1947.

5.12 Emmons, H.W. *Flow of a Compressible Fluid Past a Symmetrical Airfoil in a Wind Tunnel and in Free Air.* NACA Tech. Note 1746, 1948.

5.13 Epstein, H.T.
Albers, L.U. *The Effects of Compressibility on the Two-Dimensional Subsonic Wind-Tunnel Constriction Correction.* J. aero. Sci. Vol.15, 1948, pp.144-150.

5.14 Drougge, G. *Note on Wall Interference in Two-Dimensional Flow at Subsonic and Transonic Speeds.* FFA (Sweden) Report 40, 1951.

5.15 Perl, W.
Moses, H.E. *Velocity Distributions on Symmetrical Airfoils in Closed Tunnels by Conformal Mapping.* NACA Tech. Note 1642, 1948.

5.16 Moses, H.E. *Velocity Distributions on Arbitrary Airfoils in Closed Tunnels by Conformal Mapping.* NACA Tech. Note 1899, 1949.

5.17 Whitehead, L.G. *Two-Dimensional Wind-Tunnel Interference.* ARC R & M 2802, 1950.

5.18 Thom, A. *Tunnel Wall Effect from Mass Flow Considerations.* ARC R & M 2442, 1947.

5.19 von Doenhoff, A.E.
Abbott, F.T. *The Langley Two-Dimensional Low-Turbulence Pressure Tunnel.* NACA Tech. Note 1283, 1947.

5.20 Franke, A.
Weinig, F. *Die Korrektur der Anströmgeschwindigkeit und des Anströmwinkels in einem Hochgeschwindigkeitskanal mit geschlossener Meßstrecke infolge der Verdrängungsströmung in Tragflügelmodellen.* Deutsche Luftfahrtforschung Forschungsbericht 1171, 1939. (Translated as MAP R & T 259, ARC Report 10.268.)

5.21 Batchelor, G.K. *Interference on Wings, Bodies and Airscrews in a Closed Tunnel of Octagonal Section.* Report ACA-5 (Australia), 1944.

5.22 Woods, L.C. *The Theory of Subsonic Plane Flow.* Cambridge University Press, 1961.

5.23 Herriot, J.G. *Blockage Corrections for Three-Dimensional-Flow Closed-Throat Wind Tunnels, with Consideration of the Effect of Compressibility.* NACA Report 995, 1950.

5.24 Vasy, G.S. *The Drag of Streamline Bodies of Revolution in a Wind Tunnel.* Acta Tech. Acad. Sci. Hung. (Hungary) Vol.18, 1957, pp.317-322.

5.25 Evans, J.Y.G. *Corrections to Velocity for Wall Constraint in any 10 × 7 Rectangular Subsonic Wind Tunnel.* ARC R & M 2662, 1949.

5.26 Lamb, H. *On the Effect of the Walls of an Experimental Tank on the Resistance of a Model.* ARC R & M 1010, 1926.

5.27 Vincenti, W.G.
Graham, D.J. *The Effect of Wall Interference upon the Aerodynamic Characteristics of an Airfoil Spanning a Closed-Throat Circular Wind-Tunnel.* NACA Report 849, 1946.

5.28 Watson, G.N. *The Use of a Series of Bessel Functions in Problems Connected with Cylindrical Wind-Tunnels.* Proc. Roy. Soc. Series A, Vol.130, 1930, pp.29-37.

5.29 Lock, C.N.H. *The Interference of a Wind Tunnel on a Symmetrical Body.* ARC R & M 1275, 1929.

5.30 Göthert, B. *Windkanalkorrekturen bei hohen Unterschallgeschwindigkeiten unter besonderer Berücksichtigung des geschlossenen Kreiskanals.* Deutsche Luftfahrtforschung Forschungsbericht 1216, 1940. (Translated as NACA Tech. Memo. 1300.)

5.31 Göthert, B. *Windkanalkorrekturen bei hohen Unterschallgeschwindigkeiten.* Lilienthal-Gesellschaft für Luftfahrtforschung, Bericht 127, 1940, pp.114-12

5.32 Wieselsberger, C. *Windkanalkorrekturen bei kompressibler Strömung.* Lilienthal-Gesellschaft für Luftfahrtforschung, Bericht 127, 1940, pp.3-7. (Translated as MAP R & T 379, ARC Report 11,199.)

5.33 Vendrey, F. *Theoretical Corrections for Long Rankine Ovoids in a Closed or Open Tunnel of Circular Cross-Section.* ARC Report 14,239, 1951. (Unpublished.)

5.34 Lock, C.N.H.
Johansen, F.C. *Wind Tunnel Interference on Streamline Bodies.* ARC R & M 1451, 1931.

5.35 Fage, A. *On the Two-Dimensional Flow Past a Body of Symmetrical Cross-Section Mounted in a Channel of Finite Breadth.* ARC R & M 1223, 1929.

5.36 Schmitz, G. *Beitrag zur Geschwindigkeitskorrektur in Windkanälen bei kompressibler Unterschallströmung.* Z. Flugwiss. Vol.5, 1957, pp.169-172.

5.37 Ludwieg, H. *Widerstandskorrektur in Hochgeschwindigkeitskanälen.* Deutsche Luftfahrtforschung Forschungsbericht 1955, 1944. (Translation in NACA Tech. Memo. 1163.)

5.38 Taylor, G.I. *The Force Acting on a Body Placed in a Curved and Converging Stream of Fluid.* ARC R & M 1166, 1928.

5.39 von Baranoff, A. *Zur Frage der Kanalkorrektur bei kompressibler Unterschallströmung.* Deutsche Luftfahrtforschung Forschungsbericht 1272, 1940. (Translated as NACA Tech. Memo. 1162.)

5.40 Hensel, R.W. *Rectangular-Wind-Tunnel Blocking Corrections Using the Velocity-Ratio Method.* NACA Tech. Note 2372, 1951.

5.41 Thom, A.
Jones, M. *Tunnel Blockage Near the Choking Condition.* ARC R & M 2385, 1946.

5.42 Nair, W.A.
Gamble, H.E. *The Effect of Model Size on Measurements in the RAE High Speed Tunnel. Drag of Two-Dimensional Symmetrical Aerofoils at Zero Incidence.* ARC R & M 2527, 1944.

5.43 Ackeret, J.
et al. *Untersuchungen an gepfeilten und ungepfeilten Flügeln bei hohen Unterschallgeschwindigkeiten.* Z. ang. Math. Phys. (ZAMP) Vol.1, 1950, pp.32-42.

5.44 Goldstein, S.
Young, A.D. *The Linear Perturbation Theory of Compressible Flow, with Applications to Wind-Tunnel Interference.* ARC R & M 1909, 1943.

5.45 Tsien, H.S.
Lees, L. *The Glauert-Prandtl Approximation for Subsonic Flows of a Compressible Fluid.* J. aero Sci., Vol.12, 1945, pp.173-187, 202.

5.46 Lock, C.N.H.
et al. *Determination of Profile Drag at High Speeds by a Pitot Traverse Method.* ARC R & M 1971, 1943.

5.47 Adamson, J.E. *An Experimental Investigation of Wind-Tunnel Interference in the RAE 5 ft Open-Jet Circular Tunnel.* ARC R & M 1897, 1941.

5.48 Katzoff, S.
et al. *Linear Theory of Boundary Effects in Open Wind Tunnels with Finite Jet Lengths.* NACA Report 976, 1950.

5.49 Vandrey, F. *Der Düseneinfluss auf die Windkanalkorrekturen bei ebener Strömung.* Jahrbuch der Deutschen Luftfahrtforschung, 1942, pp.1785-1793.

5.50 Petersohn, E.	*On Maximum Model Size for Wind Tunnel Investigations at High Subsonic Mach Numbers.* FFA (Sweden) Report 23, 1948.
5.51 Loos, H.G.	*Tunnel-Wall Interference for Aerofoils and Aerofoil-Fuselage Combinations in a Tunnel with an Octagonal Section for Incompressible Flow.* NLL (Netherlands) Report A 1024, 1951.
5.52 Knechtel, E.D.	*Experimental Investigation of Two-Dimensional Tunnel-Wall Interference at High Subsonic Speeds.* NACA Tech. Note 3087, 1953.
5.53 Suzuki, K.	*On the Subsonic Flow of a Compressible Fluid past a Circular Cylinder Between Parallel Walls.* Proc. Phys. Math. Soc. Japan, Vol.23, 1941, pp.336-346.
5.54 Barbieux, J.	*Contribution à l'Étude de l'Effet de Paroi en Écoulement Plan Incompressible.* Publ. Sci. Tech. Min. Air France 304, 1955.
5.55 von Kármán, T. Burgers, J.M.	*General Aerodynamic Theory - Perfect Fluids. Airfoils and Airfoil Systems of Finite Span.* "Aerodynamic Theory" (ed. W.F.Durand) Vol.II, Div. E, Chap, IV, Sect. 44, Julius Springer, Berlin, 1935.
5.56 Pankhurst, R.C. Holder, D.W.	*Wind Tunnel Technique.* Chap. 8, pp.396-398. Pitman, London, 1952. (Reprinted in 1965.)
5.57 Wuest, W.	*Verdrängungkorrekturen für rechteckige Windkanäle bei verschiedenen Strahlbegrenzungen und bei exzentrischer Lage des Modells.* Z. Flugwiss, Vol.9, 1961, pp.15-29 and Errata p.362.
5.58 Cramer, H. Kolberg, F.	*Windkanalkorrekturen angestellter Körper bei kompressibler Unterschallströmung.* Z. ang. Math. Mech. (ZAMM) Vol.40, 1960, pp.65-74.
5.59 Fuchshuber, R.	*Étude Mathématique de l'Influence des Dimensions Finies de la Veine d'Air autour d'un Modèle dans les Souffleries pour le Domaine de l'Écoulement Compressible Subsonique.* Publ. Sci. Tech. Min. Air France 376, 1961.

ADDITIONAL REFERENCES FOR CHAPTER V

Abdurahiman, P.V.	*Two-Dimensional Compressible Flow past a Solid Body Symmetrically Placed in a Channel.* ARC R & M 2443, 1947.
Bateman, T.E.B. Haines, A.B.	*A Comparison of Results in the ARA Transonic Tunnel on a Small and a Large Model of a Slender Wing.* ARC R & M 3287, 1961.
Berndt, S.B.	*Approximate Calculation of the Influence of Wall Boundary Layers upon the Blockage Interference in a High Speed Wind Tunnel.* FFA (Sweden) Report 45, 1952.
Fuchshuber, R.	*Über die Berechnung randbedingter Geschwindigkeitskorrekturen bei Windkanälen mit geschlossener und offener Meßstrecke im Bereich kompressibler Unterschallströmung.* Dissertation Tech. Hoch., Aachen, 1956.
Katzoff, S. Finn, R.S.	*Determination of Jet-Boundary Corrections to Cowling-Flap-Outlet Pressures by an Electrical Analogy Method.* NACA ARR 4B23 (NACA/TIB/602), 1944.
Sanders, J. Pounder, J.R.	*Wall Interference in Wind Tunnels of Closed Rectangular Section.* NRC (Canada) Report AR-7, 1949.
Thom, A. Klanfer, L.	*Tunnel-Wall Effect on an Aerofoil at Subsonic Speeds.* ARC R & M 2851, 1951.
Whitehead, L.G.	*Two-Dimensional Wind-Tunnel Interference.* ARC R & M 2802, 1950.
Woods, L.C.	*Compressible Subsonic Flow in Two-Dimensional Channels. The Direct and Indirect Problems.* ARC Report 14,838, 1952. (Unpublished.)
Woods, L.C.	*Compressible Subsonic Flow in Two-Dimensional Channels.* Aeron. Quart. Vol.6, 1955, pp.205-220, 254-276.
Wright, R.H. Donaldson, C. du P.	*Comparison of Two-Dimensional Air Flows about an NACA 0012 Airfoil of 1-Inch Chord at Zero Lift in Open and Closed 3-Inch Jets and Corrections for Jet-Boundary Interference.* NACA Tech. Note 1055, 1946.

TABLE 5.I

Functions Giving the Distribution of Solid Blockage along Bodies in Circular Tunnels (Ref.5.33)

ξ	H	-I	ξ	H	-I
0.0	0.000	0.000	2.0	0.439	0.048
0.1	0.040	0.010	2.2	0.449	0.043
0.2	0.080	0.020	2.4	0.456	0.038
0.3	0.119	0.029	2.6	0.463	0.034
0.4	0.155	0.038	2.8	0.468	0.030
0.5	0.190	0.045	3.0	0.472	0.027
0.6	0.220	0.052	3.2	0.476	0.024
0.7	0.250	0.057	3.4	0.478	0.021
0.8	0.276	0.060	3.6	0.481	0.019
0.9	0.300	0.063	3.8	0.483	0.017
1.0	0.322	0.064	4.0	0.485	0.015
1.1	0.342	0.064	4.2	0.486	0.014
1.2	0.359	0.064	4.4	0.487	0.013
1.3	0.374	0.063	4.6	0.488	0.012
1.4	0.387	0.062	4.8	0.489	0.011
1.5	0.399	0.060	5.0	0.490	0.010
1.6	0.409	0.058	6.0	0.493	0.007
1.7	0.418	0.055	7.0	0.495	0.005
1.8	0.426	0.052	8.0	0.496	0.004
1.9	0.433	0.050	9.0	0.497	0.003
2.0	0.439	0.048	10.0	0.498	0.002

For closed and open circular tunnels respectively

$$\epsilon_s(x) = [H(\xi_1) - H(\xi_2)]\,\frac{A_m}{C} \tag{5.39}$$

and

$$\epsilon_s(x) = [I(\xi_1) - I(\xi_2)]\,\frac{A_m}{C}\,. \tag{5.59}$$

where

$$\left.\begin{aligned} \xi_1 &= \frac{x + \frac{1}{2}a}{R} \\ \xi_2 &= \frac{x - \frac{1}{2}a}{R} \end{aligned}\right\}\,,$$

x is measured from the centre of the body, and for slender bodies $a \fallingdotseq l$ (Ref.5.2). Note that $H(-x) = -H(x)$, $I(-x) = -I(x)$.

λ_2 is defined in equation (5.3).

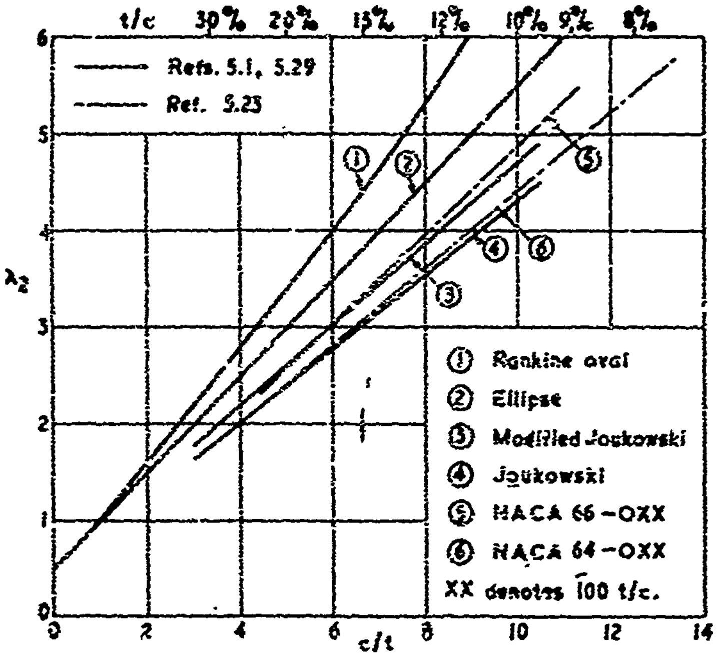

Fig. 5.1 Aerofoil-shape parameter

λ_3 is defined in equation (5.17).

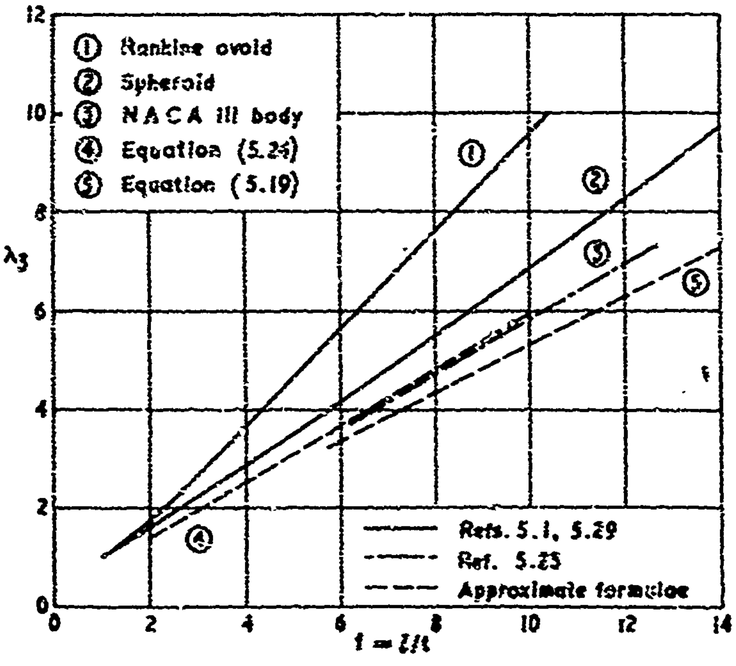

Fig. 5.2 Body-shape parameter

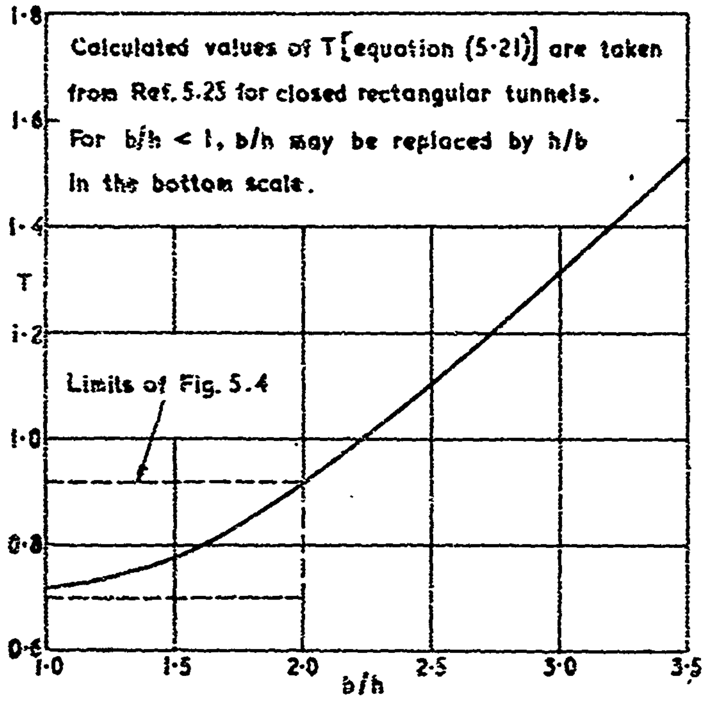

Fig.5.3 Tunnel-shape parameter for small models

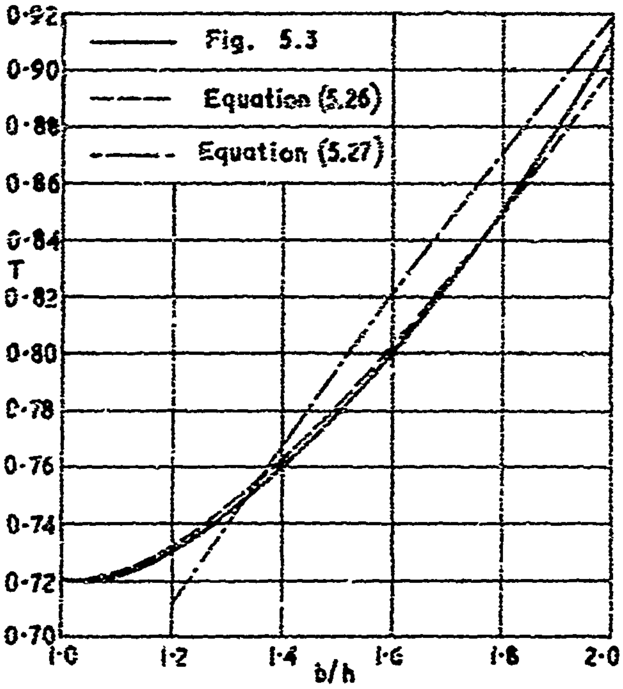

Fig.5.4 Tunnel-shape parameter from various formulae

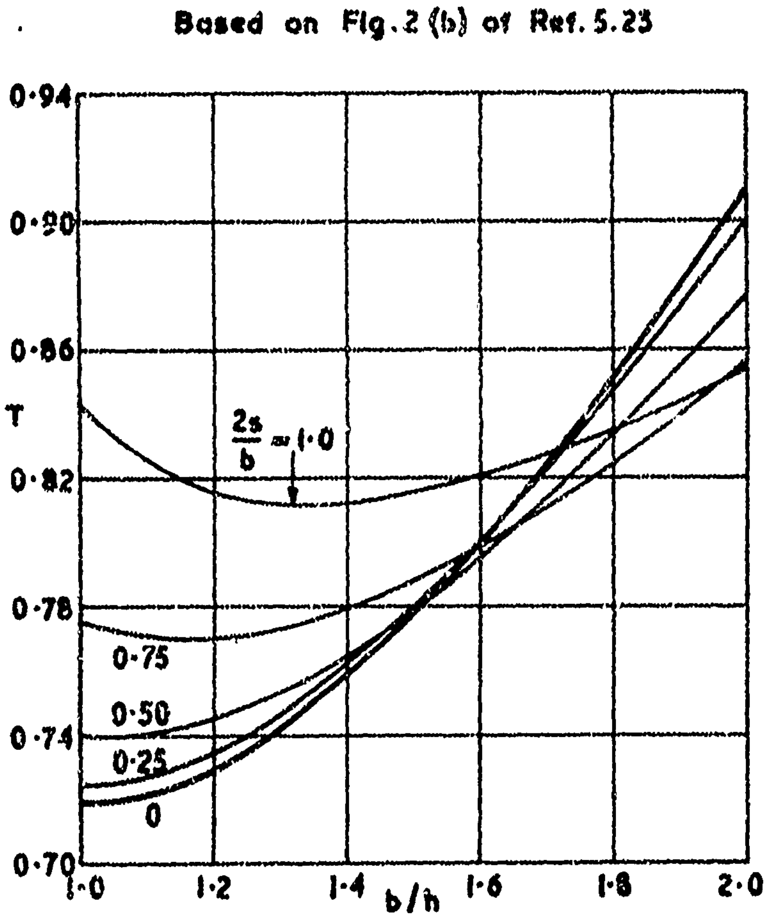

Fig. 5.5 Tunnel-shape parameter for large-span models

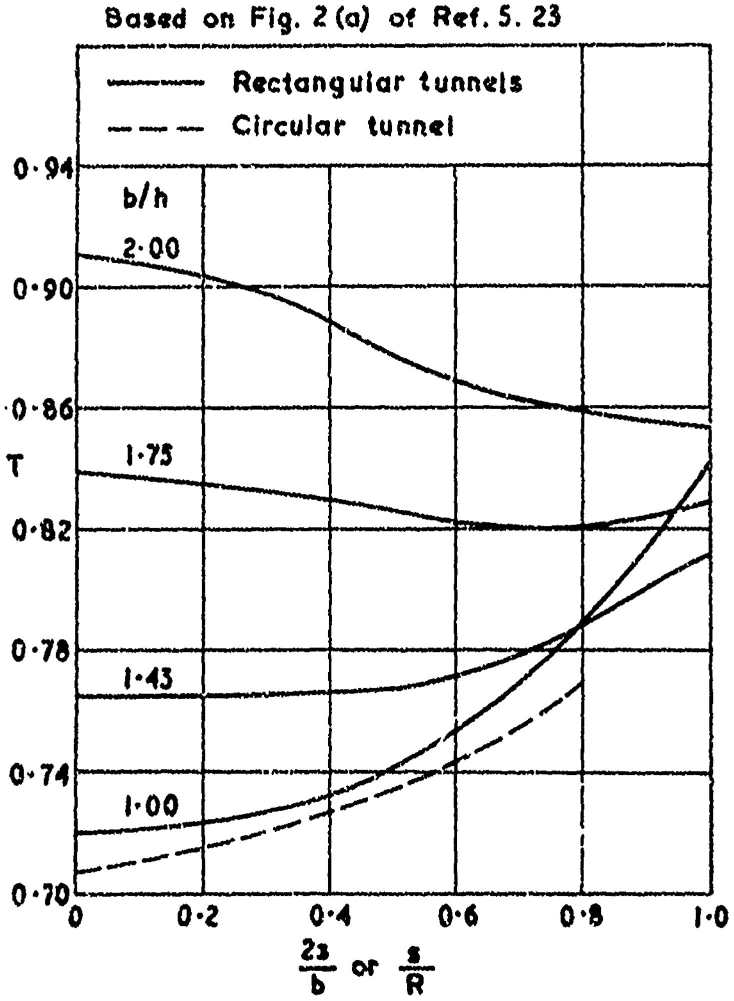

Fig. 5.6 Effect of model span on T for various closed tunnels

Based on Fig.2 of Ref. 5.33

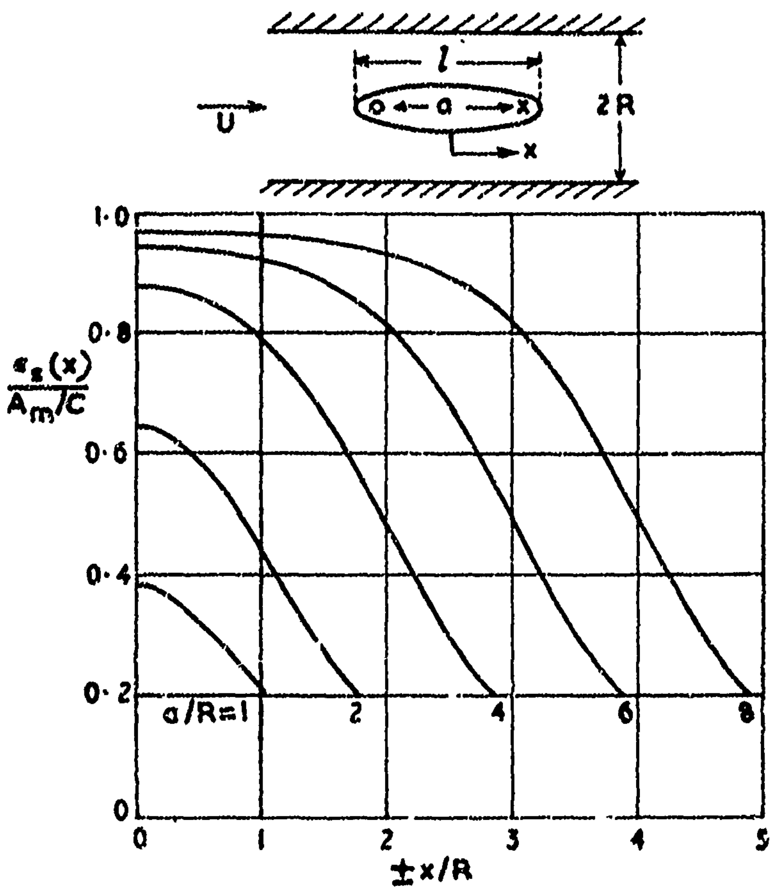

Fig.5.7 Distribution of solid blockage along bodies in closed circular tunnel

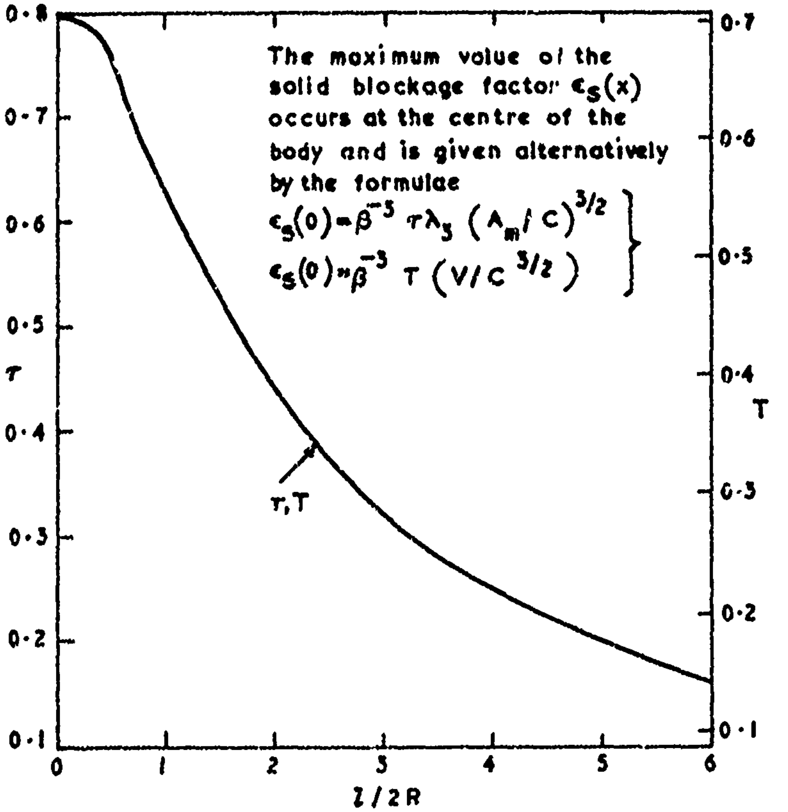

The maximum value of the solid blockage factor $\epsilon_S(x)$ occurs at the centre of the body and is given alternatively by the formulae

$$\left.\begin{aligned}\epsilon_S(0) &= \beta^{-3}\,\tau\lambda_3\,(A_m/C)^{3/2}\\ \epsilon_S(0) &= \beta^{-3}\,T\,(V/C^{3/2})\end{aligned}\right\}$$

Fig.5.8 Approximate values of tunnel-shape parameters for long bodies in closed circular tunnels

Based on Fig.1 of Ref.5.33

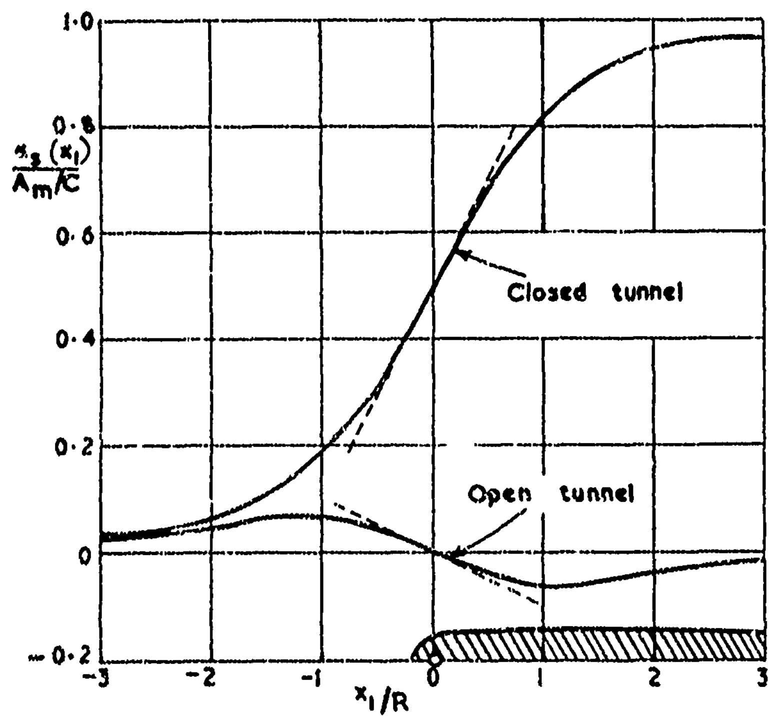

Fig.5.9 Blockage factors for semi-infinite bodies of revolution in circular tunnels

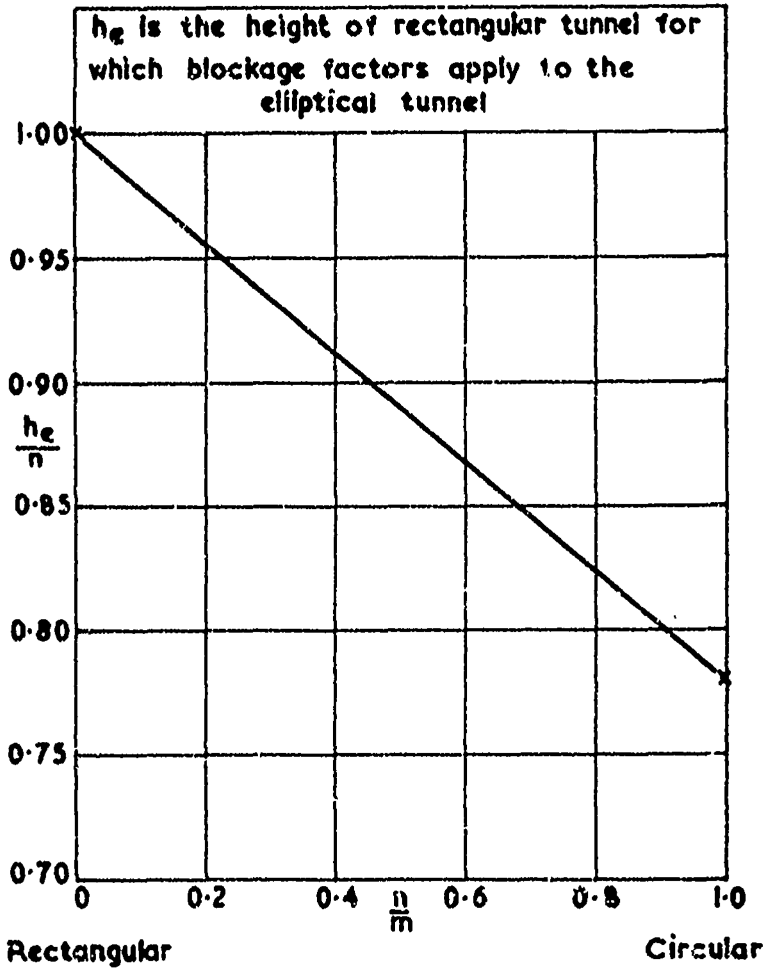

Fig.5.10 Blockage at centre section of wing spanning an elliptical tunnel

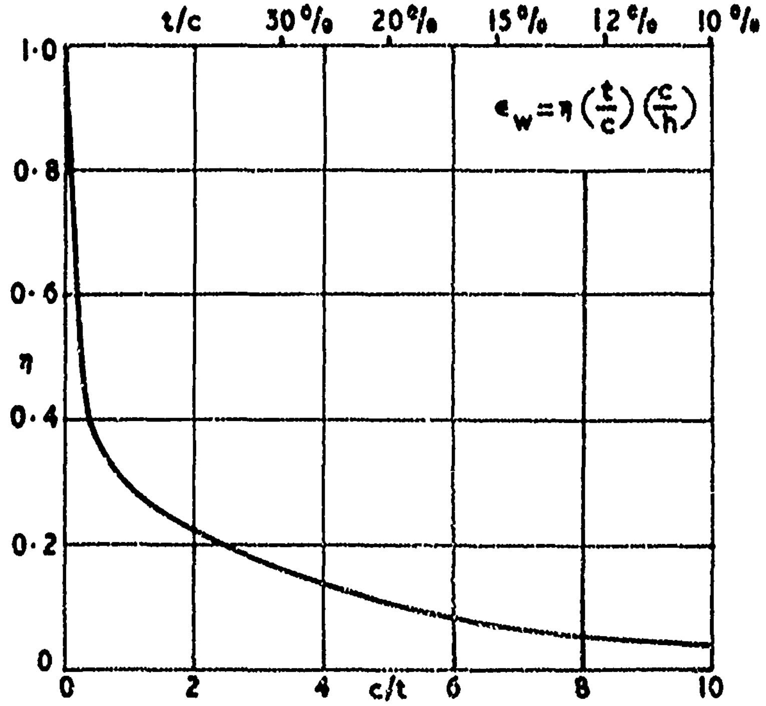

Reproduced from Fig.28 of Ref.5.1

Fig.5.11 Glauert's two-dimensional wake-blockage factor

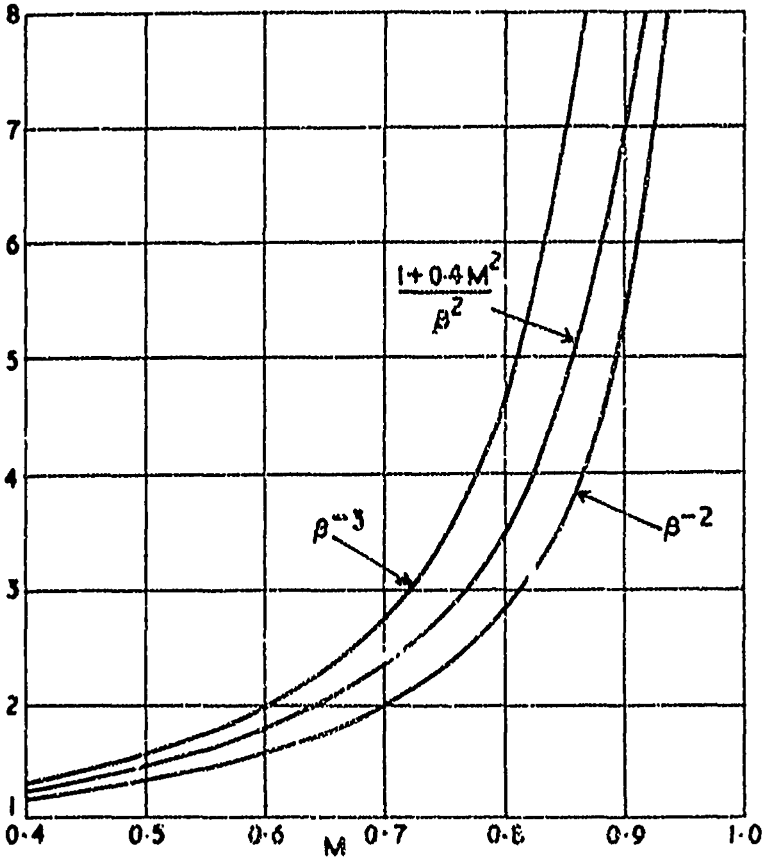

Fig.5.12 Simple compressibility factors used in blockage equations

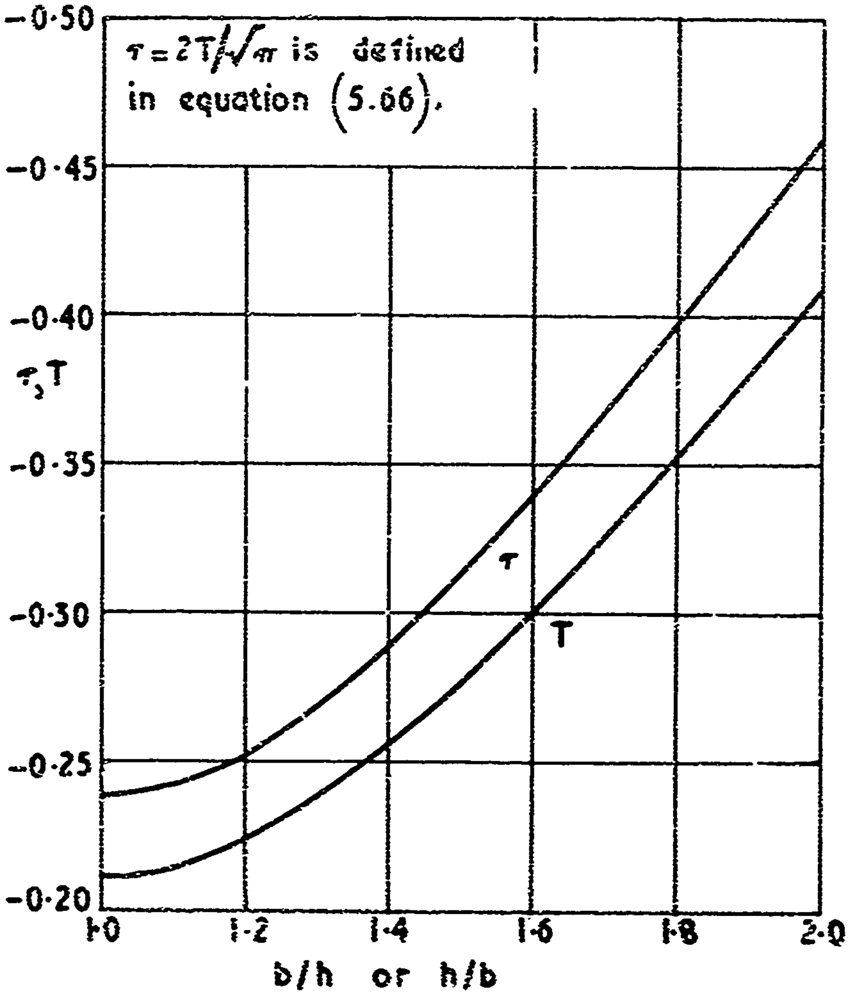

Fig. 5.13 Tunnel-shape parameters for small models in open rectangular tunnels

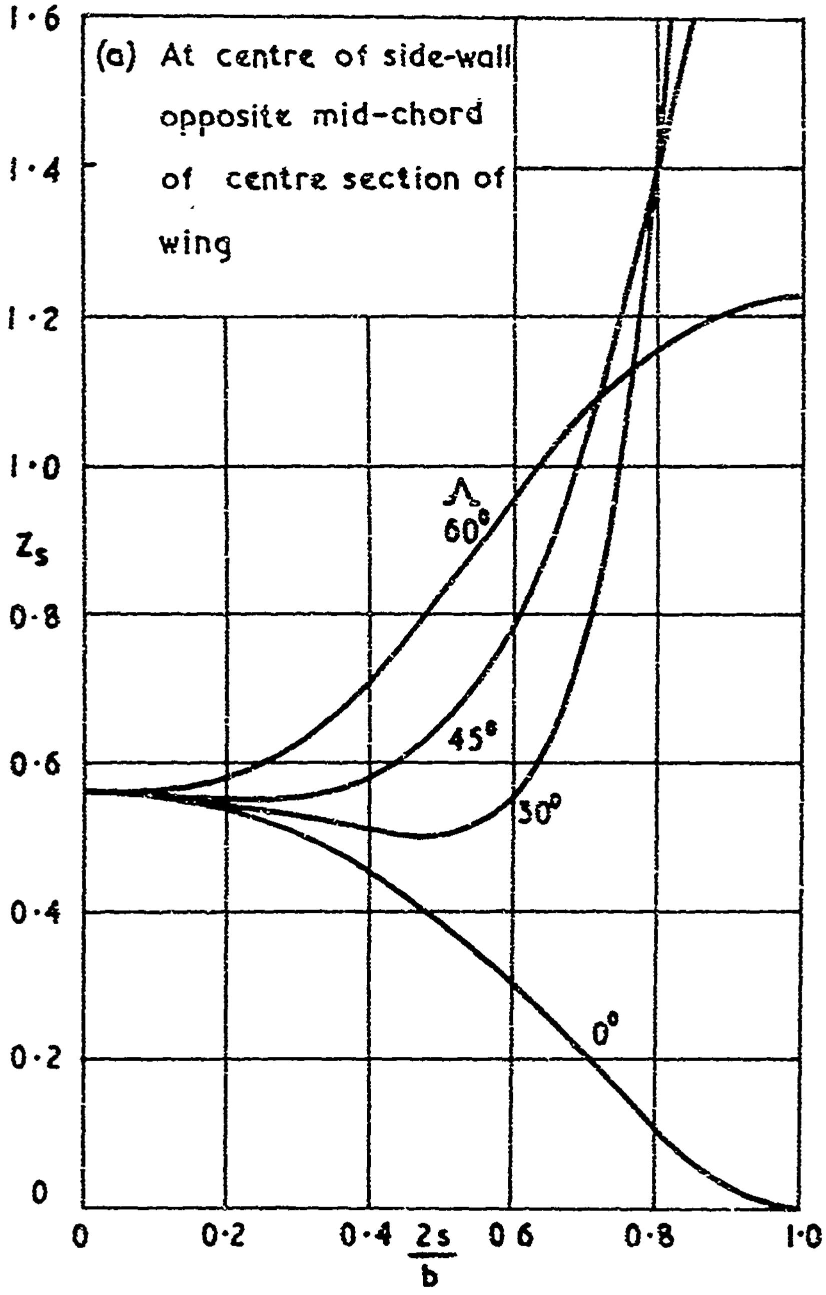

Based on Fig. 6 of Ref. 5.40

Fig. 5.14(a) Effect of model span and sweepback on wall-velocity ratio $Z_s (b/h = \sqrt{2})$

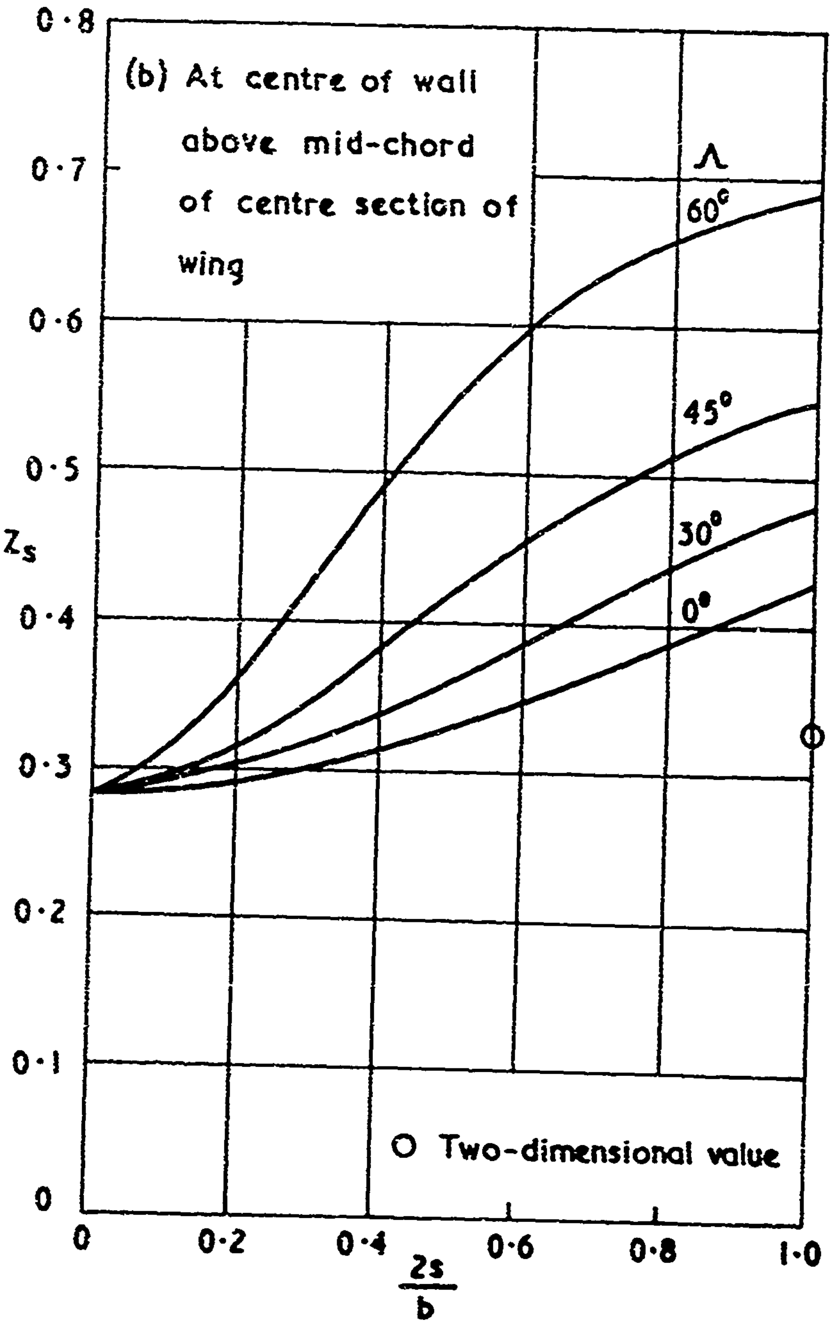

Based on Fig. 5 of Ref. 5.40

Fig. 5.14(b) Effect of model span and sweepback on wall-velocity ratio $Z_s (b/h = \sqrt{2})$

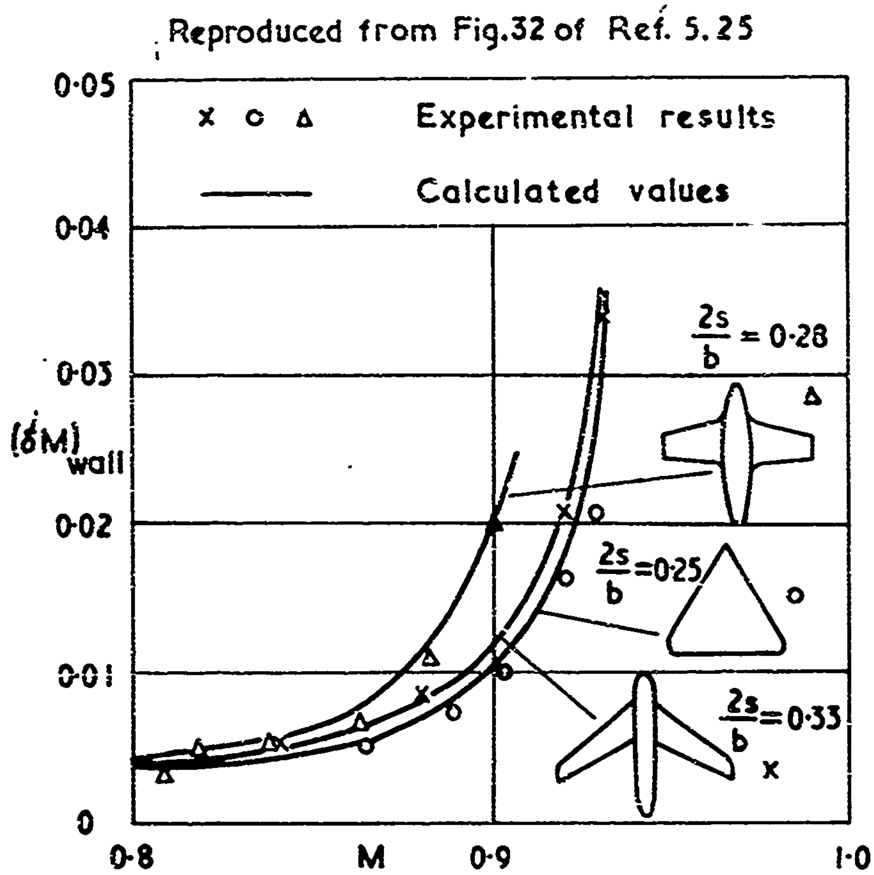

Fig. 5.15 Examples of calculated and experimental Mach number increments at side-wall of 10 ft × 7 ft tunnel

CHAPTER VI

WALL INTERFERENCE IN TUNNELS WITH VENTILATED WALLS

by

E.W.E.Rogers

Aerodynamics Division, National Physical Laboratory,
Teddington, Middlesex, England

BLANK PAGE

CONTENTS

Page

LIST OF TABLES 345

LIST OF FIGURES 345

NOTATION 348

6.1 INTRODUCTION 351

6.2 BOUNDARY CONDITIONS FOR WALLS WITH LONGITUDINAL SLOTS 353

6.3 TWO-DIMENSIONAL BLOCKAGE IN TUNNELS WITH LONGITUDINAL SLOTS 357
- 6.3.1 Solid Blockage 357
- 6.3.2 Longitudinal Pressure Gradient Due to Solid Blockage 360
- 6.3.3 Wake Blockage 361

6.4 THREE-DIMENSIONAL BLOCKAGE IN TUNNELS WITH LONGITUDINAL SLOTS 362
- 6.4.1 Circular Tunnel 362
- 6.4.2 Rectangular Tunnel with Slotted Roof and Floor 365
- 6.4.3 Rectangular Tunnel with Slots on Each Wall 367

6.5 LIFT INTERFERENCE IN TUNNELS WITH LONGITUDINAL SLOTS 369
- 6.5.1 Two-Dimensional Tunnel 369
- 6.5.2 Circular Tunnel 372
- 6.5.3 Rectangular Tunnel with Slotted Roof and Floor 375
- 6.5.4 Rectangular Tunnel with Slots on Each Wall 378

6.6 SOME GENERAL REMARKS ON INTERFERENCE EFFECTS IN TUNNELS WITH LONGITUDINAL SLOTS 379

S.7 THE PERFORATED WALL 380

6.8 TWO-DIMENSIONAL BLOCKAGE IN TUNNELS WITH PERFORATED WALLS 383
- 6.8.1 Solid Blockage 383
- 6.8.2 Wake Blockage 384

6.9 THREE-DIMENSIONAL BLOCKAGE IN TUNNELS WITH PERFORATED WALLS 385
- 6.9.1 Circular Tunnel 385
- 6.9.2 Rectangular Tunnel 386

Page

6.10 LIFT INTERFERENCE IN TUNNELS WITH PERFORATED WALLS 386
6.10.1 Two-Dimensional Tunnel 386
6.10.2 Circular Tunnel 387
6.10.3 Rectangular Tunnel 388

6.11 APPLICATION OF CORRECTION FACTORS 389

REFERENCES 391

ADDITIONAL REFERENCES 395

TABLE 397

FIGURES 398

LIST OF TABLES

Page

Table 6.I Summary of Results 397

LIST OF FIGURES

Fig.6.1 Notation and geometry for longitudinal slots 398

Fig.6.2 Solid-blockage factors for two-dimensional aerofoil in a slotted tunnel 399

Fig.6.3 Values of slot and porosity parameters required to give zero solid blockage for a two-dimensional aerofoil 400

Fig.6.4 Effect of aerofoil size on solid-blockage factor in ideal slotted tunnel 401

Fig.6.5 Effect of model size on slot parameter for zero blockage (F_c) in ideal slotted tunnel 402

Fig.6.6 Distribution of solid-blockage factor along two-dimensional ideal slotted tunnel 403

Fig.6.7 Longitudinal pressure gradient at the model associated with solid blockage 404

Fig.6.8 Solid-blockage factor for small three-dimensional model in circular slotted tunnel 405

Fig.6.9 Values of slot and porosity parameters required to give zero solid blockage for a small three-dimensional model in a circular tunnel 406

Fig.6.10 Solid-blockage factor for a small model in rectangular tunnels with ideal slotted roof and floor 407

Fig.6.11 Solid-blockage factor for large wings in rectangular tunnels with ideal slotted roof and floor 408

Fig.6.12 Estimated solid-blockage factor for small model in square tunnel with ideal slotted walls 409

Fig.6.13 Collapse of existing results for solid-blockage interference in ideal slotted tunnels 410

Page

Fig.6.14 Influence of porosity parameter on lift interference for small two-dimensional aerofoil in a slotted tunnel 411

Fig.6.15 Lift interference for two-dimensional aerofoil in an ideal slotted tunnel 412

Fig.6.16 Values of slot and porosity parameters required to give zero upwash interference for a small three-dimensional model in a circular tunnel 413

Fig.6.17 Lift-interference parameter for circular and square ideal slotted tunnels 414

Fig.6.18 Lift-interference parameter for models in a square ideal slotted tunnel with solid side-walls 415

Fig.6.19 Lift-interference parameter for models in ideal slotted tunnel with solid side-walls 416

Fig.6.20 Streamline-curvature correction in ideal slotted tunnel with solid side-walls 417

Fig.6.21 Influence of viscosity on lift-interference parameter for models in square slotted tunnel with solid side-walls 418

Fig.6.22 Influence of viscosity on lift-interference parameter for models in slotted tunnel with solid side-walls 419

Fig.6.23 Values of slot and porosity parameters required to give zero lift interference in slotted rectangular tunnels with solid side-walls 420

Fig.6.24 Effect on lift interference of discrete slots in the roof and floor 421

Fig.6.25 Lift-interference parameter for small wings in rectangular tunnels with ideal slotted walls 422

Fig.6.26 Variation of blockage with wall porosity in two-dimensional perforated tunnel 423

Fig.6.27 Distribution of solid-blockage factor along two-dimensional perforated tunnel 424

Fig.6.28 Blockage factor for small model in perforated circular tunnel 425

Fig.6.29 Lift interference in a two-dimensional perforated tunnel 425

Page

Fig.6.30 Lift interference for a small model in a perforated circular tunnel 426

Fig.6.31 Lift-interference parameter for small wing in special types of perforated tunnel 427

Fig.6.32 Comparison of exact and approximate values of δ_0 for closed and open rectangular tunnels 428

Fig.6.33 Estimated lift-interference parameter for small wing in perforated rectangular tunnels of different porosity 429

NOTATION

a	width of slot (Fig.6.1)
A	cross-sectional area of aerofoil
A_e	equivalent value of A (Section 6.3.2)
A_n	coefficient in Equation (6.67)
b	breadth of tunnel
c	chord of aerofoil
$\bar{c}$	geometric mean chord of wing
$\bar{\bar{c}}$	aerodynamic mean chord of wing in Equation (6.64)
C	cross-sectional area of tunnel
C_D	drag coefficient = (drag)/$\frac{1}{2}\rho U^2 S$
C_L	lift coefficient = (lift)/$\frac{1}{2}\rho U^2 S$
C_m	= (pitching moment about quarter-chord axis)/$\frac{1}{2}\rho U^2 S\bar{c}$
d	periodic spacing of slots (Fig.6.1)
f	thickness of slat (Fig.6.1)
F	non-dimensional slot parameter (Fig.6.1)
F_0	value of F giving zero interference
h	height of tunnel
I_0, I_1	modified Bessel functions (Ref.6.27)
$I_{A,B,C,D}$	Integrands in Equations (6.18), (6.23), (6.28), (6.51)
$I_{E,F,G,H}$	Integrands in Equations (6.52), (6.58), (6.84), (6.95)
K	geometric slot parameter in Equation (6.2)
K_0, K_1	modified Bessel functions (Ref.6.27)
l	distance between source and sink ($\simeq$ c)
M	Mach number of undisturbed stream

n	outward normal distance from tunnel boundary
N	number of equally spaced slots in a single wall
p	pressure
p_c	pressure in plenum chamber
P	porosity parameter defined by Equation (6.6)
q	variable of integration
r	radial distance from axis of circular tunnel
R	radius of circular tunnel
s	semi-span of wing
S	reference area of model
T	shape parameter of tunnel (Chapter V)
U	velocity of undisturbed stream
v_n	velocity normal to perforated wall
V	volume of model
V_e	equivalent volume of model (Chapter V)
w_i	interference upwash velocity
x	distance downstream of model
y	spanwise distance from axis of tunnel
z	distance upwards from model
α	incidence of aerofoil (in radians)
β	$= (1 - M^2)^{\frac{1}{2}}$
δ_0	list interference parameter for a small model
δ_1	lift interference parameter associated with streamline curvature
δp	pressure drop across a slot
Δ	prefix denoting increment due to wall correction
ϵ	blockage factor, $\Delta U/U$ (Section 6.3)

ζ	=	$\tan^{-1}(\beta/P)$
θ		cylindrical co-ordinate
μ	=	$\cot^{-1}(\beta/P)$
ρ		density of undisturbed stream
σ	=	2s/b
Φ		perturbation velocity potential
Φ_r	=	Φ(row) in a tunnel of infinite height
Φ_s	=	$(\Phi - \Phi_r)$, contribution from slotted roof and floor
Ψ		solid-blockage parameter for slotted tunnels in Equation (6.46)
Ω_s, Ω_w		blockage-factor ratio in Equations (6.16), (6.24)
Ω'_s		limit of Ω_s as slotted walls become fully open

Subscripts

B	denotes effect of blockage.
c	denotes closed tunnel.
g	denotes effect of velocity gradient (buoyancy).
i	denotes quantity induced by tunnel walls.
m	denotes model alone.
s	denotes solid blockage.
w	denotes wake blockage.

WALL INTERFERENCE IN TUNNELS WITH VENTILATED WALLS

E.W.E.Rogers

6.1 INTRODUCTION

The use of wind tunnels with partially-open, or ventilated, walls for transonic investigations is now widespread, and such tunnels are inevitably employed for tests at subsonic speeds, a fixed wall geometry usually being retained throughout the speed range. Ventilated walls may be of several different types, but frequently the openings consist of longitudinal slots or circular perforations; these allow the air to pass between the working section and the surrounding plenum chamber or tank. The ventilated walls may constitute the complete tunnel boundary or, alternatively, the side-walls of the tunnel may be solid, with glass windows, thus easing the problems of viewing or supporting the model.

The boundaries of the ventilated wind tunnel influence the flow about the model in a similar manner to the boundaries of the more conventional closed or open-jet tunnel. Indeed, these two types may often be regarded as the extreme limits within which the amount of wall ventilation may be varied. Fortunately, many of the wall-interference effects are of opposite sign in the two extreme geometries, and hence by using a partially-open tunnel it is possible to reduce, or even eliminate, these effects. Such considerations sometimes determine the design of the wall geometry to be used; frequently, however, the need to reduce shock-wave reflection effects at transonic and low supersonic speeds may be more important and become the basis of the tunnel design$^{6.32}$. Indeed for tunnels with perforated walls, where shock-wave reflection can be considerably reduced by careful choice of wall geometry, some degree of wall interference may have to be accepted, because the criteria for wave-reflection elimination and zero subsonic wall interference will probably be incompatible.

In general it is not possible to remove all types of subsonic wall interference by choosing a particular wall geometry; corrections are therefore required to many of the measured quantities, but very often these are not applied. One important reason for this apparent neglect is that the necessary corrections are frequently very small, partly because the model may be small in relation to the tunnel, and partly because the chosen wall geometry may well lie close to that needed to eliminate the particular interference effect. In addition, the theoretical potential-flow approach to the problems of ventilated-wall interference is sometimes felt to be less soundly based than when applied to tunnels with uniform boundaries, particularly since the effects of viscosity on the flow through the ventilations may be of considerable significance, yet difficult to estimate. The approach developed by, say, Baldwin et al. (Ref.6.1; 1954), in which the general effects of viscosity (particularly on the flow through longitudinal slots) may be allowed for, is of great value in meeting this type of criticism. The analysis is inevitably made more complicated, however, and knowledge of the porosity characteristics of the wall is required. This can often only be found by direct experiment.

Though much analysis has been undertaken in the general field of ventilated wind-tunnel interference, the supporting experimental checks on the theory (as opposed to tests demonstrating that certain interference effects are small) are at present insufficient to confirm or modify much of the theoretical work. Theory, however, does form a useful and general frame of reference against which the tunnel operator must often make his own assessment.

Interest in the use of mixed boundaries to minimize wall interference was aroused as early as 1931, when Theodorsen[6.2] discussed the interference experienced by a small lifting wing in tunnels having a combination of open and closed boundaries, and suggested that constraint effects could be reduced considerably by using these unconventional types of working section. These ideas were subsequently extended by many authors[6.3-6.12], both lift and blockage interference being considered. A few experimental tests were also made[6.4,6.10,6.11]. The blockage factors appropriate to rectangular tunnels having one or more completely open walls have recently been given by Wuest (Ref.6.50; 1961) who used an electronic computer and by this means was able to calculate the effects of displacing the model from the tunnel axis.

In terms of present-day tunnel configurations, these papers may be regarded as dealing with working sections having one or two longitudinal slots of considerable width. There are, however, certain disadvantages in using a small number of slots. For example, the flow in the working section may deteriorate due to jet instability[6.2], and the flow field in the neighbourhood of the model will tend to be rather distorted. The power requirements of the tunnel may also be large. For such reasons, working sections having multiple longitudinal slots have been adopted and much of the modern analysis has been concerned with this type of boundary.

The use of perforated walls to produce a partly-open boundary seems to have arisen from considering the characteristics of porous walls, where the flow through the wall corresponds to a slow viscous motion, and in which the pressure drop across the wall is proportional to the mass flow passing through it.

It is convenient therefore to divide the discussion of wall interference into two sections, dealing with tunnels having (a) longitudinal slots and (b) perforations. This is largely a matter of convenience since, as Maeder and Wood (Ref.6.13; 1956) show so elegantly, both types of ventilation are particular cases of a more general boundary condition; the proposed arrangement however does correspond to the major division in wind-tunnel construction, even though there are certain tunnels with walls which in effect combine slots and perforations.

Historically, and perhaps also practically, the elimination of solid-blockage effects has been considered of more importance than the removal of lift-interference effects, probably because it was felt that the test Mach number could then be accurately determined, particularly at high subsonic speeds. It is proposed therefore to discuss blockage interference initially and subsequently to consider lift interference, particularly the value likely to be present in a tunnel designed for zero-blockage conditions. It will be assumed that the lift and blockage corrections are independent and additive, and hence that it is sufficient to calculate the blockage effects of zero model lift. A summary of the results to be presented in this chapter is included at its end, as Table 6.I.

6.2 BOUNDARY CONDITIONS FOR WALLS WITH LONGITUDINAL SLOTS

The first attempt to calculate the lift interference experienced by a small wing in a tunnel having multiple longitudinal slots was made in 1940 by Pistolesi[6.14] for a circular tunnel. Similar results were obtained in 1953 by Matthews[6.15] in an independent analysis, which was more detailed than the earlier work and allowed for variations in slot configuration, wing span and loading. The blockage of a slender body in a slotted circular wind tunnel was discussed by Wright and Ward (Ref. 6.16; 1948), again using the exact boundary conditions. An extension of this method to a two-dimensional aerofoil was made in 1950 by Tomlinson[6.51].

It proved difficult however to apply these methods in practice due to the complexity associated with the mixed nature of the boundary; for example, to satisfy the correct boundary conditions for a source-sink doublet placed on the axis of a circular-slotted tunnel, an infinite set of linear simultaneous equations arises in the calculation of the interference functions. Even with certain simplifying assumptions, extensive numerical work is often required. Difficulties of this type led to the consideration of a simpler, though less exact, wall condition by an approach attributed in Reference 6.17 to Busemann. This assumed that the real slotted wall could be replaced by an equivalent homogeneous boundary whose influence near the model would be very similar to that of the real wall. Since this influence may be imagined as a weighted mean of the effects due to the slots and the solid slats, it seems that the equivalent wall would give a close representation of the flow near the tunnel centre, provided that the dimensions of the tunnel were large compared with the distance between adjacent slots. The calculations and discussions of Davis and Moore (Ref. 6.17; 1953) confirm the validity of this argument, and show that the simpler analysis based on the equivalent boundary gives, in general, correction effects which are in very close agreement with those calculated by the earlier exact methods.

The linearized boundary condition of the equivalent wall has been derived by more than one method. (See References 6.1, 6.13, 6.17 to 6.20). In most cases the cross-flow approaching a single slot and slat is considered, and this leads to a simple homogeneous boundary condition for subsonic flow, which is assumed to apply along the entire length of the tunnel working section and is thus independent of x :

$$\frac{\partial \Phi}{\partial x} + K \frac{\partial^2 \Phi}{\partial x \partial n} = 0 , \qquad (6.1)$$

where Φ is the perturbation velocity potential, x is measured in the stream direction and n along the outward normal to the wall surface. The parameter K , having the dimensions of length, is defined by

$$K = \frac{d}{\pi} \log_e \operatorname{cosec} \frac{\pi a}{2d} . \qquad (6.2)$$

Here, the slats are assumed to be of small thickness normal to the cross-flow direction, d is the periodic spacing of the slots, and a is the slot width (Fig.6.1); the open area ratio a/d must be small, d being a small fraction of the tunnel dimensions. Equation (6.1) should be compared with the exact conditions, represented usually by

$$\left.\begin{aligned} \frac{\partial\Phi}{\partial n} &= 0 \quad \text{at the slats} \\ \frac{\partial\Phi}{\partial x} &= 0 \quad \text{at the slots} \end{aligned}\right\} . \tag{6.3}$$

The boundary condition used by Woods in Sections 7.30 to 7.32 of Reference 6.19 (1961) is somewhat different and overcomes certain difficulties involved in the assumption that the calculations are being made for a position whose distance from the wall is large compared with the slot spacing. This alternative boundary condition would seem to be of most value when only a few widely spaced slots are present. Goethert (Ref.6.18; 1957) in a more exact analysis of the cross-flow near the slots shows that Equation (6.2) may be regarded as the first term of a power series in the open-area ratio a/d ; unless this ratio is small, higher-order terms may be significant.

Wood[6.57] discusses the validity of the linearized boundary condition in Equation (6.1) with particular emphasis on the large transverse velocities which can occur in the neighbourhood of narrow slots when large models are tested, and on the significance of the displacement of the free boundary from the contour of the slotted wall. These considerations lead to the non-linear homogeneous boundary condition

$$\frac{\partial\Phi}{\partial x} + \left(\frac{\pi + 2}{\pi}\right)^2 \frac{d^2}{2Ua^2}\left(\frac{\partial\Phi}{\partial n}\right)^2 = 0 , \tag{6.4}$$

which implies a similarity between the transverse flow in the slot and a two-dimensional Helmholtz jet. Reference 6.57 includes a measured velocity distribution along the wall, that appears to justify Wood's non-linear calculations for a non-lifting two-dimensional aerofoil. Further applications of this non-linear boundary condition have not so far been made, and the analysis in the present chapter is based on linear boundary conditions.

So far the flow has been assumed inviscid, so that there is no pressure drop across the slot boundary, apart from that associated with changes in fluid velocity. In practice, the effects of viscosity may well be of importance, particularly if the slot width is small compared with the wall boundary-layer thickness. Equation (6.1) then needs to be modified. Baldwin et al.[6.1] do this by adopting the homogeneous boundary condition for a porous wall[6.21,6.45], in which the average velocity normal to the wall is assumed to be proportional to the pressure drop (δp) through the wall (see Section 6.7). This is a linearized approximation to the viscous flow through a porous medium and leads to the boundary condition

$$\frac{\partial\Phi}{\partial x} + \frac{1}{P}\frac{\partial\Phi}{\partial n} = 0 . \tag{6.5}$$

where P is a porosity parameter defined by

$$\delta p = \frac{\rho U}{P} \frac{\partial \Phi}{\partial n} . \tag{6.6}$$

Here U is the free-stream velocity, $\partial\Phi/\partial n$ the velocity normal to the wall, and ρ the fluid density. As mentioned in Section 6.7, P may be determined experimentally for any given wall by measuring δp for various values of $\rho(\partial\Phi/\partial n)$.

It is assumed therefore that, for a slotted wall having viscous effects within the slots, a boundary condition

$$\frac{\partial \Phi}{\partial x} + K \frac{\partial^2 \Phi}{\partial x \partial n} + \frac{1}{P} \frac{\partial \Phi}{\partial n} = 0 \tag{6.7}$$

may be used; alternatively, if the porosity parameter is found not to be linear with $\partial\Phi/\partial n$, a more complex condition may be required (Appendix B of Reference 6.1). Solutions based on Equation (6.7) will include the following special cases:

the closed wall ($K \to \infty$ or $P = 0$),
the open jet ($K = 0$ and $P \to \infty$),
the perforated wall ($K = 0$),
the inviscid slotted wall ($P \to \infty$).

The perforated wall will be discussed in Sections 6.7 to 6.10. The last case will henceforward be referred to as an "ideal" slotted wall.

Alternatively the effects of viscosity in the slot region may be represented by considering the slots to be covered with a porous or perforated material; a more complicated boundary condition is then required[6.18]. In some wind tunnels perforated cover plates have been fixed across the slots, so that the pressure drop can be increased artificially to match the local outflow characteristics in free air.

Much of the existing analysis for interference effects in slotted-wall tunnels is based on an inviscid boundary condition similar to Equation (6.1), and it is now possible to estimate the required corrections for a wide range of models and tunnel cross-sections for this ideal slotted wall. Some of the experimental checks that have been made in References 6.23 and 6.24 suggest however that the ideal slotted wall condition $P \to \infty$ may not always be achieved; indeed for typical working-section configurations P may be of order unity and not greatly influenced by the stream Mach number. Much more information is required on this point, and it is here perhaps sufficient to point out that the ideal slotted-wall correction factors may sometimes need to be applied with caution; fortunately interference corrections have been evaluated in several cases for the more general boundary condition (6.7), and these are discussed below. The assumption of an ideal slotted wall, however, is valuable in enabling a general picture to be obtained of wall-interference effects in slotted tunnels, especially the trends with slot geometry and model size.

It will also be assumed (unless stated to the contrary) that the slotted working section is long compared with the tunnel height or breadth and that the slots are uniformly spaced, have sharp edges, small thickness and no longitudinal taper. Further it will be assumed that the model is mounted centrally in the working section.

In certain cases, the restrictions on slot geometry may be overcome. For example, if the walls have tapered slots, Equation (6.7) may be used as the boundary condition but P , instead of representing the viscous effects in the slot flow, may now be related to the slot taper by

$$\frac{1}{P} = \frac{dK}{dx} , \qquad (6.8)$$

K being given by Equation (6.2); this matter is discussed further in Reference 6.1.

If the slats have a thickness f , a boundary condition of similar form to Equation (6.1) may be derived, but with a somewhat different definition of the parameter K (Ref. 6.52; 1957). Unfortunately, as f tends to zero this new definition of K becomes inconsistent with Equation (6.2) above. The differences are quite large and seem to arise from the way in which the slats are represented in the analysis; by doublets, when the slats have finite thickness and, in effect, by sources for the case of very thin slats. Since in practice most wind-tunnel slats are thin compared with their width, the definition of Equation (6.2) seems a reasonable one to use in such cases.

The discrete boundary conditions at a slotted wall may be satisfied if the rheo-electric analogy is employed; in this the electric potential in an electrolytic tank may be identified with the interference velocity potential, the tank being contoured to represent the tunnel section. In the exact analogical model the solid portions of the wall are insulators, whilst the slots are made of conducting material, so that a wall consisting only of a few slots and slats may readily be represented. If required, the linear homogeneous boundary condition of Equation (6.5) can also be represented by a simple analogy (Tirumalesa, Ref. 6.55; 1959). The actual profile and incidence of a two-dimensional aerofoil may be simulated in the tank, a considerable advantage if the model is a large one, and this aspect is discussed in detail in Reference 6.55.

At Birmingham University, Rushton (Ref. 6.60; 1965) has developed an electrical analogue computer to study slotted-wall interference effects. The computer consists of a rectangular array of resistors which form, in effect, a model of the wing and tunnel cross-section. The equations of the electrical network are made identical to the finite-difference form of the two-dimensional differential equation governing the velocity potential, and the resistance network can then be used to estimate the interference upwash at the wing for different types of tunnel boundary. Rushton in fact considered the interference experienced by small lifting wings in rectangular tunnels having both roof and floor slotted or all four walls slotted. With such an analogue it is possible to compare results obtained under the linear homogeneous boundary condition, discussed earlier, and for walls with ideal slots and slats; this comparison is discussed below in Section 6.5.3. The analogue method can also be used to check the significance of assumptions necessary to secure an analytical solution to a particular problem, and to give, if required, improved data for the interference corrections. Examples of this are contained in Sections 6.5.3 and 6.5.4.

6.3 TWO-DIMENSIONAL BLOCKAGE IN TUNNELS WITH LONGITUDINAL SLOTS

Blockage interference arises from both the model and its wake, the two components being called solid and wake blockage respectively. It manifests itself as an increment $\Delta U_B = \epsilon_B U$ in stream velocity at the model position. The total blockage factor ϵ_B is conveniently expressed as the sum of the solid-blockage factor ϵ_S and the wake-blockage factor ϵ_W, which are derived independently at zero model lift. Associated with both the solid- and wake-blockage increments are longitudinal velocity gradients, which impose a corresponding drag force on the model.

The analysis for slotted tunnels is rather less extensive in scope than for the closed and open tunnels, although most of the important simple cases have now been discussed. The present section is concerned with two-dimensional models spanning a slotted tunnel of height h ; the tunnel side-walls are assumed to act merely as reflection planes contributing nothing to the flow about the model.

6.3.1 Solid Blockage

If the model is small and thin, it may be represented by a two-dimensional doublet whose velocity potential in a free stream of subsonic Mach number M is

$$\Phi_m = \frac{AU}{2\pi\beta}\left[\frac{x}{x^2 + \beta^2 z^2}\right] , \qquad (6.9)$$

where A is the cross-sectional area of the model, and $\beta = (1 - M^2)^{\frac{1}{2}}$. The origin of the co-ordinate system is at the centroid of the model. In the tunnel the perturbation potential is given by

$$\Phi = \Phi_m + \Phi_i , \qquad (6.10)$$

Φ_i being the potential of the wall constraint. The latter must satisfy the general linearized equation of flow

$$\beta^2 \frac{\partial^2\Phi_i}{\partial x^2} + \frac{\partial^2\Phi_i}{\partial z^2} = 0 . \qquad (6.11)$$

The potential Φ must also satisfy the boundary condition (6.7) at the slotted walls, so that

$$\left(\frac{\partial\Phi_i}{\partial x} \pm K \frac{\partial^2\Phi_i}{\partial x\partial z} \pm \frac{1}{P}\frac{\partial\Phi_i}{\partial z}\right)_{z=\pm\frac{1}{2}h} = -\left(\frac{\partial\Phi_m}{\partial x} \pm K \frac{\partial^2\Phi_m}{\partial x\partial z} \pm \frac{1}{P}\frac{\partial\Phi_m}{\partial z}\right)_{z=\pm\frac{1}{2}h} . \qquad (6.12)$$

From Equations (6.9), (6.11) and (6.12), the interference potential may be found. Different techniques have been employed in the solution for Φ_i . Reference 6.1, for example, uses Fourier transforms

$$\left.\begin{aligned} G(g,z) &= \frac{1}{2\pi}\int_{-\infty}^{+\infty}\Phi(x,z)e^{igx}\,dx \\ \Phi(x,z) &= \int_{-\infty}^{+\infty}G(g,z)e^{-igx}\,dg \end{aligned}\right\} \qquad (6.13)$$

for both Φ_m and Φ_i . Once the solution for Φ_i is known, the solid-blockage factor can be obtained from the expression

$$\epsilon_s = \frac{\Delta U_s}{U} = \frac{1}{U}\left(\frac{\partial \Phi_i}{\partial x}\right)_{x=z=0} , \qquad (6.14)$$

conditions at the origin being taken as the mean of the distributed effect along the model. In the general case[6.1]

$$\epsilon_s = -\frac{6}{\pi^2}\left(\frac{\pi A}{6\beta^3 h^2}\right)\int_0^\infty \left\{\frac{[1 - F^2q^2 - (\beta/P)^2] + [(1 - Fq)^2 + (\beta/P)^2]e^{-2q}}{(\cosh q + Fq \sinh q)^2 + (\beta/P)^2 \sinh^2 q}\right\} q\, dq , \qquad (6.15)$$

where $q = \frac{1}{2}\beta \xi h$. The effect of slot geometry is represented by the parameter F $(= 2K/h)$, and the influence of viscosity on the slot flow by the ratio β/P . Thus, if P is assumed to be independent of stream Mach number (as certain tests suggest), the influence of the viscous slot flow will vary with M ; moreover, as the stream Mach number approaches unity, β/P tends to zero, and the ideal slotted tunnel condition is approached.

Following Reference 6.17, it is convenient to use a parameter $(1 + F)^{-\frac{1}{2}}$ to illustrate the variation of the solid-blockage effect with slot geometry. This parameter has a value of zero for the closed tunnel and unity for the open tunnel. It seems reasonable, too, to consider the ratio of ϵ_s in the slotted tunnel to its value $(\epsilon_s)_c$ in a similar tunnel with closed walls. The latter quantity is that in brackets outside the integral in Equation (6.15). Thus

$$\Omega_s = \epsilon_s/(\epsilon_s)_c = \left(\frac{6\beta^3 h^2}{\pi A}\right)\epsilon_s \qquad (6.16)$$

is considered as a function of $(1 + F)^{-\frac{1}{2}}$. This type of presentation may be of value in extending the present results for simple model shapes to more complex representations, by assuming that for a given tunnel the value of Ω_s is unchanged if the more sophisticated methods discussed in Chapter V are used for determining $(\epsilon_s)_c$.

The variation of Ω_s with $(1 + F)^{-\frac{1}{2}}$ for a two-dimensional aerofoil is shown in Figure 6.2 for two values of β/P . One, taken from Reference 6.17, corresponds to the ideal slotted tunnel $(P \to \infty)$ and indicates an almost linear variation of Ω_s from the fully closed tunnel to open-jet tunnel. The other, broken, curve has been calculated for $M = 0.8$, $P = 1.0$; the latter value, though arbitrarily chosen, may well be typical of many tunnels.

Zero solid blockage will correspond to $\Omega_s = 0$, and this is achieved in an ideal slotted tunnel for the condition

$$(1 + F)^{-\frac{1}{2}} = 0.67_7 , \qquad (6.17)$$

whence

$$F = F_0 = 1.18 .$$

For the broken curve, $F_0 = 1.0_5$. The variation of F_c with β/P to give zero blockage has been estimated by Baldwin et al.[6.1] and is reproduced as Figure 6.3.

The definition of P contained in Figure 6.1 indicates that for each value of the ratio of tunnel height to slot spacing (h/d) there is a critical value of the open-area ratio for zero solid blockage, as illustrated in the following table, where the ideal slotted tunnel is compared with one having $\beta/P = 1$.

Percentage Open-Area Ratio for Zero Solid Blockage

$\frac{h}{d}$	1	2	4	6	8	12
$100\frac{a}{d}$ for $\frac{\beta}{P} = 0$	10.0	1.6	0.4×10^{-1}	0.9×10^{-3}	0.2×10^{-4}	0.1×10^{-7}
$100\frac{a}{d}$ for $\frac{\beta}{P} = 1$	20.5	6.4	0.64	$0.6_5 \times 10^{-1}$	$0.6_5 \times 10^{-2}$	$0.6_5 \times 10^{-3}$

These values are remarkably small for the slot configurations usually employed*, and it seems doubtful whether the theoretical approach can be considered entirely valid for the two-dimensional case. On this evidence, slot configurations usual in two-dimensional tunnels would be often too open, and the solid-blockage factor would be negative. Experimentally, Pearcey et al. (Ref. 6.24; 1959) found zero-blockage conditions for a particular slot configuration $h/d = 6.37$, $a/d = 1.6\%$, for which $P = 0.37$. As Figure 6.3 shows, this would correspond to a value $\beta/P = 1.20$, though no attempt was made to measure this quantity directly.

The alternative boundary condition suggested by Woods in Section 7.31 of Reference 6.19 is claimed to be more valid for $h/d < 2$, but for greater values of this ratio there is little difference between his results and those obtained by other authors.

Maeder (Ref. 6.25; 1953) discusses the case in which the model is too large to be represented sufficiently accurately by a doublet and where use of a Rankine oval (discrete source and sink) is preferable. His theoretical curves for the ideal slotted tunnel are reproduced in Figure 6.4 for different values of the ratio $l/\beta h$, where l is the source-sink separation distance. When the aerofoil is thin, this ratio is approximately $c/\beta h$, where c is the model chord; a more accurate relationship between l and c will be found in Reference 6.26. Figure 6.4 shows a discrepancy between Maeder's curve for a very small model and that given by Davis and Moore[6.17]; this is due to an approximation contained in the analysis of Reference 6.25†. The discrepancy does not affect the estimated value of F_0 required to give zero solid blockage (Fig. 6.5) and, since most wind tunnels operate in the region between this condition and that for an open-jet, the difference between the two methods of analysis may usually be unimportant.

---

[*] For example, if h is 10 units and the slot spacing d is 1 unit, then the calculated slot width for zero interference is 6×10^{-9} units for the ideal slotted tunnel and about 7×10^{-6} units for $\beta/P = 1.0$.

[†] There is a similar discrepancy for a small three-dimensional model in a tunnel with solid side-walls and slotted roof and floor (Section 6.4.2); this is discussed by Acum (Ref. 6.34; 1961).

The problem of an aerofoil whose chord may no longer be regarded as small compared with the tunnel height is also discussed by Tirumalesa, using the rheoelectric analogy[6.55]. His results in Figure 3 of Reference 6.55 are in broad agreement with the theoretical calculations of Maeder and confirm that, as the model size increases relative to the tunnel, F_0 also increases (Fig. 6.5). For a fixed slot spacing, this corresponds to a reduction in open area ratio.

6.3.2 Longitudinal Pressure Gradient Due to Solid Blockage

In the preceding section, the velocity increment at the model position due to the solid blockage has been discussed. This increment, however, varies both along and across the working sections. The latter variation is small in the region of the model and may usually be neglected. The longitudinal velocity gradient has been detected experimentally by Wright (Ref. 6.28; 1959) and is of importance for two reasons. Firstly, if the stream velocity is measured at some position on the tunnel wall upstream of the model, this position may be itself subject to a small interference effect*. Secondly, consideration must be given to the velocity gradient, and hence the corresponding pressure gradient, along the model to see whether this influences the measured drag.

In an ideal slotted tunnel with the linearized, homogeneous boundary condition, the solid-blockage velocity increment varies symmetrically on either side of the position of a small model, so that the longitudinal pressure gradient there is zero (Fig. 6.6). Hence there is no horizontal buoyancy force, and no correction to be applied to the measured drag. On the other hand, Wood[6.57] shows that for large interference velocities, where the linear boundary condition may no longer be valid, the interference velocity may be antisymmetric on either side of the model, giving rise to a buoyancy force.

The interference symmetry is also lost if viscous effects appear at the slots and the linearized boundary condition (6.7) with finite P is used. The longitudinal velocity gradient for a two-dimensional aerofoil may be derived from the general solution for Φ_1 in Equation (19) of Reference 6.1. At the model position

$$\frac{\partial \epsilon_s}{\partial x} = \frac{24}{\pi^2 \beta h} (\epsilon_s)_c \frac{\beta}{P} \int_0^\infty I_A \, dq \ . \tag{6.18}$$

where

$$I_A = \frac{q^2}{(\cosh q + Fq \sinh q)^2 + (\beta/P)^2 \sinh^2 q}$$

and $(\epsilon_s)_c = \pi A/(6\beta^3 h^2)$ is the value of ϵ_s for a closed tunnel. The pressure gradient, $\partial p/\partial x$, is given by $-\rho U^2(\partial \epsilon_s/\partial x)$, and the magnitude of this gradient for a particular ratio, $\beta/P = 0.6$, is illustrated in Figure 6.7.

---

* In many tunnels, the stream speed is determined from the pressure in the plenum chamber surrounding the working section. The influence of the model on the plenum-chamber pressure is discussed briefly in Reference 6.49.

The pressure gradient associated with the solid blockage imposes an unwanted drag force on the model, which is given by minus the product of the pressure gradient and the equivalent area of aerofoil cross-section (A_ϵ). Now A_e may be shown to be equivalent to $6\beta^3h^2(\epsilon_s)_c/\pi$ (see Reference 6.43, for example), and it follows that the required correction to the measured drag coefficient for the wall-induced velocity gradient is

$$(\Delta C_D)_{sg} = \frac{\partial p}{\partial x}\frac{A_e}{\frac{1}{2}\rho U^2 c}$$

$$= -\frac{288}{\pi^3}\frac{\beta^2 h}{c}(\epsilon_s)_c^2\frac{\beta}{P}\int_0^\infty I_A\,dq\,, \tag{6.19}$$

where I_A is the integrand in Equation (6.18).

6.3.3 Wake Blockage

As discussed in Section 5.4.4, the presence of the wake downstream of the model gives rise to two constraint effects when the tunnel walls are solid. One is an effective velocity increment at the model position: the other is the horizontal buoyancy associated with the longitudinal velocity gradient at the model position. In the open-jet tunnel, the first effect (but not the second) is usually taken to be zero, because the boundaries of the jet can be displaced away from the tunnel axis in order to compensate for the low-velocity air in the model wake. There is then no need to increase the stream velocity in the flow outside the wake in order to maintain the same mass flow upstream and downstream of the model. Similar considerations would apply to the slotted tunnel.

Formally, the model wake is replaced by a source. The subsequent analysis has been made for an ideal slotted tunnel by Maeder$^{6.13,6.25}$ and for a tunnel with a porosity parameter P by Wright$^{6.28}$, using the techniques of Reference 6.1.

When the model is a two-dimensional aerofoil, the effective interference velocity*, $\epsilon_w U$, at the model is found to be zero, provided that the slot flow corresponds to that in an ideal slotted tunnel. The velocity gradient at the model position for this case is

$$\frac{\partial\epsilon_w}{\partial x} = -\frac{C_D c}{\pi\beta^2h^2}\int_0^\infty\frac{(1 - Fq)e^{-q}q\,dq}{\cosh q + Fq\sinh q}\,. \tag{6.20}$$

The velocity gradient associated with a single source has the same magnitude as the velocity due to a doublet of equal strength. Provided that the boundary conditions are independent of x, as in Equation (6.7) when $P \rightarrow \infty$, then the wake-blockage gradient can be identified with the solid-blockage factor ϵ_s, apart from a numerical factor. Thus for the condition $\beta/P = 0$, it follows from Equations (6.15), (6.16) and (6.20) that

---

* There may be an induced velocity at some reference point upstream of the model and in consequence an equal and opposite effective interference velocity at the model.

$$\frac{\partial \epsilon_w}{\partial x} = \frac{\pi}{12}\Omega_s \frac{C_D c}{\beta^3 h^2}\,, \qquad (6.21)$$

which becomes zero when Ω_s vanishes. Hence, in an ideal slotted tunnel, the wake-blockage velocity increment and horizontal buoyancy are eliminated if zero solid-blockage conditions are present. If this is not the case, the correction to the measured drag is

$$(\Delta C_D)_{wg} = -\Omega_s(\epsilon_s)_c C_D\,. \qquad (6.22)$$

the derivation being similar to that described in Section 5.8.2.

If the tunnel does not conform to ideal slotted conditions, the velocity increment far upstream is still zero, but at the model position by Equation (23) of Reference 6.28 there is a wake-blockage factor

$$\epsilon_w = -\frac{2}{\pi}\left[\frac{C_D c}{4\beta^2 h}\right]\frac{\beta}{P}\int_0^\infty I_s\, dq\,. \qquad (6.23)$$

where

$$I_s = \frac{[(1 + Pq)\sinh q + \cosh q]e^{-q}}{(\cosh q + Pq\sinh q)^2 + (\beta/P)^2\sinh^2 q}\,.$$

The quantity in square brackets outside the integral in Equation (6.23) is $(\epsilon_w)_c$, the value of ϵ_w for a closed tunnel, so that the ratio of the wake-blockage factors may be written as

$$\Omega_w = \frac{\epsilon_w}{(\epsilon_w)_c} = -\frac{2}{\pi}\frac{\beta}{P}\int_0^\infty I_s\, dq\,. \qquad (6.24)$$

The velocity gradient at the model and the associated drag correction are still given by Equations (6.21) and (6.22), and it follows that these vanish if the tunnel is operating under zero solid-blockage conditions.

6.4 THREE-DIMENSIONAL BLOCKAGE IN TUNNELS WITH LONGITUDINAL SLOTS

There are three main types of slotted working-section used for testing three-dimensional models: (i) circular; (ii) rectangular with slots on the top and bottom walls; and (iii) rectangular with all walls slotted. These will be considered in turn.

6.4.1 Circular Tunnel

A small three-dimensional model may be replaced by its equivalent doublet, whose potential in free air is given approximately by

$$\Phi_s = \frac{UV}{4\pi}\left[\frac{x}{(x^2 + \beta^2 r^2)^{3/2}}\right]\,, \qquad (6.25)$$

where V is the volume of the model, and $r = (y^2 + z^2)^{\frac{1}{2}}$ is the radial distance perpendicular to the tunnel axis. In cylindrical co-ordinates the velocity potential satisfies

$$\beta^2 \frac{\partial^2\Phi}{\partial x^2} + \frac{1}{r}\frac{\partial}{\partial r}\left(r\frac{\partial\Phi}{\partial r}\right) = 0 . \qquad (6.26)$$

As in Section 6.3.1, we write $\Phi = \Phi_m + \Phi_i$, which satisfies Equation (6.26) and the boundary condition at the wall (r = R),

$$\left(\frac{\partial\Phi_i}{\partial x} + K\frac{\partial^2\Phi_i}{\partial x\partial r} + \frac{1}{P}\frac{\partial\Phi_i}{\partial r}\right)_{r=R} = -\left(\frac{\partial\Phi_m}{\partial x} + K\frac{\partial^2\Phi_m}{\partial x\partial r} + \frac{1}{P}\frac{\partial\Phi_m}{\partial r}\right)_{r=R} . \qquad (6.27)$$

This corresponds to Equation (6.12). Fourier integral expressions for Φ_m and Φ_i may again be used to deduce the perturbation velocity at the model position and hence the blockage factor. Baldwin et al.[6.1] give this in a form which may be rewritten as

$$\epsilon_s = -0.40\left[\frac{0.797V}{2\pi\beta^3R^3}\right]\int_0^\infty I_c\,dq , \qquad (6.28)$$

with

$$I_c = \frac{\left\{K_0(q)I_0(q) - qF[K_1(q)I_0(q) - K_0(q)I_1(q)] - \left(q^2F^2 + \frac{\beta^2}{P^2}\right)K_1(q)I_1(q)\right\}q^2}{[I_0(q) + qFI_1(q)]^2 + \left[\frac{\beta}{P}I_1(q)\right]^2} ,$$

where for the circular tunnel F = K/R and the modified Bessel functions I_0, I_1, K_0 and K_1 are tabulated in Reference 6.27. For the ideal slotted tunnel $P \to \infty$, and I_c becomes

$$I_c = \frac{[K_0(q) - qFK_1(q)]q^2}{[I_0(q) + qFI_1(q)]} . \qquad (6.29)$$

The expression in brackets in Equation (6.28) is the solid-blockage factor for a closed circular tunnel, so that we may write

$$\Omega_s = \frac{\epsilon_s}{(\epsilon_s)_c} = -0.40\int_0^\infty I_c\,dq . \qquad (6.30)$$

The variation of Ω_s with slot geometry is shown in Figure 6.8 for the ideal slotted tunnel only. Davis and Moore[6.17] used these results to demonstrate the validity of the approximate homogeneous boundary condition (6.27) by showing that they are in good agreement with the exact calculations made by Wright and Ward[6.16].

Zero blockage in the ideal slotted tunnel occurs when the abscissa $(1+F)^{-\frac{1}{2}} = 0.798$, i.e. when $F = F_0 = 0.57$. Now for a circular tunnel with N equally-spaced slots

$$\frac{d}{R} = \frac{2\pi}{N} , \tag{6.31}$$

so that the non-dimensional slot parameter F becomes (Fig.6.1)

$$F = \frac{K}{R} = \frac{2}{N} \log_e \operatorname{cosec} \frac{\pi a}{2d} . \tag{6.32}$$

The variation of the open-area ratio with the number of slots to give zero blockage in an ideal tunnel is illustrated in the following table corresponding to $F = F_0 = 0.57$.

N	2	4	6	8	12	16	24
$100 \frac{a}{d}$	38.3	20.7	11.6	6.5	2.1	0.7	0.07

These values are far larger than those for a two-dimensional model and give reasonable slot widths even when the number of slots is large.

The effect of viscosity on F_0 is discussed in Reference 6.1, from which the present Figure 6.9 is reproduced*; certain values have been transferred to Figure 6.8 to indicate the possible trend of the curves for Ω_s . There seems to be little direct evidence as to whether the assumption of zero viscosity at the slots is reasonable or not in typical slotted circular tunnels. Nevertheless the tests of Reference 6.16, made in a tunnel with 10 slots and open-area ratio 12.5% $[(1 + F)^{-\frac{1}{2}} = 0.86]$ exhibit an interference of about the magnitude expected from the curve of Figure 6.8. It seems therefore that, if there is no information about the appropriate value of β/P for a given tunnel and the wall geometry is not far removed from that required to give zero blockage for an ideal tunnel, then it may be assumed that $\beta/P = 0$. The longitudinal pressure gradient of the model due to the solid blockage is absent for this condition only; when β/P has a finite value, the resulting velocity gradient, and hence the pressure gradient, may be calculated from Equation (34) of Reference 6.1.

The wake-blockage effects of a small three-dimensional model in a circular slotted tunnel are discussed in Reference 6.28, where the wake is replaced by a three-dimensional point source whose strength is proportional to the model drag. The expressions for the axial interference velocity ratio and the velocity gradient along the tunnel, at the model position, are

$$\Omega_w = \frac{\epsilon_w}{(\epsilon_w)_c} = -\frac{1}{\pi}\frac{\beta}{P}\int_0^{\infty} \frac{dq}{[I_0(q) + qFI_1(q)]^2 + \left[\frac{\beta}{P} I_1(q)\right]^2} \tag{6.33}$$

---

* Attention is drawn to the Errata to Reference 6.1, which corrects the original Figure 4.

and

$$\frac{\partial \epsilon_w}{\partial x} = -\frac{1}{\pi\beta R}(\epsilon_w)_c \int_0^\infty I_c \, dq = \frac{(\epsilon_w)_c \Omega_s}{0.40\pi\beta R} \, . \tag{6.34}$$

where I_c is the integrand of Equation (6.28) for the solid-blockage factor and

$$(\epsilon_w)_c = \frac{C_D}{4\beta^2}\left(\frac{S}{\pi R^2}\right) \, ,$$

S being the reference area on which the model drag coefficient is based. It follows from Equations (6.30) and (6.34) that, if the solid-blockage interference is zero, then the velocity gradient at the model due to the wake will be eliminated. Similarly it may be shown that for this flow condition ϵ_w is zero too.

When zero solid blockage is not obtained, the wake blockage may be found from Equation (6.33); the buoyancy correction to the measured drag is precisely that contained in Equation (6.22).

6.4.2 Rectangular Tunnel with Slotted Roof and Floor

In this case the model may once again be represented by the doublet whose potential in free air (Φ_m) is given in Equation (6.25). The solid side-walls require a condition of zero flow velocity normal to them and can therefore be represented by a horizontal row of doublet images spaced at distances equal to the tunnel breadth (b). The potential Φ_r of such an image-row can be derived simply from Φ_m (Ref. 6.17). Another potential Φ_s may be added to Φ_r to satisfy the conditions at the slotted walls. Thus in an ideal slotted tunnel $\Phi = \Phi_r + \Phi_s$ will satisfy

$$\left.\begin{aligned} \frac{\partial \Phi}{\partial y} &= 0 \qquad (y = \pm\tfrac{1}{2}b) \\ \frac{\partial \Phi}{\partial x} \pm K\frac{\partial^2 \Phi}{\partial x \partial z} &= 0 \qquad (z = \pm\tfrac{1}{2}h) \end{aligned}\right\} \, . \tag{6.35}$$

The formal solution for Φ_s is given in Reference 6.17. The solid-blockage incremental velocity at the model position has two components, one associated with the slotted, and the other with the solid walls; thus

$$\Delta U_s = \frac{\partial \Phi_s}{\partial x} + \frac{\partial}{\partial x}(\Phi_r - \Phi_m) \, . \tag{6.36}$$

After substitution and some manipulation[6.38] it follows that

$$\epsilon_s = \frac{\Delta U_s}{U} = \frac{V}{\beta^3 b^3}\left\{\frac{1}{2\pi}\sum_{n=1}^{\infty}\frac{1}{n^3} + \frac{2b^2}{\pi h^2}\int_0^\infty \frac{q e^{-q}(Fq - 1)}{\cosh q + Fq \sinh q}\,dq + \right.$$

$$\left. + \sum_{n=1}^{\infty}\frac{4b^2}{\pi h^2}\int_{q_0}^\infty \frac{(q^2 - q_0^2)^{\frac{1}{2}} e^{-q}(Fq - 1)}{\cosh q + Fq \sinh q}\,dq\right\} \, . \tag{6.37}$$

where $q_0 = \pi mh/b$ and, from Figure 6.1,

$$F = \frac{2b}{\pi Nh} \log_e \operatorname{cosec} \frac{\pi Na}{2b} . \tag{6.38}$$

The first term in the bracket expresses the influence of the solid side-walls, and the remainder the influence of the slotted roof and floor. In the special case $F = 0$, corresponding to a tunnel with open roof and floor, Equation (6.37) becomes[6.34]

$$(\epsilon_s)_{F=0} = \frac{V}{\beta^3 b^3} \left\{ \frac{1}{2\pi} \sum_{n=1}^{\infty} \frac{1}{n^3} - \frac{\pi b^2}{12h^2} + \frac{4b}{h} \sum_{t=1}^{\infty} t \left[\sum_{n=1}^{\infty} \frac{(-1)^n}{n} K_1 \left(\frac{2\pi nth}{b} \right) \right] \right\} , \tag{6.39}$$

and for $F \to \infty$, corresponding to a closed rectangular tunnel,

$$(\epsilon_s)_c = \frac{V}{\beta^3 b^3} \left\{ \frac{1}{2\pi} \sum_{n=1}^{\infty} \frac{1}{n^3} + \frac{\pi b^2}{6h^2} + \frac{4b}{h} \sum_{t=1}^{\infty} t \left[\sum_{n=1}^{\infty} \frac{1}{n} K_1 \left(\frac{2\pi nth}{b} \right) \right] \right\} . \tag{6.40}$$

The exponential behaviour of the Bessel function $K_1(2\pi nth/b)$ ensures rapid convergence of the series (6.39) and (6.40) which are most convenient for computation. In Figure 6.10 values of $\Omega_s = \epsilon_s/(\epsilon_s)_c$ from Equations (6.37) and (6.40) have been plotted as functions of $(1+F)^{-\frac{1}{2}}$ for representative values of h/b. As might be expected, the effect of varying F is greatest for small values of h/b; for $h > 1.17b$ zero blockage cannot be achieved. This confirms an earlier prediction of Wieselsberger (Ref. 6.7; 1942). Numerical values of $\beta^3 b^3 \epsilon_s/(8V)$ are given in Table 1 of Reference 6.34 for the complete range of $(1 + F)^{-\frac{1}{2}}$ and h/b; alternatively, the solid-blockage factor for small wings may be obtained from Figure 6.10 with the aid of the tunnel-shape parameter T from Figure 5.3 or 5.4 of Chapter V.

Maeder[6.25] has used a somewhat different technique to evaluate solid-blockage corrections and has extended his method to include the effect of model span. His result for a small model is obtained by taking only the first two terms inside the bracket in Equation (6.37). It can be shown that for large q_0

$$\frac{4b^2}{\pi h^2} \int_{q_0}^{\infty} \frac{(q^2 - q_0^2)^{\frac{1}{2}} e^{-q} (Fq - 1)}{\cosh q + Fq \sinh q} \, dq = O(q_0^{1/2} e^{-2q_0}) \tag{6.41}$$

and will be small. If $h = 1.25b$, the difference between Maeder's values of ϵ_s and those from Equation (6.37) is less than $0.0006V/(\beta b)^3$, but for smaller values of h/b it becomes appreciable. In effect, Maeder assumes the influence of the slotted roof and floor to be independent of model span. Then, for a model of span $2s$, the first term of the bracket in Equation (6.37) is replaced by

$$\frac{1}{2\pi} \sum_{n=1}^{\infty} \frac{n}{(n^2 - \frac{1}{4}\sigma^2)^2} = 0.1913 + \frac{\sigma^2 (8 - \sigma^2)}{2\pi (4 - \sigma^2)^2} + 0.0029\sigma^2 + 0.0002\sigma^4 + \ldots , \tag{6.42}$$

where $\sigma = 2s/b$. The effect of model span, shown in Figure 6.11, is obtained by adding the terms involving σ on the right-hand side of Equation (6.42) to the bracketed expression in Equation (6.37). The curves of $\epsilon_s/(\epsilon_s)_{c,\sigma=0}$ against $(1 + F)^{-\frac{1}{2}}$ are thus displaced upwards by an amount independent of F, but depending on σ and h/b. For a square tunnel zero blockage can only just be achieved if σ is as large as 0.8. Maeder's treatment does not hold when h/b is small and should be used with caution when $h/b < 1$.

The wake-blockage effects associated with a small model in an ideal slotted tunnel with ventilated roof and floor are discussed in Reference 6.28. It is there shown that ϵ_w may be taken as zero, whatever the slot geometry, and that the velocity gradient at the model vanishes when the wall is designed to eliminate solid blockage. The influence of viscous flow within the slots on the foregoing analysis, cf. Equation (6.18), does not appear to have been considered for this type of tunnel.

6.4.3 Rectangular Tunnel with Slots on Each Wall

This particular case does not seem to have been treated directly, though several authors have suggested that the solid-blockage effects for a square tunnel should be very similar to those obtained in a circular tunnel of the same cross-sectional area. If the solid-blockage factor for a small model takes the form

$$\epsilon_s = T\left(\frac{V}{\beta^3 C^{3/2}}\right) \qquad (6.43)$$

where C is the tunnel cross-sectional area, then T will depend on the tunnel shape and slot parameter F. For example, T has values of 0.706 and 0.717 for the circular and square closed tunnels respectively, and for the corresponding open tunnels, these values are −0.182 and −0.211. Thus, when the tunnel walls are close to the open-jet condition, the error in using the circular-tunnel corrections may be of consequence.

In the absence of direct information, it seems more realistic to use the existing knowledge of the blockage corrections for the open and closed square tunnels, which correspond to values of Ω_s of 1.0 and −0.294. These values may be joined by a straight line[6.33] or, better still, by a scaled version of the curve for a circular tunnel. These estimated curves for the ideal slotted square tunnel are shown in Figure 6.12 and are almost coincident in the important region near zero blockage at approximately $F = F_0 = 0.67_5$. If F is assumed to be equal to K/R', where $R' = \surd(C/\pi)$ is the radius of a circular tunnel having the same cross-sectional area, then for a square tunnel

$$F = \frac{\sqrt{\pi}K}{h} = \frac{d}{\sqrt{\pi}h}\log_e \operatorname{cosec}\frac{\pi a}{2d}$$

$$= \frac{1}{\sqrt{\pi}N}\log_e \operatorname{cosec}\frac{\pi a}{2d}\,, \qquad (6.44)$$

where N is the number of slots on each wall. For zero solid blockage, the open-area ratio a/d is given in the following table.

N	1	2	4	6	8	10
$100\frac{a}{d}$	19.5	5.8	0.53	0.05	0.004_5	0.0004

Around the tunnel periphery there will be $4N$ slots, and the open-area ratio corresponding to this number of slots in the table for the circular tunnel in Section 6.4.1 is about the same, suggesting once more the correspondence between the two types of tunnel. It seems reasonable therefore to apply to the square slotted tunnel similar influences of slot porosity to those already discussed for the circular tunnel.

The foregoing procedure may of course be applied to a tunnel of general rectangular cross-section; the appropriate values of ϵ_s for fully open and closed boundaries (Chapter V) would replace the end values of Figure 6.12. If the correspondence with the equivalent circular tunnel is maintained, then in place of Equation (6.44)

$$F = \frac{\sqrt{\pi}K}{\sqrt{bh}} = \frac{d}{\sqrt{\pi bh}}\log_e \operatorname{cosec}\frac{\pi a}{2d} . \qquad (6.45)$$

One interesting point, which perhaps strengthens the use of an approximate method similar to that at present being discussed, is revealed by replotting the known results for slotted tunnels in terms of a new parameter

$$\Psi = \frac{\Omega_s - \Omega'_s}{1 - \Omega'_s} , \qquad (6.46)$$

where Ω'_s is the value of Ω_s for the condition $F = 0$. Thus Ψ varies between unity and zero as the slotted walls change from fully closed to fully open. As Figure 6.13 shows, most of the known results lie fairly close together. Except perhaps for tunnels having a large ratio of breadth to height, some mean curve could be used to estimate the solid-blockage factor for other configurations including, for example, elliptical and octagonal sections. In particular, for rectangular tunnels with slots on each wall the blockage factor for the open-jet case must be determined first; typical values of Ω'_s for a small centrally-situated model are listed below.

$\frac{h}{b}$ or $\frac{b}{h}$	2.00	1.80	1.60	1.40	1.25	1.10	1.00
$-\Omega'_s$	0.449	0.413	0.376	0.337	0.313	0.296	0.293

The wake-blockage effects in tunnels with all four walls slotted do not seem to have been discussed. For tunnels of near-square cross-section, it would seem reasonable to calculate the appropriate velocity increment and drag correction from Equations (6.33) and (6.22) for a circular tunnel of the same cross-sectional area. For an ideal slotted tunnel, it may be assumed, by analogy with the circular tunnel and that having a slotted roof and floor, that the wake-blockage factor is zero and that the gradient at the model vanishes for the wall geometry giving zero solid blockage.

6.5 LIFT INTERFERENCE IN TUNNELS WITH LONGITUDINAL SLOTS

The induced upwash associated with the walls of a circular, slotted tunnel containing a small lifting wing was one of the first problems of this type to be considered, and in the early work of Pistolesi[6.14] the exact boundary conditions were employed. Much simplification results from the use of the equivalent homogeneous boundary conditions discussed in Section 6.2, which are valid provided that there is a reasonable number of slots; by this means the lift interference has now been evaluated for two- and three-dimensional models in the types of tunnel most frequently employed.

The lifting model is usually replaced by a simple vortex system, for example, a single bound vortex if the model is a two-dimensional aerofoil, or a trailing vortex pair in the case of a small wing. This type of representation will be sufficient for most purposes. The actual interference experienced by the model may in general be regarded as composed of two parts; an upwash (or incidence) correction at the model position, and a "streamline curvature" effect associated with the variation in the wall-induced upwash along the model length. The latter becomes of importance if this length is of the same order as the tunnel height.

Once again it is convenient to discuss separately different sorts of models and working sections. First, the two-dimensional tunnel will be considered, and then three types of working section suitable for testing three-dimensional models.

6.5.1 Two-Dimensional Tunnel

As before, the aerofoil is considered to span the tunnel breadth, the solid side-walls acting merely as reflection planes. The interference is due to the pressure of the slotted boundaries above and below the aerofoil which is replaced by a two-dimensional vortex of strength $\frac{1}{2}UcC_L$.

Wright[6.28] has developed for this particular case the approach contained in Reference 6.1, which allows for viscous effects within the slots. The potential of the vortex in free air is

$$\Phi_m = -\frac{UcC_L}{4\pi}\tan^{-1}\frac{\beta z}{x} . \qquad (6.47)$$

At the slotted boundaries, the interference potential Φ_i must satisfy Equation (6.12). The method of solution is then similar to that used for the solid-blockage interference, outlined in Section 6.3.1. In the general case, the induced upwash angle at the vortex position becomes

$$\frac{w_i}{U} = \frac{1}{U}\frac{\partial\Phi_i}{\partial z} = -\frac{cC_L}{2\pi h}\frac{\beta}{P}\int_0^\infty \frac{dq}{[\sinh q + Pq\cosh q]^2 + \left[\frac{\beta}{P}\cosh q\right]^2} . \qquad (6.48)$$

Consider first the ideal slotted tunnel (P → ∞); in this case Equation (6.48) reduces to the limit

$$\frac{w_i}{U} = -\frac{cC_L}{4h(1+F)} , \tag{6.49}$$

which is independent of stream Mach number. This lift interference becomes zero when the tunnel walls are closed ($F \to \infty$) and has the value $-\frac{1}{4}(c/h)C_L$ for an open-jet tunnel ($F = 0$). For the condition of zero solid blockage in an ideal slotted tunnel ($F_0 = 1.18$) the lift interference is about 0.46 of that predicted for a two-dimensional open jet. Because it is proportional to c/h, the interference may be of considerable magnitude.

Holder (Ref. 6.58; 1962) has evaluated Equation (6.48) for a range of values of β/P. His results are presented in Figure 6.14 in terms of the parameter

$$\delta_0 = \frac{hw_i}{UcC_L} . \tag{6.50}$$

The induced upwash interference disappears for the condition $P = 0$, which represents a wall with extremely high resistance to cross-flow. In this condition, an important limiting case is the closed tunnel ($P = 0$, $F \to \infty$) in which δ_0 is known to be zero from earlier work on upwash interference. One important feature revealed by Figure 6.14 is that, for a given slot geometry (constant F), the upwash interference decreases as the viscous effects grow. This suggests that in practice the actual interference is likely to be smaller than that predicted by Equation (6.49). The experiments described in Reference 6.24 provide evidence of such a trend, but the effect may not be attributed with certainty to the influence of viscous flow within the slots.

The general expression for the induced upwash angle along the tunnel axis may sometimes be required; Equation (6) of Reference 6.28 simplifies to give

$$\frac{w_i}{U} = -\frac{cC_L}{2\pi h}\int_0^\infty I_D \, dq , \tag{6.51}$$

where

$$I_D = \frac{\dfrac{\beta}{P}\cos\left(\dfrac{2qx}{\beta h}\right) + \left[(1 - Fq)(\sinh q + Fq\cosh q) - \left(\dfrac{\beta}{P}\right)^2\cosh q\right]e^{-q}\sin\left(\dfrac{2qx}{\beta h}\right)}{[\sinh q + Fq\cosh q]^2 + (\beta/P)^2\cosh^2 q} .$$

For an ideal slotted tunnel ($P \to \infty$) Equations (6.49) and (6.51) are inconsistent. It is explained in Reference 6.28 that the uniform upwash corresponding to Equation (6.49) must be added to Equation (6.51) to make w_i vanish in the limit as $x \to -\infty$. Fortunately, if P is finite, there is no singularity in I_D at $q = 0$ and consequently no difficulty at $x = -\infty$.

For a completely closed tunnel, the upwash vanishes both far upstream and at the model position. The well-known lift-interference corrections for an aerofoil in a tunnel with closed boundaries result from the streamline curvature and are proportional to $(c/h)^2$, when higher-order terms are neglected. The streamline curvature effect in a slotted-wall tunnel at $x = 0$, can be obtained by differentiating Equation (6.51):

$$\frac{c}{U}\frac{\partial w_i}{\partial x} = -\frac{c^2 C_L}{\pi\beta h^2}\int_0^\infty I_E\,dq\ , \tag{6.52}$$

where

$$I_E = \frac{[(1 - Pq)(\sinh q + Pq\cosh q) - (\beta/P)^2\cosh q]qe^{-q}}{[\sinh q + Pq\cosh q]^2 + (\beta/P)^2\cosh^2 q}\ .$$

As Glauert[6.43] points out, the correction to incidence, $\Delta\alpha$ is the value of w_i/U at the mid-chord of the aerofoil. The representative vortex must be placed at the centre of pressure, and the mid-chord is approximately at a distance $c(\frac{1}{4} + C_m/C_L)$ downstream. Then

$$\begin{aligned}\Delta\alpha &= \frac{w_i}{U} + \frac{c}{U}\frac{\partial w_i}{\partial x}\left(\frac{1}{4} + \frac{C_m}{C_L}\right)\\ &= \frac{cC_L}{h}\,\delta_0 + \frac{c^2}{\beta h^2}\,\delta_1(\tfrac{1}{4}C_L + C_m)\ ,\end{aligned} \tag{6.53}$$

where, by Equations (6.49), (6.51) and (6.52),

$$\left.\begin{aligned}\delta_0 &= \frac{hw_i}{UcC_L} = -\frac{1}{4(1+P)} &&\text{when}\quad P\to\infty\\ \delta_0 &= -\frac{1}{2\pi}\int_0^\infty I_D\,dq &&\text{when}\quad P\ \text{is finite}\\ \delta_1 &= \frac{\beta h^2}{UcC_L}\frac{\partial w_i}{\partial x} = -\frac{1}{\pi}\int_0^\infty I_E\,dq &&\text{for all}\quad P\end{aligned}\right\}\ . \tag{6.54}$$

The residual corrections due to streamline curvature are conveniently expressed as equivalent increments to the coefficients of lift and pitching moment about the quarter-chord point.

$$\left.\begin{aligned}\Delta C_L &= -\frac{\pi}{2\beta}\frac{c}{U}\frac{\partial w_i}{\partial x} = -\frac{\pi}{2}\left(\frac{c}{\beta h}\right)^2\delta_1 C_L\\ \Delta C_m &= \frac{\pi}{8\beta}\frac{c}{U}\frac{\partial w_i}{\partial x} = \frac{\pi}{8}\left(\frac{c}{\beta h}\right)^2\delta_1 C_L\end{aligned}\right\}\ . \tag{6.55}$$

For a closed tunnel $\delta_0 = 0$ and $\delta_1 = \pi/24$, and Equations (6.53) and (6.55) become identical to Equations (2.16) and (2.17) of Chapter II.

For the ideal slotted tunnel $\beta/P = 0$ and

$$I_E = \frac{(1 - Pq)qe^{-q}}{\sinh q + Pq\cosh q}\ . \tag{6.56}$$

For zero solid blockage when $F = F_0 = 1.18$, Wright[6.28] has evaluated $\delta_1 = -0.027$, which is small relative to the corresponding values for closed and open tunnels. Values of δ_0 and δ_1 at other values of F may be obtained from Figure 6.15, where the abscissa $(1 + F)^{-1}$ is a useful parameter for presenting lift-interference curves. Zero streamline curvature occurs when $F = 1.59$.

Tirumalesa[6.55] has used the rheoelectric analogy to treat the case where the model chord is of the same order as the tunnel height. The distribution of interference upwash along a two-dimensional model, displaced from the axis of the tunnel, is discussed in Reference 6.30.

6.5.2 Circular Tunnel

Matthews[6.13] has extended the early work of Pistolesi[6.14] and provides a general solution for the correct boundary conditions; in special circumstances the method of Reference 6.15 may be of great value, and in addition it provides a check on the use of the less precise homogeneous boundary condition (Section 6.2). The linear form of this condition has been employed by several authors for a lifting wing in the centre of a circular slotted tunnel, and the method devised by Baldwin et al.[6.1] is again of significance because of the way in which it can allow for viscous effects at the slots.

In this analysis the wing is replaced by a small horse-shoe vortex, whose potential in free air is

$$\Phi_v = \frac{USC_L}{8\pi}\left(1 + \frac{x}{\sqrt{x^2 + \beta^2 r^2}}\right)\frac{\sin\theta}{r}, \tag{6.57}$$

where S is the wing planform area and x, r and θ are the cylindrical co-ordinates. The fact that the actual span (2s) is finite introduces higher-order terms which are negligible at distances large compared with the model size. The interference potential Φ_i must satisfy Equation (6.26) and the boundary condition (6.27); in Reference 6.1, Φ_i and its derivative $\partial\Phi_i/\partial z$ are obtained by a Fourier transform method.

The upwash angle at the model position may be expressed as

$$\frac{w_i}{U} = \frac{SC_L}{8\pi R^2}\left[1 - \frac{\beta}{\pi P}\int_0^\infty I_P \, dq\right]. \tag{6.58}$$

where

$$I_P = \frac{q^2}{q^2[(1 - F)I_1(q) + qFI_0(q)]^2 + (\beta/P)^2[I_1(q) - qI_0(q)]^2}$$

and, as in Equation (6.28), $F = K/R$. I_0 and I_1 are modified Bessel functions. The incidence correction is unaffected by compressibility, except through β/P.

For a small model it is convenient to express the lift interference as

$$\Delta\alpha = \frac{w_i}{U} = \frac{SC_L}{C}\delta_0. \tag{6.59}$$

C being the tunnel cross-sectional area. In the present case $C = \pi R^2$, and the interference parameter

$$\delta_0 = \frac{1}{8}\left[1 - \frac{\beta}{\pi P}\int_0^{\infty} I_P \, dq\right] . \qquad (6.60)$$

The values of $P = P_0$ required to give zero lift interference are shown in Figure 6.16 against the slot porosity parameter β/P .

Davis and Moore[6.17] have shown that a wing of uniform spanwise loading, represented as a horse-shoe vortex, in an ideal slotted tunnel gives an interference parameter

$$\delta_0 = \frac{1}{8}\sum_1^{\infty}\frac{Pn - 1}{n(Pn + 1)}\left(\frac{s}{R}\right)^{2n-2} \qquad (n = 1, 3, 5, \ldots) , \qquad (6.61)$$

which is obtained as an average along the semi-span $0 \leqslant y \leqslant s$. Even for quite large values of s/R , only the first term need be considered, so that it is sufficient to write

$$\delta_0 = \frac{1}{8}\left[\frac{P - 1}{P + 1}\right] . \qquad (6.62)$$

which is plotted as a straight line against $(1 + P)^{-1}$ in Figure 6.17. It can be shown that Equation (6.60) tends to this result, when the ideal slotted tunnel is considered by the limiting process $P \to \infty$. In Reference 6.17 Equation (6.62) is compared with the exact values obtained by Matthews[6.15] for tunnels having 4, 8 and 12 slots; excellent agreement is obtained between the two methods of solution.

The condition for zero upwash interference corresponds to the value $P_0 = 1.0$, compared with a value of 0.57 to eliminate solid-blockage effects. It is apparent therefore that it is not possible to eliminate both upwash and blockage interference simultaneously in a circular ideal slotted tunnel, but, as Figure 6.16 shows, this may well be achieved if β/P has a value around 0.7. At $P = 1.0$, the relationship between the total number of slots and the open-area ratio is as follows.

N	2	4	6	8	12	16	24
$100\left(\frac{a}{d}\right)$	24.0	8.6	3.2	1.2	0.16	0.02	0.0004

The ideal zero-blockage condition may well be the one for which the tunnel is designed; δ_0 is then −0.034, which is of the opposite sign to the correction in a solid-wall tunnel and about 27% of its magnitude.

If the model chord is of the same order as the tunnel diameter, some correction for streamline curvature may be required. For the case where β/P is not zero the curvature can be obtained as

$$\frac{\bar{c}}{U}\frac{\partial w_i}{\partial x} = \frac{\bar{c}}{U}\left(\frac{\partial^2\Phi_i}{\partial z\partial x}\right)_{x=r=0} \, ,$$

where $\bar{c}$ is the geometric mean wing chord and Φ_i is given by Equation (46) of Reference 6.1. Reynolds et al.[6.23] give curves of the corrections for a value of $F = 0.191$ appropriate to the Cooperative Wind Tunnel in California with different values of the porosity parameter P. The total correction to incidence takes the form

$$\Delta\alpha = \frac{SC_L}{\pi R^2}\left(\delta_0 + \frac{\bar{\bar{c}}}{4\beta R}\,\delta_1\right) \, , \tag{6.63}$$

where
$$\delta_1 = \frac{2\pi\beta R^3}{USC_L}\frac{\partial w_i}{\partial x}$$

is independent of Mach number. The second term in Equation (6.63) represents the increment in w_i/U associated with a displacement $\frac{1}{4}\bar{\bar{c}}$ in the streamwise direction, where the aerodynamic mean chord

$$\bar{\bar{c}} = \int_0^1 \frac{[c(y)]^2}{\bar{c}}\,d\left(\frac{y}{s}\right) \, . \tag{6.64}$$

This choice of $\Delta\alpha$ approximately eliminates any residual correction to lift, but there remains an approximate pitching-moment correction

$$\Delta C_m = \frac{\partial C_L}{\partial \alpha}\frac{\lambda x_1}{2U}\frac{\partial w_i}{\partial x} \, , \tag{6.65}$$

where the planform parameter $\lambda x_1/\bar{c}$ is discussed in Sections 3.2.4 and 3.3.4 and typical values are given in Table 3.III of Chapter III.

According to Guderley[6.20], the curvature correction is very small in an ideal slotted tunnel designed for zero solid blockage. Wright[6.28] estimates it to be about -1% of the correction appropriate to a closed circular tunnel; he adds that no adequate experimental data exist for checking the interference corrections in a circular slotted tunnel.

If the wing is so large and slender that the wing and tunnel may be treated as a slender configuration, then the Munk-Jones theory[6.41] may be used. In this case Tirumalesa[6.37] has derived a value of the lift-interference parameter,

$$\frac{C(\Delta\alpha)}{SC_L} = \delta_0 = \frac{1}{4}\left[\frac{F-1}{F+1}\right] \, , \tag{6.66}$$

which is just twice the value given for a small wing in Equation (6.62).

6.5.3 Rectangular Tunnel with Slotted Roof and Floor

As in the calculation of the solid-blockage interference, the effects of the solid side-walls may be adequately represented by a horizontal row of vortices extending in a plane containing the wing span. To the potential Φ_r associated with this row may be added a potential Φ_s, so that the total $\Phi = \Phi_r + \Phi_s$ will satisfy the boundary conditions of Equation (6.35).

The solution for a uniformly-loaded wing in an ideal slotted tunnel is set out in Equation (43) of Reference 6.17, where an average interference upwash in the plane of the wing is derived. When the analysis is completed by substituting the coefficients of the Fourier cosine series for Φ_r and $\partial\Phi_r/\partial z$, we obtain, corresponding to Equation (6.59), the interference parameter

$$\delta_0 = \frac{h}{4\pi\sigma^2 b}\left[\log_e\left(\frac{\pi\sigma}{\sin\pi\sigma}\right) - \sum_{n=1}^{\infty} A_n \sin(n\pi\sigma) - \frac{\pi\sigma^2 b}{h(1+F)}\right], \qquad (6.67)$$

where $\sigma = 2s/b$.

$$nA_n = \frac{4(b - n\pi hF)\sin(n\pi\sigma)}{(b + n\pi hF)e^{2n\pi h/b} - (b - n\pi hF)}.$$

In the limiting case of small span this reduces to

$$\delta_0 = \frac{\pi h}{24b} - \frac{\pi h}{b}\sum_{n=1}^{\infty}\frac{n}{\theta_n e^{2n\pi h/b} - 1} - \frac{1}{4(1+F)}, \qquad (6.68)$$

where $\theta_n = \frac{b + n\pi hF}{b - n\pi hF}$.

The influence of the model size on the correction factor is illustrated in Figures 6.18 and 6.19 for tunnels with h/b equal to 1.0 and 0.5. As in the case of a circular ideal slotted tunnel, the conditions for zero upwash interference do not correspond to those required for zero blockage interference. The induced upwash in this wall condition is quite large; for example, a square tunnel designed for zero solid blockage is calculated to have a lift interference of about -0.63 of the value for a closed tunnel.

Maeder et al. (Ref. 6.29; 1955) give a similar equation to (6.67) above for the interference upwash at the mid-span position; this contains an error and the correct expression is

$$\delta_\sigma = \frac{h}{4\sigma b}\left(\frac{2}{\pi\sigma} - \cot\frac{\pi\sigma}{2}\right) - \frac{h}{4\sigma b}\sum_{n=1}^{\infty} nA_n - \frac{1}{4(1+F)}, \qquad (6.69)$$

where nA_n is defined in Equation (6.67). They point out, however, that the first term is essentially associated with the side-wall image system and this does not vary with the slot parameter F. The third term is identically the incidence correction for a two-dimensional aerofoil in Equation (6.54) and thus may be imagined as giving the influence due to an aerofoil spanning the tunnel breadth and having the same total lift as the wing. These authors conclude therefore that the summation term in Equation (6.67) may often be neglected, as it merely indicates the difference in the slotted-wall case between a mean two-dimensional vortex system and an exact vortex system. The approximate equation for δ_0 then becomes

$$\delta_0 = (\delta_0)_c - \frac{1}{4}\left(\frac{1}{1+F}\right) \qquad (6.70)$$

which is independent of stream Mach number; $(\delta_0)_c$ denotes the value of δ_0 in a closed tunnel, to be found in Chapter III for different value of h/b. For a square tunnel, the discrepancy between the two equations is small, even when the ratio of model span to tunnel breadth is as small as 0.1 (Fig.6.18). At $h/b = 0.5$, however, the approximate formula is no longer valid (Fig.6.19) due to the dominant effect of the slotted boundaries. Katzoff and Barger (Ref.6.30; 1959) have discussed the limits of this approximate method and give corrections which may be applied to values of δ_0 obtained in this way. By using the results contained in Reference 6.30, it is possible to obtain easily the upwash distribution along the tunnel axis.

Wright[6.28] discusses an interesting difference between the approach of References 6.25 and 6.29 on the one hand and Reference 6.30 on the other. Katzoff and Barger ascribe the slotted-wall effect mainly to the interference on the bound vortex, whilst the effect on the trailing vortices is used merely to derive a small correction. Maeder and his associates[6.25,6.29] consider the main correction to come from the interference of the slotted walls in the presence of trailing vortices.

The streamline curvature at the model is also discussed in Reference 6.29. Similarly to Equation (6.63), the total correction to incidence is expressed as

$$\Delta\alpha = \frac{SC_L}{C}\left(\delta_0 + \frac{\frac{1}{2}\bar{c}}{\beta h}\,\delta_1\right) , \qquad (6.71)$$

where

$$\delta_1 = \frac{\beta h C}{USC_L}\,\frac{\partial w_i}{\partial x} .$$

The correction term in Reference 6.29 is equivalent to

$$\delta_1 = (\delta_1)_c - \frac{h}{2\pi b}\int_0^\infty \left[\frac{1}{Be^q - 1} + \frac{1}{e^q + 1}\right] q\,dq , \qquad (6.72)$$

where

$$B = \frac{h + Fbq}{h - Fbq}$$

and $(\delta_1)_c$ denotes the value for a closed tunnel (Chapter III). The variation with slot geometry for a tunnel with $h/b = 0.69$ is shown in Figure 6.20 as a full line. It should be noted that this result is very approximate; the limiting value $\delta_1 = -0.13$ for $F = 0$ compares with the exact value $\delta_1 = -0.21$ for an open floor and roof (Chapter III). More accurate results have been obtained by Rushton[6.41] using a three-dimensional electrical analogue, and these are shown in Figure 6.20. The difference between the two curves is quite large, particularly when the wall is designed to give zero solid blockage.

For a square ideal slotted tunnel designed to operate at zero solid blockage, the streamline curvature is about -0.28 of the value obtained in a square closed tunnel, if the model is reasonably small[6.28].

The influence of viscous flow within the slots on the results discussed in this section has been considered by Holder[6.58,6.59]. He has extended the analysis of Reference 6.17 to satisfy the boundary condition (6.7). The average interference parameter in the transverse plane of a uniformly-loaded wing can be written as*

$$\delta_0 = (\delta_0)_c - \frac{\beta}{2\pi P}\int_0^\infty \frac{dq}{[\sinh q + Fq\cosh q]^2 + \left[\frac{\beta}{P}\cosh q\right]^2} -$$

$$- \frac{\beta}{\pi P}\sum_{n=1}^{\infty}\left[\frac{\sin(n\pi\sigma)}{n\pi\sigma}\right]^2 \int_0^\infty \frac{dq}{\left(\frac{q}{\alpha_n}\right)^2[\sinh \alpha_n + F\alpha_n \cosh \alpha_n]^2 + \left[\frac{\beta}{P}\cosh \alpha_n\right]^2} , \quad (6.73)$$

where

$$\alpha_n = \left[q^2 + \left(\frac{n\pi h}{b}\right)^2\right]^{\frac{1}{2}}$$

The second term is precisely the interference upwash of a two-dimensional aerofoil in Equation (6.48). For an ideal slotted tunnel ($P \to \infty$), this reduces to the second term of Equation (6.70) and the third term of Equation (6.73) therefore represents a correction to Equation (6.70). It can be shown that Equation (6.73) reduces to Equation (6.67) in the limit as $P \to \infty$.

Equation (6.73) has been evaluated by Holder for a range of values of β/P, for a square tunnel cross-section and one where $h = 0.5b$. These results are shown in Figures 6.21 and 6.22 for the case of a very small model ($\sigma = 0$), and also where the model span is half the tunnel breadth ($\sigma = 0.5$). For a given slot geometry, the effect of the viscous flow in the slots is to increase the induced upwash, and for values of β/P greater than about unity it may no longer be possible to obtain the zero lift-interference condition. The value of F_0 for this condition is also affected by the span of the wing, the effect being particularly marked for the duplex tunnel cross-section. The variation of F_0 with β/P is shown in Figure 6.23.

The preceding discussion in this section has been based on the use of the homogeneous boundary condition at the slotted walls. By employing an electrical analogue technique, however, it is possible to obtain results for ideal slot flow in which the discrete slots and slats are represented. Thus a direct comparison between the use of exact and approximate boundary conditions may be made, and this has been done by Rushton[6.60] for the case of a small lifting wing in the centre of a rectangular tunnel with slotted roof and floor. The exact boundary conditions are represented in a linearized form by

---

* An error in Equation (9) of Reference 6.59 has been corrected here.

Equations (6.3). The interference potential Φ_i satisfies Laplace's equation subject to the discrete boundary conditions at the roof and floor in place of the homogeneous condition (6.12). The resistance network automatically solves the finite-difference form of Laplace's equation, and in Reference 6.60 the boundary conditions are applied to the voltages in finite-difference form, if necessary. Then the electrical potentials are measured on the network, and these may be equated to the velocity potentials.

Rushton has investigated the validity of the homogeneous boundary condition for an ideal slotted wall by considering a rectangular tunnel with $h/b = 0.5$. The slotted roof and floor had an open-area ratio (a/d) equal to 0.125. Two symmetrical arrangements of the slots are possible, with either a slot or a slat directly above and below the small wing. Four cases of each arrangement were considered, with a total of $N = 2,3,4$ or 6 slots forming the ventilated wall and, if necessary, half slots at the corners. For the fixed open-area ratio the slot parameter F is inversely proportional to N . The interference parameter δ_0 obtained with these discrete arrangements of slots may be compared with those deduced from Equation (6.68), and this comparison is shown in Figure 6.24 against $(1 + F)^{-1}$. It is clear that, as the number of slots is increased, the differences between the exact and the homogeneous boundary conditions become smaller, and for $N \geqslant 6$ these differences may be neglected. Further, the value of δ_0 deviates towards that for an open or closed tunnel according as a slot or slat lies directly above the wing. Some points obtained from the electrical analogue, but with the homogeneous boundary condition at the slotted wall, are plotted in Figure 6.24. These agree well with the analytical solution from Equation (6.68) and illustrate the validity of the analogue technique.

It is perhaps worth stressing that these results are for the small ratio $h/b = 0.5$ and for one particular value of the open-area ratio (0.125). More favourable results would be expected for larger h/b : many tunnels operate with an open-area ratio not very different from 0.125, and it is unusual to have fewer than six slots in a ventilated wall. One may conclude then, that in most cases of practical importance the use of the simple homogeneous boundary condition is satisfactory.

6.5.4 Rectangular Tunnel with Slots on Each Wall

The lift interference experienced by a small wing at the centre of an ideal slotted rectangular tunnel has been considered by Davis and Moore[6,17], who use a method which involves the transformation from a uniformly slotted circular tunnel. The widths of the individual slots in the rectangular tunnel vary, and their dimensions may be found by calculating the points which correspond to the slot edges in the circular tunnel. The technique therefore is less precise than that used for other cross-section shapes and geometries.

The general solution for the interference parameter δ_0 in the slotted tunnel involves elliptic functions, but very simple approximations for δ_0 may be derived. For a square tunnel, Davis and Moore suggest that

$$\delta_0 \simeq 0.137\left[\frac{F-1}{F+1}\right] , \qquad (6.74)$$

where F is defined in Figure 6.1; and for extreme rectangular cross-sections

$$\delta_0 \simeq \frac{\pi}{48}\frac{b}{h}\left[\frac{F-2}{F+1}\right] \qquad \left(\frac{h}{b} \leqslant 0.5\right) \tag{6.75}$$

and

$$\delta_0 \simeq \frac{\pi}{48}\frac{h}{b}\left[\frac{2F-1}{F+1}\right] \qquad \left(\frac{h}{b} \geqslant 2.0\right) . \tag{6.76}$$

These equations give good approximations to the limiting values of δ_c for completely closed or open tunnels. A straight line joining these limiting values results if δ_0 is plotted against $(1 + F)^{-1}$. Equation (6.74) is very similar in form to that given in Equation (6.62) for a circular ideal slotted tunnel. As shown in Figure 6.17, both these results are close to that for a square tunnel with solid side-walls and ideal slotted roof and floor. This would seem to justify in part an assumption, commonly made, that the interference in a square slotted tunnel is equal to that obtained in a circular slotted tunnel of the same cross-sectional area. Reynolds et al.$^{6.23}$ suggest that the curvature correction for a near-square tunnel with all four walls slotted may be based on the analogous Equations (6.63) and (6.65) above for the slotted circular tunnel having the same cross-sectional area.

The method of analysis proposed by Davis and Moore is rather unsatisfactory, and it is therefore particularly valuable to have results from the electrical-analogue technique for rectangular tunnels with all four walls slotted. These results, presented by Rushton in Reference 6.60, correspond to the ideal homogeneous boundary condition for slotted walls. Three tunnel geometries, with $h/b = 0.5$, 1.0 and 1.6 , are considered over the whole range of slot parameter F . In Figure 6.25 the full curves from the analogue experiments are compared with the results deduced from the linear relationship suggested by Davis and Moore. Between $h/b = 0.5$ and $h/b = 1.0$ the linear approximation does not lead to large discrepancies, but more serious errors are incurred when $h/b = 1.6$. The data given by Rushton are probably sufficient to allow corrections to be estimated for most tunnel geometries at present in use.

Zero upwash interference in a square slotted tunnel does not correspond to zero blockage; at the former condition the interference correction due to blockage is about 0.12 of the value appropriate to a square tunnel (i.e., $\Omega_s = 0.12$ in Figure 6.12). Conversely, for the square tunnel operating at zero blockage, the upwash will be about −0.28 of the closed-tunnel value. The evidence in Figures 6.13 and 6.25 does suggest, however, that both interference effects could be eliminated in a rectangular tunnel having ideal slots on each wall with $F = 0.8$ approximately and a ratio h/b between 1.4 and 1.5.

6.6 SOME GENERAL REMARKS ON INTERFERENCE EFFECTS IN TUNNELS WITH LONGITUDINAL SLOTS

In the preceding pages, an attempt has been made to outline the techniques and results at present available to correct aerodynamic data obtained in wind tunnels with longitudinally-slotted walls. It is apparent that the most important types of working section geometry and shape have been analysed, for small models at least, in sufficient detail to enable the required calculations to be made. A summary of the relevant figures and equations is given in Table 6.I.

The theory of Reference 6.1 is particularly valuable, in that for certain cases it enables some estimate to be made of the influence of viscous effects on the slots. The theory indicates that in compressible flow the primary parameter is not $1/P$, but β/P, so that the conditions required for zero blockage or zero lift interference will vary with Mach number, even if P remains constant. As the stream Mach number approaches unity, β/P will tend to zero, so that the ideal slotted tunnel conditions will be approached. However, it is just in this range that the theory itself becomes less reliable, and the magnitude of the interference effects is probably best determined by experimental comparisons. An allowance for the viscous effects, though complicating the interference correction, is of great value in suggesting a mechanism by which in real tunnels both blockage and lift interference may be eliminated or minimized for a given slot arrangement (Figs. 6.16 and 6.23). The viscous effects, linked as they are to β/P, may also be responsible for the disagreement sometimes observed between the trend with Mach number of the experimental results and that predicted for an ideal slotted tunnel[6.24, 6.28, 6.31].

It is likely that the theoretical corrections based on the linear boundary conditions of Equations (6.1) and (6.7) would have most validity when applied to reasonably small models, for with these any distortion of the flow field which may correspond to a second-order effect is likely to be small also. For larger disturbances at the boundary, the non-linear condition of Wood[6.57] must be considered. Wright[6.28] also suggests that the lift interference is less well determined than the blockage interference in a slotted tunnel, due to uncertainties in the boundary conditions for the former. This consideration is likely to be of greatest significance for two-dimensional flows because of the appearance in these cases only of the conditions at infinity upstream. Wright argues that any significant downward displacement of the tunnel flow resulting from the lift imposed on the model will cause an increase in the inflow on the wall above the wing and hence an increased boundary-layer thickness. The actual boundary condition in this region might then approach that for an open tunnel or resemble the non-linear condition of Equation (6.4).

Despite reservations of this type, the progress made in recent years towards understanding the general problem of slotted-wall interference has been considerable, due mainly to the use of the equivalent homogeneous boundary conditions. Their validity for most types of problem has been established beyond doubt, provided the disturbance due to the model is small.

It will be apparent from the foregoing text that, for a tunnel designed to have zero-blockage with a small model, the interference corrections will be considerably smaller than those appropriate to either a closed or an open tunnel. In many cases the effects of the tunnel walls can be neglected altogether; it is important, however, to consider whether this action is justified for each combination of model and tunnel, and whether the interference quantities could become comparable with the permitted tolerances in the observations.

6.7 THE PERFORATED WALL

The other form of ventilated boundary in common use contains regularly-spaced openings into the surrounding plenum chamber, the dimensions of the openings being small compared with the tunnel height or breadth. Such walls are usually called 'perforated'. The perforations may be of various shapes, but most frequently they are circular, with the axes of the holes normal to the plane of the wall. Occasionally, for reasons connected with the need to minimize wave reflection at low supersonic stream speeds, the hole axes may be inclined away from the normal.

There is an important difference in the behaviour of a wall containing an array of small perforations and one having longitudinal slots along the working section. In the former case any pressure difference between the working section and the plenum chamber is primarily due to viscous effects in the slot, the resulting pressure change being given by Equation (6.6). With a perforated wall a pressure difference is associated with a cross-flow, even if viscosity is ignored. For convenience, the solid part of the wall may be likened to a lattice of small lifting wings whose incidence is the flow inclination to the wall (v_n/U). Thus one may write approximately

$$\delta p \propto \tfrac{1}{2}\rho U^2 \frac{v_n}{U} \propto \rho U v_n \quad , \tag{6.77}$$

so that

$$\delta p \;=\; p - p_c \;=\; \frac{\rho U}{P}\, v_n \;=\; \frac{\rho U}{P}\frac{\partial \Phi}{\partial n} \; , \tag{6.78}$$

where p_c is the pressure in the plenum chamber. This is precisely the Equation (6.6) used for estimating the influence of viscosity on interference effects in tunnels with longitudinal slots. Unless otherwise stated, it will be assumed that a perforated wall has the linear pressure-drop characteristics, implied by Equation (6.78), where the porosity parameter, P , is mainly dependent on the wall geometry and stream velocity. In general, P must be determined experimentally for the particular wall geometry of interest and at the required stream Mach number. Theoretical values for P have so far only been obtained for single and multiple slots transverse to the flow direction (Refs. 6.19, 6.32, 6.42, 6.47). In the case of the single transverse slot it has been shown[6.54], contrary to Reference 6.57, that separation on the plenum-chamber side of the wall does not affect the linear form of the pressure-drop equation.

The experimental cross-flow characteristics of perforated walls are discussed in some detail by Goethert in Reference 6.32, and further information is contained in References 6.22, 6.38 and 6.47. For circular holes with axes normal to the wall there may be a small decrease in P as the stream Mach number rises. The wall boundary layer, which develops more rapidly along a perforated wall than along a longitudinally-slotted wall[6.46,6.48,6.53,6.56], may have a marked influence on the observed porosity parameter and on the range over which the linear variation of pressure difference with flow inclination is maintained. Markedly non-linear effects can be obtained at small cross-flows, if the displacement thickness of the boundary layer is large compared with the hole diameter. Similar deviations may be obtained if the wall thickness is comparable with the hole size; in addition, the hole may now act as a diffuser, so that the overall pressure change across the wall is reduced. It has also been found experimentally[6.52], that the cross-flow characteristics of a perforated wall are changed, if the working-section length is short compared with the tunnel height. These and other aspects of perforated-wall behaviour are considered in Reference 6.32; it is sufficient here to note that the theoretical analysis of boundary interference in perforated-wall tunnels assumes a pressure-drop relationship of the linear form given by Equation (6.78) and a simple linearized homogeneous boundary condition at the perforated wall, which is equivalent to Equation (6.5), viz.

$$\frac{\partial\Phi}{\partial x}+\frac{1}{P}\frac{\partial\Phi}{\partial n} = 0 . \qquad (6.79)$$

It is perhaps necessary to consider briefly the difference in the behaviour of a perforated wall, and one which is truly porous. In the latter case friction effects dominate the flow, and the pressure drop is directly proportional to the mass flow through the wall[6.44]. The equation analogous to (6.78) is then

$$\delta p = p - p_c = \frac{\rho U}{P} v_n = \frac{\rho U}{(P'U)}\frac{\partial\Phi}{\partial n} . \qquad (6.80)$$

The porosity parameter P for a perforated wall is replaced by $P'U$ and thus depends directly on the stream velocity. This is an undesirable characteristic which is partly responsible for the limited use made of porous-wall tunnels. Analyses for wall interference in tunnels with porous walls (e.g., Ref. 6.21) are immediately applicable to the perforated case, provided that the porosity parameter is defined by means of Equation (6.78). Conversely, the results set out in the subsequent sections of the present text, with perforated tunnels in mind, may be used for tunnels with porous walls.

It is apparent that an actual perforated wall may, in certain flow conditions, not conform to the behaviour of the idealized wall assumed in the analysis; to this extent it may be argued (as in Reference 6.28) that the corrections for wall-interference effects in perforated tunnels are less soundly based than in the case of longitudinally-slotted boundaries. Nevertheless, it is felt that the simple theory at present available does give a valuable indication of the approximate magnitude and trends of the interference effects in wind tunnels having perforated boundaries.

As will be shown below, the parameter determining the interference-free flow is β/P , where P is defined by Equation (6.78) and is dependent mainly on the wall geometry. Thus, to maintain a constant value of β/P over the complete range of test Mach number, the wall geometry would need to be continuously varied. In contrast, the interference-free condition for an ideal slotted tunnel is usually independent of stream Mach number and attained simply through a specific value of the geometric parameter $F = F_0$ (Fig. 6.1). This distinction is sometimes used as an argument, that the perforated wall is less suitable as a boundary for subsonic tunnels than one having longitudinal slots. However, when viscous effects are present, so that F_0 is now a function of β/P , experimental evidence suggests that the value of P for slotted walls is not greatly influenced by stream Mach number, and hence, as in the case of a perforated wall, continuous variation of wall geometry is strictly required to maintain interference-free conditions. The relative advantages of the two types of wall are then less obvious.

As the stream Mach number approaches unity, β/P tends to zero, and the perforated tunnel behaves more and more like an open jet. In this flow regime the linearized theory, on which the analysis is based, is of limited validity; the interference present must therefore be calculated from flow equations with the proper transonic approximations.

However, the choice of the geometry of a perforated wall may be influenced by considerations other than the need to minimize subsonic wall interference. For tunnels which are required to operate at transonic and low supersonic speeds, a perforated wall can be designed to reduce shock-wave reflections[6.32]; the open-area ratio of such a wall (as well as the inclination of the holes to the wall surface) may well be very different from that which would be chosen solely to satisfy the need for small wall interference at subsonic speeds. More specifically, the value of β/P for a wave-cancellation wall may be as low as 0.3, so that the tunnel behaves rather like an open-jet configuration and corrections for wall interference are far from negligible. In some cases, however, there may be an incidental advantage in operating the tunnel away from zero-interference conditions; the longitudinal pressure gradient along the tunnel axis and the streamline curvature may then be smaller, so that a more uniform interference effect is achieved over the whole length of the model.

It is clear that the actual design of a perforated wall can be a compromise between conflicting requirements. Nevertheless in the present text some stress will continue to be laid on conditions which achieve zero wall interference at subsonic speeds. Sufficient data are presented, however, to enable the corrections to be calculated for a wide range of β/P .

6.8 TWO-DIMENSIONAL BLOCKAGE IN TUNNELS WITH PERFORATED WALLS

6.8.1 Solid Blockage

The solid-blockage interference experienced by a two-dimensional model in a perforated tunnel was considered independently by Goodman (Ref. 6.21; 1950) and Kassner (Ref. 6.35; 1952). Both authors use the boundary condition (6.79). Later, a solution was obtained by Baldwin et al.[6.1] as a special case (K = 0) of the homogeneous boundary condition (6.7) for longitudinal slots with viscous flow. The interference potential Φ_i , and hence the longitudinal interference velocity increment at the model position ΔU_s , may be found similarly to that for lon tudinal slots, discussed in Section 6.3.1.

Alternatively a Fourier analysis method, or, following Kassner, a modified image method, may be employed. The solid-blockage factor ϵ_s is most conveniently expressed in terms of Ω_s , the ratio of its value in the ventilated tunnel to that in a geometrically-similar tunnel with closed walls. For a two-dimensional model in a perforated-wall tunnel a simple equation for this ratio is

$$\Omega_s = 1 - 6\left(\frac{\mu}{\pi}\right) + 6\left(\frac{\mu}{\pi}\right)^2 , \tag{6.81}$$

where $\mu = \cot^{-1}(\beta/P)$ may vary between zero and $\frac{1}{2}\pi$, the value for an open-jet tunnel. The variation of Ω_s with porosity parameter is shown in Figure 6.26. Zero solid blockage occurs when $\beta/P = 1.28$; a result close to this, but derived in a different way, was obtained by Brescia (Ref. 6.40; 1952).

The boundaries of a perforated tunnel, unlike ideal slotted walls, induce a velocity gradient along the model due to the solid blockage. At the model position this gradient may be obtained from Equation (6.18) with $F = 0$.

$$\frac{\partial \epsilon_s}{\partial x} = \frac{24}{\pi^2 \beta h} (\epsilon_s)_c \frac{\beta}{P} \int_0^{\infty} \frac{q^2 dq}{\cosh^2 q + (\beta/P)^2 \sinh^2 q} , \qquad (6.82)$$

$$\simeq \frac{12}{\pi^2 \beta h} (\epsilon_s)_c$$

if the tunnel is designed to give zero blockage ($\beta/P = 1.28$). Figure 6.27, taken from Reference 6.35, shows how ϵ_s varies along the tunnel for different wall porosities. The correction to measured drag may be calculated from Equation (6.13) with $F = 0$. The broken curve in Figure 6.27 suggests that $(\Delta C_D)_{sg}$ is roughly a maximum when $\epsilon_s(0)$ is zero.

In Section 7.28 of Reference 6.19 Woods has considered the more general problem of a two-dimensional tunnel with perforated walls of finite length. He derives a simple, but lengthy, expression for $\epsilon_s(x)$ which is shown to become consistent with Equation (6.81) when the perforated walls are of infinite streamwise extent.

6.8.2 Wake Blockage

Wright[6.28] has considered the wake-blockage effects experienced by an aerofoil in a perforated tunnel by methods similar to those of Reference 6.1. The ratio of the wake-blockage factor in the perforated tunnel to that in the closed tunnel may be denoted by Ω_w, and for the two-dimensional aerofoil

$$\Omega_w = -\frac{2}{\pi} \frac{\beta}{P} \int_0^{\infty} \frac{dq}{\cosh^2 q + (\beta/P)^2 \sinh^2 q} = -\frac{2}{\pi} \tan^{-1}\left(\frac{\beta}{P}\right) . \qquad (6.83)$$

The variation of Ω_w with β/P is shown in Figure 6.26. At zero solid blockage, Ω_w is about -0.57; for $\beta/P > 1.28$, the wake blockage would tend to counter the solid blockage.

Whereas Ω_s in Equation (6.81) tends to the correct limits $-\frac{1}{2}$ and 1 for open ($\beta/P = 0$) and closed ($\beta/P \to \infty$) tunnels respectively, Ω_w only tends to the correct limit in the former case. Just as for an ideal slotted tunnel $\Omega_w = 0$ for finite values of P, so here Ω_w is negative for finite values of β/P; neither tends to the definition $\Omega_w = 1$ for a closed tunnel. In the analysis of Reference 6.28, the model wake is represented by a single source and the interference velocity becomes zero far upstream of the model; the wake-blockage correction in Equation (6.83) is simply the interference velocity at the model position. The same is not true of a closed tunnel, unless the model wake includes a sink of equal strength far downstream.

The velocity gradient at the model position due to the wake images may also be derived formally[6.28]. The velocity gradient due to a source is closely related to the velocity increment associated with a doublet, and hence the wake-blockage gradient vanishes when the solid blockage is zero. In general, $\partial\epsilon_w/\partial x$ and the corresponding drag correction are given by Equations (6.21) and (6.22), where Ω_s now takes the appropriate value from Equation (6.81).

6.9 THREE-DIMENSIONAL BLOCKAGE IN TUNNELS WITH PERFORATED WALLS

6.9.1 Circular Tunnel

The solid blockage of a small body in a circular tunnel of radius R may be solved by similar methods to those used in considering the slotted tunnel. Goodman[6.36] provided the first solution in 1951. At the model position, the blockage-factor ratio Ω_s becomes

$$\Omega_s = -0.40 \int_0^\infty I_G \, dq \qquad (6.84)$$

with

$$I_G = \frac{[K_0(q)I_0(q) - (\beta/P)^2 K_1(q) I_1(q)]q^2}{[I_0(q)]^2 + [(\beta/P)I_1(q)]^2} ,$$

where the modified Bessel functions I_0 , I_1 , K_0 and K_1 are tabulated in Reference 6.27. The variation of Ω_s with β/P is shown in Figure 6.28, and zero solid blockage occurs for β/P equal to 1.22.

Once again the velocity gradient at the model position may be obtained directly by twice differentiating the interference velocity potential from Equation (34) of Reference 6.1; hence

$$\frac{\partial \epsilon_s}{\partial x} = (\epsilon_s)_c \frac{0.40}{\beta R} \left[\frac{\beta}{P} \int_0^\infty \frac{q^2}{[I_0(q)]^2 + [(\beta/P)I_1(q)]^2} \, dq \right] . \qquad (6.85)$$

According to Wright[6.28] the expression in square brackets is equal to 1.47 when β/P has the value 1.22 appropriate to zero solid blockage. This is confirmed by independent calculation and, not unlike the two-dimensional case in Figure 6.27, the expression is close to its maximum value that occurs near $\beta/P = 1.6$.

In considering the wake blockage, the model wake may once more be represented by a three-dimensional source. The wake-blockage factor at the model position is obtained as a special case of Equation (6.33),

$$\Omega_w = \frac{\epsilon_w}{(\epsilon_w)_c} = -\frac{1}{\pi}\frac{\beta}{P} \int_0^\infty \frac{dq}{[I_0(q)]^2 + [(\beta/P)I_1(q)]^2} . \qquad (6.86)$$

A curve of Ω_w against β/P is shown in Figure 6.28; this only vanishes for an open-jet tunnel ($\beta/P = 0$), and no perforated wall geometry will remove the wake-blockage effect. For a tunnel designed to have zero solid blockage $\Omega_w = -0.43$. As in the two-dimensional case below Equation (6.83), the limit $\Omega_w = -1$ as $\beta/P \to \infty$ cannot be identified with the definition $\Omega_w = 1$ for a closed tunnel. An expression for the variation of the wake blockage along the axis of the tunnel for different values of β/P is given in Reference 6.45. As in Equation (6.34) the gradient at the model position is

$$\frac{\partial \epsilon_w}{\partial x} = -\frac{1}{\pi \beta R} (\epsilon_w)_c \int_0^\infty I_G \, dq = \frac{(\epsilon_w)_c \Omega_s}{0.40 \pi \beta R} \qquad (6.87)$$

where I_0, defined in Equation (6.84), is identical to I_C in Equation (6.28) with $P = 0$. It follows that the wake-blockage gradient vanishes with the solid blockage.

6.9.2 Rectangular Tunnel

Blockage effects do not seem to have been considered for a rectangular tunnel having either two opposite, or all four, walls perforated. A working section with four perforated walls may be regarded as having similar interference characteristics to a circular tunnel of the same cross-sectional area, provided the height/breadth ratio is near unity. The results of Section 6.9.1, or Figure 6.28, may then be used for a small model mounted on the axis of the tunnel.

6.10 LIFT INTERFERENCE IN TUNNELS WITH PERFORATED WALLS

6.10.1 Two-Dimensional Tunnel

The lifting aerofoil may be represented by a two-dimensional vortex having the same circulation. The subsequent analysis is then very similar to that for the solid-blockage interference, and is set out in detail by Wright in Reference 6.26. The boundary-induced upwash at the model position is

$$\frac{w_i}{U} = -\frac{cC_L}{2\pi h}\cot^{-1}\left(\frac{\beta}{P}\right) . \tag{6.88}$$

Since the general expression for $\hat{w}_i/U$ becomes zero far upstream from the model, Equation (6.88) represents the complete interference upwash acting on a small aerofoil. For the closed tunnel $(P = 0)$ w_i is zero, but for any other value of P some induced upwash must be present; in the limiting case $\beta/P = 0$, the value $w_i/U = -\frac{1}{4}(c/h)C_L$ is consistent with an open tunnel. Equation (6.88) may be recast in terms of the interference parameter

$$\delta_0 = \frac{hw_i}{UcC_L} = -\frac{1}{2\pi}\cot^{-1}\left(\frac{\beta}{P}\right) , \tag{6.89}$$

which is plotted in Figure 6.29; at zero solid-blockage conditions, the correction is 0.42 of that appropriate to the open tunnel.

Wright has also considered the streamline curvature at the model position and shows that this may be expressed as

$$\frac{c}{U}\frac{\partial w_i}{\partial x} = -\frac{\pi c^2 C_L}{12\beta h^2}\left[1 - 6\left(\frac{\zeta}{\pi}\right) + 6\left(\frac{\zeta}{\pi}\right)^2\right] . \tag{6.90}$$

where $\zeta = \tan^{-1}(\beta/P) = \frac{1}{2}\pi - \mu$.

The quantity in square brackets is identical in form to that arising in the expression for the solid blockage of a two-dimensional model in Equation (6.81), but now contains $(\frac{1}{2}\pi - \mu)$ in place of μ. It follows that the streamline curvature will be zero for a value $\beta/P = 0.78$, the reciprocal of that which eliminates the solid blockage. An equation similar to (6.90) was obtained by Brescia[6.34], using a different analytical approach. The interference parameter

$$\delta_1 = \frac{\beta h^2}{UcC_L}\frac{\partial w_i}{\partial x} = -\frac{\pi}{12}\left[1 - 6\left(\frac{\zeta}{\pi}\right) + 6\left(\frac{\zeta}{\pi}\right)^2\right] \qquad (6.91)$$

is also plotted as a function of β/P in Figure 6.29; the streamline curvature in the two-dimensional perforated tunnel, designed to have zero solid blockage, is as much as 0.46 of the value appropriate to a closed tunnel. The corrections to incidence, lift and quarter-chord pitching moment are given by Equations (3.53) and (6.55).

$$\left.\begin{aligned}
\Delta\alpha &= \frac{cC_L}{h}\,\delta_0 + \frac{c^2}{\beta h^2}\,\delta_1\,(\tfrac{1}{4}C_L + C_m) \\
\Delta C_L &= -\frac{\pi}{2}\left(\frac{c}{\beta h}\right)^2\delta_1 C_L \\
\Delta C_m &= +\frac{\pi}{8}\left(\frac{c}{\beta h}\right)^2\delta_1 C_L
\end{aligned}\right\} . \qquad (6.92)$$

where the quantities δ_0 and δ_1 for a given porosity parameter may be taken from Equations (6.89) and (6.91) or from Figure 6.29.

6.10.2 Circular Tunnel

The corrections for a small wing in a circular perforated tunnel may be considered as special cases of those derived in Reference 6.1 for the general ventilated wall having both porosity and longitudinal slots. The original solution by Goodman[6.36] considered only the perforated tunnel. The induced incidence at the model position may be expressed as

$$\frac{w_i}{U} = \frac{SC_L}{8\pi R^2}\left[1 - \frac{\beta}{\pi P}\int_0^\infty I_{F0}\,dq\right] . \qquad (6.93)$$

where I_{F0} is the integrand of Equation (6.58) with the substitution $F = 0$. As in Equations (6.59) and (6.60), the interference parameter δ_0 becomes

$$\delta_0 = \frac{\pi R^2}{SC_L}\frac{w_i}{U} = \frac{1}{8}\left[1 - \frac{\beta}{\pi P}\int_0^\infty I_{F0}\,dq\right] . \qquad (6.94)$$

The variation of δ_0 with β/P is shown in Figure 6.30. Zero lift interference occurs when $\beta/P = 1.13$, compared with $\beta/P = 1.22$ required to remove the solid-blockage velocity increment. Thus, at zero solid blockage, δ_0 will be only 0.04 of its value in a closed circular tunnel. The marked contrast between this case ($F = 0$) and the ideal slotted tunnel ($\beta/P = 0$) is illustrated in Figure 6.16.

The flow curvature at the origin can be obtained directly from Equation (47) of Reference 6.1, which gives

$$\delta_i = \frac{2\pi\beta R^3}{USC_L}\frac{\partial w_i}{\partial x} = -\frac{1}{4\pi}\int_0^{\infty} I_H\,dq \ . \qquad (6.95)$$

where

$$I_H = \frac{\{q^2K_1(q)I_1(q) + (\beta/P)^2[K_1(q) + qK_0(q)][I_1(q) - qI_0(q)]\}q^2}{[qI_1(q)]^2 + (\beta/P)^2[I_1(q) - qI_0(q)]^2} \ .$$

At zero solid-blockage conditions, the streamline curvature is large, 0.59 of its value in a closed tunnel[6.28]. The corrections to incidence and pitching moment follow from Equations (6.63) and (6.65) and may be evaluated with the aid of Figure 6.30.

Goodman[6.34] points out that for the perforated tunnel a solution to the upwash at the model position may not be deduced by considering the flow in a plane far downstream. In the closed or ideal slotted tunnel, for example, the upwash at this position is twice that at the model, and this analogy may be used to simplify the analysis. The homogeneous boundary condition for the perforated circular tunnel is

$$\frac{\partial\Phi}{\partial x} + \frac{1}{P}\frac{\partial\Phi}{\partial r} = 0 \ ; \qquad (6.96)$$

since $\partial\Phi/\partial x = 0$ in the distant wake, the boundary condition at infinity downstream reduces to

$$\frac{\partial\Phi}{\partial r} = 0 \ , \qquad (6.97)$$

the boundary condition for a closed tunnel. It is necessary therefore to consider the three-dimensional flow at the model position in solving the interference problem.

Goethert[6.32] suggests a physical reason for this behaviour of the perforated wall. The wall, acting like a lattice of elementary wings, generates free vortices at positions away from the axis of the tunnel. The distant-wake analogy holds true for each elementary vortex; but, since these are not all generated in the transverse plane of the model, $x = 0$, the analogy does not hold for the complete vortex system.

6.10.3 Rectangular Tunnel

The interference experienced by a small lifting wing in a rectangular tunnel seems only to have been partially solved, the major contribution coming from an early paper by Goodman (Ref. 6.39; 1951). He considers the case of a wing mounted between two infinite perforated walls, either vertical or horizontal. The wing itself is replaced in the analysis by an infinitesimal horse-shoe vortex. For vertical walls, the interference upwash at the wing is given by .

$$\begin{aligned}\delta_0 &= \frac{C}{SC_L}\frac{w_i}{U}\\ &= \frac{\pi h}{24b}\left[1 - \frac{12}{\pi^2}\int_0^{\infty}\frac{[\{(\beta/P)^2\sinh^2 q + \cosh^2 q\}^{\frac{1}{2}} - (\beta/P)\sinh q]q\,dq}{\cosh^2 q\,\sinh q}\right] \ , \end{aligned} \qquad (6.98)$$

and this may be expected to hold if h/b is large enough. Similarly, if h/b is small enough, Goodman's result for horizontal perforated walls may be used,

$$\delta_0 = \frac{\pi b}{48h}\left[1 - \frac{24}{\pi^2}\int_0^\infty \frac{q\,dq}{\{(\beta/P)^2\cosh^2 q + \sinh^2 q\}^{\frac{1}{2}}\cosh q}\right] . \qquad (6.99)$$

Values of $(b/h)\delta_0$ from Equation (6.98) and of $(h/b)\delta_0$ from Equation (6.99) are plotted against porosity parameter in Figure 6.31; zero lift interference occurs for $\beta/P = 0.81$ and 1.50 respectively. The equations become identical to Equations (6.75) and (6.76) in the limiting cases of closed $(\beta/P \to \infty)$ and open jet $(\beta/P = 0)$ tunnels. Some idea of the range of applicability may be obtained from Figure 6.32 where these limiting results are compared with exact values calculated from the usual image methods (Chapter III). For the closed tunnel, it would seem that the horizontal walls have negligible influence when $h/b > 1.25$, and the vertical walls when $h/b < 0.4$. Similarly, for the open jet, the discrepancies can be ignored unless $0.8 < h/b < 2.5$.

Unfortunately, many existing tunnels are nearly square, and it would seem best in these cases to estimate δ_0 from the curve of Figure 6.30 for a circular tunnel. This is reproduced in Figure 6.31 and suggests that the tunnel with vertical walls only is a good approximation for $\beta/P > 2.0$, and the tunnel with roof and floor only is useful for $\beta/P < 0.5$. For the intermediate range of β/P, curves of δ_0 against h/b in Figure 6.33 have been estimated graphically by identifying the square and circular tunnel and using the asymptotic formulae (6.98) and (6.99) for large and small h/b.

Goodman does not consider the curvature induced by the perforated boundaries, but it may be obtained as a direct extension of his analysis.

6.11 APPLICATION OF CORRECTION FACTORS

The ways in which blockage and lift interference may be used to correct the measured quantities are discussed in Sections 5.8 and 3.2.4 respectively.

The blockage factor $\epsilon_B = \epsilon_s + \epsilon_w$ determines the increment to the measured Mach number by means of the equation

$$\Delta M = (1 + 0.2M^2)M\epsilon_B ; \qquad (6.100)$$

in addition, there are corrections to other stream quantities, such as density and Reynolds number. Alternatively, corrections may be applied to the measured force and pressure coefficients. If corrections, such as Equation (6.100), are applied to stream quantities, then there remains a correction to drag coefficient due to longitudinal pressure gradient,

$$\begin{aligned}\Delta C_D &= -\frac{2V_e}{S}\frac{\partial\epsilon_B}{\partial x}\\ &= -\frac{2V_e}{S}\frac{\partial\epsilon_s}{\partial x} - C_D\epsilon_s , \qquad (6.101)\end{aligned}$$

where the equivalent volume of the model V_s may be estimated from Equation (5.89) and Figure 5.2. In two-dimensional flow $(\Delta C_D)_{sg}$, the first term on the right hand side of Equation (6.101), is given by Equation (6.19).

The interference upwash on a lifting model

$$\frac{w_i}{U} = \frac{SC_L}{C}\left(\delta_0 + \frac{x}{\beta h}\,\delta_1\right) \tag{6.102}$$

leads to incremental corrections to incidence, drag, lift and pitching moment. For a three-dimensional model in a rectangular tunnel

$$\left.\begin{aligned} \Delta\alpha &= \frac{SC_L}{C}\left(\delta_0 + \frac{\bar{\bar{c}}}{2\beta h}\,\delta_1\right) \\ \Delta C_D &= \frac{SC_L^2}{C}\,\delta_0 \\ \Delta C_L &= 0 \\ \Delta C_m &= \frac{\partial C_L}{\partial \alpha}\,\frac{SC_L}{C}\,\frac{\lambda x_1}{2\beta h}\,\delta_1 \end{aligned}\right\} . \tag{6.103}$$

where the planform parameter $\lambda x_1/\bar{c}$ is discussed and tabulated in Chapter III. Corresponding formulae for a circular tunnel are given in Equations (6.63) and (6.65). In two-dimensional flow there is no correction to drag; the corrections to incidence, lift and pitching moment are given by Equations (6.92). In correcting the pitching moment for a complete aircraft model, care must be taken to evaluate the change in interference upwash between the wing and the tail surface; the linear dependence of w_i/U on x, assumed in Equation (6.102), may not be accurate enough.

The evaluation of interference corrections requires the knowledge of ϵ_s, ϵ_w, $\partial\epsilon_s/\partial x$, δ_0 and δ_1. Table 6.I is a guide to the available information for tunnels with slotted or perforated walls.

REFERENCES

6.1 Baldwin, B.S. et al. *Wall Interference in Wind Tunnels with Slotted and Porous Boundaries at Subsonic Speeds.* NACA Tech. Note 3176, 1954.

6.2 Theodorsen, T. *The Theory of Wind-Tunnel Wall Interference.* NACA Report 410, 1931.

6.3 Rosenhead, L. *Interference Due to Walls of a Wind-Tunnel.* Proc. Roy. Soc. Series A, Vol. 142, 1933, pp. 308-320.

6.4 Tani, I., Taima, M. *Two Notes on the Boundary Influence of Wind Tunnels of Circular Cross Section.* Aero. Res. Inst. (Tokyo) Report 121, 1935.

6.5 de Haller, P *L'Influence des Limites de la Veine Fluide sur les Caractéristiques Aérodynamiques d'une Surface Portante.* Communication de l'Institut d'Aérodynamique de l'Ecole Polytechnique Fédérale. (ETH, Zürich), 1934.

6.6 Toussaint, A. *Experimental Methods – Wind Tunnels. Influence of the Dimensions of the Air Stream.* "Aerodynamic Theory" (ed. W.F. Durand), Vol. III, Div. I, Chap. III, Julius Springer, Berlin, 1935, pp. 290-299.

6.7 Wieselsberger, C. *Über den Einfluss der Windkanalbegrenzung auf den Widerstand insbesondere im Bereiche der kompressiblen Strömung.* Luftfahrtforschung, Vol. 19, 1942, pp. 124-128.

6.8 Kondo, K. *The Wall Interference of Wind Tunnels with Boundaries of Circular Arcs.* Aero. Res. Inst. (Tokyo) Report 126, 1935.

6.9 Kondo, K. *Boundary Interference of Partially Closed Wind Tunnels.* Aero. Res. Inst. (Tokyo) Report 137, 1936.

6.10 Theodorsen, T., Silverstein, A. *Experimental Verification of the Theory of Wind-Tunnel Boundary Interference.* NACA Report 478, 1934.

6.11 Van Schliestett, G. *Experimental Verification of Theodorsen's Theoretical Jet-Boundary Correction Factors.* NACA Tech. Note 506, 1934.

6.12 Riegels, F. *Korrekturfaktoren für Windkanäle elliptischen Querschnitts mit teilweise offener und teilweise geschlossener Meßstrecke.* Luftfahrtforschung, Vol. 16, 1939, pp. 26-30. (Translated as NACA Tech. Memo. 1310.)

6.13 Maeder, P.F., Wood, A.D. *Transonic Wind Tunnel Test Sections.* Z. ang. Math. Phys. Vol. 7, 1956, pp. 177-212.

6.14 Pistolesi, E. — (i) *On the Interference of a Wind Tunnel with a Mixed Boundary.* Pont. Accad. Sci. Vol. 4, No. 9, 1940. (Unpublished translation by Cornell Aero. Lab., 1949.)
(ii) *On the Interference of a Wind Tunnel with Mixed Contour.* Pont. Accad. Sci. Vol. 7, No. 5, 1943. (Unpublished translation by NACA, 1951.)

6.15 Matthews, C.W. — *Theoretical Study of the Tunnel-Boundary Lift Interference Due to Slotted Walls in the Presence of the Trailing-Vortex System of a Lifting Model.* NACA Report 1221, 1955.

6.16 Wright, R.H.
Ward, V.G. — *NACA Transonic Wind-Tunnel Test Sections.* NACA Report 1231, 1955. (First issued as R.M.L8J06, 1948.)

6.17 Davis, D.D.
Moore, D. — *Analytical Study of Blockage- and Lift-Interference Corrections for Slotted Tunnels Obtained by the Substitution of an Equivalent Homogeneous Boundary for the Discrete Slots.* NACA RM L53E07b (NACA/TIB/3792), 1953.

6.18 Goethert, B.H. — *Properties of Test Section Walls with Longitudinal Slots in Curved Flow for Subsonic and Supersonic Velocities (Theoretical Investigations).* Arnold Eng. Dev. Center, AEDC-TN-55-56, 1957.

6.19 Woods, L.C. — *The Theory of Subsonic Plane Flow.* Cambridge University Press, 1961.

6.20 Guderley, G. — *Simplifications of the Boundary Conditions at a Wind-Tunnel Wall with Longitudinal Slots.* Wright Air Dev. Center, Tech. Report 53-150, 1953.

6.21 Goodman, T.R. — *The Porous Wall Wind Tunnel, Pt.II. Interference Effect on a Cylindrical Body in a Two-Dimensional Tunnel at Subsonic Speeds.* Cornell Aero. Lab. Report AD-594-A-3, 1950.

6.22 Stokes, G.M.
et al. — *An Experimental Study of Porosity Characteristics of Perforated Materials in Normal and Parallel Flow.* NACA Tech. Note 3085, 1954.

6.23 Reynolds, W.G.
et al. — *Boundary Interference Studies in the Slotted Test Section of the Southern California Cooperative Wind Tunnel for the Mach Number Range 0.4 to 1.3.* CWT Report P-19, 1959.

6.24 Pearcey, H.H.
et al. — *Some Effects of Wind Tunnel Interference Observed in Tests on Two-Dimensional Aerofoils at High Subsonic and Transonic Speeds.* AGARD Report 296, 1959.

6.25 Maeder, P.F. — *Theoretical Investigation of Subsonic Wall Interference in Rectangular Slotted Test Sections.* Brown Univ. Div. of Eng. Tech. Report WT-11, 1953.

6.26 Borden, A. *Wall Corrections for Flow About Two- and Three-Dimensional Symmetrical Bodies in Rectangular Channels of Infinite and Finite Length.* David W. Taylor Model Basin, Report 804, 1954.

6.27 Watson, G.N. *A Treatise on the Theory of Bessel Functions.* 2nd Edition. Cambridge University Press. 1944.

6.28 Wright, R.H. *The Effectiveness of the Transonic Wind Tunnel as a Device for Minimizing Tunnel-Boundary Interference for Model Tests at Transonic Speeds.* NASA paper presented at AGARD meeting on Interference Effects. AGARD Report 294, 1959.

6.29 Maeder, P.F. et al. *Experimental Investigation of Subsonic Wall Interference in Rectangular Slotted Test Sections.* Brown Univ. Div. of Eng. Tech. Report WT-16, 1955.

6.30 Katzoff, S., Barger, R.L. *Boundary-Induced Downwash Due to Lift in a Two-Dimensional Slotted Wind Tunnel.* NASA Tech. Report R-25, 1959.

6.31 Rao, D.M., Ramaswamy, M.A. *Measurements of Two-Dimensional Zero-Lift Interference of Ventilated Boundaries at Speeds up to Sonic.* Z. ang. Math. Phys. Vol.11, 1960, pp.327-334.

6.32 Goethert, B.H. *Transonic Wind Tunnel Testing.* AGARDograph 49, 1961.

6.33 Squire, L.C. *A Comparison of Test Results from Three Transonic Tunnels for Two Sets of Geometrically Similar Models.* RAE Tech. Note Aero.2679, ARC Report 22,059, 1960.

6.34 Acum, W.E.A. *Note on the Evaluation of Solid-Blockage Corrections for Rectangular Wind Tunnels with Slotted Walls.* ARC R & M 3297, 1961.

6.35 Kassner, R.R. *Subsonic Flow over a Body between Porous Walls.* Wright Air Dev. Center, Tech. Report 52-9, 1952.

6.36 Goodman, T.R. *The Porous Wall Wind Tunnel, Pt.IV. Subsonic Interference Problems in a Circular Tunnel.* Cornell Aero. Lab. Report AD-706-A-2, 1951.

6.37 Tiramalesa, D. *Lift Interference for Low Aspect Ratio Wings in Transonic Wind Tunnels.* J. aero. Soc. India, Vol.11, 1959, pp.79-82.

6.38 Chew, W.L. *Cross-Flow Calibration at Transonic Speeds of Fourteen Perforated Plates with Round Holes and Airflow Parallel to the Plates.* Arnold Eng. [illegible] Center AEDC-TR-54-65, 1955.

6.39 Goodman, T.R. *The Porous Wall Wind Tunnel, Pt.V. Subsonic Interference on a Lifting Wing between Two Infinite Walls.* Cornell Aero. Lab. Report AD-706-A-3, 1951.

6.40 Brescia, R. *Wall Interference in a Perforated Wind Tunnel.* NACA Tech. Memo. 1429. (Translated from Atti della Accademia delle Scienze di Torino, Vol. 87, 1952-3.)

6.41 Jones, R.T. *Properties of Low-Aspect-Ratio Pointed Wings at Speeds Below and Above the Speed of Sound.* NACA Report 835, 1946.

6.42 Maeder, P.F. *Some Aspects of the Behavior of Perforated Transonic Wind Tunnel Walls.* Brown Univ. Div. of Eng. Tech. Report WT-15, 1954.

6.43 Glauert, H. *Wind Tunnel Interference on Wings, Bodies and Airscrews.* ARC R & M 1566, 1933.

6.44 Muskat, M. *Flow of Homogeneous Fluids through Porous Media.* McGraw-Hill, 1937, pp. 55-120.

6.45 Carroll, J.B.
Rice, J.B. *Analytical and Experimental Studies of Wall Interference in Perforated Wind Tunnels.* Wright Air Dev. Center, Tech. Report 56-240, 1956.

6.46 Lukasiewicz, J. *Effects of Boundary Layer and Geometry on Characteristics of Perforated Walls for Transonic Wind Tunnels.* Aerospace Eng., Vol. 20, April 1961, pp. 22-23, 62-68.

6.47 Maeder, P.F. *Investigation of the Boundary Condition at a Perforated Wall.* Brown Univ. Div. of Eng. Tech. Report WT-9, 1953.

6.48 Maeder, P.F.
Stapleton, J.F. *Investigation of the Flow through a Perforated Wall.* Brown Univ. Div. of Eng. Tech. Report WT-10, 1953.

6.49 Hill, J.A.F.
et al. *Mach Number Measurements in High-Speed Wind Tunnels.* AGARDograph 22, 1956.

6.50 Wuest, W. *Verdrängungskorrekturen für rechteckige Windkanäle bei verschiedenen Strahlbegrenzungen und bei exzentrischer Lage des Modells.* Z. Flugwiss, Vol. 9, pp. 15-19 and Errata p. 362, 1961.

6.51 Tomlinson, R.C. *The Theoretical Interference Velocity on the Axis of a Two-Dimensional Wind Tunnel with Slotted Walls.* ARC CP 181, 1953.

6.52 Chen, C.F.
Mears, J.W. *Experimental and Theoretical Study of Mean Boundary Conditions at Perforated and Longitudinally Slotted Wind Tunnel Walls.* Brown Univ. Div. of Eng. Tech. Report WT-25, 1957.

6.53 Maeder, P.F.
Hall, J.F. *Investigation of Flow over Partially Open Wind Tunnel Walls.* Brown Univ. Div. of Eng. Tech. Report WT-19, 1955.

6.54 Hill, J.A.F.	*An Analytical Study of Flow through a Perforated Wall.* United Aircr. Corp. Report R-95630-9, 1953.
6.55 Tirumalesa, D.	*Wall Interference in Transonic Wind Tunnels.* J. Aero. Soc. India, Vol. 11, 1959, pp. 53-67.
6.56 Maeder, P.F. Thommen, H.U.	*On the Boundary Layer at Perforated Walls.* Z. angew. Math. Phys. Vol. 9b, 1958, pp. 438-453.
6.57 Wood, W.W.	*Tunnel Interference from Slotted Walls.* Quart. J. Mech. appl. Math. Vol. 17, 1964, pp. 125-140.
6.58 Holder, D.R.	*Upwash Interference in a Rectangular Wind Tunnel with Closed Side Walls and Porous Slotted Floor and Roof.* ARC R & M 3322, 1962.
6.59 Holder, D.R.	*Upwash Interference on Wings of Finite Span in a Rectangular Wind Tunnel with Closed Side Walls and Porous-Slotted Floor and Roof.* ARC R & M 3395, 1963.
6.60 Rushton, K.R.	*Studies of Slotted-Wall Interference Using an Electrical Analogue, Part II. Particular Examples of Slotted-Wall Tunnel Interference.* ARC R & M 3452, 1965.
6.61 Rushton, K.R.	Private Communication, 1965.

ADDITIONAL REFERENCES FOR CHAPTER VI

Brescia, R.	*Studio dell'Interferenza delle Gallerie Aerodinamiche con Pareti a Fessure in Correnti Compressibili.* Atti della Accademia delle Scienze di Torino, Vol. 88, 1953-54.
Gale, A.E.	*Wall Corrections for Transonic Wind Tunnels. Part I: A Lifting Model in a Circular Slotted Tunnel.* MIT Aero. Eng. Dept. TACP Report 3, 1954.
Guderley, G.	*Theoretical Remarks on Wind Tunnels with Slotted Walls.* Wright Air Dev. Center Tech. Report 52-8, 1952.
Guderley, G.	*Wall Corrections for a Wind Tunnel with Longitudinal Slots at Subsonic Velocities.* Wright Air Dev. Center Tech. Report 54-22, 1954.
Maeder, P.F.	*Investigation of Tunnel Boundary Interference on Two-Dimensional Airfoils Near the Speed of Sound.* Brown Univ. Div. of Eng. Tech. Report WT-6, 1951.

Nelson, W.J. Bloetscher, F.	*An Experimental Investigation of the Zero-Lift Pressure Distribution over a Wedge Airfoil in Closed, Slotted, and Open-Throat Tunnels at Transonic Mach Numbers.* NACA RM L52C18 (NACA/TIB/3241), 1952.
Tirumalesa, D.	*Some Aspects of Interference in Ventilated Wall Transonic Wind Tunnels.* NAL (Bangalore) Tech. Note TN-AE-12-61, 1961.
Vandrey, F. Wieghardt, K.	*Experiments on a Slotted Wall Working Section in a Wind Tunnel.* ARC CP 206. 1952.
Whitcomb, C.F. Osborne, R.S.	*An Experimental Investigation of Boundary Interference on Force and Moment Characteristics of Lifting Models in the Langley 16- and 8-foot Transonic Tunnels.* NACA RM L52L29 (NACA/TIB/3642), 1953.
Woods, L.C.	*On the Theory of Two-Dimensional Wind Tunnels with Porous Walls.* Proc. Roy. Soc., Series A, Vol.233, 1955, pp.74-90.
Woods, L.C.	*On the Lifting Aerofoil in a Wind Tunnel with Porous Walls.* Proc. Roy. Soc., Series A, Vol.242, 1957, pp.341-354.
Wright, R.H. Barger, R.L.	*Wind-Tunnel Lift Interference on Sweptback Wings in Rectangular Test Sections with Slotted Top and Bottom Walls.* NASA Tech. Report R-241, 1966.

TABLE 6.I

Summary of Results

Tunnel section	*Walls*	*Model**	*Blockage*		*Lift*	
			Figs.	*Eqns.*	*Figs.*	*Eqns.*
Two-dimensional	Slotted	Small	6.2 6.3	6.15 6.23	6.14 6.15	6.48
Two-dimensional	Slotted	Large	6.4 to 6.7	6.18 6.20	6.15	6.51 6.54
Two-dimensional	Perforated	Small	6.26	6.81 6.83	6.29	6.89
Two-dimensional	Perforated	Large	6.27	6.82	6.29	6.91
Circular	Slotted	Small	6.8 6.9	6.28 6.33	6.16 6.17	6.58
Circular	Slotted	Large	–	6.34	–	6.61 6.63
Circular	Perforated	Small	6.28	6.84 6.86	6.30	6.94
Circular	Perforated	Large	–	6.85 6.87	–	6.95
Rectangular	Slotted roof and floor	Small	6.10	6.37	6.21 to 6.24	6.70 6.73
Rectangular	Slotted roof and floor	Large	6.11	–	6.18 to 6.23	6.67 6.73 6.72
Rectangular	All slotted	Small	6.12	–	6.17 6.25	6.74 6.75 6.76
Rectangular	Perforated	Small	–	–	6.31 6.33	6.98 6.99
General	Slotted	Small	6.13	6.46	–	–

* "Large" denotes that the effect of longitudinal pressure gradient, streamline curvature, length or span of model is considered.

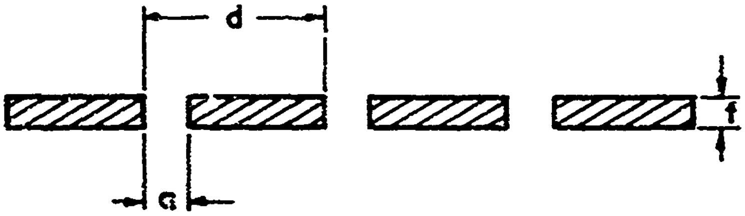

Open area ratio is $\frac{a}{d}$

$$K = \frac{d}{\pi} \log_e \operatorname{cosec} \frac{\pi a}{2d}$$

(a) For a tunnel of height h and breadth b with solid side-walls

$$F = \frac{2K}{h} = \frac{2d}{\pi h} \log_e \operatorname{cosec} \frac{\pi a}{2d}$$

$$= \frac{2b}{\pi N h} \log_e \operatorname{cosec} \frac{\pi a}{2d}$$

where N is the number of slots in the roof or floor

(b) For a circular tunnel of radius R

$$F = \frac{K}{R} = \frac{2}{N} \log_e \operatorname{cosec} \frac{\pi a}{2d}$$

(c) For a rectangular tunnel with evenly spaced slots on all four walls

$$F = \frac{\sqrt{\pi} K}{\sqrt{bh}} = \frac{d}{\sqrt{\pi bh}} \log_e \operatorname{cosec} \frac{\pi a}{2d}$$

Fig. 6.1 Notation and geometry for longitudinal slots

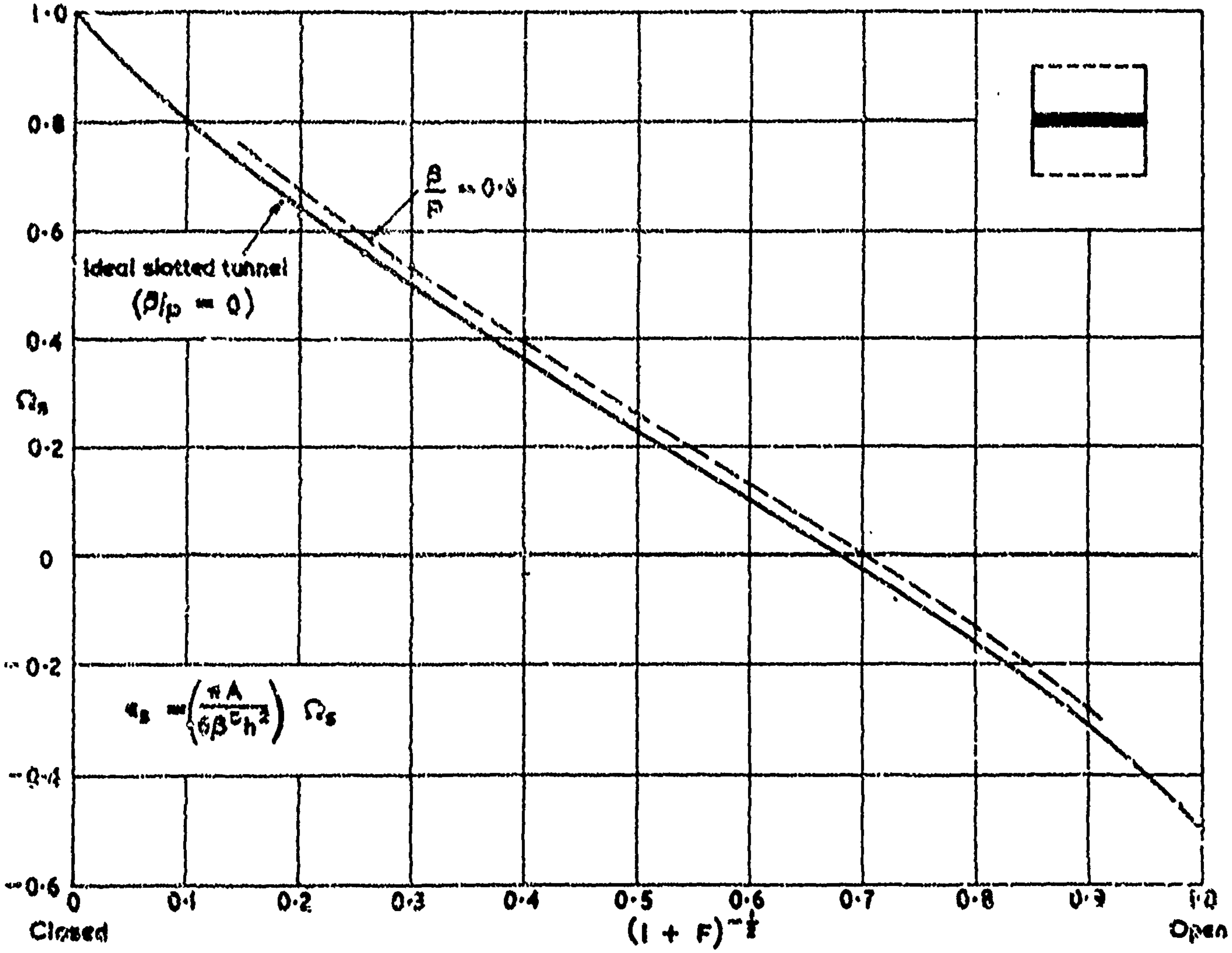

Fig. 6.2 Solid-blockage factors for two-dimensional aerofoil in a slotted tunnel

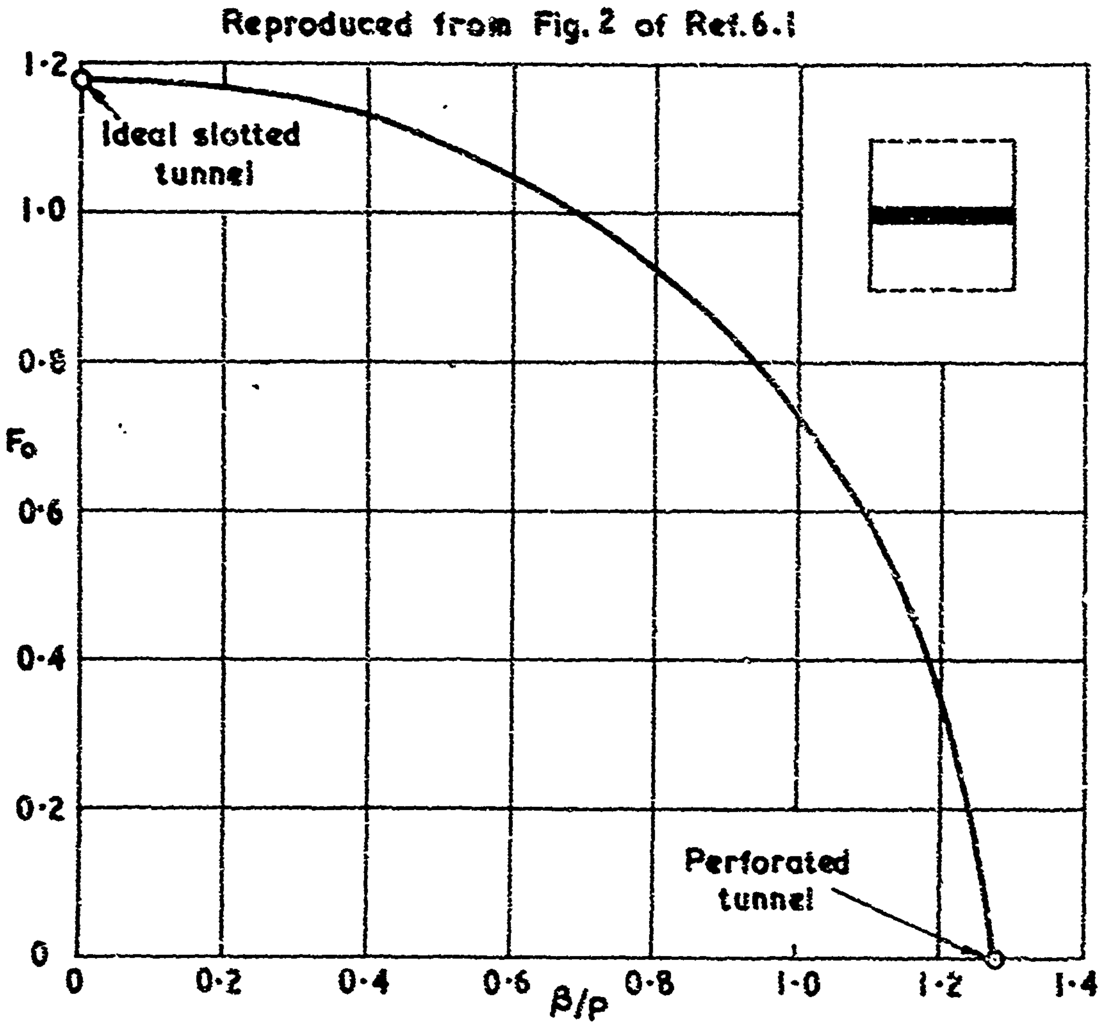

Fig. 6.3 Values of slot and porosity parameters required to give zero solid blockage for a two-dimensional aerofoil

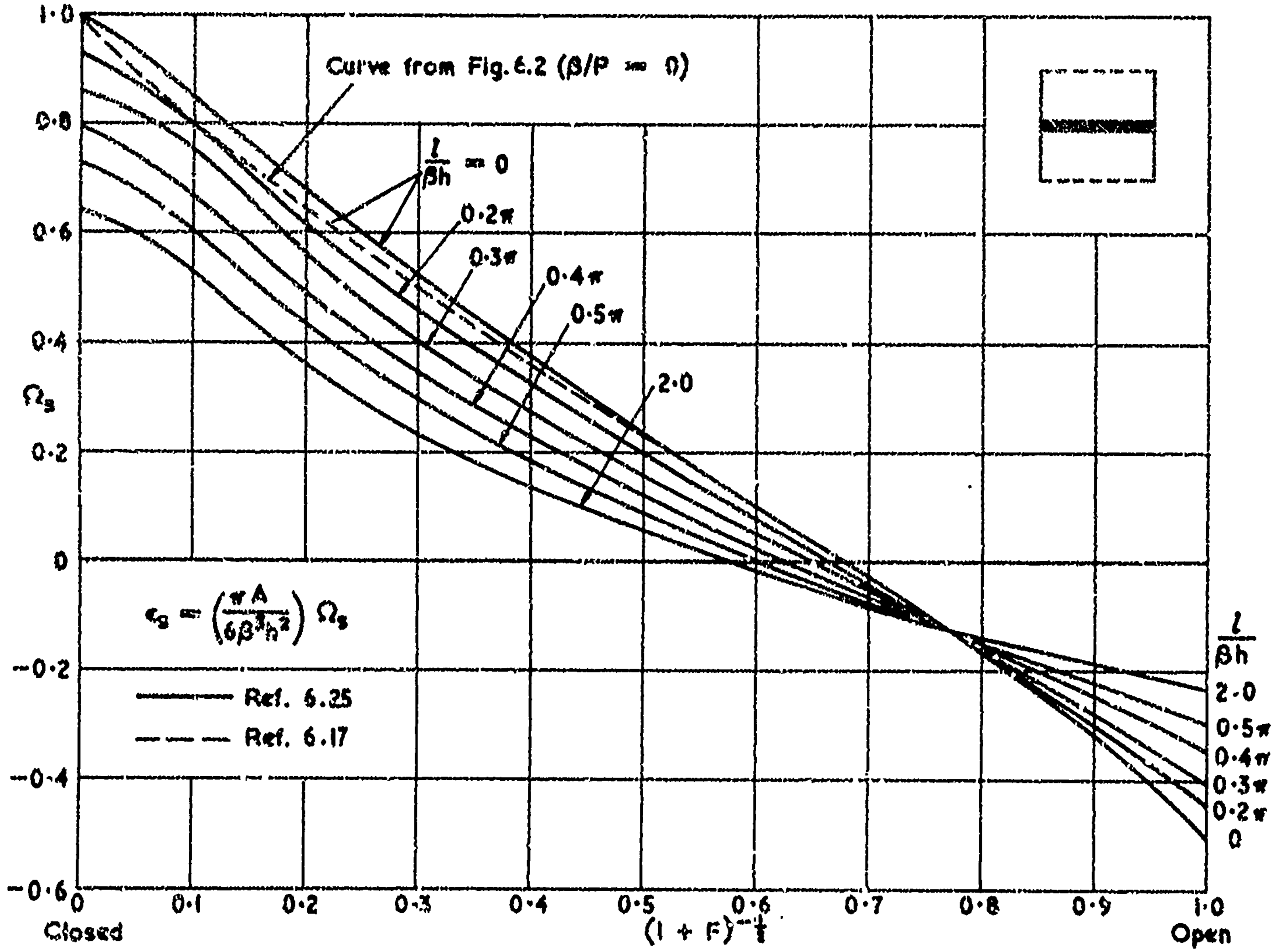

Fig. 6.4 Effect of aerofoil size on solid-blockage factor in ideal slotted tunnel

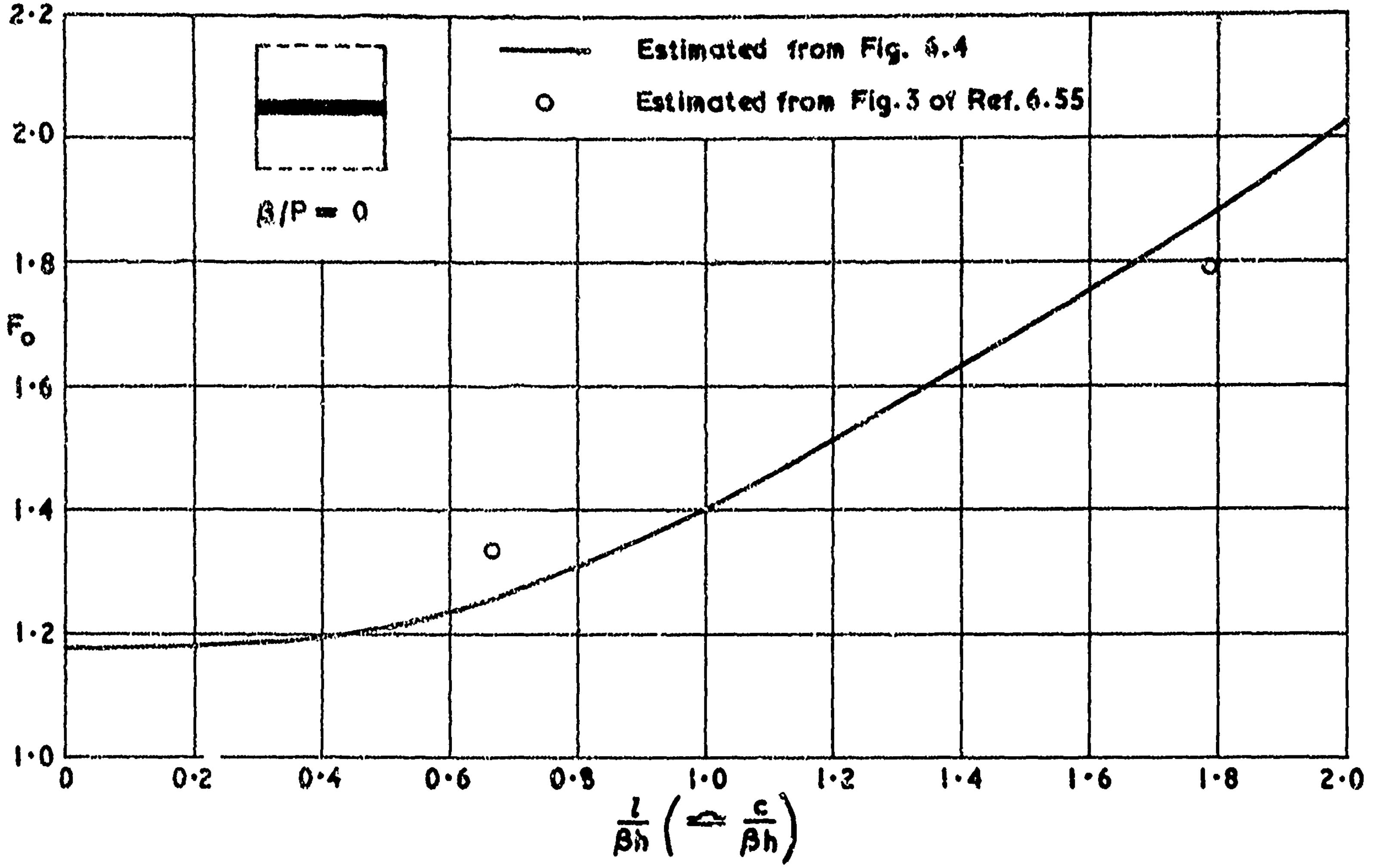

Fig. 6.5 Effect of model size on slot parameter for zero blockage (F_0) in ideal slotted tunnel

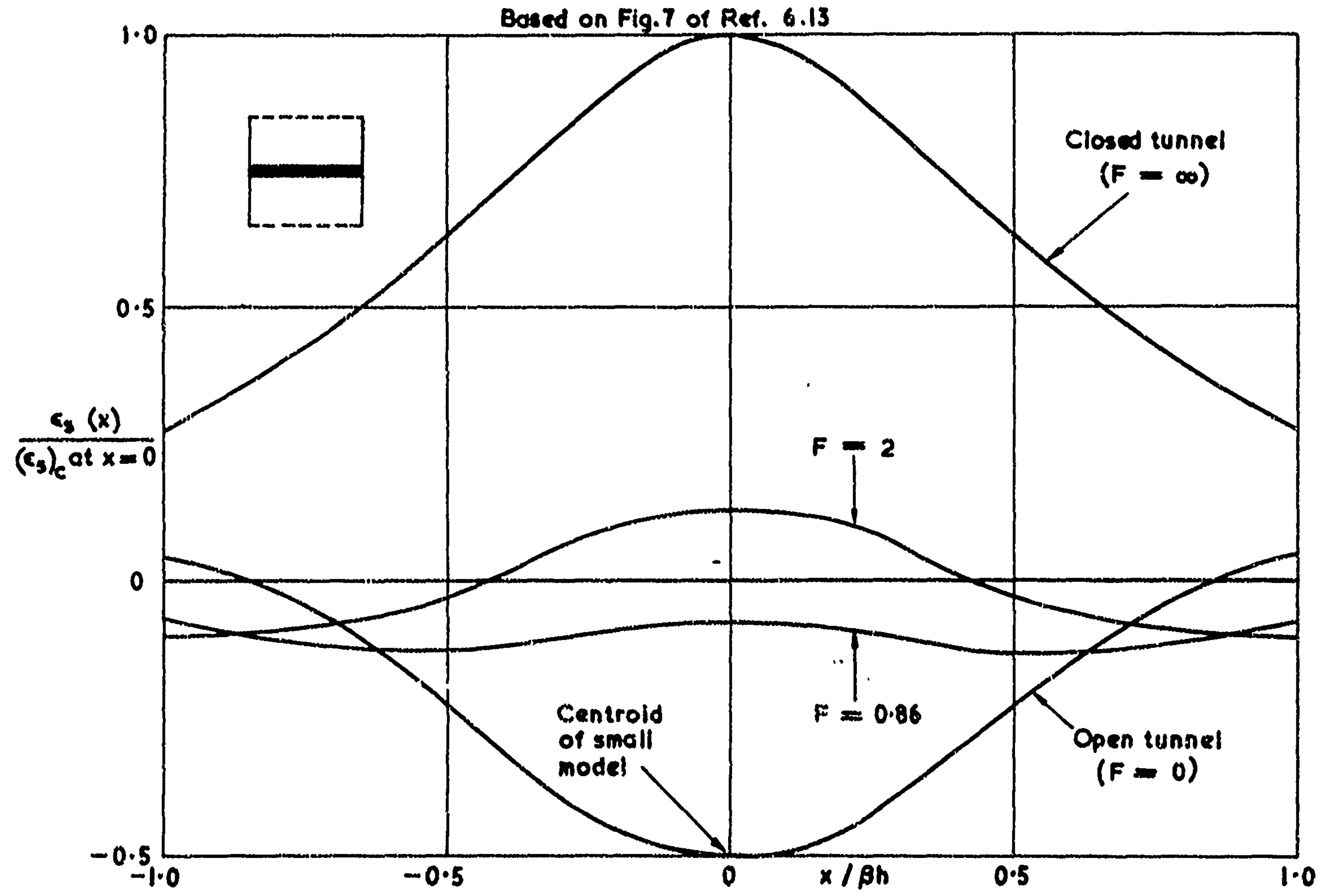

Fig. 6.6 Distribution of solid-blockage factor along two-dimensional ideal slotted tunnel

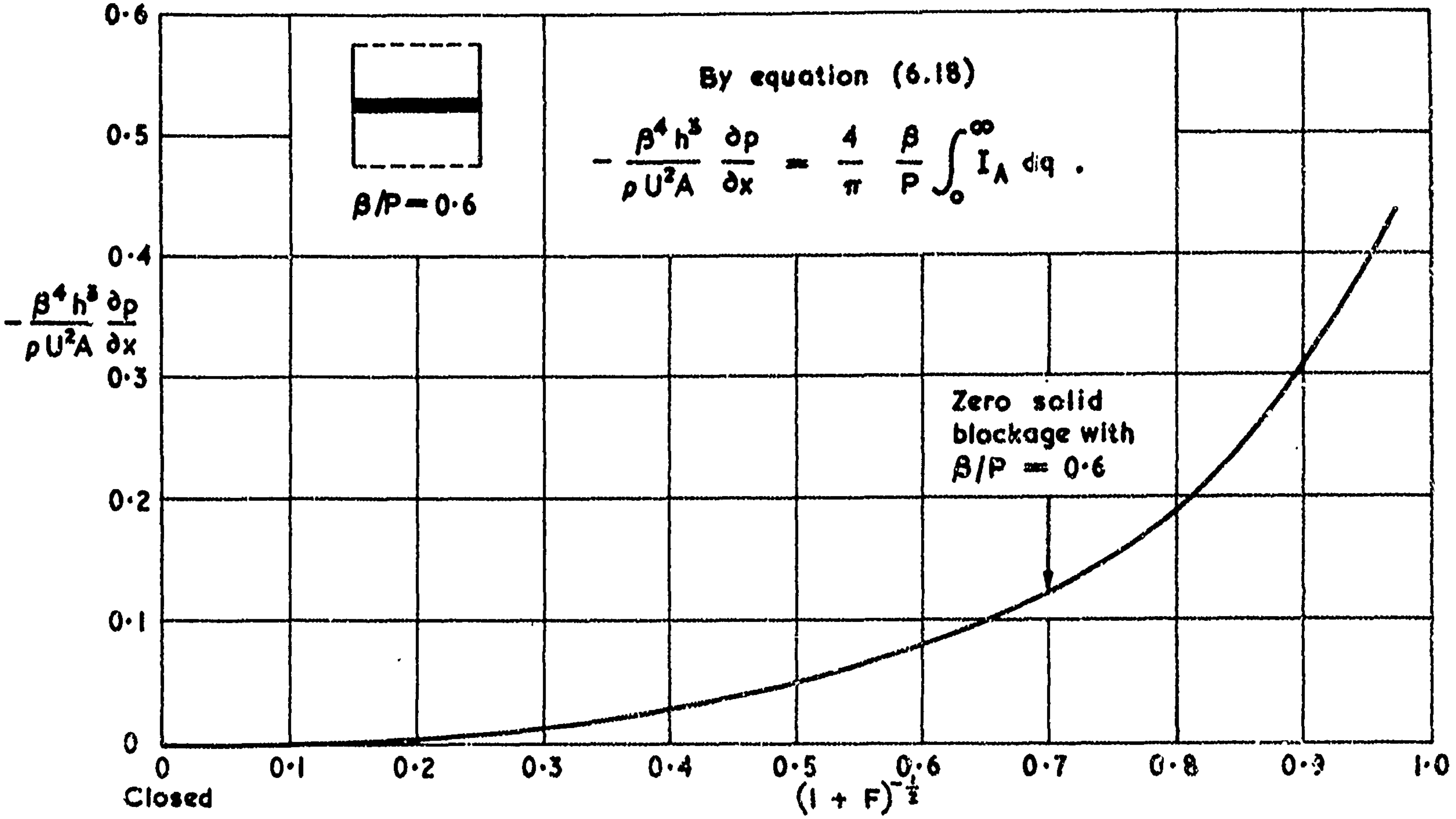

Fig.6.7 Longitudinal pressure gradient at the model associated with solid blockage

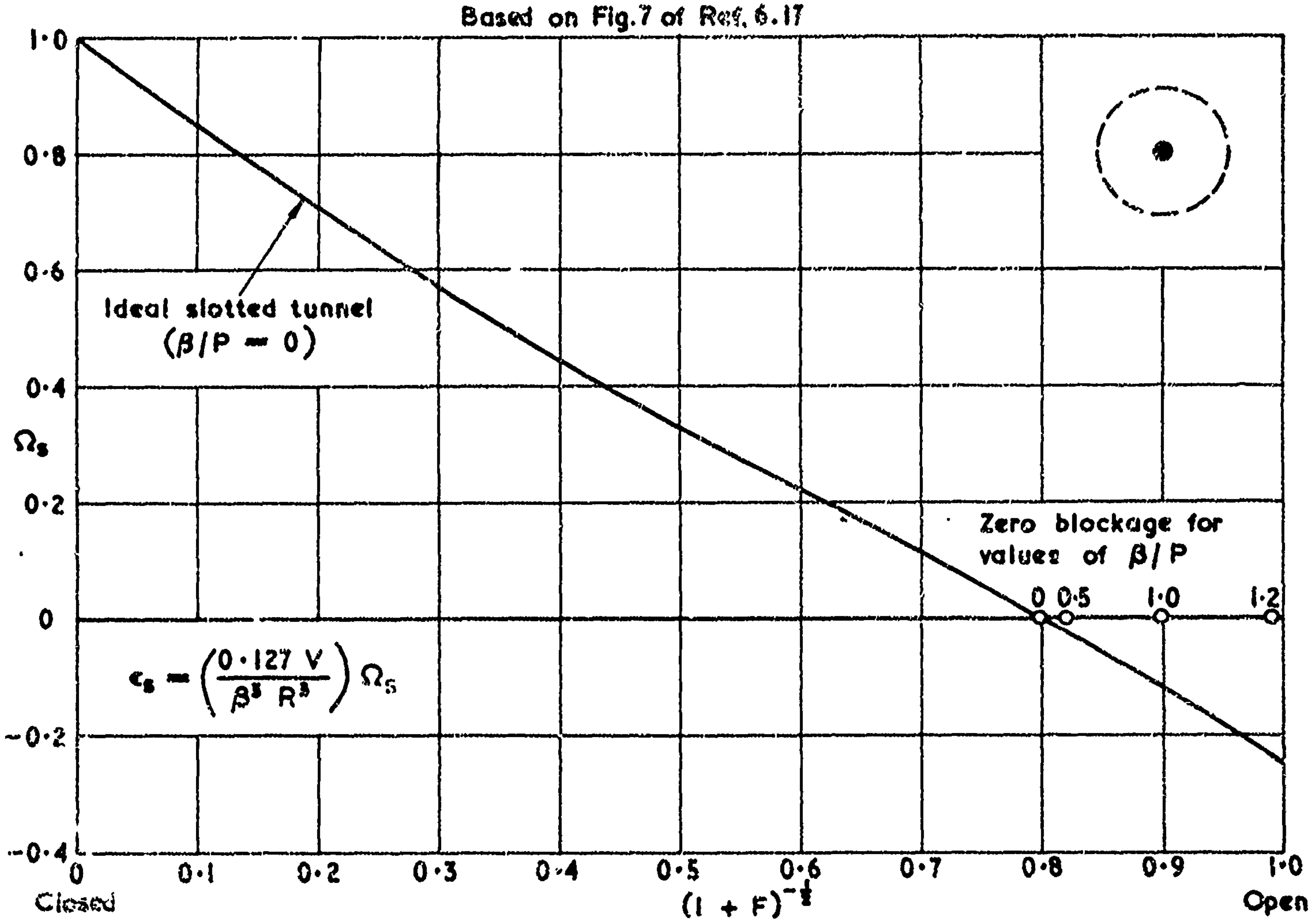

Fig. 6.8 Solid-blockage factor for small three-dimensional model in circular slotted tunnel

Reproduced from corrected Fig. 4 of Ref. 6.1

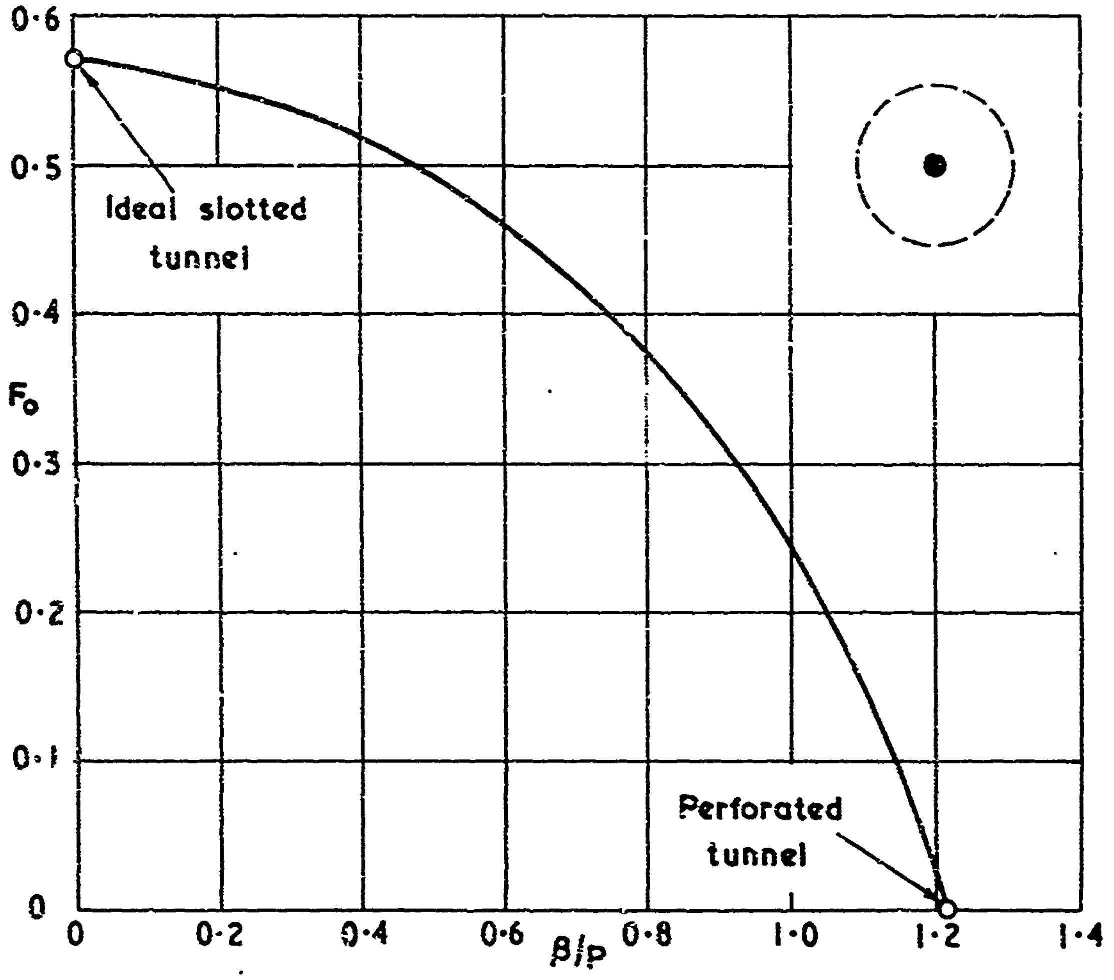

Fig. 6.9 Values of slot and porosity parameters required to give zero solid blockage for a small three-dimensional model in a circular tunnel

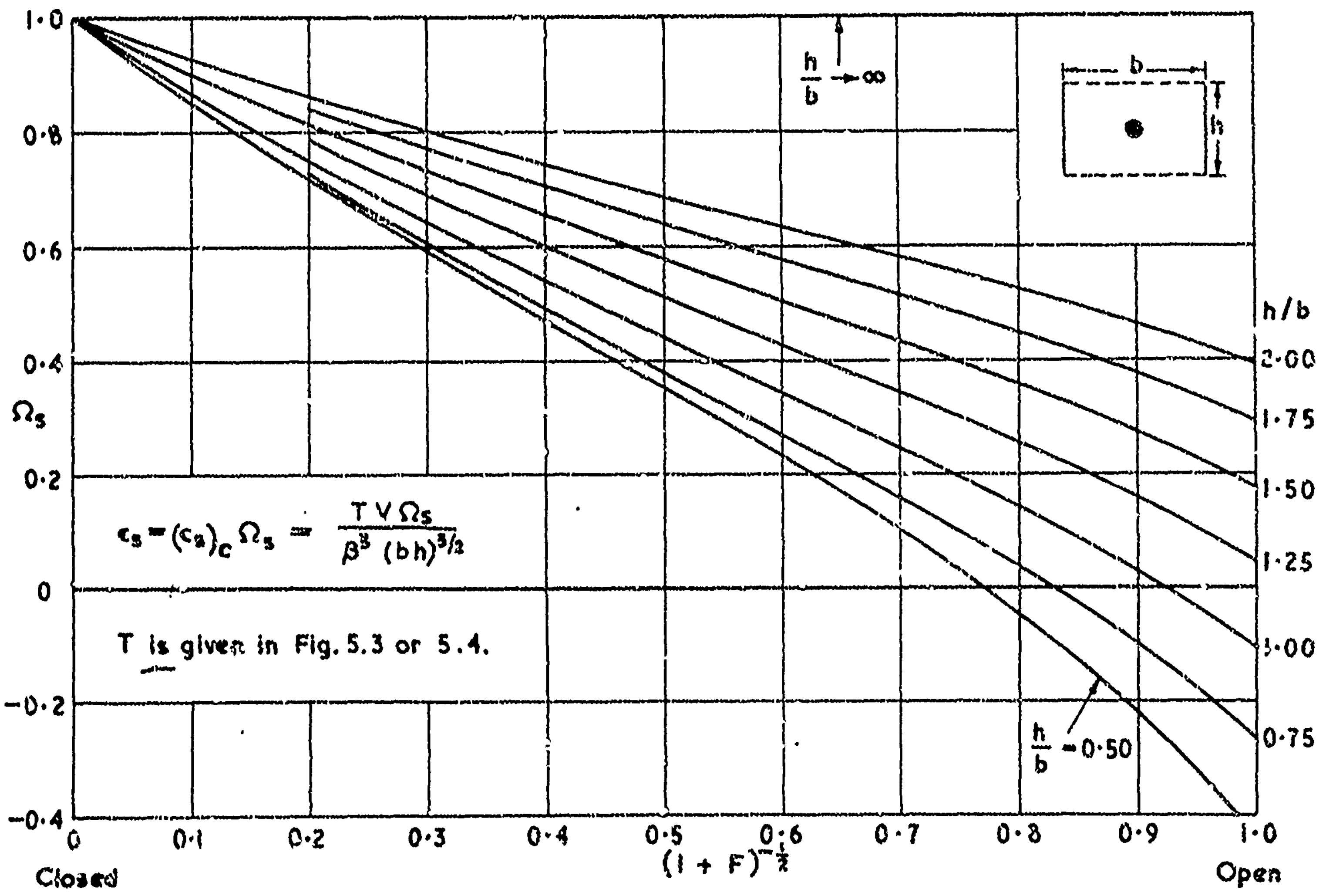

Fig. 6.10 Solid-blockage factor for a small model in rectangular tunnels with ideal slotted roof and floor

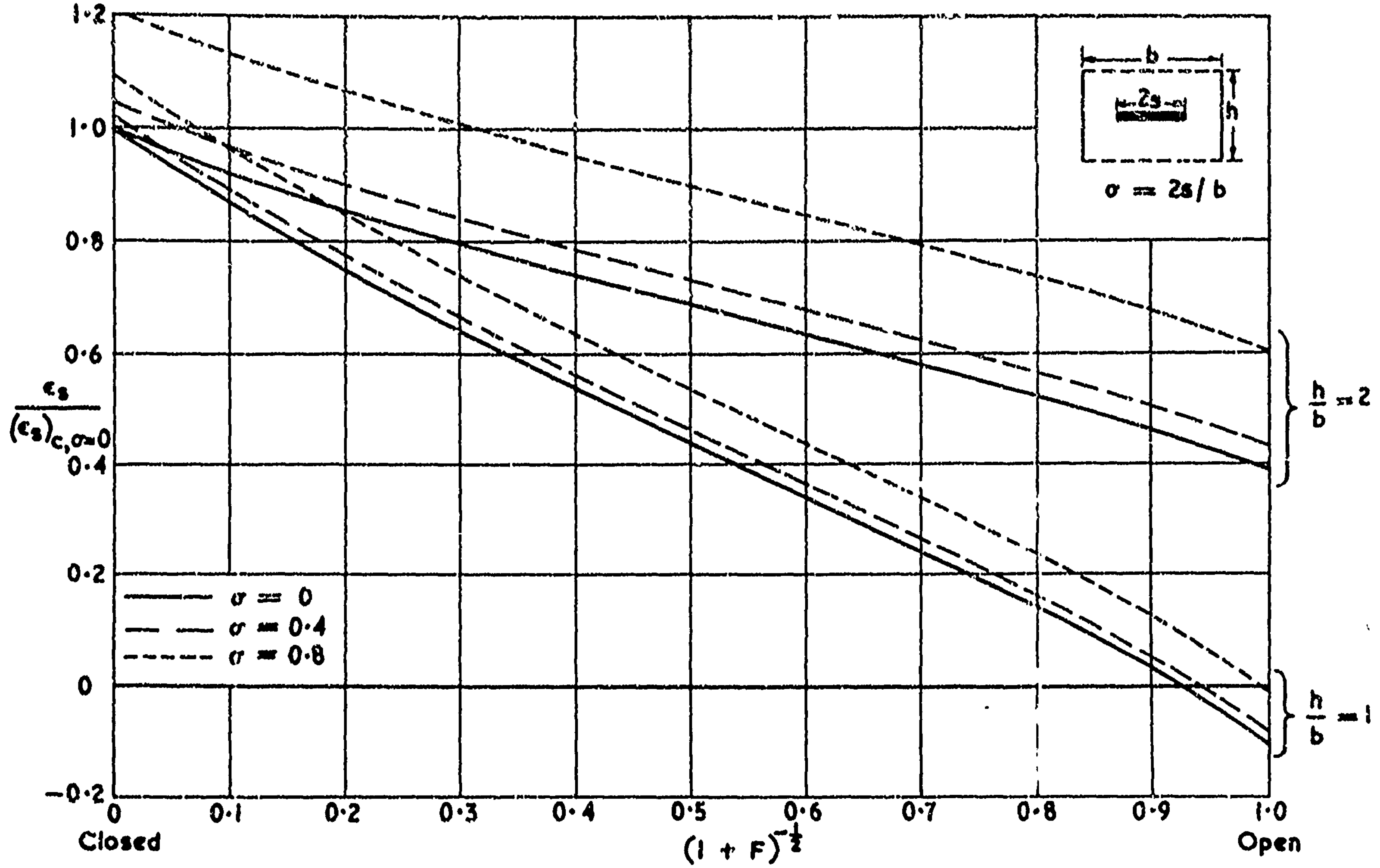

Fig.6.11 Solid-blockage factor for large wings in rectangular tunnels with ideal slotted roof and floor

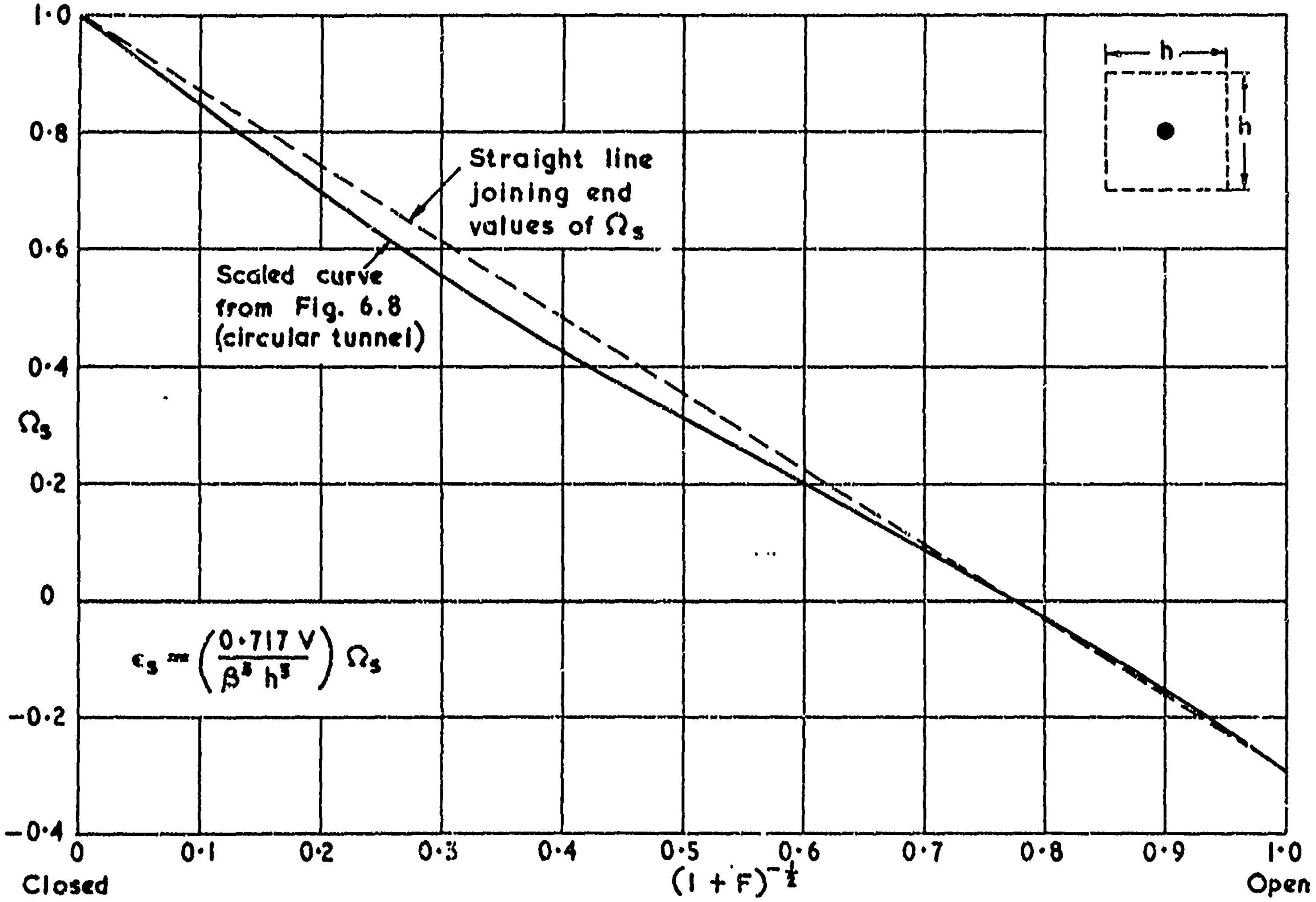

Fig. 6.12 Estimated solid-blockage factor for small model in square tunnel with ideal slotted walls

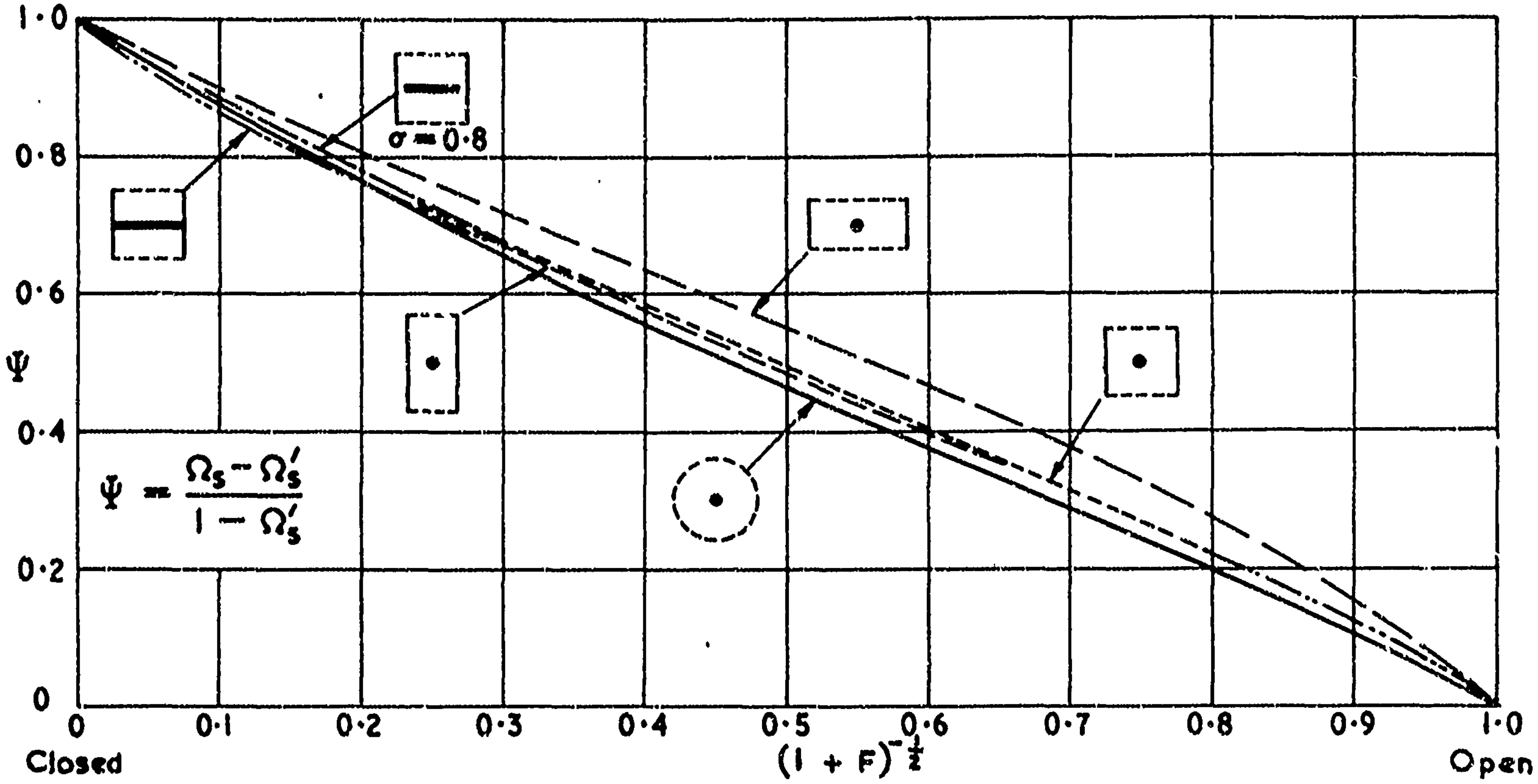

Fig. 6.13 Collapse of existing results for solid-blockage interference in ideal slotted tunnels

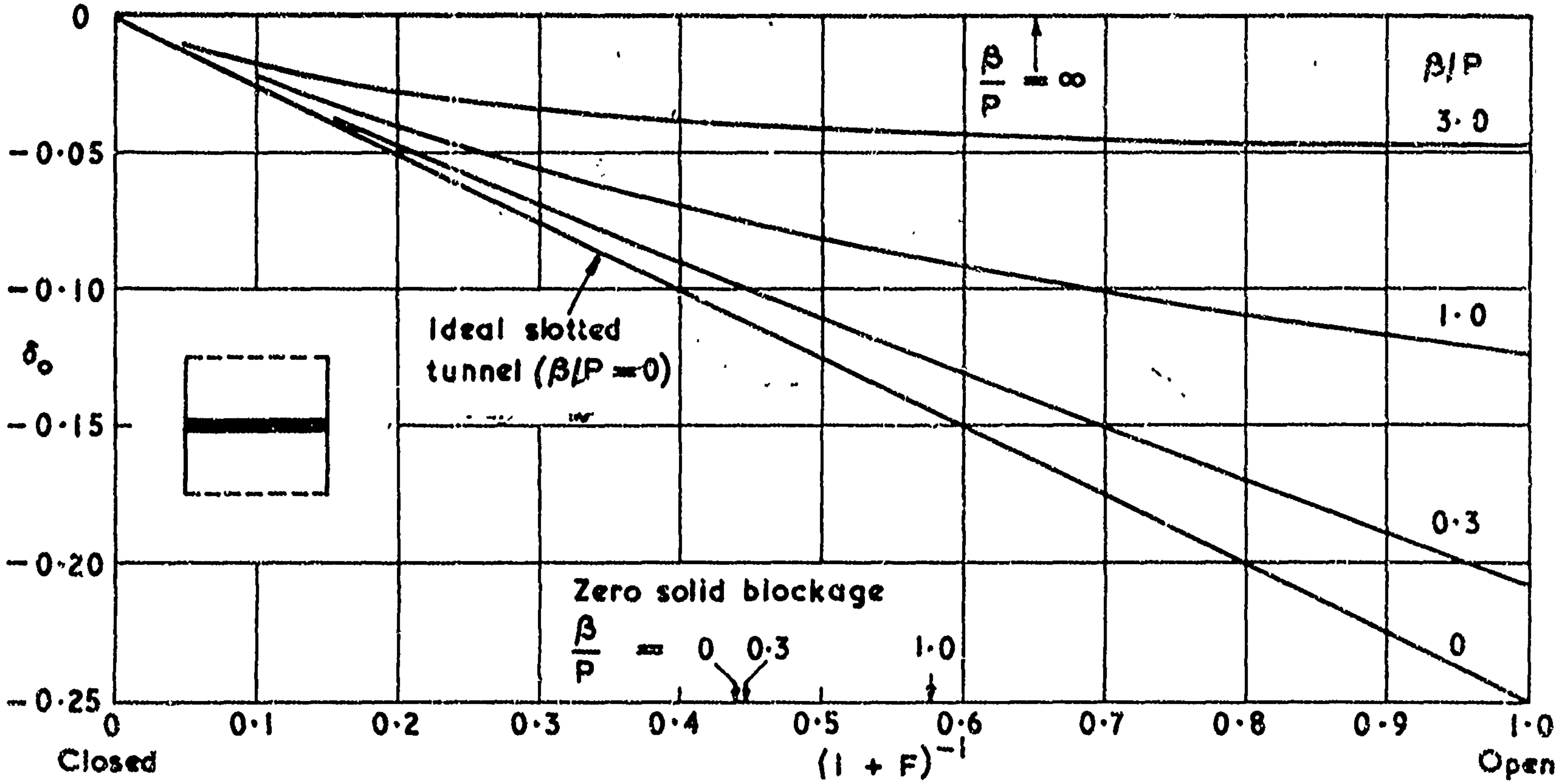
Based on Fig. 1 of Ref. 6.58

Fig. 6.14 Influence of porosity parameter on lift interference for small two-dimensional aerofoil in a slotted tunnel

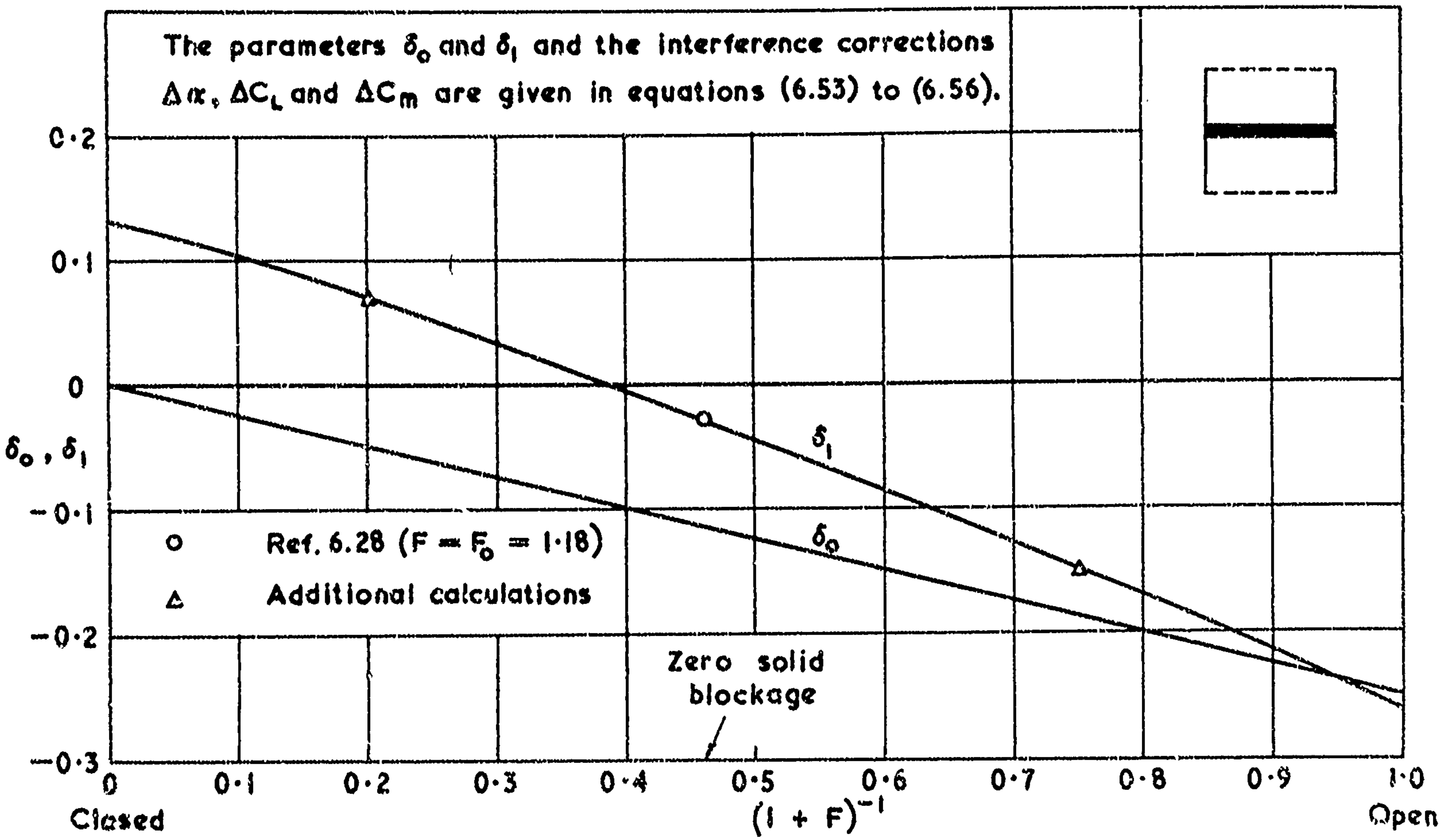

Fig. 6.15 Lift interference for two-dimensional aerofoil in an ideal slotted tunnel

Based on Fig.1 of Ref. 6.23

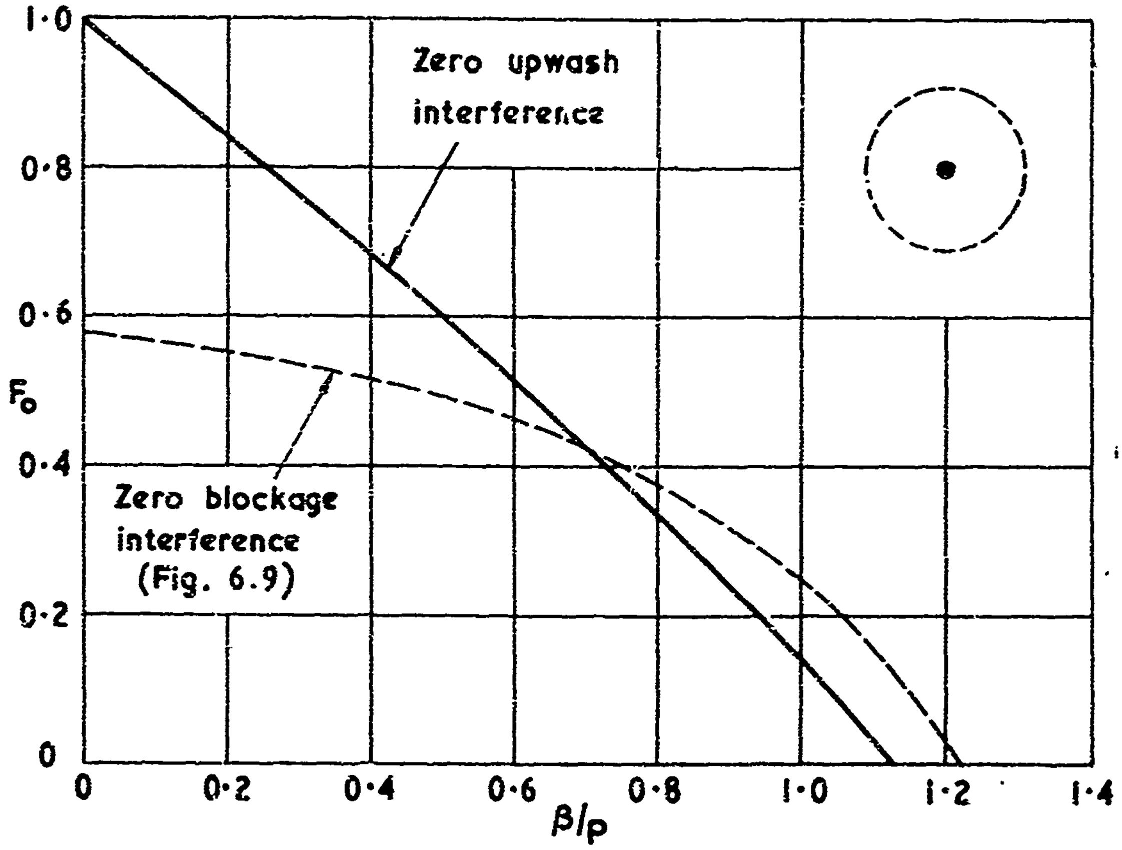

Fig. 6.16 Values of slot and porosity parameters required to give zero upwash interference for a small three-dimensional model in a circular tunnel

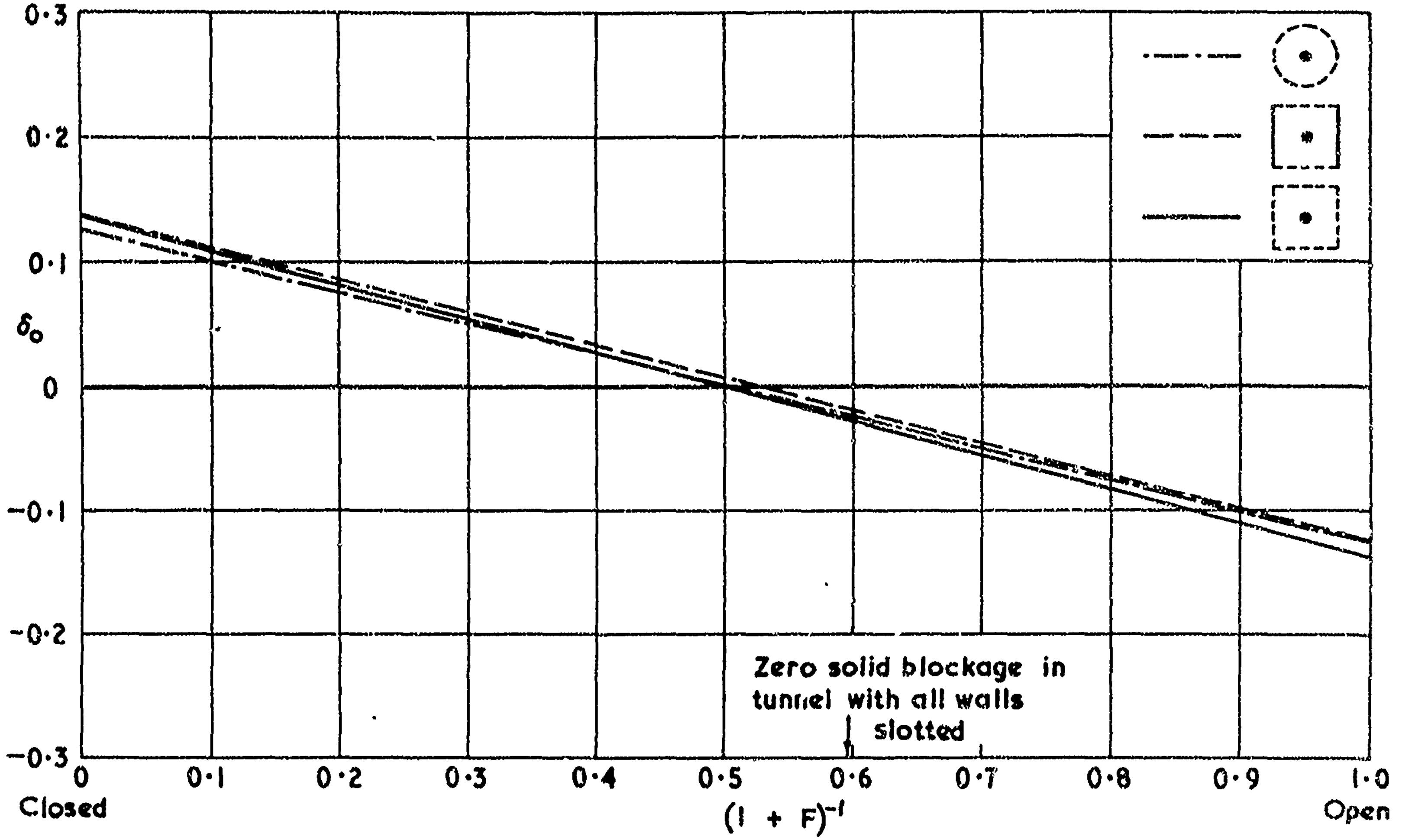

Fig. 6.17 Lift-interference parameter for circular and square ideal slotted tunnels

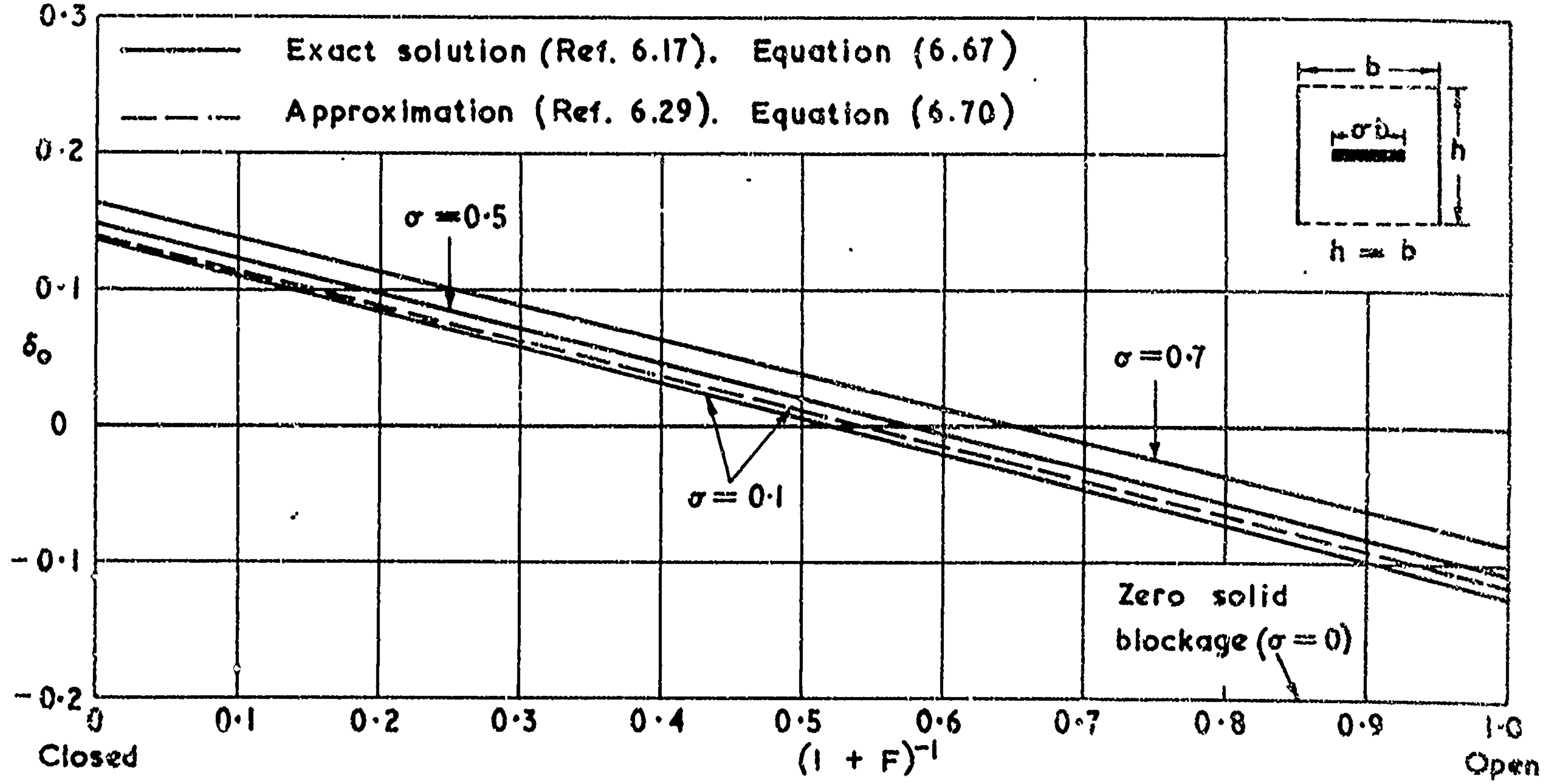

Fig. 6.18 Lift-interference parameter for models in a square ideal slotted tunnel with solid side-walls

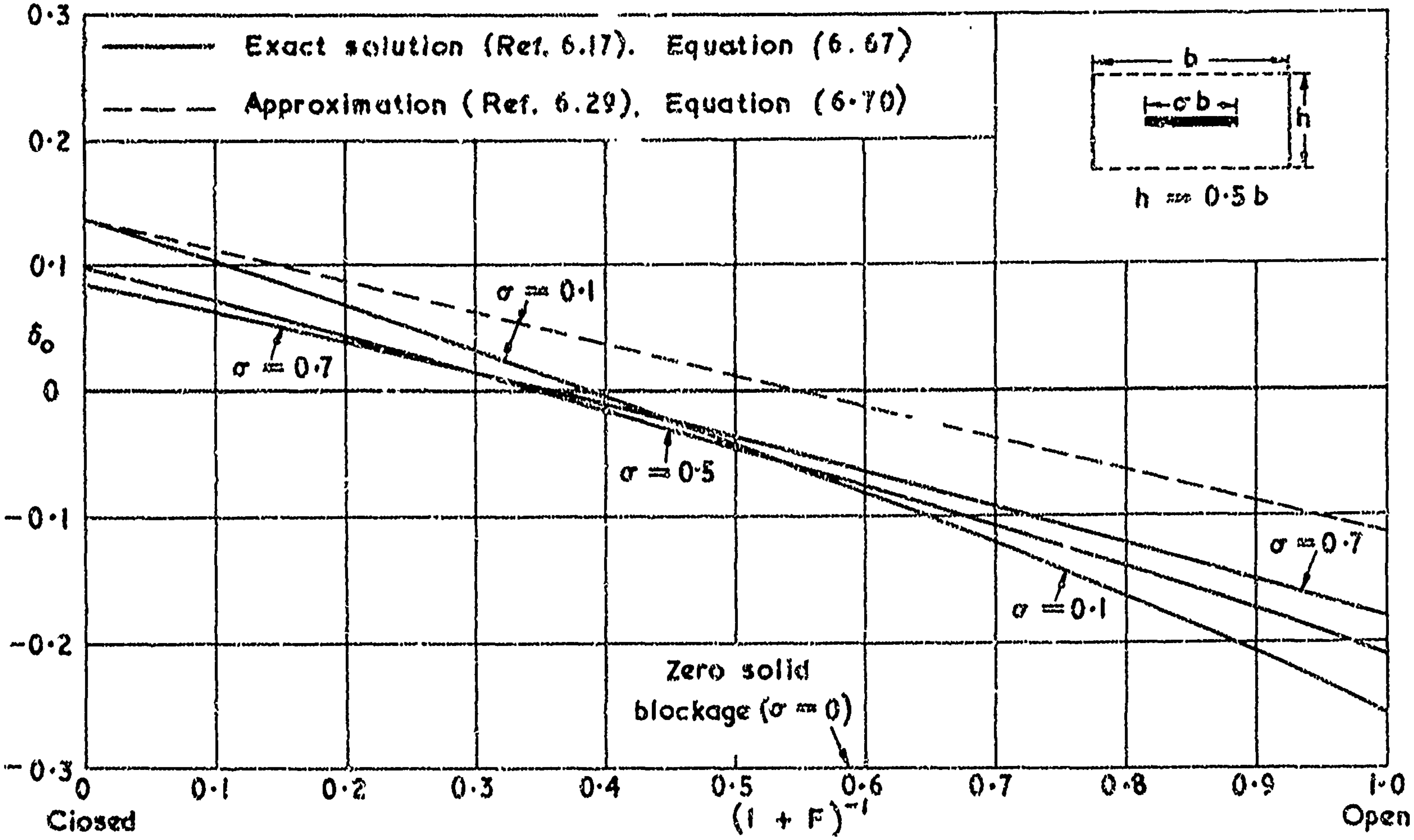

Fig. 6.19 Lift-interference parameter for model in ideal slotted tunnel with solid side walls

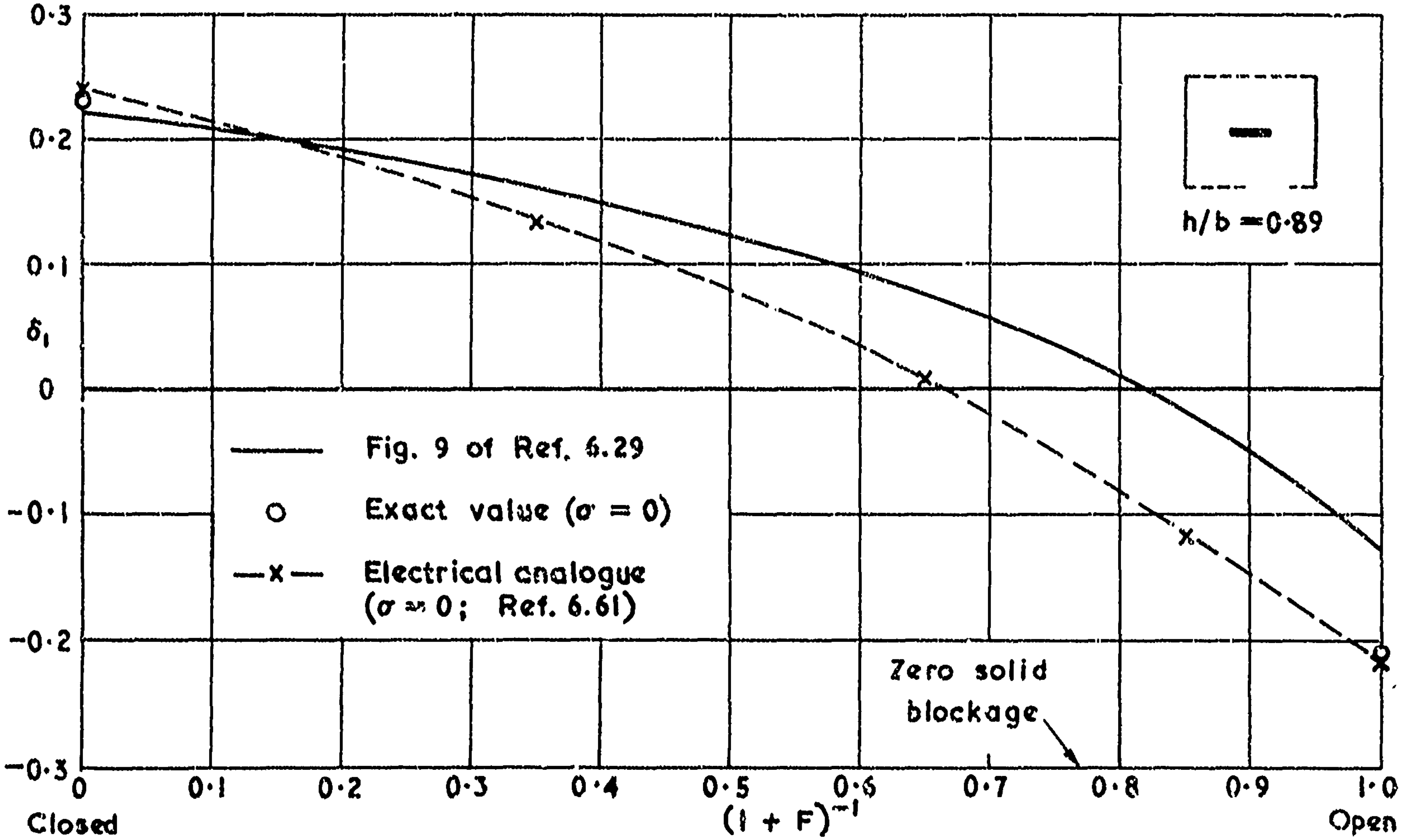

Fig. 6.20 Streamline-curvature correction in ideal slotted tunnel with solid side-walls

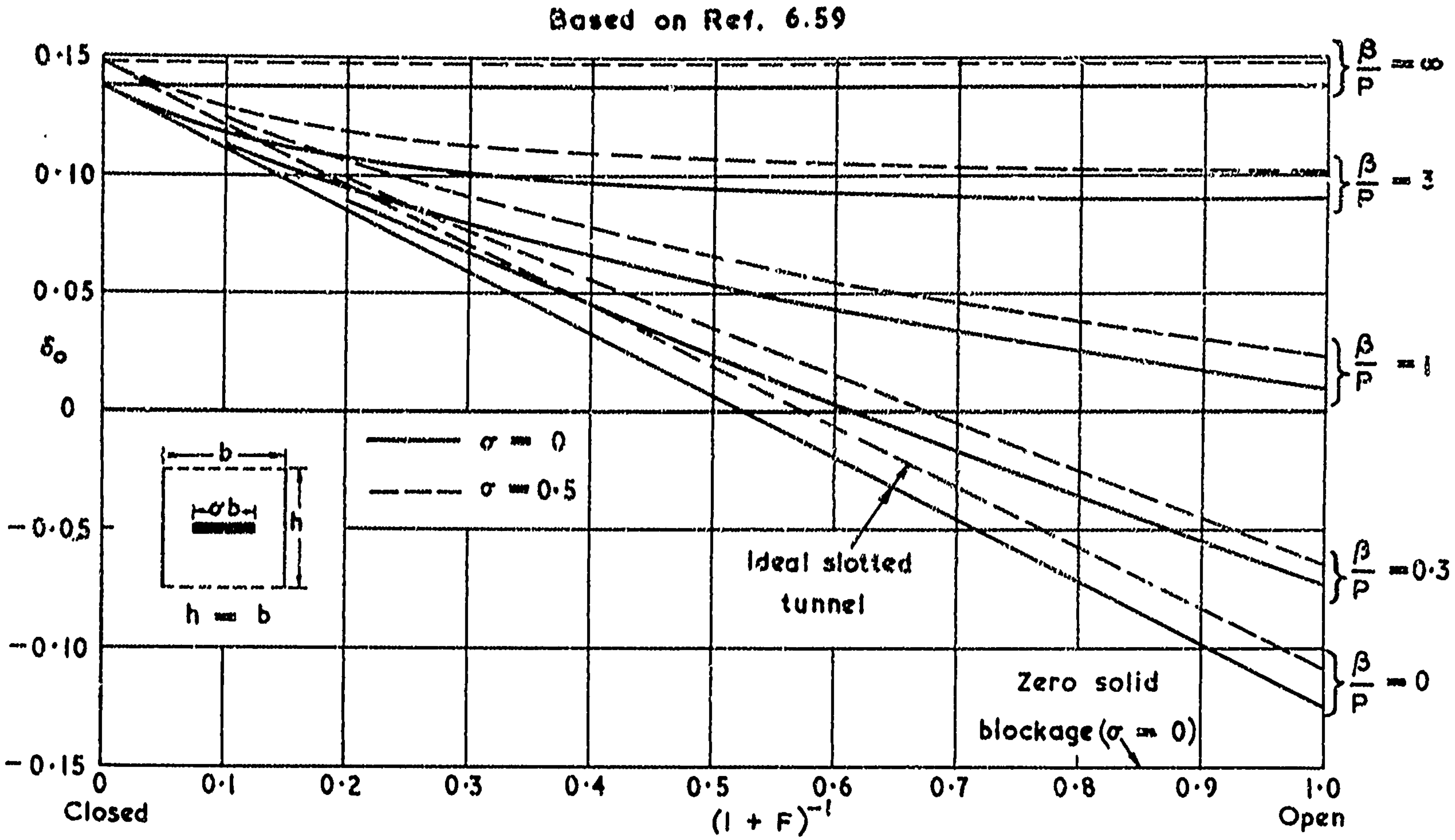

Fig. 6.21 Influence of viscosity on lift-interference parameter for models in square slotted tunnel with solid side-walls

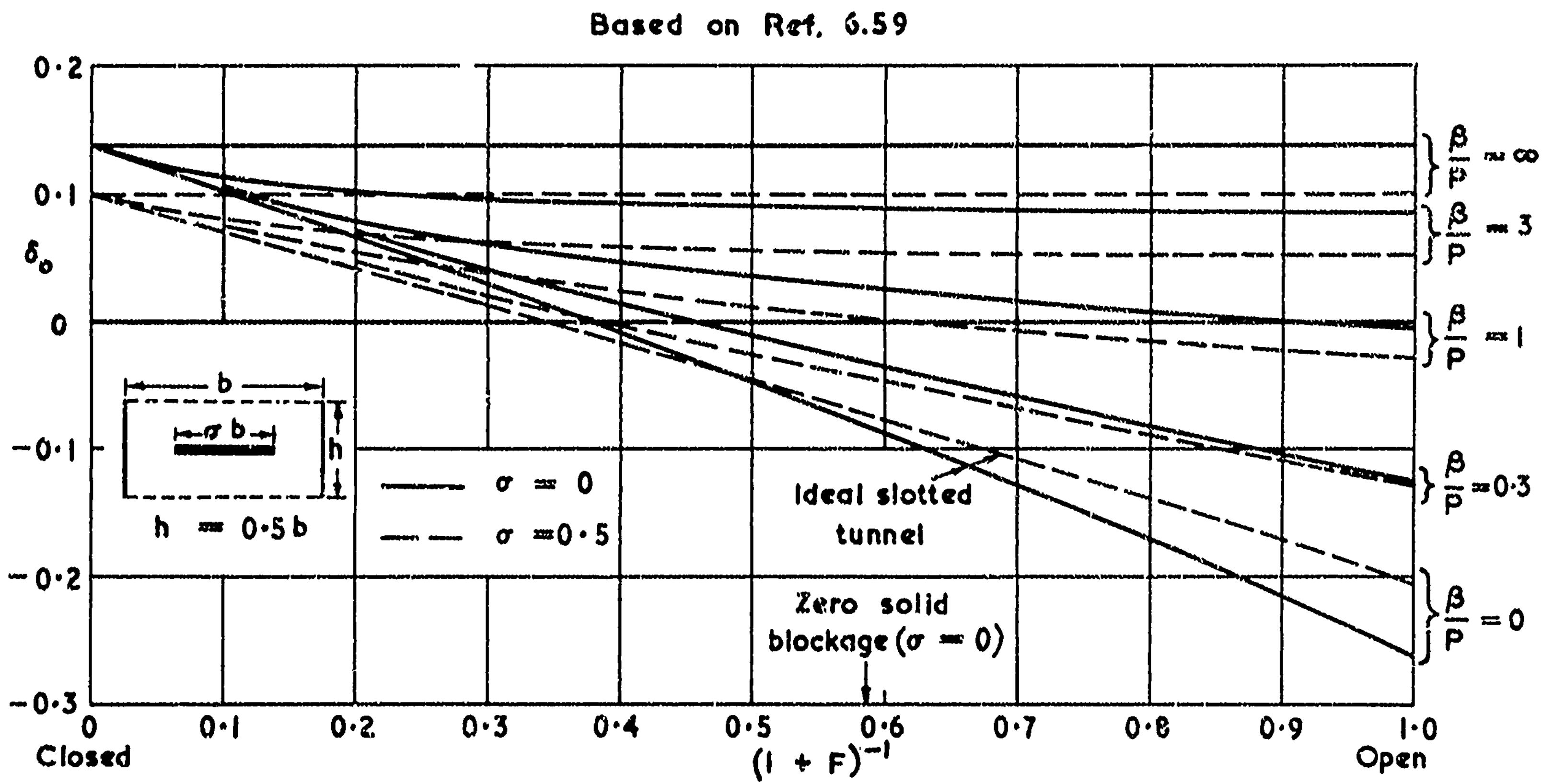

Fig. 6.22 Influence of viscosity on lift-interference parameter for models in slotted tunnel with solid side-walls

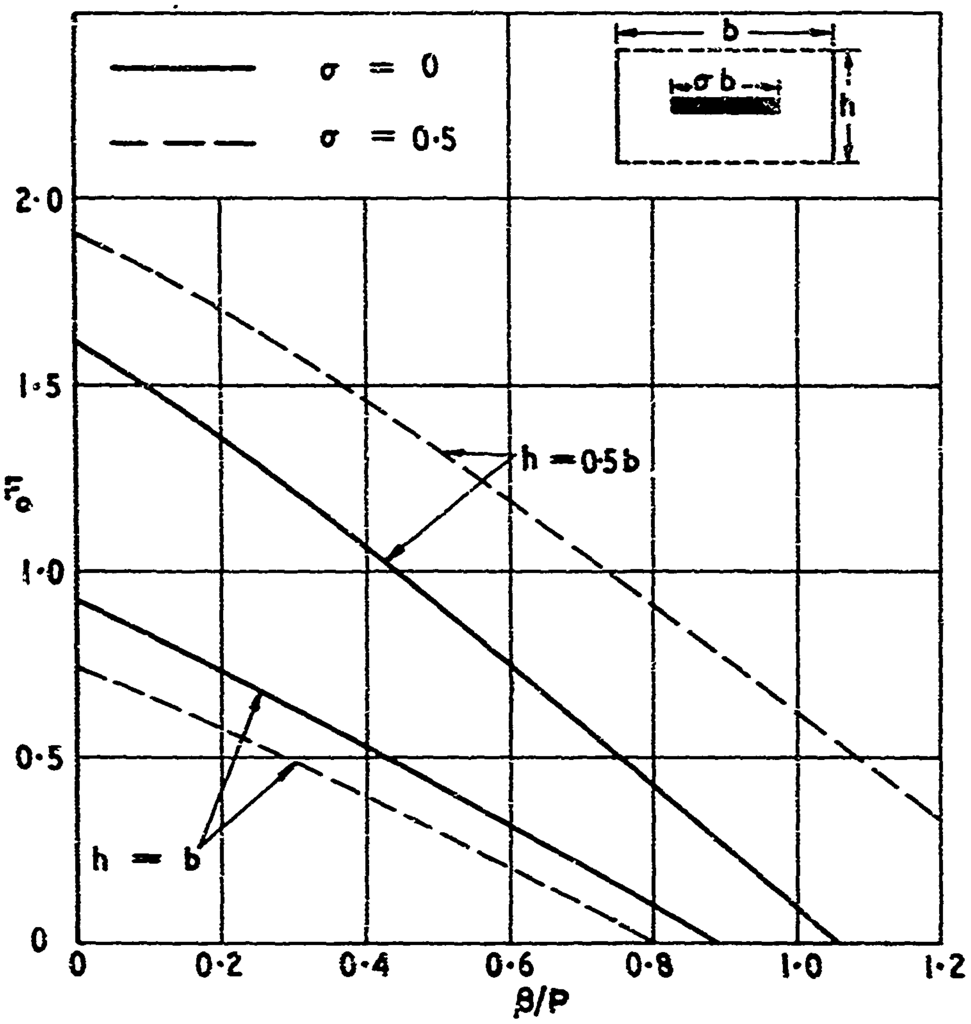

Fig. 6.23 Values of slot and porosity parameters required to give zero lift interference in slotted rectangular tunnels with solid side-walls

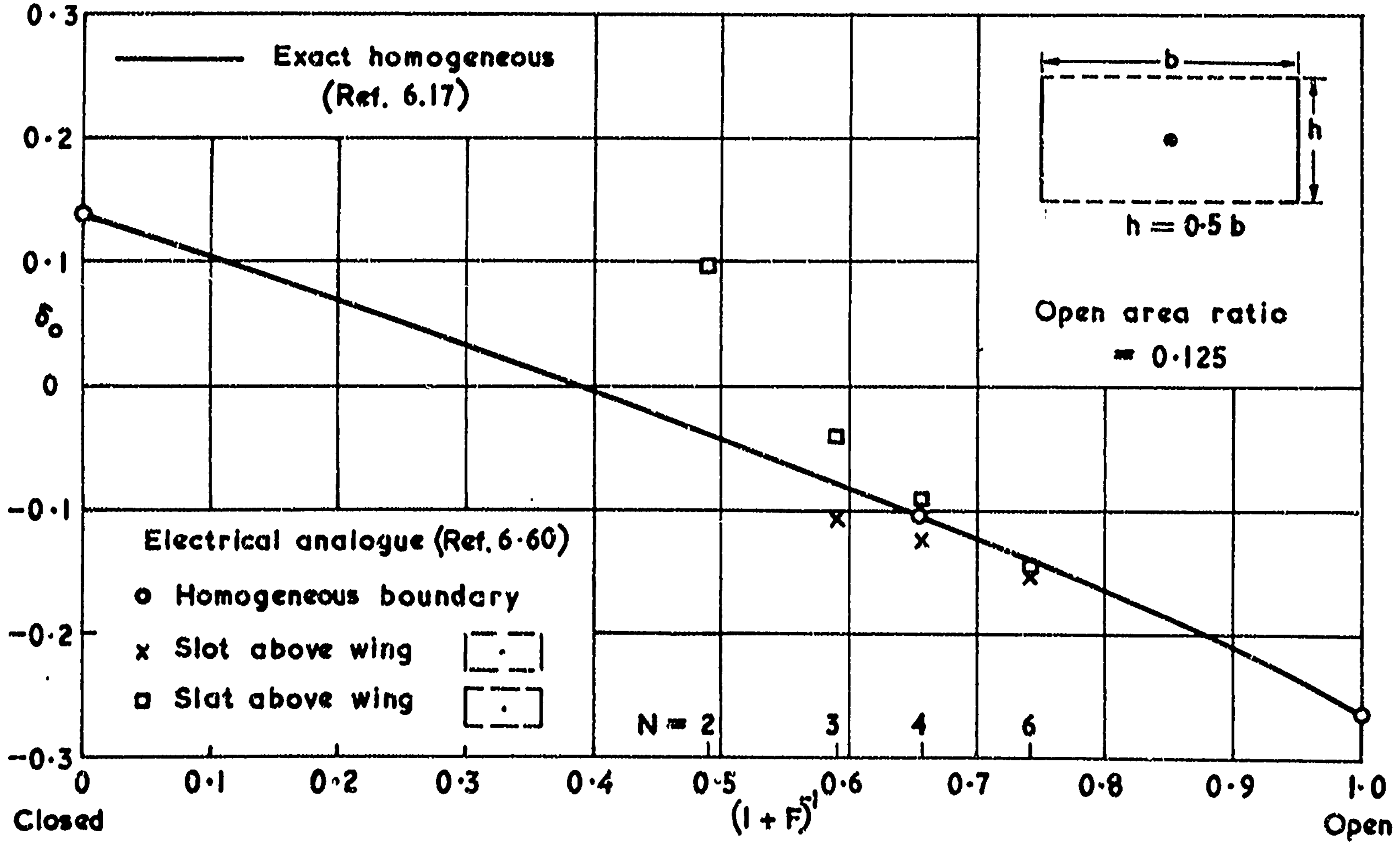

Fig. 6.24 Effect on lift interference of discrete slots in the roof and floor

Based on Ref. 6.60

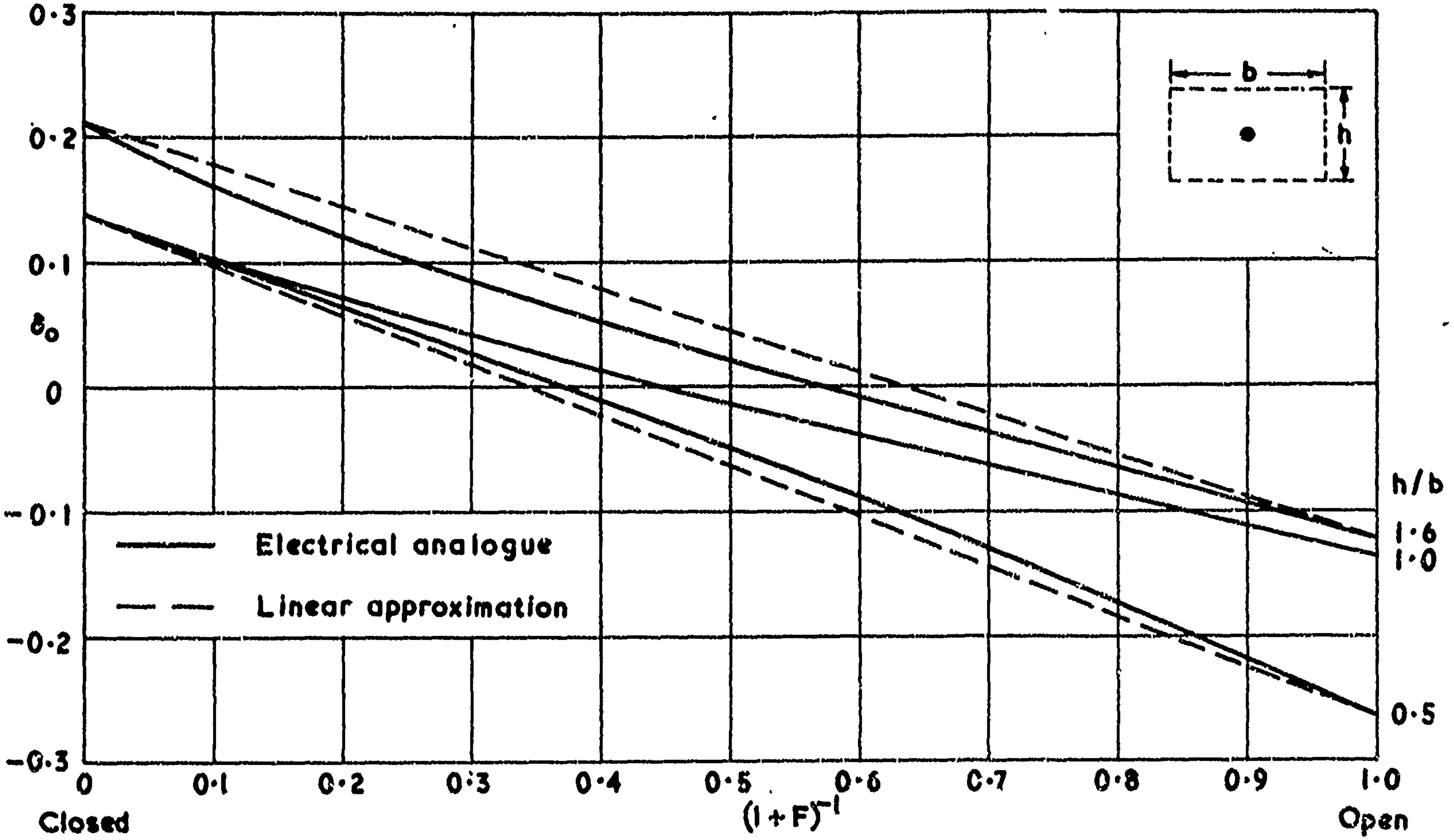

Fig. 6.25 Lift-interference parameter for small wings in rectangular tunnels with ideal slotted walls

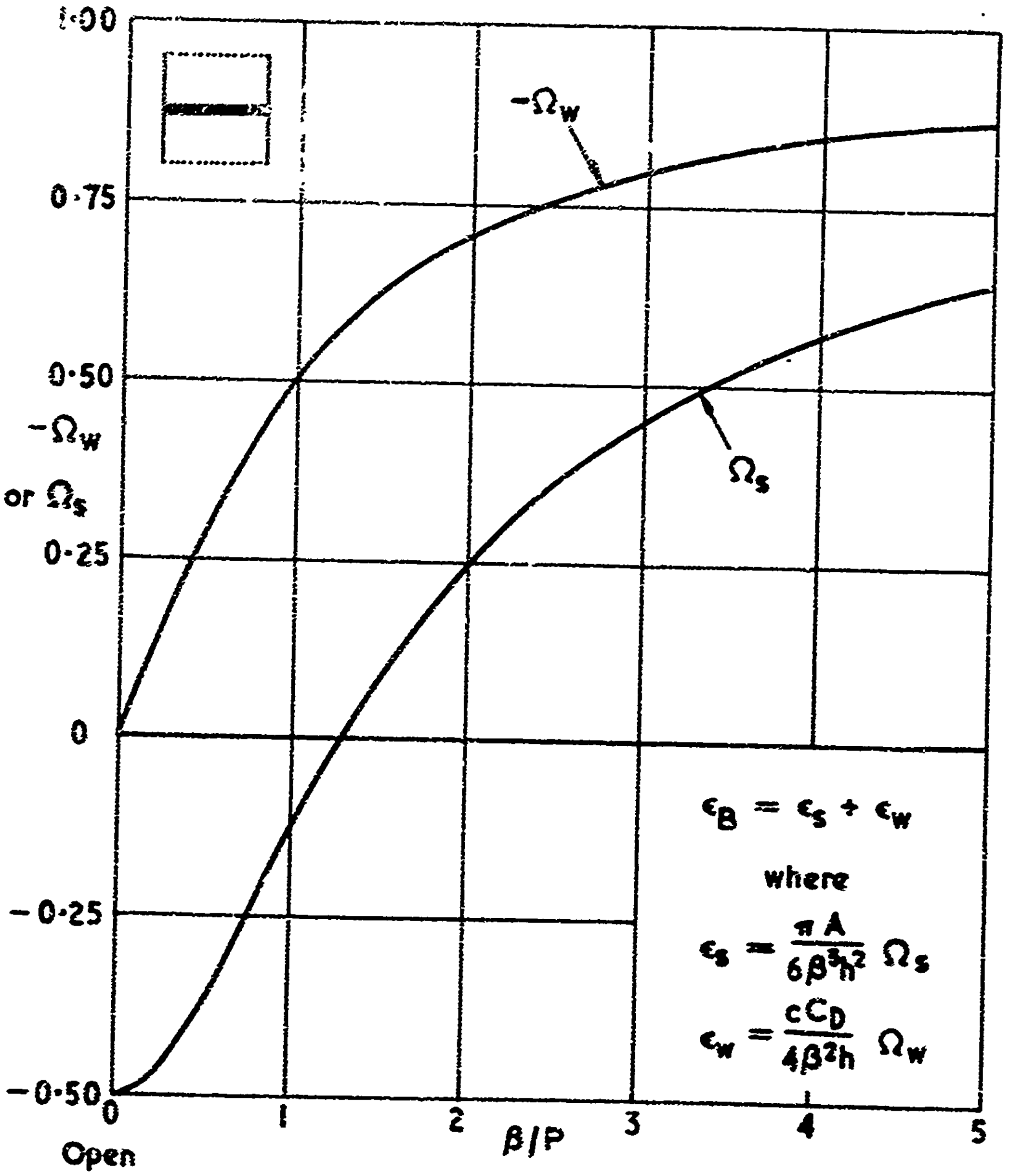

Fig. 6.26 Variation of blockage with wall porosity in two-dimensional perforated tunnel

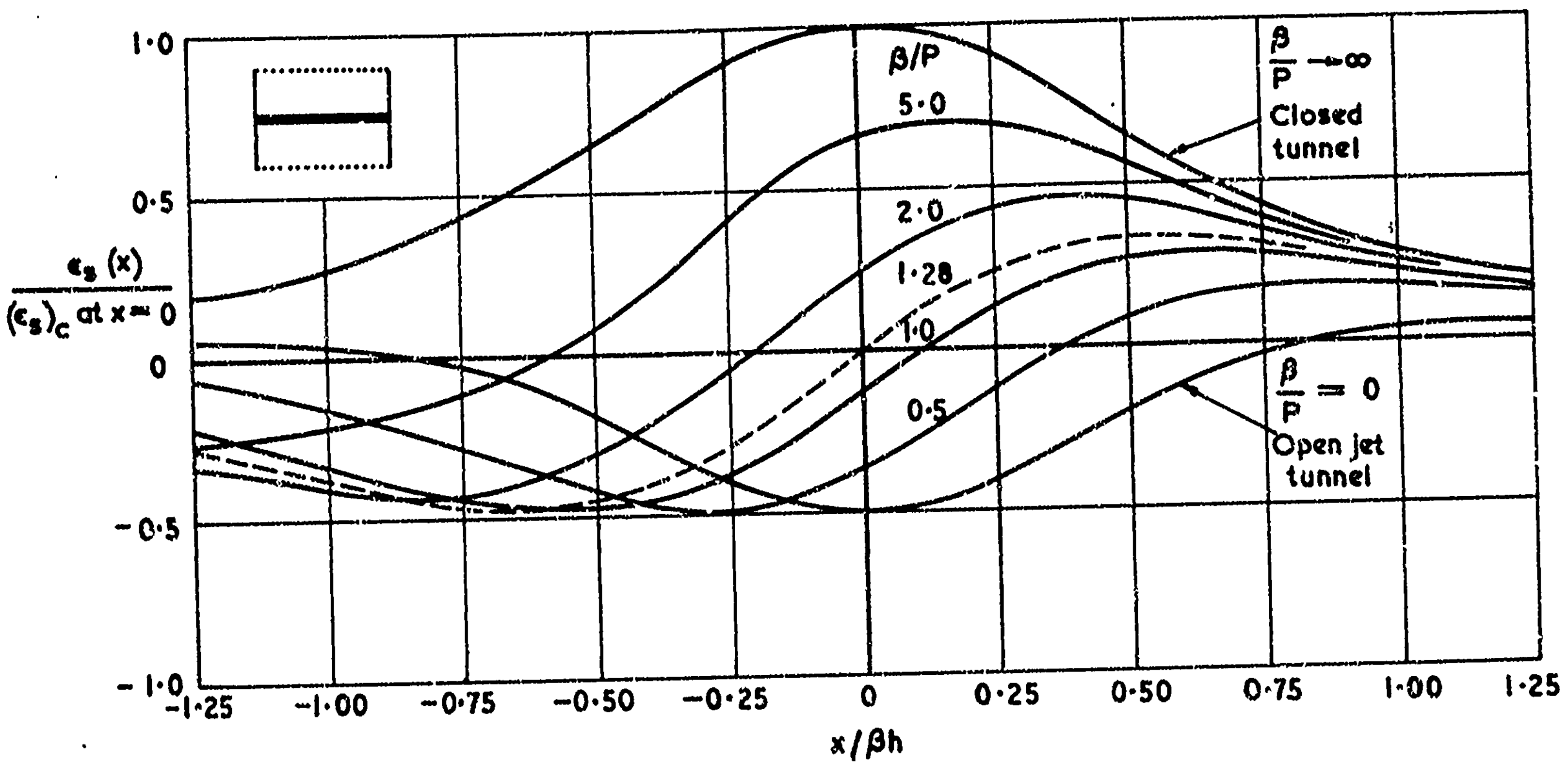

From Fig.13 of Ref.6.35

Fig. 6.27 Distribution of solid-blockage factor along two-dimensional perforated tunnel

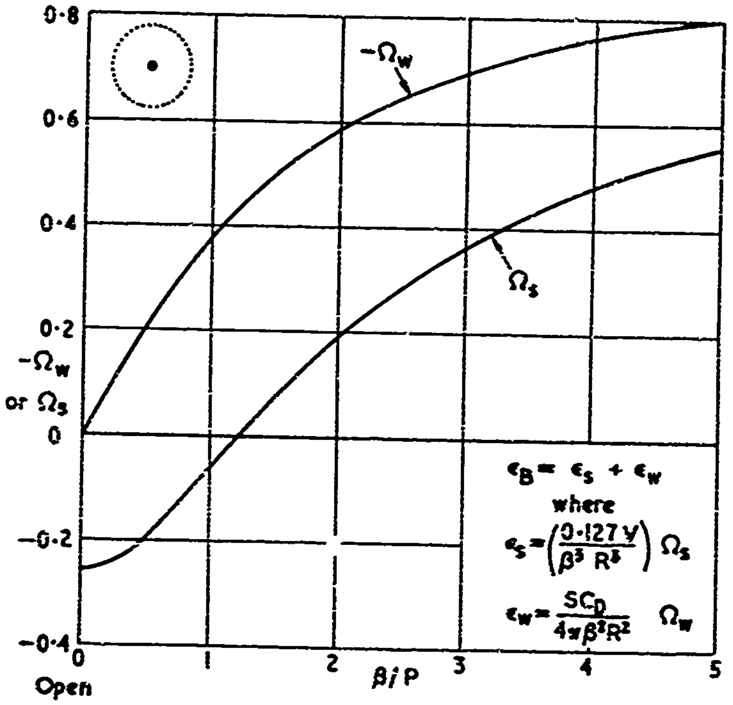

Fig. 6.28 Blockage factor for small model in perforated circular tunnel

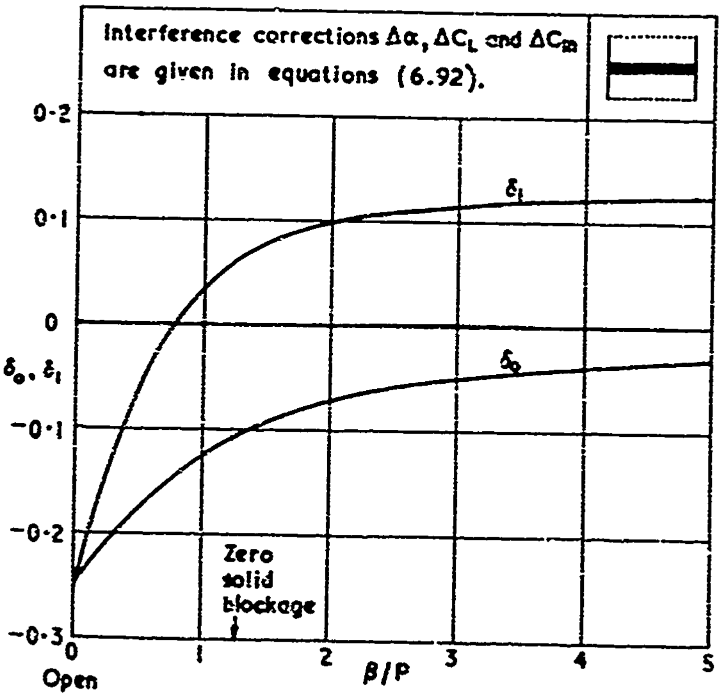

Fig. 6.29 Lift interference in a two-dimensional perforated tunnel

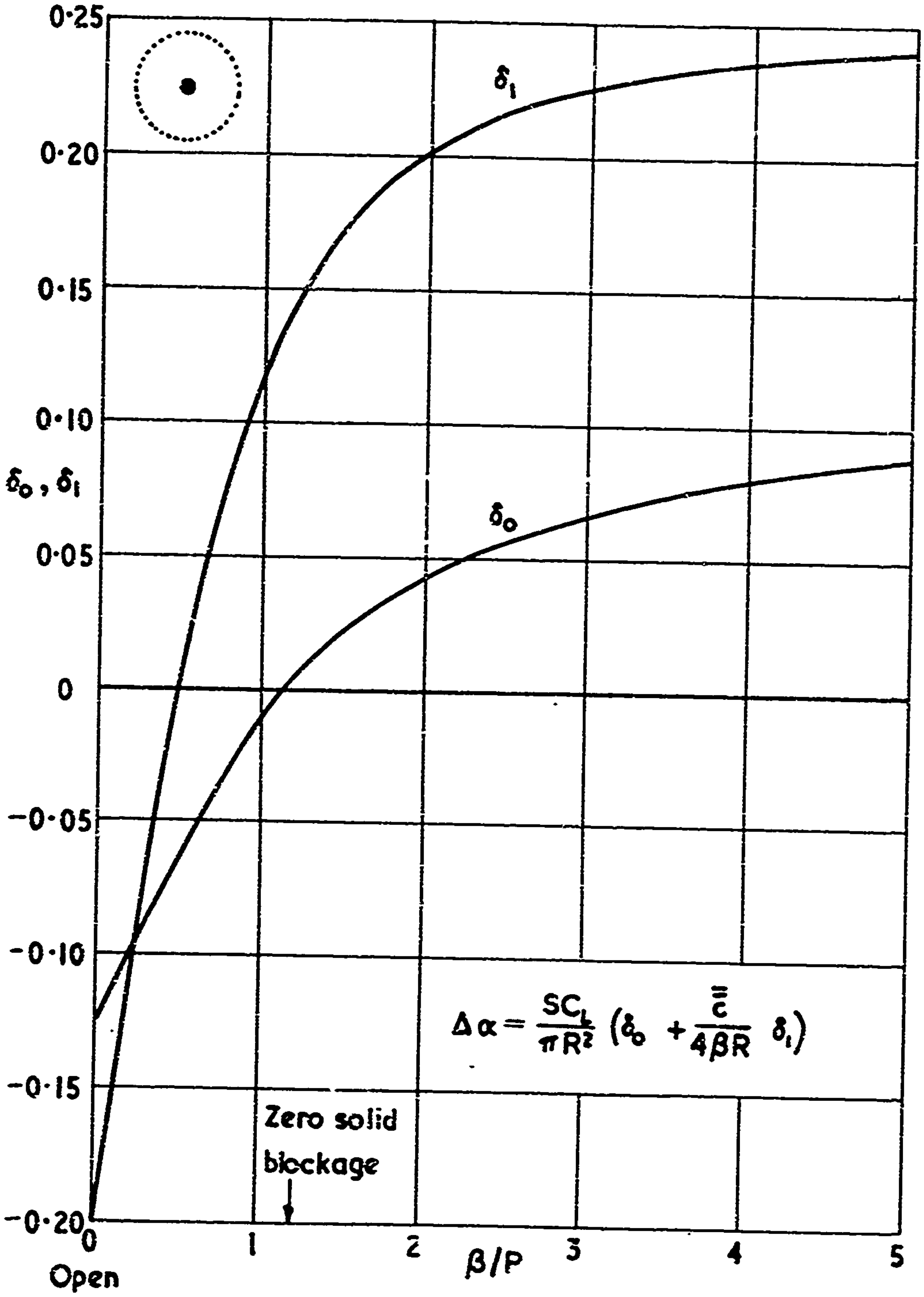

Fig. 6.30 Lift interference for a small model in a perforated circular tunnel

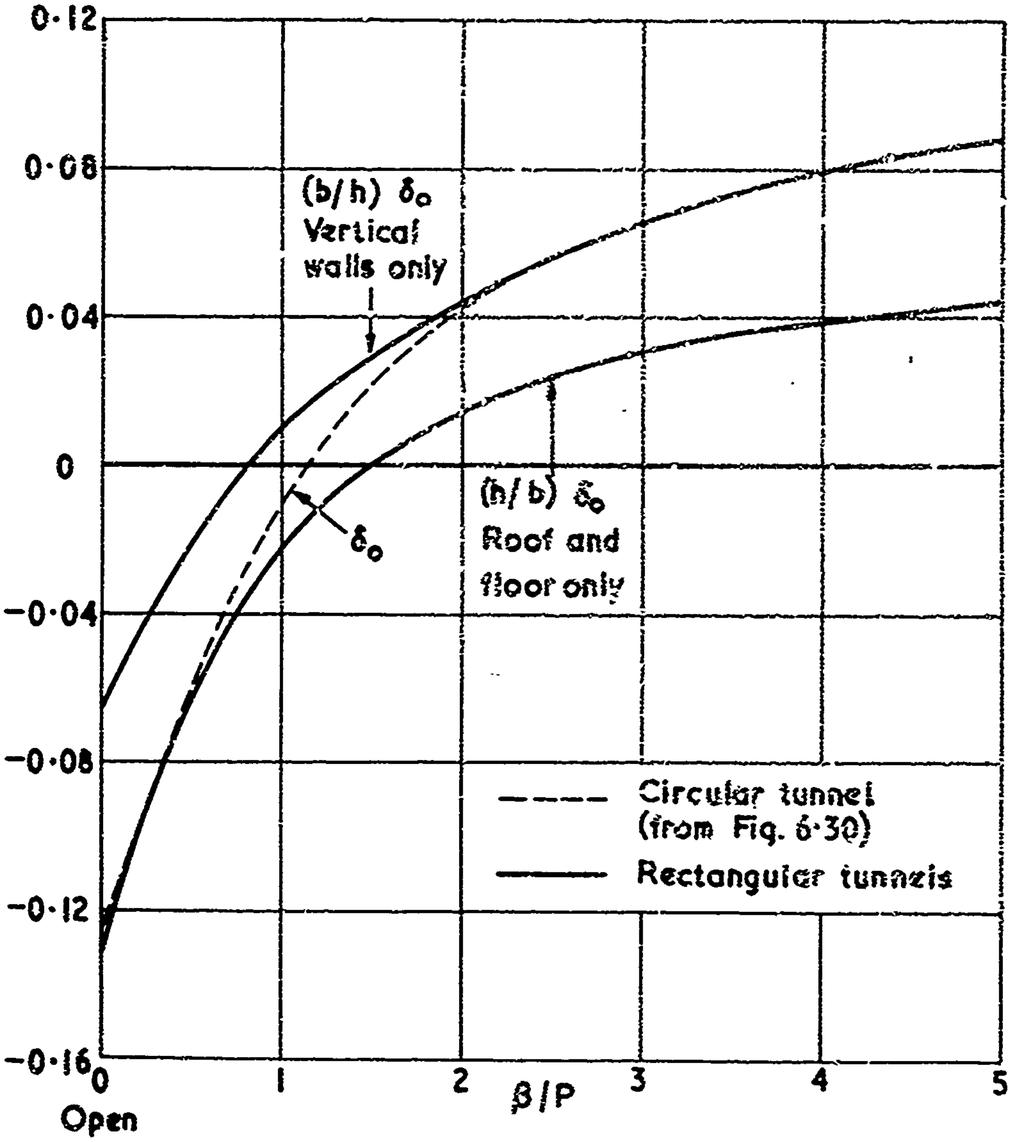

Fig. 6.31 Lift-interference parameter for small wing in special types of perforated tunnel

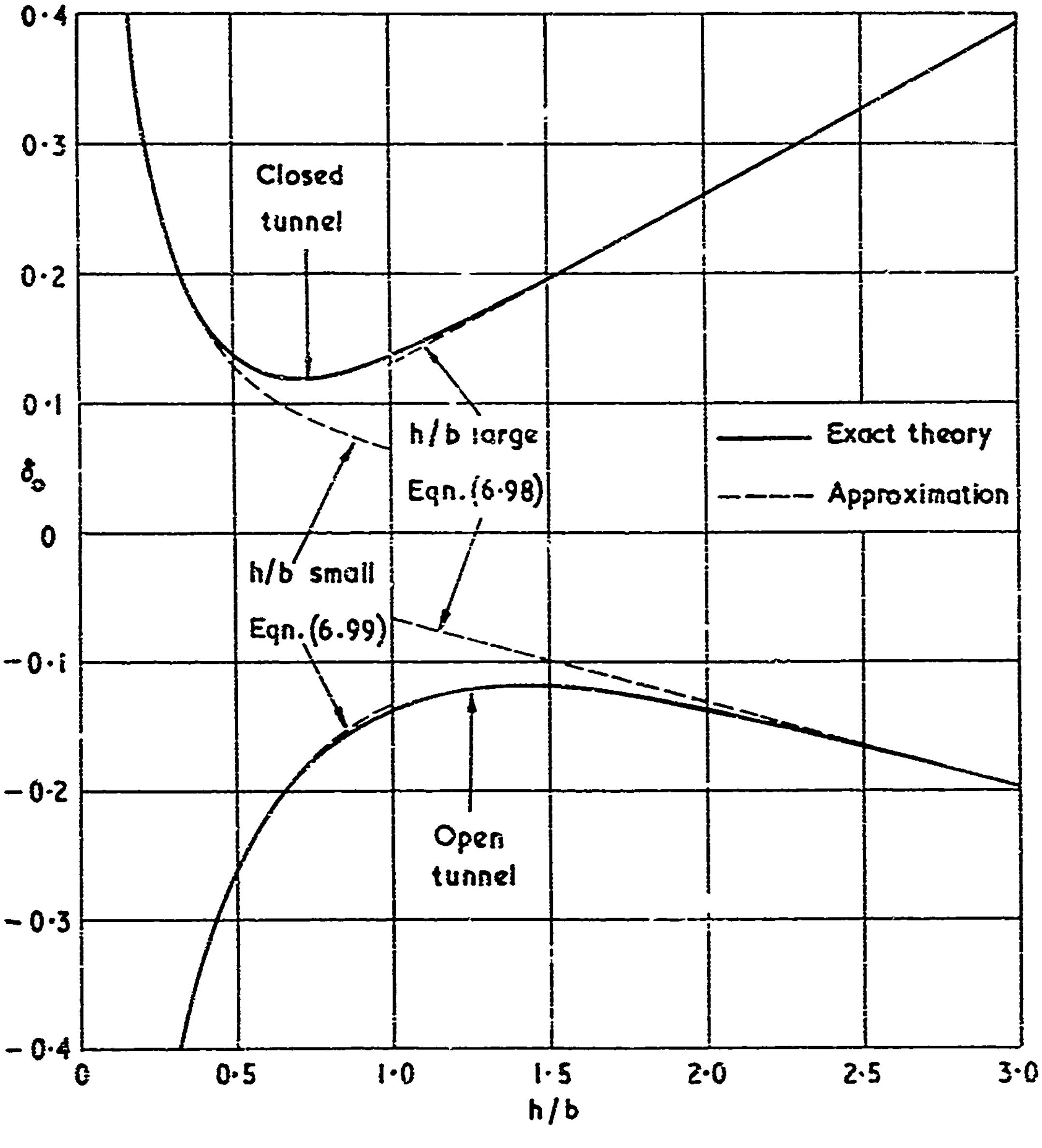

Fig. 6.32 Comparison of exact and approximate values of δ_0 for closed and open rectangular tunnels

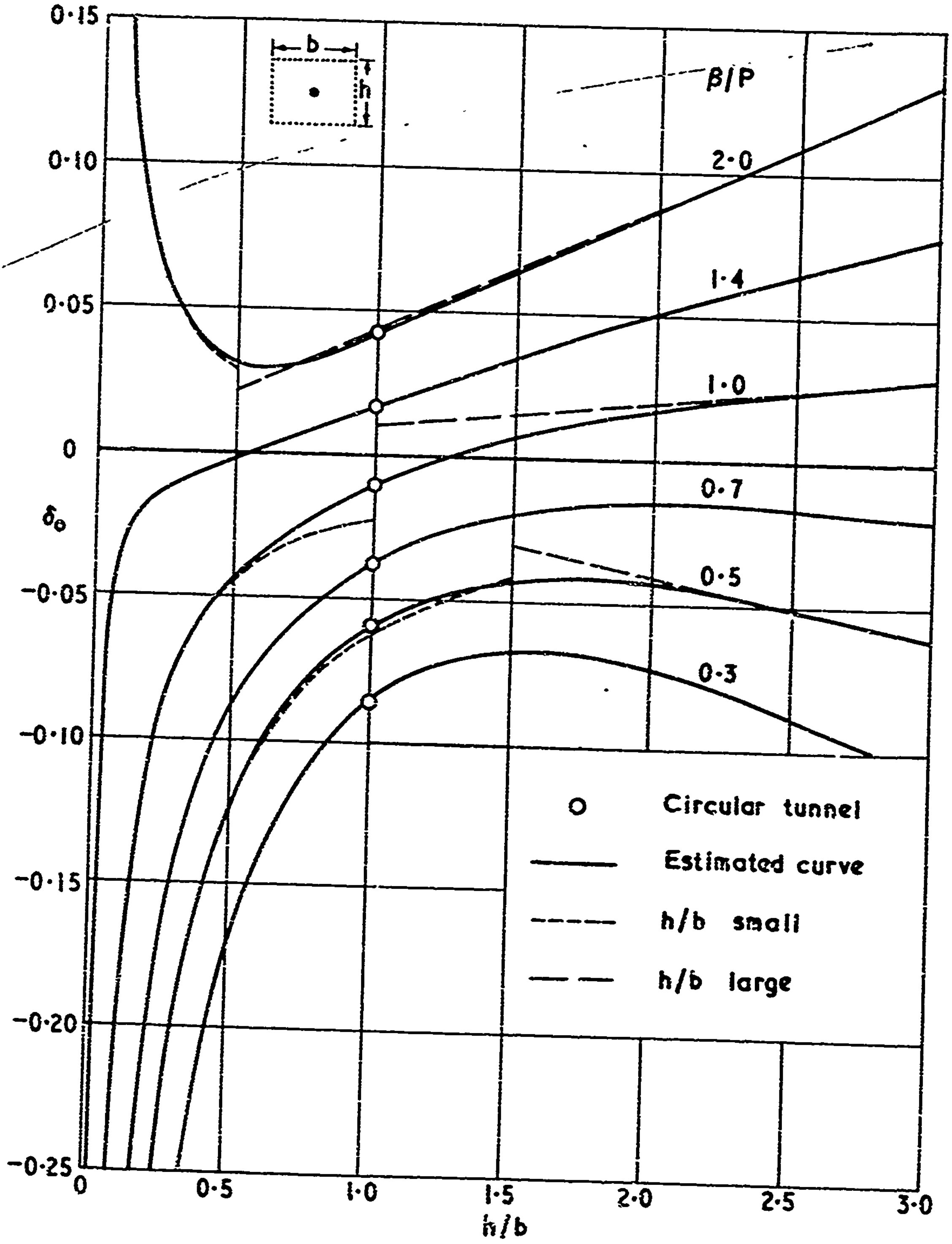

Fig. 6.33 Estimated lift-interference parameter for small wing in perforated rectangular tunnels of different porosity

CHAPTER VII

BLUFF BODIES AND HIGH-LIFT SYSTEMS

by

E.C.Maskell

Aerodynamics Department, Royal Aircraft Establishment,
Farnborough, Hampshire, England

CONTENTS

Page

LIST OF FIGURES 434

NOTATION 435

7.1 INTRODUCTION 437

7.2 BLOCKAGE EFFECTS ON BLUFF BODIES 438

7.3 LIFTING WINGS WITH SEPARATED FLOW 441
  7.3.1 Stalled Wings 441
  7.3.2 Wings with Hinged or Split Flaps 442
  7.3.3 Slender Wings with Leading-Edge Vortices 443

7.4 V/STOL CONFIGURATIONS 444
  7.4.1 Lifting Rotors 444
  7.4.2 Jet-Flaps in Closed Tunnels 446
  7.4.3 More General Configurations 448

REFERENCES 449

ADDITIONAL REFERENCES 450

FIGURES 452

LIST OF FIGURES

		Page
Fig.7.1	Model of flow past a bluff body	452
Fig.7.2	Invariance of C_D/k^2 for non-lifting square plates	452
Fig.7.3	Blockage effect on drag and base pressure for non-lifting square plates	453
Fig.7.4	Blockage effect on drag and base pressure for non-lifting two-dimensional plates	454
Fig.7.5	Variation of blockage factor with fineness ratio	455
Fig.7.6	Drag analysis for a lifting wing	456
Fig.7.7	Blockage corrections applied to lift and drag for two sizes of delta-wing-body combination	457
Fig.7.8	Wake of small rotor represented by a semi-infinite row of vertically directed doublets	458
Fig.7.9	Wake of a small rotor at non-zero angle of attack and its image below the floor of a closed tunnel	459
Fig.7.10	Interference parameter against wake skew-angle for small lifting rotors in closed rectangular tunnels	460
Fig.7.11	Interference parameter against breadth to height ratio of rectangular tunnels for rotors of different skew angle	461
Fig.7.12	Upwash interference against skew angle for a wake of horizontal doublets in closed rectangular tunnels	462
Fig.7.13	Effect of angle of attack on the interference parameter for small lifting rotors in a closed square tunnel	463
Fig.7.14	Assumed relationship between total downwash and interference upwash for a jet-flap wing	464
Fig.7.15	Typical constraint corrections for a jet-flap wing with 50° jet deflection	465

NOTATION

A	aspect ratio of wing
b	breadth of tunnel
B	cross-sectional area of wake at plane 2 (Fig.7.1)
c	chord of wing
C	cross-sectional area of tunnel
C_D	drag coefficient = D/qS
C_{Do}	profile drag coefficient
C_{Ds}	separated-flow component of C_D (Fig.7.6)
C_{Dv}	vortex-induced drag coefficient
C_J	jet momentum coefficient = momentum/qS
C_L	lift coefficient = lift/qS
C_p	pressure coefficient
C_{pb}	base-pressure coefficient
C_T	thrust coefficient = thrust/qS
D	drag
h	height of tunnel
k	base-pressure parameter in Equation (7.1)
l	length of body
l	distance along wake of lifting rotor
m =	B/S
p_b	base pressure
q	dynamic pressure of undisturbed stream
R	radius of vortex ring
s	semi-span of wing
S	area of planform of wing, reference area

t	thickness of body
U	velocity of undisturbed stream
w	z-component of velocity
w_0	upward velocity induced at centre of rotor
w_i	interference upwash velocity
W	non-dimensional downwash in Equation (7.13)
W_1	= W for vertically directed doublets in Equation (7.14)
W_2	= W for horizontally directed doublets in Equation (7.15)
x	streamwise distance
y	spanwise distance
z	upward distance
α	incidence of wing
Γ	circulation
δ_0	upwash interference parameter in Equation (7.18)
δ_h	upwash interference parameter for wake of horizontal doublets
δ_w	non-dimensional w_i in Equation (7.17)
Δ	prefix denoting increment due to wall interference
ϵ	blockage factor $= \Delta U/U$
ζ	$= 2z/h$
η	$= 2y/h$
θ	blockage factor for bluff-body flow in Equation (7.6)
ξ	$= 2x/h$
ρ	$= (\xi^2 + \eta^2 + \zeta^2)^{\frac{1}{2}}$
τ	angle of deflection of jet flap
χ	wake skew-angle of lifting rotor

Subscript

c	denotes corrected value.

BLUFF BODIES AND HIGH-LIFT SYSTEMS

E.C.Maskell

7.1 INTRODUCTION

The extent to which it is possible to establish corrections for boundary constraint on a given flow depends largely on the extent to which a theory of the corresponding unlimited flow has been developed. Thus, for any unlimited flow that is well represented by classical aerofoil theory, it is usually possible to derive constraint corrections more or less rigorously, as the foregoing chapters have shown. But for other kinds of flow field, some of which have assumed great practical importance in recent years, the situation is much less satisfactory, because the mechanism of non-streamline flows is much less well understood. The difficulty in such cases is a fundamental one, that of establishing a mathematical model of a flow that is sufficiently realistic and, at the same time, amenable to theoretical development; its resolution has been attempted in relation to only the few specific problems which form the basis of the present chapter.

The feature of an external flow that distinguishes one kind of flow field from another is the manner in which the wake, in particular the near wake, forms behind the body and interacts with the flow over the body itself. For most streamline flows this interaction is accounted for adequately, if the wake is represented simply as a plane sheet of streamwise trailing vortices. This is because the wake behind a streamline body is, by definition, thin, and because significant distortion from a plane sheet usually occurs too far downstream of the trailing edge to have much effect on the near field of the body.* In the flows considered here at least one of these simplifying properties is absent. In consequence, the appropriate mathematical models are both more difficult to justify on physical grounds, and less tractable theoretically than the streamline flow model.

The flows in question fall into two distinct groups, the first of which is typified by the flow past a bluff body. The wake in this case is far from thin, and its interaction with the near field of the body is not well understood. However, constraint corrections in closed tunnels have been derived by Maskell (Ref.7.1; 1963) by a method which relies heavily on limited experimental evidence. An interesting conclusion from this work is that distortion of the wake under constraint makes a significant contribution to the large blockage correction derived.

The second group of problems has arisen from increasing practical interest in recent years in V/STOL aircraft. The flows in this group are therefore of a kind in which lift is obtained, directly or indirectly, by the downward deflection of jets or slipstreams. Here the paths of jets or slipstreams are important features of the flows, which might be greatly affected by boundary constraint. Realistic mathematical models can usually be constructed if the effects of mixing at the boundaries of the jets or slipstreams are ignored, so that, in principle, the appropriate interactions can be taken into account. In practice, however, the resulting mathematical models are intractable. Considerable simplification is therefore inevitable, and the problem is to establish what kinds of simplification are justifiable.

---

* The slender wing is an important exception, in which the wake develops initially in the form of leading-edge vortices, often from the apex of the wing.

The most promising approaches to problems of this kind have been concerned with flows that can be regarded as essentially single-wake flows. Two examples are the flow past a helicopter, in which the dominant wake is evidently the slipstream of the rotor, and the flow past a jet-flap, in which the jet sheet simply replaces the usual trailing-vortex sheet. Heyson (Ref. 7.2; 1960) has treated the helicopter problem, using a simple linear approximation to the jet path. The method is physically convincing at the limits of hovering flight, and high forward speed. But, in general, interaction between the slipstream and the external flow would be expected to lead to a curved slipstream. However, until the effect of this curvature has been investigated for the helicopter in an unlimited stream, its neglect in the constraint problem is plainly inevitable. The flow past a jet-flap wing is more closely related to streamline flow, and has been treated as a simple extension of classical aerofoil theory by Maskell and Spence (Ref. 7.3; 1959). The further extension to the problem of boundary constraint has been given by Maskell (Ref. 7.4; 1959), who points out that distortion of the jet path by the constraint results in an effective change in the jet momentum coefficient. However, here again the approximation to the jet path employed in the theory is, to some extent, open to question, although there seems little doubt that a correction of the order of magnitude of that derived by Maskell is necessary.

More general V/STOL configurations employ multiple wakes, in that they usually consist of combinations of lifting wings with the deflected slipstreams of fans or jets in which the vortex wakes of the wings would be expected to follow markedly different paths from the slipstreams. The main problem, again, is to decide how necessary it is for these paths to be represented correctly. Heyson (Ref. 7.5; 1962) has proposed an extension of his lifting-rotor theory to the general flow, and there is evidence that the method has given plausible corrections in certain cases. However, the basic model is less convincing, on physical grounds, when applied to multiple-wake problems, which therefore seem to require much more attention. It is likely that the aerodynamics of such flows will often depend crucially on the mutual interference between the different wakes and slipstreams, and hence that it may be vital to determine, and interpret, the effect of boundary constraint on this interference. For purposes of this kind a more realistic mathematical model than Heyson's would be needed. But little further progress can be expected until the basic theory of such flows has advanced a great deal.

7.2 BLOCKAGE EFFECTS ON BLUFF BODIES

Following a comment by Glauert on the nature of the blockage effect associated with a thick bluff-body wake, Fage and Johansen (Refs. 7.6 and 7.7; 1927-28) made what appears to have been the first serious attempt to establish the magnitude of the effect experimentally, for the particular case of a two-dimensional flat plate normal to a wind stream. They tested several such plates, of different sizes, and so determined the drag coefficient corresponding to an unlimited stream by extrapolation of their measurements to zero size.

However, the attempt of Glauert to develop a correction formula in Equation (17.13) or (18.5) of Reference 7.8 was less successful - partly, perhaps, because he sought to make it too comprehensive. With greater understanding of the differences between the properties of the wakes of streamline and bluff bodies, it now seems unrealistic to suppose that the wall constraint on a bluff-body flow can be broken down into separate solid-blockage and wake-blockage effects. This sub-division is a physically realistic, and therefore useful, procedure when the influence of the wake on the form of the pressure field over the body can be regarded as a second-order effect, as it can be, for the most part, in streamline flow. But the pressure field over a bluff body depends crucially on the wake structure, and generally bears little relation to the inviscid, attached-flow, field of the body, from which the conventional solid-blockage effect derives.

The bluff-body flow evidently needs to be represented, from the outset, by a mathematical model that is quite different from that appropriate to streamline flow. But since very little is known about the internal mechanics of a bluff-body wake, there is little prospect of constructing a flow model that bears more than a superficial resemblance to the observed flow. The best that can be done at the present time is to ensure that the external effects of the wake are adequately reproduced in the model, and to take such account as is necessary of the internal field through empirically determined auxiliary equations designed to match the behaviour of the model under constraint to observation.

Maskell (Ref.7.1; 1963), has pointed out that the observed properties of the forward part of a bluff-body wake (i.e. forward of any substantial pressure recovery) are well represented by a model incorporating a stream surface extending downstream from the edge of the body; the static pressure on the stream surface is supposed constant, and equal to the base pressure p_b as far as the plane 2 in Figure 7.1, where the cross-sectional area of the wake is a maximum. The corresponding constant velocity he writes as kU. Then, if wall constraint is to be exactly equivalent to a simple increase in stream velocity, the form of the pressure distribution over the body must be invariant under constraint, and it follows that

$$\frac{C_D}{k^2} = \frac{C_D}{1 - C_{pb}} = \text{constant} \qquad (7.1)$$

independent of boundary constraint, where C_{pb} is the base-pressure coefficient, C_D is the drag coefficient D/qS, q the dynamic pressure of the undisturbed stream, and S a representative area of the body. It follows, also, that the velocity U_c of the unlimited stream which gives rise to a pressure distribution identical to that observed is such that $k_c U_c = kU$, and hence that

$$\frac{U_c^2}{U^2} = \frac{k^2}{k_c^2} = \frac{C_D}{C_{Dc}} . \qquad (7.2)$$

The relation (7.1) has been shown to hold experimentally (Fig.7.2) for a set of geometrically similar sharp-edged square plates, and is supposed to hold generally for incompressible flow in closed tunnels.

A further relation between the variables defining the flow model can de derived by considering the conservation of momentum within the control surface bounded by the walls of the wind tunnel, the surface of the body and the constant-pressure surface bounding the effective wake, and two planes normal to the undisturbed velocity vector - plane 1 lying upstream of the body, and plane 2 located where the cross-sectional dimensions of the wake are greatest. Neglecting certain supposedly small contributions, Maskell[7.1] has concluded that the momentum balance reduces approximately to

$$C_D = m(k^2 - 1 - mS/C) \tag{7.3}$$

where $m = B/S$, B is the cross-sectional area of the wake at the plane 2, and where $(mS/C)^2$ is taken to be negligibly small.

In order to complete the set of equations necessary to define the blockage effect completely, one further relation is required, to account for the distortion of the wake under constraint. The auxiliary relation adopted by Maskell can be put in the form

$$\frac{m}{m_c} = 1 - \frac{C_D - C_{Dc}}{(k^2 - 1)(k_c^2 - 1)} \frac{S}{C} \tag{7.4}$$

if terms of $O(S/C)^2$ are ignored, and is well supported by limited experimental data obtained with a series of square flat plates.

Equations (7.1) to (7.4) yield the correction formula

$$\frac{k^2}{k_c^2} = 1 + \frac{C_D}{k_c^2 - 1} \frac{S}{C} + O(S/C)^2 \tag{7.5}$$

which may be written, alternatively, in the more conventional form

$$\frac{\Delta q}{q} = \theta \frac{C_D S}{C} . \tag{7.6}$$

Here $\Delta q = q_c - q$ is the effective increase in dynamic pressure of the undisturbed stream due to contraint, $C_D S/C$ is the usual wake-blockage parameter, and

$$\theta = \frac{1}{k_c^2 - 1} \tag{7.7}$$

is the so-called blockage factor for the bluff-body flow.

If both the drag and the average base-pressure coefficient $C_{pb} = 1 - k^2$ are measured, k_c^2, and hence θ, can be determined from Equation (7.5) - most conveniently, perhaps, by means of the iteration formula

$$(k_c^2)_n = k^2 \left\{ 1 + \frac{1}{(k_c^2)_{n-1} - 1} \frac{C_D S}{C} \right\}^{-1} \tag{7.8}$$

where $(k_c^2)_n$ is the nth approximation to k_c^2, and the initial value $(k_c^2)_0 = k^2$. In this way Fail, Lawford and Eyre (Ref.7.9; 1957) have concluded that the blockage factor for rectangular flat plates varies with aspect ratio A in the following manner:

A	1	2	5	10	20	∞
θ	2.77	2.70	2.41	2.13	1.47	0.96

It turns out that the blockage factor varies very little in the interval $1 < A < 10$, where it lies roughly in the range $\theta = (5/2) \pm (1/4)$. In this range, therefore, the constant value $\theta = 5/2$ is unlikely to lead to appreciable error in practice.

The correction formulae from Equation (7.5) appropriate to drag and base pressure are given in both Figures 7.3 and 7.4. For square and two-dimensional flat plates respectively the theoretical straight lines against $C_D S/C$ are shown compared with experimental results. The blockage factor θ varies from about five times to twice the corresponding quantity for the wake blockage of streamline bodies (Chapter V).

More recent studies of blockage effects on bluff bodies are described in References 7.10 and 7.11. Lefebvre[7.10] gives results rather similar to those of Reference 7.1, and relates the geometric and aerodynamic blockage with particular reference to circular cones. Calvert[7.11] compares experiments on blunt-based bodies of revolution with the predictions of Reference 7.1 and concludes that the theory gives a good estimation of the blockage correction for fineness ratios $l/t < 3$, as shown in Figure 7.5. In the range $3 < l/t < 5.5$ Maskell's theory still leads to reasonable results, but the methods of Chapter V are more appropriate to the more slender non-lifting bodies.

7.3 LIFTING WINGS WITH SEPARATED FLOW

7.3.1 Stalled Wings

The breakdown of streamline flow past a wing of finite span gives rise to regions of separated flow that bear some resemblance to bluff-body wakes, and would therefore be expected to lead to blockage effects similar in kind to those treated in Section 7.2. In fact, experimental measurements by Kirby and Spence (Ref.7.12; 1955) in the wakes of models of particular delta-wing and swept-wing aircraft suggest that, for wings of moderate to small aspect ratio, the localised regions of separated flow that develop as such wings begin to stall resemble axisymmetric bluff-body wakes surprisingly closely. Furthermore, Fail et al.[7.9] have observed a strong tendency to axial symmetry in the wakes of non-axisymmetric bluff bodies. And Maskell has been led to suppose the tendency to axial symmetry in the separated flow region to be universal, within the practical range of wing shapes, and to give rise to the blockage factor $\theta = 5/2$ appropriate to most bluff-body flows.

However, the formulae derived in Section 7.2 cannot be applied directly to the partially stalled lifting wing, because its total drag is only partially related to the separated-flow regions. There are two other contributions to the total drag: the vortex-induced drag D_v, and the momentum defect associated with the wake within the streamline regions of the flow and corresponding to the conventional profile drag D_0. Hence, the drag coefficient that occurs in the blockage parameter is not the total drag coefficient C_D, but its separated-flow component

$$C_{DS} = C_D - C_{Dv} - C_{D0} . \qquad (7.9)$$

There remains the problem of determining the drag coefficient C_{DS} from normal experimental observations of lift and drag. Since great accuracy is not usually necessary, Maskell suggests that the most logical procedure is to define C_{DS} by extrapolation from the measured properties of the unstalled wing. Linear extrapolation of the appropriate part of the measured $C_D \sim C_L^2$ relation, sketched in Figure 7.6, is usually sufficient. But visual observation of the flow development, allowing the onset of flow separation to be located, obviously helps to identify the point at which the bluff-body type of blockage effect begins to make its appearance. It will be noticed that the procedure ensures that the derived C_{DS} is zero for the unstalled wing, as it should be.

It is convenient, in practice, to combine the blockage correction corresponding to separated flow with that appropriate to streamline flow in the following manner,

$$\frac{q_c}{q} = 1 + \frac{1}{2}\frac{S}{C}\left(C_{DR} + C_{D0}\right) + \frac{5}{2}\frac{S}{C}\left(C_D - C_{Dv} - C_{D0}\right) , \qquad (7.10)$$

where, for the sake of completeness, a drag coefficient C_{DR} associated with the support rig - and assumed here to correspond to streamline flow - has been included. The composite formula reduces automatically to the correct formula for streamline flow at incidences below that at which flow separation first occurs.

The effectiveness of the correction formula is indicated in Figure 7.7, which shows the results of applying it to data obtained with two models of an aircraft having a delta wing of aspect ratio 3.

For a stalled wing of infinite span there is no vortex-induced drag, and the drag coefficient appropriate to the blockage parameter is the total C_D if, as is usual, the total drag is predominantly due to the separated flow. The problem in this case is to assign a value to the blockage factor θ, and no doubt the best procedure is to measure the pressure distribution over the upper surface of the aerofoil and to derive the appropriate factor from Equation (7.5). However, from the limited experimental evidence available, θ seems unlikely to differ greatly from unity once the stall is fully developed.

7.3.2 Wings with Hinged or Split Flaps

Hinged or split flaps deflected near the trailing edges of wings also give rise to regions of separated flow similar to bluff-body wakes. It is reasonable to suppose, therefore, that the theory of Section 7.2 can again be used to calculate the blockage effect.

In this case the situation is much the same as that treated in Section 7.3.1, but with the important difference that some separated flow is present at all angles of incidence when the flaps are deflected. However, there is still a range of incidence over which the separated flow is restricted to the wakes of the flaps themselves, and in which the appropriate C_{Dv} can probably be defined with sufficient accuracy. Then, if C_{D0} is determined from the clean wing (i.e. with flaps undeflected), Equation (7.10) can be used as before, with C_{Ds} (= $C_D - C_{Dv} - C_{D0}$) non-zero at all angles of incidence.

The above procedure, though plausible, must be regarded as less well established than the application to stalled wings considered in Section 7.3.1, because it has been much less severely tested. In any event, for flap aspect ratios that are greater than 10, say, a blockage factor of 5/2 is most likely inappropriate. It would be reasonable to expect θ to fall as flap aspect ratio increases, roughly according to the table in Section 7.2.

7.3.3 Slender Wings with Leading-Edge Vortices

At angles of incidence less than some critical value, flow separation from the leading edges of slender wings gives rise to a characteristic vortex flow that bears no resemblance whatever to the bluff-body wake. In fact this kind of "separated flow" is much better regarded as a generalized form of the classical streamline flow. It is essentially steady, with a thin wake, but one that originates from all the edges of the wing, and not only from the trailing edge. The rolling-up of the wake, which is taken to occur predominantly downstream of the trailing edge in the classical flow model to form the so-called tip vortices, therefore begins at the apex of a slender wing and forms leading-edge vortices. In consequence, the appropriate blockage correction is of the streamline-flow kind, viz.,

$$\frac{q_c}{q} = \tfrac{1}{4} C_{D0} \frac{S}{C}, \qquad (7.11)$$

where C_{D0} is the profile-drag coefficient.

However, at the critical angle of incidence, the leading-edge vortices are said to break down. Their structure changes from the orderly streamline form to something much more unsteady, and generally enclosing substantial regions of reversed flow which, once again, bear some resemblance to axisymmetric bluff-body wakes. At the critical incidence, the vortex breakdown occurs in the neighbourhood of the trailing edge of the wing and, as incidence is increased, the point of breakdown moves forward towards the apex. At angles of incidence below the critical, vortex breakdown may still occur, but not sufficiently close to the wing to affect its near field materially.

It seems reasonable to suppose that a blockage effect similar to that experienced by a bluff body will be felt by the slender wing at angles of incidence higher than the critical. Moreover, since the regions of separated flow in the wake of a partially stalled wing of moderate sweepback have a similar vortex structure to that which follows vortex breakdown on more slender wings, it also seems reasonable to suppose that the same blockage factor $\theta = 5/2$ will be appropriate in both cases.

The point at which the higher blockage factor becomes applicable is perhaps best identified from visual observations of the vortex flow. However, there is some evidence to suggest that the procedure outlined in Section 7.3.1 may be satisfactory as most empirical $C_D \sim C_L^2$ curves for slender wings appear to exhibit a linear region for a substantial range of incidence below the critical.

7.4 V/STOL CONFIGURATIONS

7.4.1 Lifting Rotors

A wholly self-consistent mathematical model of a lifting rotor seems to follow from the apparently simple assumptions that the rotor itself can be represented as a uniformly loaded actuator disc, and that the effects of mixing between the slipstream and the external flow can be ignored. Thus a uniform rise in total head would be supposed to occur across both the rotor disc and the interface between the slipstream and the external flow. And the precise shape of this interface would be such as to make it a stream surface across which the static pressure varies continuously. However, such a model is not yet amenable to theoretical treatment, even for an unlimited mainstream, and further simplifying assumptions must be introduced.

In general, the interaction between slipstream and mainstream, implied in the boundary conditions at the interface, would be expected to result in a slipstream following a curved path and having cross-sections that become increasingly distorted downstream of the rotor disc. Of these two effects on the geometry of the slipstream, the former seems much the more important, since it implies a continuous transfer of downward momentum from the slipstream to the external flow downstream of the rotor. But theory has not yet advanced far enough to allow even this effect to be accounted for adequately, and the best that can be done at present is, following Heyson (Ref.7.2; 1960), to replace the true path of the slipstream by an appropriate linear approximation.

Heyson represents the rotor slipstream by a skewed elliptic vortex cylinder of uniform strength $d\Gamma/dl$, where Γ is the circulation associated with a length l along the skewed slipstream. The velocity field of the rotor in free air can then be calculated by integrating the Biot-Savart expression for the velocity field of a vortex element over the surface of the vortex cylinder. In particular, the upward induced velocity w_0 at the centre of the rotor, and normal to its tip-path plane, is given by

$$w_0 = -\frac{1}{2}\frac{d\Gamma}{dl} . \qquad (7.12)$$

In general, the upwash w associated with the semi-infinite vortex cylinder can be written in the form

$$w = w_0 \frac{S}{C}\left\{-\frac{2b}{\pi h}\bar{w}\left(\frac{2x}{h}, \frac{2y}{h}, \frac{2z}{h}\right)\right\} . \qquad (7.13)$$

where b and h are respectively the breadth and height of the wind-tunnel test section, C is its cross-sectional area, and S is the area of the rotor disc.

An alternative expression for the singularities representing the slipstream follows from the fact that each elementary vortex ring is exactly equivalent to a uniform doublet sheet, circumscribed by the ring, of total strength $\frac{1}{4}\Gamma R^2$, where R is the radius of the circular element. In consequence, the far field of the rotor reduces to the field of a semi-infinite line of point doublets, directed vertically downwards if the rotor disc is in a horizontal plane. Equation (7.12) relates the strength of the line of doublets to the upwash at the centre of the rotor, and the function W in the expression (7.13) reduces, in the far field*, to

$$W_1(\xi,\eta,\zeta) = \frac{\xi^2+\eta^2}{\rho^3(\rho+\zeta\cos\chi-\xi\sin\chi)} - \left\{\frac{\zeta+\rho\cos\chi}{\rho(\rho+\zeta\cos\chi-\xi\sin\chi)}\right\}^2 , \qquad (7.14)$$

where $\rho^2 = \xi^2+\eta^2+\zeta^2$ and χ is the skew angle of the wake defined in Figure 7.8.

The upwash field thus derived is related strictly to Cartesian axes fixed in the rotor, such that the axis Oz is normal to the rotor disc with z measured positive along the thrust line. It gives the true upwash relative to wind axes only if the rotor disc is at zero incidence. However, if the elementary doublets representing the slipstream are supposed always to be directed normal to the rotor disc, they are readily resolved into components directed horizontally forwards and vertically downwards, in wind axes, and the associated component fields can be superposed to yield the complete upwash field of the rotor at incidence (Fig.7.9).

Heyson expresses the upwash field due to a line of horizontally-directed doublets of strength $\frac{1}{4}\Gamma R^2$ in the form of Equation (7.13), as before, and the corresponding upwash function is

$$W_2(\xi,\eta,\zeta) = -\frac{\xi\zeta}{\rho^3(\rho+\zeta\cos\chi-\xi\sin\chi)} - \frac{(\xi-\rho\sin\chi)(\zeta+\rho\cos\chi)}{\rho^2(\rho+\zeta\cos\chi-\xi\sin\chi)^2} . \qquad (7.15)$$

The derivation of tunnel-wall corrections is now fairly straightforward, once the slipstream skew angle χ is known. Following usual practice in helicopter theory, Heyson takes

$$\tan\chi = -\frac{U\cos\alpha}{U\sin\alpha + w_c} , \qquad (7.16)$$

an expression for which there is some experimental support, and ignores any possible effect of constraint on χ in the immediate vicinity of the rotor. However, it is evident that, as the true slipstream approaches the floor of the wind tunnel its curvature increases rapidly. This effect is represented in Heyson's model by supposing that the slipstream follows its initial path until it strikes the tunnel floor, and then continues downstream coincident with the tunnel floor, as shown in Figure 7.9.

In consequence, there are two basic elements in the derivation of corrections. These are obtained by considering slipstreams composed of vertical and horizontal doublets, together with their first reflections in the tunnel floor, as illustrated in Figure 7.9. It will be noticed that the parts of the slipstreams coincident with the floor cancel each other when the doublets are vertically directed. but reinforce each other in the second case. Their upwash fields are readily obtained by superposition of fields from Equations (7.14) and (7.15) respectively.

---

* Heyson[7.2] gives also the general expression $W(\xi,\eta,\zeta)$ for a skewed cylinder of radius R.

Heyson considers two wind-tunnel configurations, both having solid lower boundaries. He then takes the remaining boundaries to be either wholly solid or wholly free, and expresses the interference velocity at the centre of the test section in the form

$$w_i = \delta_w \frac{S}{C} w_0 . \tag{7.17}$$

Some indication of its dependence on χ , α and b/h , for the two types of tunnel, is provided in Figures 7.10 to 7.13, where for consistency with the foregoing chapters

$$\delta_0 = -\tfrac{1}{4}\,\delta_w \quad , \tag{7.18}$$

is plotted. In particular, it should be noted that at high forward speeds, when slipstream skew angles are close to 90°, the corrections are the same as those for a wing, as they evidently should be; at very low speeds, i.e., small skew angles, they are largely determined by the floor of the wind tunnel, and the interference upwash at the rotor is large.

Heyson points out that care is needed in the interpretation of the interference field. In hover, and at low forward speeds, the rotor performance is governed primarily by the change in inflow rather than by the change in effective incidence. He suggests, therefore, that a possible interpretation of the results is that the interference velocity corresponds to a change in rate of climb (or sink) between corresponding wind-tunnel and free-air conditions.

7.4.2 Jet-flaps in Closed Tunnels

The main differences between a jet-flap and a conventional trailing-vortex wake are that the vortex representation of the jet sheet includes bound-vortex elements of strength proportional to the jet-momentum coefficient C_J and that there is local curvature of the sheet. The presence of these bound-vortex elements gives rise to a substantially larger circulation about the wing than would otherwise occur; in consequence, the effect of wind-tunnel constraint on their strength must be considered carefully. There will be additional curvature of the jet sheet due to constraint, leading to stronger bound vortices in the jet than would occur in an unlimited stream with the same jet-momentum coefficient C_J and jet-deflection angle τ . It is essential, therefore, that this wall-induced curvature be taken into account.

Maskell (Ref.7.4; 1959) has considered the constraint problem for the jet-flap in a closed wind-tunnel, as an extension of the unlimited-stream theory given by Maskell and Spence[7.3]. The main problem is one of interpretation. The interference velocity field can be largely determined as for a three-dimensional wing, so that the interference upwash at the wing and at infinity downstream are known. However, it is the variation of upwash between these limits that determines the curvature of the jet path, and hence the bound-vortex strength, and Maskell chooses to represent this variation by an interpolation that leads to a simple interpretation of the effect of the induced curvature. He points out that, if the interference upwash w_i is related linearly to the total downwash $-w$ in the manner shown in Figure 7.14, the induced curvature is equivalent to an increment ΔC_J in jet-momentum coefficient. The particular choice of interpolation in w_i is, of course, open to question. But the conclusion that the effect can be interpreted as a correction to C_J seems sound, and the order of magnitude derived by Maskell is probably correct.

The first-order effects of constraint are obtained as a correction to incidence

$$\Delta\alpha = \delta_0 \frac{SC_L}{C}\left[1 + \frac{2C_J}{\pi A}\right]^{-1} . \tag{7.19}$$

where δ_0 takes the classical value from Chapter III, and a correction to jet-momentum coefficient

$$\frac{\Delta C_J}{C_J} = \frac{\Delta\alpha}{\tau + \alpha + (w/U)_\infty} , \tag{7.20}$$

where

$$\left(\frac{w}{U}\right)_\infty = -\frac{2C_L}{\pi A + 2C_J} . \tag{7.21}$$

The application of the corrections requires some care, since the lift and thrust forces measured in the wind tunnel are of the same order of magnitude. In consequence, when these forces are resolved normal and parallel to the effective stream direction, increments to lift and thrust coefficients result, of magnitude

$$\left.\begin{aligned} \Delta C_L &= C_T\Delta\alpha + \Delta C_J \sin(\tau + \alpha) \\ \Delta C_T &= -C_L\Delta\alpha + \Delta C_J \cos(\tau + \alpha) \end{aligned}\right\} , \tag{7.22}$$

where $\Delta\alpha$ and ΔC_J are given in Equations (7.19) and (7.20). If a drag coefficient is defined according to

$$C_D = C_J - C_T , \tag{7.23}$$

then

$$\Delta C_D = \Delta C_J - \Delta C_T$$

and Equations (7.22) can be expressed in the alternative form

$$\left.\begin{aligned} \frac{\Delta C_L}{\Delta\alpha} &= -C_D + C_J\left(1 + \frac{\sin(\tau + \alpha)}{\tau + \alpha + (w/U)_\infty}\right) \\ \frac{\Delta C_D}{\Delta\alpha} &= C_L + C_J\left(\frac{1 - \cos(\tau + \alpha)}{\tau + \alpha + (w/U)_\infty}\right) \end{aligned}\right\} . \tag{7.24}$$

The corrections from Equations (7.19) to (7.22) for a typical wind-tunnel experiment[7.13] are plotted in Figure 7.15. For comparison, the effect of ignoring the correction to ΔC_J, as in Glauert's[7.8] classical theory, is also shown. However, there is, as yet, no experimental confirmation that the magnitudes of the corrections are adequate in practice.

Reference should be made to Maskell's[7.4] original paper for a discussion of the effect of boundary constraint on the performance of the tailplane of a jet-flap aircraft.

7.4.3 More General Configurations

More general V/STOL configurations must be expected to require representation by mathematical models incorporating more than one wake or slipstream. If the overall performance of a configuration of this kind depends crucially on the mutual interference between the different lifting elements and their wakes or slipstreams, there seems little prospect of deriving adequate wind-tunnel corrections until the nature of the interference is better understood than it is at present. Much depends on the importance of bound vorticity of the kind included in a jet sheet and related to its curvature. But this problem has not yet been considered generally.

It may be that the jet-flap effect can be largely ignored in relation to jets and slipstreams of initially circular cross-section. Nevertheless, fair approximations to the true paths of the elements of the multiple wakes, and to their relative vortex or doublet strengths, would no doubt prove essential. Provided that Heyson's lifting-rotor model is adequate for the single-rotor case, it can be extended, plausibly, to twin rotors with separate wakes. But the combination of, say, a fan with a conventional lifting wing appears to be too complex to handle in this manner.

Heyson (Ref.7.5; 1962) has suggested that such general problems might be treated by a simple extension to his lifting-rotor theory, in which the multiple wakes are approximated by a single mean rotor wake, the parameters of which are determined by the measured lift and drag. He has given an extremely comprehensive theory based on this simple concept and tables of interference factors in a series of reports[7.5, 7.14–7.17], to which reference should be made for the detailed corrections. But the theory would seem to be most plausible when a single wake or slipstream predominates.

Several experimental studies have been made of wind-tunnel interference on V/STOL configurations, notably by Grunwald[7.18, 7.19] and by Davenport and Kuhn[7.20]. The broad conclusion from these particular investigations seems to be that Heyson's general theory accounts for most of the interference effects on lift and drag, but may fail to correct pitching moments adequately. Further work is needed before these conclusions can be generalized to other configurations. Similar caution is advocated in an independent review by Templin[7.21], who discusses the magnitude of wall interference by Heyson's theory in relation to acceptable sizes of model and wind tunnel.

REFERENCES

7.1 Maskell, E.C. *A Theory of the Blockage Effects on Bluff Bodies and Stalled Wings in a Closed Wind Tunnel.* ARC R & M 3400, 1963.

7.2 Heyson, H.H. *Jet-Boundary Corrections for Lifting Rotors Centered in Rectangular Wind Tunnels.* NASA Tech. Report R-71, 1960.

7.3 Maskell, E.C., Spence, D.A. *A Theory of the Jet Flap in Three Dimensions.* Proc. Roy. Soc., Series A, Vol.251, 1959, pp.407-425.

7.4 Maskell, E.C. *The Interference on a Three-Dimensional Jet-Flap Wing in a Closed Wind Tunnel.* ARC R & M 3219, 1959.

7.5 Heyson, H.H. *Linearized Theory of Wind-Tunnel Jet-Boundary Corrections and Ground Effect for VTOL-STOL Aircraft.* NASA Tech. Report R-124, 1962.

7.6 Fage, A., Johansen, F.C. *On the Flow of Air behind an Inclined Flat Plate of Infinite Span.* ARC R&M 1104, 1927. Proc. Roy. Soc., Series A, Vol.116, 1927, pp.170-197.

7.7 Fage, A., Johansen, F.C. *The Structure of Vortex Sheets.* ARC R & M 1143, 1928. Phil. Mag., Vol.5, 1928, pp.417-441.

7.8 Glauert, H. *Wind Tunnel Interference on Wings, Bodies and Airscrews.* ARC R & M 1566, 1933.

7.9 Fail, R., et al. *Low-Speed Experiments on the Wake Characteristics of Flat Plates Normal to an Air Stream.* ARC R & M 3120, 1957.

7.10 Lefebvre, A.H. *A Method of Predicting the Aerodynamic Blockage of Bluff Bodies in a Ducted Airstream.* Coll. Aero. (Cranfield) Report 188. ARC Report 27,859, 1965.

7.11 Calvert, J.R. *Blockage Corrections for Blunt-Based Bodies of Revolution.* J. Roy. aeron. Soc., Vol. 70, 1966, pp.532-533.

7.12 Kirby, D.A., Spence, A. *Low-Speed-Tunnel Model Tests on the Flow Structure behind a Delta-Wing Aircraft and a 40 deg Swept-Wing Aircraft at High Incidences.* ARC R & M 3078, 1955.

7.13 Foster, D.N. Private communication, 1966.

7.14 Heyson, H.H. *Tables of Interference Factors for Use in Wind-Tunnel and Ground-Effect Calculations for VTOL-STOL Aircraft. Part I - Wind Tunnels Having Width-Height Ratio of 2.0.* NASA Tech. Note D-933, 1961.

7.15 Heyson, H.H.	*Tables of Interference Factors for Use in Wind-Tunnel and Ground-Effect Calculations for VTOL-STOL Aircraft. Part II - Wind Tunnels Having Width-Height Ratio of 1.5.* NASA Tech. Note D-934, 1961.
7.16 Heyson, H.H.	*Tables of Interference Factors for Use in Wind-Tunnel and Ground-Effect Calculations for VTOL-STOL Aircraft. Part III - Wind Tunnels Having Width-Height Ratio of 1.0.* NASA Tech. Note D-935, 1961.
7.17 Heyson, H.H.	*Tables of Interference Factors for Use in Wind-Tunnel and Ground-Effect Calculations for VTOL-STOL Aircraft. Part IV - Wind Tunnels Having Width-Height Ratio of 0.5.* NASA Tech. Note D-936, 1961.
7.18 Grunwald, K.J.	*Wall Effects and Scale Effects in V/STOL Model Testing.* Presented at Aerodynamic Testing Conference at Washington, March 1964.
7.19 Grunwald, K.J.	*Experimental Study of Wind-Tunnel Wall Effects and Wall Corrections for a General-Research V/STOL Tilt-Wing Model with Flap.* NASA Tech. Note D-2887, 1965.
7.20 Davenport, E.E., Kuhn, R.E.	*Wind-Tunnel-Wall Effects and Scale Effects on a VTOL Configuration with a Fan Mounted in the Fuselage.* NASA Tech. Note D-2560, 1965.
7.21 Templin, R.J.	*The Choice of Working Section Size and Shape for V/STOL Wind Tunnels.* NRC (Canada) Quarterly Bulletin DME/NAE 1965(4), 1965.

ADDITIONAL REFERENCES FOR CHAPTER VII

Butler, S.F.J., Williams, J.	*Further Comments on High-Lift Testing in Wind Tunnels with Particular Reference to Jet-Blowing Models.* AGARD Report 304, 1959.
Duquenne, R., Werlé, H.	*Effets de Paroi sur une Aile avec Soufflage.* AGARD Report 305, 1959.
Ganzer, V.M., Rae, W.H.	*An Experimental Investigation of the Effect of Wind Tunnel Walls on the Aerodynamic Performance of a Helicopter Rotor.* NASA Tech. Note D-415, 1960.
Heyson, H.H.	*Wind-Tunnel Wall Interference and Ground Effect for VTOL-STOL Aircraft.* J. Am. Helicopt. Soc., Vol.6, 1961, pp.1-9.

de Jager, E.M. *Two-Dimensional Tunnel-Wall Corrections for a Wing with a Blown Flap between Two Parallel Walls.* NLR (Netherlands) Report W.8, 1961.

de Jager, E.M., van Spiegel, E. *Calculated Tunnel-Wall Corrections for Two-Dimensional High-Lift Wings.* NLL (Netherlands) Report MP.181, 1959.

Kuhn, R.E., Naeseth, R.L. *Tunnel-Wall Effects Associated with VTOL-STOL Model Testing.* AGARD Report 303, 1959.

Wells, W.J. *Wind Tunnel Corrections for a Helicopter Rotor in Forward Flight.* United Aircr. Corp. Report M-0554-4, 1955.

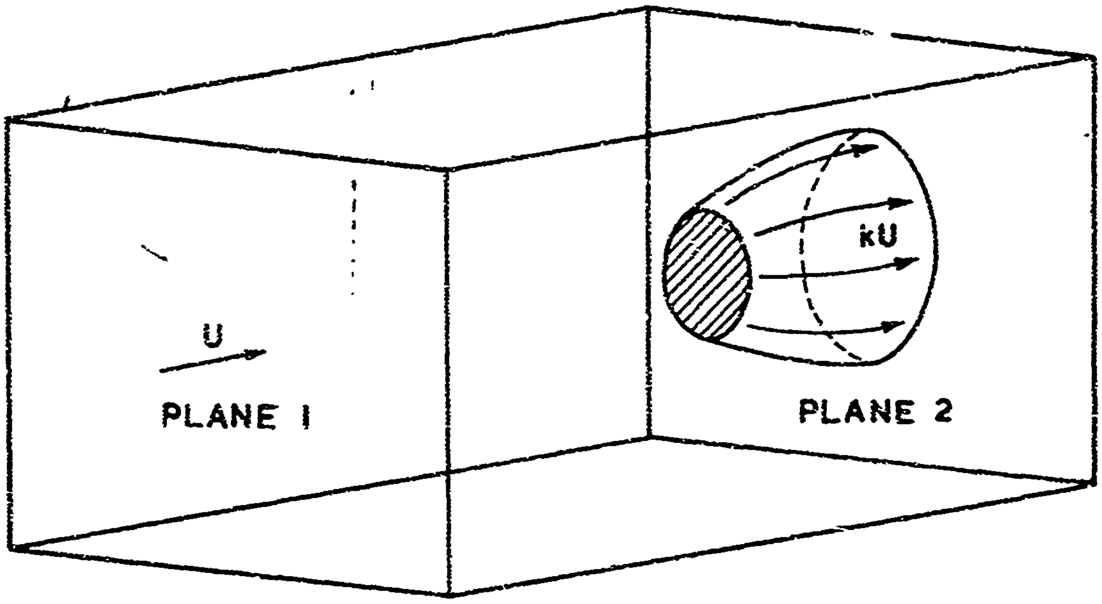
U
PLANE I
kU
PLANE 2

Fig.7.1 Model of flow past a bluff body

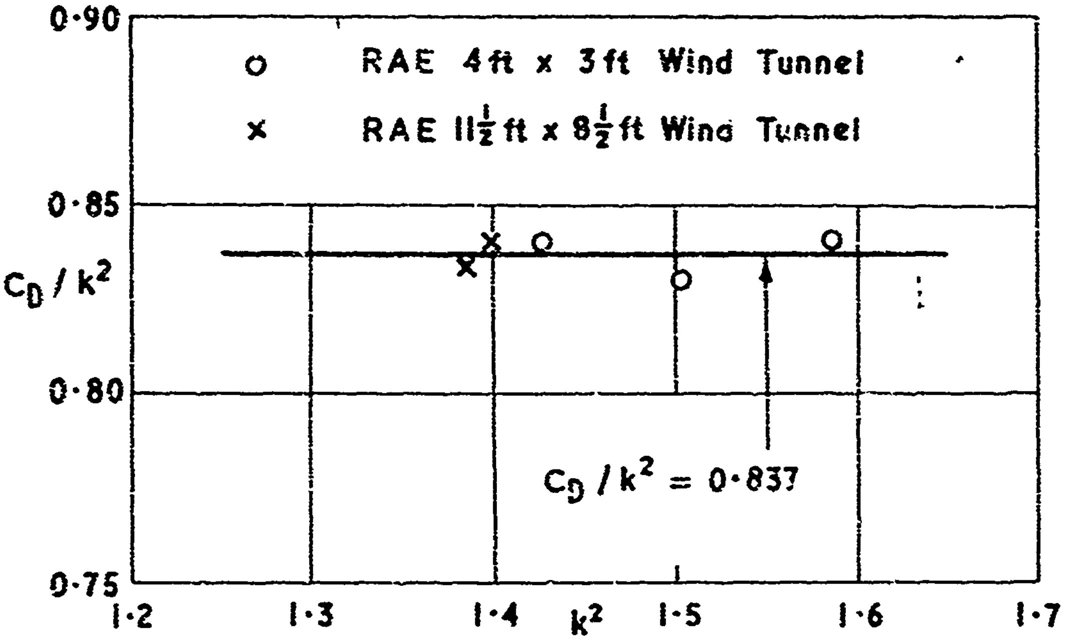

Fig.7.2 Invariance of C_D/k^2 for non-lifting square plates

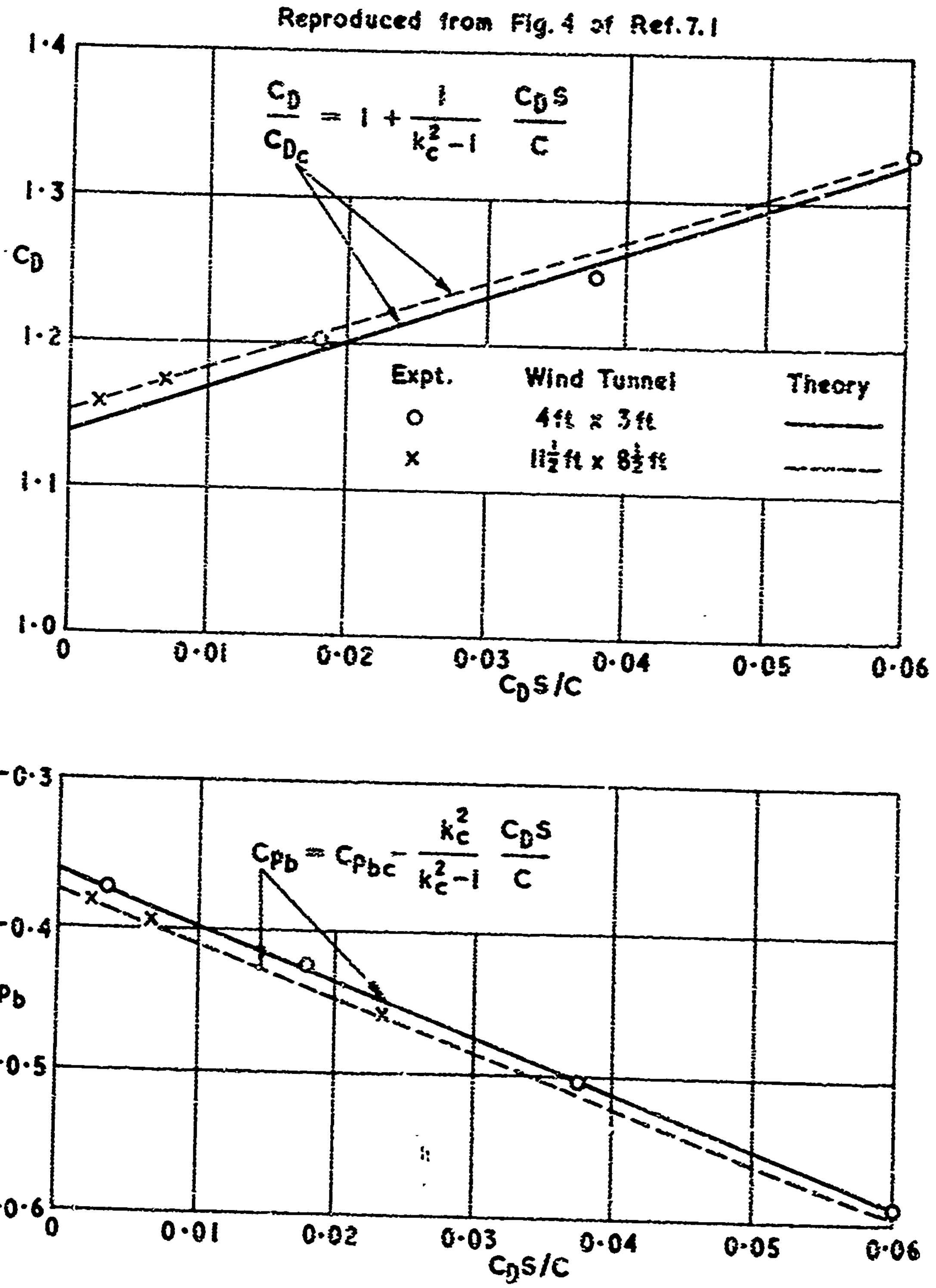

Fig. 7.3 Blockage effect on drag and base pressure for non-lifting square plates

Reproduced from Fig.5 of Ref. 7.1

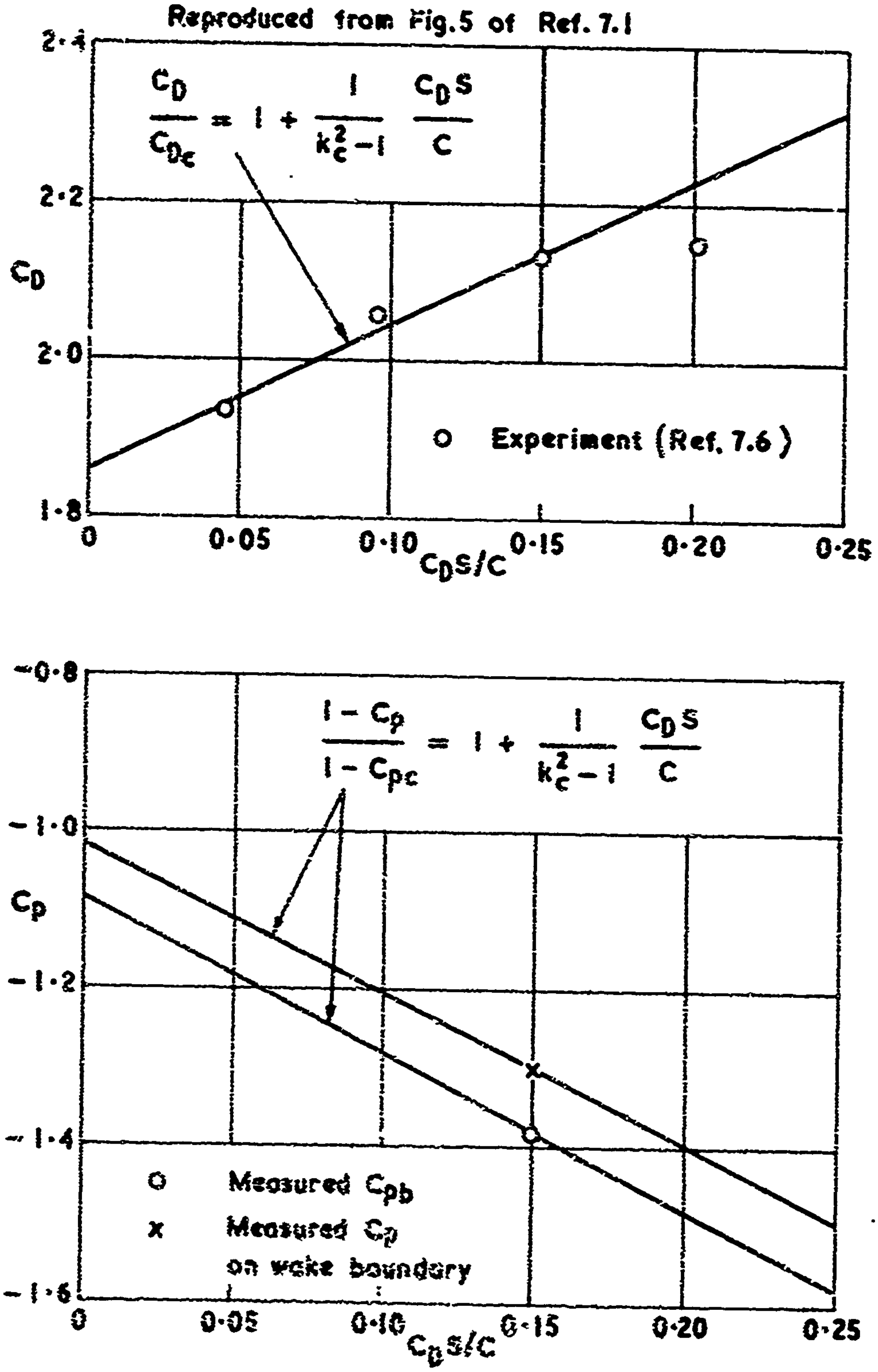

Fig. 7.4 Blockage effect on drag and base pressure for non-lifting two-dimensional plates

Based on Fig.2 of Ref.7.II

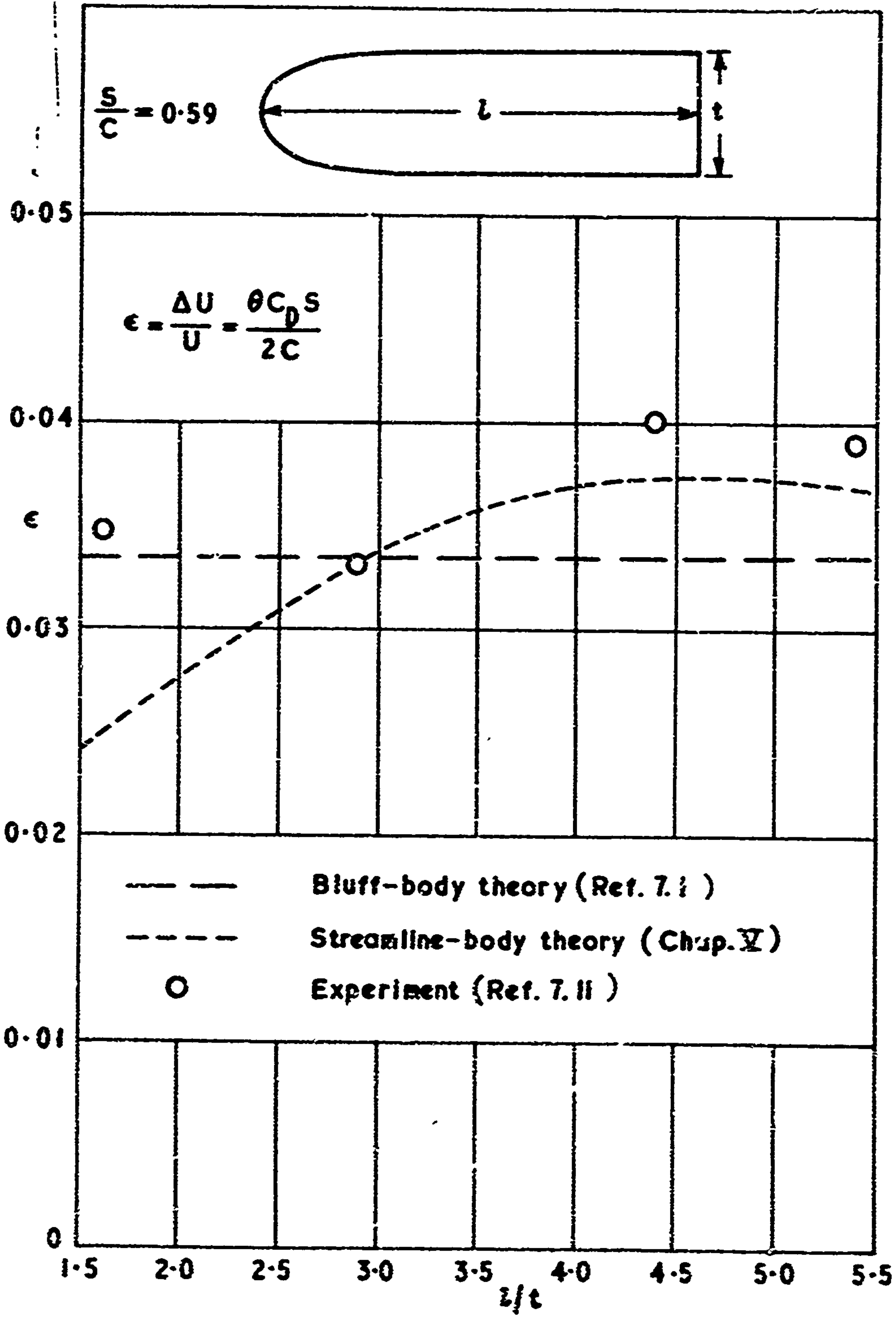

Fig. 7.5 Variation of blockage factor with fineness ratio

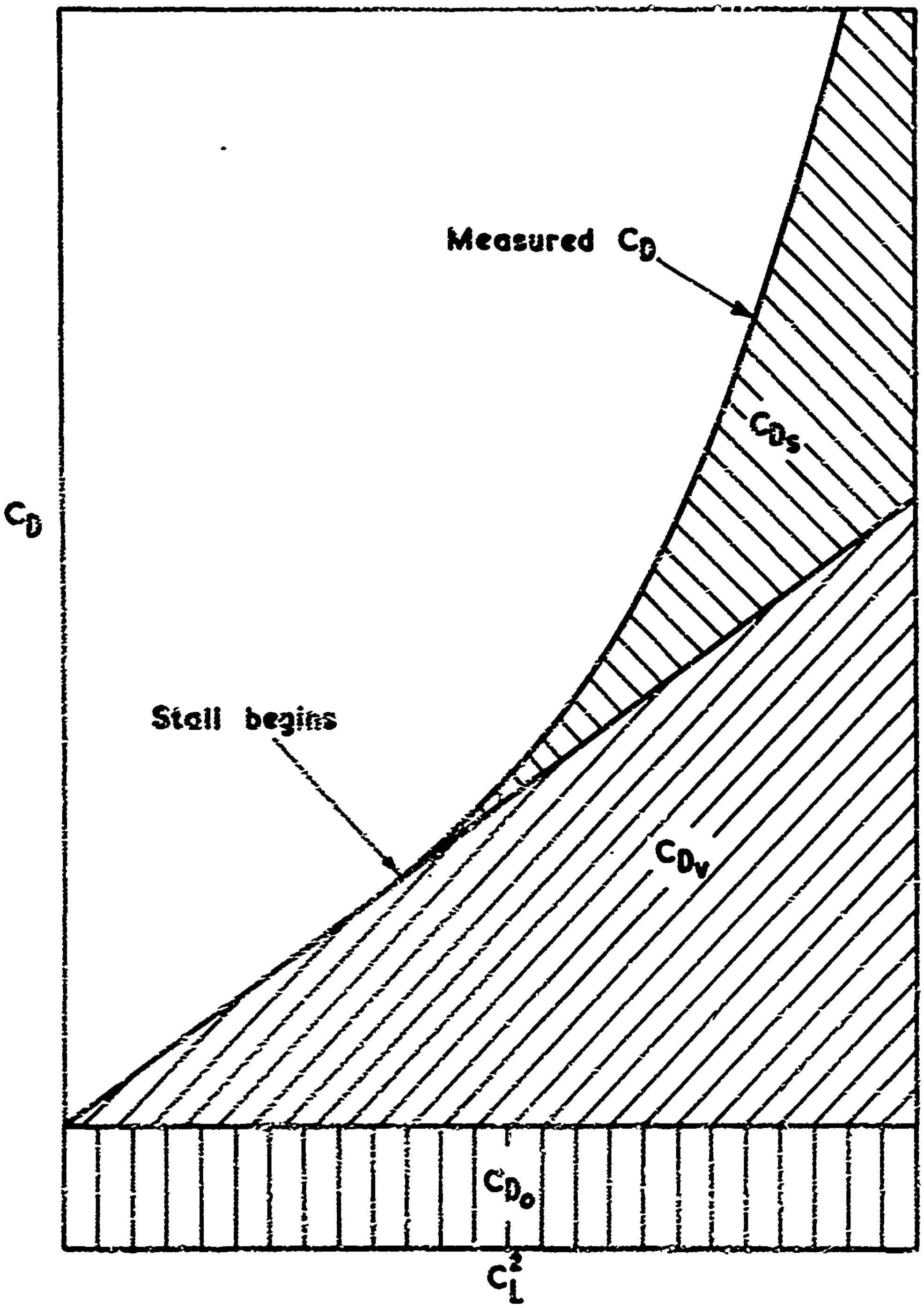

Fig.7.6 Drag analysis for a lifting wing

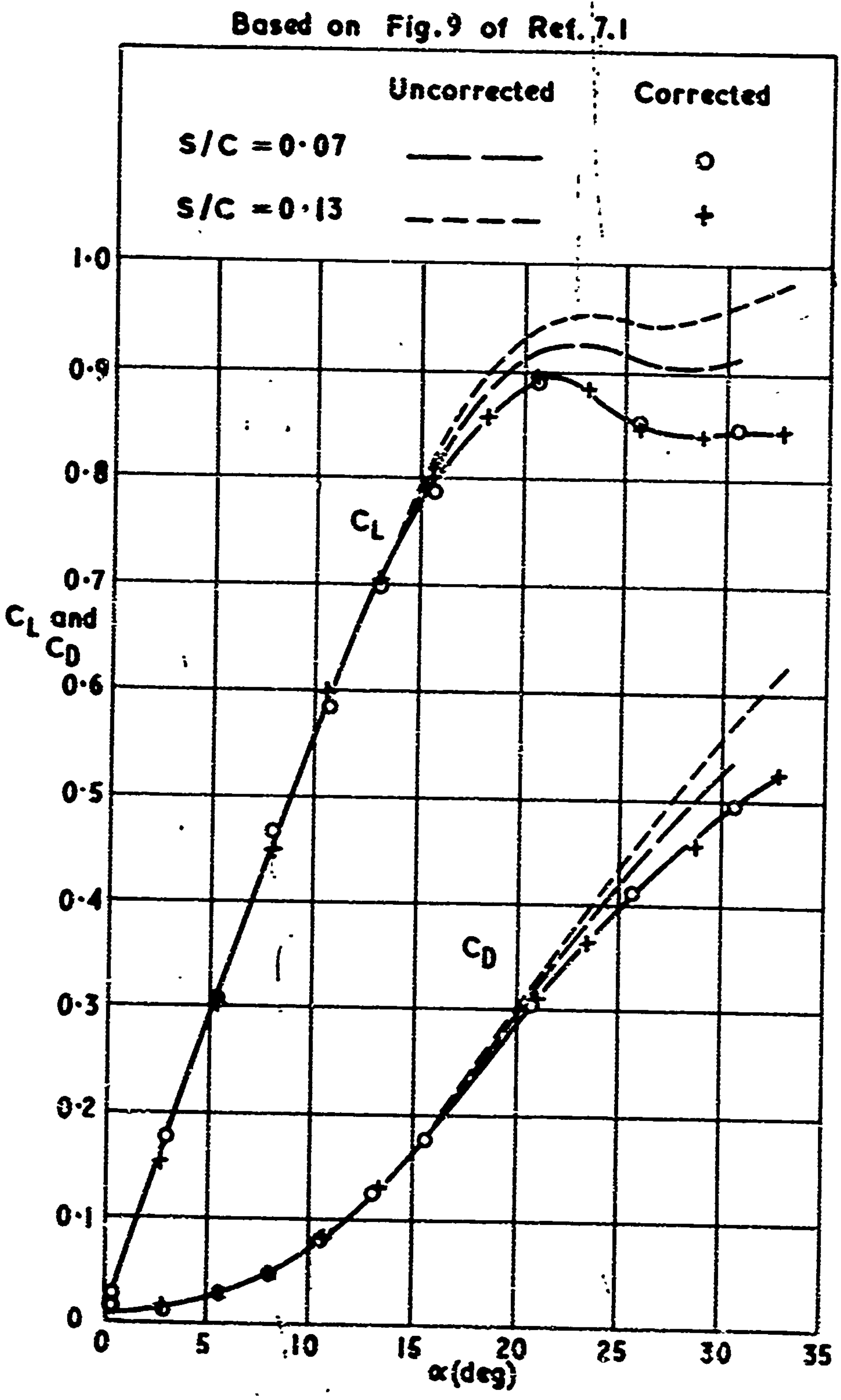

Fig. 7.7 Blockage corrections applied to lift and drag for two sizes of delta-wing-body combination[1]

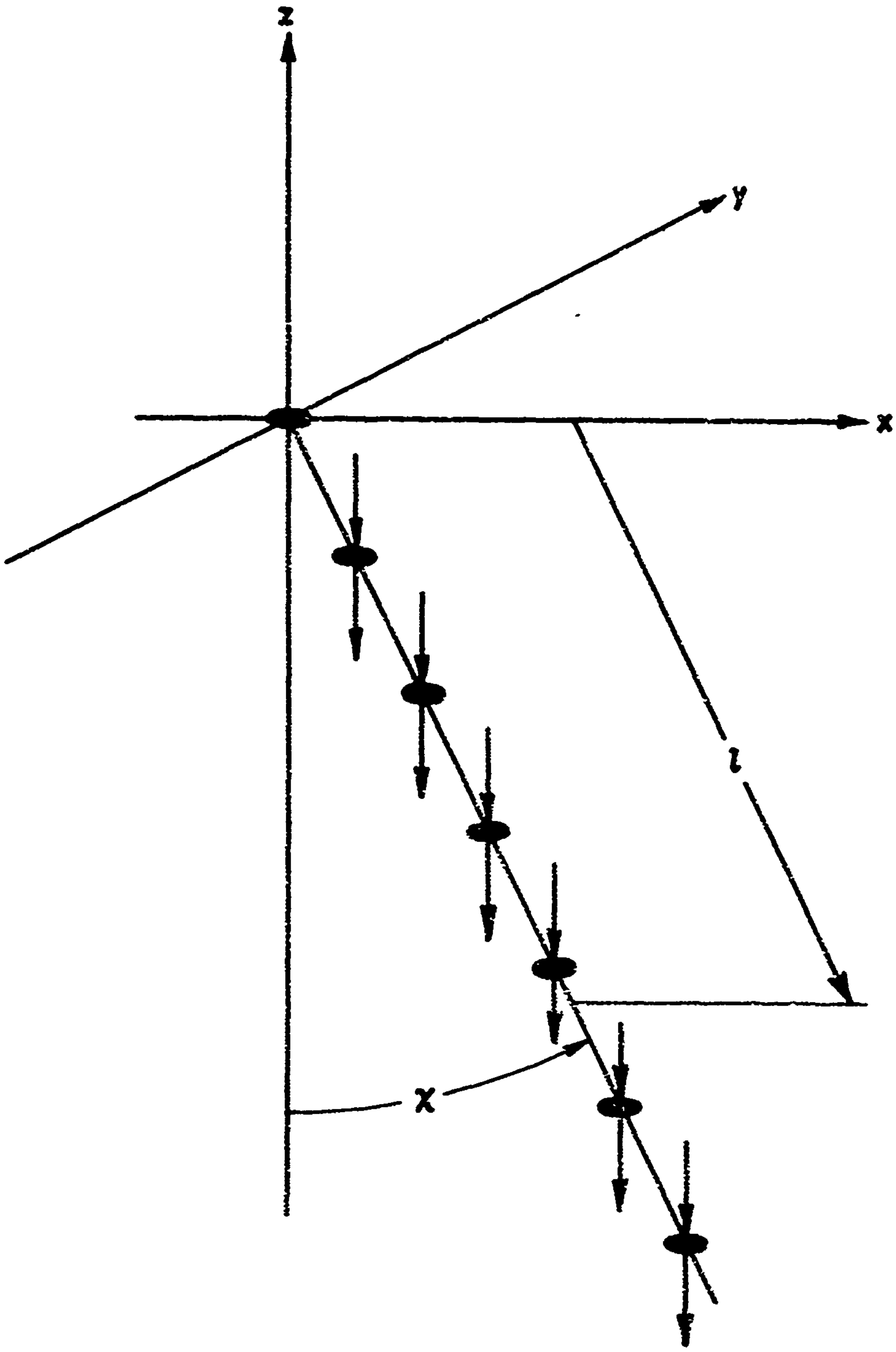

Fig.7.8 Wake of small rotor represented by a semi-infinite row of vertically directed doublets

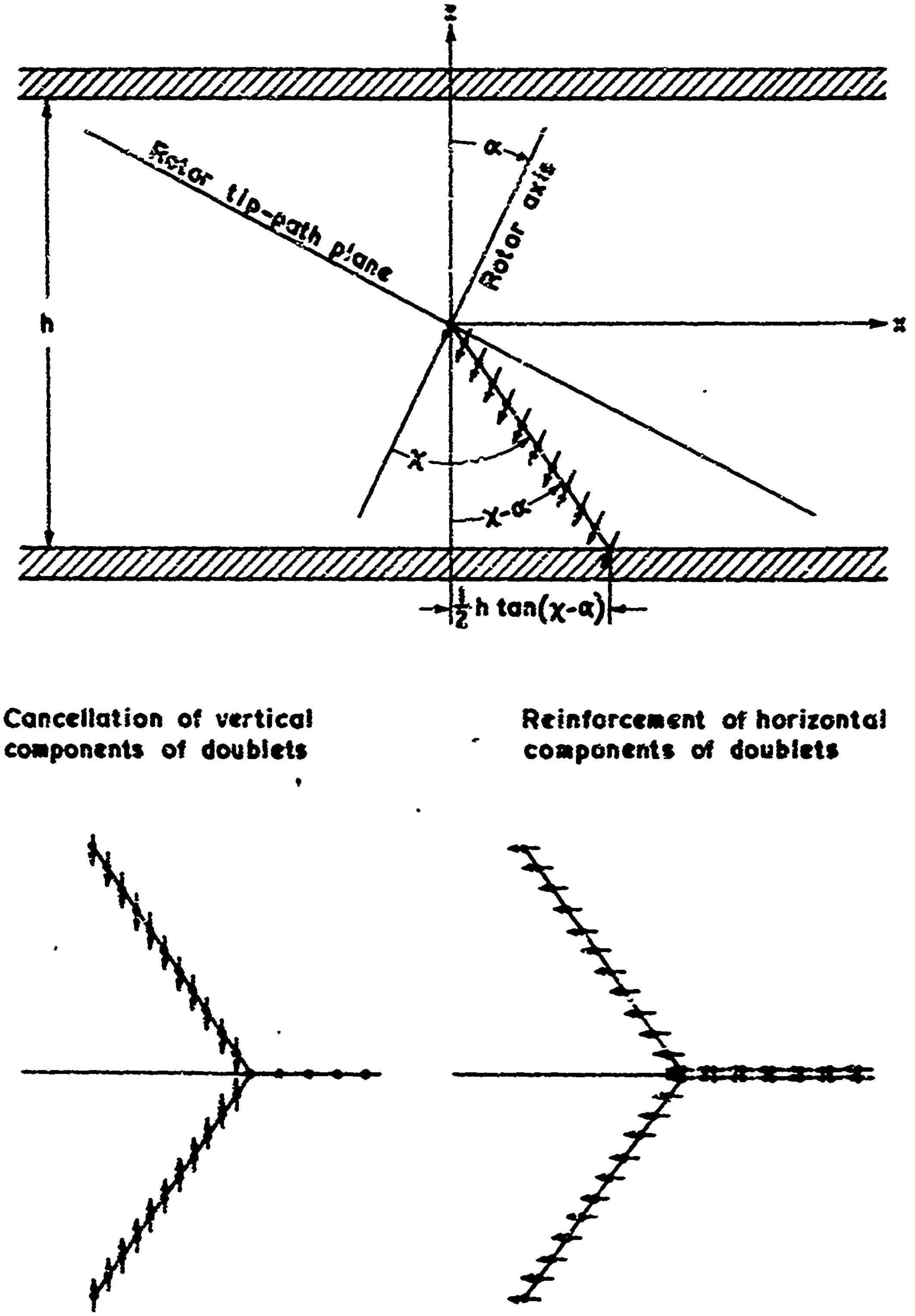
z
α
Rotor axis
Rotor tip-path plane
h
x
χ
χ-α
$\frac{1}{2}h\tan(\chi-\alpha)$
Cancellation of vertical components of doublets
Reinforcement of horizontal components of doublets

Fig. 7.9 Wake of a small rotor at non-zero angle of attack and its image below the floor of a closed tunnel

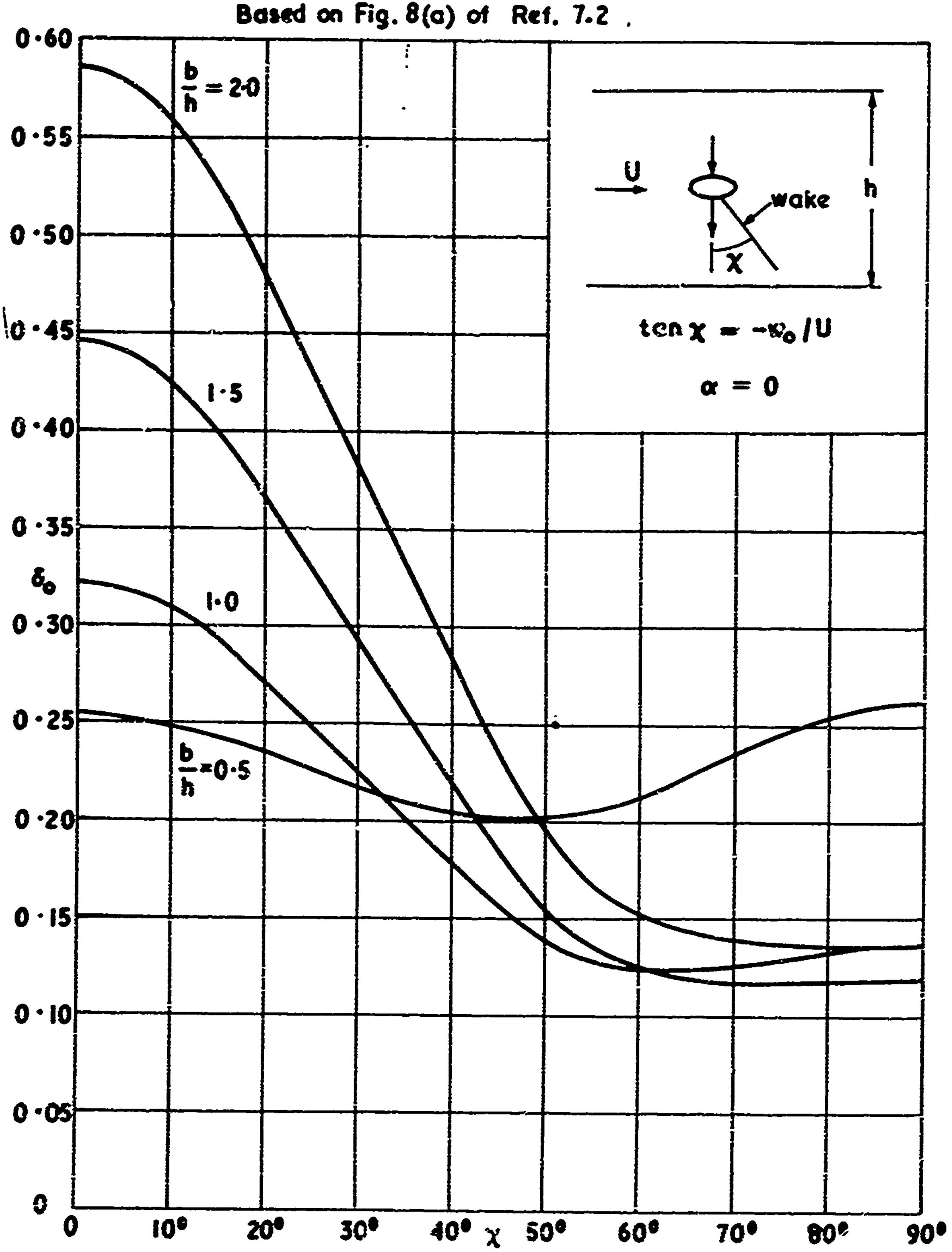
Based on Fig. 8(a) of Ref. 7.2 .

Fig.7.10 Interference parameter against wake skew-angle for small lifting rotors in closed rectangular tunnels

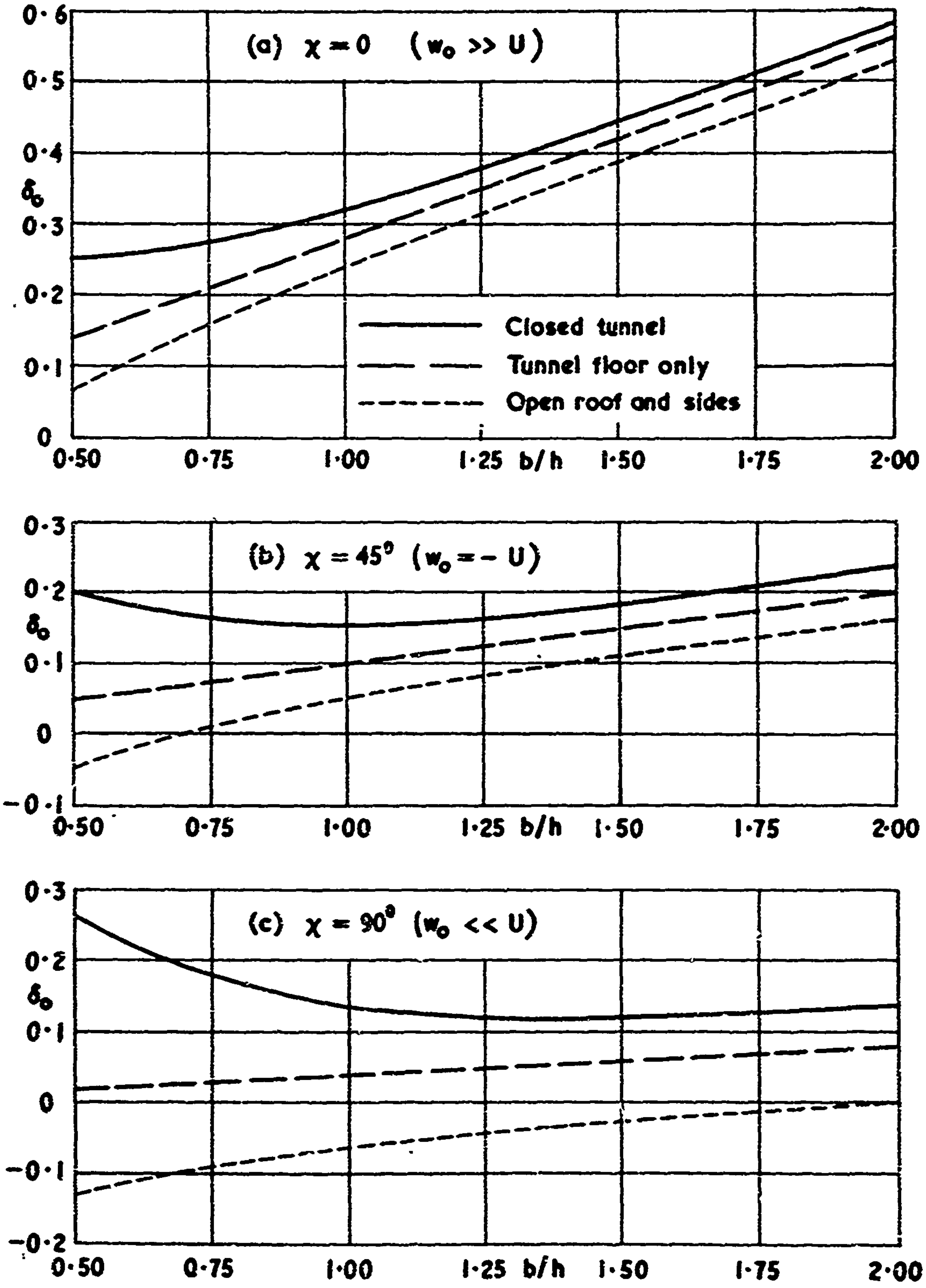

Fig. 7.11 Interference parameter against breadth to height ratio of rectangular tunnels for rotors of different skew angle

Based on Fig. 14(a) of Ref. 7.2

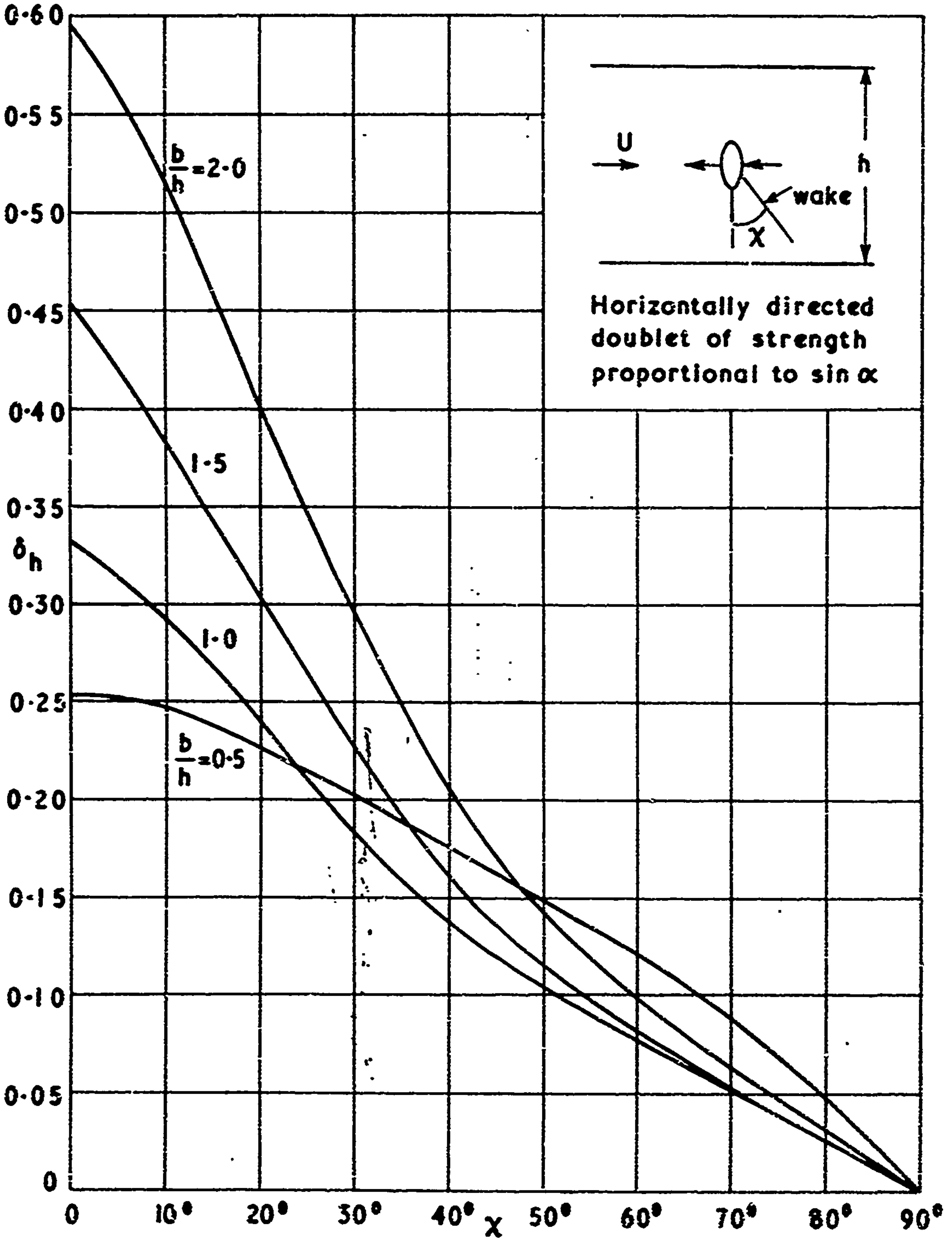

Fig. 7.12 Upwash interference against skew angle for a wake of horizontal doublets in closed rectangular tunnels

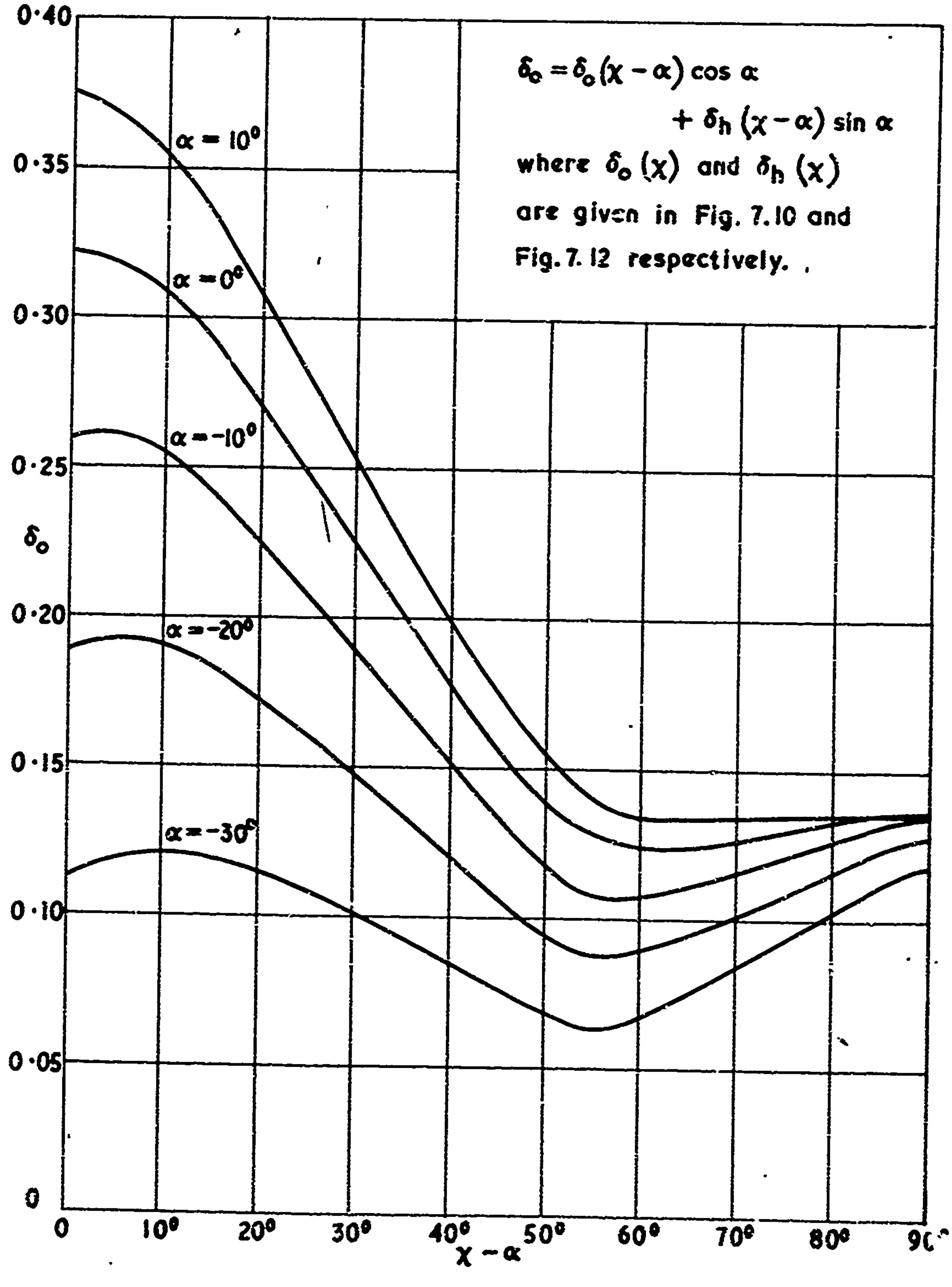

Fig. 7.13 Effect of angle of attack on the interference parameter for small lifting rotors in a closed square tunnel

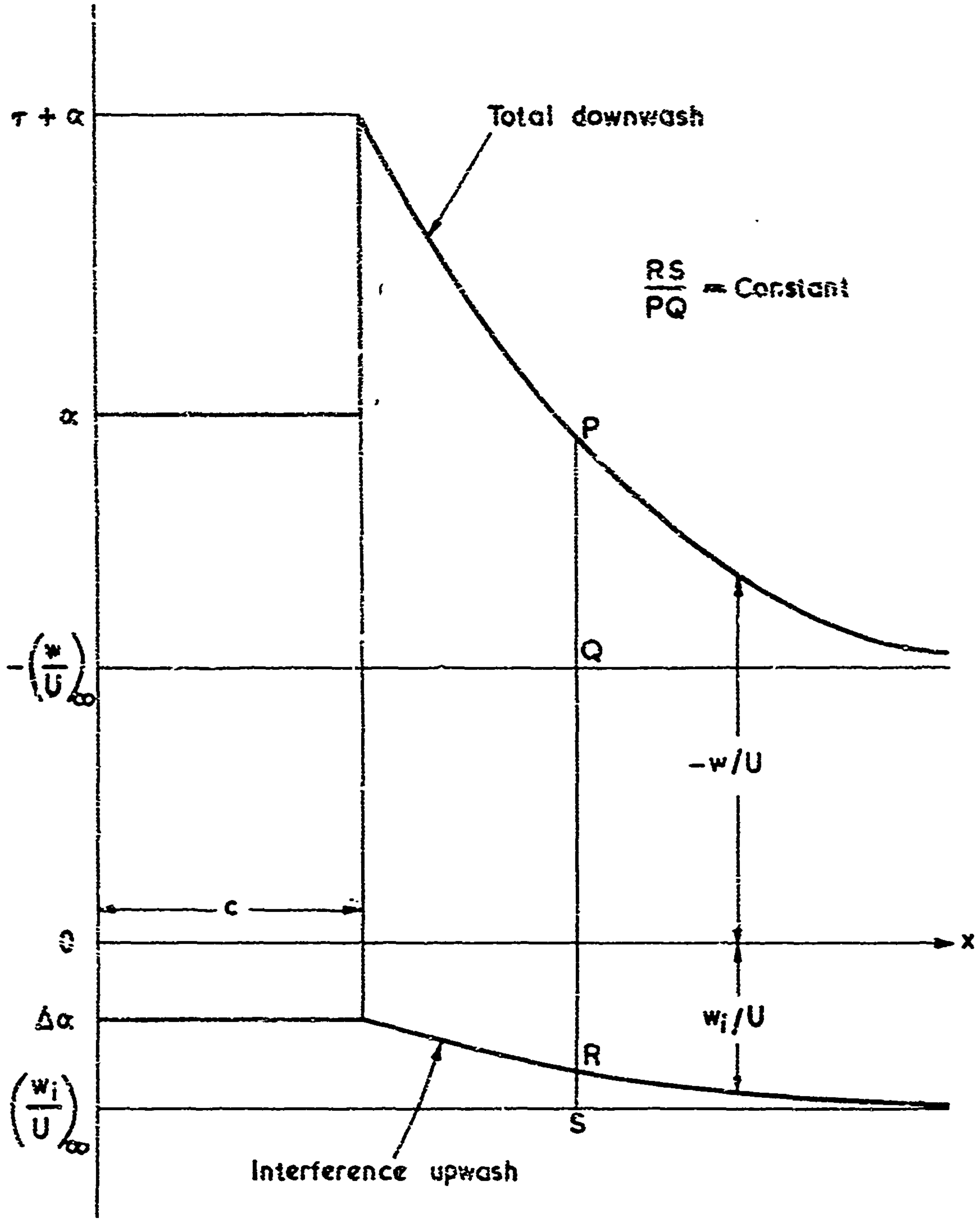
τ + α
Total downwash
RS/PQ = Constant
α
P
Q
$-\left(\frac{w}{U}\right)_\infty$
$-w/U$
c
0
x
Δα
w_i/U
R
S
$\left(\frac{w_i}{U}\right)_\infty$
Interference upwash

Fig. 7.14 Assumed relationship between total downwash and interference upwash for a jet-flap wing

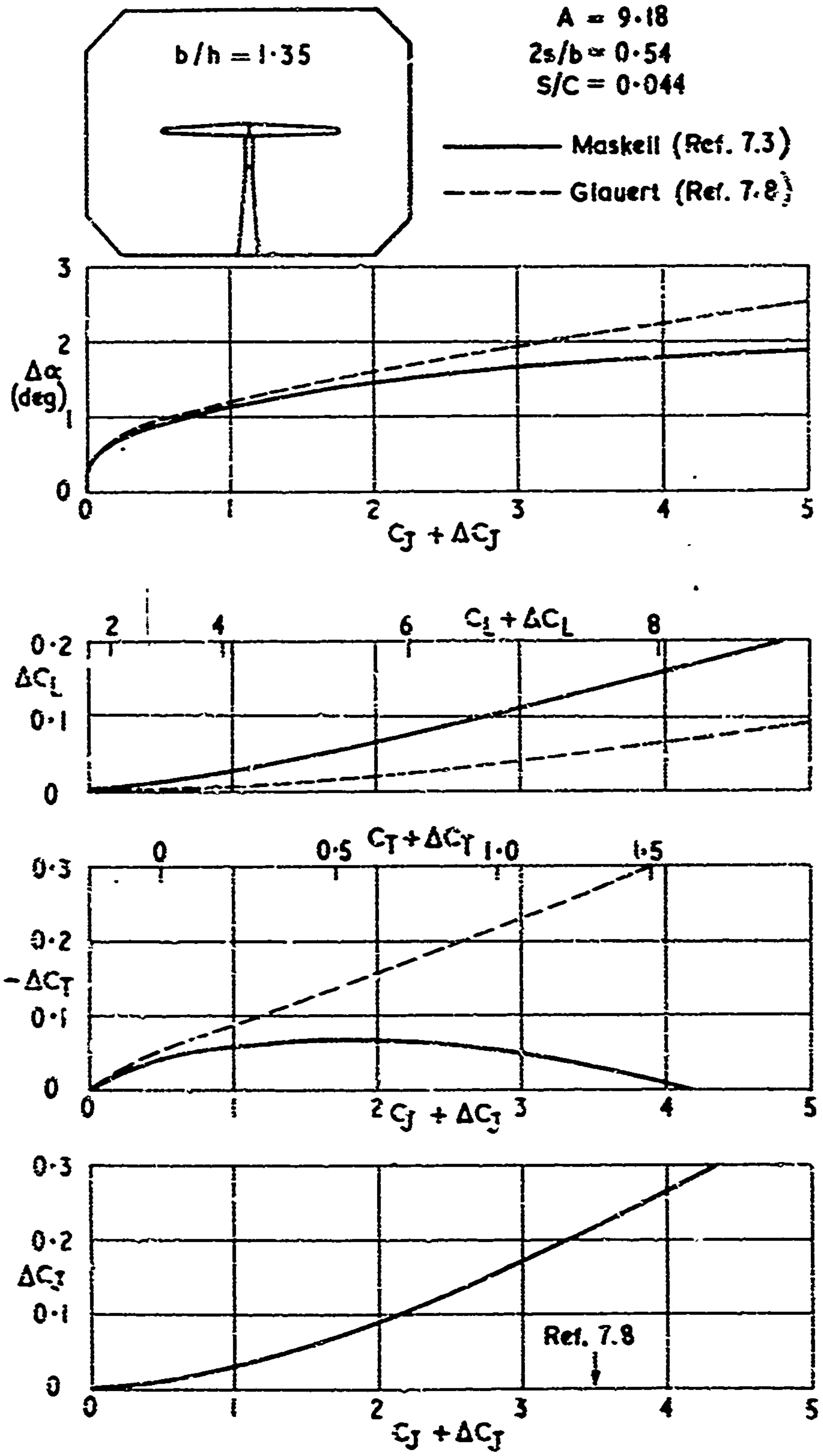

Fig. 7.15 Typical constraint corrections for a jet-flap wing with 50° jet deflection